A STUDY OF GPS AND OTHER NAVIGATIONS SYSTEMS FOR HIGH PRECISION NAVIGATION AND ATTITUDE DETERMINATIONS

WAN-XUAN FU

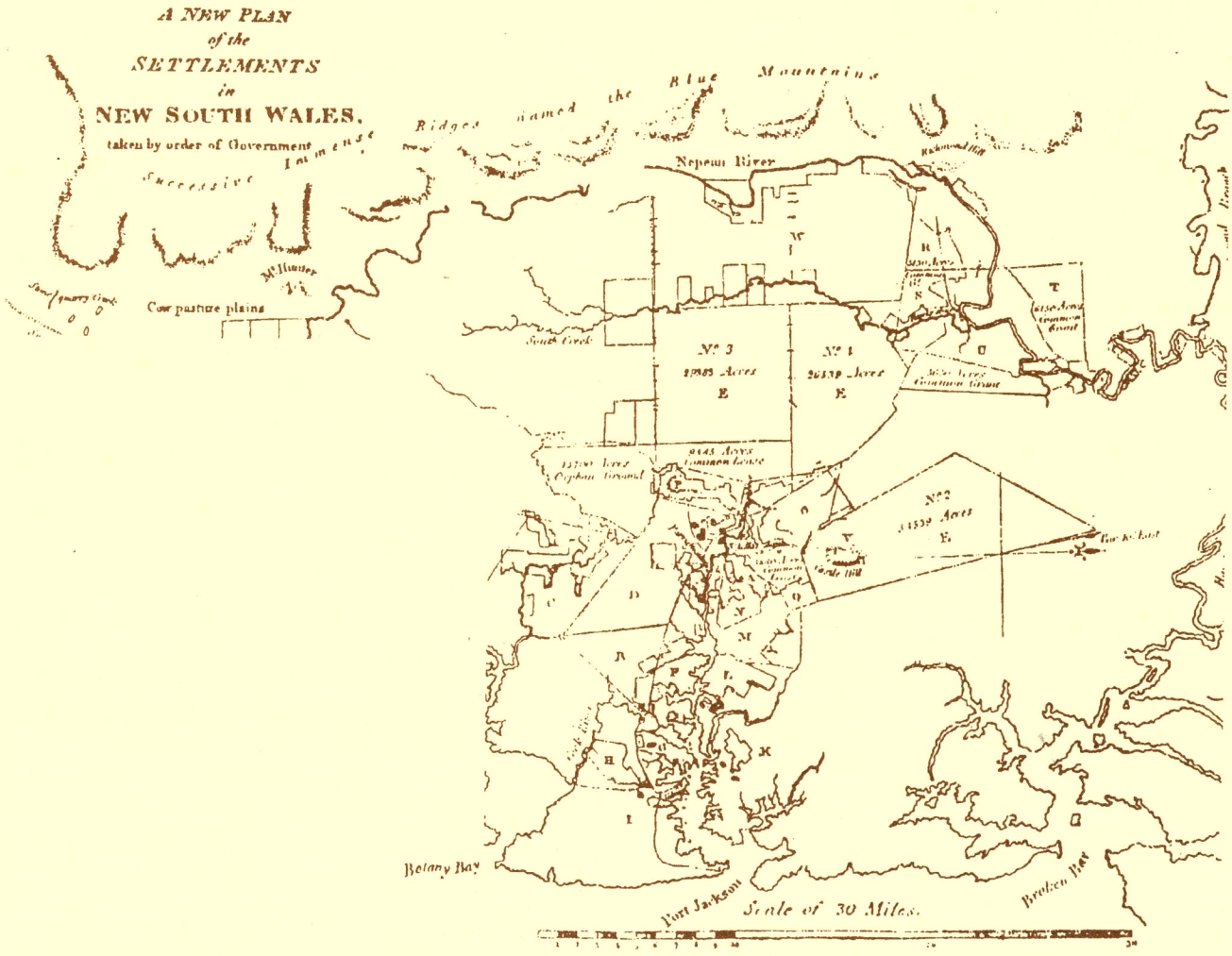

UNISURV S-45, 1996

Reports from

SCHOOL OF GEOMATIC ENGINEERING

THE UNIVERSITY OF NEW SOUTH WALES SYDNEY NSW 2052 AUSTRALIA

UNISURV REPORT S-45, 1996

A STUDY OF GPS AND OTHER NAVIGATIONS SYSTEMS FOR HIGH PRECISION NAVIGATION AND ATTITUDE DETERMINATIONS

WAN-XUAN FU

Completed, January, 1996
Received: August, 1996

SCHOOL OF GEOMATIC ENGINEERING
UNIVERSITY OF NEW SOUTH WALES
SYDNEY NSW 2052
AUSTRALIA

COPYRIGHT ©

No part may be reproduced without written permission

National Library of Australia

Card No. and ISBN 0 85839 069 8

ABSTRACT

Since 1960's the navigation techniques have experienced a revolutionary advance, which due to the advent of some new kinds of navigation systems, such as inertial navigation system and satellite navigation system, under the background of rapid development of computer technologies, optimal estimation and modern control theory. All navigation information can now be used jointly and optimally, and the integrated navigation system has become standard navigation tool.

This research involved the analysis and investigation of navigation systems (mainly the GPS and integrated navigation systems) and navigation computation for high precision navigation and attitude determination, especially for marine application. The emphasis of the research was to find new methods and concepts to deal with the traditional navigation problems.

The navigation models were analyzed in both time and frequency domains and the model's stability, controllability and observability with GPS observables were introduced in order to facilitate the navigation filter design.

New kind of filters, such as frequency-discriminating filters and separated-bias Kalman filter, were introduced to navigation data processing, and these filters are useful for GPS data smoothing, cycle slip detection and repair and ambiguity resolution in both static and kinematic modes.

Based on the navigation system and equipment operation and error analysis, a closed-loop dead reckoning integration with other navigation systems (GPS, Omega, Loran-C and radar) was proposed in order to obtain a good system frequency response and facilitate the body's manoeuvre detection and system quality control.

To use GPS potential efficiently, a new GPS observable "Doppler created phase" was introduced and associate algorithms were developed. This new observable can be used in both static and kinematic positioning (if the data rate is high enough) using low-cost navigation receivers (output C/A code and

Doppler only), and theoretically an accuracy of equivalent to a phase-floating-ambiguity solution can be expected.

Extensive analysis was given to the attitude determination using GPS, and its limits, potential and alternative implementation are also presented.

The software development and data processing validated the proposed theory and algorithms. The results and statistic tests were illustrated by the different kind of plots including the correlograms and periodograms.

TABLE OF CONTENTS

LIST OF TABLES

LIST OF FIGURES

ACKNOWLEDGEMENTS

First of all I wish to express my deep appreciation to Associate Professor Chris Rizos, my supervisor, for his valuable suggestions and encouragement throughout this research. Without his support and inspiration, this thesis would not have been finished.

I want to thank specially Mr. Bernie Hirsch for helping in my software refinement, GPS receiver performance analysis and data collections.

I also want to thank my fellow students and all colleagues at the School of Geomatic Engineering, UNSW, for providing an atmosphere in which it is very enjoyable to work.

Appreciation would be given to the Oceanographic Branch, CSIRO, Australia, for supporting the research, and I thank the crew of M.S. FRANKLIN for the successful experiment and happy voyage.

CHAPTER 1

INTRODUCTION

1.1 Navigation and Positioning

Navigation can be loosely defined as the techniques *by which a craft is given guidance to travel from one known location to another.* Hence navigation is not only concerned with determining position, but also determining a trajectory to be followed and ensuring that the actual track matches, as far as possible, the planned trajectory (Logsdon, 1992).

There are two functions navigation has therefore to fulfil: **positioning** and **guidance**. The relation between positioning and guidance is conceptionally illustrated in Fig.1.1. Here, it is assumed a vessel is underway with speed V from the origin of an arbitrary Cartesian coordinate system to a destination point B, passing a danger d at a minimum distance r. OAB is the planned trajectory, C is the initial planned course with a course error ΔC. At each position fix, the true track and drift are estimated and a new course (C1, C2,and C3) is determined in order to return the vessel to the planned track. The true track deviates from the planned track due to the effects of wind, current and the errors of the course and speed-to-steer. The relationship between heading, course, water speed and ground speed is shown in Fig.1.2 (where the effects of wind and current have been exaggerated).

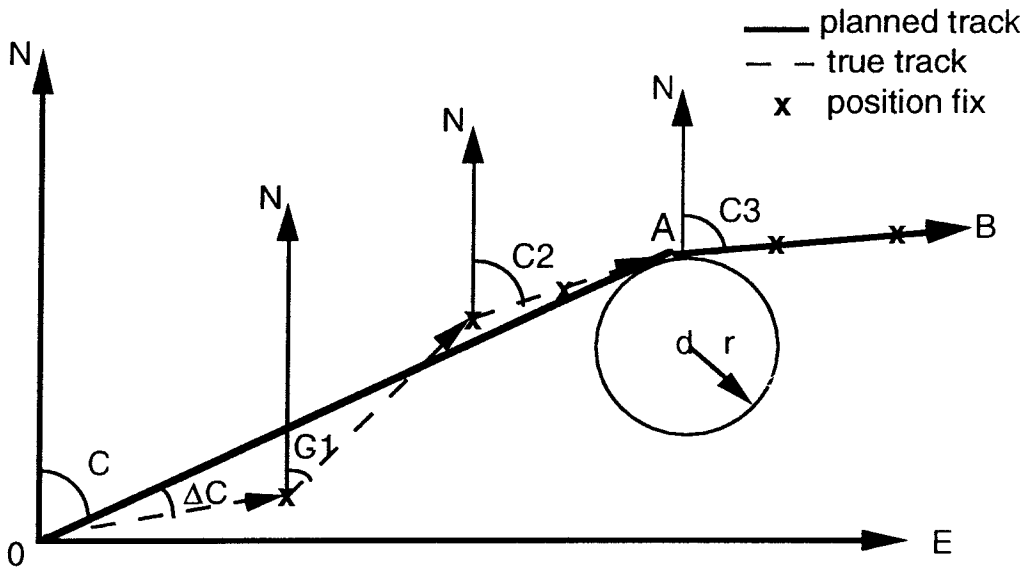

Figure 1.1. The Navigation procedure: positioning and guidance.

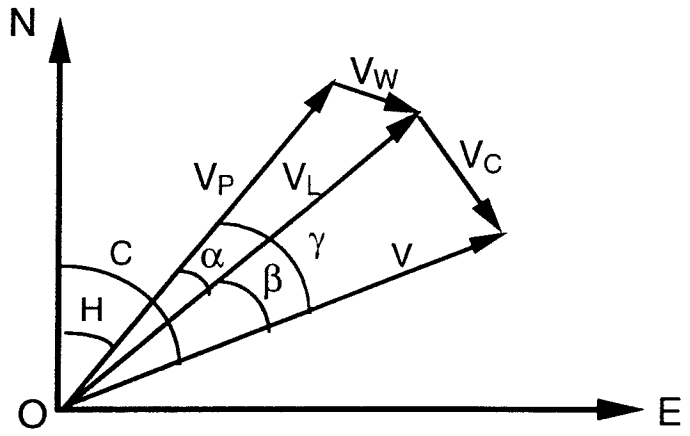

Figure 1.2. Relationship between course, heading and speed relative to water and ground.

where

O	centre of mass of vessel	N	north direction
V_p	vessel's propelling speed	E	east direction
V	vessel's ground speed	V_L	vessel's speed relative to water
H	heading	V_W	leeway speed caused by wind
α	leeway angle	β	current set angle
γ	total set angle	C	course-made-good
V_C	current speed		

Heading H can be provided by a gyrocompass, the speed relative to water V_L by a sensor such as a vessel's speed log, course C and ground speed V are usually determined from consecutive position fixes.

A vessel's trajectory is usually determined as a set of discrete positions using navigation systems, relying on observations to targets whose locations are known. Theoretically, in order to recover the *continuous* true trajectory from such discrete position data, the positioning interval should be less than half of the shortest period of the trajectory variation. In other words, the positioning rate (or frequency) should be at least twice the highest frequency of trajectory variation (Oppenheim & Schafer, 1989) for positioning at equal intervals. Otherwise only a smoothed or mean trajectory can be assumed to have been determined.

In general there are two basic methods of navigation: **position fixing** and **dead reckoning**. Position fixing is accomplished using information from navigation systems external to the vessel, such as GPS, Loran-C, Omega, etc. Their positioning precision can be represented by the error ellipse (or ellipsoid) which is dependent on the observation geometry and measurement noise. The positioning process can be discrete, or continuous. On the other hand, dead reckoning (DR) is based on information obtained from navigation sensors attached to the vessel which measure the vessel's heading, or course and speed, such as gyrocompass, speed log and inertial navigation systems (INS). In the case of a *pure* DR system there is no need to exchange information with the outside world, as it is entirely self-contained. However, the navigation accuracy generally degrades with time, as illustrated in Fig.1.3.

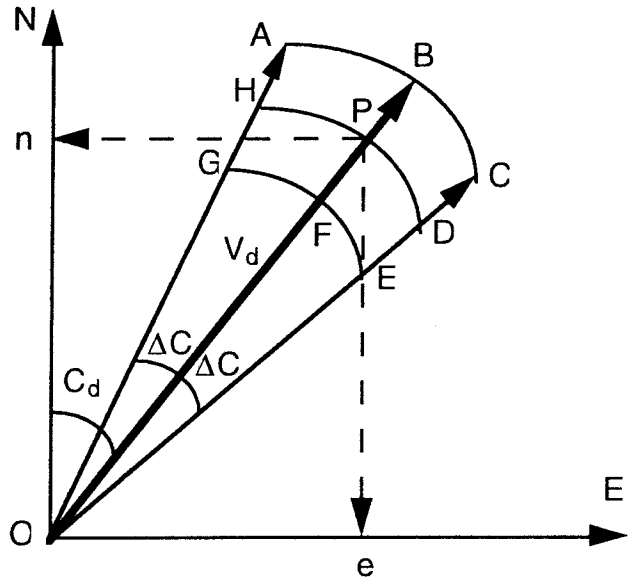

Figure 1.3. Dead reckoning and the growth of position error.

In Fig.1.3 0 is the known start position at time t(0), P is the DR position at time t(k) determined from the DR course C_d and speed V_d, obtained from gyrocompass, speed log or INS output. $0P = V_d\ [t(k) - t(0)]$ is the DR distance. The DR position in a local geographic frame can be expressed as:

$$0e = V_d\ [t(k) - t(0)]\ \sin C_d \qquad (1.1)$$

$$0n = V_d\ [t(k) - t(0)]\ \cos C_d \qquad (1.2)$$

It is apparent that the DR distance error $FP = PB = \Delta V \cdot [t(k) - t(0)]$ and the DR error due to course error is $PH = PD \approx 0P \cdot \Delta C = V \cdot [t(k) - t(0)] \cdot \Delta C$, where ΔC and ΔV are the course and speed uncertainty attributable to the gyrocompass, speed log or INS errors, as well as wind and current uncertainty. The DR position is inside the area ABCDEFGH at time t(k), and this area can be expected to increase with time. Although the DR system can give a continuous trajectory, its error growth must be controlled by regular position fixing. The choice of appropriate navigation system, sensors and methodology depends on the application and the associated navigation requirements.

1.2 Navigation Requirements

There are several phases of any vessel's journey. When on the open seas a vessel's planned trajectory is likely to be a straight line and the position fixing rate need not be high. When the vessel approaches the coast, however, the position fixing interval may need to be shortened, as in general, a higher accuracy is required. When travelling within a navigation channel in a harbour, or within confined waters, the vessel has to be kept on a specified trajectory, and any deviation from this trajectory should be detected and corrected with minimum delay.

Maritime navigation requirements generally have a well structured classification according to the three distinct phases of operation namely: the ocean phase [Table 1.1]; coastal phase [Table 1.2]; and the harbour approach and harbour phase [Table 1.3]. These tables are based on U.S. Federal Radionavigation Plan (FRP, 1988) requirements and are reproduced here for the sake of "bench marking", and to aid in the assessment of emerging navigation technologies (Krakiwsky et al.,1990). In the Tables the accuracy is stated in terms of the marginal confidence region ± 2 drms (distance root mean square) which has an associated probability of 95%. The status of current navigation systems is summarized in Fig. 1.4 (Logsdon, 1992). For a discussion concerning the future of navigation systems see, for example, Heywood (1992), Krakiwsky et al., (1990).

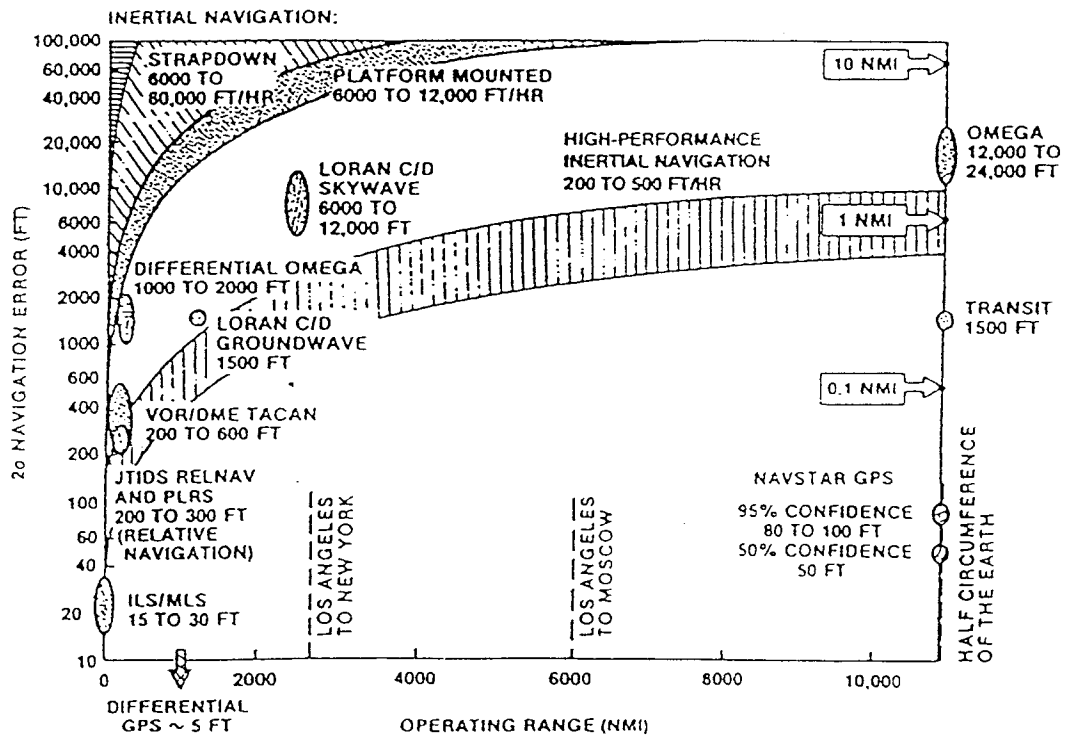

Figure 1.4. Range and accuracy comparisons for various navigation systems.

Table.1.1 Marine requirements-Ocean Phase (After U.S. FRP, 1988)

REQUIREMENTS	MEASURES OF MINIMUM PERFORMANCE CRITERIA TO MEET REQUIREMENTS							
	ACCURACY (2 drms)		COVERAGE	AVAIL ABILITY	RELIA BILITY	FIX INTERVAL	FIX DIMENSION	CAPACITY
	PREDICTABLE	RELATIVE						
Safety of Navigation - All Craft	2-4 nm (3.7-7.4 km) minimum 1-2 nm (1.8-3.7 km) Desirable	-	Worldwide	99% fix at least every 12 hours	**	15 minutes or less desired; 2 hours maximum	Two	Unlimited
Large Ships Maximum Efficiency	0.1-0.25 nm* (185-460 m)	-	Worldwide, except Polar regions	99%	**	5 minutes	Two	Unlimited
Resource Exploration	10-100 m*	-	Worldwide	99%	**	1 minute	Two	Unlimited
Search Operations	0.1-0.25 nm (460 m)	185	National maritime SAR regions	99%	**	1 minute	Two	Unlimited

* Based on stated user need.
** Dependent upon mission time.

Table.1.2 Marine requirements-Coast Phase (After U.S. FRP, 1988)

REQUIREMENTS	MEASURES OF MINIMUM PERFORMANCE CRITERIA TO MEET REQUIREMENTS							
	ACCURACY (2 drms)		COVERAGE	AVAIL ABILITY	RELIA BILITY	FIX INTERVAL	FIX DIMENSION	CAPACITY
	PREDICTABLE	RELATIVE						
Safety of Navigation - All Ships	0.25 nm (460 m)	-	Coastal waters	99.7%	**	2 minutes	Two	Unlimited
Safety of Navigation - Recreation Boats & Other Smaller Vessels	0.25 nm-2 nm	-	Coastal waters	99%	**	5 minutes	Two	Unlimited
Commercial Fishing (including Commercial Sport Fishing)	0.25 nm (460 m)	-	Coastal/ fisheries areas	99%	**	1 minute	Two	Unlimited
Resource Exploration	10-100 m*	-	Coastal areas	99%	**	1 second	Two	Unlimited
Search Operations, Law Enforcement	0.25 nm (460 m)	300 ft (90 m)	Coastal/ fisheries areas	99.7%	**	1 minute	Two	Unlimited
Recreational Sports Fishing	0.25 nm (460 m)	-	Coastal areas	99%	**	5 minutes	Two	Unlimited

* Based on stated user need.
** Dependent upon mission time.

Table.1.3 Marine requirements-Harbour Approach and Harbour Phase (After U.S. FRP, 1988)

REQUIREMENTS	MEASURES OF MINIMUM PERFORMANCE CRITERIA TO MEET REQUIREMENTS							
	ACCURACY (2 drms)		COVERAGE	AVAIL ABILITY	RELIA BILITY	FIX INTERVAL	FIX DIMENSION	CAPACITY
	PREDICTABLE	RELATIVE						
Safety of Navigation - Large Ships & Tows	25-65 ft *** (8-20 m)	-	Harbours & harbour approaches	99.7%	**	6-10 seconds	Two	Unlimited
Safety of Navigation - Smaller Ships	***	-	Harbours & harbour approaches	99.7%	**	***	Two	Unlimited
Resource Exploration	1-5 m*	-	Harbours & harbour approaches	99%	**	1 second	Two	Unlimited
Fishing, Recreational and Other Small Vessels	***	-	Harbours & harbour approaches	99.7%	**	***	Two	Unlimited

* Based on stated user need.
** Dependent upon mission time.
*** Varies from one harbour to another.

In general, INS have not been in common use for civilian maritime applications. However, with the rapid development of computer technology and the advent of new low-cost, medium accuracy inertial sensors such as fibre-optic gyros, vibrating-rate gyros and solid-state accelerometers, there may be an increasing application of these sensors for land, air and sea navigation (for more details the reader is referred to, for example, Liu et al., 1990; Norling, 1990; Karnick, 1992; Bader, 1993).

1.3 Development of Marine Navigation Technology in the 20th Century

There have been three distinct phases in the development of marine navigation technology in this century.

1.3.1 Phase One (1900-1945)

The gyrocompass was introduced at the beginning of the century and several prototype radio aids such as Consol, Loran, the radio direction finder and radar at the end of World War II. Nevertheless, there was little change in the practice of navigation compared to that during the 19th century. The navigator still relied on the compass, log, sextant and chronometer to fix and compute his position using simple navigation techniques and observation models. The position fixing frequency was dependent on the visibility of the landmark and celestial bodies, and a few nautical miles of position error was common in the ocean. Near-coast, the positioning accuracy was nearly inversely proportional to the distance from a visible landmark.

1.3.2 Phase Two (1946-1960)

The medium and long range radio aids such as Loran, Decca and Omega, were fully developed and put into operation. Statistical estimation methods were used for position determination, and sophisticated mathematical models of the earth's geometry and signal propagation were used within navigation computation. However, the navigation information obtained from different navigation sensors

were generally used independently, and the position discrepancy had to be resolved using the navigator's judgement.

1.3.3 Phase Three (1961-present)

Computer technologies, optimal estimation and modern control theory, inertial navigation and satellite navigation systems develop rapidly. All navigation information can be used jointly and optimally, and the integrated navigation system has become the standard navigation tool.

1.4 Motivation of the Thesis

The navigation computation requires three basic models: the dynamic model, the observation model and the computation model.

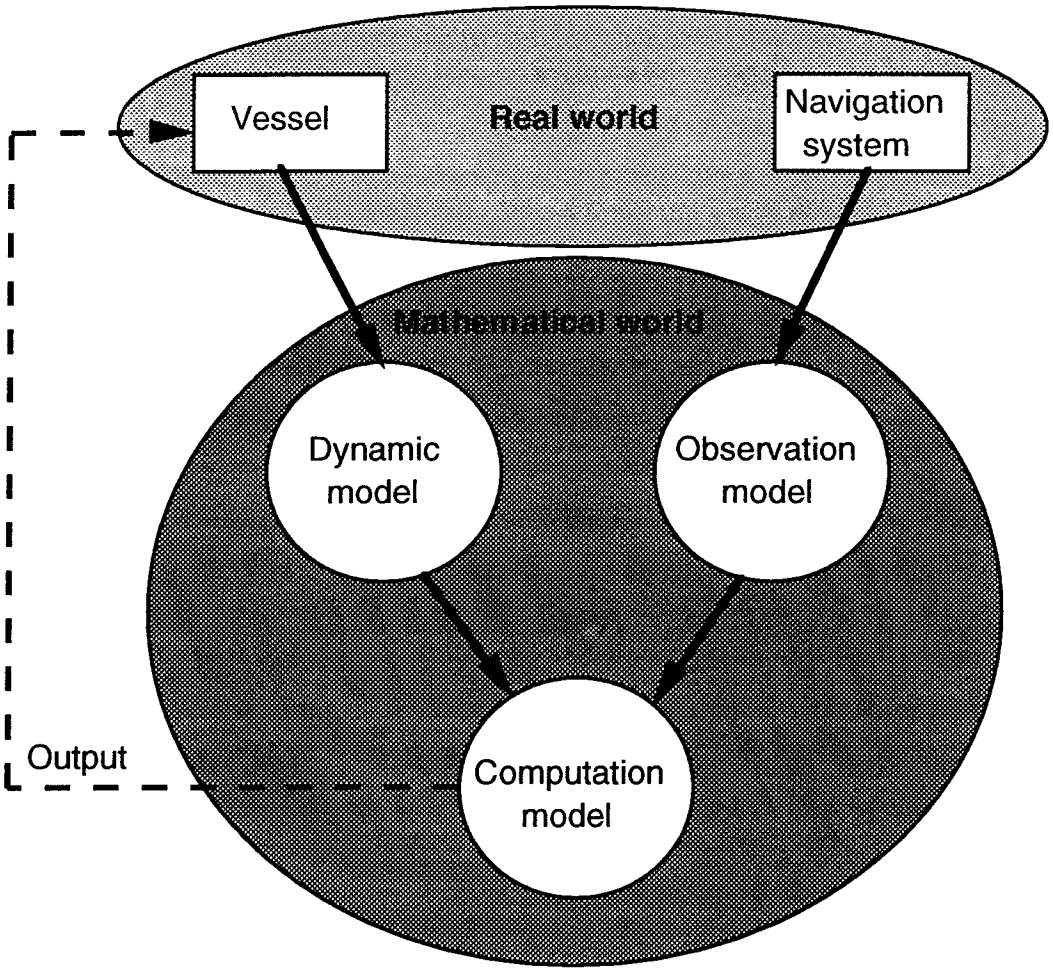

Figure 1.5. The navigation computation procedure and its linkages.

The **dynamic model** is the mathematical description of the vessel's dynamics. Ideally it should be a true duplication and mapping of the vessel's state in the real world. However, some model approximation is inevitable, for example the navigation condition (or environment) is unpredictable, and the approximation causes the navigation error to increase with time if there is no external navigation information available.

The set up of the **observation model** addresses two considerations: (a) how to fully and optimally use the information provided by the navigation system, and (b) how to map the vessel's dynamics into the observation domain. Hence the observation model is closely related to the dynamic model and to the navigation system performance.

The **computation model** may be a filter whose structure and performance is closely dependent on the navigation requirements and the observations available. The computation model should correctly and optimally integrate the dynamic and observation models, and it's performance will directly affect the accuracy and quality of navigation.

This thesis is a report on investigations into the dynamic, observation and computation models as well as the **total system model**, which can be referred to simply as **navigation model**, in both the time and frequency domains. Sometimes the observation and system dynamic characteristics can be discussed more clearly, and more easily dealt with, in the frequency domain, rather than in the usual time domain. For example, time-invariant navigation models have been used for many years, yet the stability of the models, which can be derived easily by analysing the models in the frequency domain, has not been fully investigated. Another example is the application of frequency-discriminating filters (or digital filters) to GPS measurement series processing. This thesis proposes some new mathematical models which can be used for the precise determination of a vessel's position and/or attitude. Also the relationship between the three models and alternative sensor integration strategies has been investigated.

1.5 Outline of the Dissertation

Chapter 2 introduces the basic navigation coordinate systems and the relevant transformation procedures, including the velocity and acceleration transformations. The Attitude determination problem is closely related to the topic of coordinate system, hence it is also introduced in this chapter.

Chapter 3 presents a brief description of several radio aids and navigation sensors, such as Omega, Loran-C, radar, gyrocompass and Doppler-log, as well as the inertial navigation system (INS).

Chapter 4 describes the GPS observables and error models, the smoothed code measurements, and some new Doppler-created phase algorithms.

Chapter 5 discusses the integrated navigation system and describes different integration strategies and structures, especially for the integration of GPS with dead reckoning systems.

Chapter 6 presents the navigation models and such characteristics as model **stability**, **controllability** and **observability**, especially for the case of coloured measurement noise for different observation modes.

Chapter 7 discusses the basic filters used for navigation, including polynomial fitting, Least Squares, digital filter and the Kalman filter. A bias-separated filter is proposed which has particular application to GPS phase data processing.

Chapter 8 presents the data processing examples for position and attitude determination using a variety of models developed by the author.

Chapter 9 summarizes the findings, draws conclusions and makes recommendations for future research.

Appendix 1 discusses the unified semi-analytic inertial navigation system mechanization.

Appendix 2 describes the strapdown inertial navigation system mechanization.

Appendix 3 discusses the inertial navigation error model and the integration of a north-directed inertial navigation system and GPS.

Appendix 4 describes the Bartlett and Portmanteu tests.

Appendix 5 discusses the federated Kalman filter algorithms.

Appendix 6 contains the plots of smoothed code measurements.

1.6 Contributions of the Research

The contributions of the research carried out by the author are summarized as below:

1) Development of a closed-loop GPS and dead reckoning integrated navigation system model, having high performance across wide frequency bands, and which is independent of the vehicle's dynamics.

2) Development of an algorithm for the computation of the transition matrix of a time-varying system using dead reckoning sensor output, which simplifies and reduces the total computational load.

3) Development of a phase-smoothing code measurement algorithm which can be used for real-time GPS data processing.

4) Digital filters for data smoothing (especially useful for single frequency GPS data), and cycle slip detection and repair have been developed. The algorithms are suitable for use with high sampling rate data and real-time applications.

5) Development of Doppler-created phase processing algorithms for high precision static and kinematic positioning using low-cost GPS receiver output (code range and Doppler only).

6) Introduction of the concept of stability of navigation models to assist in the theoretical understanding of navigation models, hence aid to navigation model design.

7) Introduction of the concept of controllability and observability of the navigation models for the GPS observables, in one-way and differential modes, to assist in the design of stable and convergent navigation filters.

8) The frequency response characteristics of polynomial fitting, and the cause of the "wiggle effect" are studied, and the criteria for the selection of polynomial order are given for data of different dynamic characteristics.

9) Development of a bias-separated filter for GPS data processing, that is especially useful for GPS carrier phase ambiguity resolution and state estimation.

CHAPTER 2

AN INTRODUCTION TO COORDINATE SYSTEMS FOR NAVIGATION

A solid body motion in space has six degrees-of-freedom and can therefore be described by six parameters. Typically these are chosen to be the three translation parameters of the body's centre of mass and three rotation parameters about the body's centre of mass. Hence the states of a body, can be described by its translation state (expressed in position, velocity, acceleration), and its rotation state (typically attitude angle and attitude angle rate). For navigation computation purposes, several Cartesian systems or frames are required. The transformation matrix of the body's position, velocity, acceleration and angular velocity, etc., between any two of these frames is generally an orthogonal matrix, and all the body's states (except attitude angle) are vectors in these frames.

2. 1 Cartesian Coordinate Systems

The three most fundamental reference systems for navigation are the space-fixed (or inertial), the earth-fixed and the geographic coordinate systems (Fig. 2.1).

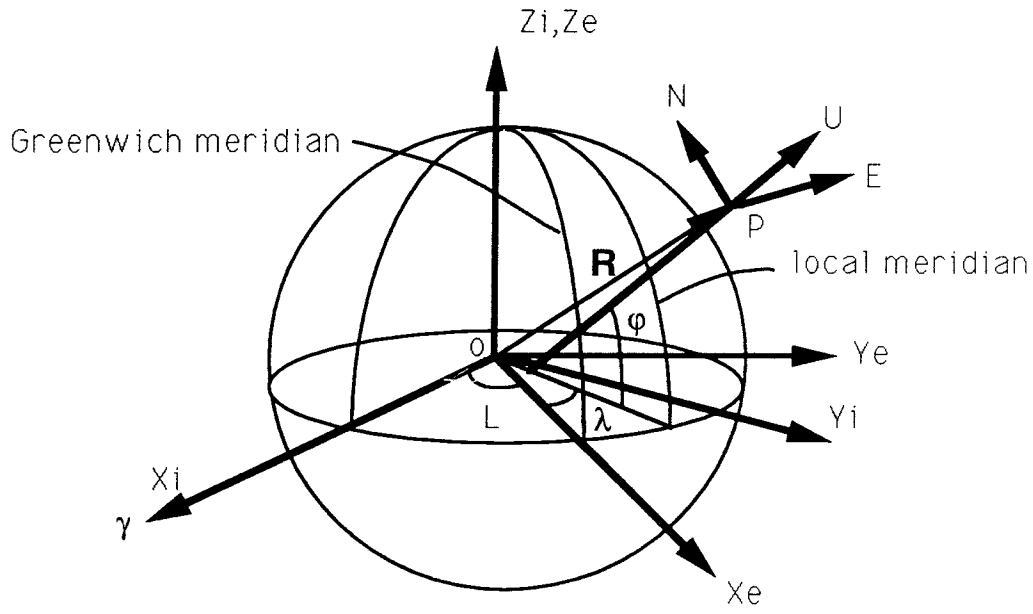

Figure 2.1. Space-fixed, earth-fixed and geographic frames.

where:

- γ Vernal Equinox
- L Greenwich sidereal time
- φ, λ geographic latitude and longitude
- P position of body's mass centre
- **R** position vector of P

2.1.1 The Inertial Frame (Xi, Yi, Zi)

In this frame Newton's law is valid and there are no accelerations of the frame. In practice, a frame that has its origin at the geocentre of the earth, and which is non-rotating relative to the stars, can be considered to be an inertial frame for navigation applications in the vicinity of the earth, and hence the gravitational effects of the sun and planets can be neglected. Conventionally the *Xi* axis points to the Vernal Equinox in the equatorial plane, the *Zi* axis is coincident with the earth's angular velocity vector and the *Yi* axis is in the equatorial plane and completes a right-handed orthogonal frame with the other two axes. This is the basic frame for GPS satellite orbit computations and inertial navigation sensor measurements.

2.1.2 The Earth Frame (Xe,Ye,Ze)

This is an earth-centred and earth-fixed frame, which rotates relative to the inertial frame around the spin axis of the earth with an angular velocity of about 15 deg./hr. Its origin is the geocentre, the *Ze* axis is coincident with the spin axis of the earth and the *Xe* and *Ye* axes are located in the equatorial plane. The *Xe* axis is the line of intersection of the Greenwich meridian plane with the equatorial plane. This frame is the basis of navigation computation and ground-based navigation systems such as Omega, Loran-C and radar (Kayton, 1969). The earth frame is related to the concept of a geodetic datum (Krakiwsky et al., 1971). For most navigation purposes the earth is assumed to be an ellipsoid and the body's position is represented by the triplet of geographic latitude, longitude and ellipsoidal height. Different values of the reference ellipsoid parameters correspond to different frames, for example, the WGS-84 system (Decker, 1986) being one very commonly used nowadays.

2.1.3 The Geographic Frame (E, N, U)

The origin of this frame is at the location of body's centre of mass and its axes align with the *east*, *north* and *up* directions. *Up* is defined to be coincident with the normal to the reference ellipsoid and is perpendicular to the E-N plane. It is a translating and rotating frame relative to the earth frame, as a consequence of the body's motion. The translation velocity relative to the earth frame $\mathbf{V}_{eg}$ is:

$$\mathbf{V}_{eg} = \frac{d\mathbf{R}}{dt} \tag{2.1}$$

The angular velocity relative to the earth frame can be expressed as:

$$\omega_{eg} = \dot{\lambda}\mathbf{i}_{\Omega} - \dot{\varphi}\mathbf{i}_{E} \tag{2.2}$$

where $\mathbf{i}_{\Omega}$, $\mathbf{i}_{E}$ are the unit vectors in the directions of the earth rotation and east, and (modified from Farrell, 1976):

$$\dot{\lambda} = \frac{V_E}{R_M} = \frac{V_{eg}\cos\kappa\sin C}{R_M} \tag{2.3}$$

$$\dot{\varphi} = \frac{V_N}{R_N} = \frac{V_{eg}\cos\kappa\cos C}{R_N} \tag{2.4}$$

where

$$R_M = \frac{A}{(1 - f^2 \sin^2\varphi)^{\frac{1}{2}}} + h \tag{2.5}$$

$$R_N = \frac{A(1 - f^2)}{(1 - f^2 \sin^2\varphi)^{\frac{3}{2}}} + h \tag{2.6}$$

Here λ, φ are the geographic longitude and latitude of the origin of the geographic frame P, C is the body's course, A is the semi-major axis of the ellipsoid and f is the ellipsoid flattening. The relationship between $\mathbf{V}_{eg}$, $\mathbf{V}_E$, $\mathbf{V}_N$ and elevation angle κ is illustrated in Fig. 2.2.

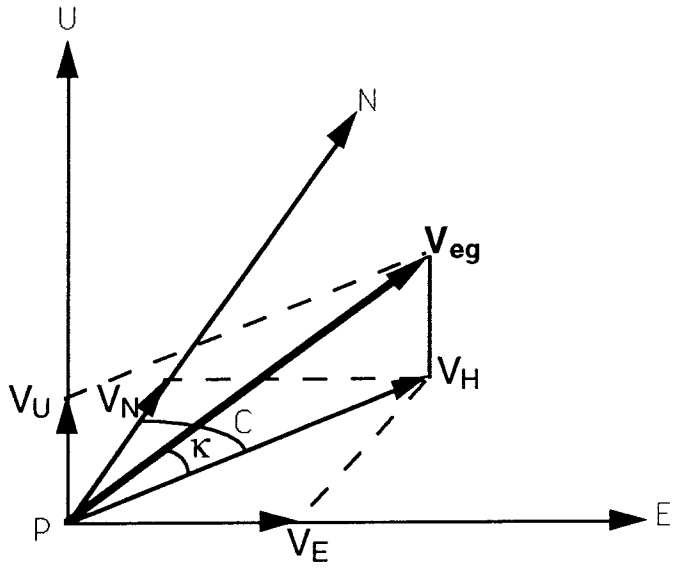

Figure 2.2. Velocity decomposition relating the geographic frame.

Because the east angular velocity corresponds to a decreasing of φ, the sign of the second term of eqn (2.2) is minus. $\mathbf{i}_\Omega$ can be decomposed as:

$$\mathbf{i}_\Omega = \cos\varphi\mathbf{i}_N + \sin\varphi\mathbf{i}_U \tag{2.7}$$

where $\mathbf{i}_N$, $\mathbf{i}_U$ are the unit vectors in the directions of north and up of the geographic frame, and eqn (2.2) can now be rewritten as:

$$\omega_{eg} = -\dot{\varphi}\mathbf{i}_E + \dot{\lambda}\cos\varphi\mathbf{i}_N + \dot{\lambda}\sin\varphi\mathbf{i}_U \qquad (2.8)$$

Projecting the angular velocity of earth rotation Ω into the geographic frame:

$$\Omega = \Omega\cos\varphi\mathbf{i}_N + \Omega\sin\varphi\mathbf{i}_U \qquad (2.9)$$

Hence the angular velocity of the geographic frame relative the the inertial frame is:

$$\begin{aligned}\omega_{ig} &= \Omega + \omega_{eg} \\ &= -\dot{\varphi}\mathbf{i}_E + (\dot{\lambda} + \Omega)\cos\varphi\mathbf{i}_N + (\dot{\lambda} + \Omega)\sin\varphi\mathbf{i}_U \qquad (2.10)\end{aligned}$$

The translation velocity relative to the inertial frame is:

$$\mathbf{V}_{ig} = \frac{d\mathbf{R}}{dt} + \Omega \times \mathbf{R} \qquad (2.11)$$

The geographic frame is the reference frame for the body's attitude computation.

2.1.4 The Tangent Frame

This frame is also defined as a geographic frame except that its origin is at a certain fixed reference location on the earth. It is an earth-fixed frame and is used for relative navigation to (or from) some reference point. The origin of the frame is typically taken to be the destination site, guidance radar station, reference station of GPS, or other convenient point. Its angular velocity relative to the inertial frame can also be expressed by eqn (2.9).

2.1.5 The Body Frame (P, R, Y)

The origin of this frame is the centre of mass of the body. In the case of marine navigation the *P* axis points to the vessel's starboard, the *R* axis points to the forward direction of the vessel's centre line, and the *Y* axis is perpendicular to the vessel's deck and up (Fig.2.3). *P* , *R* and *Y* are the axes which define the pitch, roll and yaw of the vessel.

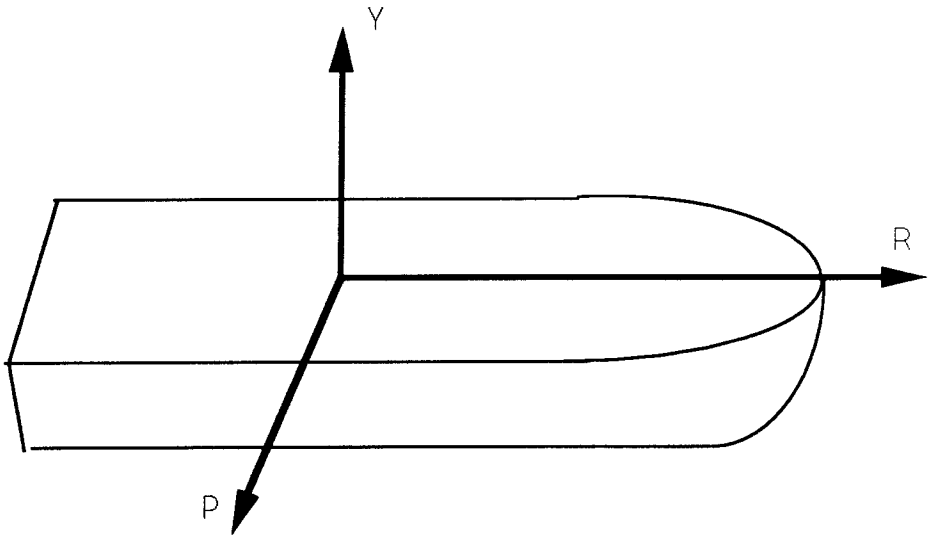

Figure 2.3. The body frame.

The body frame is a rotating frame relative to the geographic frame and the Euler angles, which are defined as the rotation angles around the *P*, *R* and *Y* axes, are the attitude angles of the body (Ishilinskii, 1965; Beggs, 1983). The body's angular velocity relative to the geographic frame can be expressed as:

$$\omega_{gb} = \dot{p}\mathbf{i}_P + \dot{r}\mathbf{i}_R + \dot{y}\mathbf{i}_Y \qquad (2.12)$$

where p, r, y are the pitch, roll and yaw angles, and $\mathbf{i}_P$, $\mathbf{i}_R$, $\mathbf{i}_Y$ are the unit vectors of the *P*, *R* and *Y* axes.

2.2 Transformation of Position

2.2.1 Transformation between Orthogonal Frames

The transformation of position between two orthogonal frames is straightforward (adapted from Seeber, 1993):

$$\mathbf{R}_Q = \mathbf{C}_S^Q (\mathbf{R}_S - \Delta\mathbf{R}_S^Q) \qquad (2.13)$$

where:

$\mathbf{R}_Q$, $\mathbf{R}_S$ coordinates in the Q and S frames

$\Delta\mathbf{R}_S^Q$ coordinates of the origin of the Q frame in the S frame

The direction cosine matrix $\mathbf{C}_S^Q$ is:

$$\mathbf{C}_S^Q = \begin{bmatrix} \cos(\widehat{X_Q X_S}) & \cos(\widehat{X_Q Y_S}) & \cos(\widehat{X_Q Z_S}) \\ \cos(\widehat{Y_Q X_S}) & \cos(\widehat{Y_Q Y_S}) & \cos(\widehat{Y_Q Z_S}) \\ \cos(\widehat{Z_Q X_S}) & \cos(\widehat{Z_Q Y_S}) & \cos(\widehat{Z_Q Z_S}) \end{bmatrix} \qquad (2.14)$$

The elements of eqn (2.14) are the direction cosines between the axes of the Q and S frame. Only three elements of the total nine direction cosines are independent, hence by using three independent parameters the relative relationship of the two frames can be determined. These three parameters are chosen to be the three rotation angles α, β, γ between the two frames as shown in Fig. 2.4.

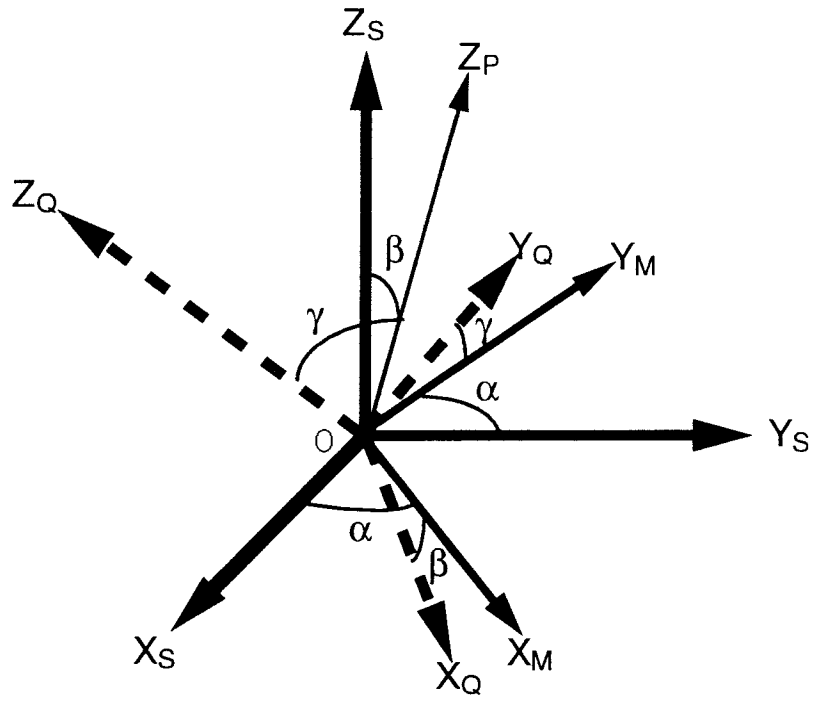

Figure 2.4. Rotation transformation of frames.

The rotation sequence in Fig. 2.4 is: XsYsZs to $X_M Y_M Z_S$ by rotating through the α angle about the OZs axis, $X_M Y_M Z_S$ to $X_Q Y_M Z_P$ by rotating through the β angle about the OY_M, $X_Q Y_M Z_P$ to $X_Q Y_Q Z_Q$ by rotating through the γ angle about OX_Q. The direction cosine matrix (eqn(2.14)) can be written as:

$$\mathbf{C}_S^Q = \mathbf{C}_P^Q \, \mathbf{C}_M^P \, \mathbf{C}_S^M \qquad (2.15)$$

where

$$\mathbf{C}_S^M(\alpha) = \begin{bmatrix} \cos\alpha & \sin\alpha & 0 \\ -\sin\alpha & \cos\alpha & 0 \\ 0 & 0 & 1 \end{bmatrix} \tag{2.16}$$

$$\mathbf{C}_M^P(\beta) = \begin{bmatrix} \cos\beta & 0 & -\sin\beta \\ 0 & 1 & 0 \\ \sin\beta & 0 & \cos\beta \end{bmatrix} \tag{2.17}$$

$$\mathbf{C}_P^Q(\gamma) = \begin{bmatrix} 1 & 0 & 0 \\ 0 & \cos\gamma & \sin\gamma \\ 0 & -\sin\gamma & \cos\gamma \end{bmatrix} \tag{2.18}$$

The reverse transformation is:

$$\mathbf{R}_S = \Delta\mathbf{R}_S^Q + \mathbf{C}_Q^S\,\mathbf{R}_Q \tag{2.19}$$

$$\mathbf{C}_Q^S = \left[\mathbf{C}_S^Q\right]^{-1} = \left[\mathbf{C}_S^Q\right]^T = \mathbf{C}_M^S\,\mathbf{C}_P^M\,\mathbf{C}_Q^P \tag{2.20}$$

$$\mathbf{C}_Q^P = \left[\mathbf{C}_P^Q\right]^{-1} = \left[\mathbf{C}_P^Q\right]^T = \mathbf{C}_P^Q(-\gamma) \tag{2.21}$$

$$\mathbf{C}_P^M = \left[\mathbf{C}_M^P\right]^{-1} = \left[\mathbf{C}_M^P\right]^T = \mathbf{C}_M^P(-\beta) \tag{2.22}$$

$$\mathbf{C}_M^S = \left[\mathbf{C}_S^M\right]^{-1} = \left[\mathbf{C}_S^M\right]^T = \mathbf{C}_S^M(-\alpha) \tag{2.23}$$

The basic transformations between frames therefore are:

1) inertial frame to earth frame: $\mathbf{C}_S^M(L)$

2) earth frame to geographic frame: $\mathbf{C}_P^Q(\pi/2 - \varphi)\mathbf{C}_S^M(\pi/2 + \lambda)$

3) geographic frame to body frame: $\mathbf{C}_M^P(r)\mathbf{C}_P^Q(p)\mathbf{C}_S^M(y)$

Because an angle is not a vector, the sequence of the transformation is important. For small rotation angles $\Delta\alpha, \Delta\beta, \Delta\gamma$, the computation can be simplified by assuming that the small angles are vectors. By neglecting the high order terms, the small angle rotation can be expressed as (modified from Britting, 1971) :

$$\Delta \mathbf{C}_S^Q \approx \mathbf{I} + \begin{bmatrix} 0 & \Delta\gamma & -\Delta\beta \\ -\Delta\gamma & 0 & \Delta\alpha \\ \Delta\beta & -\Delta\alpha & 0 \end{bmatrix} = \mathbf{I} + \Delta\theta = \begin{bmatrix} 1 & \Delta\gamma & -\Delta\beta \\ -\Delta\gamma & 1 & \Delta\alpha \\ \Delta\beta & -\Delta\alpha & 1 \end{bmatrix} \quad (2.24)$$

and

$$[\Delta\theta]^T = -\Delta\theta \quad (2.25)$$

2.2.2 Transformation between Non-Orthogonal Frames

For physical frames, such as the accelerometer frame, the gyro frame in inertial systems and the GPS antenna triad for attitude determination, are not exactly orthogonal because of the inevitable small assembly errors. These errors can also be expressed in the form of small angles between the axes of the ideal frame (X_I, Y_I, Z_I) and the physical frame (X_P, Y_P, Z_P), which are decomposed into two separate, independent rotations about the ideal frame axis, as illustrated in Fig. 2.5.

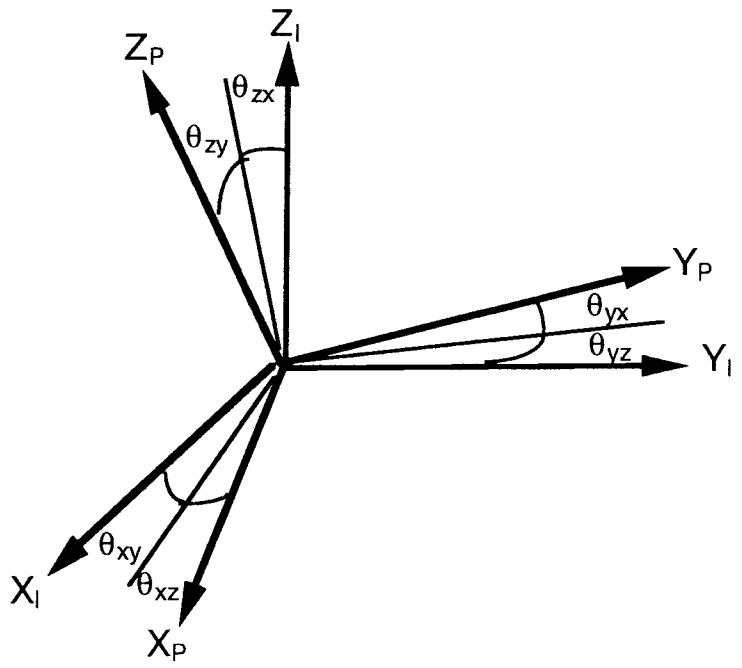

Figure 2.5. Non-orthogonal transformation.

The transformation from the physical frame to the ideal frame therefore is:

$$\mathbf{C}_P^I = \begin{bmatrix} 1 & -\theta_{yz} & \theta_{zy} \\ \theta_{xz} & 1 & -\theta_{zx} \\ -\theta_{xy} & \theta_{yx} & 1 \end{bmatrix} \tag{2.26}$$

2.3 Transformation of Velocity and Acceleration

The equation defining the transformation of velocity can be derived from eqn (2.13) as:

$$\begin{aligned} \mathbf{V}_Q = \frac{d\mathbf{R}_Q}{dt} &= \frac{d\left[\mathbf{C}_S^Q (\mathbf{R}_S - \Delta\mathbf{R}_S^Q)\right]}{dt} \\ &= \dot{\mathbf{C}}_S^Q (\mathbf{R}_S - \Delta\mathbf{R}_S^Q) + \mathbf{C}_S^Q (\dot{\mathbf{R}}_S - \Delta\dot{\mathbf{R}}_S^Q) \\ &= \dot{\mathbf{C}}_S^Q (\mathbf{R}_S - \Delta\mathbf{R}_S^Q) + \mathbf{C}_S^Q (\mathbf{V}_S - \Delta\mathbf{V}_S^Q) \end{aligned} \tag{2.27}$$

where $\mathbf{V}_Q$, $\mathbf{V}_S$ are the velocities in the Q and S frame respectively, and $\Delta\mathbf{V}_S^Q$ is the relative velocity of the S and Q frame.

The derivative of $\mathbf{C}_S^Q$ is obtained as follows:

$$\dot{\mathbf{C}}_S^Q = \lim_{\Delta t \to 0} \frac{\mathbf{C}_S^Q(t+\Delta t) - \mathbf{C}_S^Q(t)}{\Delta t} \tag{2.28}$$

In Δt time, the angle augment is small and hence:

$$\mathbf{C}_S^Q(t+\Delta t) \approx [\mathbf{I} + \Delta\theta]\, \mathbf{C}_S^Q(t) \tag{2.29}$$

Substituting eqn (2.29) into eqn (2.28) :

$$\dot{\mathbf{C}}_S^Q = \lim_{\Delta t \to 0} \frac{\Delta\theta}{\Delta t}\, \mathbf{C}_S^Q(t) = \omega_{SQ}^S\, \mathbf{C}_S^Q(t) \tag{2.30}$$

where

$$\lim_{\Delta t \to 0} \frac{\Delta\theta}{\Delta t} = \lim_{\Delta t \to 0} \begin{bmatrix} 0 & \frac{\Delta\gamma}{\Delta t} & -\frac{\Delta\beta}{\Delta t} \\ -\frac{\Delta\gamma}{\Delta t} & 0 & \frac{\Delta\alpha}{\Delta t} \\ \frac{\Delta\beta}{\Delta t} & -\frac{\Delta\alpha}{\Delta t} & 0 \end{bmatrix}$$

$$= \begin{bmatrix} 0 & \omega_{SQ}^z & -\omega_{SQ}^y \\ -\omega_{SQ}^z & 0 & \omega_{SQ}^x \\ \omega_{SQ}^y & -\omega_{SQ}^x & 0 \end{bmatrix} = \omega_{SQ}^S \tag{2.31}$$

where ω_{SQ}^x, ω_{SQ}^y, ω_{SQ}^z are the angular velocities of the S frame relative to the Q frame.

According to eqns (2.19) and (2.20) the velocity transformation from the Q frame to the S frame is:

$$\mathbf{V}_S = \dot{\mathbf{R}}_S = \Delta\dot{\mathbf{R}}_S^Q + \dot{\mathbf{C}}_Q^S\, \mathbf{R}_Q + \mathbf{C}_Q^S\, \dot{\mathbf{R}}_Q$$

$$= \Delta\mathbf{V}_S^Q + \dot{\mathbf{C}}_Q^S\, \mathbf{R}_Q + \mathbf{C}_Q^S\, \mathbf{V}_Q \tag{2.32}$$

where

$$\dot{\mathbf{C}}_Q^S(t) = \frac{d\left[\mathbf{C}_S^Q(t)\right]^T}{dt} = \left[\omega_{SQ}^S\, \mathbf{C}_S^Q(t)\right]^T = -\,\mathbf{C}_Q^S(t)\omega_{SQ}^S \qquad (2.33)$$

Eqn (2.32) can be written as:

$$\begin{aligned}\mathbf{V}_S &= \Delta\mathbf{V}_S^Q + \mathbf{C}_Q^S\,\mathbf{V}_Q + \dot{\mathbf{C}}_Q^S\,\mathbf{R}_Q \\ &= \Delta\mathbf{V}_S^Q + \mathbf{C}_Q^S\left[\mathbf{V}_Q - \omega_{SQ}^S\,\mathbf{R}_Q\right] \\ &= \Delta\mathbf{V}_S^Q + \mathbf{C}_Q^S\left[\mathbf{V}_Q + \omega_Q \times \mathbf{R}_Q\right]\end{aligned} \qquad (2.34)$$

where

$$\omega_Q = \left[\begin{array}{ccc} \omega_{SQ}^x & \omega_{SQ}^y & \omega_{SQ}^z \end{array}\right]^T$$

The geometrical meaning of eqn (2.34) is apparent: supposing S is a fixed frame, Q is a moving and rotating frame relative to the S frame and R_Q are the coordinates of a body in the Q frame, then $\Delta\mathbf{V}_S^Q$ is the translation velocity of the Q frame relative to the S frame, $\mathbf{V}_Q$ is the velocity of the body relative to the Q frame, and the term of the cross product is the tangential velocity caused by the rotation of the Q frame relative to the S frame.

The transformation of acceleration can be derived directly from eqn (2.34):

$$\begin{aligned}\mathbf{a}_S &= \Delta\mathbf{a}_S^Q + \dot{\mathbf{C}}_Q^S\left[\mathbf{V}_Q + \omega_Q \times \mathbf{R}_Q\right] \\ &\quad + \mathbf{C}_Q^S\left[\dot{\mathbf{V}}_Q + \dot{\omega}_Q \times \mathbf{R}_Q + \omega_Q \times \dot{\mathbf{R}}_Q\right] \\ &= \Delta\mathbf{a}_S^Q + \mathbf{C}_Q^S\left[\omega_Q \times(\mathbf{V}_Q + \omega_Q \times \mathbf{R}_Q)\right] \\ &\quad + \mathbf{C}_Q^S\left[\dot{\mathbf{V}}_Q + \dot{\omega}_Q \times \mathbf{R}_Q + \omega_Q \times \mathbf{V}_Q\right] \\ &= \Delta\mathbf{a}_S^Q + \mathbf{C}_Q^S\left[\dot{\mathbf{V}}_Q + 2\,\omega_Q \times \mathbf{V}_Q + \dot{\omega}_Q \times \mathbf{R}_Q + \omega_Q \times \omega_Q \times \mathbf{R}_Q\right]\end{aligned} \qquad (2.35)$$

where:

$\Delta \mathbf{a}_S^Q$	translation acceleration between the Q and S frame
$\dot{\mathbf{V}}_Q$	acceleration of the body relative to the Q frame
$2\,\omega_Q \times \mathbf{V}_Q$	Coriolis acceleration cause by the motion of the body on the rotating frame Q relative to the S frame
$\dot{\omega}_Q \times \mathbf{R}_Q$	tangential acceleration caused by the rotation of the Q frame
$\omega_Q \times \omega_Q \times \mathbf{R}_Q$	centripetal acceleration caused by the rotation of the Q frame

Assuming there is a GPS antenna located at P, its position vector in the geographic frame is ρ. The centre of mass of the body is at A, its position vector is **R**, and its speed vector is $\mathbf{V}_{eg}$ in the earth frame. The angular velocity of the geographic frame relative to the earth frame is ω_{eg}. The angular velocity of the body frame relative to the geographic frame is ω_{gb}, the antenna velocity relative to the earth frame is $\mathbf{V}_{eb}$, as illustrated Fig. 2.6.

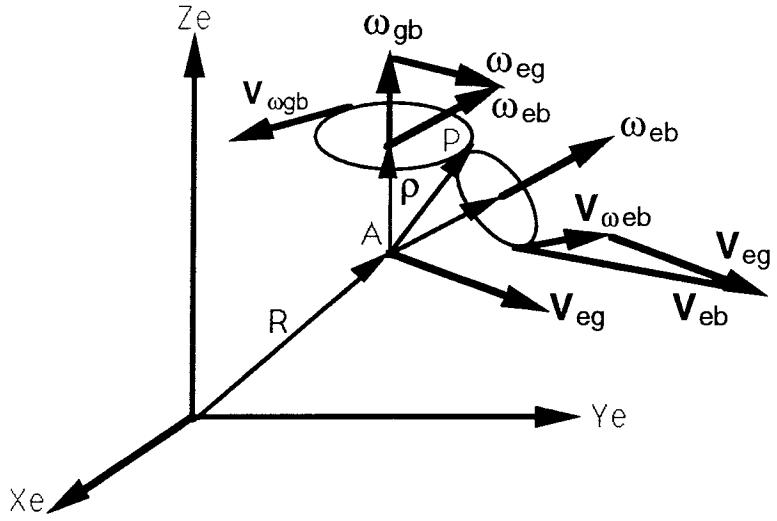

Figure 2.6. Composition of velocity.

According to eqn (2.34) and Fig. 2.6, the antenna velocity $\mathbf{V}_{\omega gb}$ relative to the geographic frame is:

$$\mathbf{V}_{\omega gb} = \omega_{gb} \times \rho \tag{2.36}$$

The acceleration of the antenna relative to the geographic frame is:

$$\dot{\mathbf{V}}_{\omega gb} = \dot{\omega}_{gb} \times \rho + \omega_{gb} \times \dot{\rho}$$
$$= \dot{\omega}_{gb} \times \rho + \omega_{gb} \times \omega_{gb} \times \rho \qquad (2.37)$$

The antenna velocity relative to the earth frame is:

$$\mathbf{V}_{eb} = \frac{d\mathbf{R}}{dt} + \omega_{eb} \times \rho = \frac{d\mathbf{R}}{dt} + (\omega_{eg} + \omega_{gb}) \times \rho$$
$$= \mathbf{V}_{eg} + \mathbf{V}_{\omega eb} \qquad (2.38)$$

where $\mathbf{V}_{\omega eb}$ is the tangential velocity caused by the rotation of the body frame relative to the earth frame. For a low speed body, ω_{eg} is usually a small value compared to ω_{gb}, except at high latitude, and can be neglected, see eqns (2.3), (2.4) and (2.8).

The acceleration of the antenna relative to the earth frame can be obtained from eqn (2.35) as:

$$\dot{\mathbf{V}}_{eb} = \frac{d^2\mathbf{R}}{dt^2} + \dot{\omega}_{eb} \times \rho + \omega_{eb} \times \omega_{eb} \times \rho \qquad (2.39)$$

There are no Coriolis acceleration terms in eqn (2.37) and (2.39) because the antenna is fixed in the body frame. GPS measurements are only sensitive to the linear and tangential acceleration components $d^2\mathbf{R}/dt^2$ and $\dot{\omega}_{eb} \times \rho$.

2.4 GPS Attitude Determination

With the exception of inertial navigation systems, GPS is the only potential six degree-of-freedom navigation system having the ability to provide attitude information. The compatible attitude determination accuracy of GPS to that of INS is based on the potential centimetre level accuracy of kinematic positioning using GPS carrier phase measurements for short baselines (Mader, 1986; Hatch, 1986; Remondi, 1992). The first results of experiments of GPS attitude determination were presented by Brown (1982) of the Draper Laboratory. Since the experiments of GPS triads on a rotating base carried out by the Trimble Navigation company (Trimble, 1987), GPS attitude determination techniques have developed rapidly and have been applied successfully to spacecraft control (Cohen et al., 1993), artillery pointing (Jurgens et al., 1991),

and marine and air navigation (Fu, 1991; Cohen et al., 1992; Diefes et al., 1993).

The body's attitude (pitch, roll and yaw angles) can be determined by fixing three or more GPS antennas in a non-colinearl pattern which forms at least two coplanar vectors. The typical configuration is a three antenna triad whose axes are parallel to the axes of body frame. Under the assumption of rigidity, the antenna locations remain fixed in the body frame and the translation between the centre of mass and the triad has no effect on attitude determination. The positioning of the antennas in the body frame $\mathbf{D}_b$ can be carried out using GPS static surveying techniques because the relationship between the geographic frame and the body frame can be determined at that moment. Once in motion, the locations of the antennas in the geographic frame frame $\mathbf{D}_g$ are determined using GPS interferometry techniques and the geographic frame is set up by the position of one of the antennas. At any given epoch the antenna locations in the two frames are related as follows:

$$\mathbf{D}_g = \mathbf{C}_b^g \mathbf{D}_b \tag{2.40}$$

where

$$\mathbf{C}_b^g = \left[\mathbf{C}_M^P(r)\mathbf{C}_P^Q(p)\mathbf{C}_S^M(y)\right]^T =$$

$$\begin{bmatrix} \text{cosycosr-sinysinpsinr} & \text{-sinycosp} & \text{cosysinr+sinysinpcosr} \\ \text{sinycosr+cosysinpsinr} & \text{cosycosp} & \text{sinysinr-cosysinpcosr} \\ \text{-cospsinr} & \text{sinp} & \text{cospcosr} \end{bmatrix} \tag{2.41}$$

The instantaneous value of the attitude angles can be determined as follows (adapted from Graas et al., 1992):

$$\mathbf{C}_b^g = \mathbf{D}_g\mathbf{D}_b^T\left[\mathbf{D}_b\mathbf{D}_b^T\right]^{\sim -1} \tag{2.42}$$

where ~ -1 denotes the generalized matrix inverse. Eqn (2.42) can be changed to a more convenient form for computations (modified from Xinhua Qin et al., 1992):

$$\mathbf{C}_b^g(j,k) = \left[\mathbf{D}_g^{ij} \;\; \mathbf{D}_g^{ik} \;\; \mathbf{D}_g^{ij}\times\mathbf{D}_g^{ik}\right]\left[\mathbf{D}_b^{ij} \;\; \mathbf{D}_b^{ik} \;\; \mathbf{D}_b^{ij}\times\mathbf{D}_b^{ik}\right]^{-1} \tag{2.43}$$

where $\mathbf{D}_g^{ij}$, $\mathbf{D}_b^{ik}$ refer to the baselines between the i and j antennas and between the i and k antennas in the geographic frame and the body frame respectively. (If there are three baselines, four $\mathbf{C}_b^g$ can be obtained from the four independent combinations of the baselines, and an average $\mathbf{C}_b^g$ can be obtained.) The attitude angles can be computed as follows:

$$p = \sin^{-1}[\mathbf{C}_b^g(3,2)] \tag{2.44}$$

$$r = \sin^{-1}\left[-\frac{\mathbf{C}_b^g(3,1)}{\cos p}\right] \tag{2.45}$$

$$y = \sin^{-1}\left[-\frac{\mathbf{C}_b^g(1,2)}{\cos p}\right] \tag{2.46}$$

(The signs of p, r and y are determined by the right-hand rule and the definitions of pitch and roll angles are in the range of -90 to +90 degrees and the yaw angle in the range of -180 to +180 degrees.)

For one baseline, or a so-called pointing system, the azimuth and elevation angles are computed as:

$$Az = \tan^{-1}\left[\frac{D_E}{D_N}\right] \tag{2.47}$$

$$El = \sin^{-1}\left[\frac{D_U}{D}\right] \tag{2.48}$$

where D is the baseline length, D_E, D_N and D_U are the components of the baseline in the east, north and up directions.

2.4.1 GPS Interferometry

The principle of GPS interferometry is illustrated in Fig. 2.7 (modified from Brown et al., 1982)

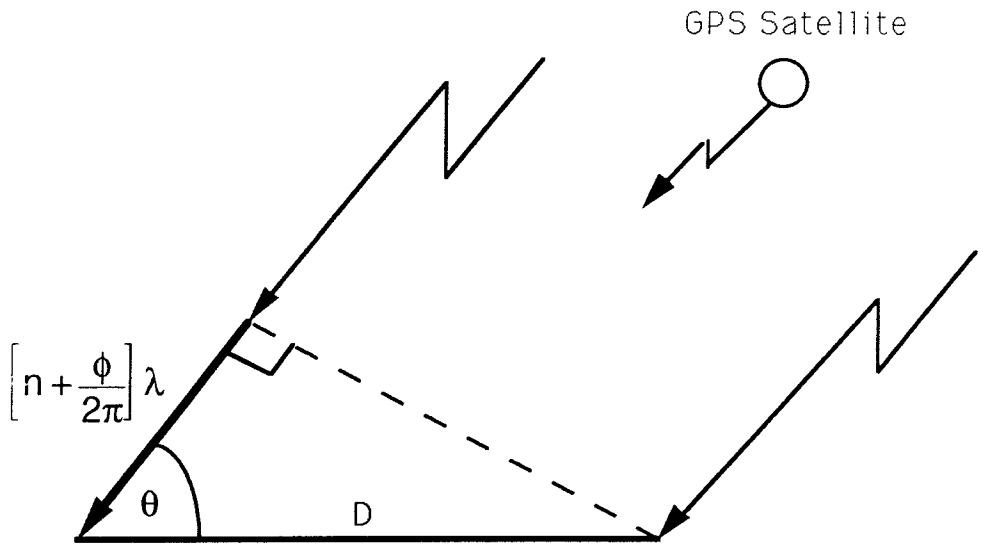

Figure 2.7. GPS interferometry principle.

Neglecting the measurement bias and noise it can be seen that:

$$\left[n+\frac{\phi}{2\pi}\right]\lambda = D\cos\theta \qquad (2.49)$$

where:

- D baseline length
- n integer number of carrier wavelengths
- ϕ measured phase difference
- λ wavelength of the GPS carrier signal
- θ angle that the line-of-sight (LOS) to the satellite subtends on the baseline

Eqn (2.49) can be rewritten as:

$$\left[n+\frac{\phi}{2\pi}\right]\lambda = D\mathbf{l}_D{}^*\mathbf{l}_i \qquad (2.50)$$

where:

- $\mathbf{l}_D$ unit vector in the direction of the baseline
- $\mathbf{l}_i$ unit vector in the direction of the satellite i
- * dot product

Some GPS attitude determination systems (ADS), such as the AN/PSN-9 pointing unit of Texas Instruments Inc., measure the between-site differenced phase measurements internally. However, in general, the attitude

determination computation uses double-differenced carrier phase measurements to eliminate common measurement biases. For the double-differenced phase measurement eqn (2.50) can be rewritten as:

$$\left[\nabla n + \frac{\nabla\phi}{2\pi}\right]\lambda = D\mathbf{l}_D^*[\mathbf{l}_i - \mathbf{l}_j] = D\mathbf{l}_D^*\mathbf{l}_{ij} \qquad (2.51)$$

where ∇n, $\nabla\phi$ are the double-differenced ambiguity and phase measurement involving satellites i and j.

For ambiguity resolution eqn (2.51) can be rewritten as:

$$\nabla n = \frac{D}{\lambda}\mathbf{l}_D^*[\mathbf{l}_i - \mathbf{l}_j] - \frac{\nabla\phi}{2\pi} = \frac{D}{\lambda}\mathbf{l}_D^*\mathbf{l}_{ij} - \frac{\nabla\phi}{2\pi} \qquad (2.52)$$

Differentiating eqn (2.52), we have the ambiguity error equation as:

$$d\nabla n = \frac{dD}{\lambda}\mathbf{l}_D^*\mathbf{l}_{ij} + \frac{D}{\lambda}d\mathbf{l}_D^*\mathbf{l}_{ij} + \frac{D}{\lambda}\mathbf{l}_D^*d\mathbf{l}_{ij} - \frac{d\nabla\phi}{2\pi} \qquad (2.53)$$

The ambiguity error (here a real value ambiguity is assumed) can be analyzed for each error source contained in eqn (2.53):

1) The baseline length error dD:
The maximum ambiguity error is equal to dD/λ when $\mathbf{l}_D$ is parallel to $\mathbf{l}_{ij}$, which means that for a horizontal baseline a large ambiguity error can be induced when the satellite elevations are low. The ambiguity error is zero when $\mathbf{l}_D$ is perpendicular to $\mathbf{l}_{ij}$.

2) The baseline attitude error $d\mathbf{l}_D$:
For a fixed baseline length D, $d\mathbf{l}_D$ causes the original baseline vector **D** to rotate to a new direction, and the second term of eqn (2.53) can be expressed as:

$$d\nabla n = \alpha \times \frac{D^*}{\lambda}\mathbf{l}_{ij} \qquad (2.54)$$

where α is the rotation vector attributable to the $d\mathbf{l}_D$. For a small rotation angle α the maximum ambiguity error is:

$$d\nabla n = \alpha \frac{D}{\lambda} \qquad (2.55)$$

in case of a 1 metre baseline, if α is less than 5.5 degrees, the ambiguity error will be less than half the L1 wavelength and will have no effect on the integer ambiguity resolution. If the baseline attitude can be determined to better than 5.5 degrees, the integer ambiguity can be obtained instantaneously for 1 metre baseline, and a 0.55 degrees attitude accuracy for 10 metre baseline, etc. When $\mathbf{l}_{ij} = \mathbf{l}_i - \mathbf{l}_j = 0$ (meaning that the satellites i and j are in the same direction and the PDOP value is infinitely large for three observed satellites), the ambiguity error is zero for errors dD or $d\mathbf{l}_D$. Generally speaking, small value of $\mathbf{l}_{ij}$ implies a large PDOP value and will cause a lower ambiguity error for fixed dD or $d\mathbf{l}_D$.

3) LOS error $d\mathbf{l}_{ij}$:

The effect of $d\mathbf{l}_{ij}$ is similar to that of $d\mathbf{l}_D$, and causes the baseline to rotate. The source of $d\mathbf{l}_{ij}$ is primarily the position error of the reference antenna, and satellite ephemeris error, as shown in Fig. 2.8.

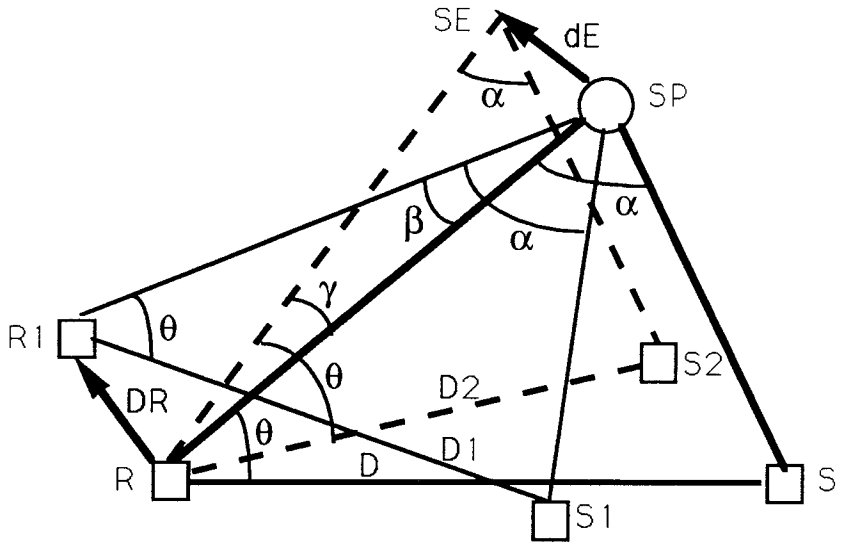

Figure 2.8. The effects of orbit and reference site errors.

In Fig. 2.8 R,S and **D** are the reference site, remote site and true baseline vector, R1,S1,and **D**1 are the reference site, remote site and baseline vector assuming reference site error **DR**, S2 and D2 are the remote site and baseline vector assuming ephemeris error DE. SE is the satellite position implied by ephemeris data and SP is the true satellite position. From Fig.2.8 it can be seen that for a fixed baseline length D the effects of the reference site position

error and the ephemeris error cause a rotation of the baseline vector D. The rotation angles β, γ are the subtended angles of the reference site error at the satellite and the subtended angle of the ephemeris error at the reference site respectively. Considering the large distance between the satellite and the reference site, β, γ are small angles and are negligible for short baseline. For example β = 0.17 arc minute for a 1 km reference site error and γ = 0.017 arc minute for a 100 metre ephemeris error, and both are negligible if the baseline length is less than 300 m,

4) The measurement error $d\nabla\phi$:
After double-differencing the measurements, the only error sources remaining for a short baseline are multipath and measurement noise, both of which directly affect ambiguity determination.

2.4.2 Ambiguity Resolution of ADS

Most ADS use modified Least Squares search methods (for details of Least Squares search methods see Hatch, 1989; Hatch, 1990; Frei, 1991; Abidin, 1993; Teunissen, 1994). Considering the a priori knowledge of the relative positions of the ADS antennas in the body frame, there are some constraints for the baseline vectors: one constraint for the length of the first baseline vector, one length and one angle constraint for the second vector, and three position constraints for the remaining vectors. The constraints can be expressed as follows:

$$\mathbf{D}_i^T \mathbf{D}_i = [\mathbf{D}_i + \Delta\mathbf{D}_i]^T[\mathbf{D}_i + \Delta\mathbf{D}_i] = |\mathbf{D}_i|^2 \qquad (2.56)$$

$$\mathbf{D}_i^T \mathbf{D}_j = [\mathbf{D}_i + \Delta\mathbf{D}_i]^T[\mathbf{D}_j + \Delta\mathbf{D}_j] = \text{constant} \qquad (2.57)$$

where $\mathbf{D}_i$, $\mathbf{D}_j$ are the ith and jth baseline vectors, $\Delta\mathbf{D}_i$, $\Delta\mathbf{D}_j$ are the changes in the baseline vectors.

For double-differenced measurements, the primary satellites for the ambiguity search reduce to three for the first vector and two for the second vector, and the remaining vectors are only used for testing the ambiguity resolution.

For a single baseline, the ambiguity solution must be on the surface of a sphere of radius D1 and for the first measurement the search is along the whole baseline length in the first measurement vector direction:

$$\frac{-D_1}{\lambda} - \frac{\Delta\varphi_1}{2\pi} \leq n_1 \leq \frac{D_1}{\lambda} - \frac{\Delta\varphi_1}{2\pi} \tag{2.58}$$

For the second ambiguity n2, the search range can be reduced by projecting the second measurement to the first measurement as (adapted from Quinn, 1993.):

$$\frac{-\varphi_{2max}}{\lambda} - \frac{\Delta\varphi_2}{2\pi} \leq n_2 \leq \frac{\varphi_{2max}}{\lambda} - \frac{\Delta\varphi_2}{2\pi} \tag{2.59}$$

where

$$\pm\varphi_{2max} = \Delta\varphi_1 (\mathbf{l}_1^T\mathbf{l}_2) \pm \sqrt{\left[1 - (\mathbf{l}_1^T\mathbf{l}_2)^2\right]\left[D_1^2 - \Delta\varphi_1^2\right]} \tag{2.60}$$

$\mathbf{l}_1$, $\mathbf{l}_2$ are the unit vectors of the first and second double-differenced measurements.

For the second baseline, the search range can be determined directly by using the constraint in eqn (2.57). In this case, the only uncertainty of the second baseline is related to the rotations about the first baseline. If the second baseline is orthogonal to the first one, the spherical surface of the possible position of the second baseline relative to the first shrinks to a great circle band AB , see Fig. 2.9 (which is a plane figure). If the second baseline is not orthogonal to the first, the great circle band will shrink into a small circle band CD. The smaller the angle between the two baseline the smaller is the circle band until the two baseline is lined up, the circle band becomes a point P on the surface of the sphere.

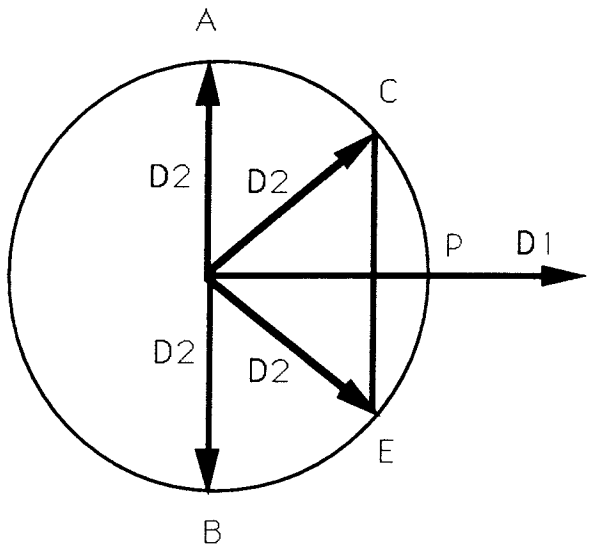

Figure 2.9. The search range of the second baseline.

From an ambiguity resolution point of view, the angle between the two baselines should be small, but the effective length in the orthogonal direction to the first baseline also becomes small and the potential of the attitude determination will decrease in that direction until the two baselines line up and the system degenerates into a pointing system (Jurgens et al., 1991). Adroit System Inc. (ibid.) developed a pointing system based on the above principles. The system uses three co-linear GPS antennas to form a short baseline of less than one carrier wavelength, and a long baseline. The short baseline is intended for ambiguity resolution initialization of the long baseline, and the long baseline is used for azimuth and elevation determination.

Another aid to resolving the ambiguity for an ADS is the changing observation geometry due to the body's attitude change. Assuming there are three non-coplanar baselines $\mathbf{D}_1$, $\mathbf{D}_2$ and $\mathbf{D}_3$, expanding eqns (2.56) and (2.57), it can be seen that:

$$2\Delta\mathbf{D}_i^T\,\mathbf{D}_i = -\,\Delta\mathbf{D}_i^T\Delta\mathbf{D}_i \qquad (2.61)$$

$$\Delta\mathbf{D}_j^T\,\mathbf{D}_i + \Delta\mathbf{D}_i^T\,\mathbf{D}_j = -\,\Delta\mathbf{D}_i^T\Delta\mathbf{D}_j \qquad (2.62)$$

Combining eqns (2.61) and (2.62), a measurement equation can be derived (modified from Cohen et al., 1991):

$$\begin{bmatrix} \Delta\mathbf{d}_2^T & \Delta\mathbf{d}_1^T & 0 \\ \Delta\mathbf{d}_3^T & 0 & \Delta\mathbf{d}_1^T \\ 0 & \Delta\mathbf{d}_3^T & \Delta\mathbf{d}_2^T \\ 2\Delta\mathbf{d}_1^T & 0 & 0 \\ 0 & 2\Delta\mathbf{d}_2^T & 0 \\ 0 & 0 & 2\Delta\mathbf{d}_3^T \end{bmatrix} \begin{bmatrix} \mathbf{D}_1 \\ \mathbf{D}_2 \\ \mathbf{D}_3 \end{bmatrix} = - \begin{bmatrix} \text{diag}\,(\Delta\mathbf{d}_1^T\Delta\mathbf{d}_2) \\ \text{diag}\,(\Delta\mathbf{d}_1^T\Delta\mathbf{d}_3) \\ \text{diag}\,(\Delta\mathbf{d}_3^T\Delta\mathbf{d}_2) \\ \text{diag}\,(\Delta\mathbf{d}_1^T\Delta\mathbf{d}_1) \\ \text{diag}\,(\Delta\mathbf{d}_2^T\Delta\mathbf{d}_2) \\ \text{diag}\,(\Delta\mathbf{d}_3^T\Delta\mathbf{d}_3) \end{bmatrix}$$

(2.63)

where

$$\Delta\mathbf{d}_k = \left[\Delta\mathbf{D}_k^1\ \Delta\mathbf{D}_k^2 \cdots \Delta\mathbf{D}_k^n\right]$$

for measurements at n different times and k = 1, 2, 3.

The baseline vectors can be determined by Least Squares estimation on the condition that a large attitude change guarantees the estimation accuracy, and the axis of the attitude change should not be parallel to any baseline vector, otherwise the normal matrix will be rank-deficient. A similar equation to eqn (2.63) can be derived for the two baseline case.

2.4.3 Some Comments Regarding ADS

1) Achievable attitude accuracy:

The achievable attitude accuracy, or the angular resolution, is dependent on the baseline length and can be expressed as:

$$\sigma_A = \frac{\sigma_L}{D} \qquad (2.64)$$

where σ_L is the standard deviation of the baseline length, and D is the baseline length. The achievable accuracy σ_A can be expressed in radians (where 1 milliradian $\approx$ 0.057 degree). For a 1 metre baseline and 1 mm baseline error the angular resolution is therefore 1 milliradian.

2) The attitude DOP:

The azimuth DOP can be derived by differentiation of eqn (2.47) :

$$d(Az) = \frac{1}{\sqrt{D_N^2 + D_E^2}}\left[\frac{D_N dD_E - D_E dD_N}{\sqrt{D_N^2 + D_E^2}}\right]$$

$$= \frac{1}{D_h}[\cos\alpha dD_E - \sin\alpha dD_N] \qquad (2.65)$$

where α is the azimuth angle and

$$D_h = \sqrt{D_N^2 + D_E^2} \qquad (2.66)$$

The azimuth accuracy can be written as:

$$\delta_{AZ} = \frac{1}{D_h}\sqrt{\cos^2\alpha\sigma_{rE}^2 + \sin^2\alpha\sigma_{rN}^2}$$

$$= \frac{\sigma_p}{D_h}\sqrt{\cos^2\alpha D_{EE} + \sin^2\alpha D_{NN}} \qquad (2.67)$$

where σ_{rE}, σ_{rN} are the standard deviations of the east and north components, σ_p is double-differenced phase measurement noise, D_{EE} and D_{NN} are the diagonal terms of the cofactor matrix corresponding to the east and north components under unit measurement standard deviation. The azimuth DOP is defined as:

$$AZDOP = \sqrt{\cos^2\alpha D_{EE} + \sin^2\alpha D_{NN}} \qquad (2.68)$$

Hence

$$\delta_{AZ} = \frac{\sigma_p}{D_h} AZDOP \qquad (2.69)$$

The elevation DOP (ELDOP) is derived from eqn (2.48).That is:

$$d(El) = \frac{dD_U}{\sqrt{D^2 - D_U^2}} = \frac{dD_U}{D_h} \qquad (2.70)$$

The ELDOP is:

$$\delta_{EL} = \frac{\sigma_U}{D_h} = \frac{\sigma_p}{D_h} VDOP \qquad (2.71)$$

Hence

$$ELDOP = VDOP \qquad (2.72)$$

If D_h is in the R or P axis direction of the body frame, then eqn (2.71) is the pitch or roll error.

The above AZDOP and ELDOP definition is similar to those proposed by Brown & Evans (1990) derived from uncorrelated double-differenced measurements by Gram-Schmidt orthogonalization (Balakrishnan, 1987) and the use of baseline length D instead of the horizontal baseline length D_h in eqns (2.69) and (2.71). For a small elevation angle, D and D_h are not significantly different (but not in the case of a large elevation angle).

3) Computational considerations:

The attitude angle and error computations discussed above are perhaps the best understood means of attitude expression, but they are far from robust. This lack of robustness can be seen by examining eqns (2.44)-(2.46) for the case of $p=90^o$. Note that although p can be recovered, r and y are lost (corresponding to $D_h=0$). This situation corresponds to the 'gimbal-lock' problem of a three-gimbal ring platform in INS in which the outer and inner gimbal rings are coplanar and the platform loses one degree-of-freedom (O'Donnell, 1964). In practice eqns (2.44)-(2.46) can be used for $p \leq 60^o$. One solution to the problem is to add another roll 'gimbal ring' to form a 'four ring' system. The 'roll ring' added is controlled by the pitch angle to make the 'outer ' and inner rings nearly orthogonal at all times. This will make the computation of the direction cosine matrix complicated because now the pitch and roll angles are a function of the 'outer roll ring' attitude. Another solution is using quaternion parameterization instead of the direction cosine matrix (Klein et al., 1965; Farrell, 1976). Although many parameterizations of the direction cosine matrix are possible, quaternions offer conciseness, efficiency, and stability not possible with other parameterizations. The implementation of quaternion parameterization algorithms for GPS ADS is still under development.

4) Length or angle:

The above methods are based on the baseline vector computation in order to derive attitude information, and this induces some problems. An alternative approach is to derive the attitude angles directly from the GPS measurements. Considering that the baseline vector change corresponds to the attitude change for the baselines with fixed lengths, the linearized measurement equation for the attitude can be derived from eqn (2.51) as:

$$\nabla\tilde{\phi} = \frac{2\pi}{\lambda}\left[\hat{\mathbf{D}}_k \times \mathbf{l}_{ij}\right]^T \alpha + \Delta n_{ij}^k + b_{ij}^k + v_{ij}^k \qquad (2.73)$$

where $\hat{\mathbf{D}}_k$ is the estimated kth baseline vector in the geographic frame, α is the attitude error and Δn_{ij}^k, b_{ij}^k, v_{ij}^k are the ambiguity, bias and measurement noise. Eqn (2.73) avoids the computation of the direction cosines, and is suitable for sequential estimation algorithms. Furthermore, after ambiguities are resolved, three measurements are enough for attitude determination. Eqn (2.73) is based on the assumption that the attitude error is small, hence the initial value should be quite accurate, and a high measurement data rate is necessary to update the baseline vector $\hat{\mathbf{D}}_k$. Generally speaking, this method is more suitable for a low dynamic body, or a body with an INS installed.

5) Angle and angle rate:

The rate of change of attitude information is contained in the between antennas Doppler (or phase-rate) measurements. According to eqn (2.51) the phase-rate measurement can be written as:

$$\frac{\nabla\dot{\phi}}{2\pi}\lambda = D\dot{\mathbf{l}}_D{}^*\mathbf{l}_{ij} + D\mathbf{l}_D{}^*\dot{\mathbf{l}}_{ij} \qquad (2.74)$$

Similarly, the attitude change can be measured by the delta-range measurements. If the data rate is high enough (at least twice that of the attitude change frequency of about 10 Hz for a land-vehicle to perhaps 50 Hz for a helicopter, according to Cannon, 1993) the attitude change envelope can be recovered from the Doppler measurements.

6) Two or more antennas:

Two antennas form a pointing system, while three antennas comprise a full ADS with one angular redundancy. For a three antenna-two baseline system the optimal configuration is an orthogonal frame formed by the antennas

(although the frame need not necessarily be parallel to the body frame), with the longest effective baselines that can be obtained. Adding more antennas will increase the ambiguity resolution efficiency and quality, and the accuracy of the attitude determination by permitting direction cosine averaging and orthogonalization.

7) Independent or integrated systems:

The independent ADS can work 24 hours a day, anywhere in the world. The potential accuracy of long baseline-high performance ADS can be compatible to that of a high performance INS without solution drift, and system calibration and alignment (Karels et al.,1994; McMillan et al., 1994). The ADS attitude update rate is between 1 to 10 Hz (Cohen,1992; Diefes, 1994), which is much lower than that of an INS, which can be as high as 100 Hz. Therefore it is only suitable for relatively low dynamic bodies. The main problem with GPS ADS is GPS signal reliability and quality (which can be monitored by supporting navigation systems). For an ADS comprising 1 metre baselines, if the attitude error is under 5.5 degrees there will be no ambiguity and cycle slip problems, and this requirement is achievable even using a low cost fibre-optic gyro INS or gyrocompass. Furthermore, the bandwidth of the tracking loop of the INS-aided GPS receiver can be narrowed and the measurement noise reduced. Although an INS can be calibrated by the position and velocity information obtained by a single GPS receiver, the accuracy of the calibration is not very high considering the inherent point positioning accuracy of GPS. The accurate attitude information offered by an ADS can be used directly for monitoring the gyro drift, which is the main error source of the INS. Through integration of GPS ADS, position, velocity and attitude calibrations can be obtained for the INS, while high accuracy position, velocity and attitude information at a high output data rate are available to the user.

8) Dedicated or non-dedicated receiver:

A dedicated ADS receiver is designed especially for attitude determination. The signal received by the separate antennas are processed by channels which are under the control of a common oscillator and hence good signal synchronization is obtained. All common mode errors of the system are cancelled because the phase observables in each channel are synthesized from only one replica code generator and one replica carrier generator, to produce simultaneous interferometric measurements between the antennas. The carrier tracking bandwidth is optimized according to the ratio of signal to noise, typically 1/20 Hz for dynamic movement to 4 g (Jurgens et al., 1992), and

a 0.15 mm static double-differenced measurement noise is claimed (Brown et al., 1990). For antennas which have a relatively large gain for the signals of low elevation satellites, a minimization of multipath and the interference effects of neighbouring antennas through the use of a choke ring or other such devices together supporting software optimized for attitude determination in real time, high system performance can be expected. In the case of a 1 metre static baseline, sub-milliradian azimuth accuracy has been reported (Ferguson et al., 1991; Charles et al., 1993). Generally, the elevation (or pitch and roll) accuracy is about 2 to 3 times worse than that of azimuth because of the inherently large estimated height error of GPS. The azimuth accuracy in dynamic mode is not very consistent, ranging from 0.5 milliradian for a 1 metre baseline (Brown et al., 1990) to 2 milliradian for a 3 m metre baseline, and 1 to 4 milliradian for a 50 metre baseline (McMillan, 1994), depending on the systems used, the body's dynamics, the operational environment and the satellite geometry.

A non-dedicated GPS receiver ADS is more versatile and is therefore potentially cheaper than a dedicated system. The performance depends on the characteristics of the receivers used. Agreement between GPS and INS attitude at a level of 3-7 arcminutes for 7-10 metre baselines was reported using NovAtel GPSCard^{TM} receivers (Cannon, 1994). In another experiment the mean errors of 5.2 and 11 milliradian and maximum errors of 21.1 and 53 milliradian for azimuth and elevation were reported for a 1 metre baseline using Magnavox GPS Engine^{TM} receivers with low dynamics (Cannon, 1992). Usually, only post-processed attitude information is available from such non-dedicated systems.

CHAPTER 3

NAVIGATION AND NAVIGATION SYSTEMS

In this chapter the basis for the development of the mathematical models for navigation is presented. The navigation systems and sensors generally used in marine navigation are discussed. Emphasis is placed on the inertial navigation and dead reckoning systems, as well as the optimal integration of these with GPS and other navigation systems.

3.1 Navigation Systems

3.1.1 Omega

Omega is a terrestrial RF based system (for background details the reader should refer to proceedings of the 12th Annual Meeting of International Omega Association, Hawai, 1987; Forssell, 1991). Eight continuous wave (CW) stations are located around the world transmitting time-shared signals on four very low (VL) frequencies (10.2, 11.33, 13.6, and 11.05 kHz). Each station is identified by a further-unique frequency which also contributes to improving the measurement accuracy.

Omega is a hyperbolic positioning system and the positioning function is based on phase difference measurements. Phase ambiguity can be resolved if the navigator knows his approximate position to within about 36 n.m. (nautical mile). The main advantage of Omega is its nearly global coverage and an availability of 97% to 99% (Warren, 1990). The main disadvantage of Omega however is its low positioning accuracy, typically only of the order of 4 n.m. (mainly caused by the unpredictable effects of VL wave propagation). The Omega signals effectively propagate in the waveguide formed by the earth's surface and the D-region of the ionosphere, hence it is the condition of these two surfaces which most affect Omega phase lag error. The height of the ionosphere is primarily affected by solar illumination, which produces a

pronounced diurnal component to the Omega phase lag. In addition, the earth's surface conductivity along the signal path has a significant effect on the phase lag. These factors can be modelled and compensated to a large extent, and are available to users as "Phase Propagation Corrections" (McMillan,1988). In addition to refraction effects, the positioning accuracy of Omega is influenced by station-vessel geometry, the station pairs used, and the time of day. The accuracy can however be improved by using Omega in differential mode. There are some reference transmitters in Europe and on the North American coast which compute the propagation error and transmit this information on a special communication channel to users within their operating area. The accuracy of differential Omega is claimed to be of the order of 0.5 n.m. when within 100 n.m. of a reference transmitter (Morris et al., 1989). This accuracy is still not adequate for navigation within confined waters, hence Omega has only been suitable for navigation in the open seas.

3.1.2 Loran-C

Loran-C is also a terrestrial RF based system in which one master transmitting station and two to four secondary stations form a chain. The transmitters utilize the same 100 kHz carrier frequency, but transmit pulses in time sharing mode within a certain interval. The coarse measurements are used to find the approximate times of arrival of the pulses, and then the phase of the carrier is measured to obtain a better accuracy. The time delay of arrival of signals from the transmitters of the master and secondary stations provides range difference information, or equivalently a hyperbolic line of position. The coverage of Loran-C is limited by the effective range of ground wave propagation. This range is of the order of 2000-3000 km over sea during the day and about 30% less at night. If the signal propagates over land the range decreases by at least 10-15% (Last et al., 1993) . The Loran-C errors are primarily phase lag errors and corrections for these errors known as PF (Primary Factor), SPF (Secondary Phase Factor) and ASF (Additional Secondary Factor) are modelled and calculated to improve the accuracy of time delay measurements (Enge et al., 1988). Loran-C can also operate in differential mode and tests have demonstrated accuracies of the order of 8-10 m for short-ranges from the reference station (Forssell, 1991). Differential Loran-C is a promising means of navigation in narrow waters. Loran-C chains, conventional and differential,

have been set up mainly along the European, North American and North African coasts, as well as the Russian and China coasts. The Russian counterpart of Loran-C is called Chayka ("sea gull").

3.1.3 Radar

Although the main function of radar is collision avoidance, radar is still a important tool for coastal and near harbour navigation, especially during conditions of restricted visibility.

The principle of radar is quite simple. Pulses of short wavelength are generated by a radar transmitter and radiated in a narrow beam by means of a directional and rotary aerial. When they encounter a object, the pulses will be reflected by the object and a radar receiver detects the returning echo. By accurately measuring the time elapsed between the transmission of the pulse and reception of the echo the distance to the object is determined. The direction of the aerial gives the bearing to the object. Typically, marine radars use the X-band (10 GHz, wavelength 3 cm) and S-band (3 GHz, wavelength 10 cm) radio signals. The S-band signal is used in wet weather to decrease the absorption effect of atmospheric humidity. X-band and S-band signals propagate along nearly straight lines and the maximum operating range, or radar horizon, is nearly equal to the visual range (Terheyden, 1986), defined by the approximation relation:

$$R = 2.23\left[\sqrt{Hra} + \sqrt{Hob}\right] \qquad (3.1)$$

where:

R radar horizon in n.m.
Hra height of radar aerial above sea level (in metres)
Hob height of object above sea level (in metres)

The radar impulse duration is about 0.05 to 1.5 μs corresponding to about 15 to 450 m of pulse length. The radar range resolution or range discrimination is equal to half the pulse length. The bearing resolution is about 0.6^0 to 2^0, which is the horizontal beam width of the radar pulse. Hence the range measurements are more precise than the bearing measurements, and the

basic position fixing method by radar is the "range-range" mode. The position accuracy of radar fix is primarily dependent upon the identification of the objects and the geometric shape, which effects the power of the reflected radar pulses. From a radar beacon set up in some area, precise radar measurements can be obtained.

3.2 Inertial Navigation System (INS)

INS is a self-contained navigation system whose heart is the Inertial Measuring Unit (IMU) comprising gyroscopes (gyro) and accelerometers as well as the platform. Gyros and accelerometers measure INS platform's angular variation or angular velocity and linear accelerations in relation to a certain reference system. Once the INS is supplied with initial position and attitude information, it is capable of continuously updating the platform's position, ground speed and attitude. Because an IMU measures non-gravitational acceleration, INS has to take into account the effects of gravity and earth rotation. Another source of error is imperfections in the IMU: gyro drift error, bias and scale factor errors of gyro and accelerometer, assembly error and initial alignment error. All the errors have different signatures and mathematical expressions, depending on the structure of the INS and the mechanization of the navigation equations. Generally speaking, these errors have bias and long oscillation period (low frequency) characteristics. The INS platform's speed and position are derived by integration of the IMU measured accelerations and hence their errors will increase with time. Compared to other navigation systems INS has good high frequency performance and is very sensitive to rapid changes of the platform's states. On the other hand, the positioning characteristics of GPS and other radio navigation systems are those that can be described as "averaging" and are therefore not very sensitive to the high frequency noise, and have only a good low frequency performance.

The following analysis, and the contents of Appendix 1, provides a full summary, modification/unification and simplification of the INS mechanization and error analysis based on the following materials: Britting, 1971; Farrell, 1976; Schwarz, 1979; Schwarz, 1980; Caspary, 1987; Schröder et al.,1988; Huddle, 1989.

The INS model simplification assumes that the second or higher order errors of gyro, accelerometer and platform can either be neglected or modelled as noise due to the availability of a high calibration rate for the INS by external navigation systems such as GPS. The height channel of an INS is included in the system model and mechanization. The reason is that for marine vessels the mean value of the height change about the centre of mass of the vessel can be considered to be zero, and can therefore be used as a constraint for the height channel of the INS. Furthermore, the height can be obtained from GPS measurement and the time integration in the INS height channel can be restricted to the short periods between GPS measurement epochs, avoiding a large system positive feedback which will cause the height channel to become instable. In this way the accurate height change and change rate can be obtained from the INS height channel and the GPS measurements. This fact is useful for GPS measurement corrections such as cycle slip detection and SA compensation (Wong et al.,1988; Hein G. et al.,1988; Loomis, 1990; Negast et al., 1990; Lipp et al.,1994).

There are two main classes of INS in use: the analytic system (strapdown system) and the semi-analytic system (platform system), as indicated in Fig. 3.1.

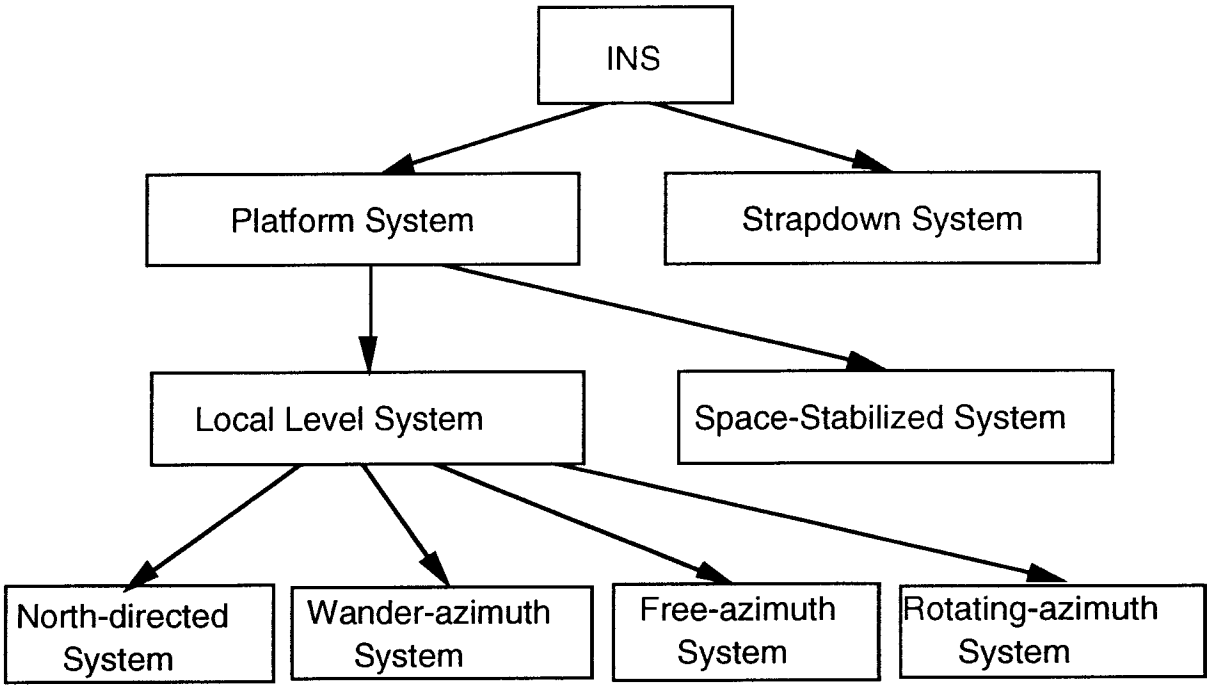

Figure 3.1. Specifications of INS.

For all INS systems the basic navigation equation is (see Appendix 1.1):

$$\dot{\mathbf{V}} = \mathbf{a} - (2\Omega + \omega) \times \mathbf{V} + \mathbf{g} \qquad (3.2)$$

where **a** is the output of the accelerometers, Ω is the angular velocity of earth rotation, ω is the platform's angular velocity relative to the earth, **V** is the platform's velocity relative to the earth and **g** is the acceleration due to earth gravity.

All inertial navigation systems perform the following functions:

1) Instrument a reference frame.
2) Measure specific force.
3) Have knowledge of the gravitational field.
4) Time integrate the specific force to obtain velocity and position.

The structure and function of INS are illustrated in Fig. 3.2.

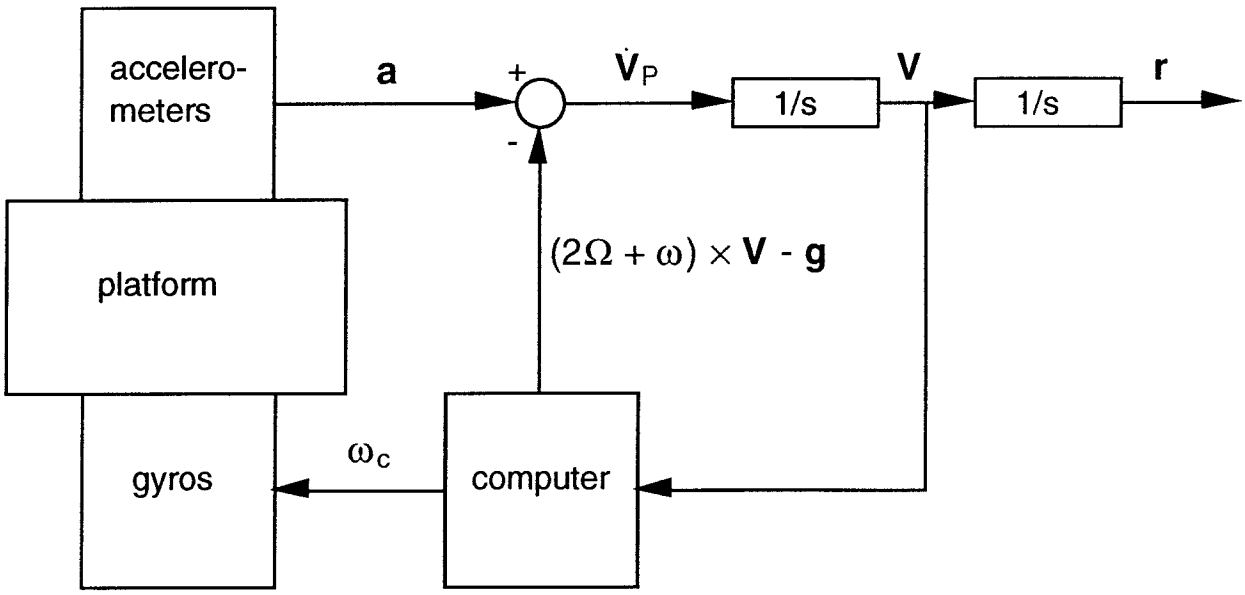

Figure 3.2. The structure of an INS.

where:

- **a** output of accelerometer
- **Vp** platform's velocity relative to earth
- Ω earth's angular velocity
- ω platform's angular velocity relative to earth
- ω_c platform's command
- g gravitational acceleration

3.2.1 Semi-Analytic INS

The IMU of a semi-analytic INS is a stabilized platform. The platform is usually stabilized in either the inertial space or a local level frame. It's main components are: 1) three one-degree freedom gyros or two two-degree freedom gyros, 2) two or three accelerometers, 3) three gimbal rings (for pitch or roll angle that is larger than 90^0, there is a fourth gimbal ring to prevent the rings from "gimbal-lock"), 4) servo loops (see Caspary, 1987).

3.2.1.1 Local Level Systems

For local level stabilized systems the sensitive axes of the gyros and accelerometers comprise a Cartesian coordinate frame, and follows the local level by making the undamped oscillation period of the platform equal the Schuler period (84.4 minutes). The azimuth of the platform can be fixed in any direction or left totally relaxed. When there is no torque acting on the gyro, the spin axis of an ideal gyro is fixed in a certain direction in inertial space. In order to make the platform follow the inertially rotating local level frame, there is a need to put torque through the servo system of the platform to compensate for the earth's rotation and the platform's movement. Because the platform is kept in local level orientation and the outputs of two horizontal accelerometers have no components of the earth gravity (and hence there is no need to compensate it), high navigation precision is available but at a cost of a complicated platform mechanism.

There are different kinds of local level systems depending on the method of azimuth gyro control:

1) North-directed system:

The platform keeps tracking the geographic frame whose origin is of the platform centre. The body's attitude and course are obtained directly from the platform attitude and the computation burden is therefore light. Its main defect is that the platform should be kept north-directed at all times. In high latitude regions where east-west velocity causes a large longitude change rate, the platform requires a large torque to be applied to the azimuth gyro to make the platform north-seeking, see eqns (A.1.2.8) to (A.1.2.10), and a large scale factor error is induced. When at the pole, the platform needs an infinitely large torque to make the platform change 180 degree in azimuth instantly, something that is impossible to accomplish. Furthermore it requires a long time for initial alignment to force the platform into a north-directed state. In practice, a north-directed system is only capable of working satisfactorily in regions where latitude is less than 60 degrees.

2) Wander-azimuth system:

This type of system only compensates for the perpendicular component of the earth's rotation. The azimuth of the platform is not fixed in any direction, and it varies according to the platform's east-west velocity and latitude, see eqn (A.1.3.1). There is no need to compensate the platform's east-west velocity, hence the system can function in high latitudes. Compared with a north-directed system, the body's position and attitude cannot be obtained directly because the platform's frame is not coincident with the geographic frame due to azimuth wandering. More computations are therefore required to calculate the direction cosine matrix and the earth curvature, which changes with azimuth and latitude.

3) Free-azimuth system:

This type of system has no command torque applied to the azimuth gyro. The azimuth of the platform can settle down in any direction in the local level, and keeps changing even if the platform is stationary, see eqn (A 1.4.1). Because only small torque is applied to the azimuth gyro to compensate for the gyro drift, the effects of gyro scale factor error and Coriolis acceleration is also small. Free-azimuth systems can function in high latitude regions but the navigation computer workload is larger than that of the wander-azimuth system.

4) Rotating-azimuth system:

This system is based on the fact that the effects of the drift of horizontal gyros and the bias of accelerometers can be reduced if the platform is rotated around it's vertical axis. A constant torque is applied to the azimuth gyro to make the platform rotate relative to inertial space with a constant angular velocity, see eqn (A.1.5.1). Although this procedure can reduce the constant errors of horizontal gyros and accelerometers, if the scale factor error of the azimuth gyro is large, then the large constant torque will induce large error. To overcome this problem, a periodic direction-changing torque can be applied to the azimuth gyro instead of a constant one, a so-called oscillating-azimuth system results. Both rotating and oscillating systems can function in high latitude regions and both need gyros of high dynamic performance, and a powerful computer to guarantee navigation computation precision.

3.2.1.2 Space-Stabilized Systems

The platform of such systems physically realizes an earth-centred, inertially non-rotating frame. The platform is stabilized in inertial space and the sensitive axes of the accelerometers point in fixed directions in inertial space. Except for small compensation torques applied to the gyros to account for acceleration sensitivity, anisoelastic effects, temperature sensitivity, the gyros are uncommanded and there is no compensation for earth rotation and platform attitude change. Hence the output of each accelerometer includes the components of the earth gravity, which vary with position and have to be compensated for. The mechanism of the space-stabilized platform is much simpler than those of local-stabilized platforms. The navigation precision mainly depends on the quality of the compensation of the earth gravity. The space-stabilized system is principal used in survey practice INS, with the GEOSPIN of Honeywell being a typical example (see Eissfeller, 1989, for details).

3.2.2 Analytic Systems

Analytic systems have no physical platforms, and the gyros and accelerometers are mounted directly to the body. The gyros and accelerometers measure the angular velocity and acceleration of the body relative to inertial space and the directions of the accelerometers change according to the changes of body's attitude. Setting up of the frame, determining the body's attitude and performing the computations are all carried out by a navigation computer. Hence there is an analytic platform within the system which can be implemented mathematically in different local level systems, such as local geographic frame, wander-azimuth frame, etc. (see Appendix 2).

For a stationary base, the error propagation characteristics of a strapdown system are similar to that of a platform system. The errors of a strapdown system also consist of three components: Schuler oscillation, Foucault oscillation and 24 hour oscillation.

Compared with the platform system, a summary of the characteristics of the strapdown INS system (SINS) is presented below:

1) Because there are no complicated platform mechanisms and associated servo system, the hardware of the SINS is simpler and easier to maintain, and hence its cost is correspondingly lower. The reliability of the system is high: for example, the MTBF (Mean Time Between Failure) for a laser gyro SINS is 2000 to 4000 hours, while for the platform system the MTBF is 500 to 1000 hours (Stieler et al., 1982)

2) The body's attitude, course, position, velocity, acceleration, angular velocity and angular acceleration are all provided by the computer. There is no need for any intermediate loops and sensors, and hence the information can be transferred directly to navigation, guidance and other control systems.

3) SINS impose high requirements for the inertial devices, especially the gyro which has to operate across a large dynamic range. Vibrations and other external interference will deteriorate the performance of the devices. Usually, the precision of an accelerometer working on a vibrating base is one order less than

that working on a stationary base, and this will directly influence the navigation precision obtained.

4) The accelerometers are subjected to the components of the earth gravity as the body rolls and pitches, reducing the measurement accuracy and exciting cross-axis errors. The accelerometer bias errors accumulate.

5) The body's motion induces unique sensor errors (torquer error, anisoinertia, output axis angular acceleration), which can be partly compensated.

6) Most SINS use the optical gyros, such as the ring laser gyro (RLG), fibre-optic gyro (FOG), and hence exhibit high reliability and excellent input axis stability due to their solid-state configuration (and solid-state accelerometers, such as silicon micromachined accelerometer and quartz vibrating beam accelerometer). The random walk drift of a RLG and FOG is of the order of 10^{-3}deg./$\sqrt{h}$ (Stieler et al.,1982; Killian, 1994), compared with 10^{-6}deg./$\sqrt{h}$ for electrostatically suspended gyroscopes (ESG) (Adams et al.,1981). A disadvantage of the optical gyros is that they are sensitive to the gradient of temperature and its noise floor is set by quantum effects (shot noise and spontaneous emission). For the RLG it requires a special technique to eliminate the 'lock-in' effect, or working dead zone (Stieler et al.,1982; Stieler,1982).

7) SINS have a high requirement for scale factor accuracy and linearity of the gyro torquer. For example, a working angular velocity of 50 deg/sec and gyro drift rate of 0.01 deg/h of a platform system of medium precision requires that the scale factor error be less than 2×10^{-4}. But for a strapdown system working under angular velocity 1 deg/sec and gyro drift rate 0.01 deg/h, the scale factor should be less than 3×10^{-5}. The larger the working angular velocity, the larger the error caused by scale factor error.

8) The SINS computer must be fast enough to do all calculations in a few milliseconds, with long enough wordlength to preserve computational precision. Generally speaking, the computation speed of strapdown system should be about 50 times that of a platform system.

9) The inertial device cannot rotate as a platform system does and the errors of the devices cannot be calibrated in the system alignment, and the system initial alignment is also difficult. Hence SINS rely on sensor models, with real-time calibration of the inertial errors. The error of initial alignment is large and will influence the navigation precision.

Summarizing the errors, for an unaided SINS an accuracy of 1 mile-an-hour using optic-gyro which has a typical scale factor accuracy 50 ppm is generally accepted. In contrast, the accurate platform system is a 1 mile-a-day system, which has a heading error less than 0.001deg/h (Lawrence, 1993).

3.2.3. INS Errors

The main INS error sources are:
1) Structure error: assembly error of accelerometers and gyros.
2) Device error: gyro drift and accelerometer bias.
3) Digital to analog conversion error: scale factor errors of accelerometer, gyro, and torque sensors.
4) Initial state error: initial attitude, velocity and position errors of platform.
5) Correction error: errors introduced by other navigation system for INS error calibration..

The local-level INS error analysis is presented in Appendix 3.

The INS error characteristics of local-level systems can be summarized as follows (in which points 3 to 7 are for north-directed systems) :

1) Generally speaking, in the case of moving base, eqns (A.3.3.2) to (A.3.3.4), (A.3.4.11) to (A.3.4.13), (A.3.5.3) to (A.3.5.4) can be linearized and used as the state equations of dynamic estimation, oyherwise only numerical solutions of the errors can be obtained. For a stationary base the errors can be expressed as analytic solutions of a set of linear-constant differential equations, eqns (A.3.4.18) to (A.3.4.19), (A.3.5.5) to (A.3.5.6).

2) Except for the free-azimuth system, the semi-analytic systems usually have oscillation errors which have three different periods: 84.4 minutes for the Schuler

oscillation, a 24 hour oscillation and the Foucault oscillation whose period varies with latitude, see eqns (A.3.6.9) and (A.3.6.9). (The Foucault oscillation is the envelope of the Schuler oscillation, or the Schuler oscillation can be considered to be the carrier component of the Foucault oscillation.)

3) The position, velocity and attitude errors of a north-directed INS caused by accelerometer biases and initial attitude errors are oscillation errors with the Foucault oscillation and the Schuler oscillation, see Table A.3.6.7 and Table A.3.6.10.

4) The platform drift rates mainly cause 24 hour oscillation errors along with the Schuler and Foucault oscillations. The horizontal components of the platform drift rate E_x and E_z cause the longitude errors which increase with time, see Table A.3.6.8.

5) The initial location errors have little effect on horizontal attitude, see Table A.3.6.9. The horizontal attitude errors are primarily a kind of oscillation which combine both the Foucault and Schuler oscillations, see Table A.3.6.8. The initial longitude error has no effect on latitude error. The initial latitude error causes oscillation errors in both latitude and longitude, the oscillation period is nearly 24 hours and the longitude error is latitude-dependent. If the initial alignment of system is perfect, then the Schuler oscillation component will be eliminated from each error and the 24 hour oscillation will be the main term responsible for position and azimuth errors.

6) The latitude, longitude and velocity errors consist of three oscillations: Foucault, Schuler and a 24 hour oscillation (the main part), see Table A.3.6.7 to A.3.6.10. Because the Foucault oscillation is the envelope of the Schuler oscillation, therefore if there is a damping system to eliminate the Schuler oscillation, it will also eliminate the Foucault oscillation.

7) The gyro drift causes the platform to drift directly, and is proportional to platform commands, see eqns (A.3.3.2) to (A.3.3.4). Assuming the minimum platform command equals 30 deg/h and the platform drift rate is less than 0.003°/h, the scale factor error should be less than 1×10^{-4} and assembly error less than 20". The horizontal attitude errors are mainly depend on the accelerometer biases. If the initial alignment is not perfect, or the biases of

accelerometer are changed, there will be Schuler oscillation terms in the attitude errors.

8) In the case of a wander-azimuth system the platform frame is generally not coincident with the geographic frame, hence the drifts of three gyros will all cause position errors which increase with time. Assuming 45° latitude and the drift rates of azimuth and north gyros being equal to 0.01deg/h, it will approximately cause a 0.84nm/h position error.

9) In the case of a free-azimuth system there are only Schuler oscillation and 24 hour oscillation (but no Foucault oscillation). In the case of a rotating-azimuth system the horizontal gyro drift errors will be modulated and averaged, but not in the case of the drift of azimuth gyro.

10) The navigation errors caused by random error sources are divergent, and the divergent speed is proportional to $\sqrt{t}$, see eqns (A.3.7.1) and (A.3.7.2).

11) The height and vertical velocity errors of INS increase with time and have to be constrained by external height measurements.

12) In the stationary base, the eigenfunction of SINS errors is the same as local-level systems, see eqn (A.3.6.2), and the error propagations have the same oscillation characteristics as those of local-level systems.

13) INS needs external navigation equipment to provide system initial alignment and device calibration, and on-the-fly error correction and calibration, in order to guarantee navigation accuracy.

3.3 Navigation Equipment

The navigation equipment referred to here is mounted on a body or vessel and performs the function of dead reckoning (DR). For marine applications there are mainly two types of equipment used: gyrocompass for the heading direction and speed log for the velocity measurement.

3.3.1 Gyrocompass

A gyrocompass is actually a gyro of two degree-of -freedom mounted on gimbal rings or supporting system, and using the property of direction-fixing and precession relative to inertial space to make the spin axis of the gyro meridian seeking. The ideal gyrocompass indicates true north or meridian direction.

There are essentially two types of gyrocompass: single-rotor types such as the Sperry type, Brown type and Arma-Brown type, and double-rotor types such as the Anschutz type, Plath and Arma type. About the principle of the north seeking of gyrocompass, please see Fabeck, (1980); Christou, (1983).

3.3.1.1 Gyrocompass Errors

The gyrocompass can be considered to be a linear-stable-underdamped second order system, and its undamped natural frequency is the Schuler frequency making it independent of a body's manoeuvre. The total dynamic response of a gyrocompass in the stationary base is (the following equations are modified from Christou ,1983):

$$\alpha(t) = \alpha_T + \alpha_{SS} \qquad (3.3)$$

where:

- $\alpha(t)$ deviation angle of the gyro spin axis from the meridian
- α_T transient response
- α_{SS} steady state response

and

$$\alpha_T = \alpha_m e^{-\sigma t} \cos(ft - \psi) \qquad (3.4)$$

where α_m is approximately equal to the initial deviation angle of the gyro spin axis from the meridian:

$$\alpha_m = \left\{[\alpha(0)]^2 + \left[\frac{\sigma}{f}\alpha(0) + \frac{1}{f}\dot{\alpha}(0)\right]^2\right\}^{\frac{1}{2}} \approx \alpha(0) \tag{3.5}$$

and

σ damping coefficient

f damped natural frequency which is a function of latitude and its period is about 100 to120 minutes (Terheyden & Zickwolff, 1983)

$$\psi = tg^{-1}\left[\frac{\sigma}{f}\alpha(0) + \frac{1}{f}\dot{\alpha}(0)/\alpha(0)\right] \approx 0 \tag{3.6}$$

$$\alpha_{SS} = -\gamma\, tg\varphi \tag{3.7}$$

where γ is the deviation angle of the gyrocompass gravity centre to the east.

From eqns (3.3) to (3.7) it can be seen that the transient response of a gyrocompass is a damped, periodic oscillation and will be zero as time increases. The steady state response, called the damping error or latitude error, is a function of latitude. At low latitude its value is very small because γ is small, but at high latitude this value will increase enormously. The latitude error is corrected by setting the latitude corrector of the gyrocompass to the correct latitude of the body's position. At steady state, the spin axis of the gyro will settle in nearly the meridian direction with a deviation of the latitude error and will be nearly parallel to the local level.

In a stationary base, the direction of the gyro spin axis is in coincidence with the horizontal component of the earths rotation, and the precession of the axis is equal to the vertical component of the angular velocity of the earth's rotation. The horizontal component of the earth's rotation is the useful part and the directive force of a gyrocompass is directly proportional to it. Therefore at the equator the directional force is a maximum and at the poles it is zero. At high latitudes, the directive force is so small, and the damping period is so large, that the gyrocompass cannot return to north direction rapidly in the presence of interference torque, and the latitude error increases so quickly that the gyrocompass becomes useless. In general, gyrocompasses can only operate satisfactorily in the region of latitude < 70 degrees.

When a body is moving, the angular velocity of the body relative to the inertial space is equal to the sum of the angular velocity of the earth's rotation and the angular velocity of the body relative to earth, see eqn (2.10). Assuming the body is moving with constant velocity V relative to the earth with course H, the gyrocompass is now searching the dynamic north, not the true north because it is incapable of distinguishing between the angular velocities of the earth and the body and it senses the resultant inertial angular velocity instead, as shown in Fig. 3.3.

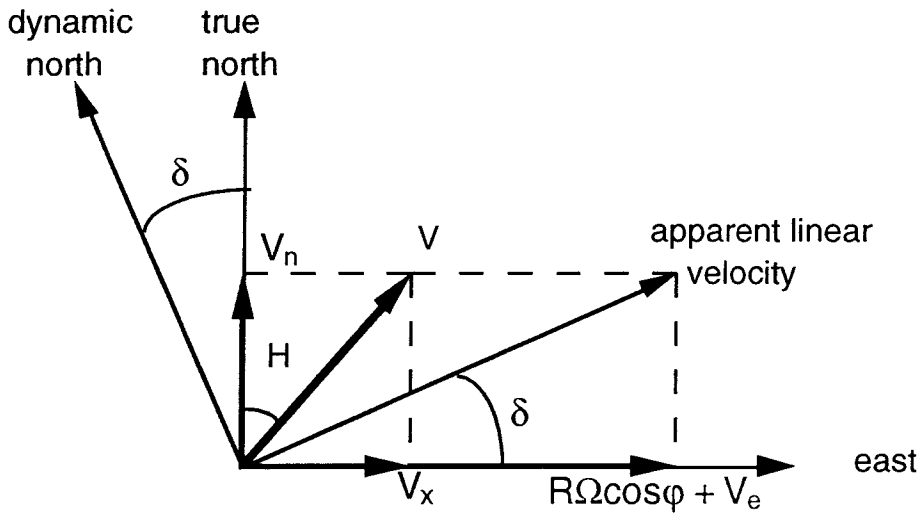

Figure 3.3. Course and speed error of gyrocompass.

The total dynamic response of the gyrocompass in a moving base is the same as eqn (3.3), but the steady state response has an additional term δ:

$$\alpha_{SS} = -\gamma \, tg\varphi + tg^{-1}\left[\frac{V \cos H}{R\Omega \cos\varphi + V \sin H}\right] \qquad (3.8)$$

δ is the deviation angle of true north from dynamic north. It is a small angle and its minimum value (zero degree) is obtained when travelling in an easterly direction (H = 90°) and the maximum value occurs when travelling in a northerly direction. The speed and course error of a gyrocompass can be corrected using the outputs of log and gyrocompass itself approximately.

The inertial force caused by a body's acceleration can be decomposed in north-south and east-west components. The east-west component causes a moment

whose direction is parallel to the gyro spin axis and does not cause the gyro to precess. The north-south component causes a moment, which causes the gyro spin axis to precess. A north acceleration make it precess towards the west and a south acceleration towards the east. Therefore the acceleration error is proportional to cosH.

The inertial force caused by the pitching and rolling of the body also imparts moments to the spin axis of a gyrocompass to make it deviate from the meridian. For a vessel, the moments have periodic oscillations and their periods are much shorter than the damped oscillation period of input and output axes of gyrocompass (100 to 120 minutes). The deviation angle, called the pitching-rolling error, is proportional to the product of the two horizontal components of acceleration caused by the pitching-rolling, and deviates towards one direction because the signs of the horizontal components of the acceleration change at the same time. The acceleration caused by pitching and rolling in rough seas can induce an error as great as 20 degrees. There are mainly two kinds of compensation for the pitching-rolling error depending on the structure of gyrocompass. For a double-rotor gyrocompass, the double-rotors are so arranged that an additional precession freedom is present and the precession around the north-south axis (spin axis) of the gyrocompass is stabilized. This precession period is increased from a few second to 10-20 min (Terheyden & Zickwolff, 1983) to make the system insensitive to horizontal oscillation of acceleration. For a single-rotor gyrocompass, a built-in liquor-ballistic mechanism is used to delay and damp the effect of the north-south component against the east-west component to eliminate the harmful torque about the input axis of the gyrocompass.

Other gyrocompass error sources are the gimballing error which is due to an imperfect support system, and random error. In the case of a gyrocompass aboard a vessel, well adjusted for latitude and speed and course, its deviation can be under 0.5 degree, and the deviation is kept constant for all heading directions.

3.3.2 Speed Log

The function of the vessel's log is to measure velocity and distance travelled. There are quite a number of logs, operating on different physical principles, among them being the Doppler log used in this study (Fig.3.4).

3.3.2.1 Doppler Log Principle

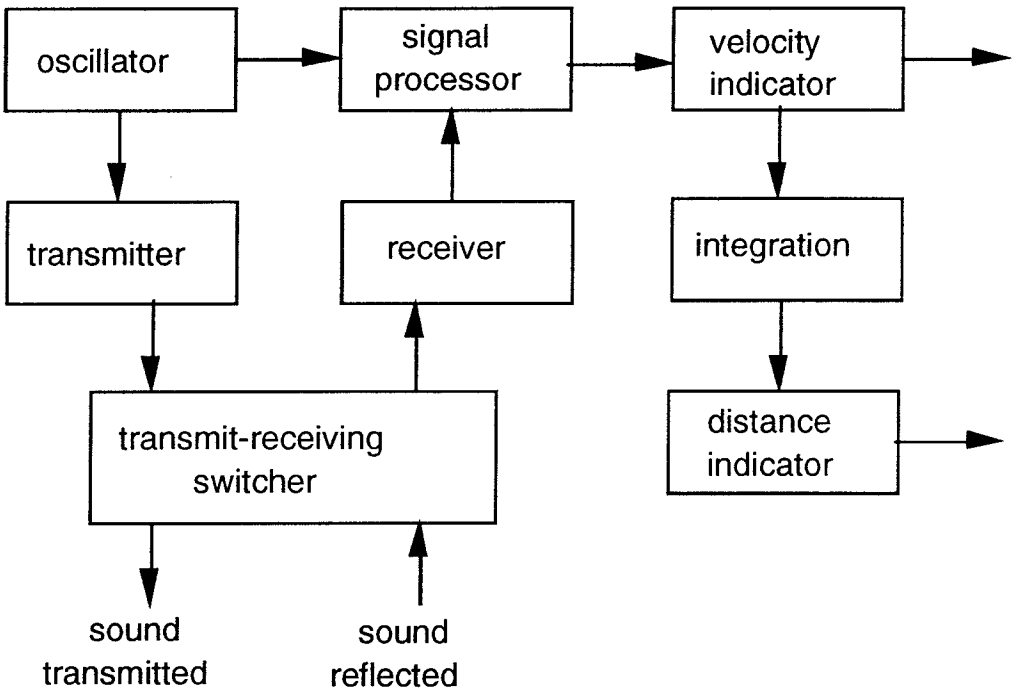

Fig.3.4. Doppler log blockchart.

The principle of the Doppler log is that the vessel's velocity is proportional to the frequency shift between the acoustic signal transmitted from the vessel and that received back by the vessel. This Doppler frequency shift is due to the relative motion of the sound source and the propagation medium. The Doppler frequency f_d equals:

$$f_d = f \frac{C + V\cos\alpha}{C - V\cos\alpha} \qquad (3.9)$$

where:

- f transmitted frequency of the sound wave
- C propagation speed of the sound wave in water
- α angle between the vessel's speed vector and the sound wave

A transmitting transducer below the vessel continuously emits a beam of sound vibrations in the water at an angle α (usually 60^{o} to the keel) in the forward direction. A second transducer receives the echo caused by diffuse reflection from the sea-bed or sea water layer. A third transmitting transducer directs a sound beam in a backward direction and a fourth receiving transducer receives its echoes. This arrangement is called the Janus configuration (Sonnenberg, 1978).

Because C is approximately 1500 m/sec in sea water and is quite large compared to the vessel's speed, by expansion and neglecting high order terms in eqn (3.9):

$$f_f = f\left(1 + \frac{2V}{C}\cos\alpha\right) \tag{3.10}$$

$$f_b = f\left(1 - \frac{2V}{C}\cos\alpha\right) \tag{3.11}$$

$$V = \frac{C}{4f\cos\alpha}\left(f_f - f_b\right) \tag{3.12}$$

where:

- f_f Doppler frequency measured by the forward transducer
- f_b Doppler frequency measured by the backward transducer

3.3.2.2 Doppler Log Errors

Actually C and α are not constant. α varies as the vessel pitches. For the Janus configuration the vertical movement of the vessel does not influence the Doppler shifts because of the equal Doppler shift changes for the forward and backward beams. By using the Janus configuration, the error caused by pitching will be reduced because the resulting Doppler shifts are not affected since the increase

and decrease of the speeds of the forward and backward beams are nearly the same, and the difference of the Doppler shifts of forward and backward beam is also not changed, see eqns (3.10) to (3.12). With a trim angle of 10^{o}, the relative error of speed measured is about 1%.

The speed of sound C depends on water temperature and (to a smaller degree) on the salinity and water pressure (Terheyden & Zickwolff, 1983):

$$dc \,/\frac{m}{s} \approx 3.6 \times dT \,/c^{o}$$

$$dc \,/\frac{m}{s} \approx 1.2 \times dS \,/‰$$

$$dc \,/\frac{m}{s} \approx 0.2 \times dp \,/bar$$

where:

- dc variation of the speed of sound
- dT variation of temperature of sea water
- dS variation of salinity of sea water
- dp variation of pressure of sea water

Because of temperature differences in the ocean layers, sound waves do not travel in a straight line. Instead, they follow a curved path, resulting in bending, splitting and distortion of the directed sound waves. A sound beam bends away from a layer of high temperature, and bends towards a layer of low temperature (Navpapers, 1963). The horizontal layers of sea water of different temperature, salinity and pressure have no influence on the measurements of the Doppler log because the reverse frequency change of the echo will cancel out the first frequency change of the transmitting beam. The frequency drift of the transmitter has no influence on the measurement of log because the Doppler shifts received by the forward and backward transducers change by the same value with the same sign, and the quotient $(f_f - f_b) / f$ is not changed.

The measurements of the Doppler log depend solely on the speed of the sound waves. If there is a 5^{o} C temperature change it will cause a change of sound speed, and result in a measurement error of the vessel's speed of about 1.2%. Some equipment uses a thermistor or velocimeter mounted near the

transducers. Deviations of the sound speed from the normal value are passed to the system computer for correction of its calculation. Other logs (those of Krupp and Thomson CSF (Sonnenberg, 1978)) apply automatic methods of correction for changes in the sound speed by using a large number of electrostrictive elements of PZT material. The elements are fed with voltages that differ in phase and the sound waves have the same phase difference. The sound propagation is always perpendicular to a wave front and the wave front is controlled by the distance between the electrostrictive elements. This method keeps $C / \cos\alpha$ constant.

In general, the sound beam of a Doppler log is absorbed and scattered by the mass of water between 200 to 400 metre depth, the so-called deep scattering layer (DSL). When reflections are received from this layer the speed of the vessel is determined relative to that layer, and not relative to the sea bottom. Generally a Doppler log of the navigation type can only measure the ground speed of a vessel in waters up to a depth of about 200 metres. The depth penetrated by the sound wave is dependent on the sound wave frequency transmitted (the higher the frequency, the greater the depth). Apart from the effect of the DSL, the water at 10 to 30 metres below the vessel's keel also causes an echo, called 'water track' (as opposed to 'bottom track'). Some Doppler logs such as the Krupp Atlas type can work in both ' bottom track' or 'water track' modes.

The following average performance is based on data supplied by producers of Doppler log (Sonnenberg, 1978):

Accuracy:	0.2 to 0.5 per cent of the distance travelled, plus 20 metres/hour drift of the set. For high speeds, e.g. 20 to 40 knots, about 1.0 per cent.
Velocity range:	up to between 30 and 100 knots alongships, up to between 8 and 10 knots athwartships.
Minimum depth:	about 0.3 - 0.5 metre.

Frequency of vibration in water: 100 to 600kHz.

CHAPTER 4

GPS MODELS

Operation of the NAVSTAR Global Positioning System (GPS) is the responsibility of the Joint Program Office (JPO), under the direction of the U.S. Department of Defense (DoD). GPS is an all-weather, space-based radio navigation system which satisfies the requirements for the U.S. military to accurately determine position, velocity, and time in a common reference system, anywhere on or near the earth, on a continuous basis.

The GPS system consists of the space segment, control segment and user segment, and supports two positioning service: the Standard Positioning Service (SPS) and the Precise Positioning Service (PPS). The SPS signal consists of the L1 frequency, the Coarse/Acquisition (C/A) code and the unencrypted portion of the navigation message. SPS is available world-wide for civil use and its positioning accuracy is 100 m horizontal (2 dRMS), which is roughly equivalent to 76 m SEP (Spherical Error Probable). The true SPS velocity accuracy is classified though 0.5 to 1.5m/sec velocity error have been reported (Cannon, 1993). In most cases, SPS positioning accuracy satisfies the requirements for ocean and coastal navigation for civil marine use. The PPS signal comprises the clear SPS plus the encrypted signals and data transmitted by the GPS satellite. Specifically, the PPS signal consists of the L1 and L2 frequency, the Y code (which is the encrypted form of the P code), and the Selective Availability corrections. Selective Availability (SA) and Anti-Spoofing (A-S) are the two methods used by the control segment to restrict access to the PPS, and the hostile imitation of the PPS signal. The PPS is available to the U.S. and allied military use, and limited civil use under stringent conditions. The objective positioning accuracy offered by the PPS is 16 m SEP, though accuracies of 8 m SEP have been reported (Jules, 1991), while the velocity standard deviation is about 0.01m/sec. SA and A-S are presently activated continuously on the Block II operational satellites.

4.1 GPS Observables

The complete signal leaving the satellite antenna can be represented by (Wells et al., 1987):

$$A_cC(t)D(t)\sin(2\pi f_1 + \phi_c) + A_pp(t)D(t)\cos(2\pi f_1 + \phi_{p1}) + A_pP(t)D(t)\cos(2\pi f_2 + \phi_{p2}) \quad (4.1)$$

where:

A_c, A_p	modulation amplitudes of the C/A and P codes
C(t)	C/A code with a chip rate = 1.023 Mbps; period = 1 ms; chip length = 1023 bits and wavelength ≈ 293 m
P(t)	P code with a chip rate = 10.23 Mbps; period = 266 days; 9 hour, 45 minute, 55.5 seconds; chip length = 235,469,592,765,000 bits; and wavelength ≈ 29.3 m
D(t)	data sequence with a data rate = 50 bps; frame length = 1500 bits; frame period = 30 seconds; the detail see (for details see Van Dierendonck et al., 1980)
ϕ_c, ϕ_{p1}, ϕ_{p2}	small phase noise and oscillator drift components of C/A, L1 P code and L2 P code
f_1, f_2	the nominal frequencies of the L1 and L2 carrier waves, (The wavelength of L1 ≈ 19 cm, and the wavelength of L2 ≈ 21 cm)

The entire signal modulation and synchronization is controlled by the main satellite oscillator with a fundamental frequency of 10.23 Hz. The navigation data D(T) has a bandwidth of 100 Hz. Due to the modulation of the code signal, the power spectrum density (PSD) of the GPS signal is spread. The bandwidths of the P code and C/A code are 20 MHz and 2 MHz respectively. The spread spectrum of the GPS signal makes it much less sensitive to interference and jamming. The modulation errors, including phase noise and quadrature, are all less than 5^0, the equipment group delay is less than 3 ns (2 σ) (Wells et al.,1987) and the RMS clock transition time difference between the C/A code and P code clock is less than 5 nsec (Spilker, 1980).

The observation equations for code, carrier phase and range-rate are (adapted from Rizos & Grant, 1990):

$$P = \rho + d_{ephem} + c\,(dt - dT) + d_{ion} + d_{trop} + d_{mul} + \varepsilon_p \tag{4.2}$$

$$\Phi = \rho + d_{ephem} + c\,(dt - dT) + \lambda N - d_{ion} + d_{trop} + d_{mul} + \varepsilon_\Phi \tag{4.3}$$

$$D = \dot{\rho} + \dot{d}_{ephem} + c\,(\dot{dt} - \dot{dT}) - \dot{d}_{ion} + \dot{d}_{trop} + \dot{d}_{mul} + \varepsilon_D \tag{4.4}$$

where:

ρ	geometric range between the satellite and receiver antennas
d_{ephem}	satellite ephemeris error
dt:	satellite clock error
dT	receiver clock error
d_{ion}	ionospheric refraction error
d_{trop}	tropospheric refraction error
d_{mul}	multipath error
λN	carrier phase ambiguity
ε_p, ε_ϕ, ε_D	measurement noise

The superscript dot in eqn (4.4) refers to the derivative with respect to time.

4.2 GPS Erros

4.2.1 Satellite Errors

1) Ephemeris error:

The primary perturbing forces for the GPS satellites are earth-mass attraction, solar radiation pressure, lunar and solar gravity. The nominal broadcast orbital error is of the order of 5 to 25 m, with error peaks which have reached 80 m in the past, and but which remain within 5 to 10 m now that GPS has been declared fully operational (Lachapelle, 1990). For relative positioning, the vector error caused by orbital error is approximately (Kleusberg, 1993):

$$\text{vector error (m)} \approx \frac{d}{20{,}000} \times \text{orbit error (m)} \tag{4.5}$$

where d is the baseline length in km.

For point positioning, the ephemeris error will bias the final position results in a systematic way, depending on the receiver-satellite geometry. For most navigation applications the ephemeris error is ignored.

2) Clock error:
The GPS satellites carry several frequency standards of the Rubidium and Cesium beam type. The Rubidium standards exhibit deterministic drift characteristics. The Cesium standards normally do not exhibit higher order deterministic drift in frequency over the time periods of interest. They can be characterized as a frequency offset plus random variations in frequency. Any other characteristics are only observable over very long periods of time (over a day or two). A second order polynomial function is adequate for representing the drift characteristics of a satellite clock, and it also absorbs any secular relativistic effects. In fact, for a reasonable time period a first order polynomial already suffices to describe a Cesium frequency drift, though not for the Rubidium frequency drift. The second order representation of clock error is uploaded to the space vehicles as a part of the navigation message at least once a day by the Master Control Station (via the network of Upload Stations) and the average prediction error is about 5-10 ns (1-3 m). The prediction accuracies and reliabilities of the satellite ephemeris and clock depend on the age of the data upload, represented in the navigation message as AODE (Age Of Data Ephemeris) and AODC (Age Of Data Clock). For 24 hours of data age, the orbital error can increase 2 times and the clock error 6 times (Russell , et al, 1980).

3) Multipath:
Satellite multipath occurs when the transmitted signal bounces off part of the satellite, before travelling down to the ground-based receivers. There are several possible reflecting surfaces which can become prominent depending upon the satellite-receiver elevation and satellite altitude. Although the simultaneous presence of more than one multipath effect can lead to an increasing chance of non-coherent interference of signals and reduce the total multipath effect, as the satellite signals have a common time origin it can also give rise to a beat pattern with a larger amplitude than that which an individual reflection could produce. The satellite multipath effect is expected to be of the

order of a few centimetres for baselines of a few hundred kilometres (Young, 1985), but it cannot be eliminated by differencing data between two receivers.

4) Selective Availability:

For the Standard Positioning Service, Selective Availability (SA) is the largest of all the errors attributable to the space segment. The implementation of SA is known to be a combination of clock dithering (δ-type SA) and manipulation of the ephemeris data (ε-type SA). The orbital error term caused by SA has been estimated to be up to 100 m with a correlation time of 3 minutes (Kremer et al., 1989). However, little evidence has been found of ε-type SA at present. The clock dithering is implemented through the injection of errors in the satellite clock drift term. Because the timing for all GPS satellites is controlled by one master oscillator or frequency standard, clock dithering effects appear on code, carrier and Doppler measurements simultaneously. The satellite clock frequency error can be 5.6×10^{-12} under SA compared with 2.2×10^{-12} for the SA-free case. Data analysis results provided by the JPO, and processed by DOT (U.S. Department of Transport) indicate 1-sigma pseudo-range errors of about 30 metres, the Doppler measurement dispersion distribution is around 0.86 ns/sec, the range-rate errors are of the order of 0.13 m/sec, and acceleration errors of about 0.0037 m/sec^2 with a 3 minute correlation time (Kremer et al., 1989). Differential GPS can largely overcome the effect of SA. Experiments carried out by Rocken & Meertens (1991) showed that SA modulated GPS carrier frequency in the range of -2 Hz to +2 Hz over several minutes, and the maximum effect of the satellite clock dithering on double-difference phase residuals grew as a function of the clock synchronization error as 0.04 cm/msec, and it increased as a function of baseline length at the rate of about 0.014 cm/100km. If the GPS receivers remain synchronized to better than 10 msec, the SA dithering effect on double-difference processing techniques can be neglected. For point processing the dithering effect is apparent. For example, if HDOP equals 2, the velocity error range could be -0.76 m/sec to +0.76 m/sec, according to $\pm$ 2 Hz frequency change, hence some real time estimation techniques of SA may have to be considered (Matchett, 1985).

4.2.2 Propagation Errors

1) Ionospheric refraction error:

The time delay induced by the earth's ionosphere is directly proportional to the TEC (Total Electron Content) along the path from the satellite to the receiver antenna, and is proportional to the inverse square of the signal frequency. The mean ionospheric delay at night is on the order of 10 m at the zenith and 50 m during the day. At low satellite elevation angles the ionospheric delay can be 3 times these values. In regions near the geometric equator, or near the poles, the delays and the latitudinal gradients of the ionosphere can be very larger, particularly during periods of magnetic storms or intense solar activity. For the dual frequency user, the ionospheric effect can be compensated (adapted from Spilker, 1980):

$$d_{ion}(L1) = \frac{\Delta\rho}{\left[\frac{f_{L1}}{f_{L2}}\right]^2 - 1} \approx 1.5336\ \Delta\rho \qquad (4.6)$$

where $d_{ion}(L1)$ is the ionospheric delay of the L1 code signal; f_{L1}, f_{L2} are the L1, L2 carrier frequencies and $\Delta\rho$ is the difference between the L1 and L2 code measurements.

For a single frequency user, the ionospheric delay can be compensated for by applying the Ionospheric Correction Algorithm (ICA) (Klobuchar, 1987). The eight coefficients of this algorithm are transmitted as part of the satellite's navigation message, and approximately 60% of the ionospheric error can be accounted for using this algorithm (Feess & Stephens, 1987).

Similar relations exist for the Doppler or range-rate measurements. The range-rate ionospheric delay can be expressed as (modified from Seeber, 1993) :

$$\dot{d}_{ion} \approx -\frac{1}{\sin\theta}\,\frac{40.3}{f^2}\,\frac{d(TEC)}{dt} \qquad (4.7)$$

where:

- θ satellite elevation angle
- f signal frequency

and

$$\dot{d}_{ion}(L1) \approx (D_{L2} - D_{L1}) \frac{f_{L2}^2}{f_{L1}^2 - f_{L2}^2} \approx 1.5336\,(D_{L2} - D_{L1}) \tag{4.8}$$

where D_{L1}, D_{L2} are the L1 and L2 range-rate measurements.

Again, large Doppler ionospheric delay occurs during the day, and when the ionospheric effect attains its maximum or minimum value during the day the Doppler ionospheric delay is zero. The corrections of the Doppler ionospheric error for a single frequency user are not practical by modelling techniques as in the case of phase delay, due to the impossibility of predicting, except in a statistical or stochastic manner, the small undulations in the ionosphere which produce Doppler errors on time scales of a few seconds to minutes, hence a commonly used model is a first order Markov process.

Apart from the time delay and polarization change caused by the TEC, other ionospheric effects are the amplitude scintillation causing the signal to fade or enhance, phase scintillation causing rapid changes in signal delay, and clutter causing partial signal reflection. All these effects will cause a rapid change of signal Doppler frequency and degrade the signal detection and tracking, sometimes causing cycle slips. For most navigation purposes, the residuals of the ionospheric effect after IAC correction are neglected, though the ionospheric effect can be significantly reduced by differential navigation techniques. For real-time precise positioning, the IAC residuals can be modeled as a first order Gauss-Markov process (Goad, 1990) with an approximate 3 hour time constant and 2 m standard deviation (Coco et al., 1991).

2) Tropospheric refraction error:
The tropospheric refraction error is a function of the satellite elevation angle, the antenna height, the atmospheric pressure, temperature (dry component) and water vapour (wet component). Approximately 90% of the tropospheric error is attributable to the dry component and is easier to model than the wet component. The commonly used tropospheric error models are those due to Saastamoinen (1973) and Hopfield (1971). A standard atmospheric condition is assured for the computation of the tropospheric delay error in navigation applications because the true atmospheric profile cannot be easily obtained. The tropospheric residuals after model correction are of the order of 0.1 m (1σ), which is adequate for most navigation users (Martin, 1980).

Consideration of the rates of change of the ionospheric and tropospheric delay errors indicates that the propagation gradient are of the order of metres per hour. Evaluation of the combined effects of vertical gradient, spatial gradient and geometrical motion defines a gradient bound of (ibid.):

$$\frac{d\Delta L}{dt} \leq 10 \frac{\text{metres}}{\text{hour}} = 2.75 \times 10^{-3} \frac{\text{metre}}{\text{second}} \qquad (4.9)$$

The Doppler measurement ensemble RMS value due to the propagation gradient is approximately equal to the measurement noise of the receiver. This gradient RMS value has a functional dependency on the satellite elevation angle similar to the ionospheric and tropospheric errors (cosecant of elevation angle). The propagation gradient can be modelled as a first order Markov process.

3) Receiver multipath:
The receiver multipath error is a function of the antenna type and environment. The environment includes the geometry of the signal reflector and its electromagnetic properties. These properties determine the strength, polarization, and phase of the multipath signal at the antenna. Multipath is also a function of the antenna gain and polarization pattern. For stationary GPS receivers the multipath effect can add short and long periodic errors to the receiver and these periodicities generally range from a few minutes to tens of minutes (Bosloper, 1990). Long periods arise when the satellite elevation is high and the rate of change of the elevation is small. The long periodic multipath effects with period of tens of minutes have the potential to bias the results for short observation session. A strong multipath effect can cause total signal fade out and cycle slip.

The code modulation of the GPS signal provides an inherent rejection to multipath interference signals which does not occur within one code width (one chip length) of the direct signal time delay. For moving receivers the multipath of the P code has been determined to be a noise-like or quasi-random measurement error whose ensemble statistics have a RMS value of 1.0 to 3.0 metres (Martin, 1980). For a standard delay loop receiver, the multipath of the C/A code is considered to have a RMS value an order of magnitude greater than that of P code. For a receiver with a narrow-spacing correlator, the multipath of double-differenced C/A code measurements can be reduced to the 0.5 m level,

either in static or kinematic mode (Cannon & Lachapelle, 1992), and the carrier phase multipath does not exceed 0.25 of the carrier wavelength (Lachapelle, 1990).

It is believed that the multipath effects on Doppler measurements can be considered to be white noise of the same magnitude as the measurement noise in a dynamic situation.

4.2.3 Receiver Errors

1) Clock errors:
Receiver clock errors (bias and drift) are usually estimated as part of the navigation solution. Most navigation receivers are equipped with good quality ovenized quartz clocks. Over short periods of up to several seconds, the performance of the quartz clock is as good, or better, than that of a cesium clock, but it will degrade with time, and different stochastic behaviour of the clocks, white noise, flicker noise and random walk, appear for different time intervals (Rizos & Grant, 1990).

There are two problems with modelling the clock errors. The first one is the flicker noise. Although some people have tried to model the flicker noise using the frequency response method (Landau, 1988) or ARIMA (AutoRegressive Integrated Moving Average) model (Percival, 1976), these models are actually approximations of flicker noise using white noise and random walk, based on the Allan variance analysis of the clock behaviour. Both the frequency response and ARMA models are based on the assumption that the PSD (Power Spectrum Density) of the clock error is rational or can be expressed by the response of a linear system incited by white noise, but the PSD of flicker noise is not rational. It is similar to a half-integration system, and this system is physically non-retractable. A simple combination of a white noise and random walk model is more practical and computationally efficient. Secondly, the Allan variance is an expression of stochastic behaviour of clock frequency standards that does not include the deterministic drift or trend of the clock. For different types of clocks, their Allan variances are different, but for clocks of the same type, the Allan variances can also be different. Consequently, approximate or reference values have to be adopted for modelling the clock errors. Popular models of receiver clock error are constant velocity and constant acceleration models with white noise as the system inputs, see section 6.1.

2) Receiver noise and resolution:

The receiver noise and resolution errors result from the processing of signals by the receiver hardware and software. The GPS receiver carrier and code phase measurements are implemented digitally to achieve the best tracking performance which can be expected to approach ideal theoretical performance limit, with the only significant performance losses due to the finite sampling interval. The resolution of GPS measurements depends on the quantizations of code, carrier phase and Doppler measurements. The quantizations are exponentials of the number two and if the quantizations are 1/64 of code chips or carrier phase wavelength, the corresponding quantization sizes for P code, C/A code, L1 carrier phase and Doppler are 0.46 m, 4.6 m, 0.0025 m and 0.0025 m/sec respectively. The quantization error is a uniform distribution over the quantization sizes and assumed to be white, hence the resultant errors (1 σ) are :

P code	0.266 m
C/A code	2.66 m
L1 carrier phase	0.0017 m
L1 Doppler	0.0017 m/sec

Generally, the receiver tracking loop noise for the code and phase can be expressed as (modified Martin, 1980; Jurgens et al., 1992) :

$$\sigma^2 = \frac{K_1 B_n \Delta^2}{(C/N_0)} \qquad (4.10)$$

where:

- σ^2 variance of the code or phase tracking loop noise
- K_1 code or phase mechanization constant
- B_n one-sided tracking loop bandwidth
- Δ code chip length or carrier phase wavelength
- C/N_0 signal-to-noise ratio

For a standard second order delay-lock loop, B_n is usually chosen as 3 Hz and yields a steady state delay tracking error of approximately 3 and 5 nsec for 3g and 5g steady accelerations respectively. The value of the code and phase tracking loop noise is at the same level as the quantization error.

The delta-range is defined as a range change over a specific time interval and the effect of the measurement noise will be to increase the noise of the phase by $\sqrt{2}$ (given that the time interval is sufficient to insure independent samples). The Doppler or range-rate measurement noise is at the same level as that of delta-range, considering the time averaging procedure of the Doppler and range-rate measurement mechanization.

The code and carrier phase loop models for covariance analysis should generally be approximated as a first order Markov process with an exponential autocorrelation function. This approximation is valid for code and carrier phase loop implementations that utilize first order loop filter algorithms, and may be altered accordingly for higher order mechanization implementations. If the sampling period of the measurements is comparable to the correlation time of the loop, the correlated nature of the loop noise must be accounted for in the estimation process by an augmented state formulation or by other forms of mechanization compensation. Assuming the internal noises of the receiver such as tracking loop noise, quantization error, thermal noise, etc., are all white and the code and phase loops are time-invariant and operate linearly, the distribution of the final receiver noise will be (or almost will be) Gaussian because white noise passing through any linear time-invariant system tends to become a Gaussian distribution, regardless of the amplitude distribution of the noises (Lynn, 1992). About the effect of DGPS temporal correlation, see Roberts & Cross, (1993).

4.2.4 Cycle Slips

The GPS carrier phase can be written as:

$$\Phi(t) = \text{fractional}[\Phi(t_0)] + \int_{t_0}^{t} D_s(\tau)\, d\tau \qquad (4.11)$$

where D_S is the range-rate of the L1 or L2 carrier waves.

The carrier phase measurement actually is the phase change, or range change, from the initial epoch to the present. The one-way ambiguity N is defined as:

$$N = \text{integer}\left[f \frac{\rho(t_0)}{C} \right] \qquad (4.12)$$

where $\rho(t_0)$ is signal propagation path at the initial epoch t_0.

If no cycle slips have occurred, the ambiguity remains a constant and can be modelled as a random constant.

Theoretically, the cycle slip can be represented as:

$$C_s(\text{cycle}) = \text{integer}\left[\int_{t1}^{t2} D_s(\tau)\, d\tau \right] \qquad (4.13)$$

where t2, t1 are the time interval of signal interruption. The cycle slip can be detected by inspecting the signal-to-noise ratio of the receiver tracking loops, because if receiver loses signal lock, the signal-to-noise ratio should be zero, and can therefore be used as the indicator of cycle slip occurrence. The cycle slip can be repaired using a knowledge of the Doppler counts if the interval of signal interruption is small compared to the averaging time of the Doppler measurement, and considering the high internal data sampling rate of the receiver.

The carrier phase measurement, including cycle slips, can be expressed as :

$$\Phi_s(t) = \Phi(t) + \sum_{s=1}^{m} \tilde{C}_s\, u(t - t_s) \qquad (4.14)$$

where u is a step function. Cycle slip amplitude $\tilde{C}_s$, occurrence time t_s and occurrence number m are all random variables and do not follow a Gaussian distribution.

The Doppler and range-rate measurements are derived from the averaged internal carrier phase change of the receiver. The averaging length depends on the internal data rate of the receiver. If the receiver can detect the cycle slip, it can be "over jumped" and actually has no effect on the averaging if the cycle slip occurs over a short time period compared to the averaging time, otherwise the cycle slip will also be averaged and will lose its integer character. For delta-range measurements, which can be considered to be the integral or summation

of the Doppler or range-rate between epochs, the cycle slip will affect the output at that epoch as an integer if it cannot be detected by the receiver.

4.2.5 Summary of GPS Errors

From the point of view of error theory, each error source consists of systematic component and random component. The different definitions in the time and frequency domain can be summarized according to Fig.4.1.

In this thesis, the systematic error component is defined as a bias irrespective of it's time-variant or time-invariant nature, and the random error component as noise. Therefore each error source such as atmospheric error, clock error, etc., consists of bias and noise, called atmospheric bias, clock bias, clock drift bias and atmospheric noise and clock noise respectively. The error definition adopted here is not only for the purpose of clarity but also considers the distinction between the stochastic properties of the systematic and random errors, and the different processing strategies for GPS measurements.

Except for the ambiguity of the phase measurement, all biases of GPS measurements are generally non-stationary. The biases are temporally or spatially correlated, hence also called coloured noise. The dominant part of the biases generally changes slowly and its power is concentrated in a narrow frequency area, hence the bias can be referred to as low frequency noise (narrow band noise). The bandwidth of the power spectrum density (PSD) depends on the bias correlation time. A wide bandwidth corresponds to a short correlation time and a brief time-averaging for the bias smoothing.The PSD of the biases are generally mixed together and have some overlap. The biases can be eliminated or significantly reduced by differencing in time or space, or modelled mathematically. The prominent and consistent changing features in time and space of the biases can be modelled partly by deterministic functions and the remaining part may be modeled stochastically (Chatfield,1989). For navigation applications, the practical method for correcting the biases is through the use of deterministic models and the remaining errors are considered as noise.

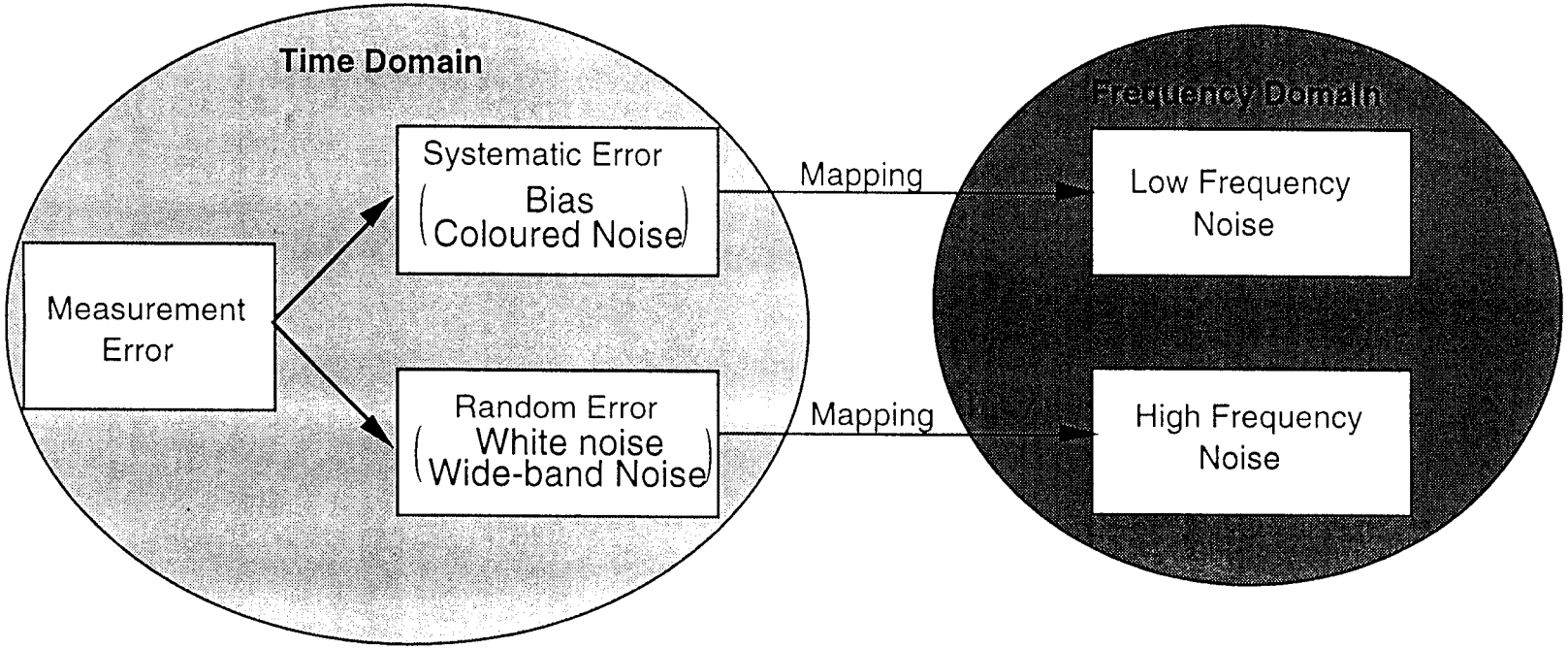

Figure 4.1 Characteristics of GPS errors

Compared to the bias models, the noise can only be modelled as white noise or a purely indeterministic process whose only characteristics in time domain is uncorrelated (independent for Gaussian noise) and its power spectrum spreads across the whole frequency range (wide-banded). Here, the noise is defined as being zero mean, stationary white noise and its PSD is constant across the whole frequency range. Because most of the noise power is distributed in the high frequency region, the noise can be referred to as high frequency noise which can be suppressed by a low-pass filter. The total GPS measurement noise is modelled as Gaussian white noise with a standard deviation:

$$\sigma_n = \sqrt{\sigma^2_{ephem} + \sigma^2_{ion} + \sigma^2_{trop} + \sigma^2_{mult} + \sigma^2_{SA} + \sigma^2_{res} + \sigma^2_{rn}} \tag{4.15}$$

where σ_n is the standard deviation of the measurement noise. The terms under the square root are the variances of the noises for ephemeris, ionospheric, tropospheric and multipath errors, SA, and the variances of measurement resolution and receiver noise. The receiver clock biases are estimated directly within the navigation solution and their residuals are hence absorbed by the receiver noise. It is assumed that the above terms are all noise-like, with zero means and limited standard deviations, and that they are independent of each other and none has a dominating effect on the resultant noise. Hence the resultant total measurement noise will follow a Gaussian distribution with zero mean as the Lindberg-Feller Theorem claimed.

For Doppler measurement noise, the same relationship exists:

$$\sigma_{nD} = \sqrt{\sigma^2_{ephemD} + \sigma^2_{ionD} + \sigma^2_{tropD} + \sigma^2_{multD} + \sigma^2_{SAD} + \sigma^2_{resD} + \sigma^2_{rnD}} \tag{4.16}$$

where the terms in the square root are the change rate (or gradient) noise of ephemeris, ionosphere, troposphere,etc..

Generally, except for SA and sometimes the ionospheric effect, the remaining biases are modelled in practice as noise on the Doppler or range-rate.

If the UERE (User Equivalent Range Error) is known, the point positioning error is approximated by the UERE timing the corresponding DOP value. The same procedure is valid for velocity determination using Doppler measurements and

the DOP values for Doppler and range measurements can be considered to be the same (Fu, 1993).

4.3 The GPS Observation Equations

The linearized observation equations for code and carrier phase can be written as:

$$p - \rho_0 = \mathbf{H}\begin{bmatrix}\Delta x\\ \Delta y\\ \Delta z\end{bmatrix} + \sum \text{bias} + \text{noise} \tag{4.17}$$

$$\rho_0 = \sqrt{(x_s - x_0)^2 + (y_s - y_0)^2 + (z_s - z_0)^2} \tag{4.18}$$

where ρ, ρ_0 are the measured and nominal geometric range values. x_s, y_s, z_s are the coordinates of the satellite antenna, and x_0, y_0, z_0 are the nominal coordinates of the receiver antenna. Δx, Δy, Δz are the position errors of the receiver antenna. The observation matrix is:

$$\mathbf{H} = \begin{bmatrix}\frac{\partial\rho}{\partial x} & \frac{\partial\rho}{\partial y} & \frac{\partial\rho}{\partial z}\end{bmatrix} = \begin{bmatrix}-\cos\alpha & -\cos\beta & -\cos\gamma\end{bmatrix} \tag{4.19}$$

where $\cos\alpha$, $\cos\beta$, $\cos\gamma$ are the direction cosines of the satellite.

The linearized observation equation for range-rate is :

$$\dot{\rho} - \dot{\rho}_0 = \mathbf{H}_D\begin{bmatrix}\Delta x\\ \Delta y\\ \Delta z\\ \Delta\dot{x}\\ \Delta\dot{y}\\ \Delta\dot{z}\end{bmatrix} + \sum \text{bias} + \text{noise} \tag{4.20}$$

where

$$\dot{\rho} = \frac{(x_s - x)(\dot{x}_s - \dot{x}) + (y_s - y)(\dot{y}_s - \dot{y}) + (z_s - z)(\dot{z}_s - \dot{z})}{\rho} \tag{4.21}$$

and

$$\mathbf{H}_D = \left[\frac{\partial\dot{\rho}}{\partial x} \; \frac{\partial\dot{\rho}}{\partial y} \; \frac{\partial\dot{\rho}}{\partial z} \; \frac{\partial\dot{\rho}}{\partial \dot{x}} \; \frac{\partial\dot{\rho}}{\partial \dot{y}} \; \frac{\partial\dot{\rho}}{\partial \dot{z}}\right]$$

$$= [\mathbf{H}_1 \quad \mathbf{H}] \tag{4.22}$$

where

$$\mathbf{H}_1 = \left[\frac{\partial\dot{\rho}}{\partial x} \quad \frac{\partial\dot{\rho}}{\partial y} \quad \frac{\partial\dot{\rho}}{\partial z}\right]$$

$$= \left[\frac{(\dot{x}_s - \dot{x}) + \dot{\rho}\cos\alpha}{\rho} \quad \frac{(\dot{y}_s - \dot{y}) + \dot{\rho}\cos\beta}{\rho} \quad \frac{(\dot{z}_s - \dot{z}) + \dot{\rho}\cos\gamma}{\rho}\right] \tag{4.23}$$

Usually the body's speed is much smaller than that of the satellite (approximately 4km/sec), the magnitude of the elements in eqn (4.23) is of the order of 10^{-4}, and a 1 km position error will cause 0.1m/sec Doppler measurement error. Neglecting H1, the geometric strength of the Doppler measurement will therefore be the same as that of range.

4.4 The Secondary Observables

The secondary observables are the linear combinations of the primary observables: range, phase and Doppler. Their main function is to eliminate or reduce some of the biases, which have close cross-correlation across different sites, satellites and frequencies. They can be expressed as a linear transformation of the primary observables:

$$\mathbf{Z}_s = \mathbf{D}\,\mathbf{Z}_m \tag{4.24}$$

where:

- $\mathbf{Z}_s$ secondary observable
- $\mathbf{Z}_m$ primary observable
- **D** transformation matrix

The measurement noise of the secondary observable becomes:

$$\mathbf{R}_s = \mathbf{D}\,\mathbf{R}_m\,\mathbf{D}^T \qquad (4.25)$$

where $\mathbf{R}_s$, $\mathbf{R}_m$ are the variances of the secondary and primary observables. The correlation introduced by the transformation is usually ignored in practice.

About the commonly used secondary observables, single, double, triple differenced measurements and L3, L4, L5, L6 and other linear combinations of the dual-frequency measurements, see Rizos (1991).

4.4.1 Code, Phase and Doppler Combination

To make full use of the information contained within all the GPS observables, and in an optimal manner, linear combinations of the different GPS observables can be used to create new observables. One class of these is what we refer to as the "smoothed code measurements". There are several forms of smoothed code measurements: Doppler smoothed, phase smoothed, or via digital filter (DF) algorithms. The smoothed code measurements preserve the basic properties of the code signals, and their bias errors largely remain, only the high frequency noise of the code measurements is reduced.

Real data processing results are presented to support the performance analysis of phase smoothed code and the DF methods. Because there were no dual frequency Doppler data available, only a theoretical analysis of the Doppler smoothed code technique is presented.

4.4.1.1 Doppler Smoothed Code

The Doppler smoothed pseudo-range algorithms are based on the following relations (Hatch, 1982):

$$D_1(k) = \Delta\rho(k) + \Delta B(k) - \left[\frac{f_2}{f_1}\right] \Delta I(k) \qquad (4.26)$$

where

$$\Delta\rho(k) = \rho(k) - \rho(k-1)$$

$$\Delta B(k) = B(k) - B(k-1)$$

$$\Delta I(k) = I(k) - I(k-1)$$

D1 L1 Doppler measurement
ρ geometric range between satellite and receiver
B range measurement biases, excluding ionospheric bias
I ionospheric bias
k, k-1 the current and previous epoch
f_1 = 1575.42 MHz, f_2 = 1227.6 MHz

The L2 Doppler measurement is:

$$D_2(k) = \Delta\rho(k) + \Delta B(k) - \left[\frac{f_1}{f_2}\right] \Delta I(k) \qquad (4.27)$$

D1 and D2 in eqns (4.26) and (4.27) are in fact delta-range and can be obtained directly from the Doppler measurements if the receiver outputs Doppler count instead of delta-range. No distinction is made between the definitions of delta range and Doppler measurements, and are all referred to as Doppler in order to hence preserve the notation of Hatch's paper.

The L3 Doppler measurement (the so-called ionospheric free combination) is:

$$D_3(k) = \frac{f_1^2}{f_1^2 - f_2^2} D_1(k) - \frac{f_2^2}{f_1^2 - f_2^2} D_2(k) \qquad (4.28)$$

The equivalent code range differences M_1, M_2 for L1 and L2 can be mapped from the above equations as:

$$M_1(k) = 2\,D_3(k) - D_1(k) = \Delta\rho(k) + \Delta B(k) + \left[\frac{f_2}{f_1}\right]\Delta I(k) \tag{4.29}$$

$$M_2(k) = 2\,D_3(k) - D_2(k) = \Delta\rho(k) + \Delta B(k) + \left[\frac{f_1}{f_2}\right]\Delta I(k) \tag{4.30}$$

The initial range values can be smoothed using N Doppler measurements (modified from Hatch, 1982):

$$\overline{P_1}(0) = \frac{\sum_{i=0}^{N}\left[P_1(i) - \sum_{j=0}^{i} M_1(j)\right]}{N} = \overline{\rho(0) + B(0) + \left[\frac{f_2}{f_1}\right] I(0)} \tag{4.31}$$

$$\overline{P_2}(0) = \frac{\sum_{i=0}^{N}\left[P_2(i) - \sum_{j=0}^{i} M_2(j)\right]}{N} = \overline{\rho(0) + B(0) + \left[\frac{f_1}{f_2}\right] I(0)} \tag{4.32}$$

where $M_1(0)=0$, $M_2(0)=0$, and P_1, P_2 are the L1 and L2 pseudo-range measurements. The superscript bar denotes the mean value.

The smoothed code measurements are (modified from ibid):

$$\hat{P}_1(i) = \overline{P_1(0)} + \sum_{j=1}^{i} M_1(j) = \rho(i) + B(i) + \left[\frac{f_2}{f_1}\right] I(i) \tag{4.33}$$

$$\hat{P}_2(i) = \overline{P_2(0)} + \sum_{j=1}^{i} M_2(j) = \rho(i) + B(i) + \left[\frac{f_1}{f_2}\right] I(i) \tag{4.34}$$

A recursive algorithm derived from eqns (4.31) and (4.32) for real-time applications is:

$$\hat{P}_1(N+1) = \frac{N}{N+1}\left[\hat{P}_1(N) + M_1(N+1)\right] + \frac{1}{N+1} P_1(N+1) \tag{4.35}$$

$$\hat{P}_2(N+1) = \frac{N}{N+1}\left[\hat{P}_2(N) + M_2(N+1)\right] + \frac{1}{N+1} P_2(N+1) \tag{4.36}$$

There are some problems with the above algorithm. For example, there must be both L1 and L2 Doppler measurements in order to form the ionospheric-free range changes M_1 and M_2. The method assumes that the noise of the Doppler measurement is small compared to that of the code measurement and can therefore be neglected. In fact the Doppler can only considered to be of the order of 100 times better than the P code measurements. From eqn (4.31) it can be seen that:

$$\overline{P_1}(0) = \frac{\sum_{i=0}^{N}\left[P_1(i) - \sum_{j=0}^{i} M_1(j)\right]}{N}$$

$$= \frac{\sum_{i=0}^{N} P_1(i) - [N\,M_1(1) + (N-1)\,M_1(2) + (N-2)\,M_1(3) + \cdots + M_1(N)]}{N} \tag{4.37}$$

Assuming the code and Doppler measurements are independent and the measurement errors are white noise, the variance of $\overline{P_1}(0)$ can be written as:

$$\mathrm{Var}[\overline{P_1}(0)] = \frac{(N+1)\sigma_{P_1}^2 + \left[N^2 + (N-1)^2 + (N-2)^2 + \cdots + 1\right]\sigma_{M_1}^2}{N^2}$$

$$= \frac{(N+1)\sigma_{P_1}^2}{N^2} + \frac{17}{6}\frac{[N(N+1)(2N+1)]\,\sigma_{D_1}^2}{N^2} \tag{4.38}$$

where

$$\sigma_{M_1}^2 = 4\,\sigma_{D_3}^2 + \sigma_{D_1}^2 \approx 17\sigma_{D_1}^2$$

and $\sigma^2_{P_1}$, $\sigma^2_{D_1}$, $\sigma^2_{D_3}$ are the variances of the L1 code, Doppler and L3 Doppler measurements.

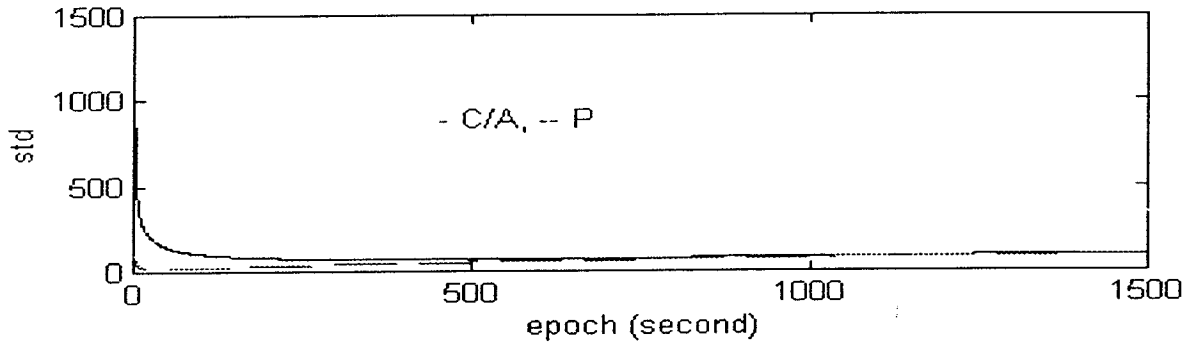

Figure 4.2 Initial state of Doppler smoothed code

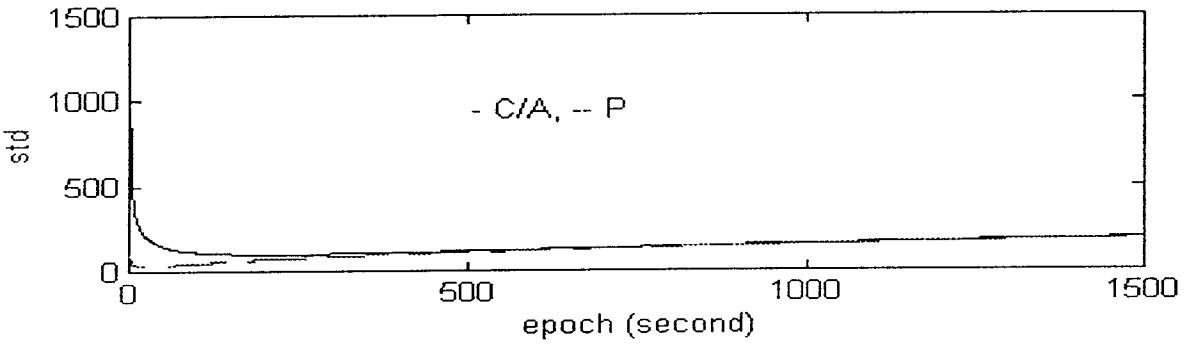

Figure 4.3 Doppler smoothed code

Assuming that for the P code measurements $\sigma_{P_1} = 100\,\sigma_{D_1}$ and for C/A code measurements $\sigma_{P_1} = 1000\,\sigma_{D_1}$, then by differentiation of eqn (4.38), the best smoothed initial values (also the best smoothed values) are obtained at N = 43 for P code and N = 430 for C/A code. Fig.4.2 illustrates this, where the standard deviation is normalized by the standard deviation of the Doppler measurement, and the standard deviations of the initial value are 22.02 σ_{D_1} and 34.87 σ_{D_1}, while the standard deviation of the best smoothed values are 69.07 σ_{D_1} and 109.91 σ_{D_1} respectively. The standard deviations of the smoothed initial values will increase approximately at a rate of $\sqrt{17N/3}\,\sigma_{D1}$. This suggests that the recursive algorithms (4.35) and (4.36) should only be used when $N \leq 43$ and $N \leq 430$. Beyond that point the initial values should be fixed at the best smoothed values and the subsequent smoothed values should be obtained from eqns (4.33) and (4.34).

The summation of M_1 and M_2 causes the standard deviation of the smoothed code measurement to increase at a rate of $\sqrt{17N}\,\sigma_{D1}$ (see Fig.4.3). Hence for $N \geq 588$ in the case of P code and $N \geq 58824$ for C/A code, the Doppler will no longer contribute to the smoothing of the code measurements.

If the noises of M_1 and M_2 are white, it is obvious from eqns (4.33) and (4.34) that the noise of smoothed code becomes a random walk series. The covariance for two smoothed code measurements at epochs N1 and N2 is approximately $17\,N1\sigma_{D_1}^2$ for N1 < N2 and hence the Doppler smoothed code measurement is no longer independent. The same analysis can be applied for the L2 code smoothing.

4.4.1.2 Phase Smoothed Code

The carrier phase measurement can be used to define the range change quantity to overcome the problem of the increasing noise intensity of Doppler smoothing. If there are L1 and L2 carrier phase measurements, and there are no cycle slips during smoothing, the range change can be derived from two phase measurements:

$$\begin{aligned}\Delta\Phi_1(k) &= \Phi_1(k) - \Phi_1(0) \\ &= \rho(k) + B(k) - \left[\frac{f_2}{f_1}\right][I(k) - I(0)] - \rho(0) - B(0)\end{aligned} \tag{4.39}$$

$$\begin{aligned}\Delta\Phi_2(k) &= \Phi_2(k) - \Phi_2(0) \\ &= \rho(k) + B(k) - \left[\frac{f_1}{f_2}\right][I(k) - I(0)] - \rho(0) - B(0)\end{aligned} \tag{4.40}$$

$$\begin{aligned}\Delta\Phi_3(k) &= \frac{f_1^2}{f_1^2 - f_2^2}\Delta\Phi_1(k) - \frac{f_2^2}{f_1^2 - f_2^2}\Delta\Phi_2(k) \\ &= \rho(k) + B(k) - \rho(0) - B(0)\end{aligned} \tag{4.41}$$

whereΦ_1, Φ_2, Φ_3 are L1, L2 and L3 carrier phase measurements.

The ionosphere-corrected range changes can be formed from the L1, L2 and L3 observables:

$$\begin{aligned}\Delta M_1(k) &= 2\Delta\Phi_3(k) - \Delta\Phi_1(k) \\ &= \rho(k) + B(k) + \left[\frac{f_2}{f_1}\right][I(k) - I(0)] - \rho(0) - B(0)\end{aligned} \tag{4.42}$$

$$\begin{aligned}\Delta M_2(k) &= 2\Delta\Phi_3(k) - \Delta\Phi_2(k) \\ &= \rho(k) + B(k) + \left[\frac{f_1}{f_2}\right][I(k) - I(0)] - \rho(0) - B(0)\end{aligned} \tag{4.43}$$

and the phase smoothed code range is:

$$\begin{aligned}\hat{P}_1(N) &= \frac{\sum_{i=0}^{N}[P_1(i) - \Delta M_1(i)]}{N} + \Delta M_1(N) \\ &= \rho(N) + B(N) + \left[\frac{f_2}{f_1}\right] I(N)\end{aligned} \tag{4.44}$$

$$\begin{aligned}\hat{P}_2(N) &= \frac{\sum_{i=0}^{N}[P_2(i) - \Delta M_2(i)]}{N} + \Delta M_2(N) \\ &= \rho(N) + B(N) + \left[\frac{f_1}{f_2}\right] I(N)\end{aligned} \tag{4.45}$$

Note the similarity of these formulae to eqns (4.33) and (4.34), except that there is no summation term for the ΔM quantities.

The recursive forms are:

$$\hat{P}_1(N+1) = \frac{N}{N+1}\left[\hat{P}_1(N) + \Delta M_1(N+1) - \Delta M_1(N)\right] + \frac{P_1(N+1)}{N+1} \tag{4.46}$$

$$\hat{P}_2(N+1) = \frac{N}{N+1}\left[\hat{P}_2(N) + \Delta M_2(N+1) - \Delta M_2(N)\right] + \frac{P_2(N+1)}{N+1} \tag{4.47}$$

Under the assumption that the noise of the carrier phase measurements is white, the standard deviation of phase smoothed code measurements will decrease and converge to a steady state error of $\sqrt{17}$ times the standard deviation of the phase measurement, and the uncertainties of the initial values decrease with increasing N (see Fig.4.4). Another contrast with the Doppler smoothed code measurements is that the noise of phase smoothed code measurements is dominated by the noise of ΔM_1 and ΔM_2 as well as the code measurement which are white noise, and hence the noise of the phase smoothed codes can be considered to be white noise and the phase smoothed codes can be considered to be independent measurements which will simplify subsequent data processing.

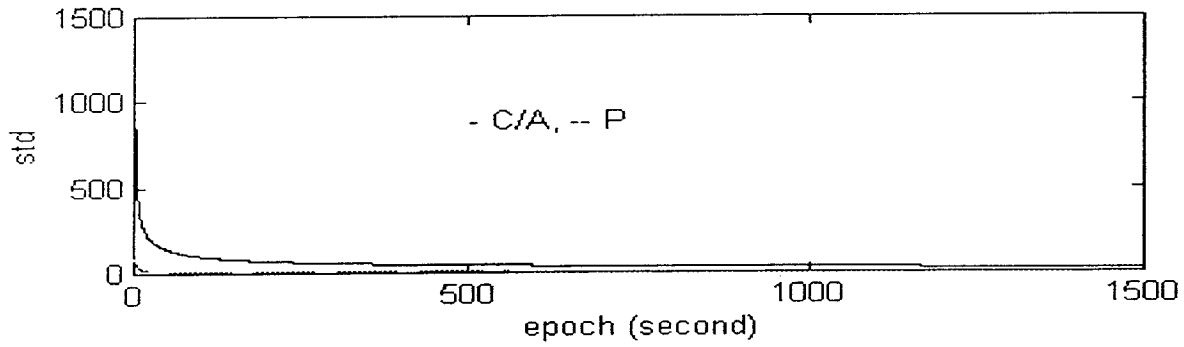

Figure 4.4 Phase smoothed code

If cycle slips are present in the phase measurement, or a restart of the smoothing at the time of occurrence of cycle slip is required, or the cycle slip can be detected and repaired using Doppler measurements as

$$
\begin{aligned}
\Delta M_1(k+1) &= 2\Delta\Phi_3(k+1) - \Delta\Phi_1(k+1) \\
&= \rho(k+1) + B(k+1) \\
&\quad + \left[\frac{f_2}{f_1}\right][I(k+1) - I(0)] - \rho(0) - B(0) \\
&= \Delta M_1(k) + \Delta\rho(k+1) \\
&\quad + \Delta B(k+1) + \left[\frac{f_2}{f_1}\right]\Delta I(k+1) \\
&= \Delta M_1(k) + M_1(k+1) \\
&\approx \Delta M_1(k) + \Delta\rho_D(k)
\end{aligned}
\tag{4.48}
$$

and

$$
\Delta\rho_D(k) = \int_{t_k}^{t_{k+1}} D_{1,2}(t)\, dt \approx \left[\frac{D_{1,2}(k+1) - D_{1,2}(k)}{2}\right][t_{k+1} - t_k] \tag{4.49}
$$

where $D_{1,2}$ (k+1) and $D_{1,2}$ (k) are the L1 or L2 Doppler measurement at time t_{k+1} and tk, $t_{k+1} - t_k$ is the epoch interval.

For a high data sampling rate, the ionospheric effect change is small between epochs, hence single frequency Doppler measurement can be considered to be equivalent to the phase-rate at that instant and the error introduced thus is negligible:

$$
\Phi_{1,2}(k+1) - \Phi_{1,2}(k) \approx \Delta\rho_D(k) \tag{4.50}
$$

4.4.1.3 Digital Filtered Code

In the case of single frequency GPS receivers the code measurements can be smoothed in the frequency domain using a frequency discriminating digital filter which will be simply referred to here as the DF. The intention of using a DF is the same as for the Doppler and phase smoothing algorithms, that is to ensure that the code biases are left unchanged but that the large code measurement noise is smoothed. In the frequency domain it is assumed that the low frequency components consisting of GPS measurement dynamics and measurement biases should be preserved, but that the high frequency noise must be

depressed, hence the DF should be a low-pass filter. There are basically two kinds of low-pass DF (LDF) for this task: the IIR (Infinite Impulse Response) DF and FIR (Finite Impulse Response) DF (Proakis & Manolakis, 1992). The direct computation algorithms of eqns (4.33), (4.34), and (4.44), (4.45), are actually a type of FIR DF, while the recursive algorithms (4.35), (4.36), and (4.46), (4.47), are similar to an IIR DF.

In contrast to the Doppler and phase smoothing code methods, the DF for single frequency measurements filters the code measurements directly, using the characteristics of the PSD (Power Spectral Density) of the code measurements, and hence no other measurements (such as Doppler and phase) are needed.

Considering the simplicity and stability characteristics of the FIR DF, a low-pass FIR DF to smooth the GPS data is preferable.

In order to compute the PSD of the data by discrete Fourier transformation, a second order differencing is used to make the measurement data stationary, otherwise the PSD components of the deterministic trends caused by the satellite motion, antenna dynamics and the close-correlated biases will dominate the periodogram.

Concerning the PSD distribution in the periodogram of the GPS measurements the following comments can be made under a high measurement sampling frequency:

1) The constant components and deterministic trends of the measurements are at zero, or near zero, frequency (Chatfield, 1989).

2) The bandwidths of the measurement biases can be estimated by their correlation times, assuming they are approximately the system constants of the biases (Norman, 1992). The larger the correlation time, the narrower the bandwidth.

3) The correlation time of SA is assumed to be 3-5 minutes, and atmospheric delay a few minutes to few hours and their PSDs are concentrated in a narrow band near zero frequency under a high measurement rate.

4) The correlation time of the multipath effect can be zero to a few tens minutes, and its PSD can spread across the whole frequency range.

5) The PSD of antenna dynamics depends on the period of the antenna state change. As the trajectory of the antenna mainly consists of first and second order curves with limited period, its PSD is band-limited and mainly in the low frequency region. Generally speaking the attitude change of the antenna has a shorter period than other antenna states.

6) There is a lengthy transition of the PSD from low frequency to high frequency and there is no distinct and explicit boundary between them.

Figures (A.6.29) to (A.6.32), (A.6.45) to (A.6.49) and (A.6.61) to (A.6.64) are the periodograms of C/A code measurement acceleration for individual satellites. The frequency axis is from 0 to the Nyquist (0.5 Hz for a 1 Hz sampling rate).

The cut-off frequency, or the main lobe, of the LDF for GPS measurement smoothing should be larger than the widest bandwidth of the biases. The transition region of the LDF amplitude response is not required to decline sharply, hence no high order DF is needed. The stop-band should have lower sidelobes and the pass-band should have a unit gain with linear phase response.

A FIR LDF of order 12 is chosen for code measurement smoothing. The order 12 is chosen so as not to cause a long delay of the data output of the LDF. The cut-off frequency is 0.4 π based on the assumption that the shortest period of the antenna attitude change is caused by a ship's roll, and for a ship of moderate size its rolling period is approximately 10 seconds which is equivalent to a frequency of 0.2 π. This cut-off frequency makes the LDF pass-band include the lengthening transition up to 0.4π of the PSD of C/A code measurement acceleration. The LDF is designed by Hamming window because it has a moderate transition width of the main lobe and has a lower sidelobe (- 43 dB) compared to other windows such as rectangular, Hann and Blackman (Norman, 1992). The LDF system function H(z) is:

$$H(z) = \sum_{k=-6}^{6} b(k)\, z^{-k} \qquad (4.51)$$

$$b(k) = [0.004,0,-0.0233,-0.0335,0.0716,0.2824,0.3976,0.2824,$$
$$-0.0335,-0.0233,0,0.004]$$

where z is the z transform operator.

In eqn (4.51) the system function H(z) is written in non-casual form because the LDF output is delayed for half of its order steps to compensate the phase response delay of the DF.

The LDF amplitude response and phase response are shown in Fig.4.5 and Fig.4.6, respectively.

Assuming the measurement noise is white, then the noise of the LDF smoothed code measurement is no longer white and its covariance sequence is:

$$\gamma(m) = \sigma_x^2 \sum_{k=-6}^{6} b(k)\, b(k+m) \tag{4.52}$$

and its variance is:

$$\gamma(0) = \sigma_x^2 \sum_{k=-6}^{6} b^2(k) \approx 0.33\sigma_x^2 \tag{4.53}$$

where σ_x^2 is the code measurement variance.

The autocorrelation of the noise is:

$$\alpha(m) = \frac{\gamma(m)}{\gamma(0)} \qquad \text{for } |m| \le 12$$

$$\alpha(m) = 0 \qquad |m| > 12 \tag{4.54}$$

where $\alpha(1) = 0.7$ and when $|m| \ge 2$, $\alpha(m) < 0.22$.

The performance of the LDF is tested using the filtered data residuals. Assuming only the C/A measurement noise, which is supposed to be white, is depressed by the LDF, the residuals (the difference of the C/A measurement and the smoothed C/A measurement) should also be white noise with zero mean. The whiteness of the residuals can be checked by Bartlett and Portmanteau tests (Vandaele, 1983).

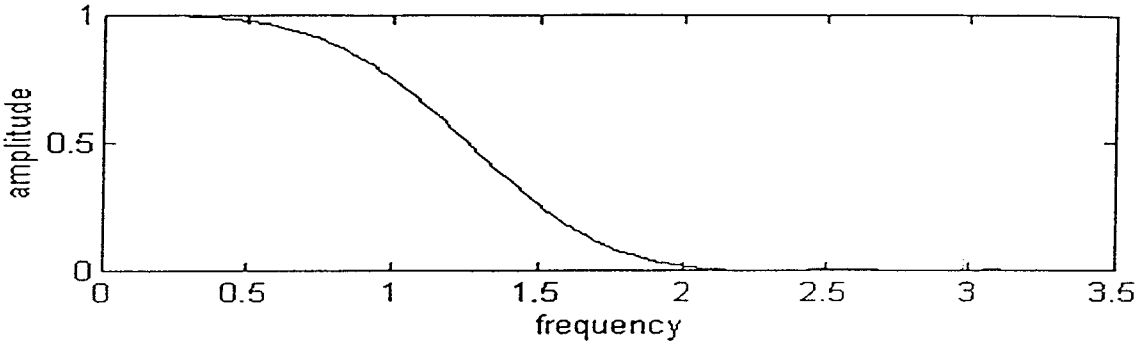

Figure 4.5 Amplitude response of the FIR

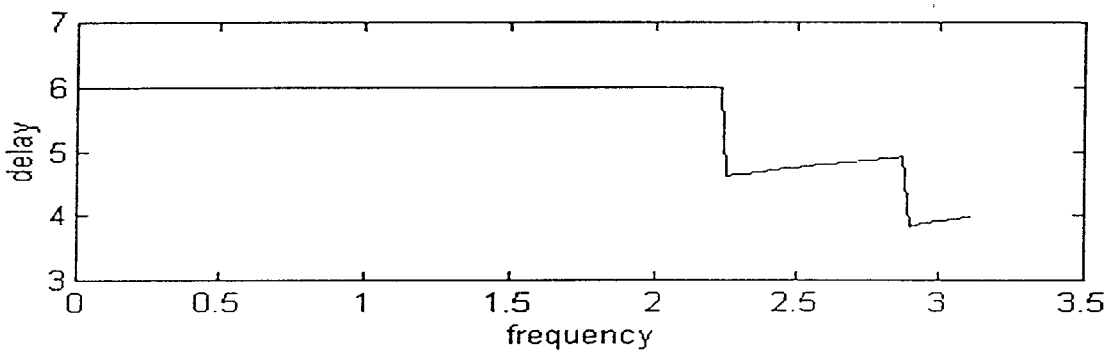

Figure 4.6 Group delay of the FIR

4.4.1.4 Data Processing

The following examples illustrate the performance of the smoothed code using the phase smoothing algorithm and the LDF. Receivers which have dual-frequency Doppler output are comparatively rare, and no data from such receivers was available for analysis.

The data for the test were collected by two Trimble SST receivers, one of which was stationary (Gas station), and the other one was sited onboard a ship sailing along the east coast of Australia (Bow station), during the time 0200-0300 UTC, 24/05/91. Satellites 2, 6, 15 and 19 were tracked at the 1 Hz rate. The measurements were C/A code, L1 and L2 carrier phases. Cycle slips in the phase data were cleaned up prior to smoothing.

The performances of the phase and LDF smoothing algorithms are shown in the plots in Appendix 3: residual plots show the convergence of long term smoothing. The RMS values of the residuals can be considered as the improvements of the C/A measurements after smoothing. The acceleration plots show the smoothing effects and the data fitting. The autocorrelation plots show the residual whiteness.

In each of the autocorrelation plots two dashed lines are added to show the limits of the Bartlett test. If the autocorrelation curve is inside the limits, the autocorrelation is supposed to be zero with a probability of 98%.

Fig.A.6.1 to Fig.A.6.4 and Fig.A.6.13 to Fig.A.6.15 are the plots of the accelerations of C/A (thin lines) and phase smoothed C/A (bold lines) for the Gas and Bow stations.

In the case of the phase smoothed C/A measurements for the Gas station, the mean values of the residuals are biased (see Fig.4.7), and the autocorrelations of the residuals for Gas station are not fading rapidly, hence the residuals are not white noise according to the Bartlett test (see Fig.A.6.9 to Fig.A.6.12). Although the phase smoothing code measurements try to preserve the original behaviour, only the ionospheric bias is considered during the smoothing. In fact the multipath effects of the code measurements are depressed along with the noise during smoothing, thus a correlation and bias are introduced into the residuals. The autocorrelation of satellite 19 shows an undamped sine wave pattern which indicates there was a high intensity component with period 60 seconds in the satellite 19 C/A measurements, and this periodicity is also seen in its residual (see Fig.A.6.8). This long period component does not appear in the periodograms (the PSD is in units of metre^2/(sec^{2}Hz), and 0 to 64 of the abscissa correspond 0 to π) because it is deleted by the data differencing before the PSD is computed. From the PSD plots, Fig.A.6.29 to Fig.A.6.32, it appears that the position information of the GPS phase and code measurement is confined in a very narrow low frequency region and the corresponding frequency pass-band width of the phase smoothing is very narrow.

For the Bow station, the autocorrelations of the residuals for satellites 2, 6 and 15 are small for large lags and passed the Bartlett test, see Fig.A.6.25 to Fig.A.6.27. The Q statistic values of the Portmanteau test for lag 23 are 45.4, 42.38 and 85.26 respectively for satellite 2, 6, 15. The χ^2 statistic value for degree of freedom of 23 is 44.2, given a significant level of 0.005, hence only the residuals of satellite 6 are uncorrelated. There are dominant frequency components of 7 and 30 second periods in the residuals of satellite 19, see Fig.A.6.32. It indicates that the pass-band is widened now compared to the stationary case. The component of the 30 second period is not presented in the PSD plots because of the impact of differencing, and note the larger high frequency components in Fig.A.6.32 than those in Fig.A.6.30, which include the amplification of high frequency noise and aliasing effects.

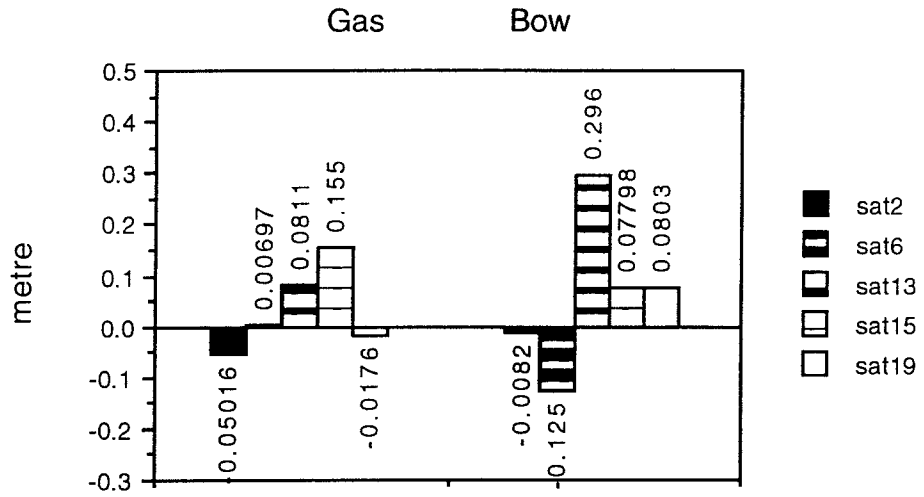

Figure 4.7 Means of phase smoothed C/A residuals

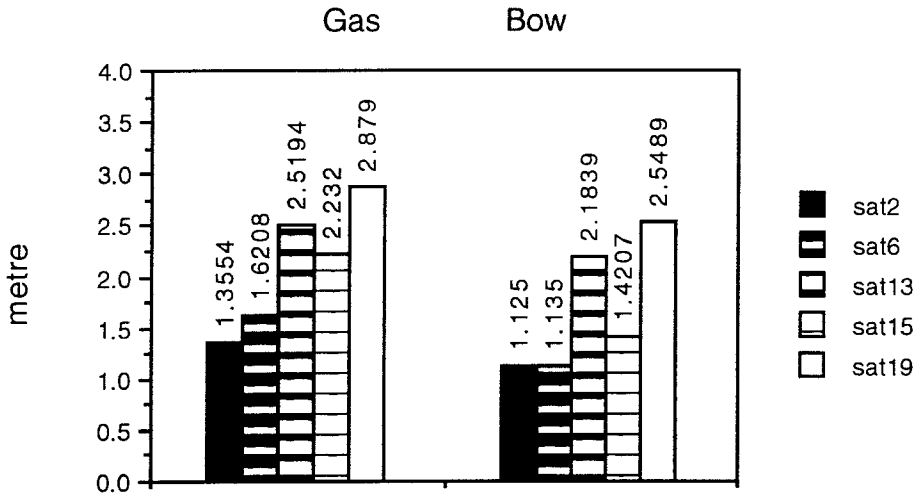

Figure 4.8 RMS of phase smoothed C/A residuals

The smoothing effect of the LDF on code measurement is illustrated in Fig.A.6.33 to Fig.A.6.64.The LDF smoothed C/A measurements follow the patterns of the C/A measurements very closely. The mean values of the residuals are much less than those of phase smoothing, see Fig.4.9, and the smoothing is unbiased. There is a large high frequency component in the C/A measurement of satellite 19, along with the 30 second period component (see Fig.A.6.40), and the pass-band is wider than that of the phase smoothing (see Fig.A.6.45 to Fig.A.6.48 and Fig.A.6.60 to Fig.A.6.64). The autocorrelations of the residuals for satellites 2, 6 and 15 of large lags are decaying rapidly and passed the Bartlett test, but not the Portmanteau test for small lags. Considering the large autocorrelation values of lag 1, the residuals of satellite 2, 6 and 15 can be modelled as an MA(1) series with coefficient 1 because the autocorrelations of lag 1 is -0.5 and the

autocorrelations for lag > 1 can be considered to be zero (see Fig.A.6.41 to Fig.A.6.43 and Fig.A.6.57 to Fig.A.6.59).

The low frequency component of 60 second period appeared in satellite 19 can be eliminated by a notch filter cascaded with the LDF.

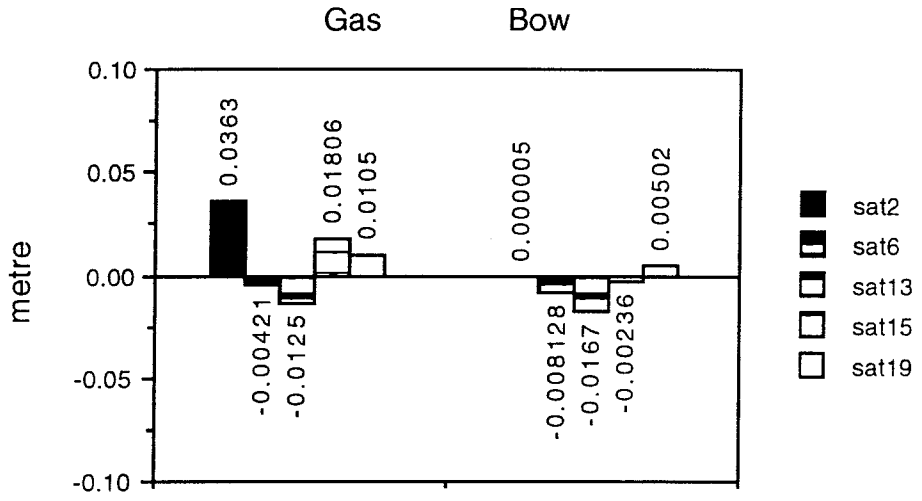

Figure 4.9 Means of FIR smoothed C/A residuals

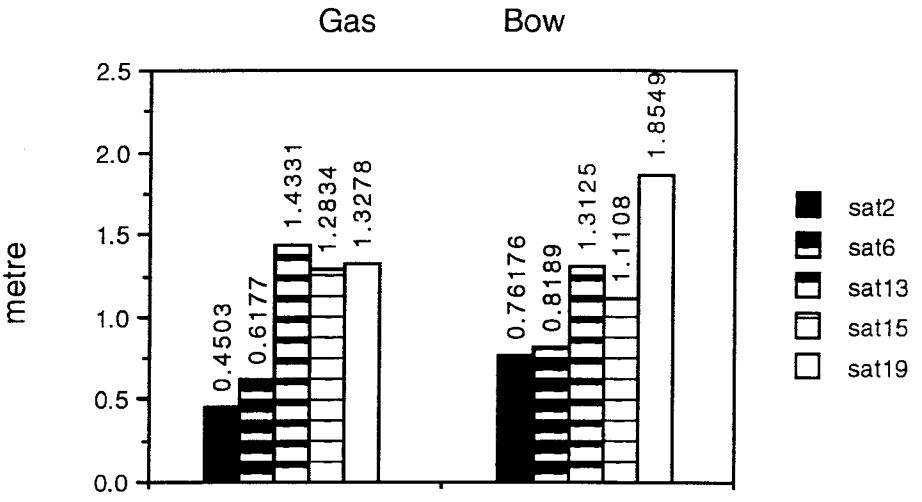

Figure 4.10 RMS of FIR smmothed C/A residuals

4.4.1.5 Summary Comments on Smoothing

If dual-frequency Doppler or phase measurements are available, the GPS code measurement can be smoothed using these measurements, and most of the code measurement biases remain unchanged.

The Doppler smoothing technique is unstable. After a short period the error of Doppler smoothing is increasing with time and the smoothed data is correlated. The Doppler smoothing technique however is insensitive to the presence of cycle slips. High data sampling rate is preferable to obtain accurate delta-range or integrated Doppler.

The phase smoothing technique is stable if cycle slips are detected and repaired. The error of the smoothing is decreasing with time and converges to a fixed value, and the convergence time is dependent on the uncertainty of the initial value. High data sampling frequency is preferable to accelerate the smoothed data convergence.

Both Doppler and phase smoothing techniques are insensitive to the antenna dynamics. The pass-band width of their frequency response is changed automatically when the antenna dynamics change. Both Doppler and phase smoothing algorithms can be implemented easily for real-time applications.

The FIR LDF is one of the large family of digital filters. The smoothing by the FIR LDF of order 12 is stable. The smoothing is purely based on the frequency response of the code signals themselves and no other information is needed. In order to avoid distortion of the smoothed data, correct choice of the pass-band width is important. The accuracy of the smoothed data is independent of the uncertainty of initial value, and the variance of the smoothed data is mainly dependent on the pass-band width, the wider the bandwidth, the larger the variance and vice versa. The LDF algorithm is easily implemented. High data sampling rate is preferable to obtain more, and accurate, frequency information of the signals and assists in designing an appropriate DF with good performance and real-time application.

4.4.2 Doppler Created Phase Data (Doppler Phase)

There are a number of low-cost GPS navigation receivers on the market which output C/A code pseudo-range and L1 Doppler only. Although DGPS can increase the positioning accuracy of C/A code to the few metre level, a further improvement in accuracy appears difficult in view of the high noise of the C/A code measurements. On the other hand, the noise of Doppler measurement is much less than that of C/A code measurements. A reason for this is that the resolution or the quantization error of the Doppler is the same as that of a carrier phase measurement and the Doppler measurement error due to receiver noise is $\sqrt{2}$ that of carrier phase measurement (which is typically only a few millimetres). In principle, GPS Doppler has a distinct and simple relationship with the phase measurement: the integration of Doppler is the carrier phase measurement assuming the initial phase value is zero. It therefore seems plausible that a sort of "synthetic" phase data with much small measurement noise than that of C/A code could be derived from the Doppler measurements. Furthermore, this phase data could then be used as the direct observable for baseline determination using algorithms similar (if not identical) to those developed for high precision carrier phase GPS navigation (Fu, 1995).

4.4.2.1 GPS Doppler and Phase

The Doppler effect on the GPS signal is illustrated in Fig.4.11.

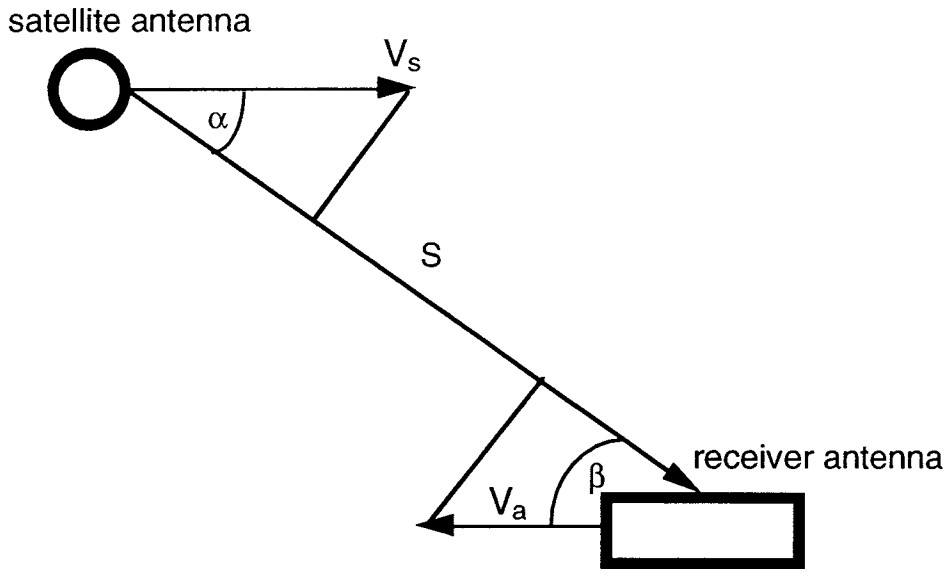

Figure 4.11. The GPS Doppler effect.

The Doppler frequency is:

$$f_D = f\left[\frac{c + V_a \cos\beta}{c - V_s \cos\alpha}\right] \approx f\left[1 - \frac{1}{c}\frac{dS}{dt}\right] \tag{4.55}$$

where:

- f nominal frequencies of L1 or L2
- c velocity of GPS signal propagation
- V_a velocity of receiver antenna
- V_s velocity of transmitter antenna
- S range between the receiver antenna and transmitter antenna

An approximation for range-rate is:

$$D = \frac{dS}{dt} = V_a \cos\beta \pm V_s \cos\alpha \tag{4.56}$$

The Doppler shift is:

$$Ds = -\frac{1}{\lambda}\frac{dS}{dt} \tag{4.57}$$

where λ is the wavelength of the L1 or L2 carrier.

The physical relationship between the carrier phase and the Doppler shift is :

$$\Phi(t) = \Phi(t_0) - \int_{t_0}^{t} Ds(\tau)\, d\tau \tag{4.58}$$

The Doppler shift or range-rate measurements usually are the averaging values of the delta-range or phase over a short period (generally not larger than half second) to reduce the influence of random noise and are independent observables.

Theoretically the nearly circular orbit and extreme distance of GPS satellites make the range change of the satellites exceptionally smooth. Clock and propagation effects do not normally destroy this smoothness, with some exceptions, such as sudden ionospheric disturbances or highly dynamic receiver motion. For a static receiver the theoretical (geometrical) value of the

maximum Doppler shift ± 5 kHz can be observed at latitude 60 degrees. The maximum Doppler shift rate is 175 mm/sec^2, or less than 1 Hz/sec and the maximum Doppler acceleration is 0.025 mm/sec^3, or less than 2×10^{-4} Hz/sec^2 (Wells et al.,1987).

The range-rate measurement can be modified from that given in eqn (4.4):

$$D = \dot{\rho} + \dot{d}_{ephem} + c\,(\dot{dt} - \dot{dT}) - \dot{d}_{ion} + \dot{d}_{trop} + \dot{d}_{mul} + b_D + \varepsilon_D \tag{4.59}$$

A bias term b_D is included to account for such effects as the group delays of the receiver tracking channels which may cause a sampling output of unsynchronized Doppler signals. For velocity determination b_D is neglected because of its small value. For Doppler phase data which involves the integration of the Doppler measurement, the long term effect of b_D has to be considered.

From eqn (4.58) a Doppler created phase measurement (referred to here simply as "Doppler phase") can be obtained:

$$\Phi_D(t) = \Phi_D(t_0) + \int_{t_0}^{t} D(\tau)\,d\tau = \Phi_{D1}(t) + \Phi_{D2}(t) \tag{4.60}$$

where

$$\Phi_{D1}(t) = \Phi_D(t_0) +$$

$$\int_{t_0}^{t} \left[\dot{\rho}(\tau)+\dot{d}_{ephem}(\tau)+c\left[\dot{dt}(\tau)-\dot{dT}(\tau)\right] -\dot{d}_{ion}(\tau)+\dot{d}_{trop}(\tau)+\dot{d}_{mul}(\tau)\right] d\tau \tag{4.61}$$

and

$$\Phi_{D2}(t) = \int_{t_0}^{t} \left[\, b_D(\tau) + \varepsilon_D(\tau)\right] d\tau \tag{4.62}$$

Assuming the integration of the Doppler biases, except for b_D and ε_D, equal the biases of corresponding phase measurements, eqn (4.61) can be written as:

$$\Phi_{D1}(t) = \Phi_D(t_0) + \rho(t) + d_{ephem}(t) + c[dt(t) - dT(t)] - d_{ion}(t) + d_{trop}(t) + d_{mul}(t) \quad (4.63)$$

The form of eqn (4.63) is similar to that of the phase measurement model of eqn (4.3). The difference is that the initial phase value $\Phi_D(t_0)$ of Doppler phase is not an integer multiple of the carrier wavelength anymore. A more important difference is the additional error terms in eqn (4.62). The unmodelled Doppler bias b_D depends on the receiver mechanization and is generally a small value and nearly constant though it has a different value for different tracking channels of the receiver. After integration of b_D a trend appears. ε_D is the Doppler measurement noise and is assumed to be white and its integration is a random walk noise.

Because the real Doppler output of a GPS receiver is a discrete time series, the integration is replaced by the summation of the Doppler measurements in discrete time to obtain the Doppler phase. Over a short time period the Doppler change can be considered as linear. The real Doppler phase measurement in discrete time can therefore be written as:

$$\Phi_D(t_k) = \Phi_D(t_0) + \sum_{i=1}^{k} \frac{[D(t_i) + D(t_{i-1})]}{2}[t_i - t_{i-1}] + v_D(t_k)$$

$$= \Phi_D(t_{k-1}) + \frac{[D(t_k) + D(t_{k-1})]}{2}[t_k - t_{k-1}] + v_D(t_k)$$

$$= \Phi_{D1}(t_k) + \Phi_{D2}(t_k) + v_D(t_k) \quad (4.64)$$

where $v_D(t_k)$ is an additional noise to account for unmodelled error and is assumed to be white noise.

More sophisticated numerical integration algorithms, such as Simpson integration etc., can be used. For static receivers and high data sampling rate (1 Hz), eqn (4.64) is adequate. An alternative is to use eqn (4.64) to integrate differenced Doppler measurements to obtain the differenced Doppler phase measurements directly.

The general model for $\Phi_{D2}(t_k)$ can be written as:

$$t_D(t_k) = t_D(t_{k-1}) + \beta(t_{k-1}) + \eta(t_k) \tag{4.65}$$

$$\beta(t_k) = \beta(t_{k-1}) + \zeta(t_k) \tag{4.66}$$

where:

$t_D(t_k)$, $\beta(t_k)$ trend and slope
$\eta(t_k)$, $\zeta(t_k)$ white noise series

Eqns (4.65) and (4.66) can be written in the state equation form as:

$$\begin{bmatrix} t_D(t_k) \\ \beta(t_k) \end{bmatrix} = \begin{bmatrix} 1 & 1 \\ 0 & 1 \end{bmatrix} \begin{bmatrix} t_D(t_{k-1}) \\ \beta(t_{k-1}) \end{bmatrix} + \begin{bmatrix} \eta(t_k) \\ \zeta(t_k) \end{bmatrix} \tag{4.67}$$

Eqn (4.67) is a model of a random trend and random walk. If $\eta(t_k)$ and $\zeta(t_k)$ are zero, eqn (4.67) becomes a deterministic trend with a constant slope.

The biases of Φ_{D1} can be eliminated by data differencing as in the case of normal phase processing. However, this is not the case for Φ_{D2} because for different receivers (different channels) the corresponding Φ_{D2} are different. The effects of Φ_{D2} could cause the baseline length to increase with observation time (for example using double or triple-difference processing methods a 20 metre baseline could increase in length to 160 metres in a nearly linear fashion over a 20 minute observation session). To control this baseline divergence, the error model (4.67) has to be augmented within an estimation procedure.

If the data sampling frequency is larger than the Nyquist frequency, Doppler phase data can also be obtained by the integration of the Doppler measurements in the kinematic case. It can be done more precisely by reconstruction of the continuous Doppler data first using the sampling equation (modified from Daubechies, 1992):

$$D(t) = \sum_n D(t_n) \frac{\sin\pi(t - t_n)}{\pi(t - t_n)} \tag{4.68}$$

where t, t_n are the continuous and discrete time arguments.

4.4.2.2 Data Processing

Three sets of experimental results are presented here based on the following system model:

$$\begin{bmatrix} \dot{\mathbf{X}}1(t) \\ \dot{\mathbf{X}}2(t) \end{bmatrix} = \begin{bmatrix} \mathbf{F}1 & 0 \\ 0 & \mathbf{F}2 \end{bmatrix} \begin{bmatrix} \mathbf{X}1(t) \\ \mathbf{X}2(t) \end{bmatrix} + \begin{bmatrix} \omega 1(t) \\ \omega 2(t) \end{bmatrix} \tag{4.69}$$

where:

$\mathbf{X}1(t)$ state vector for the remote site location

$\mathbf{X}2(t)$ augmented state vector for the trend and slope

For the static case $\mathbf{F}1$ is a zero matrix and $\omega 1(t)$ is a zero vector. $\mathbf{F}2$ can be written as:

$$\mathbf{F}2 = \begin{bmatrix} 0\ 1 & 0\ 0 & \cdots 0 \\ 0\ 0 & 0\ 0 & \cdots 0 \\ \cdots\cdots & \cdots\cdots & \cdots\cdots \\ 0\ 0 & 0\cdots & 0\ 1 \\ 0\ 0 & 0\cdots & 0\ 0 \end{bmatrix} \tag{4.70}$$

The observation equation is:

$$\begin{bmatrix} \mathbf{Z}1(t_k) \\ \mathbf{Z}2(t_k) \end{bmatrix} = \begin{bmatrix} \mathbf{H}1(t_k) & \mathbf{H}2(t_k) \end{bmatrix} \begin{bmatrix} \mathbf{X}1(t_k) \\ \mathbf{X}2(t_k) \end{bmatrix} + \begin{bmatrix} \mathbf{V}1(t_k) \\ \mathbf{V}2(t_k) \end{bmatrix} \tag{4.71}$$

where:

$\mathbf{Z}1(t_k)$, $\mathbf{Z}2(t_k)$ double-differenced Doppler phase and Doppler measurements

$\mathbf{V}1(t_k)$, $\mathbf{V}2(t_k)$ Doppler phase noise and Doppler measurement noise which are assumed to be uncorrelated to each other

Experiment 1:

The experiment was carried out at the School of Geomatic Eng., UNSW, on the 6th April, 1995. Two NovAtel receivers, which are 10 channel receivers with L1 phase, code and Doppler output were sited on surveying pillars of known location. The baseline length was 22.579 .metres.

During the session of this experiment 5 satellites were tracked: PRN 1, 14, 15, 21, and 25 and the data output rate was 1 Hz for both receivers with less than half-hour of data collected. The Doppler output of one receiver was used to create phase data and double-differenced Doppler phase and Doppler data were used as the observation within a Kalman filter. The static model was used for **F**1. The measurement noise was 2 cm for both Doppler and Doppler phase data.

The results of the baseline length are illustrated in Fig.4.13 to Fig.4.16. The difference between the phase measurements and the Doppler-created phase measurements for the remote site receiver is illustrated in Fig.4.12. Note the small differences of the slopes of the different satellites in Fig.4.12 which cannot be eliminated by differencing methods. Fig.4.13 to Fig.4.16 illustrate the results using the algorithms mentioned above. After a short transition period (a quite accurate initial position can be obtained from NovAtel C/A code measurements), the baseline and baseline components were converged to the nominal true value within less than 1 cm (the baseline of Doppler phase solution is 22.586 m) and the RMS was better than 1 cm. The results of the baseline and components were quite smooth. The maximum oscillation of the results in steady state was less than 1 cm, this means a high precision Doppler phase data (noise less than 1 cm) was obtained from the Doppler measurement. Actually during the integration of the Doppler measurements the noise of the Doppler measurements are also smoothed.

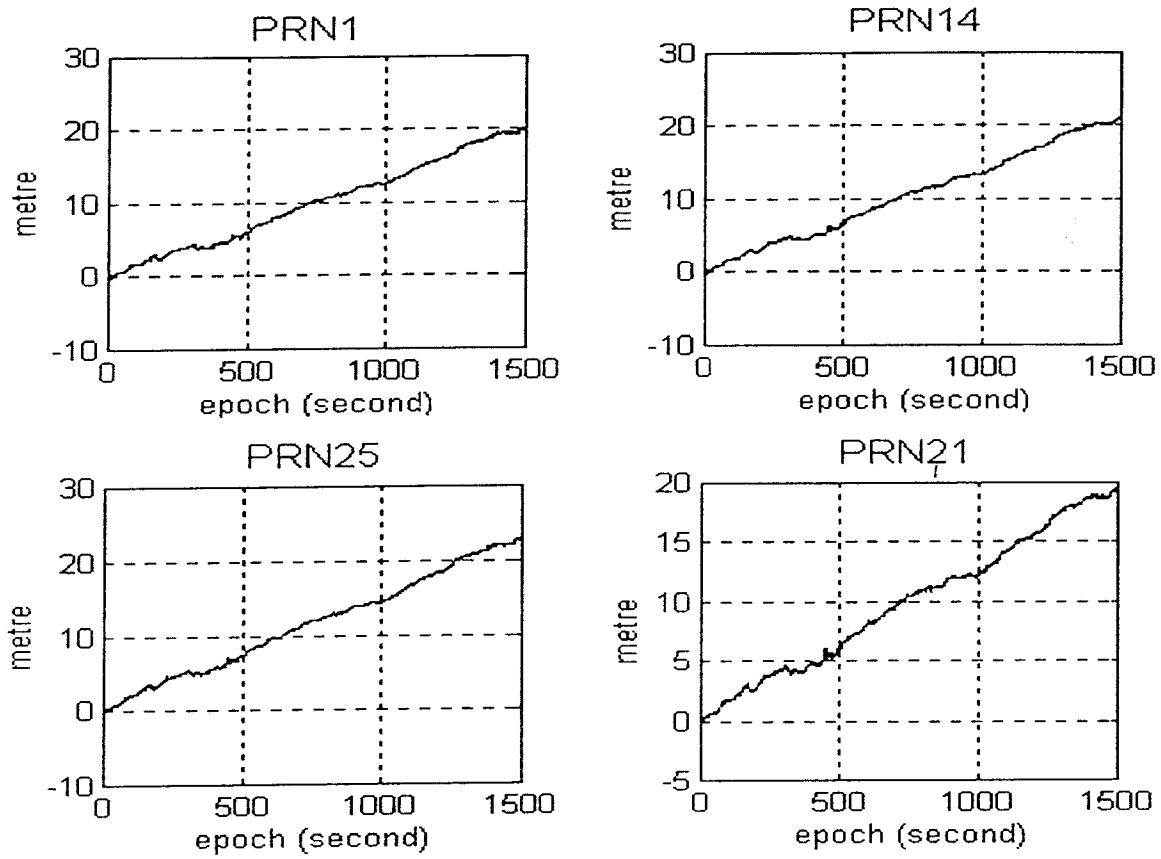

Figure 4.12 Differences between L1 phase and Doppler-phase

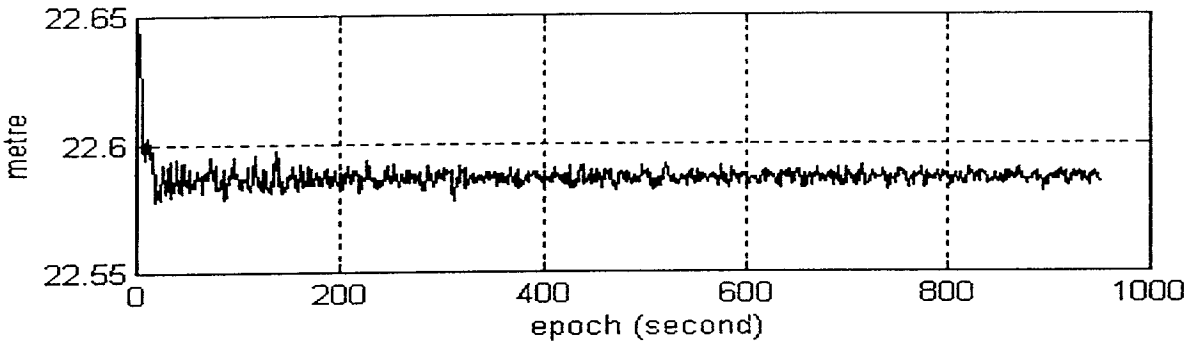

Figure 4.13 Baseline of Doppler-phase

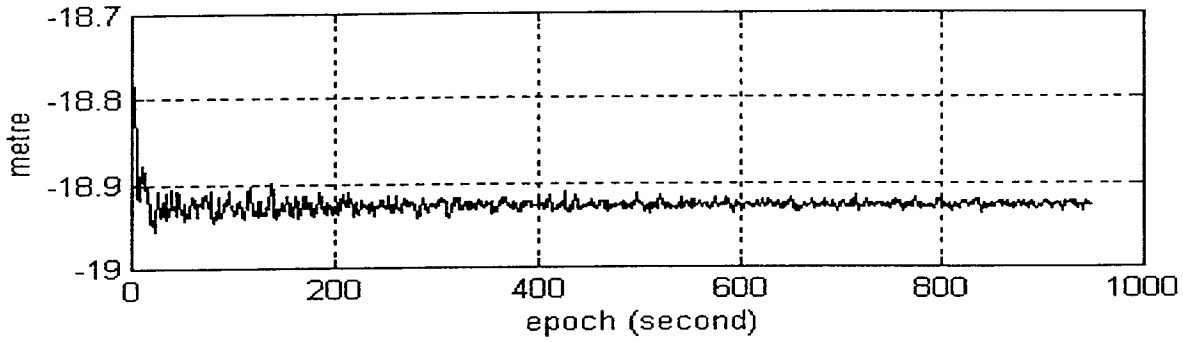

Figure 4.14 X component of the baseline

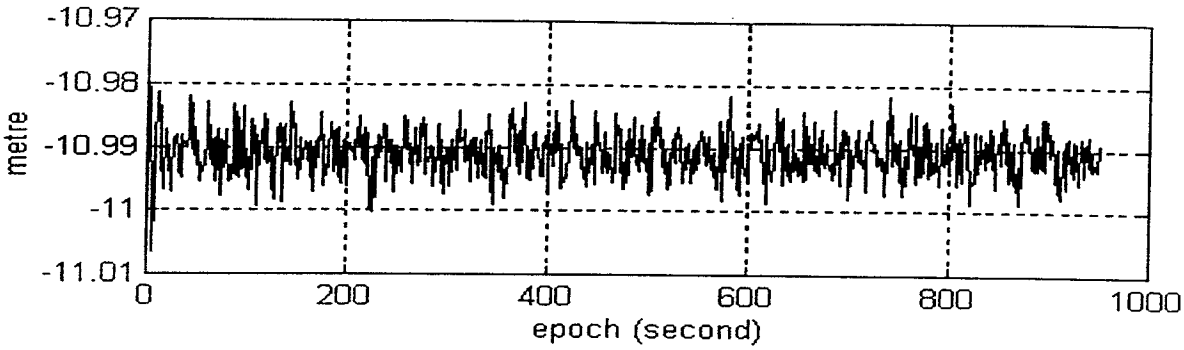

Figure 4.15 Y component of the baseline

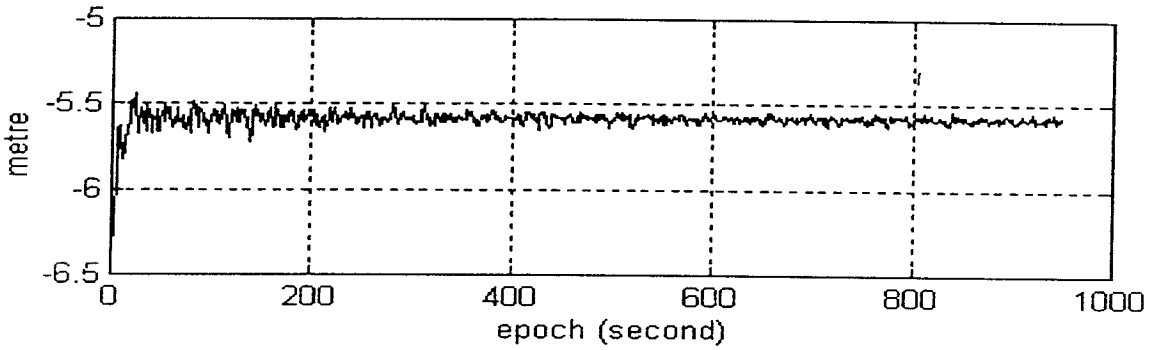

Figure 4.16 Z component of the baseline

Experiment 2:

One NovAtel receiver was sited on a surveying pillar of School of Geomatic Eng., UNSW, and another site was selected nearly 4 km away. In the first session a NovAtel receiver was used. In the second session the receiver at the remote site was replaced by a Trimble SV-6 GPS receiver whose output is L1 C/A code and Doppler, and Doppler phase data was created for the remote site. The data rate was 1 Hz for both sites, and the second session was 1 hour started at 0 hour of the 10th May, 1995. During the second session 6 satellites were observed: PRN 9, 17, 21, 23, 28 and 31. The phase data collected in the first session was processed using Leica's SKI software, and the data of the second session was processed using the Doppler phase algorithms, and the results are presented in the Fig.4.17 to Fig.4.20. There was a "Doppler jump" in epoch 193 which caused a "cycle slip" in the Doppler phase. The Doppler phase steady state results converged within 3 cm of SKI results. The slower convergence than the case for the first experiment was attributed to the large initial state uncertainty of over 10 metres and the large Doppler measurement noise (RMS 5.2 cm) of the SV-6 receiver.

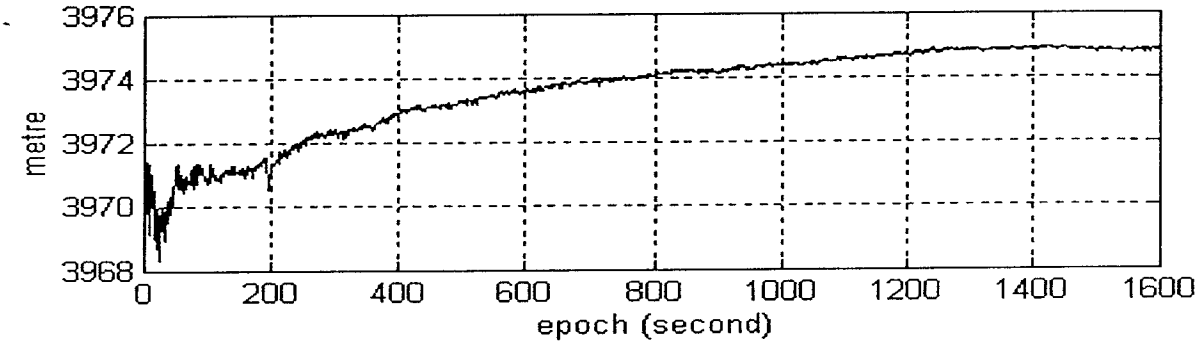

Figure 4.17 Baseline between Mather and Ewan

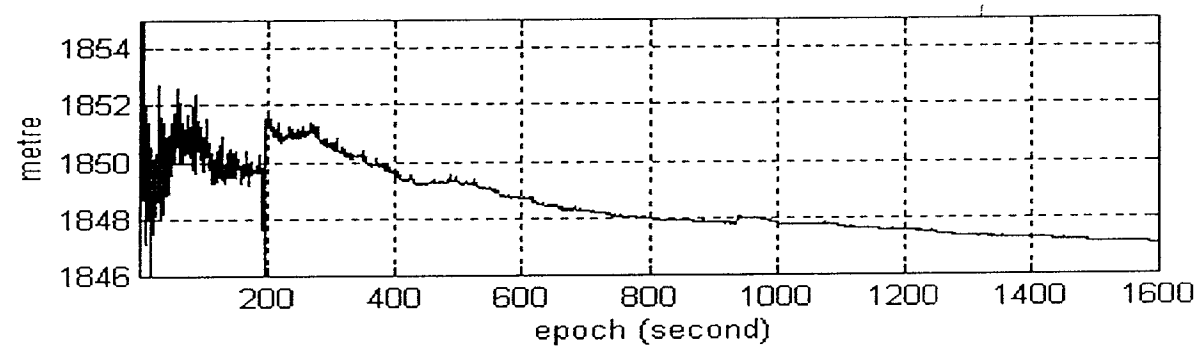

Figure 4.18 X component of the baseline

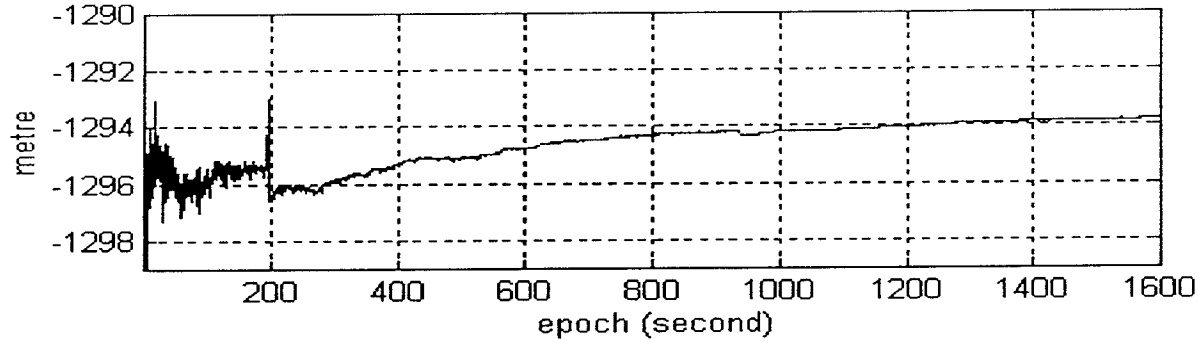

Figure 4.19 Y component of the baseline

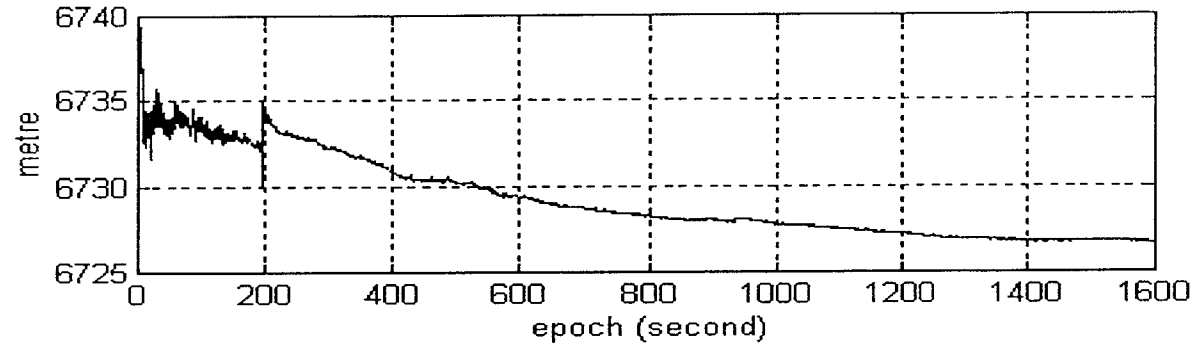

Figure 4.20 Z component of the baseline

Experiment 3:

Two Ashtech-Z12 GPS receivers were used, one was static and another was fixed aboard a moving train in South Australia. The distance between the two receivers was nearly 300 km. The Doppler phase data was used from both sites, for tracked satellites PRN 7, 2, 16, 19 and 27 collected at 1 Hz data rate. Considering the large mass and turning radius of the train, it can be assumed that 1 Hz data rate is fast enough to recover the phase measurement envelop. The results were compared with the P code solutions. The constant velocity model was used with 1m/sec*sec acceleration. The results are shown in Fig.4.21 to Fig.4.37, and Table 4.1. The mean values of the velocity difference between the P code and Doppler phase solutions is 0.0003 m/sec. The divergence between the P code and Doppler phase solutions of the baseline and components is apparently caused by the P code measurement bias (see Fig.4.26. to Fig.4.29 and Table.4.1). The nearly zero mean values of the Doppler phase innovation series indicates that the measurement bias was absorbed by the augmented bias-estimating model of eqn (4.70), and the innovation series, except of PRN 7-16, can be assumed white because they have passed the Bartlett test at a 95% confidence level (see Fig.4.34. to Fig.4.37 where the two straight lines above and below the autocorrelation are the 95% confidence limits of the Bartlett test).

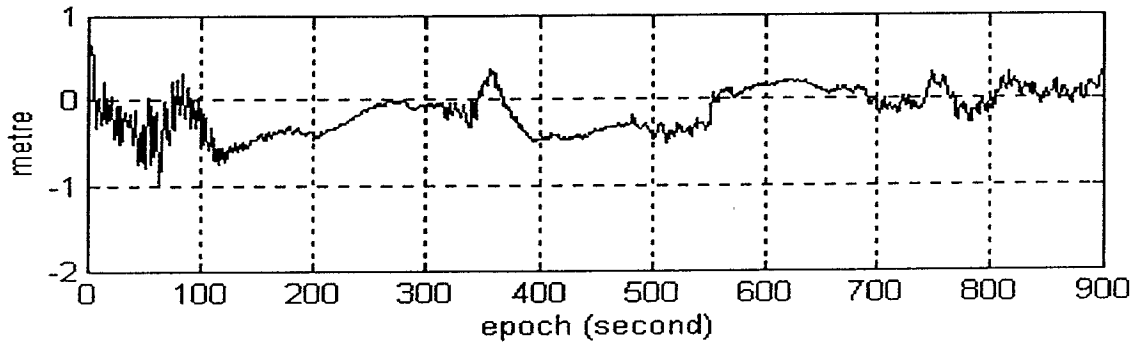

Figure 4.21. Baseline difference between P code and Doppler phase solutions.

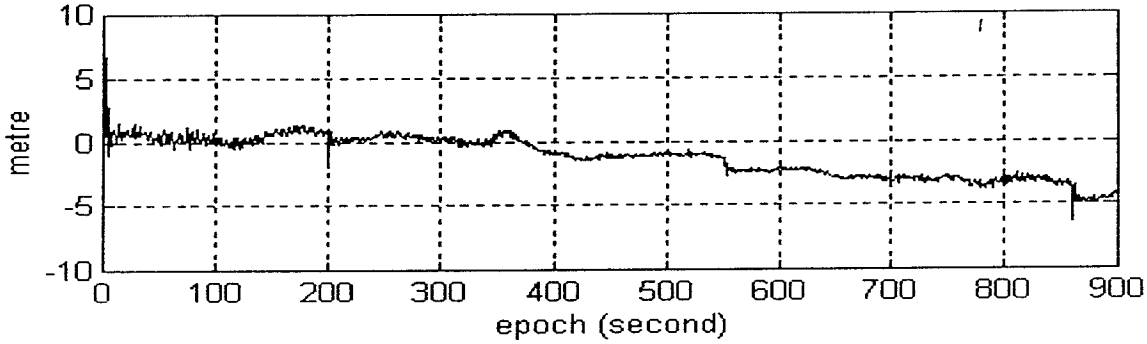

Figure 4.22. X component difference between P code and Doppler phase solutions.

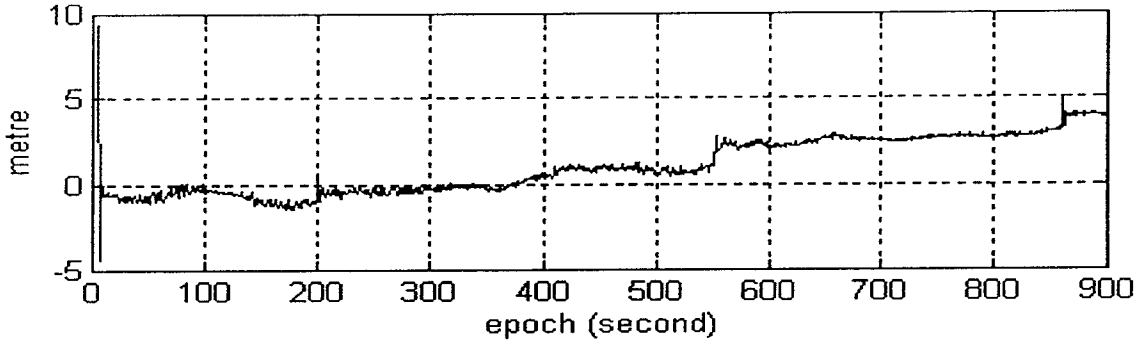

Figure 4.23. Y component difference between P code and Doppler phase solutions.

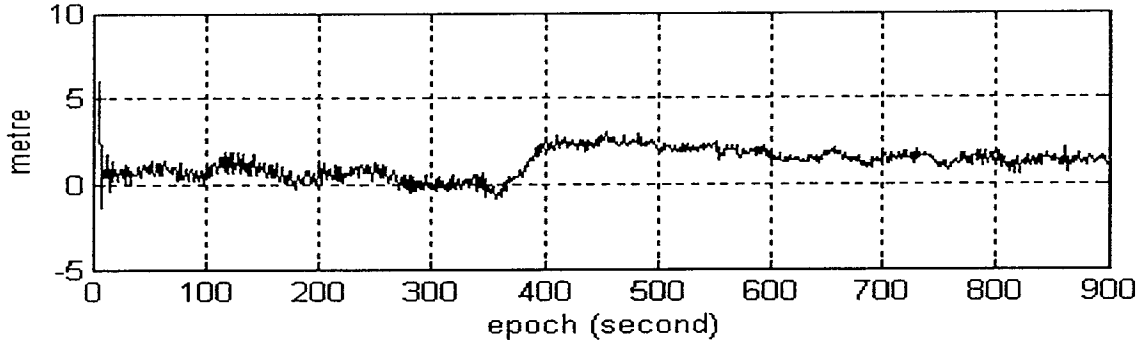

Figure 4.24. Z component difference between P code and Doppler phase solutions.

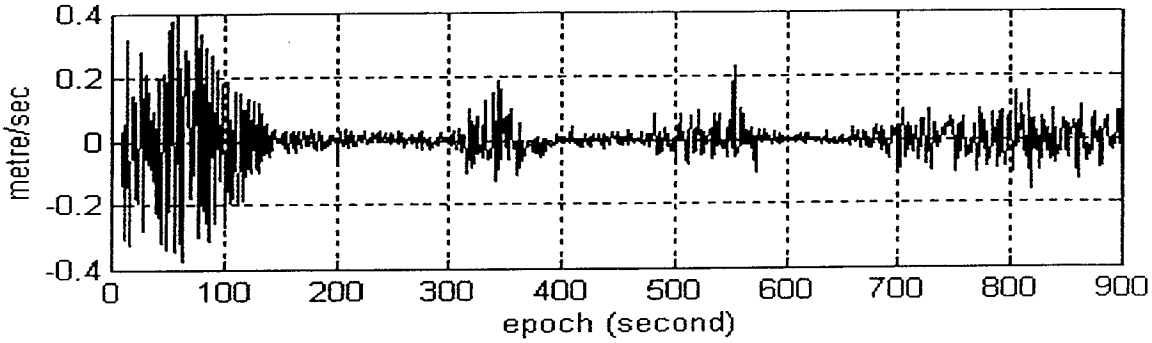

Figure 4.25. Velocity difference between P code and Doppler phase solutions.

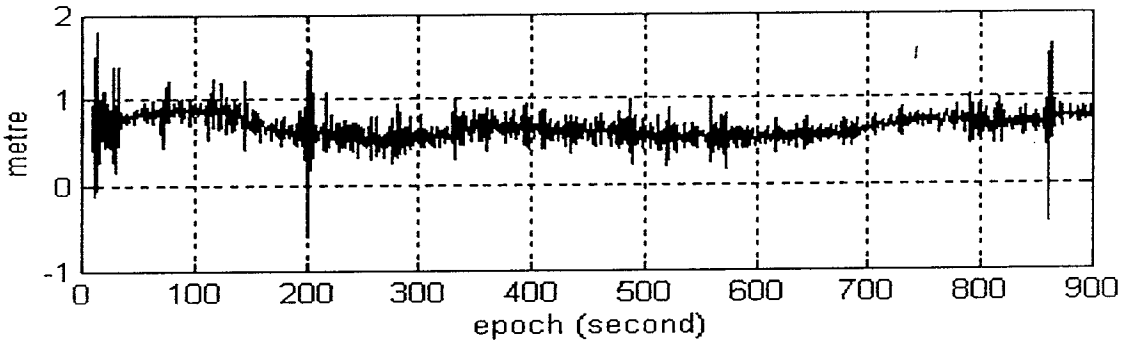

Figure 4.26. PRN 7-19 P code Innovation series.

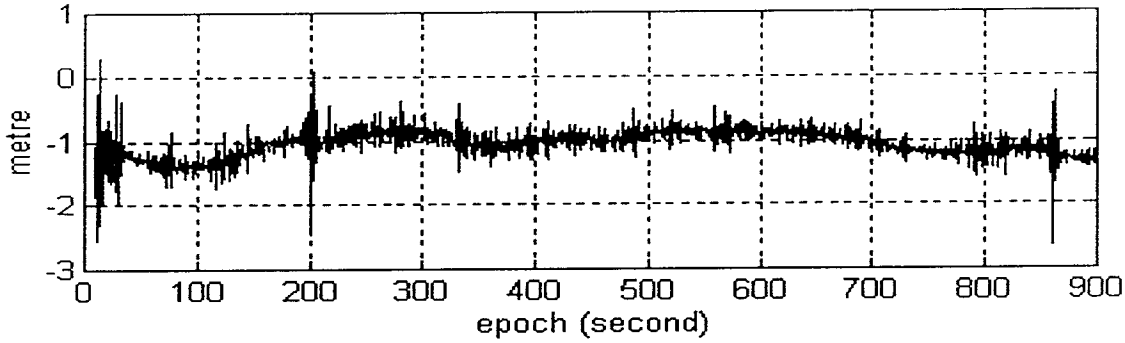

Figure 4.27. PRN 7-27 P code Innovation series.

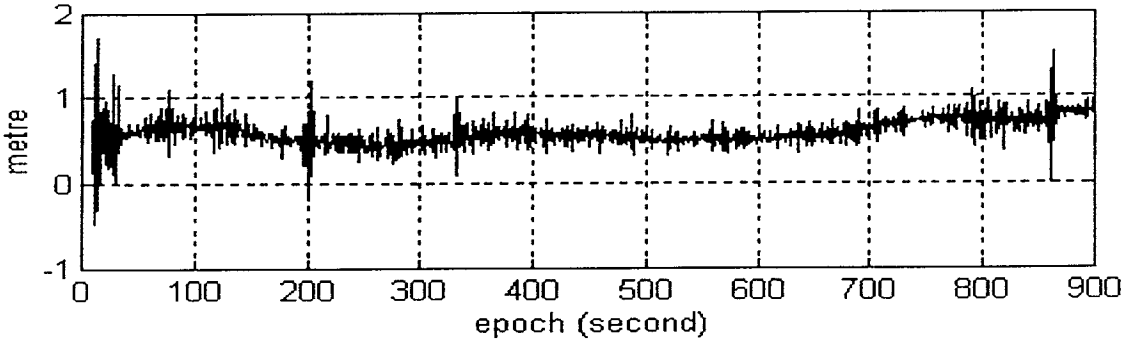

Figure 4.28. PRN 7-2 P code Innovation series.

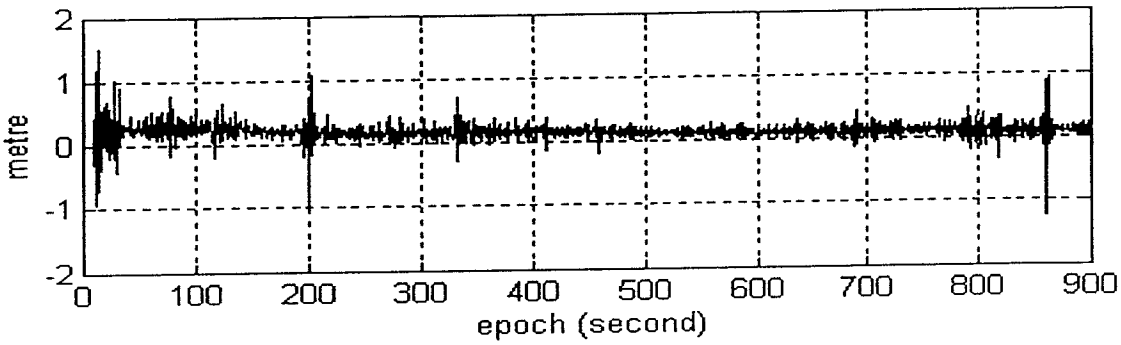

Figure 4.29. PRN 7-16 P code Innovation series.

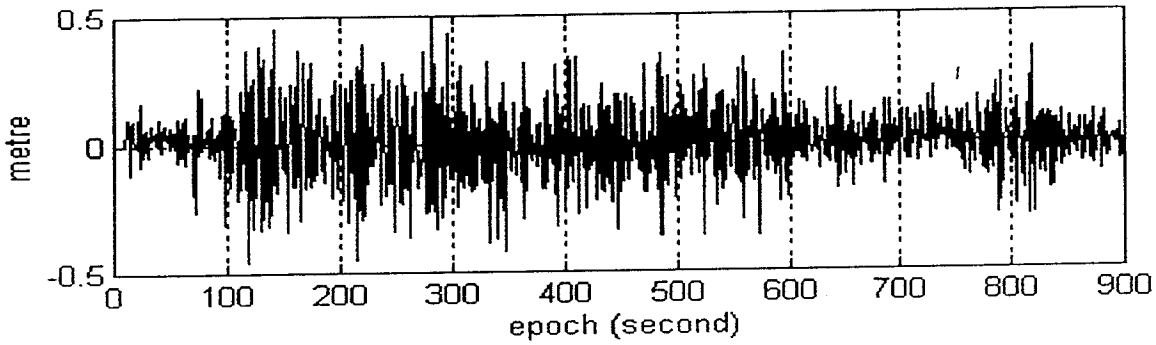

Figure.4.30. PRN 7-19 Doppler phase innovation series.

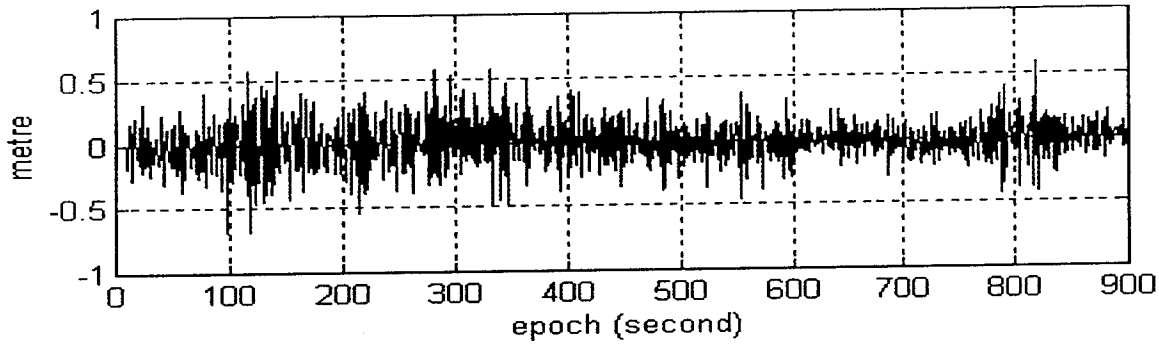

Figure.4.31. PRN 7-27 Doppler phase innovation series.

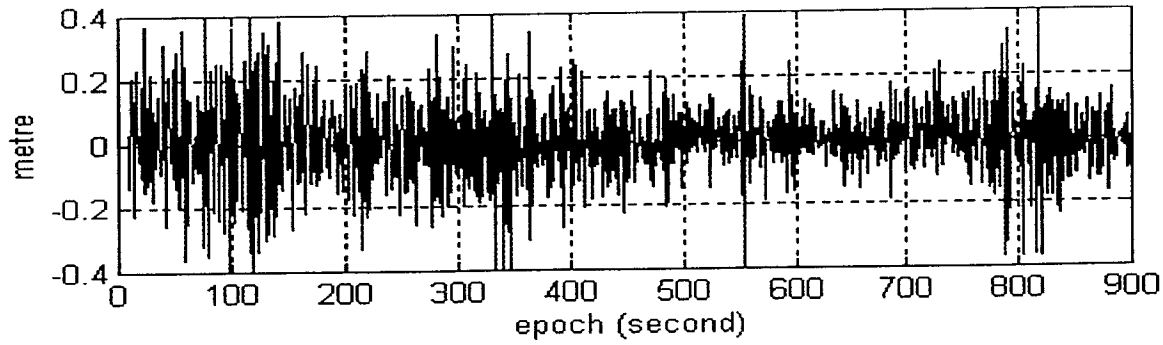

Figure.4.32. PRN 7-2 Doppler phase innovation series.

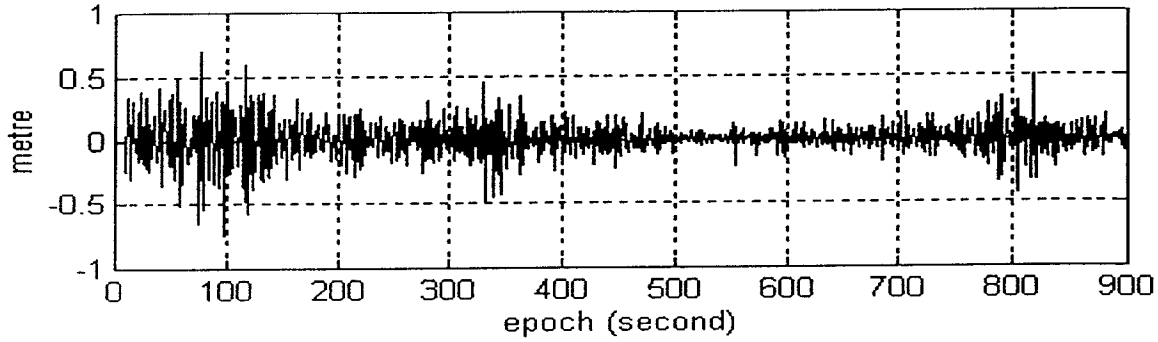

Figure.4.33. PRN 7-16 Doppler phase innovation series.

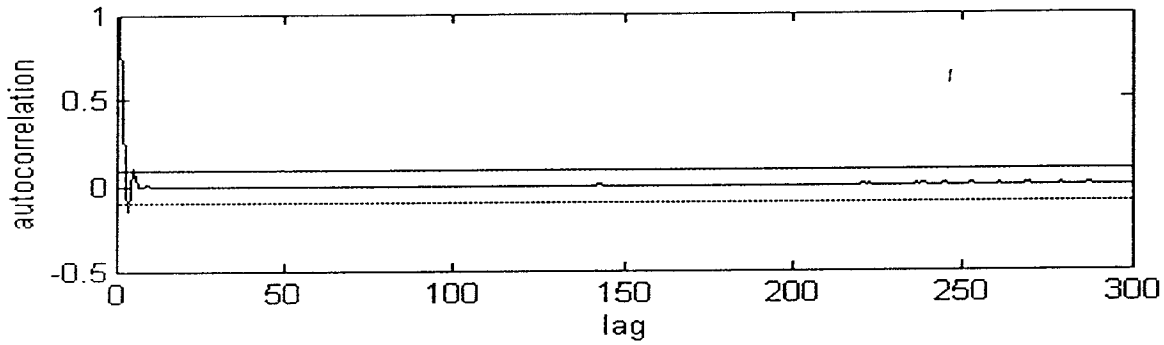

Figure.4.34. Autocorrelation of PRN 7-19 Doppler phase innovation series.

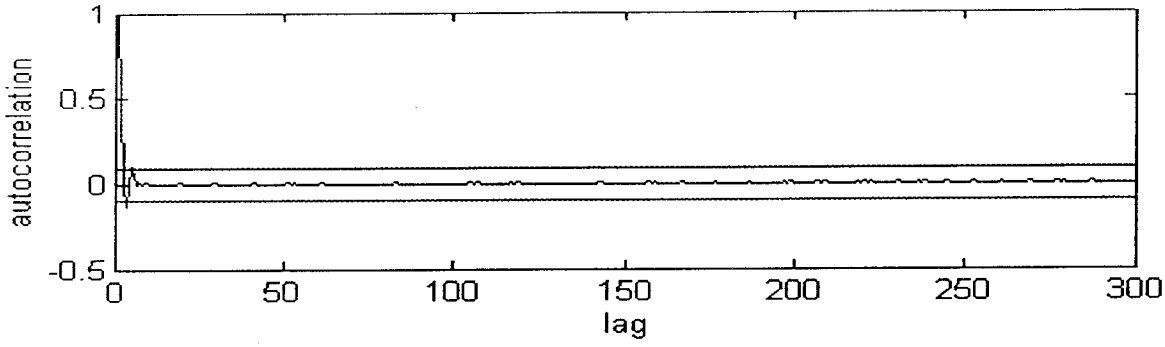

Figure.4.35. Autocorrelation of PRN 7-27 Doppler phase innovation series.

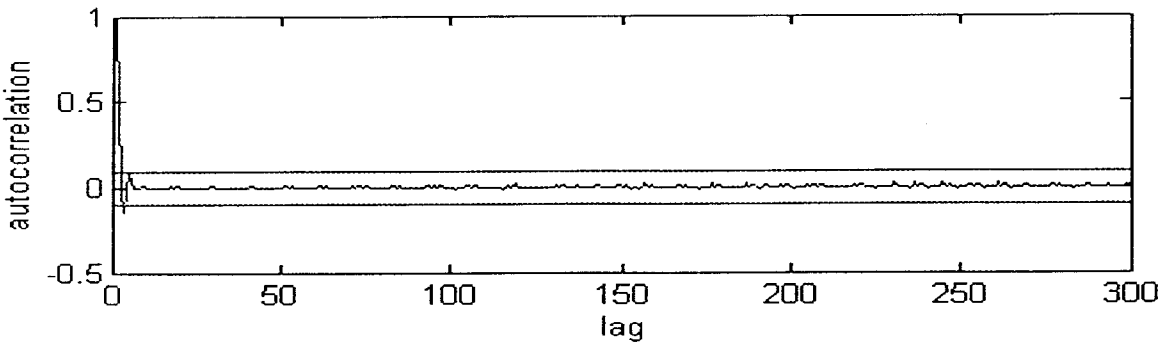

Figure.4.36. Autocorrelation of PRN 7-2 Doppler phase innovation series.

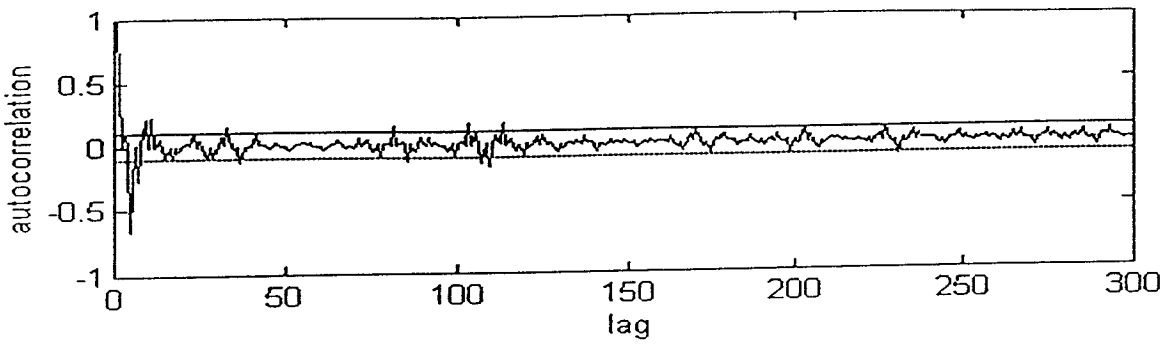

Figure.4.37. Autocorrelation of PRN 7-16 Doppler phase innovation series.

Table 4.1. Mean values of innovation series

PRN / Type	7-19	7-27	7-2	7-16
P-code	0.6628 m	-1.054 m	0.5907 m	0.1484 m
Dppler-phase	0.0028 m	-0.0039 m	0.0019 m	0.0008 m

4.4.2.3 Concluding Remarks

1) A pseudo-phase data type can be created using Doppler measurements.

2) A random trend is the primary bias for this "Doppler phase".

3) A special estimation algorithm was developed to handle the trend and cm level accuracy was obtained for a short baseline determination carried out by using Doppler phase.

4) The Doppler phase is receiver dependent.

5) If a higher than the Nyquist frequency data sampling rate is available, the method can be used in kinematic GPS applications.

6) There is "Doppler slip" when cycle slip occurs, though it can be overcome by filtering or smoothing.

Investigations are proceeding and several further static and kinematic tests are being carried out.

CHAPTER 5

THE INTEGRATED NAVIGATION SYSTEM (INNS)

The integrated navigation system makes use of modern control theory and computer technology. It consists of navigation and other associate sensors, processors, and system controllers. Among them the key devices are the processors which process the navigation information derived from the independent sensors and derive the optimal estimation and control of the body's state.

Generally INNS can be divided into two categories: global and local systems.

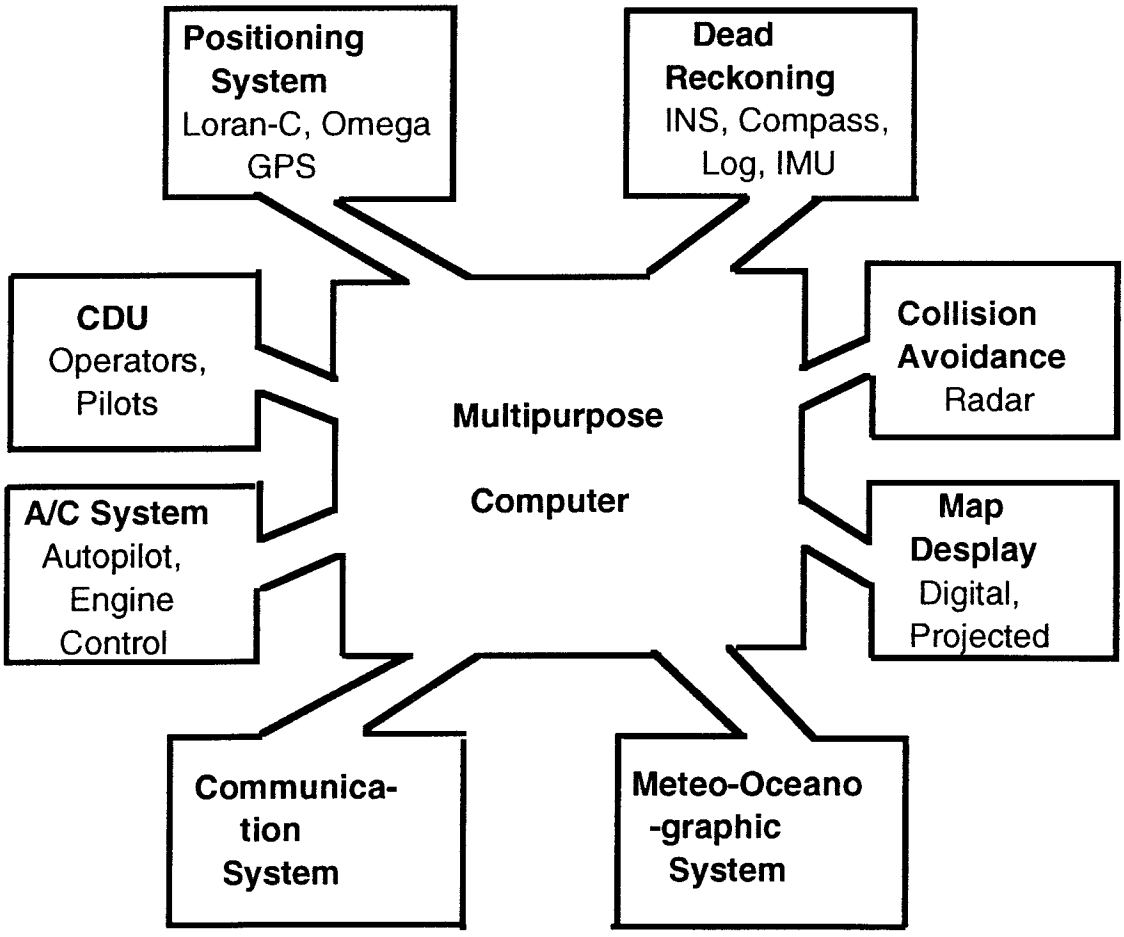

Figure 5.1. Global Integrated Navigation System.

There are a variety of global INNS depending on application, such as INA (Teldix) and Databridge (Norcontrol) systems. In the case of the INA system each local sensor processor is controlled by a central processor, and it is reported 48% of the computer time is used for data transfer and interface control, while the navigation computation only takes 9% of computer time (Terheyden & Zickwolff,1986). Another approach is the parallel implementation of multisensor integration, which can reduce the central processor work load and forms an artificial neural architecture (Bowman & Snashall, 1987).

In this thesis, only the local INNS consists of sub-systems of the global INNS (the positioning system and the DR system, and associate processors and interfaces) will be considered.

The main characteristics of an INNS is :

a) The system is robust and the performance of independent navigation sensors can be cross-checked. The integrity and reliability of the INNS is therefore increased.

b) The accuracy of navigation is higher than that of any individual navigation sensor for there is more redundant information which can be processed by the optimal filter-controller. The error sources of the navigation sensors which are independent and have different frequency characteristics can be isolated and eliminated. INNS has a good frequency response across a wide frequency range.

c) Operation of individual navigation sensors is improved and more navigation functions and a highly automatic navigation operation can be performed by the INNS.

5.1 Mechanization of INNS

There are two types of INNS mechanization: open-loop (Fig.5.2) and closed-loop (Fig.5.3) modes.

5.1.1 Open-Loop Mode

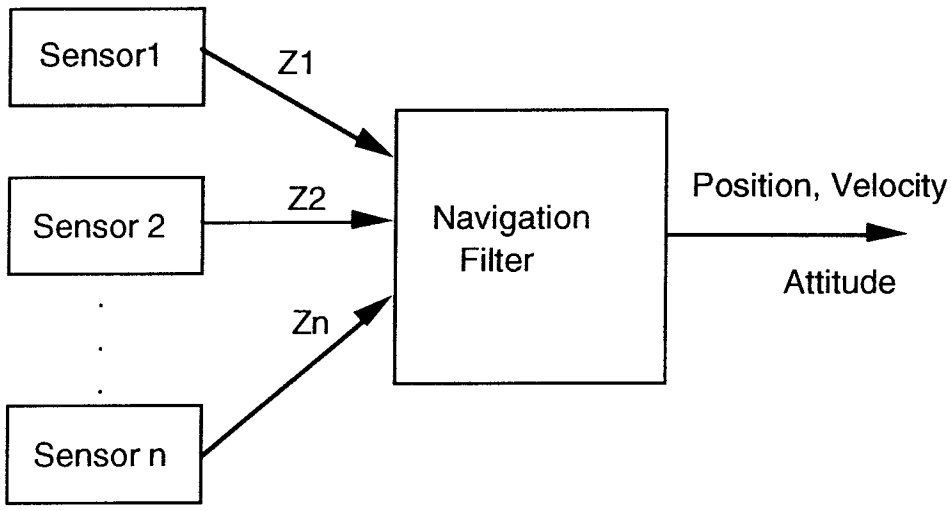

Figure 5.2. The open-loop INNS.

The open-loop mode is the simplest way to combine navigation sensors. The sensor outputs Z1, Z2, .., Zn may be the measurements of the sensors (in the case of a centralized filter), or full or reduced order estimates of the state derived from the local processors of the sensors (in the case of a decentralized filter). Generally the open-loop mode applies to the positioning system integration, and the initial alignment of INS and functions as a low-pass filter.

5.1.2 Closed-Loop INNS

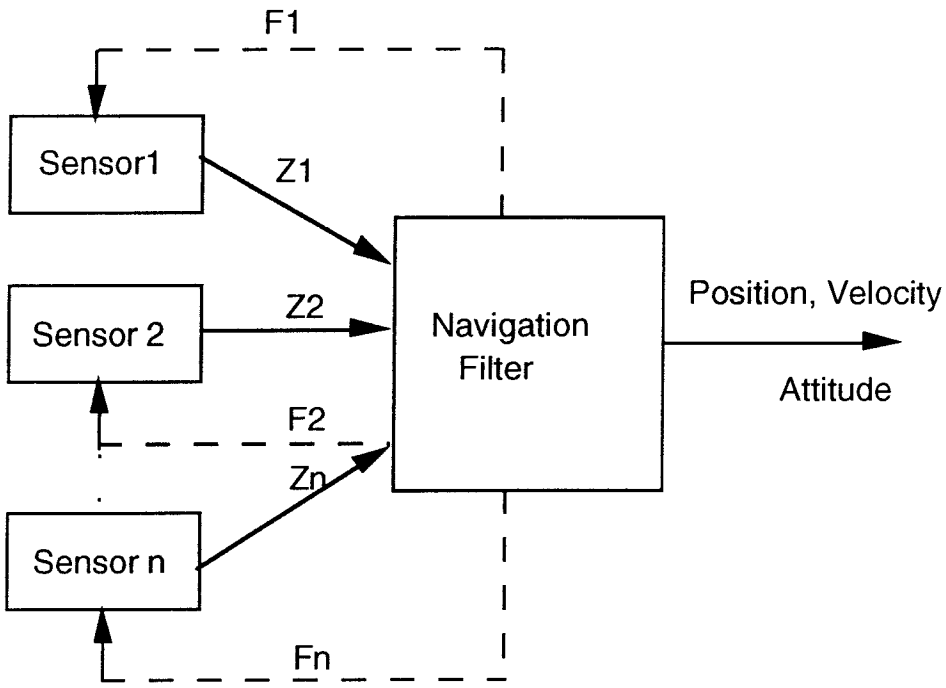

Figure 5.3. The closed-loop INNS.

The difference between the closed-loop mode and the open-loop mode is the feedback corrections F1, F2, ..., Fn, to the sensors. The feedback corrections are derived from the optimal estimation of the sensor errors and state, and are used to improve the operation of the sensors. The closed-loop mode is mainly applied to the integration of INS with other navigation sensors and functions as a low-pass or band-pass filter whose pass-band depends on the body's dynamics.

5.1.3 Decentralized Implementation

Although the centralized Kalman filtering methods can be applied to multisensor system integration, the typically large dimension of the system model and the high data rates have led in recent years to the development of decentralized parallel processing methods. Among them, one particular method of considerable usefulness to navigation was introduced by Bierman (1985), Kerr (1987) and Carlson (1990), and is called the federated Kalman filter. Algorithms

for the federated Kalman filter for the general case, modified from Carlson (1990) and Minkler (1993), are presented in Appendix 5, and its implementation is illustrated in Fig. 5.4.

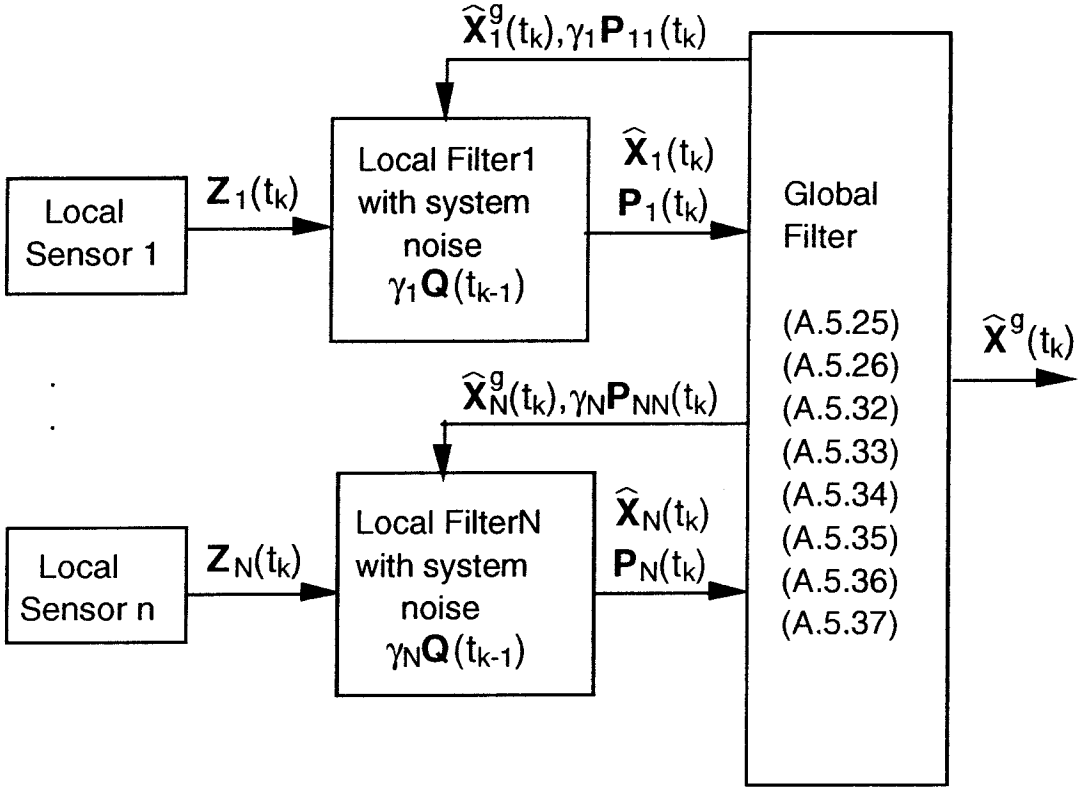

Figure 5.4. Decentralized filter architecture.

Some comments to the decentralized filter:

1) The computations of the global estimates and covariances are carried out under the dimension of local systems, especially the matrix inverse, hence the computation work load is significantly reduced compared to that of the centralized filter, see eqns (A.5.25) to (A.5.37). The algorithm provides an N-fold speed-up over a single, global filter due to parallel processing by the N local filters.

2) In most navigation applications the unique state vector is independent of the common state vector. In this case, the algorithms can be simplified further as (modified from Minkler, 1993):

$$\mathbf{P}_i(t_k) = \begin{bmatrix} \mathbf{P}_{i,c}(t_k) & 0 \\ 0 & \mathbf{P}_{i,u}(t_k) \end{bmatrix} \tag{5.1}$$

$$\hat{\mathbf{X}}^g_{iu}(t_k) = \hat{\mathbf{X}}_{iu}(t_k) \quad , i = 1, \cdots, N \tag{5.2}$$

$$\hat{\mathbf{X}}^g_c(t_k) = \left[\sum_{i=1}^{N} \mathbf{P}^{-1}_{i,c}(t_k) \right]^{-1} \sum_{i=1}^{N} \mathbf{P}^{-1}_{i,c}(t_k) \hat{\mathbf{X}}_{ic}(t_k) \tag{5.3}$$

and the estimated covariances are:

$$\mathbf{P}_c(t_k) = \left[\sum_{i=1}^{N} \mathbf{P}^{-1}_{i,c}(t_k) \right]^{-1} \tag{5.4}$$

$$\mathbf{P}_{iuc}(t_k) = \mathbf{P}_{icu}(t_k) = 0 \quad , \ i = 1, \cdots, N \tag{5.5}$$

$$\mathbf{P}_{iju}(t_k) = \begin{pmatrix} \mathbf{P}_{i,u}(t_k) & , \ i = j \\ 0 & i \neq j \end{pmatrix} \tag{5.6}$$

Block-diagonalizing is only applied to the initial and system noise covariances of the common state vector, and the estimate covariances of the common state vector for local filter resetting, see eqns (A.5.14), (A.5.18) and (A.5.38).

3) The global and local filters can operate in-step and synchronous, and all filters share a common processing cycle. Often, in practical applications, they can also operate asynchronously, usually the global filter operates at a slower rate than the local filters by using the local filters as prefilters to "compress" the local sensor data.

4) The transition matrix, observation matrix, covariances of the system noise and measurement noise of the global filter are all block-diagonal matrices, see eqns (A.5.10), (A.5.11), (A.5.14), and the global filter is completely block-observable and block-controllable. If each local filter is stable the global filter is also stable.

5) The system fault detection, identification and recovery can be carried out at several levels. First, the local filters can perform legitimate and effective screening of the local sensor measurements via residual checks. Second, the global filter incorporates each local filter output and computes a residual that can likewise be used for fault detection.

6) From a fault-tolerance viewpoint, the federated filter exhibits one serious drawback. In particular, feeding back (resetting) the estimates and covariances from the global filter introduces the possibility of cross-contamination. A fault in one sensor, if undetected by both the local and global filters, will contaminate the global solution. Feeding the solution back to the local filters will then contaminate each of them. In order to avoid this problem, a sub-optimal filter can be implemented which simply by-passes the global to local filter feedbacks, and the precision of the resultant estimates will still exceed those of any of the stand-alone local filters.

7) The merits of the decentralized filter is at the cost of filter optimality. The federated filter is conservatively optimal due to the possibility of losing information by the covariance block-diagonalizing and more emphasis is put on the measurements by setting the covariances to their upper bounds, see eqns (A.5.14), (A.5.18). For a comparative study of the performance of centralized and federated filters, see Carlson et al. (1994).

5.2 Integration of DR and GPS

The Dead Reckoning (DR) system for a ship generally comprises of gyrocompass, speed log and associated processors. The navigation function can be improved significantly by an optimal integration of DR and other navigation sensors which are based on different physical principles. The integrated navigation system can be implemented in either the open-loop or closed-loop modes.

5.2.1 Open-Loop Integration

Most radio navigation systems such as GPS, Omega and Loran-C have interfaces to operate in the open-loop mode. The navigation processor, typically a Kalman filter, may be part of a primary sensor, or functions as an independent processor as illustrated in Fig.5.5.

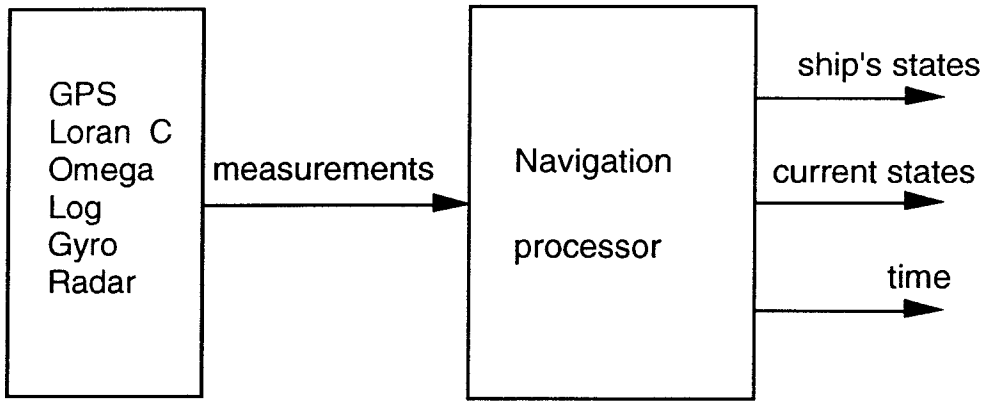

Figure 5.5. Open-loop DR integration.

The open-loop Kalman filter is based on the following model of a body's dynamics:

$$\dot{\mathbf{X}}(t) = \mathbf{F}\,\mathbf{X}(t) + \mathbf{W}(t) \tag{5.7}$$

where

$$\mathbf{X}(t) = [\mathbf{X}1(t),\ \mathbf{X}2(t)]^T \tag{5.8}$$

$$\mathbf{W}(t) = [\mathbf{W}1(t)\ \mathbf{W}2(t)]^T \tag{5.9}$$

$$\mathbf{F} = \begin{bmatrix} \mathbf{F1} & 0 \\ 0 & \mathbf{F2} \end{bmatrix} \tag{5.10}$$

where:

W1, W2	white noise representing the dynamic noise for **X**1, **X**2
F1, **F**2	constant matrices
X1	state vector for the body's state
X2	augmented state vector, whose content depends on the measurement type and the autocorrelation functions of measurement errors

The discrete measurement equation is:

$$\mathbf{Z}(t_k) = \mathbf{h}[\mathbf{X}(t_k), t_k] + \Delta\mathbf{B}(t_k) + \mathbf{V}(t_k) \tag{5.11}$$

where:

V	white noise
$\Delta\mathbf{B}(t_k)$	systematic error or bias which can be modelled as shaping filter or in the form of an ARMA model

The linearised measurement equation is generally written as:

$$\delta\mathbf{Z}(t_k) = \mathbf{H}[t_k]\,\delta\mathbf{X}(t_k) + \mathbf{V}(t_k) \tag{5.12}$$

$$\delta\mathbf{Z}(t_k) = \mathbf{Z}(t_k) - \mathbf{Z}_n(t_k) \tag{5.13}$$

where

$$\mathbf{H}[t_k] = \frac{\partial \mathbf{h}[\mathbf{X};t_k]}{\partial \mathbf{X}} \Big|_{\mathbf{x}=\mathbf{x}_n(t_k)} \tag{5.14}$$

$\mathbf{X}_n(t_k)$, $\mathbf{Z}_n(t_k)$ are the nominal values.

An open-loop system is easy to implement, however the filter performance may be sensitive to the body's dynamics. For example, if the trajectory is a straight line the filter will give a good estimate of the trajectory if a small dynamic noise **w**1 is put into the filter. On the other hand if the trajectory is not a straight line, the filter response to the change of trajectory is slow and an apparent lag and

estimation divergence from the true trajectory will occur during the body's manoeuvre. The extended Kalman filter is not very sensitive to the variation of the states because the higher order derivatives associate with the body's states other than first order terms are usually neglected in the process of linearisation of the equations. For a typical navigation problem, the dynamic equations of the system are linear, but for most measurements such as those of GPS, Omega, Loran-C and radar, they are non-linear. If a large dynamic noise is put into the filter, the constraint of the trajectory is relaxed, but the filter is more sensitive to the measurement errors and noise. Although the mean estimated trajectory of the filter can follow the body's manoeuvre, a large estimation error and an oscillation of the estimated trajectory about the true trajectory will occur, even though the true trajectory is a straight line (Meijer, 1983).

A chi-square test for the normalized innovation series of the filter was proposed as a method of monitoring the system dynamics (modified from Wolfe & Satzer, 1982):

$$\chi^2(t_k) = \partial \mathbf{Z}^T(t_k|t_{k-1}) \left[\mathbf{H}(t_k)\mathbf{P}_{k|k-1}\mathbf{H}^T(t_k) + \mathbf{R}(t_k)\right]^{-1} \partial \mathbf{Z}(t_k|t_{k-1}) \tag{5.15}$$

where:

$\partial \mathbf{Z}(t_k\|t_{k-1})$	innovation series
$\mathbf{P}_{k\|k-1}$	one step prediction of the estimate covariance
$\mathbf{R}(t_k)$	variance of measurement noise

Under the assumption that the measurement noise and dynamic noise are Gaussian white noise and the overall system model is perfect, the innovation series $\partial \mathbf{Z}(t_k|t_{k-1})$ is also a Gaussian white noise with zero mean:

$$\partial \mathbf{Z}(t_k|t_{k-1}) \sim N\left[0, \mathbf{H}(t_k)\mathbf{P}_{k|k-1}\mathbf{H}^T(t_k) + \mathbf{R}(t_k)\right] \tag{5.16}$$

The innovation series can be exploited for sensor failure detection and quality control (Salzmann, 1993), and for checking the reasonableness of the data and of the parameter estimation (Maybeck, 1982). Eqn (5.15) shows that a normalized quadratic form of the Gaussian variable $\partial \mathbf{Z}(t_k|t_{k-1})$ follows the chi-square distribution. Preliminary runs over the data serve to eliminate spurious measurement data. When obviously bad data have been removed from the data series, the threshold value of the chi-squared statistics can be set high.

Furthermore, an assumption is made that the remaining data are all sound. Then, if there are residuals which have chi-squared values exceeding the threshold, it is assumed that it is caused by the body's manoeuvre and the covariance of system dynamic noise is increased to account for the uncertainty of the manoeuvre.

There are some problems with the above method. Firstly, the chi-squared statistic is used for both data rejection and manoeuvre detection, the distinct threshold values for both purposes are difficult to determine and the effects of abnormal measurements and sudden changes in system dynamics are difficult to separate. Secondly, the increase of the covariance of body's dynamic noise will induce an increase in the filter estimation errors. If the body changes course and speed rapidly and frequently, the filter will function poorly because the driving noise is now non-stationary and the filtering steady state cannot be achieved. The optimal estimation by the Kalman filter is only obtainable at the filter steady state. Furthermore, the gain matrix of the filter will become motion dependent and large estimation error will be expected during the manoeuvre. Finally, a high data rate and a high filter updating rate are needed for the filter to follow the rapid and frequent change in the trajectory.

5.2.2 Closed-Loop Integration

A partial feedback system, or a closed-loop filter, can avoid the problems mentioned above (Fu, 1994). The state prediction of the body (position, velocity) is now derived from the outputs of dead reckoning, which in the case of a marine application are the outputs of the gyrocompass, speed log and ocean current estimation corrected for their biases by the filter feedback. As mentioned in section 3.3.1.1, the errors of the gyrocompass: the latitude error, the velocity and course error and the acceleration error, are nearly constants or have a oscillation with a comparatively long period (greater than the 84.4 minute Schuler period). The gyrocompass is very sensitive to the high frequency components of a body's state and can measure accurately the change in heading. This is also true for the speed log (Doppler log) whose error is mainly dependent on the speed of propagation of sound waves in the water (see section 3.3.2.2). In addition to the vessel's position and velocity, the errors of dead reckoning and the errors of the gyrocompass and speed log are included in the state vector and those errors estimated by the Kalman filter are fed back to the dead reckoning system to compensate their slow changing biases and

constant errors. The errors in the vessel's trajectory are now a function of the errors of the gyrocompass and speed log, which can be measured by GPS or other navigation sensors.

This configuration isolates the vessel's dynamics, which are not estimated directly by the filter. The driving noise of the filter is now the noise of the gyrocompass, log, etc., and are all stationary processes. After a short transition period, the filter will be in steady state and the innovation series can be used to monitor the quality of the measurement data and the integrity of the navigation sensors.

The filter is actually an estimator of dead reckoning errors which can be considered as constants for certain time periods, and a high filter update rate is not necessary. Furthermore, the temporary interruption of the measurement does not affect the navigation accuracy and the vessel's state can still be obtained from the dead reckoning output. The output of the dead reckoning can also be input into the navigation sensors for sensor initialization and other support functions. The closed-loop DR integration is illustrated in Fig. 5.6.

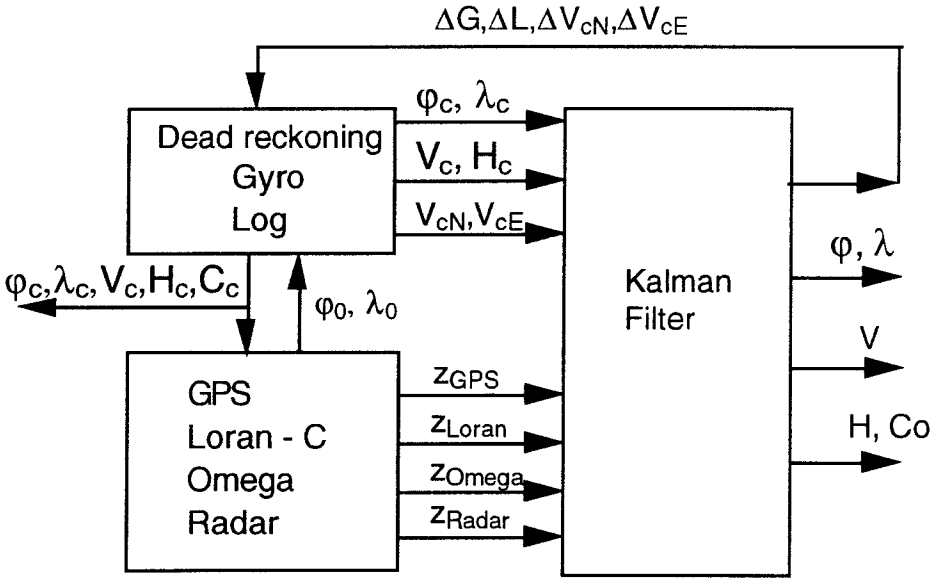

Figure 5.6. Closed-loop DR integration for a vessel.

where:

ΔG, ΔL, ΔV_{cN}, ΔV_{cE}	gyrocompass error, log error, north and east velocity errors of current
φ_c, λ_c	latitude and longitude of DR

V_L, V_c, H_c, C_c	log speed, speed relative to ground, heading and course of DR
V_{cN}, V_{cE}	north and east velocities of current
φ, λ, V, H, Co	estimated latitude, longitude, speed, heading and course
z_{GPS}, z_{Loran}, z_{Omega}, z_{Radar}	measurements of GPS, Loran-C, Omega and radar
φ_0, λ_0	initial position

The DR position is:

$$\varphi_c(t_k) = \varphi_c(t_{k-1}) + \int_{t_{k-1}}^{t_k} \frac{V_L(t)\cos[H_c(t)] + V_{cN}(t)}{R_N} dt \tag{5.17}$$

$$\lambda_c(t_k) = \lambda_c(t_{k-1}) + \int_{t_{k-1}}^{t_k} \frac{V_L(t)\sin[H_c(t)] + V_{cE}(t)}{R_M} dt \tag{5.18}$$

The log speed is:

$$V_L(t_k) = V_{Lr}(t_k) + \Delta L(t_k) \tag{5.19}$$

V_{Lr} is the output of log.

The current velocities are:

$$V_{cN}(t_k) = V_{cN}(t_k) + \Delta V_{cN}(t_k) \tag{5.20}$$

$$V_{cE}(t_k) = V_{cE}(t_k) + \Delta V_{cE}(t_k) \tag{5.21}$$

H_c is the heading of dead reckoning:

$$H_c(t_k) = H_{Gr}(t_k) + \Delta G(t_k) \tag{5.22}$$

where H_{Gr} is the the gyrocompass reading.

Speed relative to the ground and course are:

$$V_c(t_k) = \sqrt{[V_L(t_k)\cos[H_c(t_k)]+V_{cN}(t_k)]^2+[V_L(t_k)\sin[H_c(t_k)]+V_{cE}(t_k)]^2} \tag{5.23}$$

and

$$C_c(t_k) = tg^{-1}\left[\frac{V_L(t_k)\sin[H_c(t_k)] +V_{cE}(t_k)}{V_L(t_k)\cos[H_c(t_k)]+V_{cN}(t_k)}\right] + k\pi \tag{5.24}$$

Eqns (5.17) to (5.24) complete the dead reckoning procedure.

The output data rate of DR is usually high, of the order of 1 to 100 Hz. The update rate of the filter can be much lower than that of the DR, between 0.001 to 1 Hz depending on applications. During the interval of filter updating, ΔG and ΔL can be considered as constants, ΔV_{cN} and ΔV_{cE} as constants or changing linearly, and the values at t_k are easy to obtain by linear extrapolation. If the filter breaks down, the dead reckoning block can still function as a pure dead reckoning system.

Although the state equation of the Kalman filter for closed-loop DR integration can be expressed in the same form as those for the open-loop one, see eqns (5.7) to (5.10), the state vector of the closed-loop mode is different from that of open-loop one. For the DR, the state vector is:

$$\mathbf{X}1 = \begin{bmatrix} \Delta N = N_t - N_c & \text{north component error of position of DR} \\ \Delta E = E_t - E_c & \text{east component error of position of DR} \\ \Delta L = V_t - V_L & \text{velocity error of log} \\ \Delta G = H_t - H_c & \text{gyrocompass error} \\ \Delta V_{cN} = V_{tcN} - V_{cN} & \text{north component velocity error of current} \\ \Delta V_{cE} = V_{tcE} - V_{cE} & \text{east component velocity error of current} \end{bmatrix} \tag{5.25}$$

The subscripts t and c refer to the true values and the dead reckoning output values. **X**1 is expressed in the geographic frame for which the system driving noise is decoupled and stationary, and its covariance matrix is diagonal. The coefficient matrix **F**1 is not a constant matrix, because V_L and H_C vary with time. The total system model is time-variant. The filter is a combination of linearised and extended Kalman filters.

$$\mathbf{F1} = \begin{bmatrix} 0 & 0 & \cos(H_c) & -V_L\sin(H_c) & 1 & 0 \\ 0 & 0 & \sin(H_c) & V_L\cos(H_c) & 0 & 1 \\ 0 & 0 & \frac{-1}{\tau_L} & 0 & 0 & 0 \\ 0 & 0 & 0 & \frac{-1}{\tau_G} & 0 & 0 \\ 0 & 0 & 0 & 0 & \frac{-1}{\tau_{cN}} & 0 \\ 0 & 0 & 0 & 0 & 0 & \frac{-1}{\tau_{cE}} \end{bmatrix} \tag{5.26}$$

τ_L, τ_G, τ_{cN}, τ_{cE} are the time constants of log, gyrocompass and current errors. τ_G can be chosen as the damped oscillation period of gyrocompass, which is about 100-120 minutes depending on the type of gyrocompass. τ_L, τ_{cN} and τ_{cE} are dependent on the oceanographic state and are usually chosen as being a few hours.

From eqn (5.26) it can be seen that the errors of log, gyrocompass and current are all assumed to be first order Markov processes with long correlation times. The system driving noise is:

$$\mathbf{W1}(t) = \begin{bmatrix} 0 \\ 0 \\ w_L(t) \\ w_G(t) \\ w_{cN}(t) \\ w_{cE}(t) \end{bmatrix} \tag{5.27}$$

$$\mathbf{Q1} = \mathbf{E}[\mathbf{w1}\ \mathbf{w1}^T] = \begin{bmatrix} 0 & 0 & 0 & 0 & 0 & 0 \\ 0 & 0 & 0 & 0 & 0 & 0 \\ 0 & 0 & Q_L & 0 & 0 & 0 \\ 0 & 0 & 0 & Q_G & 0 & 0 \\ 0 & 0 & 0 & 0 & Q_{cN} & 0 \\ 0 & 0 & 0 & 0 & 0 & Q_{cE} \end{bmatrix} \tag{5.28}$$

$\mathbf{w1}(t)$ is zero mean white noise.

Generally speaking, the transition matrix of a time-variant system cannot be expressed by a matrix exponential. For short time intervals t_f-t_{f-1}(DR output interval) it can be assumed that the heading and velocity are constant, hence eqn (5.26) is a constant matrix during that interval and the transition matrix can be computed as:

$$\Phi 1(t_f, t_{f-1}) \approx \mathbf{I} + \mathbf{F}1(t_{f-1})\,(t_f - t_{f-1}) \tag{5.29}$$

Assuming there are m DR outputs during a filter updating interval, then:

$$\Phi 1(t_k, t_{k-1}) = \Phi 1(t_k, t_{k-1+m\Delta f})\Phi 1(t_{k-1+m\Delta f}, t_{k-1+(m-1)\Delta f})\ldots\Phi 1(t_{k-1+\Delta f}, t_{k-1}) \tag{5.30}$$

where Δf is the DR updating interval. $\mathbf{F}1(t_k)$ is determined by the output of DR.

The position transition is just a dead reckoning procedure and the transition matrix computation corresponding to the position terms can be simplified by using the intermediate speed and course as illustrated in Fig.5.7.

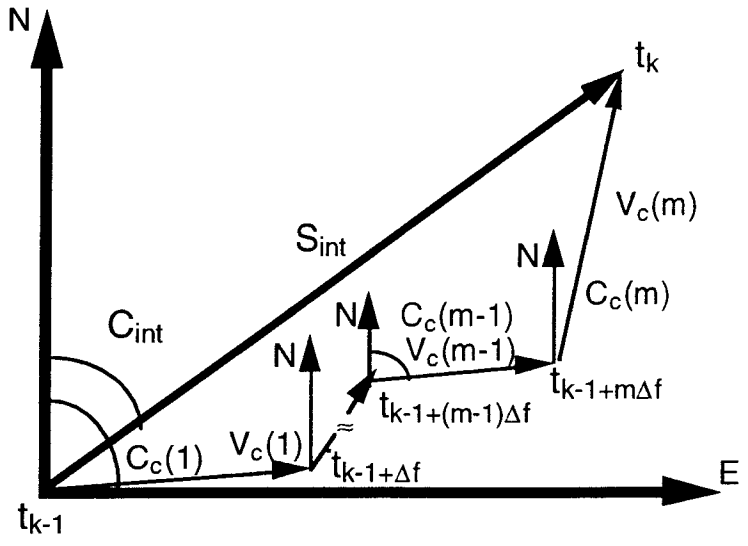

Figure 5.7. Intermediate course and speed of dead reckoning.

In Fig.5.7 $V_c(1)$, ..., $V_c(m)$ and $C_c(1)$, ..., $C_c(m)$ are the speeds and courses during DR updating intervals, obtained from eqns (5.23) and (5.24). S_{int} and C_{int} are the intermediate distance and course during the updating interval of the filter:

$$C_{int}(t_k) = tg^{-1}\left[\frac{E(t_k)}{N(t_k)}\right] + k\pi \tag{5.31}$$

$$V_{int}(t_k) = \frac{\sqrt{N^2(t_k) + E^2(t_k)}}{t_k - t_{k-1}} = \frac{S_{int}}{t_k - t_{k-1}} \tag{5.32}$$

where

$$N(t_k) = \sum_{n=1}^{m} V_c(n)\cos C_c(n)\Delta f \tag{5.33}$$

$$E(t_k) = \sum_{n=1}^{m} V_c(n)\sin C_c(n)\Delta f \tag{5.34}$$

The transition matrix can now be written as:

$$\Phi 1(t_k, t_{k-1}) \approx \mathbf{I} + \mathbf{F}1[C_{int}(t_k), V_{int}(t_k)]\ (t_k - t_{k-1}) \tag{5.35}$$

For long time intervals eqn (5.35) can still be used as an intermediate step for the computation of the transition matrix to reduce the computational burden. After the transition matrix is computed, the standard computation procedure of the Kalman filter is followed.

5.2.3. Measurements

The measurement equations of the navigation sensors are:

1) Omega:
For two transmitters i and j, the phase difference of the Omega is:

$$Z_O^{i,j}(t_k) = \frac{f_{Omega}}{C_{Omega}}[\rho_i(t_k) - \rho_j(t_k)] + \Delta O^{i,j}(t_k) + \Delta v_O^{i,j}(t_k) \tag{5.36}$$

where:

fOmega	Omega signal frequency
COmega	Omega signal propagation speed
ρ_i, ρ_j	geodesic lengths from receiver to i and j Omega transmitters

For hyperbolic navigation systems such as Omega and Loran-C, their principles are similar to the between-satellite difference mode of GPS. Omega transmitters are functioning independently and the propagation errors of the radio wave and the transmitting errors of different transmitters can be considered independent. The undifferenced Omega measurement equation can be written as:

$$Z^i_O(t_k) = f_{Omega}\left[\frac{\rho_i(t_k)}{C_{Omega}}\right] + O^i(t_k) + v^i_O(t_k) \qquad (5.37)$$

After correction of the propagation error by PPC tables (phase propagation correction), the first order terms of the correlated residual error $O^i(t_k)$ can be modelled as two first Markov processes (one weakly and the other strongly correlated), and one periodic exponentially decaying process with a period of 24 hours which is modelled as a second order Markov process (Liang & McMillan, 1982). In most cases the periodic error can be neglected. The author prefers two first order Markov process models with the correlation time T1>>T2, hence for each Omega station there are two variables augmented to the state vector. The LOP (Line Of Position) of Omega is formed by differencing the one-way measurements using a differencing operator **D**. For four stations the sequential operator **D** is:

$$\mathbf{D} = \begin{bmatrix} 1 & -1 & 0 & 0 \\ 0 & 1 & -1 & 0 \\ 0 & 0 & 1 & -1 \end{bmatrix} \qquad (5.38)$$

The linearised form of (5.37) is:

$$\delta Z^i_O(t_k) = \frac{f_{Omega}}{C_{Omega}} [-\cos\psi^i(t_k) \;\; -\sin\psi^i(t_k) \;\; 1 \;\; 1] \begin{bmatrix} \Delta N(t_k) \\ \Delta E(t_k) \\ B1^i_O(t_k) \\ B2^i_O(t_k) \end{bmatrix} + v^i_O(t_k) \qquad (5.39)$$

where:

ψ^i	bearing from the DR position to the ith Omega transmitter
$B1^i_O$, $B2^i_O$	augmented state variable for the two Markov processes
$v^i_O(t_k)$	white noise

For four Omega stations the measurement equation is:

$$\delta \mathbf{Z}_O(t_k) = \mathbf{D} \begin{bmatrix} \delta z_O^1(t_k) \\ \delta z_O^2(t_k) \\ \delta z_O^3(t_k) \\ \delta z_O^4(t_k) \end{bmatrix} \tag{5.40}$$

The covariance of measurement noise is:

$$\mathbf{D}\, E\left[\mathbf{v}_O(t_j)\ \ \mathbf{v}_O(t_k)^T\right] \mathbf{D}^T = \mathbf{D}\, \mathbf{R}_O(t_k) \mathbf{D}^T \delta_{j,k} \tag{5.41}$$

where

$$\delta_{j,k} = \begin{cases} 1 & j=k \\ 0 & j \neq k \end{cases} \tag{5.42}$$

$$\mathbf{v}_O(t_i) = \left[v_O^1(t_i) \quad v_O^2(t_i) \quad v_O^3(t_i) \quad v_O^4(t_i)\right]^T , \quad i = 1, ..., k \tag{5.43}$$

2) Loran-C:

The Loran-C measurement is much like that of Omega except that the measurement is the arrival time difference of the pulse signals from master-slave pairs of transmitters. After the correction for deterministic propagation errors SPF (Secondary Phase Factor) and ASF (Additional Secondary Phase Factor) for each station, the remaining propagation and measurement errors can be modelled as a first order Markov process and white noise:

$$Z_{M,Si}(t_k) = \frac{\rho_{M,Si}(t_k)}{C_{Loran}} + C_{M,Si}(t_k) + v_{M,Si}(t_k) \tag{5.44}$$

where C_{Loran} is the propagation speed of Loran-C signal, $Z_{M,Si}$, $\rho_{M,Si}$, $C_{M,Si}$ and $v_{M,Si}$ are the arrival time of the signal, range, measurement bias and noise of the master or ith slave stations.

The linearised Loran-C measurement equation is:

$$\delta Z_{M,Si}(t_k) = \frac{1}{C_{Loran}}[-\cos\psi_{M,Si}(t_k) \;\; -\sin\psi_{M,Si}(t_k) \;\; 1]\begin{bmatrix} \Delta N(t_k) \\ \Delta N(t_k) \\ C_{M,Si}(t_k) \end{bmatrix} + v_{M,Si}(t_k) \tag{5.45}$$

For a one master and three slave Loran-C chain, the differencing operator is:

$$\mathbf{D} = \begin{bmatrix} 1 & -1 & 0 & 0 \\ 1 & 0 & -1 & 0 \\ 1 & 0 & 0 & -1 \end{bmatrix} \tag{5.46}$$

The Loran-C measurement equation can be written as:

$$\delta \mathbf{Z}_C(t_k) = \mathbf{D}\begin{bmatrix} \delta z_M(t_k) \\ \delta z_{S1}(t_k) \\ \delta z_{S2}(t_k) \\ \delta z_{S3}(t_k) \end{bmatrix} \tag{5.47}$$

The expression of the covariance of the measurement noise is the same as eqn (5.41).

Besides the hyperbolic mode as indicated in eqn (5.47), Loran-C can be used in the range-range mode, much like the GPS pseudo-range. The Loran-C pseudo-range equation is:

$$Z_i(t_k) = \frac{\rho_i(t_k)}{C_{Loran}} + [b_r(t_k) - b_i(t_k)] + C_i(t_k) + v_i(t_k) \tag{5.48}$$

where b_r and b_i are the clock errors of the receiver and the ith transmitter.

The transmitter clock offset depends on what type of chain time control is used, and whether the transmitter is a "master" or "slave". In any event, if the station (master or slave) is under TOT (Time Of Transmission) control, then offset b_i can be assumed a constant. If the station (slave only) is under SAM (System Area Monitor) control, the offset is not a constant. The benefit of the range-range mode is that more measurements can be obtained, even from transmitters of another Loran-C chain, and the ASF can be estimated and predicted directly from the

measurements. But this mode introduces an additional error source due to clocks. Even integrated with GPS pseudo-range, the positioning accuracy is not high, 300 m to 1400 m (2dRMS) under good geometry of HDOP=2 (Enge & McCullough, 1989).

3) Radar:
Radar range can be expressed as:

$$Z_{Radard}(t_k) = \rho(t_k) + v_R(t_k) \tag{5.49}$$

where:

- ρ range to the radar detected object
- v_R white noise

The linearised radar measurement equation is:

$$\delta Z_{Rd}(t_k) = \begin{bmatrix} -\cos\psi_R(t_k) & -\sin\psi_R(t_k) \end{bmatrix} \begin{bmatrix} \Delta N_R(t_k) \\ \Delta E_R(t_k) \end{bmatrix} + v_R(t_k) \tag{5.50}$$

where:

- ΔE_R, ΔN_R the east and north range differences between radar antenna and object
- ψ_R bearing of the object

The radar azimuth measurement is:

$$Z_{Radarb}(t_k) = tg^{-1}\left[\frac{\Delta E_R(t_k)}{\Delta N_R(t_k)}\right] + v_{Rb}(t_k) \tag{5.51}$$

where v_{Rb} is white noise.

The linearised measurement equation is:

$$\delta Z_{Rb}(t_k) = \frac{1}{\rho}\begin{bmatrix} \cos\psi_R(t_k) & -\sin\psi_R(t_k) \end{bmatrix} \begin{bmatrix} \Delta N_R(t_k) \\ \Delta E_R(t_k) \end{bmatrix} + v_{Rb}(t_k) \tag{5.52}$$

4) GPS:

The pseudo-range measurement in the geographic frame is:

$$\rho(t_k) = \sqrt{[N_S(t_k) - N_c(t_k)]^2 + [E_S(t_k) - E_c(t_k)]^2 + [H_S(t_k) - H_{rc}(t_k)]^2} + \Sigma \text{bias} + v_G(t_k) \tag{5.53}$$

where:

N_s, E_s, H_s coordinates of GPS satellite in the geographic frame

N_c, E_c, H_c DR coordinates of GPS receiver in the geographic frame

v_G white noise

The linearised GPS range measurement is:

$$\delta Z_{GPS}(t_k) = \begin{bmatrix} -\cos\alpha(t_k) & -\cos\beta(t_k) & 1 \end{bmatrix} \begin{bmatrix} \Delta N(t_k) \\ \Delta E(t_k) \\ a_0(t_k) \end{bmatrix} + v_G(t_k) \tag{5.54}$$

where

$$\cos\alpha(t_k) = \frac{N_S(t_k) - N_c(t_k)}{\rho(t_k)}, \quad \cos\beta(t_k) = \frac{E_S(t_k) - E_c(t_k)}{\rho(t_k)}$$

a_0 is the receiver clock bias.

The range-rate measurement in the geographic frame is:

$$Z_D = \frac{[N_S - N_c][\dot{N}_S - \dot{N}_c] + [E_S - E_c][\dot{E}_S - \dot{E}_c] + [H_S - H_c][\dot{H}_s - \dot{H}_c]}{\rho} + \sum \text{bias} + v_D \tag{5.55}$$

where v_D is white noise.

The linearised GPS Doppler measurement equation is:

$$\delta Z_D(t_k) = [\mathbf{H}_1(t_k) \quad \mathbf{H}_2(t_k)]\, \mathbf{X}_D(t_k) + v_D(t_k) \tag{5.56}$$

$$\mathbf{H}_1 = \left[\frac{(\dot{N}_S - \dot{N}_c) + \dot{\rho}\cos\alpha}{\rho} \quad \frac{(\dot{E}_S - \dot{E}_c) + \dot{\rho}\cos\beta}{\rho} \right] \tag{5.57}$$

$$\mathbf{H}^T_2 = \begin{bmatrix} -\cos\alpha\cos H_c - \cos\beta\sin H_c \\ V_L(\cos\alpha\sin H_c - \cos\beta\cos H_c) \\ -\cos\alpha \\ -\cos\beta \\ 1 \end{bmatrix} \tag{5.58}$$

$$\mathbf{X}^T_D = [\Delta N \quad \Delta E \quad \Delta L \quad \Delta G \quad \Delta V_{cN} \quad \Delta V_{cE} \quad a_1] \tag{5.59}$$

where a1 is the receiver clock drift.

5.2.4 Augmented State Vector

The state vector **X**2 depends on the sensors being integrated. It is composed of the augmented state variables, two for each Omega transmitter and one for each Loran-C transmitter, and the receiver clock errors when GPS is also integrated:

$$\mathbf{X}2(t) = \begin{bmatrix} B_{O11} & \text{Omega bias (closely correlated) of transmitter 1} \\ B_{O12} & \text{Omega bias (weakly correlated) of transmitter 1} \\ B_{O21} & \text{Omega bias (closely correlated) of transmitter 2} \\ B_{O22} & \text{Omega bias (weakly correlated) of transmitter 2} \\ B_{C1} & \text{Loran - C bias of transmitter 1} \\ B_{C1} & \text{Loran - C bias of transmitter 2} \\ a_0 & \text{GPS receiver clock bias} \\ a_1 & \text{GPS receiver clock drift} \end{bmatrix} \tag{5.60}$$

and

$$\mathbf{F2} = \begin{bmatrix} -\frac{1}{T_{O11}} & 0 & 0 & 0 & 0 & 0 & 0 & 0 \\ 0 & -\frac{1}{T_{O12}} & 0 & 0 & 0 & 0 & 0 & 0 \\ 0 & 0 & -\frac{1}{T_{O21}} & 0 & 0 & 0 & 0 & 0 \\ 0 & 0 & 0 & -\frac{1}{T_{O22}} & 0 & 0 & 0 & 0 \\ 0 & 0 & 0 & 0 & -\frac{1}{T_{C1}} & 0 & 0 & 0 \\ 0 & 0 & 0 & 0 & 0 & -\frac{1}{T_{C2}} & 0 & 0 \\ 0 & 0 & 0 & 0 & 0 & 0 & 0 & 1 \\ 0 & 0 & 0 & 0 & 0 & 0 & 0 & 0 \end{bmatrix} \qquad (5.61)$$

where T_{Oij}, T_{Ci} are time constants for the Omega and Loran-C biases.

Eqn (5.61) is a constant matrix for two Omega and two Loran stations. The transition matrix is easy to obtained by Laplace transformation. The diagonal terms of the transition matrix for discrete time corresponding to Omega and Loran-C are:

$$e^{-\Delta t/T_{Oij}} \quad , \quad e^{-\Delta t/T_{Ci}} \qquad (5.62)$$

The transition matrix for the GPS part is:

$$\begin{bmatrix} 1 & \Delta t \\ 0 & 1 \end{bmatrix} \qquad (5.63)$$

the other elements of **F2** are zero, and

$$\mathbf{W2} \sim N(0, \mathbf{Q}_2)$$

where $\mathbf{Q}_2$ is a positive-definite diagonal matrix.

5.2.5 Some Comments

1) Navigation systems such as Omega and Loran-C are under the control of different authorities and operate in different reference systems. For INNS the transformation between local reference systems to a single computational system is essential and can be carried out in the DR block. The choice of the computational system for the specific task is essentially one of convenience. For example, the WGS-84 system may be an obvious choice from the point of view of the dominant role of GPS navigation. But in practice, nearly all marine navigation procedures are carried out on or based on the nautical chart (the digital nautical chart in future), hence the local reference system of the nautical chart may be preferable for practical applications. Here the geographic frame is selected to simplify computations by avoiding the time-varying parameters of latitude and longitude and the correlation of the system driving noise, and for the convenience of DR computation. The same reasoning applies to the time reference transformation because GPS uses GPS Time, and Omega and Loran-C are based on UTC.

2) When GPS measurements are to be integrated, more sophisticated model for the GPS measurement biases can be augmented to the system model, or the DGPS mode can be used. When using GPS carrier phase measurement, cycle slips can be detected more effectively because the effects of body's dynamics on the phase measurement are isolated by the DR.

3) The azimuth ψ of Omega and Loran-C measurement is the geodesic angle between meridian and the geodesic. For a range of 200 nm, the difference between the true spheroidal and the spherical angles is less than 1 second of arc. Usually the position of DR is very close to the true position, so for the linearisation of Loran-C measurement, the use of spherical angle instead of geodesic angle is a reasonable simplification, (even using plane angle corrected for spherical excess by the "Legendre Rule", Clark (1968), and the error introduced is much less than the signal propagation error). For Omega, the geodesic angle can be obtained from the Bessel equation and in most cases second order approximation is good enough.

4) The geometrical strength of the radio positioning aids of the INNS can be determined by HDOP (Horizontal Dilution Of Precision) :

$$HDOP = \sqrt{\text{trace}(\mathbf{A}^T\mathbf{A})^{-1}} \qquad (5.65)$$

A consists of the terms corresponding to the two horizontal position errors ΔN, ΔE of the GPS, Omega, Loran-C and radar observation matrices.

5) The quality control of INNS can be simply performed using eqn (5.15), because the manoeuvre of vessel is now isolated and the statistics of eqn (5.15) can be used for the detection of measurement outliers and the failure of devices. There are two thresholds: the error tolerance and the time tolerance. If the residual of the measurement is larger than the error tolerance, then the measurement is rejected. If the time of bad measurement occurrence for a certain device is larger than the time tolerance, then device failure is declared.

6) The model is developed in two dimensions under the assumption that the vessel's vertical displacement (precisely, the mean vertical displacement) is zero. However expansion to three dimensions is straightforward.

7) The model is different from the AN\SYN-501 (MINS-B II) system which is also a DR integration with radio navigation systems used by Canada Navy (McMillan, 1988). Firstly MINS-B II is actually an open-loop implementation. Futhermore, the gyrocompass error, which is assumed can be absorbed by the ocean current model, is not included in the state vector for computation simplification. Actually the gyrocompass error is one of the main error sources of the DR and the effect and dynamic model of the gyrocompass error should be treated differently from that of ocean current. The gyrocompass error is the vessel's attitude error and causes an equivalent course error. The correlation time of ocean current, depending on the type of the current (such as tide current or constant current), is different from that of a gyrocompass. Furthermore, the north and east velocity errors ΔV_{NG}, ΔV_{EG} caused by the gyrocompass are:

$$\Delta V_{NG} = - V_L \sin(H_c)\, \Delta G \qquad (5.65)$$

$$\Delta V_{EG} = V_L \cos(H_c)\, \Delta G \qquad (5.66)$$

ΔV_{NG}, ΔV_{EG} are heading-dependent and the current errors are not. Assuming eqns (5.65) and (5.66) are part of the ocean current errors, then the variances and correlation times of their north and east current components would also be heading-dependent.

8) During a short transient period of the filter, the filter output and the DR output is different for the closed-loop system. When the filter is in steady-state, both outputs of the filter and DR are nearly the same and the filter is now operating as a system monitor. The increase in computational workload for the closed-loop implementation is trivial compared to that of the open-loop implementation.

5.3 INS/GPS Integration

All practical INS are aided by some external navigation systems to perform the INS calibrations. The calibrations are carried out using the position, velocity, attitude information, or their combinations obtained from the external navigation systems. Especially by using range and range rate measurements of GPS it can be realized position and velocity calibrations at the same time.

5.3.1 Closed-Loop INS/GPS Integration

A closed-loop INS/GPS integration based on a centralized filter is illustrated in Fig.5.8, in which the INS is calibrated by the position and velocity obtained from the GPS range and Doppler measurements $\mathbf{Z}_p$ and $\mathbf{Z}_d$, and a negative state feedback $-\mathbf{g}\hat{\mathbf{X}}$ forms a closed-loop control for the INS, see eqn (A.3.8.20).

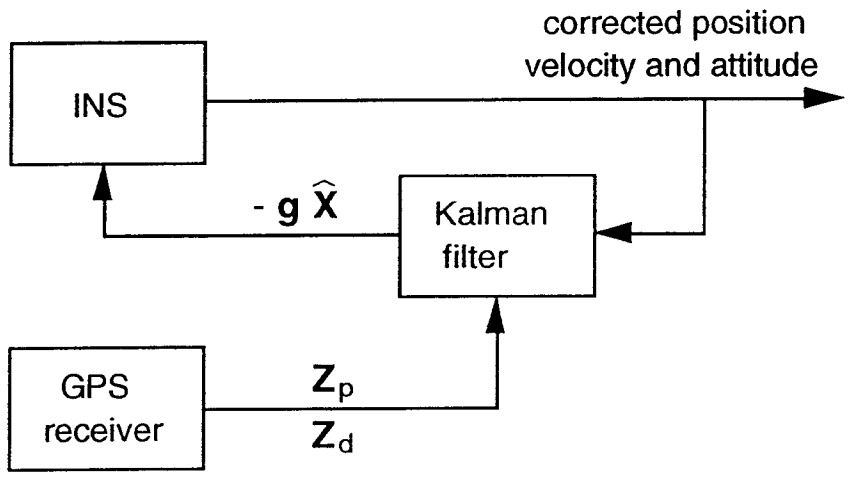

Figure 5.8. Closed-loop INS/GPS integration.

The INS itself follows the high frequency motion of the body quite accurately, and there is no need to model those dynamics explicitly in the filter. Instead, the dynamics upon which the filter is based is a set of inertial system error equations which depend on the INS mechanization, see eqns (A.3.3.2) to (A.3.3.4), (A.3.4.11) to (A.3.4.13) and (A.3.5.3) to (A.3.5.4). These are relatively well developed, well behaved, low frequency and adequately represented as linear. Because the filter is out of the INS loop and is based on linear dynamics of low frequency, its sample period can be made as long as a half minute or longer, thereby achieving practicality with respect to the amount of computer time required. The filter operates as a low-pass filter on the GPS and the high frequency noise of the GPS measurements is suppressed. At the same time, the low frequency noise of the INS is attenuated. The Kalman filter generates estimates of the errors in INS, and these are fed back into the INS to calibrate them. In this way the inertial errors are not allowed to grow unchecked and the adequacy of a linear model is enhanced.

There is a potential to feedback the estimated position and velocity into the GPS receiver which is not shown in the Fig.5.8. Although the tracking loop bandwidth of the receiver can be reduced by the direct state feedback, it is a positive feedback and the loop gain has to be controlled to be small, otherwise the INS-to-GPS-to-INS loop will become instable.

A closed-loop north-directed INS/GPS integration based on a centralized filter algorithm is presented in Appendix 3.8. More details concerning INS/GPS integration can be found in such texts as Cox, 1980; West-Vukovich et al.,1988; Eissfeller & Spietz, 1989; Henkel, 1992, Schwarz & Wei, 1994, Schwarz & Zhang, 1994.

CHAPTER 6

NAVIGATION MODELS

The navigation model, consisting of a dynamic model and an observation model, is the mathematical description of a body's motion in both the state space and the measurement space. Although the navigation model is generally well established and has been used in various implementations, for many years its dynamic characteristics and behaviour were rarely described in detail. As an example of a dynamic system, from the navigation point of view, the important characteristics of the navigation model that need to be understood are its stability, observability and controllability. Model stability is concerned with the effect of random or deterministic inputs on the model outputs. Model observability is concerned with the impact of varying model states upon the system output, and controllability is related to the effect of input upon states of the model. In the case of navigation filters, if the navigation model is not observable, the filter estimation errors along certain directions of the state space would not decrease, regardless of how many measurements are processed. For a Kalman filter if the navigation model is completely observable and controllable, this is sufficient condition to ensure the filter is stable (Maybeck,1979).

In this chapter the navigation models for GPS navigation, for both the point and differential positioning modes, are discussed. Various bias models: random constant, random walk and first order Markov process, which can be used for the improvement of the navigation filters are also discussed.

6.1 Navigation Models

Filtering in the time domain requires a navigation model consisting of the body's dynamic model and the observation model, and is expressed in state space and measurement space.

6.1.1 The Dynamic Model

Body's state: position vector **r**(t), velocity vector **v**(t) and acceleration vector **a**(t), are generally described in a R^3 Euclidean space, and is decomposed to

orthogonal coordinate components. Each coordinate component of the R^3 space can comprise of a state space of one (position), two (position and velocity) or three (position, velocity and acceleration) dimensions, or higher, depending on the body's dynamics. The state space is an orthogonal system spanned by the state variable and the state variables are linearly independent. The state vector used in GPS navigation usually comprises the correction components representing the deviation of the true trajectory from a reference (or nominal) trajectory, and obtained as a results of the linearization of the system. The correction (or the relative trajectory) to the reference trajectory in this thesis is defined as:

$$\Delta\mathbf{r}(t) = \mathbf{r}(t) - \mathbf{r}_0(t) = [x(t),\ y(t),\ z(t)]^T \tag{6.1}$$

$$\Delta\mathbf{v}(t) = \mathbf{v}(t) - \mathbf{v}_0(t) = \frac{d[\Delta\mathbf{r}(t)]}{dt} = \left[\frac{dx(t)}{dt},\ \frac{dy(t)}{dt},\ \frac{dz(t)}{dt}\right]^T \tag{6.2}$$

$$\Delta\mathbf{a}(t) = \mathbf{a}(t) - \mathbf{a}_0(t) = \frac{d^2[\Delta\mathbf{r}(t)]}{dt^2} = \left[\frac{d^2x(t)}{dt^2},\ \frac{d^2y(t)}{dt^2},\ \frac{d^2z(t)}{dt^2}\right]^T \tag{6.3}$$

where $\mathbf{r}_0$, $\mathbf{v}_0$, $\mathbf{a}_0$ are the reference (apriori) values of the body's state.

The reference trajectory should be sufficiently accurate so that the high order terms of the system linearization can either be neglected, or modelled as random noise. Under that condition the choice of the reference trajectory is arbitrary, it may be a: planned trajectory, the output of other navigation sensors, or derived from the output of GPS navigation filter. If the reference trajectory is assumed to be deterministic (for example, planned trajectory or derived from polynomial fitting), the relative trajectory and the true trajectory have the same stochastic properties, apart from their mean values. For a stochastic reference trajectory (such as the output of dead reckoning by gyrocompass and log or an inertial system), the relative trajectory is affected by low-frequency noise, and a diverging relative trajectory can result if the errors of the inertial sensors are not corrected. In any case, stationary processes $\Delta\mathbf{r}$, $\Delta\mathbf{v}$, $\Delta\mathbf{a}$ are preferable because a simple dynamic model and a long sampling interval can be used.

The following models are expressed in terms of the relative trajectory and $\Delta\mathbf{r}$, $\Delta\mathbf{v}$, $\Delta\mathbf{a}$ are simply referred to as position, velocity and acceleration vectors respectively.

6.1.1.1 Third Order System (state space of three dimensions)

$$\Delta\dddot{\mathbf{r}}(t) + \alpha\Delta\ddot{\mathbf{r}}(t) = \omega_j(t) \tag{6.4}$$

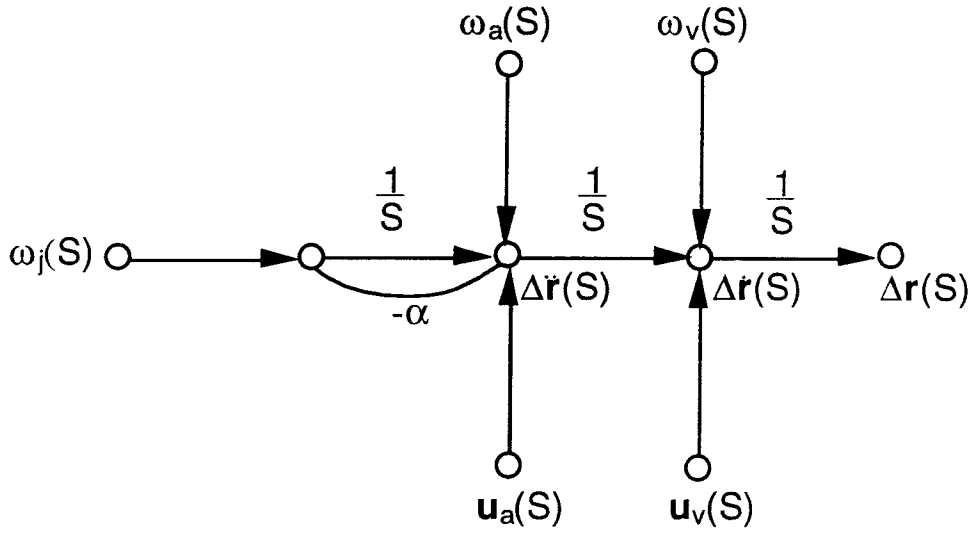

Figure 6.1. Signal flow chart of third order system.

where:

ω_j, ω_a, ω_v	3 x 1 white noise vector
$\mathbf{u}_a$, $\mathbf{u}_v$	3 x 1 bias vector
α	3 x 3 diagonal matrix, the diagonal elements $[1/t_{xa}, 1/t_{ya}, 1/t_{za}]$ are the inverse of acceleration time constants
S	the Laplace operator

For the x component the state equation is:

$$\begin{bmatrix}\dot{x}(t)\\ \ddot{x}(t)\\ \dddot{x}(t)\end{bmatrix}=\begin{bmatrix}0 & 1 & 0\\ 0 & 0 & 1\\ 0 & 0 & -1/t_{xa}\end{bmatrix}\begin{bmatrix}x(t)\\ \dot{x}(t)\\ \ddot{x}(t)\end{bmatrix}+\begin{bmatrix}1 & 0\\ 0 & 1\\ 0 & 0\end{bmatrix}\begin{bmatrix}u_{vx}(t)\\ u_{ax}(t)\end{bmatrix}$$

$$+\begin{bmatrix}1 & 0 & 0\\ 0 & 1 & 0\\ 0 & 0 & 1\end{bmatrix}\begin{bmatrix}\omega_{x1}(t)\\ \omega_{x2}(t)\\ \omega_{x3}(t)\end{bmatrix} \qquad (6.5)$$

$$E\left([\omega_{x1}(t),\ \omega_{x2}(t),\ \omega_{x3}(t)]^T\ ,\ [\omega_{x1}(t_1),\ \omega_{x2}(t_1),\ \omega_{x3}(t_1)]\right)$$

$$=\begin{bmatrix}q_{x11} & 0 & 0\\ 0 & q_{x22} & 0\\ 0 & 0 & q_{x33}\end{bmatrix}\delta(t-t_1) \qquad (6.6)$$

The discrete time solution of eqn (6.5) is:

$$\begin{bmatrix}x(t_{k+1})\\ \dot{x}(t_{k+1})\\ \ddot{x}(t_{k+1})\end{bmatrix}=\begin{bmatrix}1 & \Delta K & t_{xa}^2e^{-\Delta K/t_{xa}}+t_{xa}\Delta K-t_{xa}^2\\ 0 & 1 & t_{xa}(1-e^{-\Delta K/t_{xa}})\\ 0 & 0 & e^{-\Delta K/t_{xa}}\end{bmatrix}\begin{bmatrix}x(t_k)\\ \dot{x}(t_k)\\ \ddot{x}(t_k)\end{bmatrix}$$

$$+\begin{bmatrix}U_{x1}(t_k)\\ U_{x2}(t_k)\\ U_{x3}(t_k)\end{bmatrix}+\begin{bmatrix}W_{x1}(t_k)\\ W_{x2}(t_k)\\ W_{x3}(t_k)\end{bmatrix} \qquad (6.7)$$

where Δk is the sampling interval.

$$\mathbf{Q}_x(t_k)=E\left\{[W_{x1}(t_k),\ W_{x2}(t_k),\ W_{x3}(t_k)]^T,[W_{x1}(t_k),\ W_{x2}(t_k),\ W_{x3}(t_k)]\right\}$$

$$=\begin{bmatrix}Q_{x11}(t_k) & Q_{x12}(t_k) & Q_{x13}(t_k)\\ Q_{x21}(t_k) & Q_{x22}(t_k) & Q_{x23}(t_k)\\ Q_{x31}(t_k) & Q_{x32}(t_k) & Q_{x33}(t_k)\end{bmatrix} \qquad (6.8)$$

where

$$Q_{x11}(t_k)=q_{x11}\Delta K+q_{x22}\,\Delta K^3/3+q_{x33}C_{11}$$

$$Q_{x12}(t_k)=Q_{x21}(t_k)=q_{x22}\,\Delta K^2/2+q_{x33}C_{12}$$

$$Q_{x13}(t_k) = Q_{x31}(t_k) = q_{x33}\left[\frac{t_{xa}^3}{2}(1 - e^{-2\Delta K/t_{xa}}) - \Delta K t_{xa}^2 e^{-\Delta K/t_{xa}}\right]$$

$$Q_{x22}(t_k) = q_{x22}\Delta K + q_{x33}t_{xa}^2(\Delta K - 3t_{xa}/2 + 2t_{xa}e^{-\Delta K/t_{xa}} - t_{xa}e^{-2\Delta K/t_{xa}}/2)$$

$$Q_{x23}(t_k) = Q_{x32}(t_k) = q_{x33}t_{xa}^2(1/2 - e^{-\Delta K/t_{xa}} + e^{-2\Delta K/t_{xa}}/2)$$

$$Q_{x33}(t_k) = \frac{t_{xa}}{2} q_{x33}(1 - e^{-2\Delta K/t_{xa}})$$

$$C_{11} = \frac{t_{xa}^5}{2}\left[1+2t_{xa}^{-1}\Delta K-2t_{xa}^{-2}\Delta K^2+2t_{xa}^{-3}\Delta K^3/3-4t_{xa}^{-1}\Delta K e^{-\Delta K/t_{xa}}-e^{-2\Delta K/t_{xa}}\right]$$

$$C_{12} = \frac{t_{xa}^4}{2}\left[1-2t_{xa}^{-1}\Delta K+t_{xa}^{-2}\Delta K^2+2t_{xa}^{-1}\Delta K e^{-\Delta K/t_{xa}}-2e^{-\Delta K/t_{xa}}+e^{-2\Delta K/t_{xa}}\right]$$

and the system bias and noise U and W are the convolutions of the transition matrix and the system input.

The state equations and covariances of the y and z components take the same form as those of the x component.

When α is a zero matrix, the third order system is usually referred to as a constant acceleration model, and its state equation for the x component is:

$$\begin{bmatrix}\dot{x}(t)\\ \ddot{x}(t)\\ \dddot{x}(t)\end{bmatrix} = \begin{bmatrix}0 & 1 & 0\\ 0 & 0 & 1\\ 0 & 0 & 0\end{bmatrix}\begin{bmatrix}x(t)\\ \dot{x}(t)\\ \ddot{x}(t)\end{bmatrix} + \begin{bmatrix}1 & 0\\ 0 & 1\\ 0 & 0\end{bmatrix}\begin{bmatrix}u_{vx}(t)\\ u_{ax}(t)\end{bmatrix} + \begin{bmatrix}1 & 0 & 0\\ 0 & 1 & 0\\ 0 & 0 & 1\end{bmatrix}\begin{bmatrix}\omega_{x1}(t)\\ \omega_{x2}(t)\\ \omega_{x3}(t)\end{bmatrix} \quad (6.9)$$

The discrete time solution is:

$$\begin{bmatrix}x(t_{k+1})\\ \dot{x}(t_{k+1})\\ \ddot{x}(t_{k+1})\end{bmatrix} = \begin{bmatrix}1 & \Delta K & \Delta K^2/2\\ 0 & 1 & \Delta K\\ 0 & 0 & 1\end{bmatrix}\begin{bmatrix}x(t_k)\\ \dot{x}(t_k)\\ \ddot{x}(t_k)\end{bmatrix} + \begin{bmatrix}U_{x1}(t_k)\\ U_{x2}(t_k)\\ U_{x3}(t_k)\end{bmatrix} + \begin{bmatrix}W_{x1}(t_k)\\ W_{x2}(t_k)\\ W_{x3}(t_k)\end{bmatrix} \quad (6.10)$$

where

$$Q_{x11}(t_k) = q_{x11}\Delta K + q_{x22}\Delta K^2/2 + q_{x33}\Delta K^5/20$$

$$Q_{x12}(t_k) = Q_{x21}(t_k) = q_{x22}\Delta K^2/2 + q_{x33}\Delta K^4/8$$

$$Q_{x13}(t_k) = Q_{x31}(t_k) = q_{x33}\Delta K^3/6$$

$$Q_{x22}(t_k) = q_{x22}\Delta K + q_{x33}\Delta K^3/3$$

$$Q_{x23}(t_k) = Q_{x32}(t_k) = q_{x33}\Delta K^2/2$$

$$Q_{x33}(t_k) = q_{x33}\Delta K$$

6.1.1.2. Second Order System (state space of two dimensions)

$$\Delta\dot{\mathbf{r}}(t) + \beta\Delta\dot{\mathbf{r}}(t) = \omega_a(t) \qquad (6.11)$$

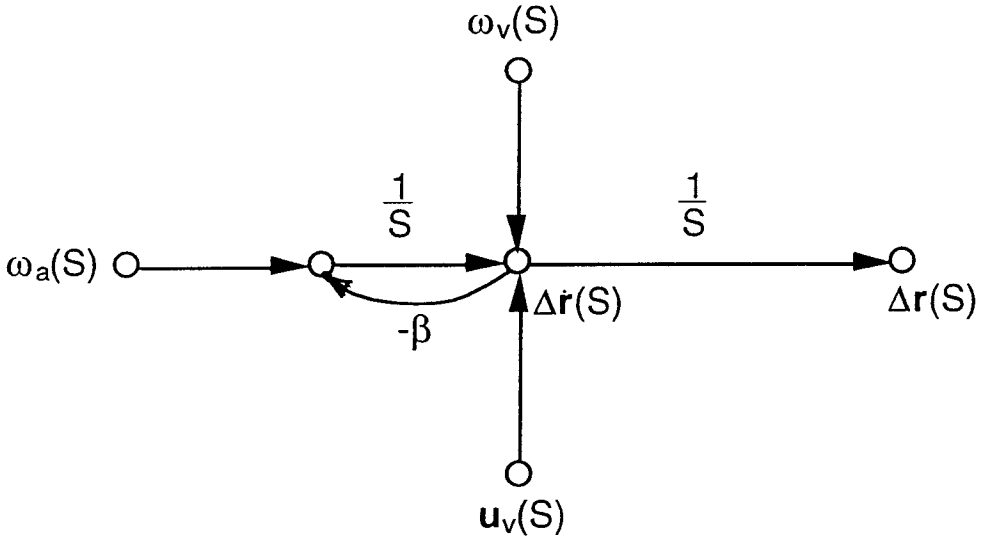

Figure 6.2. Signal flow chart of second order system.

β is a 3 x 3 diagonal matrix, the diagonal elements $[1/t_{xv}, 1/t_{yv}, 1/t_{zv}]$ are the inverse of velocity time constants. The other components are as previously defined.

The state equation of the x component is:

$$\begin{bmatrix}\dot{x}(t)\\ \ddot{x}(t)\end{bmatrix}=\begin{bmatrix}0 & 1\\ 0 & -1/t_{xv}\end{bmatrix}\begin{bmatrix}x(t)\\ \dot{x}(t)\end{bmatrix}+\begin{bmatrix}1\\ 0\end{bmatrix}u_{vx}+\begin{bmatrix}1 & 0\\ 0 & 1\end{bmatrix}\begin{bmatrix}\omega_{x1}(t)\\ \omega_{x2}(t)\end{bmatrix} \tag{6.12}$$

and

$$E\left([\omega_{x1}(t),\ \omega_{x2}(t)]^T\ ,\ [\omega_{x1}(t_1),\ \omega_{x2}(t_1)]\right) = \begin{bmatrix}q_{x11} & 0\\ 0 & q_{x22}\end{bmatrix}\delta(t-t_1) \tag{6.13}$$

The system model in discrete time is:

$$\begin{bmatrix}x(t_{k+1})\\ \dot{x}(t_{k+1})\end{bmatrix}=\begin{bmatrix}1 & t_{xv}(1-e^{-\Delta K/t_{xv}})\\ 0 & e^{-\Delta K/t_{xv}}\end{bmatrix}\begin{bmatrix}x(t_k)\\ \dot{x}(t_k)\end{bmatrix}+\begin{bmatrix}U_{x1}(t_k)\\ U_{x2}(t_k)\end{bmatrix}+\begin{bmatrix}W_{x1}(t_k)\\ W_{x2}(t_k)\end{bmatrix} \tag{6.14}$$

$$\mathbf{Q}_x(t_k) = E\left\{[W_{x1}(t_k),\ W_{x2}(t_k)]^T,\ [W_{x1}(t_k),\ W_{x2}(t_k)]\right\} = \begin{bmatrix}Q_{x11}(t_k) & Q_{x12}(t_k)\\ Q_{x21}(t_k) & Q_{x22}(t_k)\end{bmatrix} \tag{6.15}$$

where

$$Q_{x11}(t_k) = q_{x11}\Delta K + q_{x22}t_{xv}^2(\Delta K - 3t_{xv}/2 + 2t_{xv}e^{-\Delta K/t_{xv}} - t_{xv}e^{-2\Delta K/t_{xv}}/2)$$

$$Q_{x12}(t_k) = Q_{x21}(t_k) = q_{x22}t_{xv}^2(1/2 - e^{-\Delta K/t_{xv}} + e^{-2\Delta K/t_{xv}}/2)$$

$$Q_{x22}(t_k) = q_{x22}t_{xv}\ (1 - e^{-2\Delta K/t_{xv}})/2$$

When β is a zero matrix, the second order system is referred to as a constant velocity model, and its state equation for the x component is:

$$\begin{bmatrix}\dot{x}(t)\\ \ddot{x}(t)\end{bmatrix}=\begin{bmatrix}0 & 1\\ 0 & 0\end{bmatrix}\begin{bmatrix}x(t)\\ \dot{x}(t)\end{bmatrix}+\begin{bmatrix}1\\ 0\end{bmatrix}u_{vx}+\begin{bmatrix}1 & 0\\ 0 & 1\end{bmatrix}\begin{bmatrix}\omega_{x1}(t)\\ \omega_{x2}(t)\end{bmatrix} \tag{6.16}$$

The discrete time solution is:

$$\begin{bmatrix} x(t_{k+1}) \\ \dot{x}(t_{k+1}) \end{bmatrix} = \begin{bmatrix} 1 & \Delta K \\ 0 & 1 \end{bmatrix} \begin{bmatrix} x(t_k) \\ \dot{x}(t_k) \end{bmatrix} + \begin{bmatrix} U_{x1}(t_k) \\ U_{x2}(t_k) \end{bmatrix} + \begin{bmatrix} W_{x1}(t_k) \\ W_{x2}(t_k) \end{bmatrix} \tag{6.17}$$

where

$$Q_{x11}(t_k) = q_{x11}\Delta K + q_{x22}\frac{\Delta K^3}{3}$$

$$Q_{x12}(t_k) = Q_{x21}(t_k) = q_{x22}\frac{\Delta K^2}{2}$$

$$Q_{x22}(t_k) = q_{x22}\Delta K$$

6.1.1.3. First Order System (state space of one dimension)

$$\Delta\dot{\mathbf{r}}(t) + \gamma\Delta\mathbf{r}(t) = \omega_v(t) \tag{6.18}$$

γ is a 3 x 3 diagonal matrix, the diagonal elements $[1/t_{xr}, 1/t_{yr}, 1/t_{zr}]$ are the inverse of the position time constants.

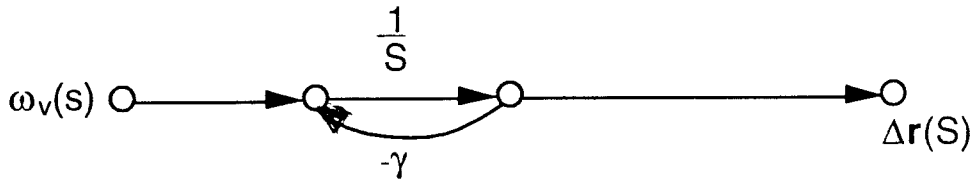

Figure 6.3. Signal flow chart of first order system.

When $\omega_v(t) = 0$, $\gamma = 0$ the first order system degenerates to a static model.
The first order model is a first order Markov process and is often used for attitude determination by GPS when the baseline length is known.

The state equation of the x component for the static model is:

$$\dot{x}(t) = 0 \tag{6.19}$$

6.1.1.4 Stability

The above models are linear, time-invariant systems and the stability of these models can be determined by the system pole position, node-by-node for each integral branch from left to right of the system signal flow charts (Fig.6.1, 6.2, 6.3). The stability referred to here is defined as the zero-input asymptotic stability, which is equivalent to the BIBO (Bounded-Input/Bounded-Output) stability for linear, time-invariant system (Maybeck, 1979), used to investigate the effects of the initial uncertainty of the system state. All system inputs are assumed to have finite covariance (finite power). A class of stable states is a linear sub-space of the state space and a system is stable if all its states are stable. For a stable state the effect of the state initial uncertainty is decreasing with time, in contrast to an unstable state in which the uncertainty of the state increases with time, and for marginally stable state the initial uncertainty remains unchanged with time at system steady state.

In the case of the third order system model (Fig.6.1) there is a first order pole $-\alpha$ at the real axis of the left half-complex plane (S plane) for the first branch hence the acceleration is stable. The second branch which consists of the two integral branches before the velocity node has two first order poles, one of which is $-\alpha$ and the other is at the zero point of the complex plane, hence the velocity is marginally stable. Similarly for the position, there is a second order pole which is at the zero point of the complex plane and position is therefore unstable. For the constant acceleration model, the acceleration is marginally stable because $-\alpha = 0$, and velocity and position are both unstable.

Aa a result of a similar analysis to that of the third order system, the velocity is stable and position is marginally stable for the second order system, and the velocity is marginally stable and the position is unstable for the constant velocity model.

In the case of the first order system, the position is stable and the static model the position is marginally stable.

The system stability under white noise input can be seen from the diagonal terms of the covariance matrices of eqns (6.8) and (6.15). Except for the acceleration of the third order system, the velocity of the second order system and the position of the first order system, the rest of the states are unstable. All states of constant acceleration and constant velocity models are unstable.

6.2 Observation Model

The observation (measurement) space is a mapping of the completely observable sub-space of the state space. The linearized observation equation can be expressed:

$$\mathbf{Z}(t_k) = \mathbf{H}_1(t_k)\mathbf{X}_1(t_k) + \mathbf{n}(t_k) + \mathbf{V}(t_k) \tag{6.20}$$

where **V** is the measurement noise and **n** is the bias, which can be modelled by a shaping filter driven by white noise $\omega_A(t)$ as:

$$\dot{\mathbf{X}}_A(t) = \mathbf{F}_A(t)\mathbf{X}_A(t) + \mathbf{B}_A(t)\omega_A(t) \tag{6.21}$$

$$\mathbf{n}(t) = \mathbf{H}_A(t)\mathbf{X}_A(t) \tag{6.22}$$

In discrete time eqn (6.21) can be expressed as :

$$\mathbf{X}_A(t_{k+1}) = \Phi_A(t_{k+1}, t_k)\mathbf{X}_A(t_k) + \mathbf{W}_A(t_k) \tag{6.23}$$

The observation equation can now be written as:

$$\begin{aligned}\mathbf{Z}(t_k) &= \mathbf{H}(t_k)\mathbf{X}(t_k) + \mathbf{V}(t_k) \\ &= [\mathbf{H}_1(t_k), \mathbf{H}_A(t_k)]\begin{bmatrix}\mathbf{X}_1(t_k) \\ \mathbf{X}_A(t_k)\end{bmatrix} + \mathbf{V}(t_k)\end{aligned} \tag{6.24}$$

where

$$E[\mathbf{V}(t_k)] = 0 \tag{6.25}$$

$$E[\mathbf{V}(t_k)\ ,\ \mathbf{V}^T(t_J)] = \mathbf{R}(t_k)\ \delta_{kJ} \tag{6.26}$$

where δ_{KJ} is the Kronecker delta function, **R** is a positive-definite matrix, and the norm of **R** satisfies $0 < |\mathbf{R}| < \infty$.

6.2.1 Pseudo-Range Observation

The observation matrix $\mathbf{H}_1$ can be obtained from the Jacobian matrix $\mathbf{J}$:

$$\mathbf{J}(t_k) = \begin{bmatrix} \frac{\partial P_1(t)}{\partial \mathbf{r}^T(t)}, \frac{\partial P_1(t)}{\partial \mathbf{v}^T(t)}, \frac{\partial P_1(t)}{\partial \mathbf{a}^T(t)} \\ \frac{\partial P_2(t)}{\partial \mathbf{r}^T(t)}, \frac{\partial P_2(t)}{\partial \mathbf{v}^T(t)}, \frac{\partial P_2(t)}{\partial \mathbf{a}^T(t)} \\ \cdots\cdots\cdots\cdots\cdots\cdots\cdots\cdots\cdots\cdots \\ \frac{\partial P_n(t)}{\partial \mathbf{r}^T(t)}, \frac{\partial P_n(t)}{\partial \mathbf{v}^T(t)}, \frac{\partial P_n(t)}{\partial \mathbf{a}^T(t)} \end{bmatrix}_{t=t_k} \tag{6.27}$$

where

$$\frac{\partial P_i(t)}{\partial \mathbf{r}^T(t)} = \left[\frac{-[r_{six}(t) - r_{rx}(t)]}{P_i(t)}, \frac{-[r_{siy}(t) - r_{ry}(t)]}{P_i(t)}, \frac{-[r_{siz}(t) - r_{rz}(t)]}{P_i(t)} \right]$$

$$= [-\cos\alpha_i \quad -\cos\beta_i \quad -\cos\gamma_i] \tag{6.28}$$

where $\cos\alpha_i$, $\cos\beta_i$ and $\cos\gamma_i$ are the direction cosines for the ith satellite. r_{six}, r_{siy}, r_{siz} are the ith satellite coordinates and r_{rx}, r_{ry}, r_{rz} the receiver antenna coordinates, and P_i is the pseudo-range measurement from the ith satellite.

$$\frac{\partial P_i(t)}{\partial \mathbf{v}^T(t)} = \frac{\partial P_i(t)}{\partial \mathbf{a}^T(t)} = [0 \quad 0 \quad 0] \tag{6.29}$$

6.2.2 Range-Rate Observation

The observation matrix $\mathbf{H}_1$ can be obtained from the Jacobian matrix $\dot{\mathbf{J}}$:

$$\dot{\mathbf{J}}(t_k) = \begin{bmatrix} \frac{\partial \dot{\mathbf{P}}_1(t)}{\partial \mathbf{r}^T(t)}, \frac{\partial \dot{\mathbf{P}}_1(t)}{\partial \mathbf{v}^T(t)}, \frac{\partial \dot{\mathbf{P}}_1(t)}{\partial \mathbf{a}^T(t)} \\ \frac{\partial \dot{\mathbf{P}}_2(t)}{\partial \mathbf{r}^T(t)}, \frac{\partial \dot{\mathbf{P}}_2(t)}{\partial \mathbf{v}^T(t)}, \frac{\partial \dot{\mathbf{P}}_2(t)}{\partial \mathbf{a}^T(t)} \\ \cdots\cdots\cdots\cdots\cdots\cdots\cdots\cdots \\ \frac{\partial \dot{\mathbf{P}}_n(t)}{\partial \mathbf{r}^T(t)}, \frac{\partial \dot{\mathbf{P}}_n(t)}{\partial \mathbf{v}^T(t)}, \frac{\partial \dot{\mathbf{P}}_n(t)}{\partial \mathbf{a}^T(t)} \end{bmatrix}_{t=t_k} \tag{6.30}$$

where

$$\dot{P}_i(t) = \frac{dP_i(t)}{dt} \tag{6.31}$$

and

$$\frac{\partial \dot{P}_i(t)}{\partial \mathbf{r}^T(t)} = \left[\frac{\dot{r}_{rx}(t)+\dot{P}_i(t)\cos\alpha}{P_i(t)}, \frac{\dot{r}_{ry}(t)+\dot{P}_i(t)\cos\beta}{P_i(t)}, \frac{\dot{r}_{rz}(t)+\dot{P}_i(t)\cos\gamma}{P_i(t)} \right] \tag{6.32}$$

$$\frac{\partial \dot{P}_i(t)}{\partial \mathbf{v}^T(t)} = [-\cos\alpha \quad -\cos\beta \quad -\cos\gamma] \tag{6.33}$$

$$\frac{\partial \dot{P}_i(t)}{\partial \mathbf{a}^T(t)} = [0 \quad 0 \quad 0] \tag{6.34}$$

The form of the augmented state vector for a GPS observation depends on how the measurement biases **n** are dealt with. The popular bias models are random constant, Markov process and random walk, or the ARMA model.

6.3 General Dynamic Model

The dynamic models of a body can now be expressed in state space as:

$$\dot{\mathbf{X}}_1(t) = \mathbf{F}_1\mathbf{X}_1(t) + \mathbf{G}_1(t)\mathbf{u}_1(t) + \mathbf{B}_1(t)\omega_1(t) \tag{6.35}$$

where:

$\mathbf{X}_1$	body's state
$\mathbf{F}_1$	system matrix
$\mathbf{u}_1$, ω_1	systematic error and dynamic noise
$\mathbf{G}_1$, $\mathbf{B}_1$	input coupling matrices and for most navigation applications they are constant and consisted of 1s and 0s

The systematic error or bias, such as sea or air current, can either be compensated as a deterministic function and have hence no influence on the stochastic estimation of the vessel's state, or they can be modelled as a shaping filter, which is also a linear time-invariant system, and augmented to the system state. The general dynamic model can be written as:

$$\dot{\mathbf{X}}(t) = \mathbf{F}\mathbf{X}(t) + \mathbf{B}(t)\omega(t) \tag{6.36}$$

where:

$\mathbf{X}$	n x1 state vector
$\mathbf{F}$	n x n constant system matrix
$\mathbf{B}$	n x p input coupling matrix
ω	p x 1 white noise

and

$$E[\omega(t),\ \omega^T(t_1)] = \mathbf{q}(t)\ \delta(t - t_1) \tag{6.37}$$

where $\mathbf{q}$ is the power spectrum density matrix of the dynamic noise.

The discrete time solution of eqn (6.36) is :

$$\mathbf{X}(t_{K+1}) = \Phi(t_{K+1},\ t_K)\mathbf{X}(t_K) + \mathbf{W}(t_K) \tag{6.38}$$

For linear, time-invariant systems, the transition matrix Φ can be considered to be in the form of a matrix exponential. A convolution form of $\mathbf{W}(t_k)$ is:

$$\mathbf{W}(t_k) = \int_{t_k}^{t_{k+1}} \Phi(t_{k+1},\ \tau)\mathbf{B}(\tau)\omega(\tau)d\tau \tag{6.39}$$

Eqn (6.39) is the less rigorous form of a stochastic integral under the assumption that the differentiation of a Wiener process is a Gaussian white noise. If an assumption can be made that $\omega(t)$ is constant during the integration interval, the Gaussian requirement for $\omega(t)$ can be dropped, and eqn (6.39) becomes a Riemann integral:

$$\mathbf{W}(t_k) = \int_{t_k}^{t_{k+1}} \Phi(t_{k+1}, \tau)\mathbf{B}(\tau)d\tau\omega(t_k) \tag{6.40}$$

and

$$E\left[\mathbf{W}(t_k), \mathbf{W}^T(t_J)\right] = \mathbf{Q}(t_k)\ \delta_{kj} \tag{6.41}$$

F and Φ are in the forms:

$$\mathbf{F} = \begin{bmatrix} \mathbf{F}_x & 0 & 0 & 0 \\ 0 & \mathbf{F}_y & 0 & 0 \\ 0 & 0 & \mathbf{F}_z & 0 \\ 0 & 0 & 0 & \mathbf{F}_A \end{bmatrix} = \begin{bmatrix} \mathbf{F}_1 & 0 \\ 0 & \mathbf{F}_A \end{bmatrix} \tag{6.42}$$

$$\begin{aligned} \omega(t) &= [\omega_x(t),\ \omega_y(t),\ \omega_z(t),\ \omega_A(t)]^T \\ &= [\omega_1(t),\ \omega_A(t)]^T \end{aligned} \tag{6.43}$$

$$\begin{aligned} \mathbf{B}(t) &= \begin{bmatrix} \mathbf{B}_x(t) & 0 & 0 & 0 \\ 0 & \mathbf{B}_y(t) & 0 & 0 \\ 0 & 0 & \mathbf{B}_z(t) & 0 \\ 0 & 0 & 0 & \mathbf{B}_A(t) \end{bmatrix} \\ &= \begin{bmatrix} \mathbf{B}_1(t) & 0 \\ 0 & \mathbf{B}_A(t) \end{bmatrix} \end{aligned} \tag{6.44}$$

$$\Phi(t_{k+1}, t_k) = \begin{bmatrix} \Phi_x(t_{k+1}, t_k) & 0 & 0 & 0 \\ 0 & \Phi_y(t_{k+1}, t_k) & 0 & 0 \\ 0 & 0 & \Phi_z(t_{k+1}, t_k) & 0 \\ 0 & 0 & 0 & \Phi_A(t_{k+1}, t_k) \end{bmatrix}$$

$$= \begin{bmatrix} \Phi_1(t_{k+1}, t_k) & 0 \\ 0 & \Phi_A(t_{k+1}, t_k) \end{bmatrix} \tag{6.45}$$

and

$$\mathbf{X}(t_k) = \begin{bmatrix} \mathbf{X}_x(t_k) \\ \mathbf{X}_y(t_k) \\ \mathbf{X}_z(t_k) \\ \mathbf{X}_A(t_k) \end{bmatrix} = \begin{bmatrix} \mathbf{X}_1(t_k) \\ \mathbf{X}_A(t_k) \end{bmatrix} \tag{6.46}$$

$$\mathbf{W}(t_k) = \begin{bmatrix} \mathbf{W}_x(t_k) \\ \mathbf{W}_y(t_k) \\ \mathbf{W}_z(t_k) \\ \mathbf{W}_A(t_k) \end{bmatrix} = \begin{bmatrix} \mathbf{W}_1(t_k) \\ \mathbf{W}_A(t_k) \end{bmatrix} \tag{6.47}$$

The terms with subscript A correspond to the augmented state vector representing the identified measurement biases. The state variables of system bias input augmented into the model are included in the $\mathbf{X}_1$ for each dimension respectively. Thus the sub-matrices corresponding to the x, y, z and augmented state vectors are decoupled and the sub-matrices corresponding to the state vectors of x, y and z coordinate components generally have the same form.

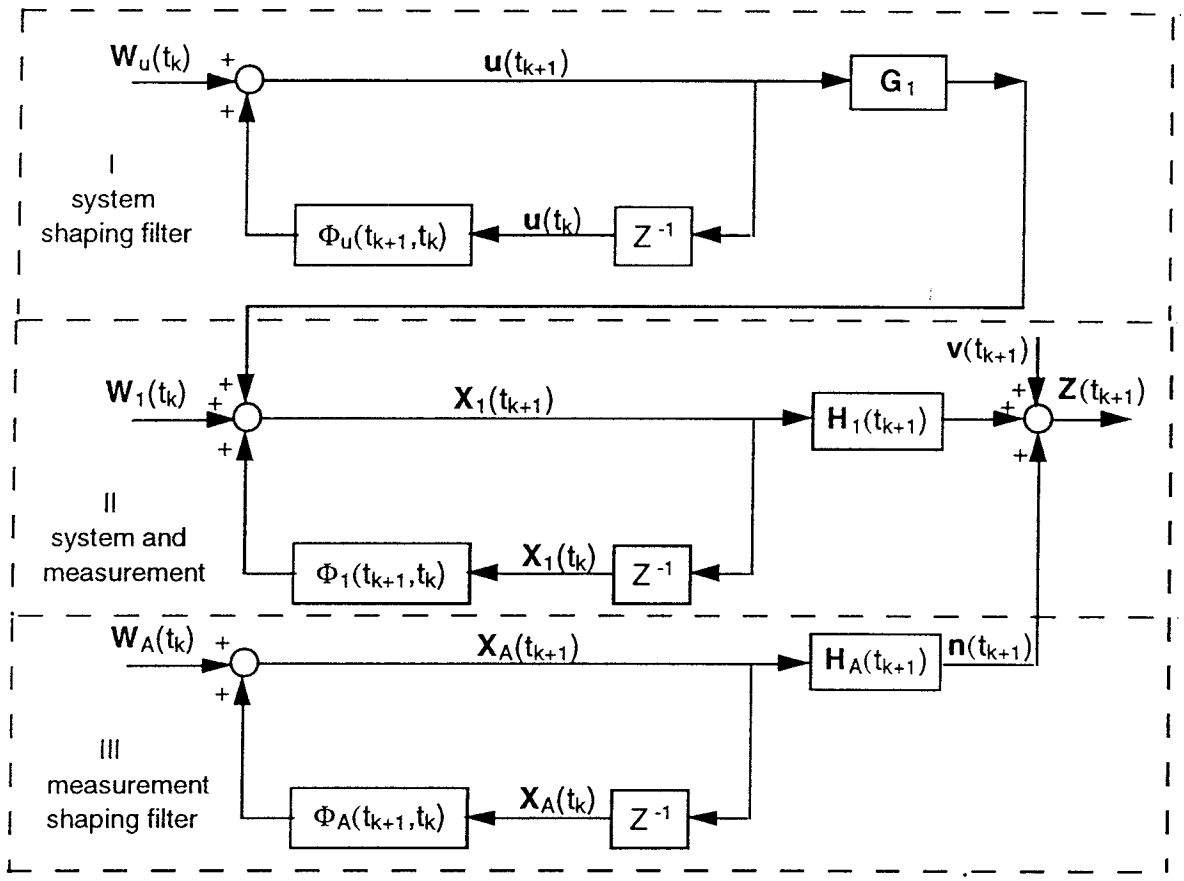

Figure 6.4. Block Chart of navigation model.

6.4 Controllability of the Navigation Model

All navigation models, except for the static model are stochastically controllable because they satisfy the condition (modified from Maybeck, 1979):

$$\alpha \mathbf{I} \le \sum_{J=i-N+1}^{i} \Phi_x(t_i, t_J)\mathbf{Q}_x(t_{J-1})\Phi_x^T(t_i, t_J) \le \beta \mathbf{I} \qquad (6.48)$$

$$0 < \alpha < \beta < \infty, \quad i \ge N$$

where Φ_x is a full rank matrix and $\mathbf{Q}_x$ is positive-definite matrix with limited strength. The same conclusion can be reached for the y, and z sub-spaces, and hence **X**1 is completely controllable. The conclusion is obvious because **B**1 matrix is full rank and every state variable is under the control of the input.

Sometimes the input coupling matrices $\mathbf{B}_x$, $\mathbf{B}_y$ and $\mathbf{B}_z$ are in following forms:

$$\begin{bmatrix} 0 & 0 \\ 0 & 1 \end{bmatrix} \text{ or } \begin{bmatrix} 0 & 0 & 0 \\ 0 & 0 & 0 \\ 0 & 0 & 1 \end{bmatrix}$$

Assuming the driving noise is the control input, the systems are completely controllable and the rank of the controllability matrix equals the dimension of the state vector n, because the systems are now in the standard controllable form and each sub-block of **F**1 is a companion matrix (see eqns (6.5), (6.9), (6.12) and (6.16)), and is completely controllable which is equivalent to the uniformly stochastic controllability matrix (Maybeck, 1982) of eqn (6.48) for a linear and time-invariant system.

Through an analysis, the following commends on the controllability of the augmented shaping filter can be made:

- Random constant is uncontrollable and marginally stable.
- First and second order Markov processed are completely controllable and stable.
- Random walk is completely controllable and unstable under random input.

For details on shaping filter structures, see Maybeck (1979), Gelb (1974).

Time series models can be used to model the biases in discrete time. For a stationary series the AR(p) (AutoRegressive) model is:

$$X_A(t_k) = \phi_1 X_A(t_{k-1}) + \phi_2 X_A(t_{k-2}) + \cdots + \phi_p X_A(t_{k-p}) + W_A(t_k) \tag{6.49}$$

or

$$\phi(B)\, X_A(t_k) = W_A(t_k) \tag{6.50}$$

$$\phi(B) = 1 - \phi_1 B - \phi_2 B^2 - \cdots - \phi_p B^p \tag{6.51}$$

where B is the delay operator. W_A is stationary white noise and p is the order of the series.

$\phi_1, \cdots, \phi_p$ are estimated by Least Squares or Kalman filter and their values should satisfy the condition that the absolute values of the characteristic roots of $\phi(B) = 0$ lie outside the unit circle to make the process stationary (stable). When $|\phi_1| < 1$, AR (1) is called a first order Markov series. The first order Markov series is different from the first order Markov process in that when $0 < \phi_1 < 1$, the autocorrelation function of AP(1) is in the exponential decaying form as that of the first order Markov process, when $-1 < \phi_1 < 0$ the autocorrelation function has an exponential decay with oscillation which can only be modelled by a second order Markov process created by a underdamped second order shaping filter. When $\phi_1 = 1$, AP(1) is a random walk series which is non-stationary because the characteristic root is at the unit circle.

Eqn (6.49) can be written in a state equation form:

$$\begin{bmatrix} X_A(t_{k-p+1}) \\ X_A(t_{k-p+2}) \\ \cdots \\ X_A(t_k) \\ X_A(t_{k+1}) \end{bmatrix} = \begin{bmatrix} 0 & 1 & \cdots & 0 & 0 \\ 0 & 0 & \cdots & 0 & 0 \\ & & \cdots & & \\ 0 & 0 & \cdots & 0 & 1 \\ \phi_p & \phi_{p-1} & \cdots & \phi_2 & \phi_1 \end{bmatrix} \begin{bmatrix} X_A(t_{k-p}) \\ X_A(t_{k-p+1}) \\ \cdots \\ X_A(t_{k-1}) \\ X_A(t_k) \end{bmatrix} + \begin{bmatrix} 0 \\ 0 \\ \cdots \\ 0 \\ 1 \end{bmatrix} W_A(t_{k+1}) \tag{6.52}$$

Eqn (6.52) is in the standard controllable form and the system is completely controllable.

The observation equation of an AR(p) is:

$$Y_A(t_k) = \begin{bmatrix} \phi_p & \phi_{p-1} \cdots & \phi_2 & \phi_1 \end{bmatrix} \begin{bmatrix} X_A(t_{k-p}) \\ X_A(t_{k-p+1}) \\ \cdots \\ X_A(t_{k-1}) \\ X_A(t_k) \end{bmatrix} + W_A(t_k) \tag{6.53}$$

For mean value non-stationary series $Z_A(k)$, it can be made stationary through differencing:

$$Y_A(t_k) = (1 - B)^d Z_A(t_k) \tag{6.54}$$

where $d \leq 2$ (usually).

Here only the AR model is given because of its equivalence to the shaping filter which is generally used within a Kalman filter. The parameter estimation of the AR model is a linear estimation and is easy to implement for real-time applications. The AR model identification by Least Squares (especially the sequential Least Squares techniques) is not only convergent for both stable and unstable systems, but its convergence rate and robustness to round-off errors is better than or equal to any other methods. The AR model has a useful structure in the general case of no a priori information compared to MA (MovingAverage) and ARMA models, and there is equivalence between the AR and MA or ARMA models. For more details see Graupe (1989).

6.5 Observability of the Navigation Model

The GPS observation equation of eqn (6.24) can be partitioned as fellows:

$$\mathbf{Z}(t_k) = \begin{bmatrix} \mathbf{Z}_P(t_k) \\ \mathbf{Z}_D(t_k) \end{bmatrix} \tag{6.55}$$

The corresponding observation matrix is:

$$\mathbf{H}(t_k) = \begin{bmatrix} \mathbf{H}_{1P}(t_k) & \mathbf{H}_{PA}(t_k) & 0 \\ \mathbf{H}_{1D}(t_k) & 0 & \mathbf{H}_{DA}(t_k) \end{bmatrix} \tag{6.56}$$

The partitioned parameter vector is:

$$\mathbf{X}(t_k) = \begin{bmatrix} \mathbf{X}1(t_k) \\ \mathbf{X}_{PA}(t_k) \\ \mathbf{X}_{DA}(t_k) \end{bmatrix} \tag{6.57}$$

The noise vector is:

$$\mathbf{V}(t_k) = \begin{bmatrix} \mathbf{V}_P(t_k) \\ \mathbf{V}_D(t_k) \end{bmatrix} \tag{6.58}$$

and

$$\mathrm{Var}[\mathbf{V}(t_k)] = \begin{bmatrix} \mathbf{R}_P(t_k) & 0 \\ 0 & \mathbf{R}_D(t_k) \end{bmatrix} = \mathbf{R}(t_k), \quad 0 < |\mathbf{R}(t_k)| < \infty \tag{6.59}$$

where $\mathbf{V}(t_k)$ is white noise

Subscripts P, D and A refer to pseudo-range (or phase), Doppler and augmented state terms for the measurements respectively.

For the deterministic system, which has no control input, the state equation is:

$$\mathbf{X}(t_{k+1}) = \Phi(t_{k+1}, t_k)\, \mathbf{X}(t_k) \tag{6.60}$$

$$\mathbf{Z}(t_k) = \mathbf{H}(t_k)\, \mathbf{X}(t_k) \tag{6.61}$$

The observability matrix of the deterministic system is (modified from Maybeck, 1982):

$$\mathbf{L}(t_0, t_{N-1}) = \begin{bmatrix} \mathbf{H}(t_0) \\ \mathbf{H}(t_1)\Phi(t_1, t_0) \\ . \\ . \\ \mathbf{H}(t_{N-1})\Phi(t_{N-1}, t_0) \end{bmatrix} \tag{6.62}$$

where $t_0 < t_{N-1} < \infty$. $\mathbf{L}$ is a l x n matrix, l is the total number of observation in N measurement epochs.

If the rank of the observability matrix $\mathbf{L}$ is equal to the dimension of the state vector n, then the system is completely observable. It means that the system state at t_0 can be uniquely determined by the observation series $\mathbf{Z}(t_0)$, $\mathbf{Z}(t_1)$, ..., $\mathbf{Z}(t_{N-1})$. It also means the total observation number l must be equal to or larger than the state vector dimension n in N measurement epochs.

The complete observability can be expressed in another form:

$$\mathbf{L}^T(t_0, t_{N-1})\,\mathbf{L}(t_0, t_{N-1}) = \sum_{k=0}^{N-1} \Phi^T(t_k, t_0)\mathbf{H}^T(t_k)\mathbf{H}(t_k)\Phi(t_k, t_0) > 0 \tag{6.63}$$

The transition matrix Φ is invertible and eqn (6.63) can be re-written as:

$$\sum_{l=k-N+1}^{k} \Phi^T(t_l, t_k)\mathbf{H}^T(t_l)\mathbf{H}(t_l)\Phi(t_l, t_k) > 0 \tag{6.64}$$

where $\Phi(t_l, t_k) = \Phi^{-1}(t_k, t_l)$

Eqn (6.64) means that if the system is completely observable, the state at t_k can be uniquely determined by the present and past observations $\mathbf{Z}(t_k)$, $\mathbf{Z}(t_{k-1})$, ..., $\mathbf{Z}(t_{k-N+1})$.

For a stochastic system model (eqns (6.24) and (6.38)) its observability can be related to eqns (6.62) and (6.63), as for any positive-definite matrix **D** there are two positive numbers μ and λ which are the maximum and minimum eigenvalues of **D** and satisfy the condition:

$$\mu(k)\,\mathbf{I} \geq \mathbf{D}(k) \geq \lambda(k)\,\mathbf{I}$$

where **I** is the identity matrix with the same dimension as **D**. Therefore:

$$\sum_{k=0}^{N-1} \Phi^T(t_k, t_0)\mathbf{H}^T(t_k)\mathbf{D}(k)\mathbf{H}(t_k)\Phi(t_k, t_0)$$

$$\geq \sum_{k=0}^{N-1} \Phi^T(t_k, t_0)\mathbf{H}^T(t_k)\lambda(k)\mathbf{H}(t_k)\Phi(t_k, t_0)$$

$$\geq \lambda(k)\sum_{k=0}^{N-1} \Phi^T(t_k, t_0)\mathbf{H}^T(t_k)\mathbf{H}(t_k)\Phi(t_k, t_0) > 0$$

If **D** is replaced by the inverse of the covariance matrix of measurement **R**, the stochastic observability condition is obtained:

$$\sum_{k=0}^{N-1} \Phi^T(t_k, t_0)\mathbf{H}^T(t_k)\mathbf{R}^{-1}(t_k)\mathbf{H}(t_k)\Phi(t_k, t_0) > 0 \qquad (6.65)$$

and

$$\sum_{l=k-N+1}^{k} \Phi^T(t_l, t_k)\mathbf{H}^T(t_l)\mathbf{R}^{-1}(t_l)\mathbf{H}(t_l)\Phi(t_l, t_k) > 0 \qquad (6.66)$$

When **R** is positive-definite and $0 < |\mathbf{R}| < \infty$, it is apparent that if the condition for deterministic complete observability is satisfied, so is the stochastic observability.

Eqn (6.66) is equivalent to the normal matrix of the Least Squares estimation as for the static case eqn (6.66) becomes:

$$\sum_{l=k-N+1}^{k} \mathbf{H}^T(t_l)\mathbf{R}^{-1}(t_l)\mathbf{H}(t_l) > 0 \qquad (6.67)$$

The following analysis concentrates on the kinematic case.

For short periods of time the geometry of the GPS satellite constellation does not undergo significant change and the observation matrices $\mathbf{H}(t_{N-1})\cdots\mathbf{H}(t_0)$ can be considered to be constant. For a time-invariant system, N can be replaced by n in eqn (6.62). This means that if in n epochs the rank of **L** is equal to n, the system is completely observable.

6.5.1 Pseud-Range Positioning Model

First, the observability of the constant acceleration model for pseudo-range point positioning is discussed. The clock error is modelled as a constant acceleration model. The total state variables are:

$$\mathbf{X} = [x, \dot{x}, \ddot{x}, y, \dot{y}, \ddot{y}, z, \dot{z}, \ddot{z}, T, \dot{T}, \ddot{T}]^T$$

If there is only one satellite available in n epochs, the observability matrix takes the form :

$$L_1 = \begin{bmatrix} H \\ H\Phi \\ \cdots \\ H\Phi^{n-1} \end{bmatrix}$$

$$= \begin{bmatrix} h_{11} & 0 & 0 & h_{12} & 0 & 0 & h_{13} & 0 & 0 & 1 & 0 & 0 \\ h_{11} & \Delta K h_{11} & \frac{\Delta K^2}{2} h_{11} & h_{12} & \Delta K h_{12} & \frac{\Delta K^2}{2} h_{12} & h_{13} & \Delta K h_{13} & \frac{\Delta K^2}{2} h_{13} & 1 & \Delta K & \frac{\Delta K^2}{2} \\ & & & & & \cdots & & & & & & \\ h_{11} & \Delta K(n-1) h_{11} & \frac{[\Delta K(n-1)]^2}{2} h_{11} & h_{12} & \Delta K(n-1) h_{12} & \frac{[\Delta K(n-1)]^2}{2} h_{12} & h_{13} & \Delta K(n-1) h_{13} & \frac{[\Delta K(n-1)]^2}{2} h_{13} & 1 & \Delta K(n-1) & \frac{[\Delta K(n-1)]^2}{2} \end{bmatrix}$$

(6.68)

where the direction cosines of the satellite are:

$h_{11} = -\cos\alpha_1, \quad h_{12} = -\cos\beta_1, \quad h_{13} = -\cos\gamma_1$

By elementary transformation Γ the observability matrix $\mathbf{L}_1$ can be transformed to $\mathbf{L}_{\Gamma 1}$:

$$\Gamma(\mathbf{L}_1) \equiv \mathbf{L}_{\Gamma 1} =$$

$$\begin{bmatrix} h_{11} & 0 & 0 & h_{12} & 0 & 0 & h_{13} & 0 & 0 & 1 & 0 & 0 \\ 0 & h_{11} & 0 & 0 & h_{12} & 0 & 0 & h_{13} & 0 & 0 & 1 & 0 \\ 0 & 0 & h_{11} & 0 & 0 & h_{12} & 0 & 0 & h_{13} & 0 & 0 & 1 \end{bmatrix} \tag{6.69}$$

It is obvious the rank of $\mathbf{L}_1$ is three. For m satellites observed in n epochs, the observability matrix can be written as:

$$\mathbf{L}_{\Gamma m} =$$

$$\begin{bmatrix} h_{11} & 0 & 0 & h_{12} & 0 & 0 & h_{13} & 0 & 0 & 1 & 0 & 0 \\ 0 & h_{11} & 0 & 0 & h_{12} & 0 & 0 & h_{13} & 0 & 0 & 1 & 0 \\ 0 & 0 & h_{11} & 0 & 0 & h_{12} & 0 & 0 & h_{13} & 0 & 0 & 1 \\ & & & & & \cdots & & & & & & \\ h_{m1} & 0 & 0 & h_{m2} & 0 & 0 & h_{m3} & 0 & 0 & 1 & 0 & 0 \\ 0 & h_{m1} & 0 & 0 & h_{m2} & 0 & 0 & h_{m3} & 0 & 0 & 1 & 0 \\ 0 & 0 & h_{m1} & 0 & 0 & h_{m2} & 0 & 0 & h_{m3} & 0 & 0 & 1 \end{bmatrix} \tag{6.70}$$

where h_{i1}, h_{i2}, h_{i3} are the direction cosines for the ith satellite and i = 1, 2, ..., m. $\mathbf{L}_{\Gamma m}$ is a 3m x n matrix. The rows and columns of $\mathbf{L}_{\Gamma m}$ are all linearly independent, and this is guaranteed as the satellites observed are not in the critical area.

From eqn (6.70) it can be seen that the rank of the observability matrix $\mathbf{L}_m$ is dependent on the total number of different satellites m observed in n epochs:

number of satellite m	rank of $\mathbf{L}_m$
1	3
2	6
3	9
4 or > 4	12

For the constant velocity model the rows and columns corresponding to the acceleration terms are not present and for each satellite there are only two rows in eqns (6.69) and (6.70). The relationship between satellite number m and the rank of the observability matrix is:

number of satellite m	rank of $\mathbf{L}_m$
1	2
2	4
3	6
4 or > 4	8

In summary:

$$\text{rank of } \mathbf{L}_m = \begin{pmatrix} m \times SD & \text{if } m < dm \\ n & \text{if } m \geq dm \end{pmatrix} \tag{6.71}$$

where:

- SD order of the navigation model which is equivalent to the dimension of the state space. The order of the clock error is the same as the order of the navigation model used
- n dimension of the state vector
- m number of satellites observed in n epochs
- dm dimension of total coordinate system (equal to the dimension of the coordinate system of the navigation model plus one corresponding to the clock error augmented to the navigation model)

The above observability matrix has been derived for the constant acceleration and constant velocity models. The same analysis can be carried out for the third order, second order and first order system models because the transition matrices of the these models are also constant and upper-triangular matrices, and an observability matrix in the similar form as eqn (6.70) can be obtained. In the following discussions only the constant acceleration and constant velocity models are dealt with but the conclusions drawn are valid also for the other models.

The conclusion that is drawn for GPS pseudo-range point positioning is that if the number of satellites observed in n epochs is equal to or larger than dm, then the navigation models are stochastically completely observable. This means that not only are the position parameter and clock bias observable but in addition the velocity, acceleration, clock drift and drift-rate can be determined from pseudo-range measurements if second order (or constant velocity) models and third order (or constant acceleration) models are used. The physical reasoning for this is obvious: the pseudo-range measurement is the direct observable of position and the position displacement is obtainable from two positions, hence the pseudo-range measurement is the indirect observable of velocity. Acceleration is the differentiation of the position displacement and this relationship is reflected in the system and transition matrices of the navigation models and the observation information is accumulated to the present epoch.

In contrast to the traditional Least Squares navigation solution of three dimensional position and clock bias from pseudo-range measurements, four or more satellites during each epoch are necessary because the Least Squares algorithm is actually working in the static mode and the system state at each epoch is considered to be independent of those obtained at other epochs, hence no velocity, acceleration, clock drift and drift-rate information is available.

6.5.2 Doppler Measurement Model

A similar procedure can be used to analyse the observability of GPS Doppler measurements. For the constant acceleration model the observability matrix for Doppler measurement can be written as:

$$\mathbf{L}_{Dm} =$$

$$\begin{bmatrix} H_{D11} & H_{D12} & H_{D13} & H_{D14} & H_{D15} & H_{D16} & H_{D17} & H_{D18} & H_{D19} & 0 & 1 & \Delta K \\ H_{D21} & H_{D22} & H_{D23} & H_{D24} & H_{D25} & H_{D26} & H_{D27} & H_{D28} & H_{D29} & 0 & 1 & 2\Delta K \\ & & & & & \cdots & & & & & & \\ H_{Dm1} & H_{Dm2} & H_{Dm3} & H_{Dm4} & H_{Dm5} & H_{Dm6} & H_{Dm7} & H_{Dm8} & H_{Dm9} & 0 & 1 & (m-1)\Delta K \end{bmatrix} \quad (6.72)$$

where

$$H_{Di1} = \frac{\dot{r}_{rx} + \dot{P}_i \cos\alpha}{P_i} \qquad H_{Di2} = (i-1)\Delta K H_{Di1} - \cos\alpha$$

$$H_{Di3} = \frac{(i-1)^2}{2}\Delta K^2 H_{Di1} - (i-1)\Delta K \cos\alpha \qquad H_{Di4} = \frac{\dot{r}_{ry} + \dot{P}_i \cos\beta}{P_i}$$

$$H_{Di5} = (i-1)\Delta K H_{Di4} - \cos\beta \qquad H_{Di6} = \frac{(i-1)^2}{2}\Delta K^2 H_{Di4} - (i-1)\Delta K \cos\beta$$

$$H_{Di7} = \frac{\dot{r}_{rz} + \dot{P}_i \cos\gamma}{P_i} \qquad H_{Di8} = (i-1)\Delta K H_{Di7} - \cos\gamma$$

$$H_{Di9} = \frac{(i-1)^2}{2}\Delta K^2 H_{Di7} - (i-1)\Delta K \cos\gamma$$

and i = 1, 2, ..., m.

For a short time period the Doppler observation matrix $\mathbf{H}_D$ can be assumed to be constant. It is obvious that the rank of the observability matrix for Doppler measurements $\mathbf{L}_{Dm}$ is less than n, because there is a zero column corresponding to the clock bias terms, hence the system is not completely observable. Furthermore, if we assume the terms of H_{Di1}, H_{Di4}, H_{Di7} which contain the Doppler effect due to the changing rates of the line-of-sight of satellites are zero during the n epochs because their values are at 10^{-4} level, then the largest possible rank of $\mathbf{L}_{Dm}$ is eight. This corresponds to a sub-space consisting of velocity, acceleration, clock drift and drift-rate which is completely observable. The null-space corresponds to the position and clock bias which are not observable, that is, the Doppler or range-rate measurements make no contributions to the determination of the position and bias terms. The physical explanation is that the Doppler measurement is a direct observable of the velocity (or position displacement) and an indirect observable of acceleration, not of the position, because the initial position cannot be determined by the Doppler measurement, and the acceleration can be derived from the differentiation of the velocity which is determined directly from the Doppler measurement. This property of the observability of Doppler measurements can be seen after an elementary transformation of eqn (6.72):

$$\Gamma(\mathbf{L}_{Dm}) = \mathbf{L}_{\Gamma Dm}$$

$$= \begin{bmatrix} 0 & h_{11} & 0 & 0 & h_{12} & 0 & 0 & h_{13} & 0 & 0 & 1 & 0 \\ 0 & 0 & h_{11} & 0 & 0 & h_{12} & 0 & 0 & h_{13} & 0 & 0 & 1 \\ & & & & & \cdots & & & & & & \\ 0 & h_{m1} & 0 & 0 & h_{m2} & 0 & 0 & h_{m3} & 0 & 0 & 1 & 0 \\ 0 & 0 & h_{m1} & 0 & 0 & h_{m2} & 0 & 0 & h_{m3} & 0 & 0 & 1 \end{bmatrix} \tag{6.73}$$

$$\text{rank of } \mathbf{L}_{Dm} = \begin{pmatrix} m \times (SD-1) & \text{if } m < dm \\ n - dm & \text{if } m \geq dm \end{pmatrix} \tag{6.74}$$

Finally, for the model consisting of both range and Doppler measurements, it can be shown that the rank of the observability matrix $\mathbf{L}_{RD}$ is equal to the rank of $\mathbf{L}_m$:

$$\text{rank of } \mathbf{L}_{RD} = \text{rank of} \begin{bmatrix} \mathbf{L}_m \\ \mathbf{L}_{Dm} \end{bmatrix} = \text{rank of} \begin{bmatrix} \mathbf{L}_{\Gamma m} \\ \mathbf{L}_{\Gamma Dm} \end{bmatrix}$$

$$= \text{rank of } \mathbf{L}_{\Gamma m} = \text{rank of } \mathbf{L}_m \qquad (6.75)$$

Note that each term of the rows of $\mathbf{L}_{\Gamma Dm}$ becomes zero by elementary transformation. Hence for the determination of position, velocity, acceleration in terms of three dimensional coordinates and the clock bias, clock drift and drift-rate using pseudo-range and Doppler, there should be at least four satellites observed in n epochs.

6.5.3 Measurement Bias Model

1)First order Markov process:

Sometimes it is required to model the measurement bias using Markov processes. These augmented state variables are decoupled from the rest of the state variable set:

$$\begin{bmatrix} X_{M1}(t_{K+1}) \\ X_{M2}(t_{K+1}) \\ X_{M3}(t_{K+1}) \\ \cdots \\ X_{Mi}(t_{K+1}) \end{bmatrix} = \begin{bmatrix} e^{-\Delta K/T_1} & 0 & 0 & \cdots & 0 \\ 0 & e^{-\Delta K/T_2} & 0 & \cdots & 0 \\ 0 & 0 & e^{-\Delta K/T_3} & \cdots & 0 \\ & & \cdots & & \\ 0 & 0 & 0 & \cdots & e^{-\Delta K/T_i} \end{bmatrix} \begin{bmatrix} X_{M1}(t_k) \\ X_{M2}(t_k) \\ X_{M3}(t_k) \\ \cdots \\ X_{Mi}(t_k) \end{bmatrix}$$

$$+ \begin{bmatrix} W_{M1}(t_K) \\ W_{M2}(t_K) \\ W_{M3}(t_K) \\ \cdots \\ W_{Mi}(t_K) \end{bmatrix} \qquad (6.76)$$

Eqn (6.76) is derived from the following shaping filter:

$$\begin{bmatrix} \dot{X}_{M1}(t) \\ \dot{X}_{M2}(t) \\ \dot{X}_{M3}(t) \\ \cdots \\ \dot{X}_{Mi}(t) \end{bmatrix} = \begin{bmatrix} \frac{-1}{T_1} & 0 & 0 & \cdots & 0 \\ 0 & \frac{-1}{T_2} & 0 & \cdots & 0 \\ 0 & 0 & \frac{-1}{T_3} & \cdots & 0 \\ & & \cdots & & \\ 0 & 0 & 0 & \cdots & \frac{-1}{T_i} \end{bmatrix} \begin{bmatrix} X_{M1}(t) \\ X_{M2}(t) \\ X_{M3}(t) \\ \cdots \\ X_{Mi}(t) \end{bmatrix}$$

$$+ \begin{bmatrix} 1 & 0 & 0 & \cdots & 0 \\ 0 & 1 & 0 & \cdots & 0 \\ 0 & 0 & 1 & \cdots & 0 \\ & & \cdots & & \\ 0 & 0 & 0 & \cdots & 1 \end{bmatrix} \begin{bmatrix} \omega_{M1}(t) \\ \omega_{M2}(t) \\ \omega_{M3}(t) \\ \cdots \\ \omega_{Mi}(t) \end{bmatrix} \qquad (6.77)$$

where T_i is the time constant. The sub-system represented by eqn (6.76) is completely controllable as the transition matrix and input coupling matrix are all diagonal matrices.

For the augmented first order Markov process model, the observation equation can be written as:

$$\mathbf{Z}(t_k) = [\mathbf{H}_1(t_k), \mathbf{H}_M(t_k)] \begin{bmatrix} \mathbf{X}(t_k) \\ \mathbf{X}_M(t_k) \end{bmatrix} + \mathbf{V}_M(t_k) \qquad (6.78)$$

$\mathbf{H}_M(t_k)$ is a m x m identity matrix.

The observability matrix for this model of the augmented first order Markov process is:

$$\mathbf{L}_M = [\ \mathbf{L}\ ,\ \mathbf{L}_{M1}\ ] \qquad (6.79)$$

where $\mathbf{L}_{M1}$ contains the terms corresponding to the augmented Markov process:

$$\mathbf{L}_{M1} = \begin{bmatrix} \mathbf{L}_{M11} \\ \mathbf{L}_{M12} \\ \cdots \\ \mathbf{L}_{M1m} \end{bmatrix} \tag{6.80}$$

and

$$\mathbf{L}_{M11} = \begin{bmatrix} 1 & 0 & \cdots & 0 \\ 0 & 1 & \cdots & 0 \\ & & \cdots & \\ 0 & 0 & \cdots & 1 \end{bmatrix} \tag{6.81}$$

$$\mathbf{L}_{M1j} = \begin{bmatrix} e^{-(j-1)\Delta k/T_1} & 0 & \cdots & 0 \\ 0 & e^{-(j-1)\Delta k/T_2} & \cdots & 0 \\ \cdots & \cdots & \cdots & \cdots \\ 0 & 0 & \cdots & e^{-(j-1)\Delta k/T_i} \end{bmatrix}, \quad j = 2, 3, \cdots, m \tag{6.82}$$

The rank of $\mathbf{L}_{M1}$ is equal to m, the number of satellites observed. By elementary transformation eqn (6.79) can be expressed as:

$$\Gamma(\mathbf{L}_M) \equiv \begin{bmatrix} \mathbf{L}_{\Gamma m} & 0 \\ 0 & \mathbf{H}_M \end{bmatrix} \tag{6.83}$$

where $\mathbf{L}_{\Gamma m}$ is the observability matrix eqn (6.70) and $\mathbf{H}_M$ is the m x m identity matrix.

Assuming the dimension of the body state and clock state vector is k and the augmented state vector has the dimension m (the number of satellites observed), then the dimension of the total state vector is n = k + m. If the number of satellites observed in n epochs is equal to or larger than dm, the rank of $\mathbf{L}_{\Gamma m}$ is k and the rank of $\mathbf{L}_M$ is k+ m = n, and hence the system with augmented Markov process is completely observable.

The same situation occurs with Doppler measurements, there are still zero columns corresponding to the position and clock bias parameters in the

observability matrix, and hence the system is not completely observable although the augmented state vector is observable.

As a conclusion it can be stated that the augmented first order Markov processes do not affect the system observability for either pseudo-range and Doppler measurements in point positioning, because the augmented Markov process belong to the completely observable and controllable sub-space and the augmented state is decoupled from other state. If the original system is completely observable, then the augmented system is also completely observable, and vice versa.

The above conclusion can be easily extended to models which have more than one first order Markov process augmented for each measurement. For example, two first order Markov processes which have different time constants to model slow and fast changing biases, as in the case of atmospheric effects and Selective Availability respectively. In this case the transition sub-matrix corresponding to the augmented Markov processes is of full rank diagonal one, as in eqns (6.76) and (6.77), with white noise as system driving noise and an identity input coupling matrix. Hence this augmented sub-system is completely controllable. The observation matrix (for four satellites) for the augmented sub-system is:

$$\mathbf{H}_M = \begin{bmatrix} 1 & 1 & 0 & 0 & 0 & 0 & 0 & 0 \\ 0 & 0 & 1 & 1 & 0 & 0 & 0 & 0 \\ 0 & 0 & 0 & 0 & 1 & 1 & 0 & 0 \\ 0 & 0 & 0 & 0 & 0 & 0 & 1 & 1 \end{bmatrix} \tag{6.84}$$

The observability matrix now is in the same form as for eqn (6.83) except that $\mathbf{H}_M$ is replaced by a unit matrix with dimension (2 x m)x(2 x m) and, as before, the augmented first order Markov processes do not change the observability of the original system.

2) Random walk:

Another popular bias model is the random walk process, which is the first order system model with $\gamma = 0$ (eqn (6.18)) and can be used to model non-stationary random processes. The point positioning model, which is the navigation model

with augmented clock error and augmented random walk, is not completely observable in a short time interval. The reason is that the position state and bias term of the clock error and the augmented random walk cannot be separated from each other. The sub-matrices of the transition matrix and observation matrix corresponding to the random walk are all identity matrices, as the same is the random constant, and the observability matrix takes the form of eqn (6.88), which is used for the augmented random constant model. Although both augmented random walk and random constant models are not observable in a short time interval, the random walk model is completely controllable and the random constant model is not.

6.5.4 Differential Mode

In the case of differenced observations some measurement biases which are augmented in the point positioning mode are eliminated. The differenced observations are a linear combination of the original measurements and hence have similar forms of observation matrices as the original ones, and the terms of the transition matrix and the observation matrix corresponding to the biases which cancel out as a result of the differencing vanish. For double-differenced pseudo-range measurements, the observation matrix can be written as:

$$\mathbf{H}^{d}(t_k) = \begin{bmatrix} h^{d}_{11} & 0 & 0 & h^{d}_{12} & 0 & 0 & h^{d}_{13} & 0 & 0 \\ h^{d}_{21} & 0 & 0 & h^{d}_{22} & 0 & 0 & h^{d}_{23} & 0 & 0 \\ & & & & \cdots & & & & \\ h^{d}_{k1} & 0 & 0 & h^{d}_{k2} & 0 & 0 & h^{d}_{k3} & 0 & 0 \end{bmatrix} \tag{6.85}$$

where k = (m-1) x (s-1), s is the GPS receiver number. For the remote receiver the measurement number is m-1 and the dimension of the coordinate system is dm = 3 because the receiver clock error is eliminated. The observability matrix for constant acceleration now takes the form:

$$\mathbf{L}^{d}_{\Gamma m} =$$

$$\begin{bmatrix}
h^{d}_{11} & 0 & 0 & h^{d}_{12} & 0 & 0 & h^{d}_{13} & 0 & 0 \\
0 & h^{d}_{11} & 0 & 0 & h^{d}_{12} & 0 & 0 & h^{d}_{13} & 0 \\
0 & 0 & h^{d}_{11} & 0 & 0 & h^{d}_{12} & 0 & 0 & h^{d}_{13} \\
 & & & & \cdots & & & & \\
h^{d}_{k1} & 0 & 0 & h^{d}_{k2} & 0 & 0 & h^{d}_{k3} & 0 & 0 \\
0 & h^{d}_{k1} & 0 & 0 & h^{d}_{k2} & 0 & 0 & h^{d}_{k3} & 0 \\
0 & 0 & h^{d}_{k1} & 0 & 0 & h^{d}_{k2} & 0 & 0 & h^{d}_{k3}
\end{bmatrix}$$

(6.86)

The criteria for determining observability is the same as for eqn (6.71), that is if k ≥ dm the system is completely observable.

For triple-differenced carrier phase measurements the observability matrix is of the same form as eqn (6.86) and dm = 3, hence if k ≥ 3 the system is completely observable. For between-site or between-satellite differenced pseudo-range measurements, the clock error is still present in the augmented state space and dm = 4, so k ≥ 4 in order to make the system completely observable.

For differenced Doppler measurements, the position is still unobservable, and velocity and acceleration is completely observable if k ≥ dm.

The system model of differenced measurement mode with augmented first order Markov processes is completely observable, as in the case of point positioning, if the original system model is completely observable. The augmented random walk model is still not completely observable in a short time interval.

For phase measurements there is another augmented state vector representing the initial cycle ambiguities. Ambiguities are modelled as random constants, which are the same as the static model:

$$\dot{\mathbf{X}}_A(t) = 0 \qquad (6.87)$$

The observability matrix for double-differenced phase measurements for the constant acceleration model is:

$$\mathbf{L}^{d}_{\Gamma m} =$$

$$\begin{bmatrix}
0 & 0 & 0 & 0 & 0 & 0 & 0 & 0 & 0 & 1 & 0 & 0 & 0 \\
0 & 0 & 0 & 0 & 0 & 0 & 0 & 0 & 0 & 0 & 1 & 0 & 0 \\
0 & 0 & 0 & 0 & 0 & 0 & 0 & 0 & 0 & 0 & 0 & 1 & 0 \\
0 & 0 & 0 & 0 & 0 & 0 & 0 & 0 & 0 & 0 & 0 & 0 & 1 \\
0 & h^{d}_{11} & 0 & 0 & h^{d}_{12} & 0 & 0 & h^{d}_{13} & 0 & 0 & 0 & 0 & 0 \\
0 & h^{d}_{21} & 0 & 0 & h^{d}_{22} & 0 & 0 & h^{d}_{23} & 0 & 0 & 0 & 0 & 0 \\
0 & h_{31} & 0 & 0 & h_{32} & 0 & 0 & h_{33} & 0 & 0 & 0 & 0 & 0 \\
0 & h^{d}_{41} & 0 & 0 & h^{d}_{42} & 0 & 0 & h^{d}_{43} & 0 & 0 & 0 & 0 & 0 \\
0 & 0 & h^{d}_{11} & 0 & 0 & h^{d}_{12} & 0 & 0 & h^{d}_{13} & 0 & 0 & 0 & 0 \\
0 & 0 & h^{d}_{21} & 0 & 0 & h^{d}_{22} & 0 & 0 & h^{d}_{23} & 0 & 0 & 0 & 0 \\
0 & 0 & h^{d}_{31} & 0 & 0 & h^{d}_{32} & 0 & 0 & h^{d}_{33} & 0 & 0 & 0 & 0 \\
0 & 0 & h^{d}_{41} & 0 & 0 & h^{d}_{42} & 0 & 0 & h^{d}_{43} & 0 & 0 & 0 & 0
\end{bmatrix} \tag{6.88}$$

Eqn (6.88) involves 5 satellites and it can be seen that the system is unobservable because columns 1, 4 and 7 of the observability matrix, corresponding to the position state, are always zero no matter how many satellites are observed. The interesting fact is although the the position is not observable, the velocity and acceleration are still observable over a short time interval because they are irrelevant to the initial position state.

It is important to emphasize that the above analysis assumes that for short time periods the observation matrices are constant. For long time periods eqn (6.88) takes the form:

$$L_1 = \begin{bmatrix} H_1 \\ H_2\Phi \\ \cdots \\ H_N\Phi^{N-1} \end{bmatrix}$$

$$= \begin{bmatrix} H_{11} & 0 & 0 & H_{12} & 0 & 0 & H_{13} & 0 & 0 & H_A \\ H_{21} & \Delta K H_{21} & \frac{\Delta K^2}{2} H_{21} & H_{22} & \Delta K H_{22} & \frac{\Delta K^2}{2} H_{22} & H_{23} & \Delta K H_{23} & \frac{\Delta K^2}{2} H_{23} & H_A \\ & & & & \cdots & & & & & \\ H_{N1} & \Delta K(N-1) H_{N1} & \frac{[\Delta K(N-1)]^2}{2} H_{N1} & H_{N2} & \Delta K(N-1) H_{N2} & \frac{[\Delta K(N-1)]^2}{2} H_{N2} & H_{N3} & \Delta K(N-1) H_{N3} & \frac{[\Delta K(N-1)]^2}{2} H_{N3} & H_A \end{bmatrix}$$

(6.89)

where

$$H_{i1} = \begin{bmatrix} \cos\alpha_{i1d} \\ \cdots \\ \cos\alpha_{ikd} \end{bmatrix}, H_{i2} = \begin{bmatrix} \cos\beta_{i1d} \\ \cdots \\ \cos\beta_{ikd} \end{bmatrix}, H_{i1} = \begin{bmatrix} \cos\gamma_{i1d} \\ \cdots \\ \cos\gamma_{ikd} \end{bmatrix}$$

are the direction cosines for the differenced mode, and i = 1, 2, ..., N, is the epoch number. H_A is a k x k identity matrix which is the corresponding terms for the double-differenced ambiguities and k is the double-differenced observation number in each epoch.

Assuming the direction cosines have significant change between epochs, or during N epochs, there will be n columns and rows of the observability matrix which are linearly independent. The rank of the matrix will be equal to the dimension of the state vector, that is, the system can become completely observable if the observation time is long enough. This observability time is dependent on the satellite geometry and the number of satellites observed and it can range from a few minutes for six or more satellites to a few tens of minute for five observed satellites. This suggests that for ambiguity determination a low sampling frequency is preferable.

The same conclusion can be reached for the augmented random walk model for triple-differenced phase or double-differenced pseudo-range measurements, because the observability matrices are the same as eqn (6.89).

For the second order system, or constant velocity model, the same conclusion can be drawn by the above analysis procedure.

For single-differenced phase measurements, the system is unobservable even after a long measurement time interval because the ambiguities are mixed together with the clock bias and the observability matrix has always one zero column which corresponds to the clock bias term.

For long distances between the reference station and the remote station, the first Markov processes can be augmented to the phase observation model to model measurement biases and estimated along with the ambiguities (about the errors in long range kinematic GPS, see Colombo, (1991)). The system is completely observable if the original system is completely observable. The augmented Markov process does not change the observability of the original system as stated before. For the augmented random walk model it will be mixed together totally with the ambiguities and the system has rank defect k, and the system is unobservable even after a long time interval because the random constant and the random walk, which are augmented together to the system model, can be replaced by one model and cannot be separated by the system:

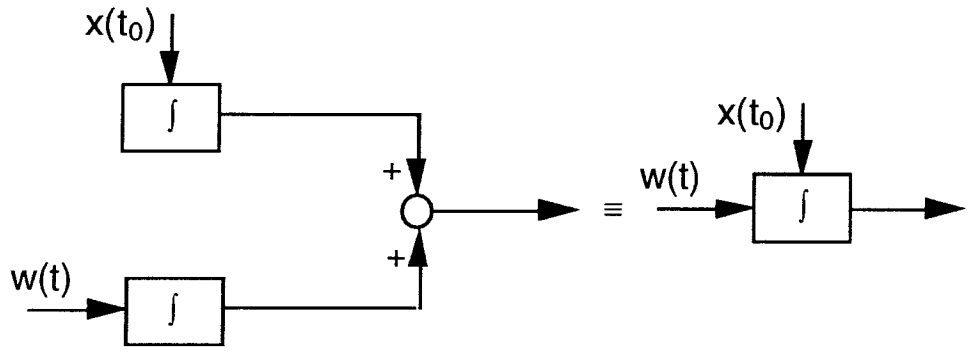

Figure 6.5. System model of random constant and random walk.

Considering the equivalence of the AP(1) model to the first order Markov process and random walk, both in the physical sense and mathematical expression, the effect of the augmented AP(1) model is the same as that of the augmented Markov or random walk process. That is if the AP(1) is stable, then the system is completely observable.

6.6 Concluding Remarks and Summary

6.6.1 The Stability and Controllability of Navigation Models

All navigation models, except for the case of the first order system model, are unstable or marginally stable and the uncertainty of the initial state is non-decreasing with time.

All navigation models, except for the case of the first order system model and static model, are unstable with random noise input and the error of the state is increasing with time.

All navigation models, except for the case of the static model, are stochastically completely controllable if the covariance of the input dynamic noise is positive-definite and has limited strength.

6.6.2 The Observability of Navigation Models

Navigation model observability analysis is made under the assumption that the covariance matrix of the GPS measurement noise is positive-definite and has limited strength.

6.6.2.1 Observability in Short Measurement Time Interval

During short time intervals, the geometry of the observed satellites undergoes no significant change and the observation matrix is time-invariant.

6.6.2.1.1 For Point Positioning

If four or more satellites are observed in n epochs (n is the dimension of the state vector), all the body's state and the receiver clock state are completely observable using pseudo-range measurements alone.

Doppler measurements give information on the body's velocity and acceleration, clock drift and drift-rate, but not the position and clock bias.

The first order Markov process can be augmented to the model and does not affect model observability.

Augmented random walk and random constant models will mix together with the position state and clock bias, and the resulting system is unobservable.

6.6.2.1.2 For Differenced Pseudo-range and Doppler Measurements

If the observation number reduction is equal to the reduction of dimension of the augmented state space, the model can be considered completely observable.

The first order Markov process can be augmented to the model and do not affect the model observability.

Random constant and random walk augmented parameters make the system unobservable.

Differenced Doppler measurements still contribute to the velocity and acceleration, clock drift and drift-rate.

6.6.2.2 Observability in Long Measurement Time Intervals

During long time spans the geometry of the observed satellites is considered to have undergone significant change and the observation matrix is time-variant.

If the model is completely observable in a short measurement time interval, it will still be completely observable in a long time interval.

The contribution of the Doppler measurements to position determination is negligible in practice.

Random walk model of measurements can be augmented to the original system, and the augmented system is completely observable if the original system has no random constant variables (ambiguities and clock bias).

6.6.2.3 For Differenced Phase Measurements

In the case of double-differenced data, the double-differenced ambiguities are completely observable in long measurement time interval both in the static and kinematic modes.

For single-differenced data the ambiguities are unobservable because the clock bias and the ambiguity terms are mixed together.

The first order Markov process can be augmented to the model and does not affect the observability of the model.

The random walk model augmented parameters will mix together with the ambiguities and the system model is then unobservable.

CHAPTER 7

NAVIGATION FILTERS

The navigation filters referred to in this chapter are the low-pass filter and high pass-filter used for navigation data processing and the estimation of a body's state.

7.1 Low-Pass Digital Filter (LDF)

The LDF is mainly used for state estimation, data smoothing and curve fitting.

7.1.1 Least Squares Polynomial Fitting (LSPF)

For GPS data processing, the LSPF used on a piecewise basis is very popular, especially for carrier phase cycle slip detection and repair, and for data smoothing.

The LSPF minimizes:

$$F(a_0, a_1, ..., a_n) = \sum_{k=1}^{m} \left\{ u_k - \left[a_0 + \sum_{i=1}^{n} a_i k^i \right] \right\}^2 \qquad (7.1)$$

where m is the number of data points, u_k is the data value at point k, n is the polynomial order and $m \geq n$. Usually n is less than 6 to avoid the polynomial "wiggle" effect (Mathews, 1992).

The coefficient of the polynomial is a solution of:

$$\mathbf{a} = \left[\mathbf{H}^T\mathbf{H}\right]^{-1} \mathbf{H}^T\mathbf{u} \qquad (7.2)$$

where

$$\mathbf{a}=\begin{bmatrix} a_0 \\ a_1 \\ a_2 \\ \cdots \\ a_n \end{bmatrix}, \quad \mathbf{u}=\begin{bmatrix} u_1 \\ u_2 \\ u_3 \\ \cdots \\ u_m \end{bmatrix}, \quad \mathbf{H}=\begin{bmatrix} 1 & 1 & \cdots & 1 & 1 \\ 1 & 2 & \cdots & 2^{n-1} & 2^n \\ 1 & 3 & \cdots & 3^{n-1} & 3^n \\ & & \cdots & & \\ 1 & m & \cdots & m^{n-1} & m^n \end{bmatrix}$$

and **H** is the Vandermonde matrix with rank n.

The polynomial fitting value is:

$$y_k = a_0 + \sum_{i=1}^{n} a_i k^i \tag{7.3}$$

Assuming that the input series **u** is non-casual and is composed of unit impulse functions, the system function of eqn (7.3) in the Z domain can be written as:

$$H(Z) = \frac{y(Z)}{u(Z)} = \frac{1 + b_1 Z^{-1} + b_2 Z^{-2} + \cdots + b_{m-1} Z^{-(m-1)}}{Z^{-f}} \tag{7.4}$$

where b_1, b_2, ..., b_{m-1} are constant, and f is the delay step.

The polynomial fitting for m data points is equivalent an (m - 1) order FIR filter. The system function and frequency response of the filter depends on the order of the polynomial n, the fitting data point m and the output delay f.

For n = 1 and m = 5, it is can be shown from eqn (7.2) that:

$$a_0 = \frac{11}{10} \sum_{k=1}^{5} u_k - \frac{3}{10} \sum_{k=1}^{5} k u_k$$

$$a_1 = \frac{1}{10} \sum_{k=1}^{5} k u_k - \frac{3}{10} \sum_{k=1}^{5} u_k \tag{7.6}$$

When f = 0 this is equivalent to a fit of the first data point. By substituting eqn (7.6) into eqn (7.3) and applying the Z transformation, the system function is:

$$H^{f=0}_{n=1,m=5}(Z) = \frac{3}{5} + \frac{2}{5}Z^{-1} + \frac{1}{5}Z^{-2} + 0 - \frac{1}{5}Z^{-4} \qquad (7.7)$$

Following the same procedure with f = 4, the system function is:

$$H^{f=4}_{n=1,m=5}(Z) = \frac{-\frac{1}{5} + 0 + \frac{1}{5}Z^{-2} + \frac{2}{5}Z^{-3} + \frac{3}{5}Z^{-4}}{Z^{-4}} \qquad (7.8)$$

Note the symmetry of the system function coefficients between eqns (7.7) and (7.8), and the fact that the amplitude responses of the two systems are the same and the group delays are symmetrical, see Fig.7.1 and Fig.7.2.

Similarly, when f = 1 and f = 3 the system functions are:

$$H^{f=1}_{n=1,m=5}(Z) = \frac{\frac{2}{5} + \frac{3}{10}Z^{-1} + \frac{1}{5}Z^{-2} + \frac{1}{10}Z^{-3} + 0}{Z^{-1}} \qquad (7.9)$$

$$H^{f=3}_{n=1,m=5}(Z) = \frac{0 + \frac{1}{10}Z^{-1} + \frac{1}{5}Z^{-2} + \frac{3}{10}Z^{-3} + \frac{2}{5}Z^{-4}}{Z^{-3}} \qquad (7.10)$$

and for the middle point f = 2:

$$H^{f=2}_{n=1,m=5}(Z) = \frac{\frac{1}{5} + \frac{1}{5}Z^{-1} + \frac{1}{5}Z^{-2} + \frac{1}{5}Z^{-3} + \frac{1}{5}Z^{-4}}{Z^{-2}} \qquad (7.11)$$

The amplitude responses and group delays of the five data points for LS first order polynomial fitting for different data fitting points are shown in Figs. 7.1 and 7.2 where the frequency is from 0 to π, and the group delay is defined as (Proakis & Manolakis, 1992):

$$\tau_g(\omega) = -\frac{d\Theta(\omega)}{d\omega} \qquad (7.12)$$

where $\Theta(\omega)$ is the system phase response and ω is the frequency. The group delay is interpreted as the time delay that a signal component of frequency ω undergos as it passes from the input to the output of the system. Note that when $\Theta(\omega)$ is linear, $\tau_g(\omega)$ = constant, and all frequency components of the input signal undergo the same time delay. An ideal filter will have a constant magnitude and linear phase characteristics within its passband, and no data distortion.

The system function of higher than first order can be obtained following the above mentioned procedure.

From the amplitude response and group delay plots (Fig.7.1 to Fig.7.6) it can be seen that the frequency response is different for different fitting points. The middle point fitting has the best performance and the least fitting error because it has the smallest sidelobe of amplitude response and has a linear phase response. Apart from the middle point, the fitting error increases because of the nonlinearity of the phase response. The sidelobe of the amplitude response and the passband width are also increased. The worst situation occurs near the end point fitting, not only because of its large sidelobe in the stopband, but also for the large distortion of the passband in both the amplitude and phase response. The situation becomes worse when the order of the polynomial increases, see Fig.7.1 to Fig.7.6. The above analysis demonstrates that the cause of the polynomial "wiggle" effect is due to the phase response nonlinearity and the amplitude response large sidelobe. This effect could cause the data extrapolation occur in the wrong direction.

Fig.7.7 to Fig.7.9 are the amplitude response plots of different data points LSPF for middle point fitting. Because they are middle point fitting, the phase responses are linear and the group delays are zero.

If middle point fitting is adopted, the algorithms can be simplified. In this case the fitting data number is chosen as an odd number and the middle point is defined as the zero point and the other points before and after the middle point are defined as being minus and plus symmetrical to the middle point: -m, -(m-1), ..., -2, -1, 0,1 ,2, ..., m-1, m for 2m + 1 data points. The polynomial fitting now can be expressed as:

$$y_0 = a_0 + \sum_{i=1}^{n} a_i k^i = a_0 \qquad (7.13)$$

The computation of a_0 can now be derived by minimizing:

$$F(a_0, a_1, ..., a_n) = \sum_{k=-m}^{m} \left\{ u_k - \left[a_0 + \sum_{i=1}^{n} a_i k^i \right] \right\}^2 \tag{7.14}$$

and the computation is simplified because all summation terms involving odd powers of m are zero:

$$\left\{ \begin{array}{l} \sum_{k=-m}^{m} a_0 + \sum_{k=-m}^{m} \sum_{i=1}^{n} a_i k^i = \sum_{k=-m}^{m} u_k \\ \sum_{k=-m}^{m} a_0 k^2 + \sum_{k=-m}^{m} k^2 \sum_{i=1}^{n} a_i k^i = \sum_{k=-m}^{m} k^2 u_k \\ \quad \cdots \\ \sum_{k=-m}^{m} a_0 k^{2L} + \sum_{k=-m}^{m} k^{2L} \sum_{i=1}^{n} a_i k^i = \sum_{k=-m}^{m} k^{2L} u_k \end{array} \right. \tag{7.15}$$

If n is even then L = n/2, if n is odd then L = (n - 1)/2. When n = 2 and n = 3, L = 1, when n = 4 and n = 5, L = 2, etc., hence for the same fitting data number 2m + 1, the middle point LS polynomial fittings for n = 2 and n = 3, n = 4 and n = 5, etc., are the same.

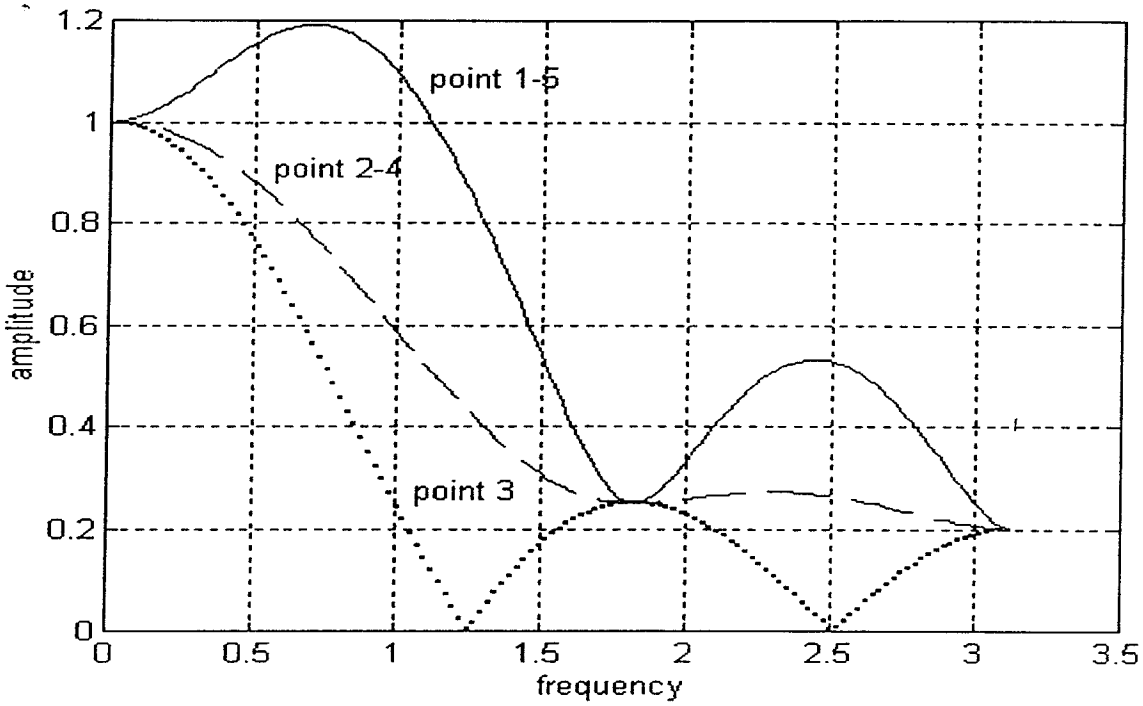

Figure 7.1. Amplitude response of first order poly-fitting for 5 data points.

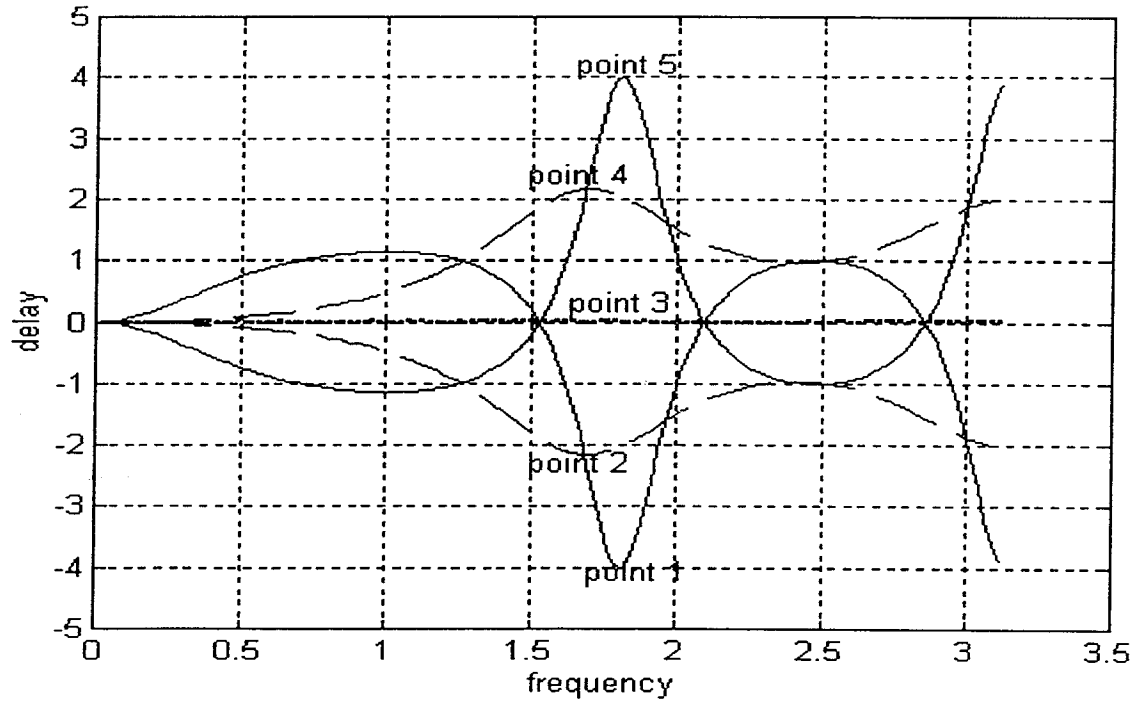

Figure 7.2. Group delay of first order poly-fitting for 5 data points.

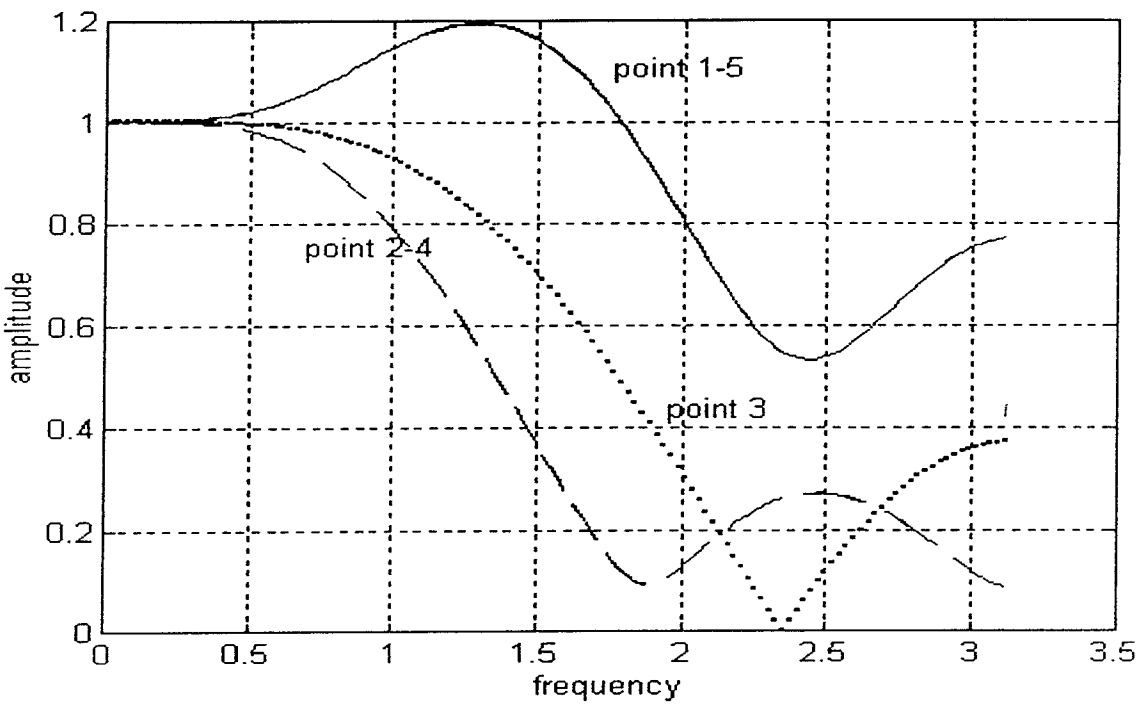

Figure 7.3. Amplitude response of second order poly-fitting for 5 data points.

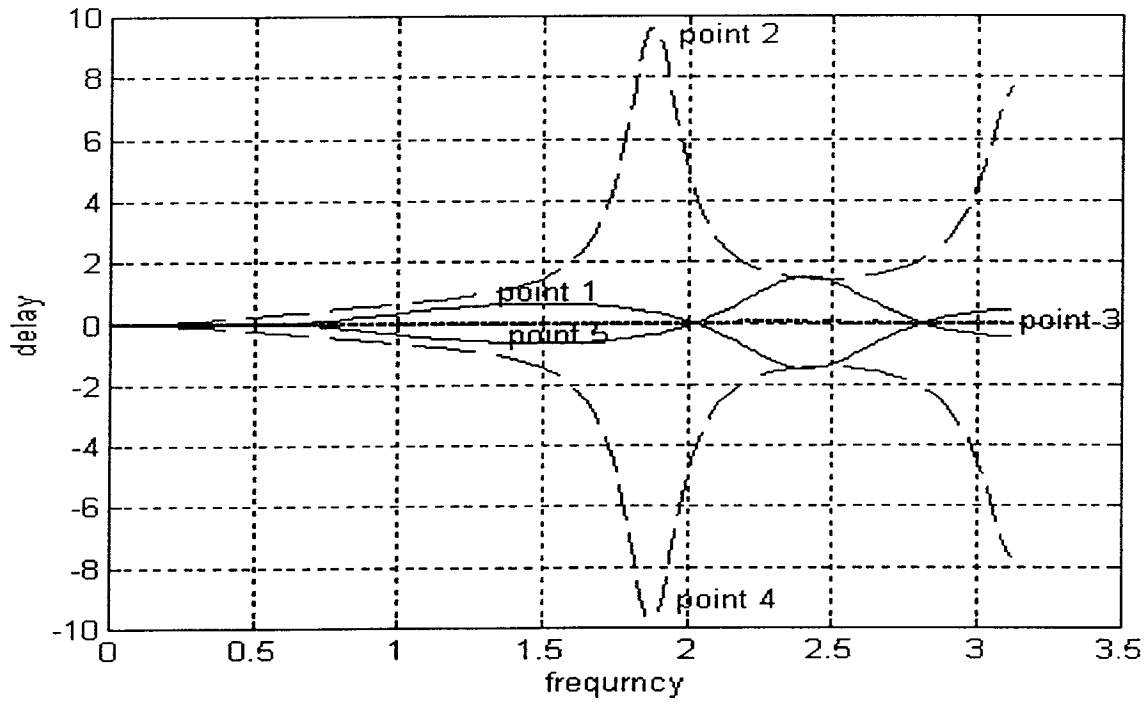

Figure 7.4. Group delay of second order poly-fitting for 5 data points.

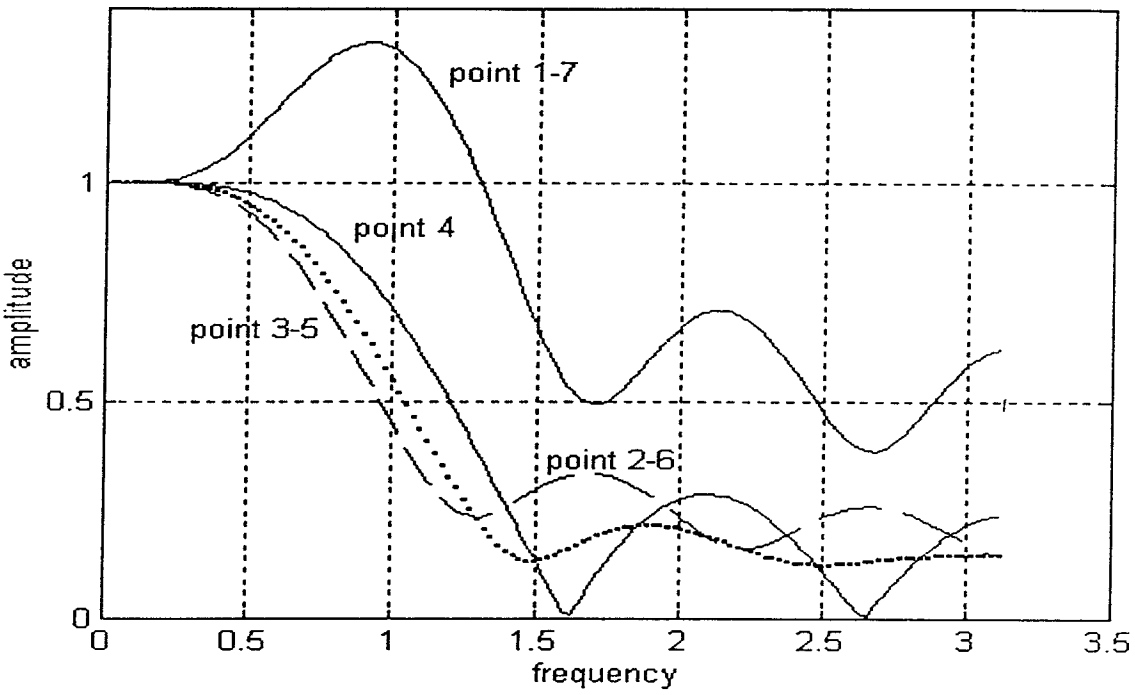

Figure 7.5. Amplitude response of second order poly-fitting for 7 data points.

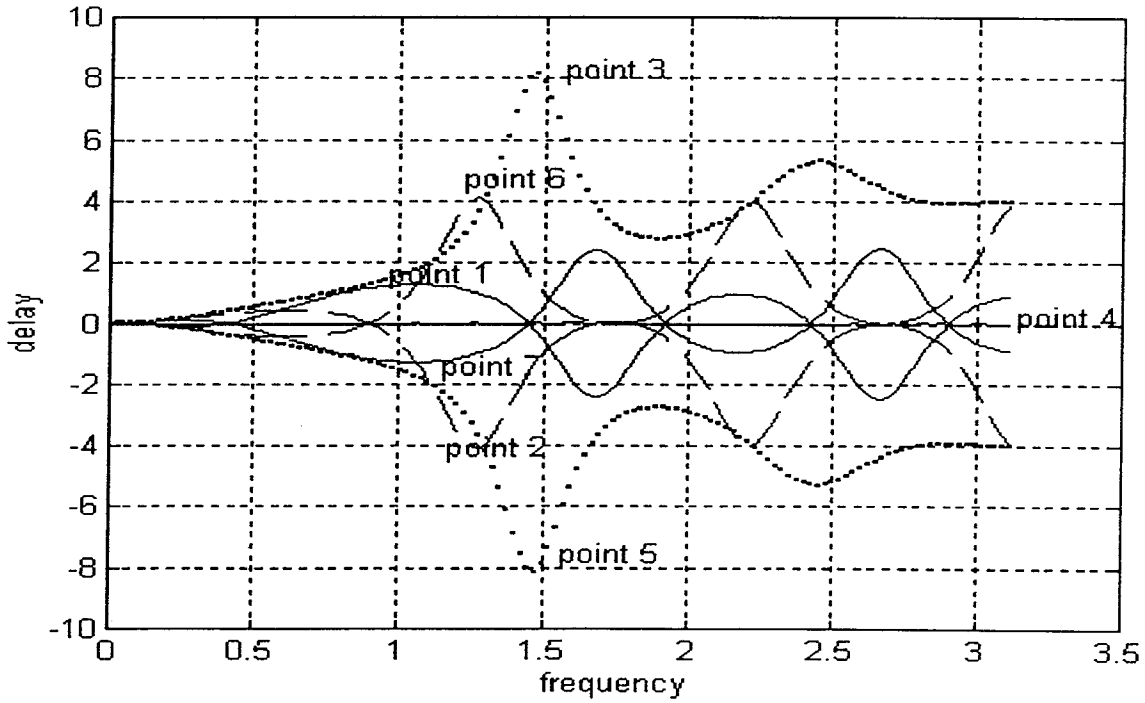

Figure 7.6. Group delay of second order poly-fitting for 7 data points.

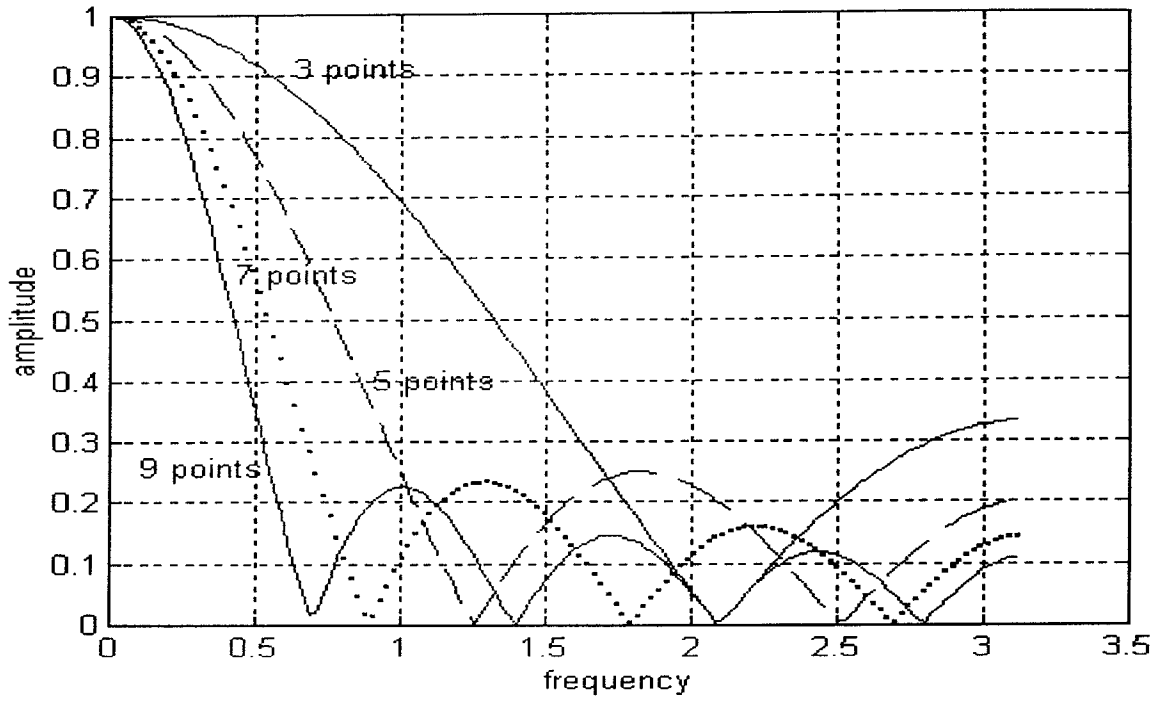

Figure 7.7. Amplitude response of first order poly-middle point fitting.

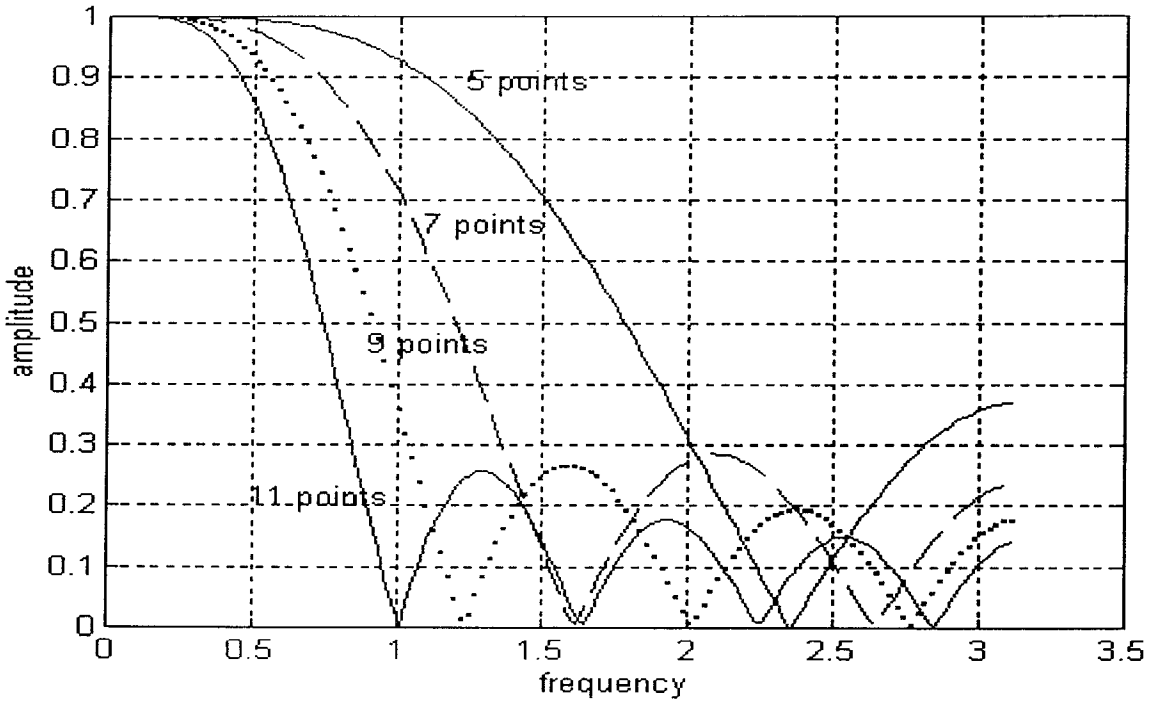

Figure 7.8. Amplitude response of second order poly-middle point fitting.

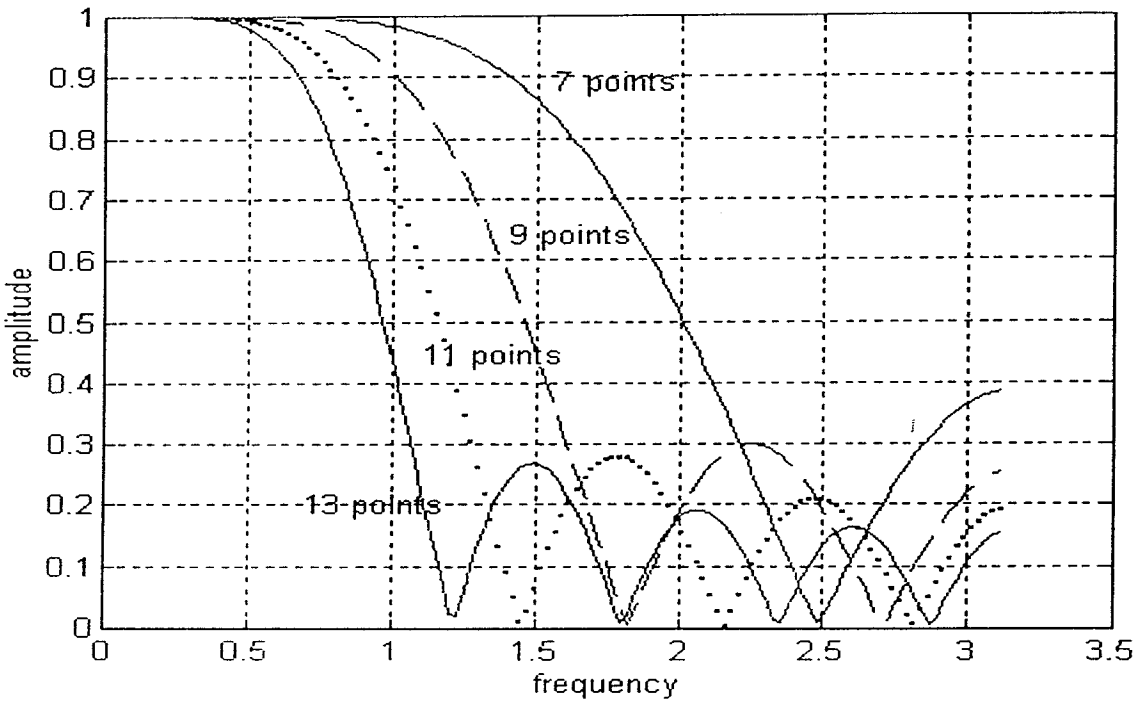

Figure 7.9. Amplitude response of fourth order poly-middle point fitting.

Remarks to LSPF:

1) The higher the order of the polynomial, the wider is its frequency response passband, the higher degree is the amplitude response tangency at $\omega = 0$ and narrower is the transition region between the passband and stopband, see Fig.7.7 to Fig.7.9. The passband width is defined as the frequency where the amplitude response decays from 1 to 0.707 (-3 dB).

2) As more data points are used for the LSPF, the narrower is the passband and the transition region and more rapid are the sidelobe "wiggles" and hence the more the envelope of the "wiggles" is squeezed towards the frequency axis (see the amplitude response plots).

3) The higher the order of the polynomial and the more data points used for the fitting, a larger deviation of the extrapolation from the real data can result because of the polynomial "wiggle" effect.

The performance of polynomial fitting can be improved by using a modified Least Squares method (Hamming, 1989), or it can be replaced by other DFs

designed in the frequency domain with a specified frequency response and filter length.

7.1.2 IIR LDF

A low-pass IIR (Infinite Impulse Response) filter known as elliptic filter, which is a combination of Chebyshev type 1 and type 2 filters exhibiting equiripple behaviour in both passband and stopband, is used for phase data fitting and cycle slip detection (Fu, 1992). The specification of the filter is based on the PSD analysis of the GPS phase data of 1 Hz sampling frequency. As an instant data jump (step function, or impulse and couple of impulse if the data is differentiated), the cycle slip behaves like high frequency noise and its power is concentrated in the high frequency area.

The specification of the filter is:

order = 5
cut-off frequency = 0.3 π
passband ripple = 0.1dB
stopband decay = 40 dB
transition region = 0.16 π

The cut-off frequency chosen is based on the consideration that there is about a 7 second roll period for a small sized ship, and that the transition region of the filter approximates the slow changing of the signal PSD transition towards the high frequency. The frequency response of the filter is shown in Fig.7.10 and Fig.7.11, and the system function is:

$$H(Z) = \frac{0.0347+0.0222Z^{-1}+0.0529Z^{-2}+0.0529Z^{-3}+0.0222Z^{-4}+0.0347Z^{-5}}{1-2.4656Z^{-1}+3.2733Z^{-2}-2.4385Z^{-3}+1.0509Z^{-4}-0.2008Z^{-5}} \quad (7.16)$$

Cycle slip detection and repair can carried out in two ways: one is similar to the LS polynomial fitting and prediction method where the DF is used to fit and predict the phase data, which can be one-way or differenced depending on the data sampling rate. The DF takes the form of an ARMA series:

$$y(k)+a(1)y(k-1)+a(2)y(k-2)+a(3)y(k-3)+a(4)y(k-4)+a(5)y(k-5)$$

$$=b(0)x(k)+b(1)x(k-1)+b(2)x(k-2)+b(3)x(k-3)+b(4)x(k-4)$$

$$+b(5)x(k-5) \tag{7.17}$$

The one step prediction is (Vadaele, 1983):

$$y(k+1) =-a(1)y(k)-a(2)y(k-1)-a(3)y(k-2)-a(4)y(k-3)-a(5)y(k-4)$$

$$+b(1)x(k)+b(2)x(k-1)+b(3)x(k-2)+b(4)x(k-3)+b(5)x(k-4) \tag{7.18}$$

Another approach is to directly filter the phase data, and the cycle slip (being high frequency noise) is eliminated by the low-pass filter. Generally the cycle slip value should be less than 10 cycles to reduce the sidelobe effect of the DF. Large cycle slip is easy to detect and repair using the DF prediction method. This is similar to data smoothing and the high frequency noise and cycle slips are all eliminated, or depressed, by the filter.

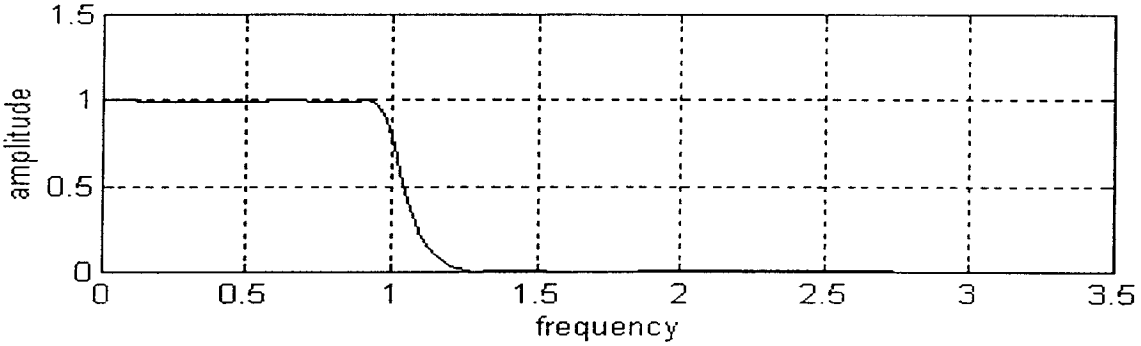

Figure 7.10. Amplitude response of the 5th order elliptic filter.

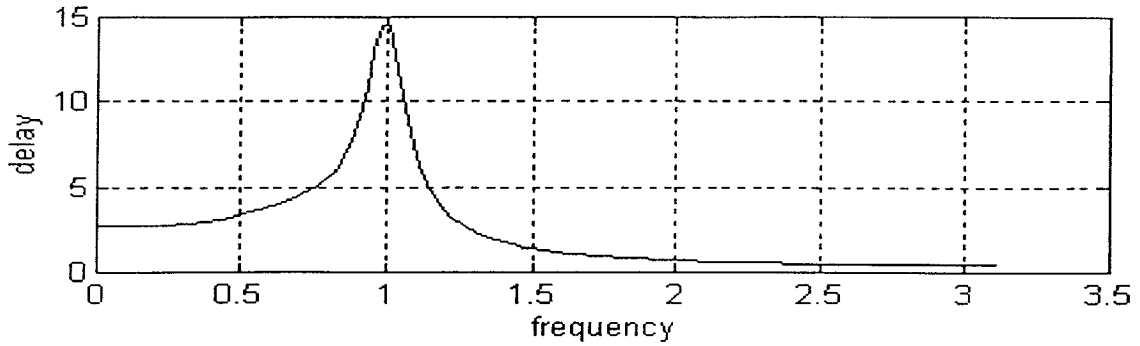

Figure 7.11. Group delay of the 5th order elliptic filter.

7.1.3 Least Squares Filter

Least Squares filter (LS) is very popular for GPS navigation, and is used within many receivers. The reason is that LS requires no information on the body's dynamics and a priori statistics of the state and measurement, except that of the second moment of the measurement noise if Markov estimation is used. If the complete observability condition is fulfilled, LS filtering is stable and convergent. The variance of LS estimation is only dependent on the satellite geometry and the variance of measurement noise. LS can be considered as a weighted-averaging procedure that smooths the random noise and its low-pass property is obvious.

The problem of LS for navigation applications is that LS operates on the static mode principle and the body's states at different epochs are considered as being totally independent. There is no information accumulation from past measurement, and only the body's position and measurement bias, which can only be modelled as random constant or white noise, can be estimated using the pseudo-range and carrier phase measurements. If the velocity and bias-rate are to be estimated, the Doppler measurements have to be used. Generally, the trajectory obtained from LS positioning is not smooth. For more details see, for example, Cross (1983).

7.1.4 Kalman Filter (KF)

For the navigation model mentioned above, the Kalman filter algorithm is (modified from Maybeck,1979):

one step prediction:

$$\widehat{\mathbf{X}}(t_k^-) = \Phi(t_k,t_{k-1})\,\widehat{\mathbf{X}}(t_{k-1}^+) \tag{7.19}$$

$$\mathbf{P}(t_k^-) = \Phi(t_k,t_{k-1})\mathbf{P}(t_{k-1}^+)\Phi^T(t_k,t_{k-1}) + \mathbf{Q}(t_k) \tag{7.20}$$

updating:

$$\mathbf{K}(t_k) = \mathbf{P}(t_k^-)\mathbf{H}^T(t_k)\left[\mathbf{H}(t_k)\mathbf{P}(t_k^-)\mathbf{H}^T(t_k) + \mathbf{R}(t_k)\right]^{-1} \tag{7.21}$$

$$\hat{\mathbf{X}}(t_k^+) = \hat{\mathbf{X}}(t_k^-) + \mathbf{K}(t_k)\left[\mathbf{Z}(t_k) - \mathbf{H}(t_k)\hat{\mathbf{X}}(t_k^-)\right] \tag{7.22}$$

$$\mathbf{P}(t_k^+) = \mathbf{P}(t_k^-) - \mathbf{K}(t_k)\mathbf{H}(t_k)\mathbf{P}(t_k^-) \tag{7.23}$$

or

$$\mathbf{P}(t_k^+) = \left[\mathbf{I} - \mathbf{K}(t_k)\mathbf{H}(t_k)\right]\mathbf{P}(t_k^-) \tag{7.24}$$

or

$$\mathbf{P}(t_k^+) = \left[\mathbf{I} - \mathbf{K}(t_k)\mathbf{H}(t_k)\right]\mathbf{P}(t_k^-)\left[\mathbf{I} - \mathbf{K}(t_k)\mathbf{H}(t_k)\right]^T + \mathbf{K}(t_k)\mathbf{R}(t_k)\mathbf{K}^T(t_k) \tag{7.25}$$

with initial condition:

$$\hat{\mathbf{X}}(t_0) = E\left[\mathbf{X}(t_0)\right] \tag{7.26}$$

$$\mathbf{P}(t_0) = \text{cov}\left[\mathbf{X}(t_0)\right] \tag{7.27}$$

Eqns (7.19) to (7.27) describe the basic Kalman filter algorithm for a linear system and for which $\mathbf{P}(t_k^+)$ is given in the three forms commonly used. Eqn (7.23) involves two symmetrical matrix subtractions, and if the measurements (carrier phase and Doppler) are very accurate, this can cause serious numerical problems, even to the extent of not assuring the positive definiteness of the **P** matrix because of the small difference between the subtrahend and minuend. Not only does eqn (7.24) fail to assure positive definiteness of the results, but it suffers additionally from the fact that the symmetry is not well preserved, because it is in the form of a product of a non-symmetric matrix and a symmetric one. Eqn (7.25), known as the Joseph form, is in the form of the sum of two symmetric matrices. The first part of (7.25) is positive-definite and the second part is positive semi-definite (n-by-n, and of rank at most m; n, m are the dimensions of state and measurements). Consequently numerical computations based on this form will be better conditioned, and better at assuring both the symmetry and positive-definiteness of $\mathbf{P}(t_k^+)$ than alternate forms (eqn (7.23), (7.24)). Furthermore, it is insensitive, to first order, to small errors in the computed filter gain $\mathbf{K}(t_k)$. For a first order error in $\mathbf{K}(t_k)$, the error in $\mathbf{P}(t_k^+)$ computed by eqn (7.25) is of second order, while the error in the alternate forms is of first order. Similarly, it is less

sensitive to arithmetic truncation error than the alternate forms, especially in the case where the measurement noise is small. Hence eqns (7.23) and (7.24) will be subject to first order truncation error effects, while eqn (7.25) will only be affected to second order. This becomes a crucial consideration for real-time applications in which the minimum computer wordlength that achieves adequate performance is sought. Although the Joseph form has some desirable characteristics, it requires considerably greater number of computations. In fact, in some cases, especially those characterized by long periods of essentially steady state behaviour, the inherently greater number of additions and multiplications leads to larger numerical errors in the Joseph form than in the alternate forms.

If the state initial conditions in some or all directions of the state space are totally unknown, the filter can be started by using the equations:

$$\mathbf{P}(t_k^+) = \left[\mathbf{P}^{-1}(t_k^-) + \mathbf{H}^T(t_k)\mathbf{R}^{-1}(t_k)\mathbf{H}(t_k)\right]^{-1} \tag{7.28}$$

$$\mathbf{K}(t_k) = \mathbf{P}(t_k^+)\mathbf{H}^T(t_k)\mathbf{R}^{-1}(t_k) \tag{7.29}$$

If $\mathbf{P}^{-1}(t_0)$ is singular, that is certain eigenvalues of $\mathbf{P}(t_0)$ go to infinity, then until $\mathbf{P}^{-1}(t_k)$ attains full rank, a unique estimate of the full state cannot be obtained.

Under the assumption that $\mathbf{P}^{-1}(t_0) = 0$ and no system driving noise, that is $\mathbf{Q}(t_k) = 0$, the Fisher information matrix:

$$\mathbf{f}(t_i,t_1) = \sum_{j=1}^{i} \Phi^T(t_j, t_i)\mathbf{H}^T(t_j)\mathbf{R}^{-1}(t_j)\mathbf{H}(t_j)\Phi(t_j, t_i) \tag{7.30}$$

has a simple relationship with the estimate covariance (Maybeck,1979):

$$\mathbf{f}(t_i,t_1) = \mathbf{P}^{-1}(t_i) \tag{7.31}$$

Note that the Fisher information matrix is directly related to the observability matrix. Eqn (7.31) shows that the larger the eigenvalues of $\mathbf{f}(t_i,t_1)$ the smaller the eigenvalues of $\mathbf{P}(t_i^+)$, and the more accurate the estimate is. If any eigenvalues of $\mathbf{f}(t_i,t_1)$ are zero, these are the directions in the state space along which the measurements give no information for the corresponding state.

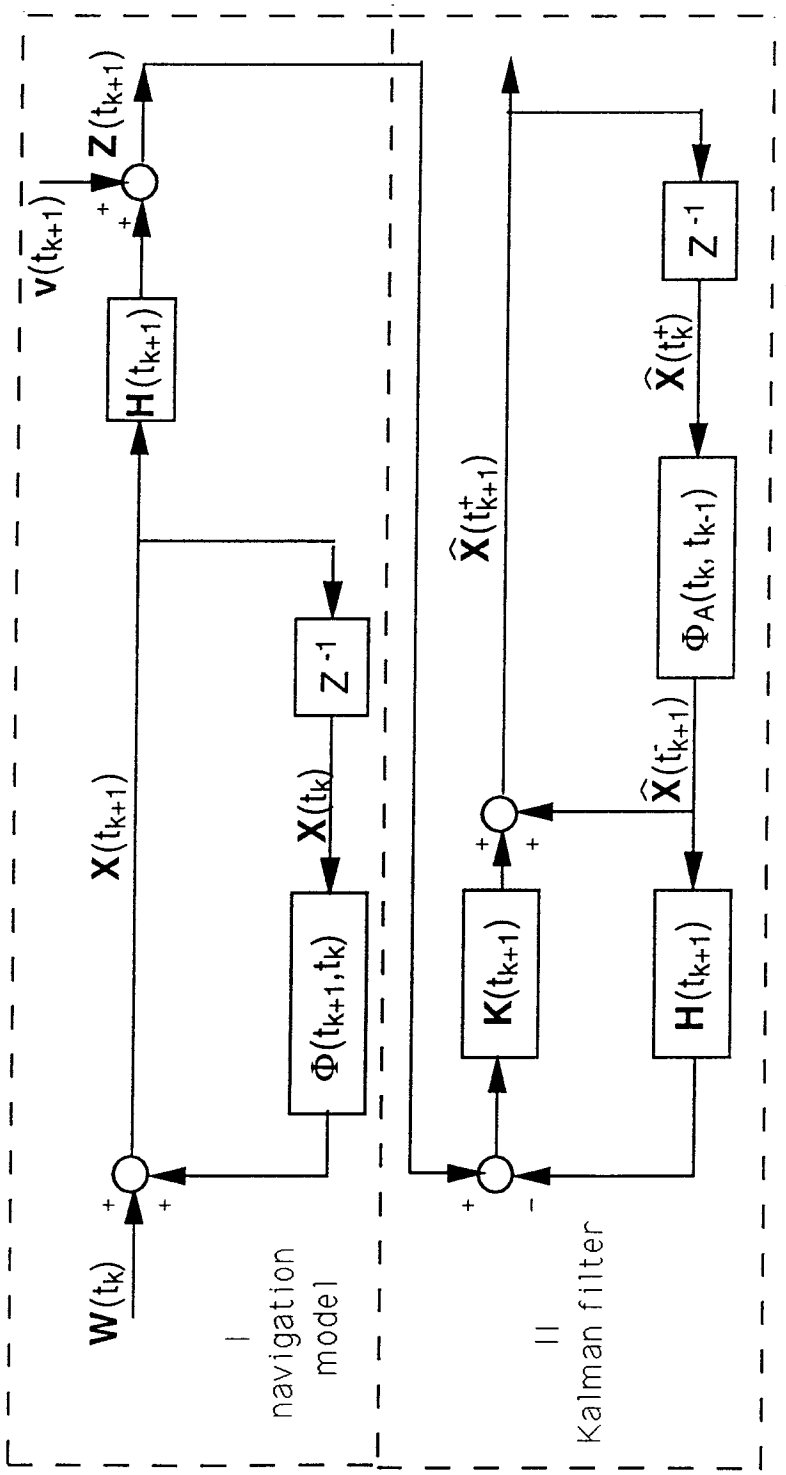

Figure 7.12. Block chart of linear discrete-time Kalman filter.

The linear discrete-time Kalman filter structure is illustrated in Fig.7.12.

- Before measurements are input into KF, they need to be linearized, either about the reference trajectory, or the one-step predicted trajectory. The KF corresponding to former mode is known as the linearized KF, and the later one is referred to as the extended KF (EKF). Both operate under the assumption that the deviations from the nominal trajectory are small enough to allow linear perturbation techniques to be employed. Generally, a first order approximation to the measurement equation is adopted, and a linearization error which is of second order of the series expansion is introduced by the process of the linearization. This linearization error can be considered as an additional measurement noise. For the EKF the linearization error is large at the beginning of filtering and decreases with increasing filtering time because the filter prediction becomes more accurate. The linearization error of the EKF can be reduced by iteration or higher order expansion.

The statistical characteristics of the KF can be summarized as follows. If the system driving noise, measurement noise and the initial state are all Gaussian processes and variables, the estimate of the KF is the minimum variance estimation:

$$\widehat{\mathbf{X}}(t_{k+1}^{+}) = E\left[\mathbf{X}(t_{k+1})/\mathbf{Z}(t_{k+1}),\ \mathbf{Z}(t_k),\ \cdots,\ \mathbf{Z}(t_1)\right] \tag{7.32}$$

If the Gaussian assumption is removed, the KF becomes a linear minimum variance estimation which is the projection of the state onto the measurement space, hence the estimation error is orthogonal to the measurement space:

$$\mathbf{e}(t_k^{+}) \equiv \left[\mathbf{X}(t_k) - \widehat{\mathbf{X}}(t_k^{+})\right] \perp \mathbf{Z}(t_k, t_1) \tag{7.33}$$

$$E\left[\mathbf{e}(t_k^{+})/\mathbf{Z}(t_k,\ t_1)\right] = 0 \tag{7.34}$$

where $\mathbf{Z}(t_k,t_1)$ is the measurement space spanned by the measurements $\mathbf{Z}(t_k)$, $\mathbf{Z}(t_{k-1})$, ..., $\mathbf{Z}(t_1)$ and the KF is an unbiased estimator which produces the smallest unconditional error covariance matrix among a class of linear estimators, whether or not the initial state, system driving noise and measurement noise are Gaussian (for more details see Anderson & Moore, 1979). The low-pass property of the KF is obvious considering that the KF estimate is the weighted mean value of the past and present measurements.

The innovation (residual) series of the KF can be written as:

$$\begin{aligned}\mathbf{r}(t_k) &= \mathbf{Z}(t_k) - \mathbf{H}(t_k)\hat{\mathbf{X}}(t_k^-) \\ &= \mathbf{H}(t_k)\mathbf{X}(t_k) + \mathbf{v}(t_k) - \mathbf{H}(t_k)\hat{\mathbf{X}}(t_k^-) \\ &= \mathbf{H}(t_k)\left[\Phi(t_k,t_{k-1})\mathbf{X}(t_k) + \mathbf{W}(t_{k-1}) - \Phi(t_k,t_{k-1})\hat{\mathbf{X}}(t_{k-1}^+)\right] + \mathbf{v}(t_k) \\ &= \mathbf{H}(t_k)\Phi(t_k,t_{k-1})\mathbf{e}(t_{k-1}^+) + \mathbf{H}(t_k)\mathbf{W}(t_{k-1}) + \mathbf{v}(t_k)\end{aligned} \tag{7.35}$$

where $\mathbf{e}(t_{k-1}^+)$, $\mathbf{W}(t_{k-1})$ and $\mathbf{v}(t_k)$ are independent of the measurements $\mathbf{Z}(t_{k-1})$, $\mathbf{Z}(t_{k-2})$, ..., $\mathbf{Z}(t_1)$, or orthogonal to the sub-space $\mathbf{Z}(t_{k-1},t_1)$. By definition, $\mathbf{r}(t_1)$, $\mathbf{r}(t_2)$, ..., $\mathbf{r}(t_{k-1})$ are linear functions of the previous measurements, so $\mathbf{r}(t_k)$ is independent of previous $\mathbf{r}(t_i)$'s. In other word, the innovation series $\mathbf{r}(t_k)$ is a white noise series and:

$$E[\mathbf{r}(t_k)] = 0 \tag{7.36}$$

$$E[\mathbf{r}(t_k)\,\mathbf{r}^T(t_k)] = \mathbf{H}(t_k)\mathbf{P}(t_k^-)\mathbf{H}^T(t_k) + \mathbf{R}(t_k) \tag{7.37}$$

Eqns (7.35) to (7.37) are based on the assumption that the mathematical model of the KF accurately depicts the real system behaviour, hence the whiteness of the innovation series and its statistics are important performance indicators of the KF. They can be exploited for KF model testing, navigation sensor failure detection or reasonableness checking of measurement data. The whiteness of the innovation series can be tested by its sample autocorrelation. If $\mathbf{X}(t_k)$ and $\mathbf{Z}(t_k)$ follow the joint Gaussian distribution, the innovation series is a Gaussian series and the statistic can be formed as:

$$\chi^2(t_k) = \mathbf{Z}^T(t_k)\left[\mathbf{H}(t_k)\mathbf{P}(t_k^-)\mathbf{H}^T(t_k) + \mathbf{R}(t_k)\right]^{-1}\mathbf{Z}(t_k) \tag{7.38}$$

and hypothesis testing of χ^2 with degree of freedom m can be carried out.

The stability of the KF can be derived by transforming the updating equation (7.22) as:

$$\begin{aligned}\hat{\mathbf{X}}(t_k^+) &= \hat{\mathbf{X}}(t_k^-) + \mathbf{K}(t_k)\left[\mathbf{Z}(t_k) - \mathbf{H}(t_k)\hat{\mathbf{X}}(t_k^-)\right] \\ &= \left[\mathbf{I} - \mathbf{K}(t_k)\mathbf{H}(t_k)\right]\Phi(t_k,t_{k-1})\hat{\mathbf{X}}(t_{k-1}^+) + \mathbf{K}(t_k)\mathbf{Z}(t_k) \\ &= \Psi(t_k,t_{k-1})\hat{\mathbf{X}}(t_{k-1}^+) + \mathbf{K}(t_k)\mathbf{Z}(t_k)\end{aligned} \tag{7.39}$$

The stability of the KF depends on the homogeneous solution of eqn (7.39). If the system represented by eqn (7.39) is uniformly asymptotically stable, then there exist positive constants β and γ such that (modified from Maybeck, 1982):

$$\left|\Psi(t_k,t_l)\right| \le \beta e^{-\gamma(t_k-t_l)} \tag{7.40}$$

where $k \ge l \ge 0$.

If the navigation model is completely controllable and observable, then condition of eqn (7.40) will be satisfied. The KF based on the navigation model is uniformly asymptotically stable, even though the navigation model itself is unstable or marginally stable. This means that the initial state uncertainty does not affect the KF estimate. Suppose $\mathbf{P}_1(t_k^+)$ and $\mathbf{P}_2(t_k^+)$ are derived from two different initial state and if the KF is stable then:

$$\left|\mathbf{P}_1(t_k^+) - \mathbf{P}_2(t_k^+)\right| \to 0 \text{ for } t_k \to \infty \tag{7.41}$$

and $\mathbf{P}_1(t_k^+)$ or $\mathbf{P}_2(t_k^+)$ are convergent and lower-bounded, which can be defined by the Cramer-Rao Lower Bound (CRLB).

Generally speaking divergence of the KF is caused by the following three phenomena:

1)The modelling error:
Since any mathematical model of a system is an approximation to reality there will always be a discrepancy between the mathematical model used to define the filter and the actual conditions under which the filter must operate. As a general rule, to avoid filtering-divergence, the modelling error should have white noise characteristics. Although the KF computes the error covariance internally, this is a valid depiction of the true errors committed of the filter only to the extent that the filter's own system model adequately portrays true system behaviour. Sometimes the estimated covariance indicates a good performance of the KF yet

the KF estimate is deviating from the true state. Generally divergence can be detected by innovation series testing.

2)The non-observability of the system:
There may be one or more state variables (or their linear combinations) that are "hidden" from the external measurements. In general, the eigenvalues of $\mathbf{P}(t_k^+)$ corresponding to the non-observable state variable will increase and the filter is instable. It can be avoided by correctly selecting the state variable (as the choice of state variable is not unique) to make the system completely observable.

3) The numerical error:
This is the integrated effect of round-off errors due to finite wordlength effects in the computer. This is particularly true for on-line applications, where computer constraints may dictate the use of fixed-point arithmetic. The numerical error mainly affects the updating of the covariance matrix, which must preserve the symmetry and positive-definiteness of the matrix. Although it is theoretically impossible for the covariance to have negative eigenvalues, such a condition can and often does result due to numerical computation effects, especially when the measurements are very accurate (eigenvalues of $\mathbf{R}(t_k)$ are small relative to those of $\mathbf{P}(t_k^-)$, this being accentuated by large eigenvalues of $\mathbf{P}(t_0)$); or some state variable, or their linear combination, is known with great precision while others are nearly unobservable; or some state variables are random constants (or pure biases) with no driving noise. In all of the above cases the covariance matrix is ill-conditioned, and this ill-conditioning can also be caused by the non-observability of the state variables. In order to overcome the divergence problem caused by numerical error square root filter algorithms can be used. Instead of $\mathbf{P}$, the square root filter algorithm results in term of $\mathbf{P}^{1/2}$ which can always be defined for a symmetrical and positive-definite matrix $\mathbf{P}$ as $\mathbf{P} = \mathbf{P}^{1/2}\mathbf{P}^{1/2}$. A related technique, known as **U-D** covariance factorization, in which $\mathbf{P}$ is factored as $\mathbf{P} = \mathbf{U}\mathbf{D}\mathbf{U}^T$ with $\mathbf{U}$ being upper triangular and $\mathbf{D}$ being a diagonal matrix, provides the same numerical benefits (double-precision is archived using single-precision algorithm) but with considerably less computational load (see Bierman,1977).

7.1.5 Separated-Bias Kalman Filter (SBKF)

For carrier phase measurements the ambiguities are modelled as random constants which are uncontrollable, for they have no driving noise. Similarly, the

gyrocompass and log errors, gyro drift, scale factor error of an INS can also be modelled as constant biases, or slow-changing biases. It is a common practice to augment the bias terms to the original system state vector. The filter then estimates the bias terms as well as those of the original system. The basic navigation models are completely controllable and observable and the filtering is stable, but as soon as the biases are augmented to the navigation models, the system becomes uncontrollable and there is an increased tendency for the calculated quantities (particularly the covariance matrix) of the filter to become ill-conditioned with time. In addition, the computational load, which can be assumed to be proportional to n^3 (n is the dimension of the state vector), increases due to the presence of augmented state variables, especially the dimension of the augmented state vector is comparable to the original one.

SBKF was first proposed by Friedland (1969). Since then it has being developed by Bierman (1973), Mendel (1976), and others, and successfully applied to various areas such as satellite orbit determination, inertial navigation etc (see, Friedland, 1983).

The SBKF flowchart is illustrated in Fig.7.13 (modified from ibid, 1983).

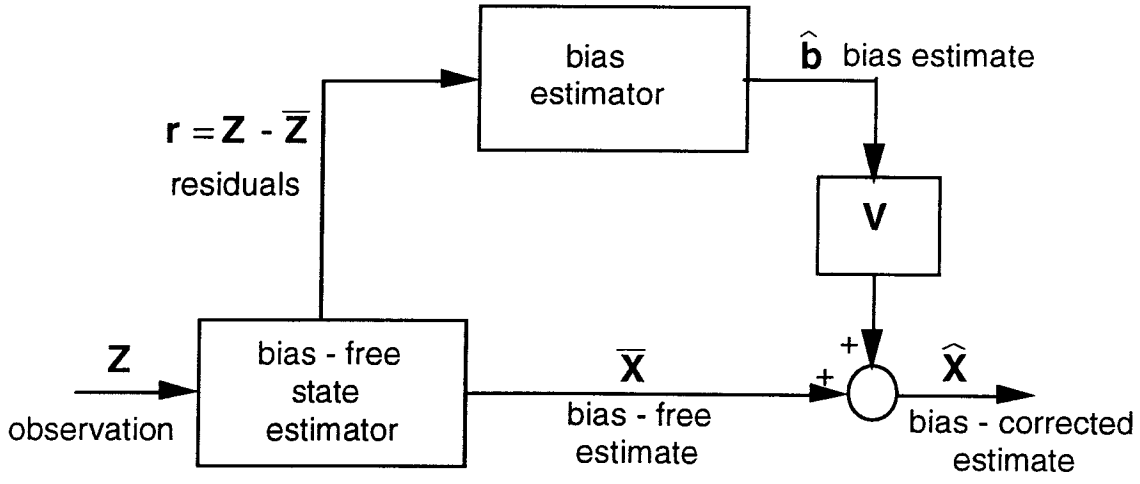

Figure 7.13. Block chart of separated bias estimator.

The SBKF consists of two KF's, the bias-free state estimator and the bias estimator. The bias-free estimator is a standard KF assuming no bias is present. The difference between the actual observation $\mathbf{Z}$ and the bias-free estimator estimated observation $\overline{\mathbf{Z}}$ is the input of the bias estimator, which outputs the optimum estimate $\hat{\mathbf{b}}$ of the unknown bias $\mathbf{b}$. The desired optimum state estimate

$\hat{\mathbf{X}}$ is the addition of the bias estimate $\hat{\mathbf{b}}$, multiplied by the correction matrix **V**, to the bias-free estimate $\bar{\mathbf{X}}$.

With the SBKF technique the estimation of the bias is essentially decoupled from the computation of the bias-free estimate of the state. Hence the bias-free estimator is a stable filter for it is based on the navigation model only, and the uncontrollable bias terms which have the same statistic property are estimated separately by the bias estimator.

The discrete-time SBKF used in GPS navigation is based on the following model equations:

$$\mathbf{X}_1(t_{k+1}) = \Phi_1(t_{k+1},t_k)\mathbf{X}_1(t_k) + \mathbf{W}_1(t_k) \tag{7.42}$$

$$\mathbf{Z}(t_k) = \mathbf{H}_1(t_k)\mathbf{X}_1(t_k) + \mathbf{C}(t_k)\mathbf{b}(t_k) + \mathbf{v}(t_k) \tag{7.43}$$

$$\mathbf{b}(t_{k+1}) = \mathbf{b}(t_k) \tag{7.44}$$

where the dimensions of $\mathbf{X}_1$ and **b** are n and r respectively, and

$$E\left[\mathbf{W}_1(t_k)\mathbf{W}_1^T(t_j)\right] = \mathbf{Q}_1(t_k)\delta_{kj} \tag{7.45}$$

$$E\left[\mathbf{v}(t_k)\mathbf{v}^T(t_j)\right] = \mathbf{R}(t_k)\delta_{kj} \tag{7.46}$$

$$E\left[\mathbf{W}_1(t_k)\mathbf{v}^T(t_j)\right] = 0 \tag{7.47}$$

The initial state is:

$$\hat{\mathbf{X}}_1(t_0) = E\left[\mathbf{X}_1(t_0)\right] \ , \ \mathbf{P}_{x1}(t_0) = \mathrm{cov}\left[\mathbf{X}_1(t_0)\right] \tag{7.48}$$

and the bias initial state depends on a priori knowledge, and generally

$$\hat{\mathbf{b}}(t_0) = 0 \ , \ \mathbf{P}_b(t_0) = \mathrm{cov}\left[\mathbf{b}(t_0)\right] \tag{7.49}$$

$$\mathrm{cov}\left[\mathbf{X}_1(t_0), \mathbf{b}(t_0)\right] = \mathbf{P}_{xb}(t_0) = 0 \tag{7.50}$$

For the standard KF, the bias **b** is augmented to the system model:

$$\mathbf{X}(t_k)=\begin{bmatrix}\mathbf{X}_1(t_k)\\ \mathbf{b}(t_k)\end{bmatrix} \tag{7.51}$$

$$\mathbf{X}(t_{k+1}) = \Phi(t_{k+1},t_k)\mathbf{X}(t_k) + \mathbf{W}(t_k) \tag{7.52}$$

$$\mathbf{Z}(t_k) = \mathbf{H}(t_k)\mathbf{X}(t_k) + \mathbf{v}(t_k) \tag{7.53}$$

where

$$\Phi(t_{k+1},t_k)=\begin{bmatrix}\Phi_1(t_{k+1},t_k) & 0\\ 0 & \mathbf{I}\end{bmatrix} \tag{7.54}$$

$$\mathbf{H}(t_k)=\begin{bmatrix}\mathbf{H}_1(t_k) & \mathbf{C}(t_k)\end{bmatrix}, \quad \mathbf{W}(t_k)=\begin{bmatrix}\mathbf{W}_1(t_k)\\ 0\end{bmatrix} \tag{7.55}$$

Φ has dimension (n+r)x(n+r), Φ_1 is nxn, **I** is rxr, **H** is sx(n+r), $\mathbf{H}_1$ is sxn, **C** is sxr, **W** is n+r and $\mathbf{W}_1$ dimension n.

The state estimate $\hat{\mathbf{X}}_1(t_k^+)$ can be obtained using a conventional KF and the covariance and gain matrices can be partitioned as:

$$\mathbf{P}(t_k^+)=\begin{bmatrix}\mathbf{P}_{x1}(t_k^+) & \mathbf{P}_{x1b}(t_k^+)\\ \mathbf{P}_{x1b}^T(t_k^+) & \mathbf{P}_b(t_k^+)\end{bmatrix} \tag{7.56}$$

$$\mathbf{K}(t_k)=\begin{bmatrix}\mathbf{K}_{x1}(t_k)\\ \mathbf{K}_b(t_k)\end{bmatrix} \tag{7.57}$$

Supposing that the bias **b** is ignored, then:

$$\mathbf{Z}(t_k) = \mathbf{H}_1(t_k)\mathbf{X}_1(t_k) + \mathbf{v}(t_k) \tag{7.58}$$

and the bias-free estimate $\overline{\mathbf{X}}_1(t_k^+)$, $\overline{\mathbf{X}}_1(t_k^-)$, $\overline{\mathbf{P}}_1(t_k^+)$, $\overline{\mathbf{P}}_1(t_k^-)$ and $\mathbf{K}_{x1}(t_k)$ can be obtained using the conventional KF:

$$\overline{\mathbf{X}}_1(t_k^-) = \Phi_1(t_k,t_{k-1})\overline{\mathbf{X}}_1(t_{k-1}^+) \tag{7.59}$$

$$\overline{\mathbf{P}}_{x1}(t_k^-) = \Phi_1(t_k,t_{k-1})\overline{\mathbf{P}}_{x1}(t_{k-1}^+)\Phi_1^T(t_k,t_{k-1}) + \mathbf{Q}_1(t_k) \tag{7.60}$$

$$\overline{\mathbf{K}}_{x1}(t_k) = \overline{\mathbf{P}}_{x1}(t_k^-)\mathbf{H}_1^T(t_k)\left[\mathbf{H}_1(t_k)\overline{\mathbf{P}}_{x1}(t_k^-)\mathbf{H}_1^T(t_k) + \mathbf{R}(t_k)\right]^{-1} \tag{7.61}$$

$$\overline{\mathbf{X}}_1(t_k^+) = \overline{\mathbf{X}}_1(t_k^-) + \overline{\mathbf{K}}_{x1}\left[\mathbf{Z}(t_k) - \mathbf{H}_1(t_k)\overline{\mathbf{X}}_1(t_k^-)\right] \tag{7.62}$$

$$\overline{\mathbf{P}}_{x1}(t_k) = \left[\mathbf{I} - \overline{\mathbf{K}}_{x1}(t_k)\mathbf{H}_1(t_k)\right]\overline{\mathbf{P}}_{x1}(t_k^-) \tag{7.63}$$

Now supposing that the bias **b** is perfectly known, then the recursive estimate of $\mathbf{X}_1$ would take the form:

$$\widetilde{\mathbf{X}}_1(t_k^-) = \Phi_1(t_k,t_{k-1})\widetilde{\mathbf{X}}_1(t_{k-1}^+) \tag{7.64}$$

$$\widetilde{\mathbf{X}}_1(t_k^+) = \widetilde{\mathbf{X}}_1(t_k^-) + \overline{\mathbf{K}}_{x1}\left[\mathbf{Z}(t_k) - \mathbf{H}_1(t_k)\widetilde{\mathbf{X}}_1(t_k^-) - \mathbf{C}(t_k)\mathbf{b}(t_k)\right] \tag{7.65}$$

and the gain matrix for this estimator is clearly identical to that of the bias-free case, as are the a priori and a posteriori error covariance matrices.

Since eqns (7.64) and (7.65) are linear in nature, the component of $\widetilde{\mathbf{X}}_1(t_k^+)$ due to the observation $\mathbf{Z}(t_k)$ is identical to the solution $\overline{\mathbf{X}}_1(t_k^+)$ obtained from eqn (7.59) and (7.62), which allows the following relationship between the two estimates to be written immediately as:

$$\widetilde{\mathbf{X}}_1(t_k^-) = \overline{\mathbf{X}}_1(t_k^-) + \mathbf{U}(t_k)\mathbf{b}(t_k) \tag{7.66}$$

$$\widetilde{\mathbf{X}}_1(t_k^+) = \overline{\mathbf{X}}_1(t_k^+) + \mathbf{V}(t_k)\mathbf{b}(t_k) \tag{7.67}$$

From eqns (7.59), (7.62), (7.64 and (7.65) it can be seen that:

$$\begin{aligned}\widetilde{\mathbf{X}}_1(t_k^-) - \overline{\mathbf{X}}_1(t_k^-) &= \mathbf{U}(t_k)\mathbf{b}(t_k)\\ &= \Phi_1(t_k,t_{k-1})\left[\widetilde{\mathbf{X}}_1(t_{k-1}^+) - \overline{\mathbf{X}}_1(t_{k-1}^+)\right]\\ &= \Phi_1(t_k,t_{k-1})\mathbf{V}(t_{k-1})\mathbf{b}(t_{k-1})\end{aligned} \tag{7.68}$$

$$\mathbf{U}(t_k) = \Phi_1(t_k,t_{k-1})\mathbf{V}(t_{k-1}) \tag{7.69}$$

Similarly, one can find that:

$$\begin{aligned}
&\tilde{\mathbf{X}}_1(t_k^+) - \bar{\mathbf{X}}_1(t_k^+) = \mathbf{V}(t_k)\mathbf{b}(t_k) \\
&= \tilde{\mathbf{X}}_1(t_{k-1}^-) - \bar{\mathbf{X}}_1(t_{k-1}^-) \\
&\quad + \bar{\mathbf{K}}_{x1}(t_k)\left[-\mathbf{H}_1(t_k)(\tilde{\mathbf{X}}_1(t_{k-1}^+) - \bar{\mathbf{X}}_1(t_{k-1}^+)) - \mathbf{C}(t_k)\mathbf{b}(t_k)\right] \\
&= \left[\mathbf{U}(t_k) - \bar{\mathbf{K}}_{x1}(t_k)(\mathbf{H}_1(t_k) + \mathbf{C}(t_k))\right]\mathbf{b}(t_k)
\end{aligned} \tag{7.70}$$

$$\mathbf{V}(t_k) = \mathbf{U}(t_k) - \bar{\mathbf{K}}_{x1}(t_k)\mathbf{S}(t_k) \tag{7.71}$$

$$\mathbf{S}(t_k) = \mathbf{H}_1(t_k)\mathbf{U}(t_k) + \mathbf{C}(t_k) \tag{7.72}$$

The measurement residual of the bias-free estimator is:

$$\begin{aligned}
\mathbf{r}(t_k) &= \mathbf{Z}(t_k) - \mathbf{H}_1(t_k)\bar{\mathbf{X}}_1(t_k^-) \\
&= \mathbf{Z}(t_k) - \mathbf{H}_1(t_k)\left[\tilde{\mathbf{X}}_1(t_k^-) - \mathbf{U}(t_k)\mathbf{b}(t_k)\right] \\
&= \mathbf{S}(t_k)\mathbf{b}(t_k) + \zeta(t_k)
\end{aligned} \tag{7.73}$$

where

$$\zeta(t_k) = \mathbf{Z}(t_k) - \mathbf{H}_1(t_k)\tilde{\mathbf{X}}(t_k^-) - \mathbf{C}(t_k)\mathbf{b}(t_k) \tag{7.74}$$

$$E\left[\zeta(t_k)\zeta^T(t_k)\right] = \mathbf{H}_1(t_k)\bar{\mathbf{P}}_{x1}(t_k^-)\mathbf{H}_1^T(t_k) + \mathbf{R}(t_k) \tag{7.75}$$

$\zeta(t_k)$ is the measurement residual of the optimal estimator assuming a perfect knowledge of the bias, and is a white noise series. It can be seen from eqn (7.73) that the measurement residual of the bias-free estimator $\mathbf{r}(t_k)$ provides a measurement relationship from which the bias vector may itself be estimated.

The bias estimator can be derived from the conventional KF assuming the measurement residual of the bias-free estimator $\mathbf{r}(t_k)$ is the measurement of the bias estimator for which $\mathbf{S}(t_k)$ is the observation matrix and $\zeta(t_k)$ is the measurement noise:

$$\hat{\mathbf{b}}(t_k^-) = \hat{\mathbf{b}}(t_{k-1}^+) \tag{7.76}$$

$$\mathbf{P}_b(t_k^-) = \mathbf{P}_b(t_{k-1}^+) \tag{7.77}$$

$$\mathbf{K}_b(t_k) = \mathbf{P}_b(t_k^-)\mathbf{S}^T(t_k)\left[\mathbf{S}(t_k)\mathbf{P}_b(t_k^-)\mathbf{S}^T(t_k) + \mathbf{H}_1(t_k)\overline{\mathbf{P}}_{x1}(t_k^-)\mathbf{H}_1^T(t_k) + \mathbf{R}(t_k)\right]^{-1} \tag{7.78}$$

$$\mathbf{P}_b(t_k^+) = \left[\mathbf{I} - \mathbf{K}_b(t_k)\mathbf{S}(t_k)\right]\mathbf{P}_b(t_k^-) \tag{7.79}$$

$$\mathbf{b}(t_k^+) = \mathbf{b}(t_k^-) + \mathbf{K}_b(t_k)\left[\mathbf{Z}(t_k) - \mathbf{S}(t_k)\mathbf{b}(t_k^-)\right] \tag{7.80}$$

Now the final estimate of the state can be obtained:

$$\hat{\mathbf{X}}_1(t_k^-) = \overline{\mathbf{X}}_1(t_k^-) + \mathbf{U}(t_k)\mathbf{b}(t_{k-1}^+) \tag{7.81}$$

$$\hat{\mathbf{X}}_1(t_k^+) = \overline{\mathbf{X}}_1(t_k^+) + \mathbf{V}(t_k)\mathbf{b}(t_k^+) \tag{7.82}$$

and

$$\begin{aligned}\mathbf{P}_{x1}(t_k^-) &= E\left\{\left[\hat{\mathbf{X}}_1(t_k^-) - \mathbf{X}_1(t_k)\right]\left[\hat{\mathbf{X}}_1(t_k^-) - \mathbf{X}_1(t_k)\right]^T\right\} \\ &= \overline{\mathbf{P}}_{x1}(t_k^-) + \mathbf{U}(t_k)\mathbf{P}_b(t_k^-)\mathbf{U}^T(t_k)\end{aligned} \tag{7.83}$$

$$\begin{aligned}\mathbf{P}_{x1b}(t_k^-) &= E\left\{\left[\hat{\mathbf{X}}_1(t_k^-) - \mathbf{X}_1(t_k)\right]\left[\hat{\mathbf{b}}(t_k^-) - \mathbf{b}(t_k)\right]^T\right\} \\ &= \mathbf{U}(t_k)\mathbf{P}_b(t_k^-)\end{aligned} \tag{7.84}$$

$$\begin{aligned}\mathbf{P}_{x1}(t_k^+) &= E\left\{\left[\hat{\mathbf{X}}_1(t_k^+) - \mathbf{X}_1(t_k)\right]\left[\hat{\mathbf{X}}_1(t_k^+) - \mathbf{X}_1(t_k)\right]^T\right\} \\ &= \overline{\mathbf{P}}_{x1}(t_k^+) + \mathbf{V}(t_k)\mathbf{P}_b(t_k^+)\mathbf{V}^T(t_k)\end{aligned} \tag{7.85}$$

$$\begin{aligned}\mathbf{P}_{x1b}(t_k^+) &= E\left\{\left[\hat{\mathbf{X}}_1(t_k^+) - \mathbf{X}_1(t_k)\right]\left[\hat{\mathbf{b}}(t_k^+) - \mathbf{b}(t_k)\right]^T\right\} \\ &= \mathbf{V}(t_k)\mathbf{P}_b(t_k^+)\end{aligned} \tag{7.86}$$

By expanding the covariance matrices obtained by the augmented KF and the bias-separated KF, it is easy to prove the equivalence of the two solutions (Ignagni, 1981) :

$$\mathbf{K}_{x1}(t_k) = \overline{\mathbf{K}}_{x1}(t_k) + \mathbf{V}(t_k)\mathbf{K}_b(t_k) \qquad (7.87)$$

If $\overline{\mathbf{K}}_{x1}$, $\mathbf{K}_b$ are chosen optimally, the estimate of the bias-separated KF is an optimum.

The bias-separated KF procedure can be summarized as following:
The bias-free estimator: eqns (7.59) to (7.63).
The matrices **U, V** and **S**: eqns (7.69), (7.70), (7.71).
The measurement residual of the bias-free estimator: eqn (7.73).
The bias estimator: eqns (7.76) to (7.80).
The updating of the final estimate: eqns (7.81) to (7.86).
The initial state of the bias-free and bias estimators is the same as the original system model.

The bias-separated KF implementation requires fewer numerical operations than the augmented-state implementation (Samant & Sorenson, 1974). Another advantage of the bias-separated KF implementation is that it avoids numerical ill-conditioning resulting from a state vector of large dimension. In the augmented-state implementation the overall process is of the order n + r, and all n + r state variables are coupled in the filter and in the covariance matrix propagation. In the bias-separated KF implementation, the maximum dimension required is the larger of n or r.

The bias-separated KF is suitable for carrier phase ambiguity estimation considering the inherent constant bias characteristics of the ambiguity. The ambiguity is now defined as the bias **b** and is separated from the body's state, and estimated separately by the bias estimator. The threshold values for the variance (the diagonal terms of the bias estimate error covariance $\mathbf{P}_b(t_k^+)$) and the tolerance of the integer of the wavelength are set up before the filtering. If the bias estimate is within the variance threshold and integer tolerance, the ambiguity can be fixed to the nearest integer and the column and the row of $\mathbf{P}_b(t_k^+)$ corresponding to the ambiguity is then set to zero. When all ambiguities are fixed, the bias estimator can be isolated and stopped, and the bias-separated KF now operates as an estimator with a perfectly known bias, which is

essentially the same as the bias-free estimator except the estimate update equation is eqn (7.65) instead of eqn (7.62).

By using the bias-separated KF the body's state and ambiguities, which are different in their stochastic characteristics and dynamic behaviour, are estimated separately and the error covariance estimation of the body's state and the ambiguities are also isolated from each other. Hence the eigenvalues of $\mathbf{P}_b(t_k^+)$ are comparable, so are $\overline{\mathbf{P}}_{x1}(t_k^+)$, although the eigenvalues of $\mathbf{P}_b(t_k^+)$ and $\overline{\mathbf{P}}_{x1}(t_k^+)$ could still have large differences. After some or all of the ambiguities are fixed, $\mathbf{P}_b(t_k^+)$ becomes positive semi-definite, but this does not affect the $\overline{\mathbf{P}}_{x1}(t_k^+)$ computation, which retains its positive-definiteness.

The implementations of the bias-free estimator and the bias estimator are actually isolated and can be operating on different steps. For example, the estimation of the ambiguity depends on the change of satellite geometry and the bias estimator can be adjusted so as to operate on a low update rate while the bias-free estimator operates on a high update rate. Otherwise a data compression technique have to be used (Colombo, 1992).

The bias-separated KF is based on a linear system and a linear observation model and is suitable for the navigation model in which the observation is linearized about a predetermined trajectory. If the the observation is linearized about the filter estimated trajectory (the EKF algorithm), some modifications need to be made. Since the linearization of the EKF is always made about the complete state estimate, the easy way to overcome the non-linear effects on the difference between $\hat{\mathbf{X}}$ and $\overline{\mathbf{X}}$ is to reset the bias computation from time to time, i.e., by setting $\overline{\mathbf{X}}$ to $\hat{\mathbf{X}}$ and, simultaneously, $\hat{\mathbf{b}}$ to zero. This operation merely resets the bias mean values and the uncertainty in the bias is not changed.

7.2 Digital Filter (DF)

The DF referred to here is the frequency discriminating DF. There are two types of DF used in GPS navigation: the high-pass DF (HDF) and the low-pass DF (LDF). The high-pass DF is used for depression of the measurement bias, while the low-pass DF is intended for the depression of the measurement noise. Both HDF and LDF can be implemented as FIR (Finite Impulse Response) or IIR (Infinite Impulse Response) filters.

The FIR filter can be described by the linear difference equation (modified from Proakis & Manolakis, 1992) :

$$y(t_n) = \sum_{k=0}^{M} b_k x(t_n - t_k) \tag{7.88}$$

where M is the filter order.

The system function of the FIR filter is:

$$H(Z) = \sum_{k=0}^{M} b_k Z^{-1} \tag{7.89}$$

where Z is the Z transform operator.

The unit impulse response of the FIR filter is:

$$h(k) = \begin{cases} b_k & 0 \le k \le M \\ 0 & \text{else} \end{cases} \tag{7.90}$$

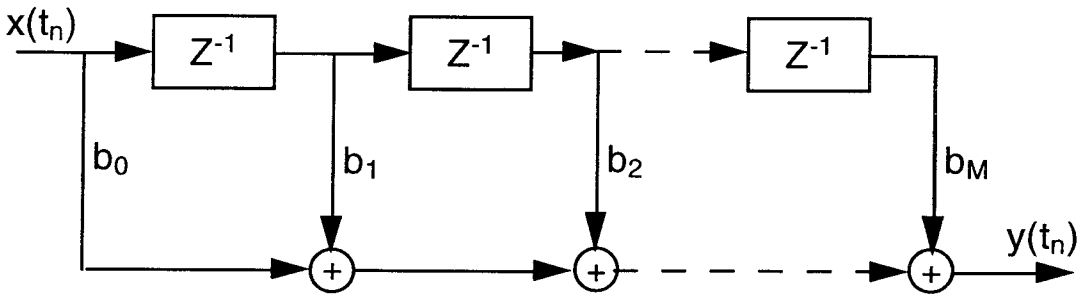

Figure 7.14. FIR filter structure.

The IIR filter can be described by the linear difference equation (ibid, 1992):

$$y(t_n) = -\sum_{k=1}^{N} a_k y(t_n - t_k) + \sum_{k=0}^{M} b_k x(t_n - t_k) \tag{7.91}$$

and the system function is:

$$H(Z) = \frac{\sum_{k=0}^{M} b_k Z^{-1}}{1 + \sum_{k=0}^{N} a_k Z^{-1}} \qquad (7.92)$$

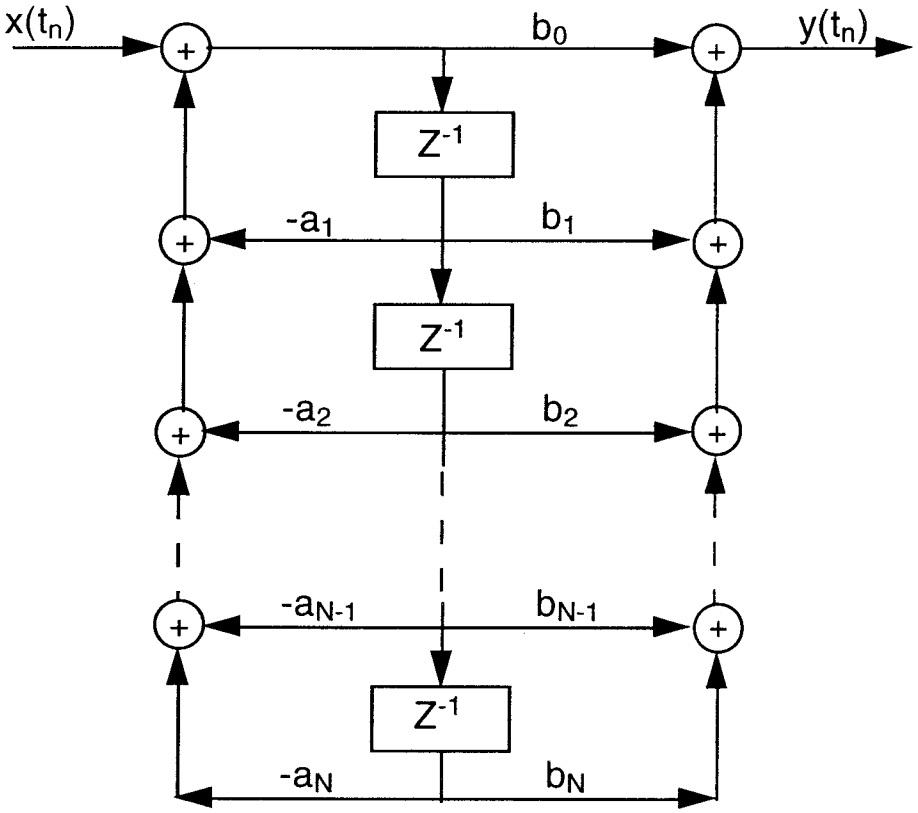

Figure 7.15. IIR filter structure.

Fig.7.14 and Fig.7.15 are only two of many different implementations of the filter, which depend on the application requirements.

The mean and covariance of the filter output can be expressed as (modified from Proakis et al., 1992) :

$$m_y(t_n) = E\left[\sum_{k=0}^{\infty} h(k)x(t_n - t_k)\right] \qquad (7.93)$$

where h(k) is the filter unit impulse response function.

where h(k) is the filter unit impulse response function.

- If x is a stationary series with mean m_x, then the output series is also a stationary series with mean value:

$$m_y = m_x \sum_{k=0}^{\infty} h(k) \tag{7.94}$$

The covariance of the output series is :

$$\gamma_{yy}(m) = \sum_{k=0}^{\infty} \sum_{j=0}^{\infty} h(k)h(j)\gamma_{xx}(k - j + m) \tag{7.95}$$

where γ_{xx} is the covariance of the input series x.

The choice of the FIR or IIR filter parameters a_K and b_K is based on the analysis of the PSD of the GPS measurements. The main differences between IIR DF and FIR DF can be summarized as follows:

IIR DF is a closed-loop system and there is a potential stability problem. FIR DF is a open-loop system and is generally stable.

For the same required system amplitude response the order of the FIR DF is at least 2 times that of the IIR DF, hence for real-time applications IIR DF is preferable if some phase distortion is tolerable or unimportant.

The system phase response of the IIR DF is, in general, non-linear and will cause a distortion of the filtered data, hence an all-pass DF has to be cascaded to compensate for the distortion if high filtering precision is required.

The system phase response of the FIR DF is linear and will cause filtered data delay for a casual filter.

As a MA series, the correlation length of the FIR DF is equal to the order of the filter. In contrast, the correlation function of the IIR DF generally exhibits a exponential decay feature.

7.2.1 HDF

The commonly used HDF in GPS is the difference operator: single, double and triple-difference. The GPS measurements can be considered as three dimensional series $x(t_k, n, m)$, where t_k is the discrete time or epoch number, n is the site number and m is the satellite number. The single, double and triple-difference can be considered to consist of independent first order differences between time, station and satellite, and the system function can be written equivalently as the first, second and third order differences:

single-difference:

$$D_1(Z) = 1 - Z^{-1} \tag{7.96}$$

double-difference:

$$D_2(Z) = \left[1 - Z^{-1}\right]\left[1 - Z^{-1}\right] \tag{7.97}$$

triple-difference:

$$D_3(Z) = \left[1 - Z^{-1}\right]\left[1 - Z^{-1}\right]\left[1 - Z^{-1}\right] \tag{7.98}$$

The amplitude response of the operators is shown in Fig.7.16, while the frequency scale of the plot is from 0 to π.

From the plot it can be seen that the low frequency components of the signals, which are the components with the frequencies less than the lower 1/3 Nyquist frequency, are attenuated and the high frequency components, which are those with the frequencies inside the upper 2/3 Nyquist frequency interval are amplified.

There is potential to use other type HDF which has better frequency response than those of difference operators.

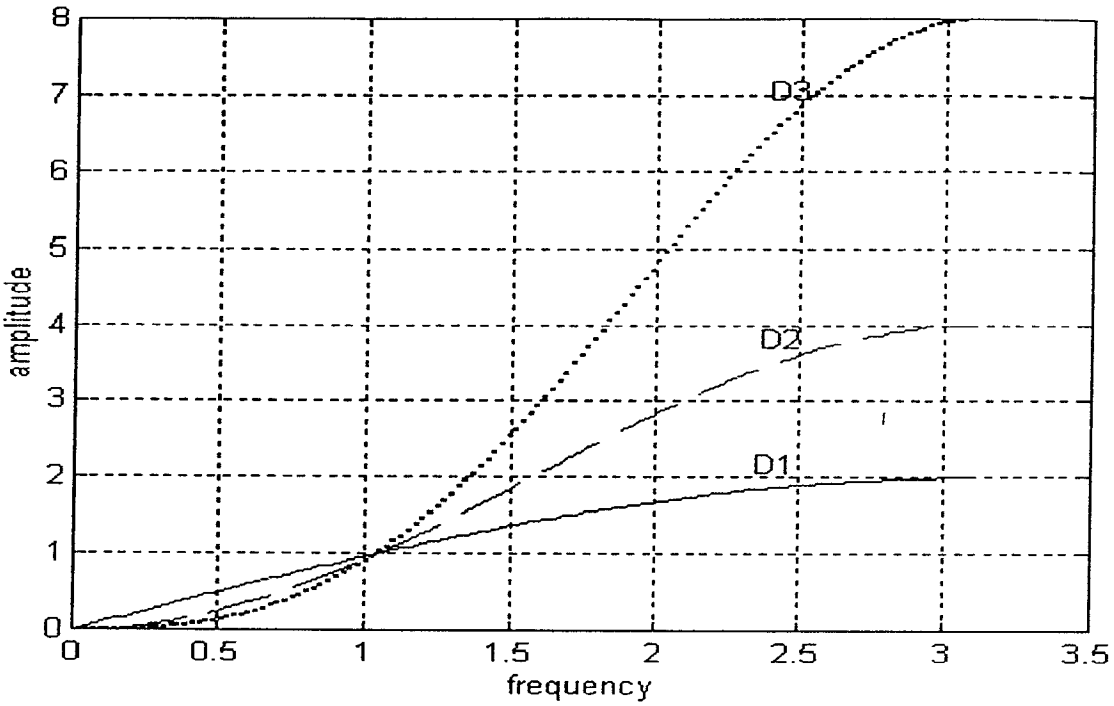

Figure 7.16. Amplitude response of first, second and third differencing operators.

CHAPTER 8

DATA PROCESSING

In this chapter a short description of the software packages used in GPS data processing is presented. The software is primarily concerned with GPS navigation, and the integration of GPS and dead reckoning technologies. The algorithms are based on the filter models discussed in previous chapters. Examples of data processing are presented as evidence of the validation of the models and the algorithms. The data processing about smoothing code measurements and baseline computation using Doppler phase are presented in section 4.4.1.4 and section 4.4.2.2 already.

8.1 Software Development

The software can be divided into two categories (Fig.8.1): the preprocessing software and the data analysis software.

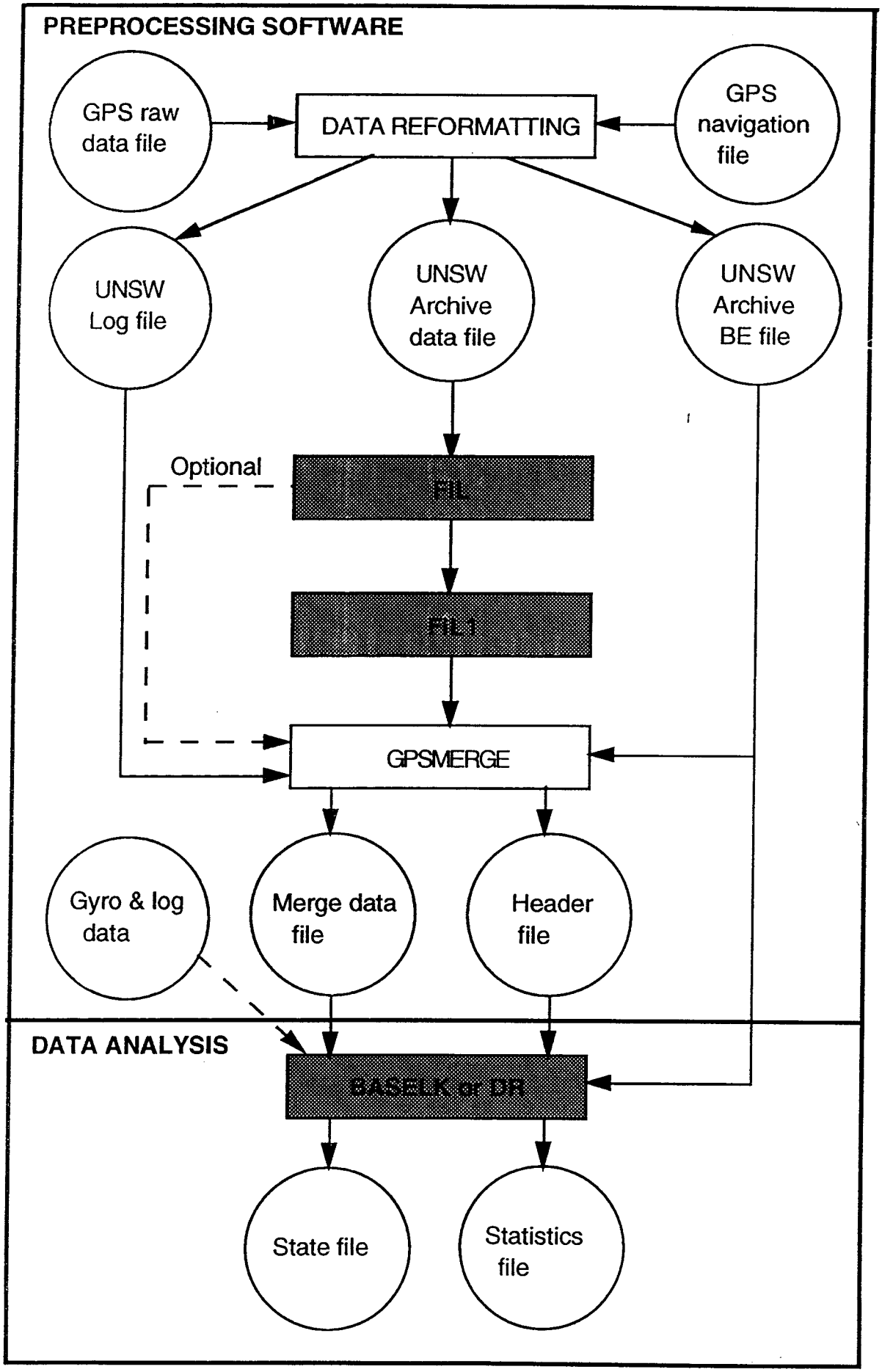

Figure 8.1 The UNSW GPS navigation software.

The navigation software developed in this thesis is influenced by the pre-existing UNSW data format and software modules. The dark-blocks in Fig. 8.1 are the newly developed software modules. The function of the navigation software is the determination of a platform's state: position, velocity, acceleration and attitude through the processing of a variety of GPS measurements: pseudo-range, phase and Doppler; and the integration of other navigation sensor data such as from a gyrocompass and speed log.

8.1.1 Preprocessing Software

8.1.1.1 Software FIL

The software FIL is a cycle slip editing program based on a 5th order elliptic IIR DF (see section 7.1.2). The IIR DF is designed for a 1 Hz data rate with cut-off frequencies of 0.1, 0.07 and 0.05 Hz corresponding to 10, 15 and 20 second oscillation periods of the platform. The IIR is implemented in the form of a lattice-ladder structure because of its build-in stability and robustness to finite-word-length effects (Proakis & Manolakis, 1992). The functional steps with this software are illustrated in Fig.8.2.

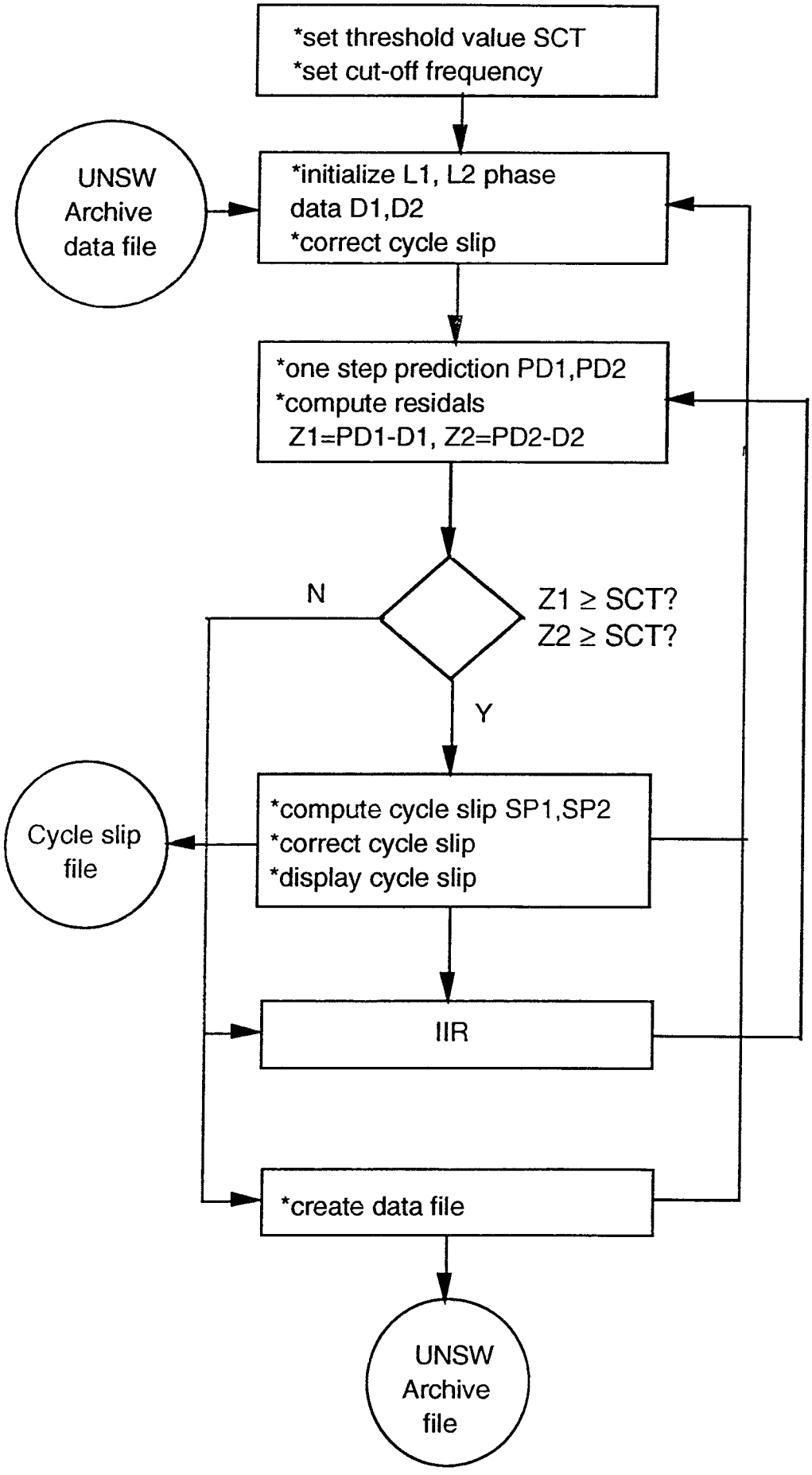

Figure 8.2. Flowchart of the program FIL.

8.1.1.2 Software FIL1

The software module FIL1 is intended for data smoothing. The pseudo-range data is smoothed using either dual-frequency Doppler data (if available), or dual-frequency phase data (if available), or using the FIR DF described in section 4.4.1.3. The phase and Doppler data can be smoothed by the FIR

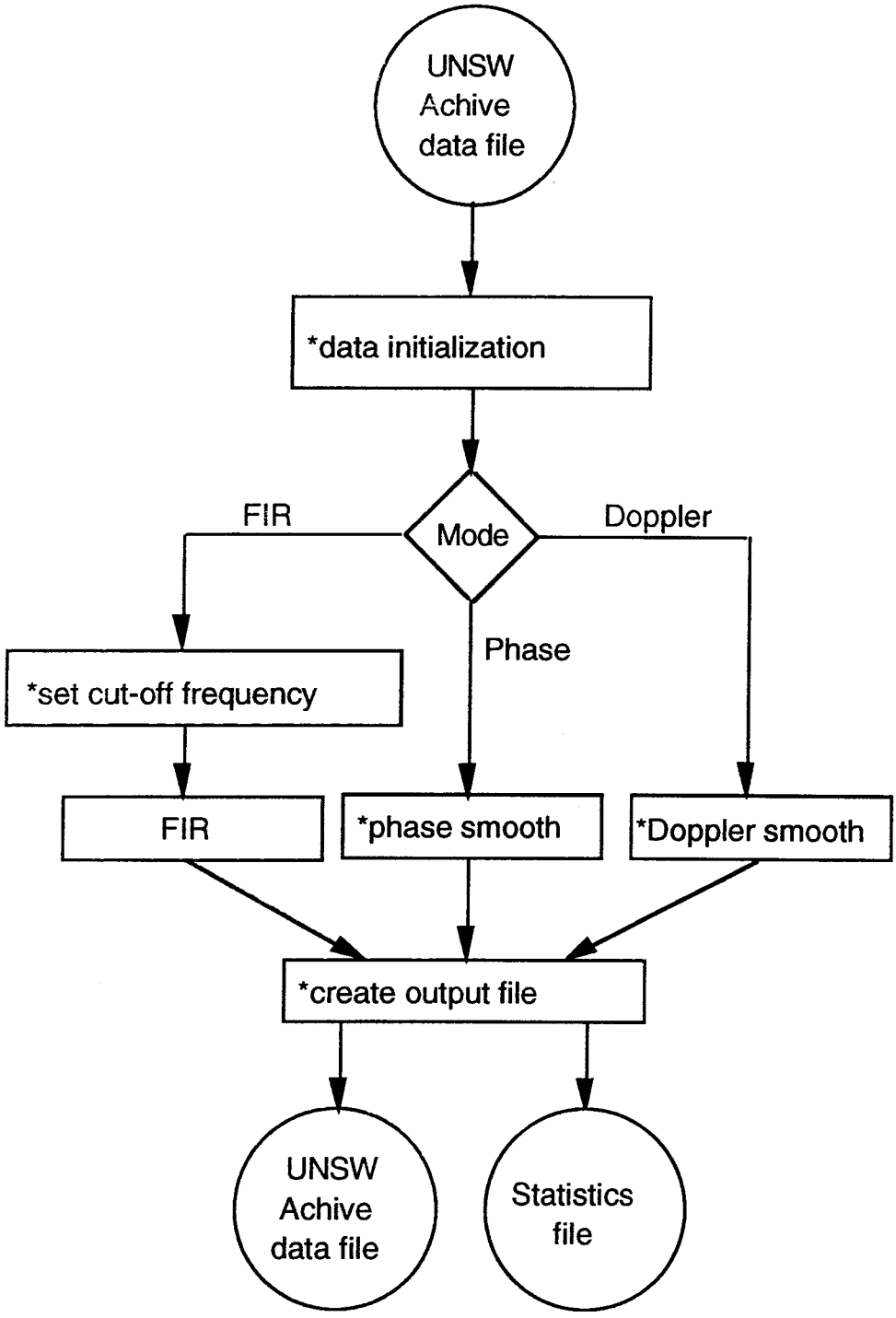

Figure 8.3. Flowchart of the program FIL1.

The function of the "data initialization" step is to remove a constant value from the measurements to be smoothed in order to reduce numerical error. The statistics file contains the residuals, the mean and RMS values of the residuals, the autocorrelations of the residuals and the results of the whiteness test of the residuals.

Both programs FIL and FIL1 operate in sequential (one data epoch at a time) mode. After initial set up and definition of the nominal values, the program can operate automatically and can be easily modified for real-time applications.

8.1.2 Data Analysis Software

There are two data analysis software packages: BASELK and DR, principally based on the bias-separated Kalman filter algorithm described in section 7.1.4. Although the data preprocessing procedures for both BASELK and DR are the same as illustrated in Fig. 8.1, the mathematical models of BASELK and DR are based on different strategies.

The BASELK is, in general, a "GPS-mainly" program. Its mathematical model and algorithms are based on the navigation and observation models discussed in chapter 6. The platform's position, velocity and acceleration are determined using undifferenced or double-differenced GPS measurements. The program can process the data from up to three GPS antennae and ten satellites simultaneously. If the data of two or three antennae mounted on the platform are available, the platform's attitude can be determined. If other navigation sensors such as gyrocompass and speed log are present, they can be integrated as extra measurements in open-loop mode. BASELK can also be used for static baseline computations. A flowchart showing the main features of BASELK is Fig. 8.4.

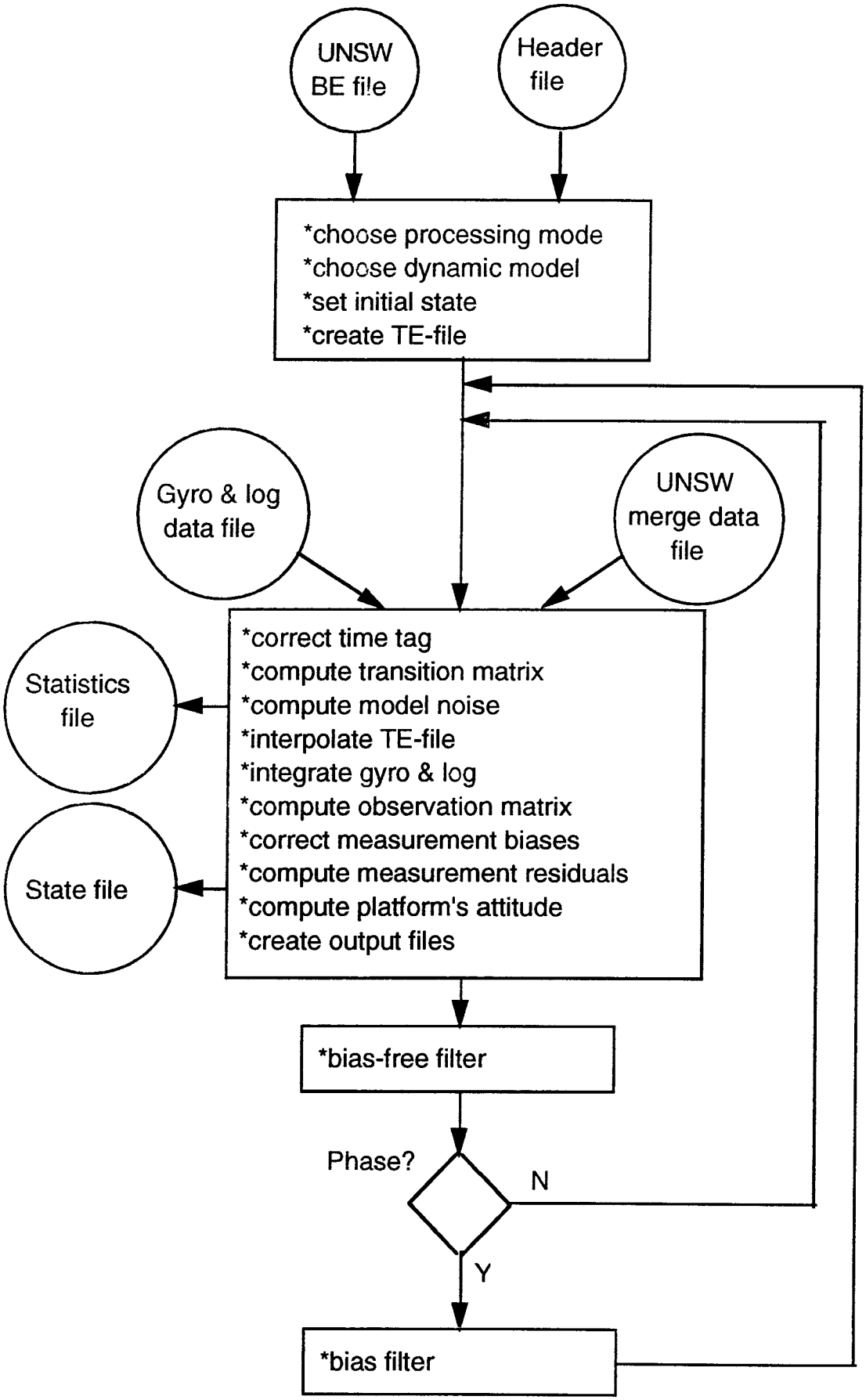

Figure 8.4. Flowchart of the BASELK program.

The state file includes the platform's estimated state: position, velocity, acceleration, attitude and baseline length. The statistics file includes residuals, residual statistics and statistical tests.

The flowchart of the DR program is basically the same as that of BASELK, except that DR is a "Dead Reckoning mainly" program and the GPS measurements are used simply for the purpose of correcting the errors of the dead reckoning sensors forming a closed-loop structure, as discussed in section 5.2. The state file now includes the platform's position, sea current correction and the corrections to the gyrocompass and speed log.

8.2 Data Processing

A kinematic data processing example is presented for a ship's state estimation.

8.2.1 Ship's Data

The ship's data were collected aboard the R.V. FRANKLIN, the oceanographic research vessel of the Division of Oceanography, CSIRO. The ship's dimensions are: overall length 55.2 m, breadth moulded 11.8 m, draft 3.8 m, displacement 1187 t. The FRANKLIN has a design speed of 13 knots. The navigation equipment aboard includes: an Arma-Brown Mk.10 gyrocompass, a Doppler speed log, two Marconi radars, a Trimble GPS receiver, a radio direction finder and an echo-sounding system. In addition there is a Vax mini-computer along with several PC's.

An Acoustic Doppler Current Profiler (ADCP) employing the Doppler principle to remotely measure speed and direction of water current over a depth range from 30 to 700 metres is also installed.

The ship's attitude can be measured by a pitching-rolling meter, and heading by gyrocompass. The ship's speed can be measured by ADCP or speed log. The accuracies of the gyrocompass, ADCP and speed log affect directly the accuracy of the current profile determination because the current vector is the difference between the ship's earth referenced speed vector and the ship's speed vector relative to water (see Fig.1.2). The speed log accuracy is approximately at the same level as that of the ADCP, the current direction accuracy is better than 1

degree and the speed accuracy is about 2% if gyrocompass, speed log and ADCP only are used. For oceanographic research into water volume temperature exchange, more accurate water current information is required. In particular the direction error of the current should be less than 0.3 degree, hence requiring that the ship's heading accuracy be better than 0.3 degree.

An investigation of ship-track and heading information for the FRANKLIN, using shore-based and ship-mounted GPS receivers was carried out during a FRANKLIN cruise, May 1991, sponsored by CSIRO and UNSW. Different data processing strategies were tested and the results were compared with the recorded ship's log, gyrocompass and ADCP data. This investigation was part of the FRANKLIN research plan for the May cruise, which included the investigation of submarine slope failure on the NSW continental margin and the biostratigraphy of the continental shelf off Sydney.

8.2.2 Equipment Implementation and Data Acquisition

Two Trimble-SST GPS receivers were installed aboard the FRANKLIN. One antenna was mounted on an extension pole rigidly fixed to the bow mast (referred to here as the Bow antenna). Another antenna was installed on top of the funnel mast (referred to here as the Fun antenna) which was about 4 metre higher than the Bow antenna. The antennae were mounted above the ship's centreline and the alignment was checked against the lumber line of the ship's standard compass. The antennae were more than 15 metre above the waterline and were well above the ship's superstructure. One 30 metre and one 20 metre long antenna cable connected the Bow and Fun antennae to the two receivers respectively, which were located inside the ship's bridge. The antenna of the third Trimble-SST receiver was set on the Mather pillar on top of the Geography and Surveying building, the University of New South Wales, Sydney. All antennas were fitted with ground planes. The GPS measurements were collected at 1 second interval during the period when a maximum number of satellites were visible. 5 satellites were observed for less than 40 minutes during the period 1430-1510 GMT each day (see Fig.8.5), and the GDOP values were all greater than 5.

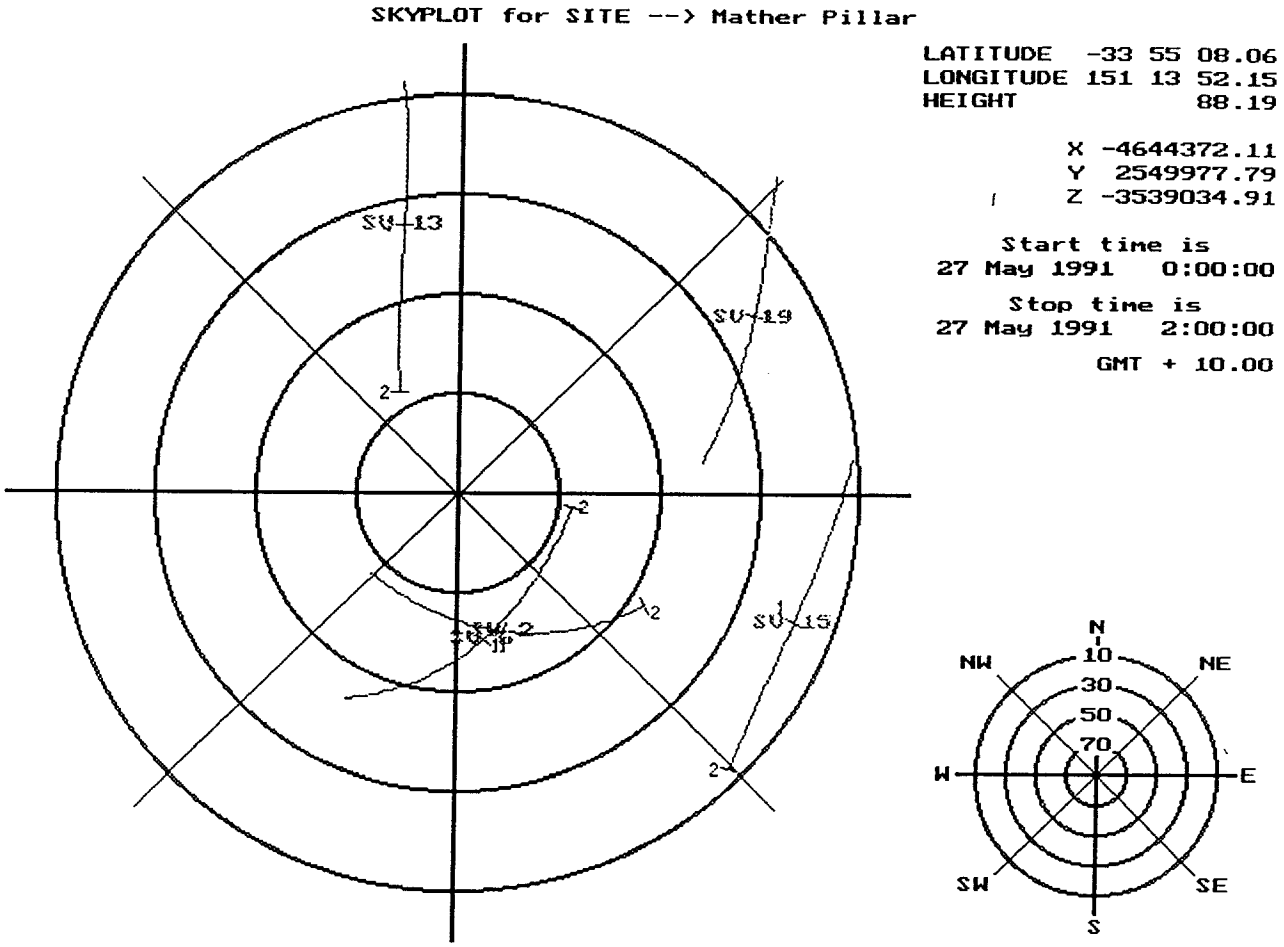

Figure.8.5 Skyplot of day 26

The nominal performance of the Arma-Brown MK. 10 gyrocompass was:

static accuracy	0.15^0
repeatability	0.25^0
follow-up speed	20^0/sec

These values assume no latitude, velocity and shock errors.

The sampling frequencies of the gyrocompass and log were 1 Hz and the data were stored on a Vax-tape. The time tag of the file is GMT and the units of the gyrocompass and log outputs are degree (0^o to 360^o) and knot.

Because the water depth was more than 750 m during the ADCP tracking periods, and no bottom-track available, that is no ground speed is available, and hence the log speed was also the speed relative to water. There were no pitch and roll data available.

The cruise began on 24 May, 1991, departing Port Jackson, Sydney at 0900 hrs and ended at 1500 hrs, 30 May, 1991, at the same port. The research area was between latitude 34^0 01' S to 35^0 10' S and longitude 150^0 50' E to 151^0 50' E (see Fig.8.6).

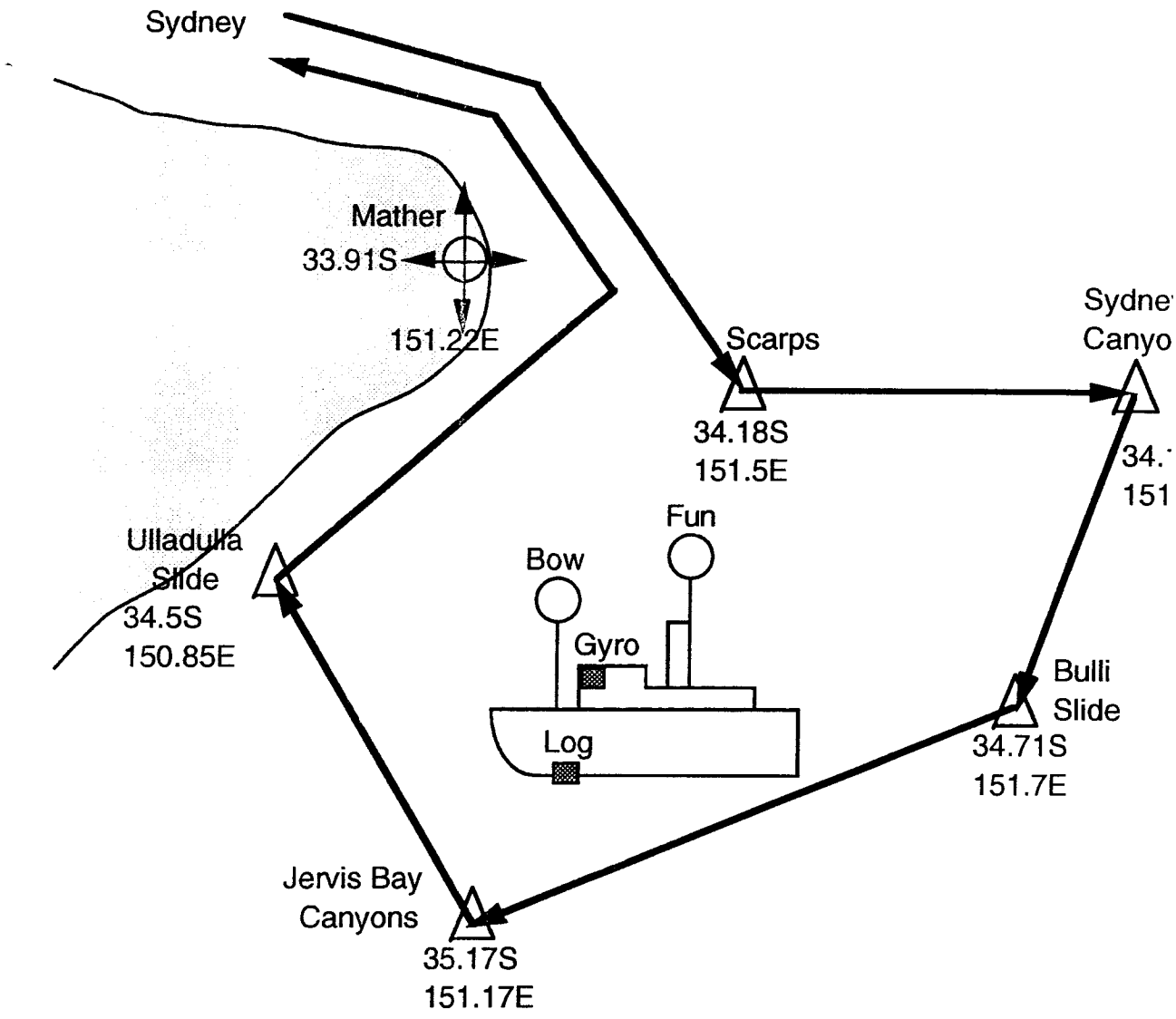

Figure 8.6. Voyage of the Franklin.

8.3 Ship's Data Processing

The measurements made can be summarized as follows:

1) The primary observable of GPS:
   C/A code
   L1 phase

2) The secondary observable of GPS:
   L1 phase-rate

3) The gyrocompass and log outputs:

heading

speed relative to water

Here only two day's results for day 26 and 28, which had the longest observation session and for which gyrocompass and log data were available, are presented.

Cycle slips in the one-way GPS phase measurements were repaired using the elliptic DF. The threshold values for cycle slips was 1 cycle for static data and 3 cycles for kinematic data which were smoothed by a FIR DF with 0.4 π cut-off frequency. In reality there were quite a few outliers in the phase data with amplitudes that were under 10 cycles and the cycle slips took pretty large values (over 1000 cycles). Although the phase data can be smoothed using the DF, only the cycle slips and outliers were cleaned up or smoothed in order to preserve the original phase measurement signature. Most cycle slips occurred for low elevation satellites at the end of each observation session.

The gyrocompass and log data were synchronized to the GPS measurement time tag.

Three different kind of data processing strategies were used: differential positioning mode, attitude mode and DR mode.

8.3.1 Differential Positioning Mode

This mode was used for differential position determination using the BASELK program. The reference station was the Mather pillar, and two remote stations were the Bow and Fun antennas. The state variables were: position, velocity. The ship's heading was derived from the position vectors of Bow and Fun. The dynamic model was the constant velocity model with 1 metre/sec*sec dynamic noise, and floating and fixed ambiguity solutions were obtained using double-differenced L1 phase data with 0.01 metre standard deviation. The distances between the reference and remote stations were 71 km and 185 km for day 26 and 28 respectively. The initial position and velocity errors were assumed to be 10 metre and 1 metre/sec respectively. The initial ambiguity uncertainty was set to 3 metres, corresponding to the C/A code measurement noise.

The results are shown in the series of Fig.8.7 to Fig.8.33 and Table 8.1 and 8.2. "M-B", "M-F" and "B-F" refer to the vectors between Mather and Bow, Mather and Fun, and Bow and Fun antennas respectively. The frequency range of the PSD plots is from 0 to π. Because only 5 satellite were observed and the satellite geometry was poor (PRN 2 and PRN 6 nearly in the same plane, and GDOP larger than 5 and 10 at the beginning and the end of the sessions), the solutions converged very slowly due to the variance of the bias estimate decreasing very slowly. Nearly 1500 epochs were needed for the solution to approach the steady state and to fix the ambiguity to integers, and the decreasing gradient of the bias variance is approximately 0.01 m^2/epoch (see the baseline plots and the heading comparison plots). The standard deviation of the estimates of the baseline components (east, north and height) of the ambiguity-fixed solution were 0.03 m, 0.067 m and 0.016 m respectively.

From the plots it can be seen that the mean value of the baseline and the heading difference between the GPS solution and the gyrocompass reading are stationary series, and the innovation series have a small bias which is less than 4 centimetre (due to the long distance between the reference and remote antennas). These remaining biases are nearly the same for both the Bow and Fun measurements and cancel out by differencing the two sets of results. Actually the separated-bias filter would deal with the slowly changing measurement bias (due to such effects as the inospheric delay) during bias estimation, and the effect of the measurement bias on ambiguity fixing was the same for both the Bow and Fun antennas (they were nearly at the same distance from the Mather antenna), hence there was no effect on the final results of the baseline between the Bow and Fun antennas. The repeatability of the baseline and heading for the two days is less than 3 mm and 0.05 degree respectively. The periodic oscillation appearing in the baseline and heading solutions is due to the ship's pitching (see the PSD and autocorrelation plots for day 28), with a period of about 5 seconds for day 28. Although periodic oscillation can be modelled by a second order underdamped system model, it will mean a doubling of the size of the bias state variable. Because only the ship's heading is of interest here, not the GPS antenna's instantaneous attitude, and the ship's rolling has no influence on the antenna pair's direction, a simple navigation model can be used and the ship's heading can be derived from the gyrocompass reading and its error correction, which is the mean value of the difference between the antenna pair direction and the gyrocompass reading.

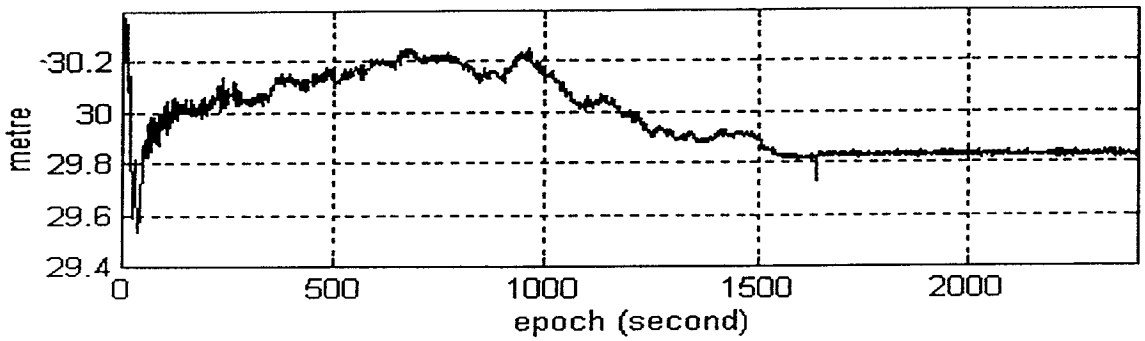

Figure 8.7. Baseline between Bow & Fun (day 26, first iteration).

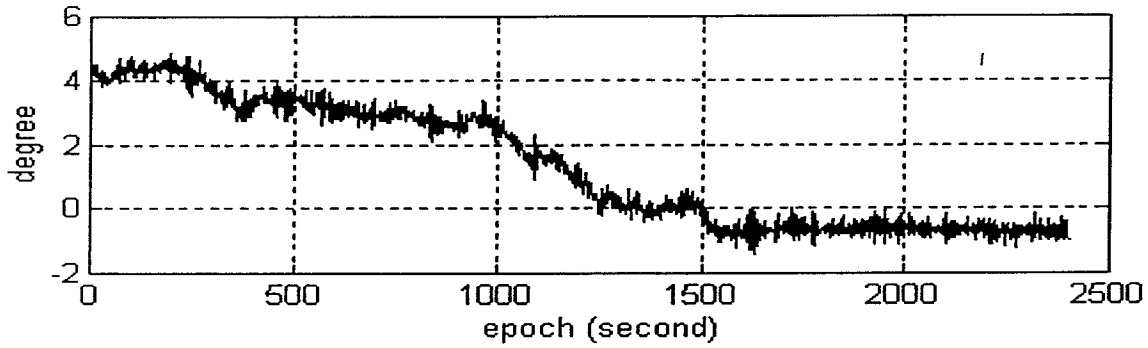

Figure 8.8. Heading difference (day 26, first iteration).

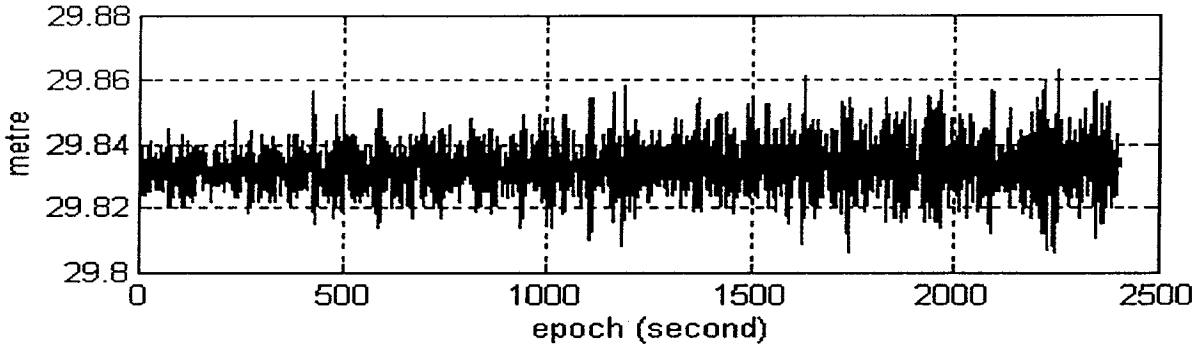

Figure 8.9. Baseline between Bow & Fun (day 26, differential mode, ambiguity fixed).

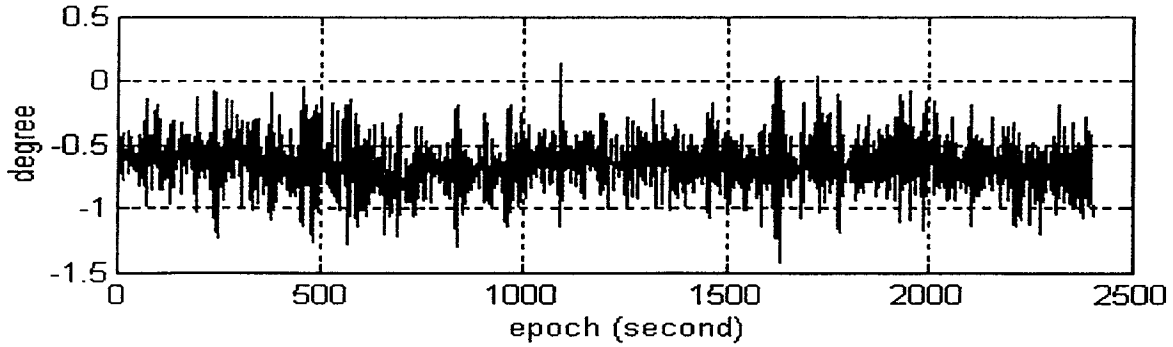

Figure 8.10. Heading difference (day 26, differential mode, ambiguity fixed).

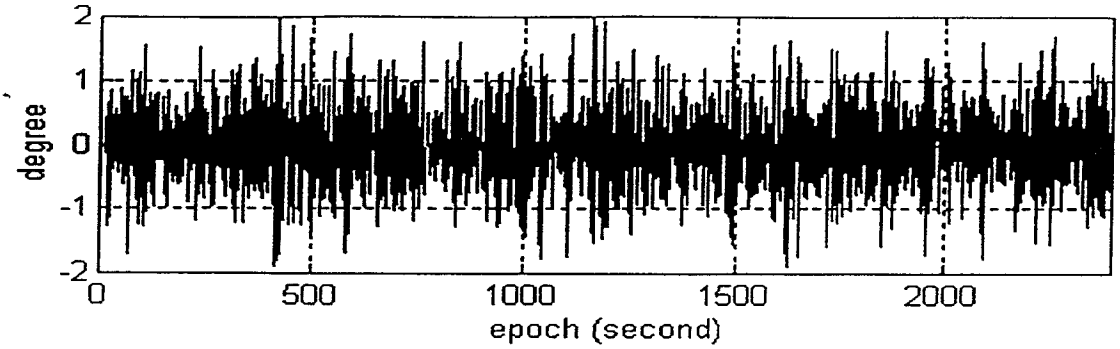

Figure 8.11. Pitch angle (day 26, differential mode, ambiguity fixed).

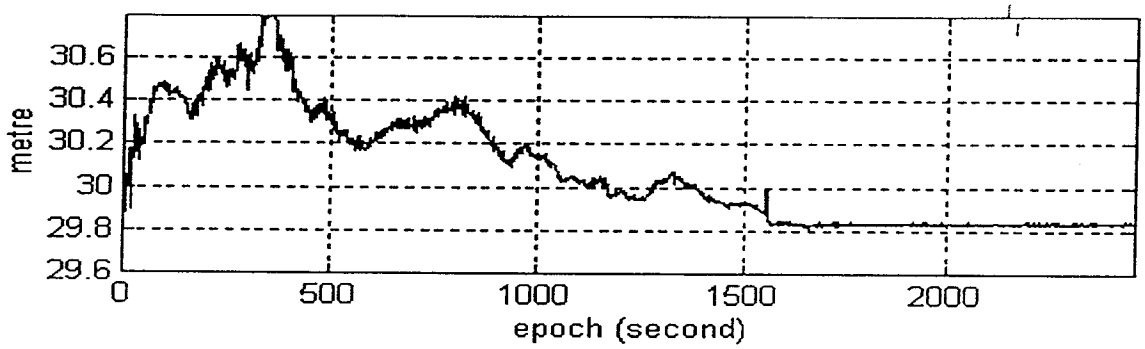

Figure 8.12. Baseline between Bow & Fun (day 28, differential mode, first iteration).

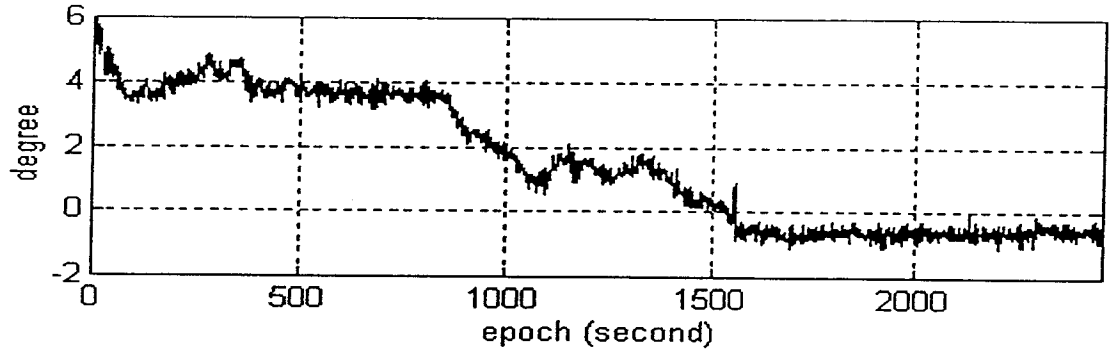

Figure 8.13. Heading difference (day 28, differential mode, first iteration).

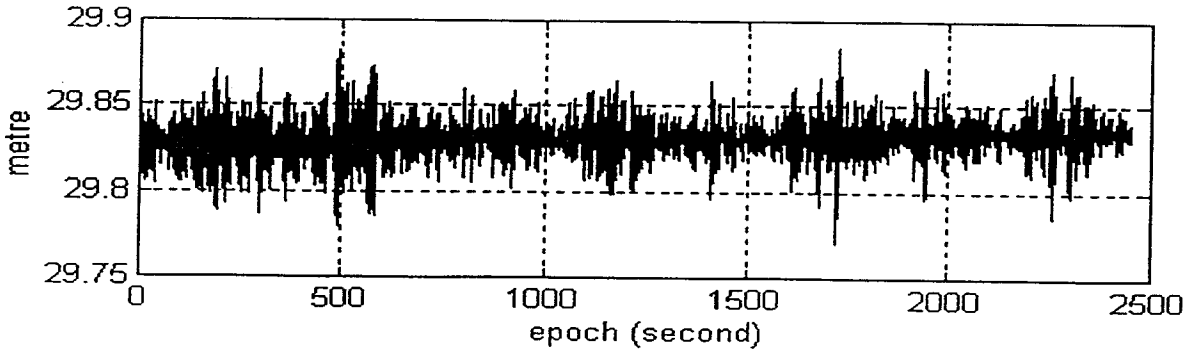

Figure 8.14. Baseline between Bow & Fun (day 28, differential mode, ambiguity fixed).

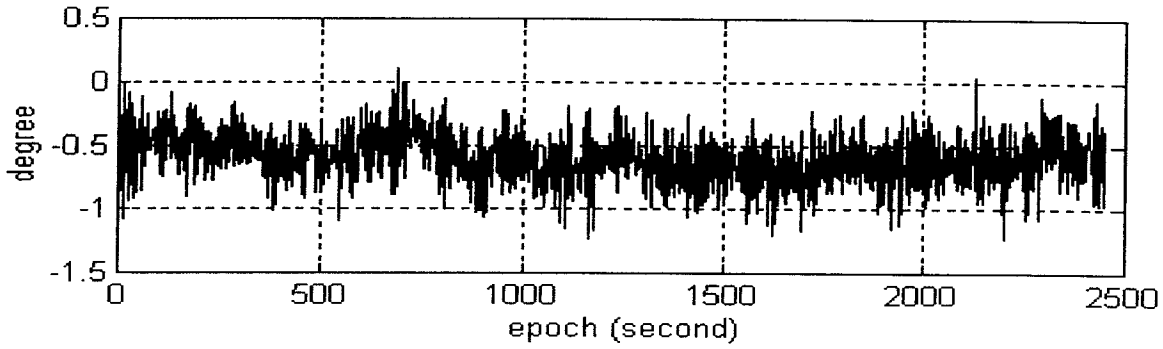

Figure 8.15. Heading difference (day 28, differential mode, ambiguity fixed)

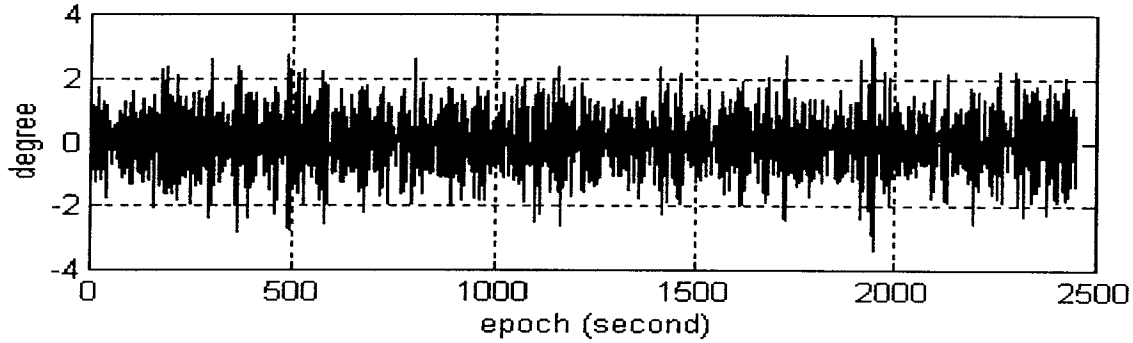

Figure 8.16 Pitch angle (day 28, ambiguity fixed)

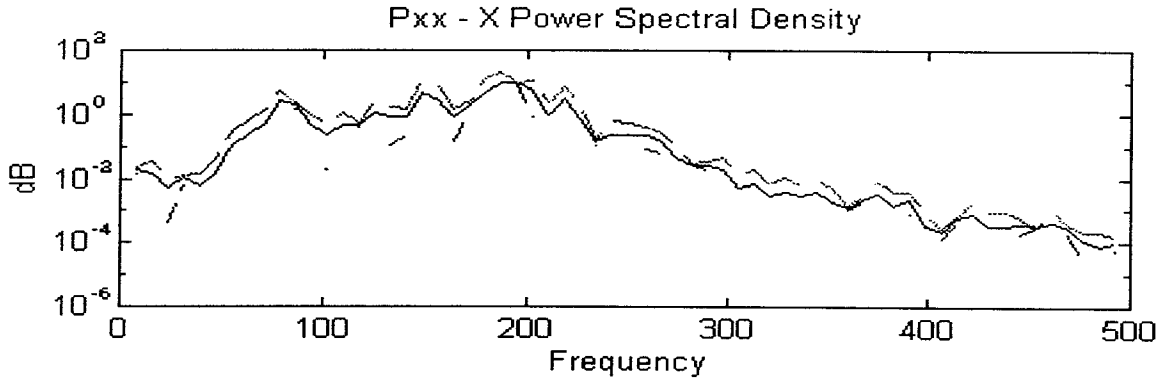

Figure 8.17. PSD of pitch (day 28, ambiguity fixed).

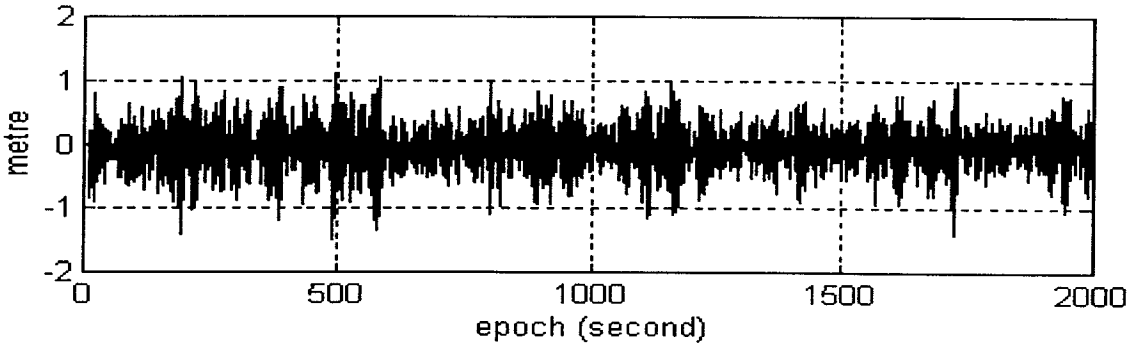

Figure 8.18. Innovation series of PRN 2-13 M-B (day 28, ambiguity fixed).

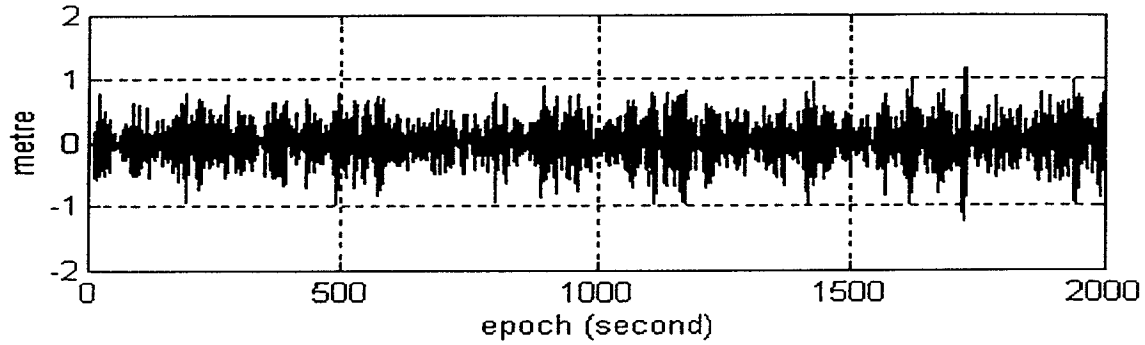

Figure 8.19. Innovation series of PRN 2-19 M-B (day 28, ambiguity fixed).

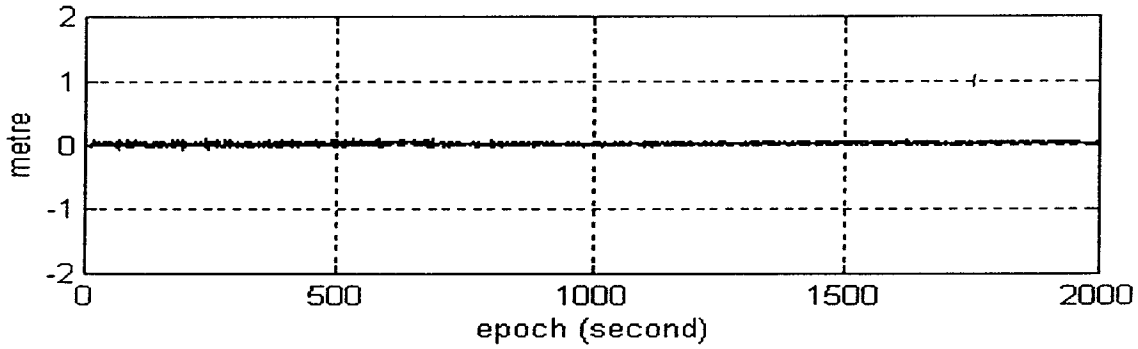

Figure 8.20. Innovation series of PRN 2-6 M-B (day 28, ambiguity fixed).

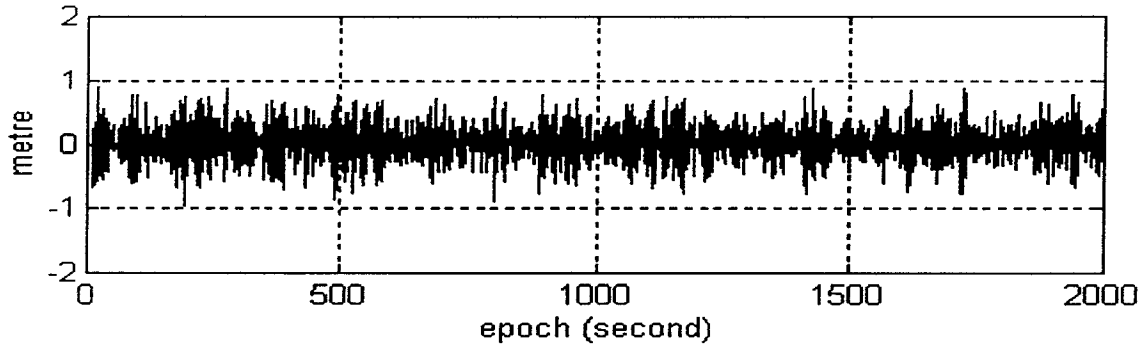

Figure 8.21 Innovation series of PRN 2-15 M-B (28/05, ambiguity fixed)

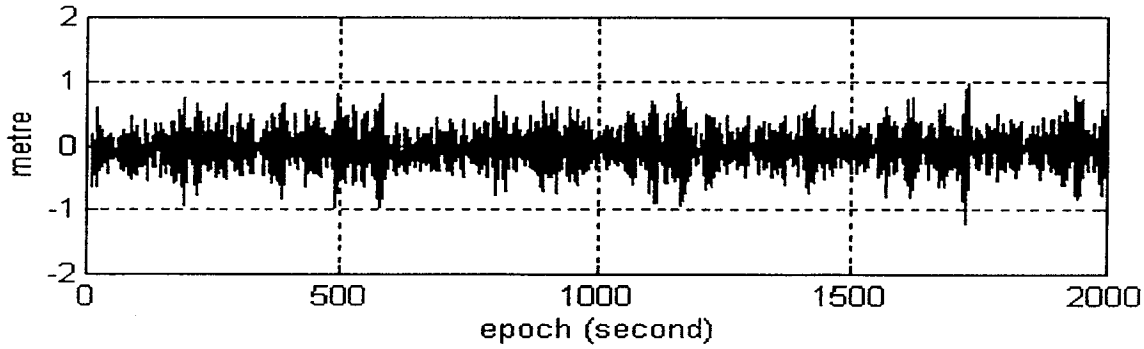

Figure 8.22. Innovation series of PRN 2-13 M-F (day 28, ambiguity fixed).

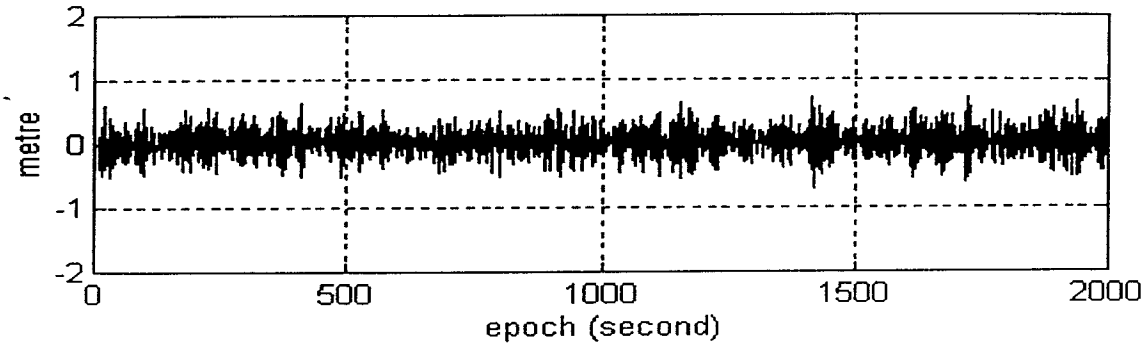

Figure 8.23. Innovation series of PRN 2-19 M-F (day 28, ambiguity fixed).

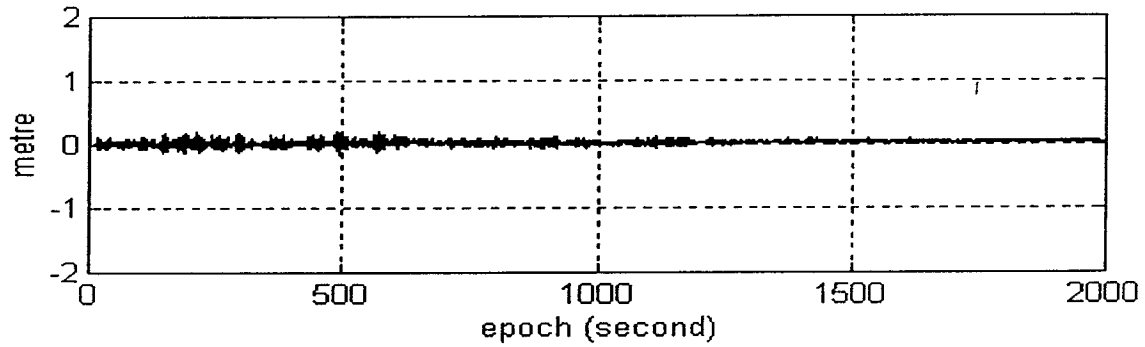

Figure 8.24. Innovation series of PRN 2-6 M-F (day 28, ambiguity fixed).

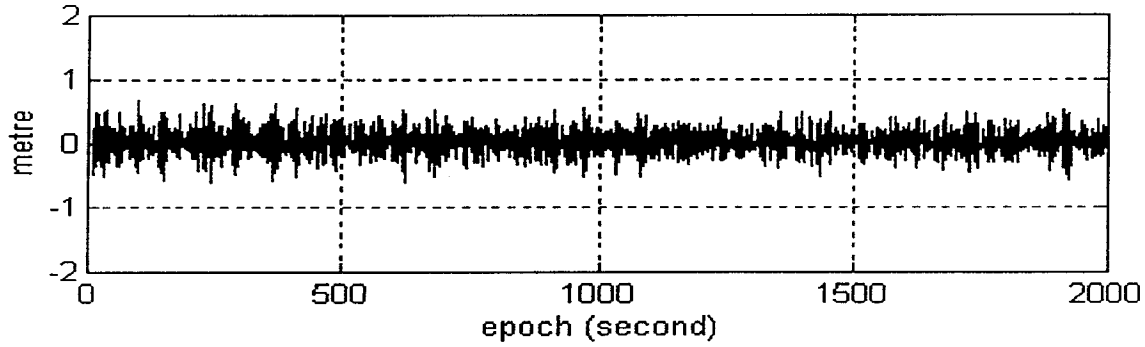

Figure 8.25. Innovation series of PRN 2-15 M-F (day 28, ambiguity fixed).

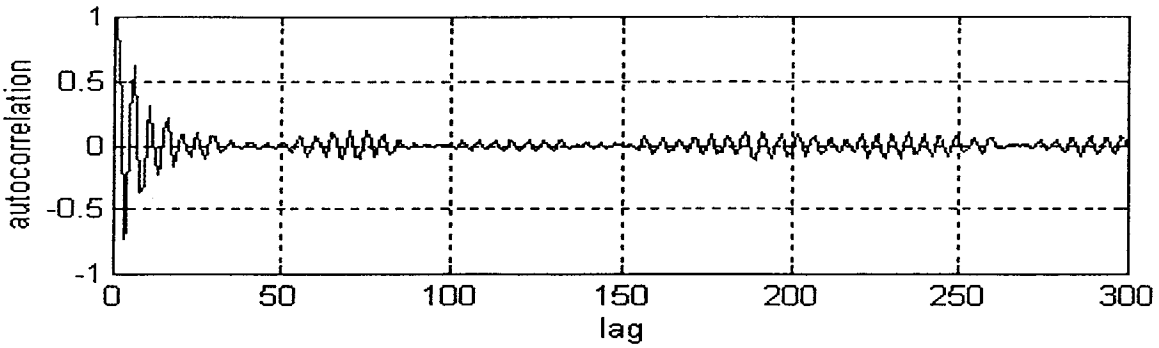

Figure 8.26. Autocorrelation of innovation series of PRN2-13 M-B (day 28, ambiguity fixed).

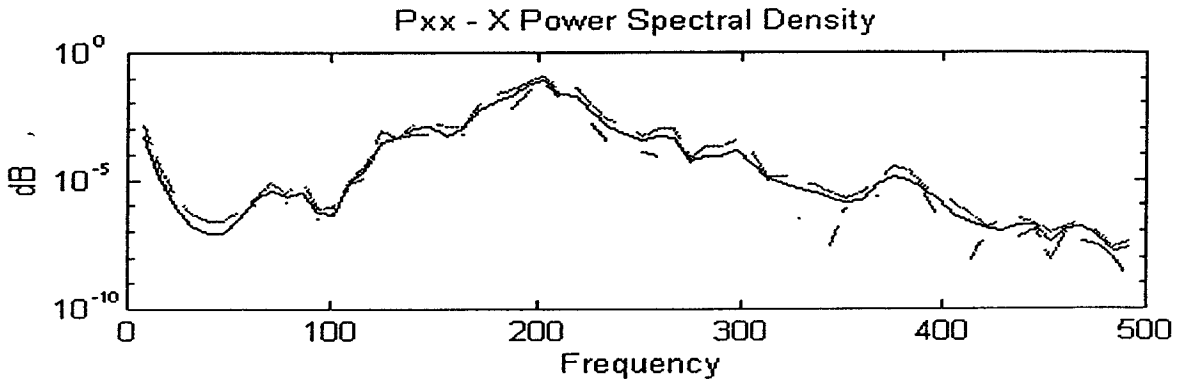

Figure 8.27. PSD of innovation series of PRN 2-13 M-B (day 28, ambiguity fixed).

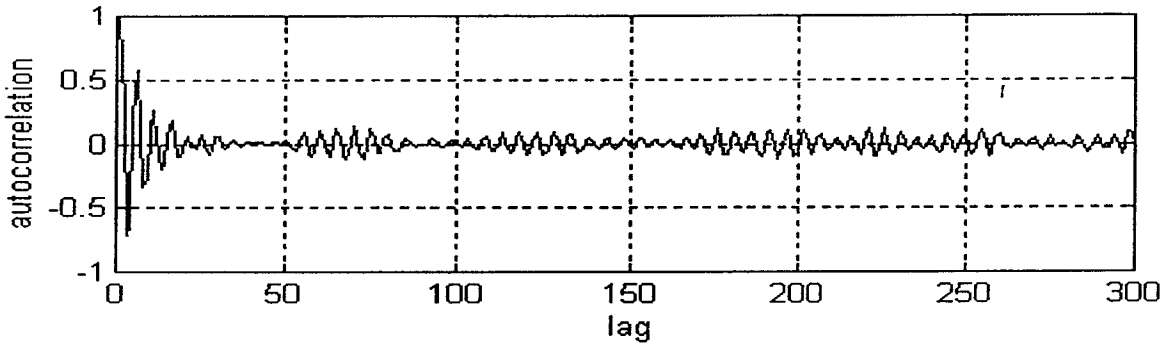

Figure 8.28. Autocorrelation of innovation series of PRN 2-19 M-B (day 28, ambiguity fixed).

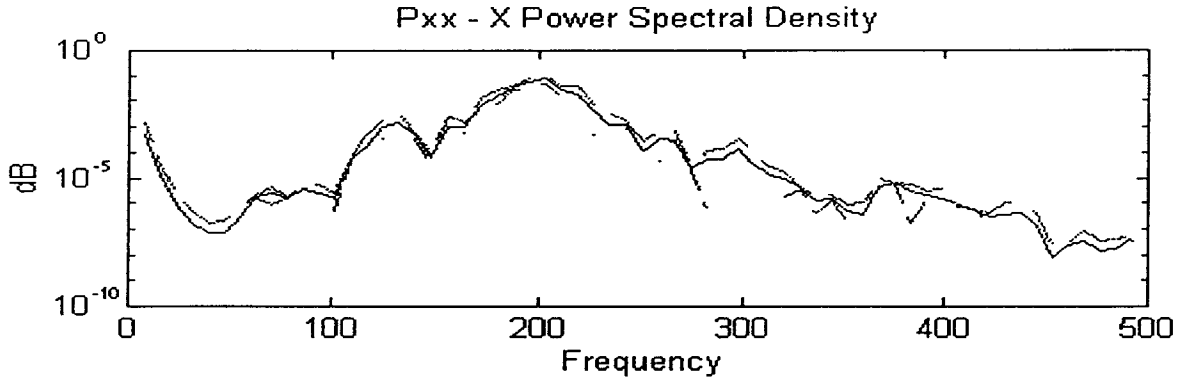

Figure 8.29. PSD of innovation series of PRN 2-19 M-B (day 28, ambiguity fixed).

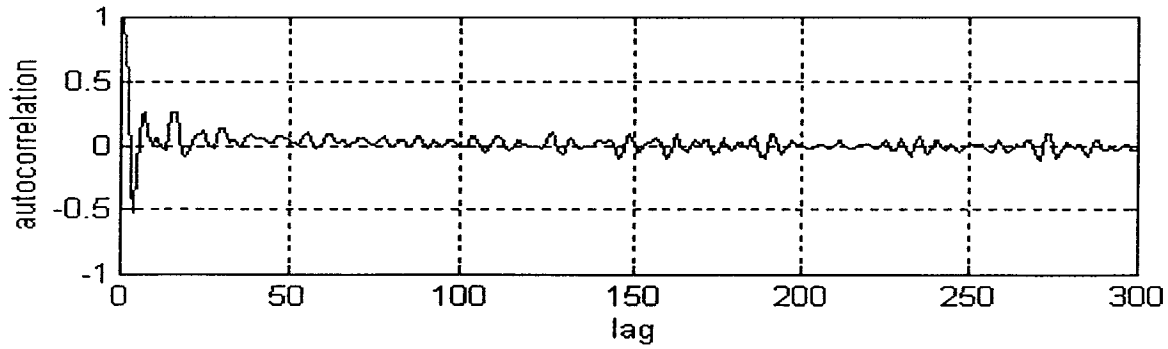

Figure 8.30. Autocorrelation of innovation series of PRN 2-6 M-B (day 28, ambiguity fixed).

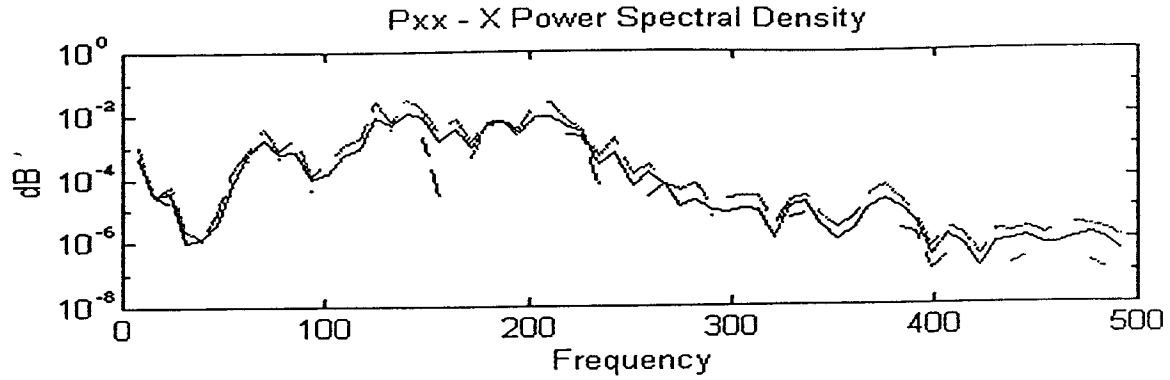

Figure 8.31. PSD of innovation series of PRN 2-6 M-B (day 28, ambiguity fixed).

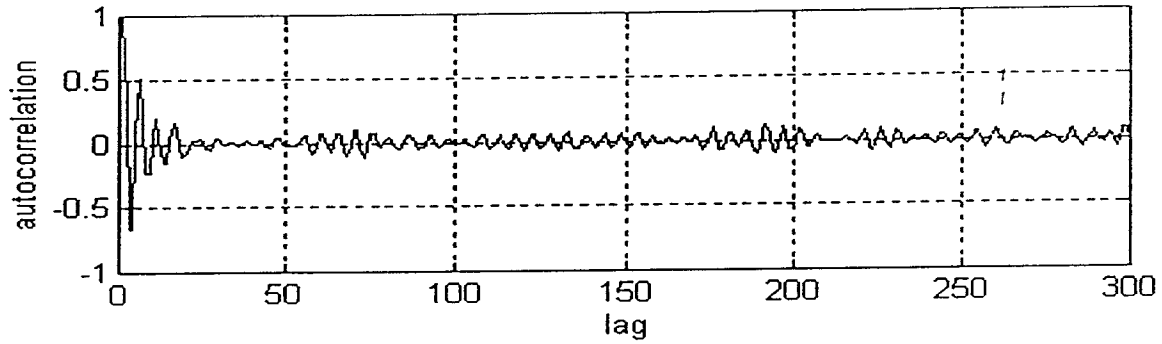

Figure 8.32. Autocorrelation of innovation series of PRN 2-15 M-B (day 28, ambiguity fixed).

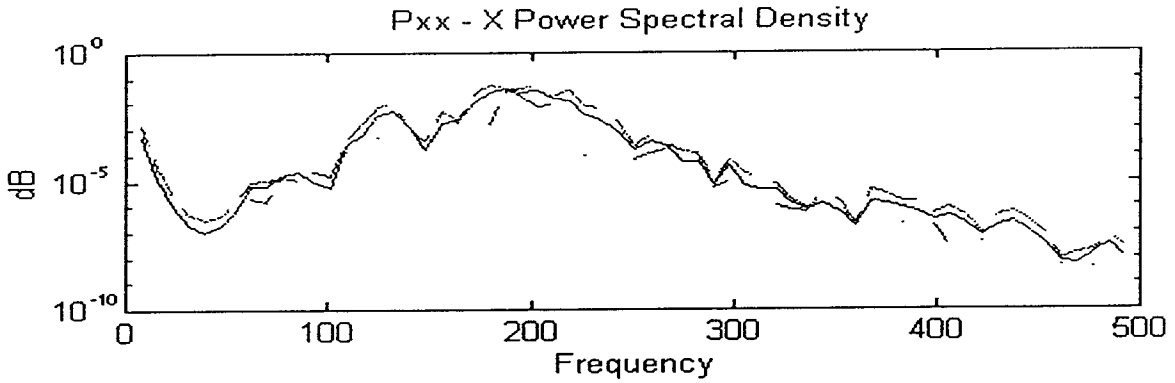

Figure 8.33. PSD of innovation series of PRN 2-15 M-B (day 28, ambiguity fixed).

Table 8.1. Mean values of ambiguity fixed solution.

Date / Type	day 26	day 28
Baseline	29.8328 m	29.8302 m
Heading difference	-0.6123 deg.	-0.5658 deg.

Table 8.2. Mean values of the innovation series (day 28).

PRN / Antenna	2-13	2-19	2-6	2-15
Bow	-0.0396 m	0.0112 m	0.0139 m	0.0211 m
Fun	-0.0400 m	0.0119 m	0.0155 m	0.0205 m

8.3.2 Attitude Mode

This mode was used for heading determination. The first order navigation model was used, and the position time constant was chosen to be 10 seconds (the approximate period of the ship's yaw). The "reference station" was the Bow antenna and the "remote station" was the Fun antenna. The measurements used were the L1 phase data and the ship's gyrocompass output, and the baseline length that was obtained as the mean value from the differential mode results. Both gyrocompass and baseline length uncertainties, 2 degrees and 10 centimetres respectively, were set to their upper bound values and used for the ambiguity initialization and constraints.

Fig.8.34 and Fig.8.35 show the baseline and heading results without heading and baseline length constraints, that is using the GPS measurements only. It can be seen that a long observation time (nearly 1500 epochs) is still needed to fix the ambiguities to integers. When the heading and baseline length constraints were applied, the ambiguities were fix to integers within 1000 epochs from the beginning of the session (see Fig.8.36).

Because the attitude determination is insensitive to the reference antenna's location, the position of the Bow antenna was chosen the location derived from the differential position mode solution. From the plots of ambiguity fixed solutions (see Fig.8.40 to 8.43. and Table 3), it can be seen that nearly the same baseline, heading and pitch results as those of differential positioning mode were obtained.

Table 8.4 shows that the mean values of the innovation series, which can be considered to be zero (comparing those of differential positioning mode which were biased), hence the estimation is clearly unbiased. There were still the pitch oscillation effect in the innovation series (see the PSD and autocorrelation plots).

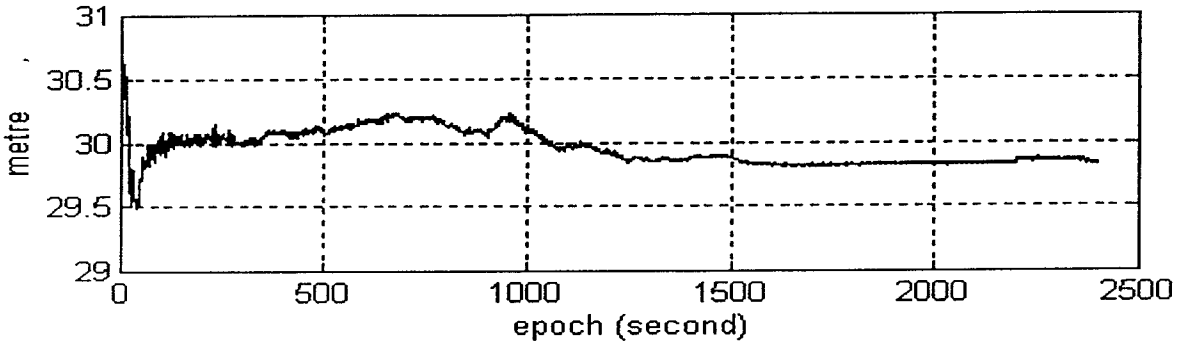

Figure 8.34. Baseline between Bow & Fun (day 26, attitude mode, no constraints).

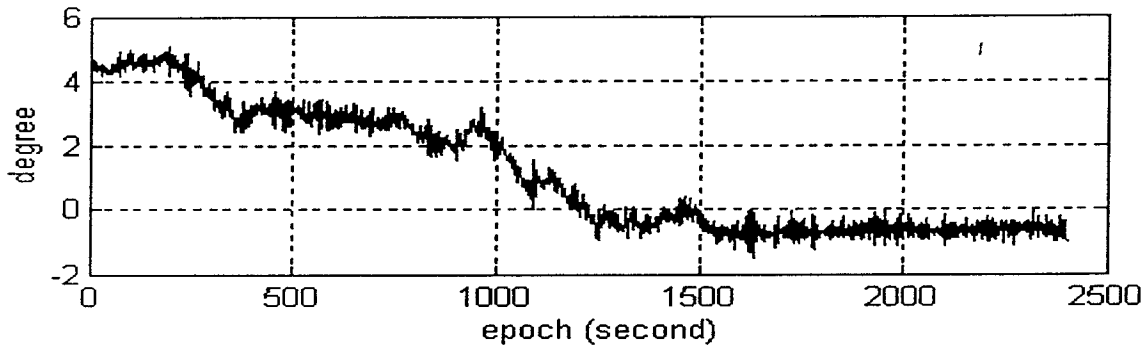

Figure 8.35. Heading difference (day 26, attitude mode, no constraints).

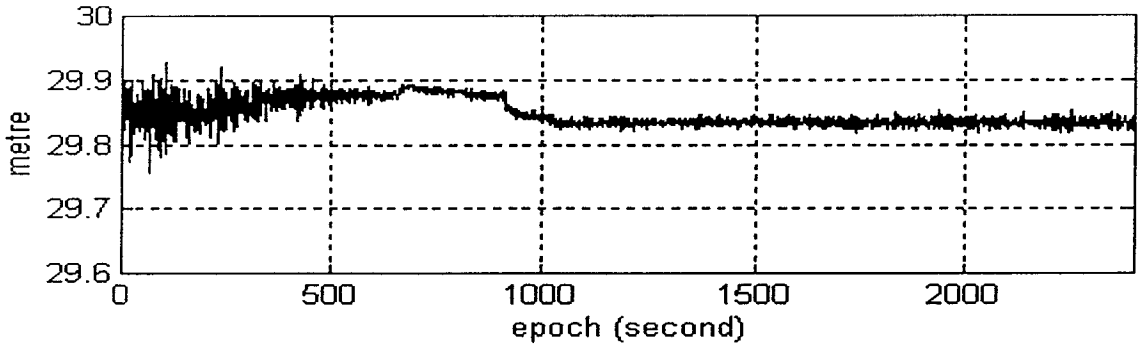

Figure 8.36. Baseline between Bow & Fun (day 26, attitude mode, constraints).

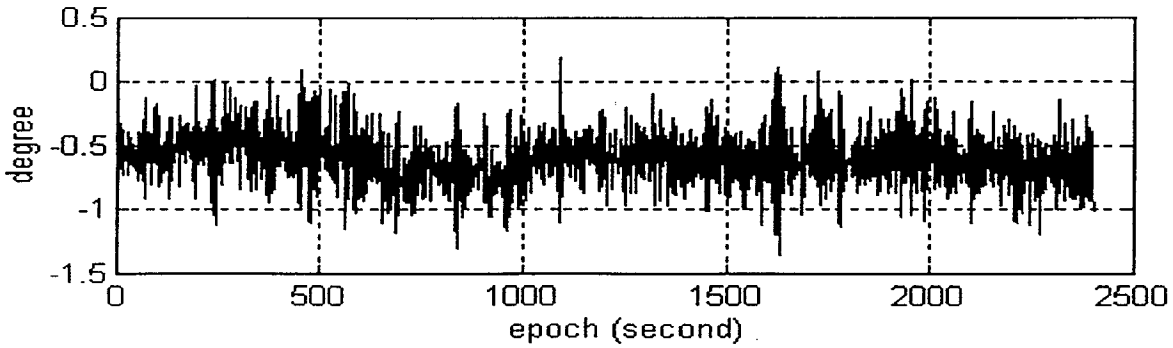

Figure 8.37. Heading difference (day 26, attitude mode, constraints).

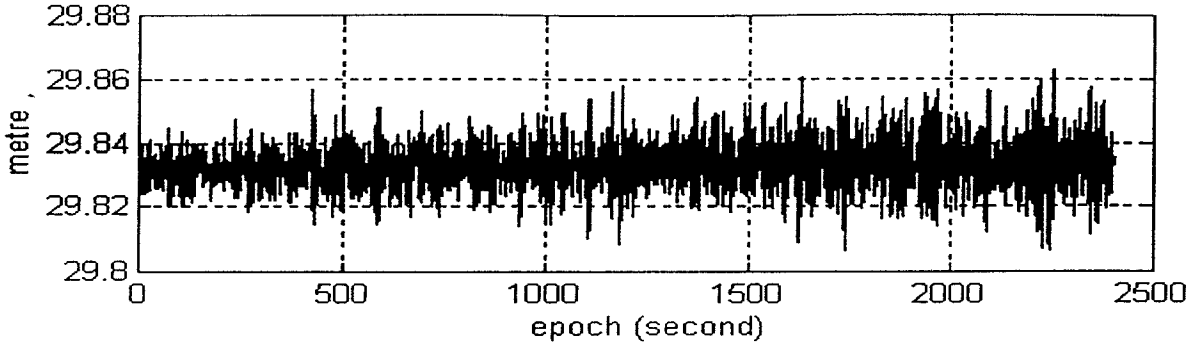

Figure 8.38. Baseline between Bow & Fun (day 26, attitude mode, ambiguity fixed).

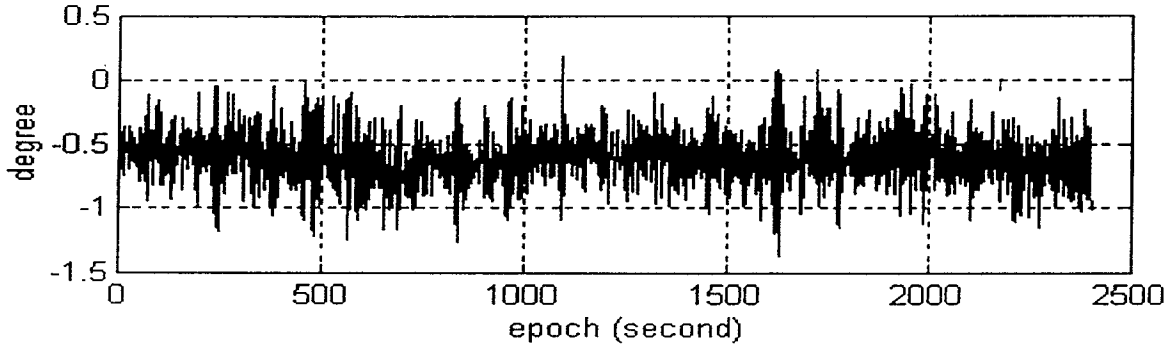

Figure 8.39. Heading difference (day 26, attitude mode, ambiguity fixed).

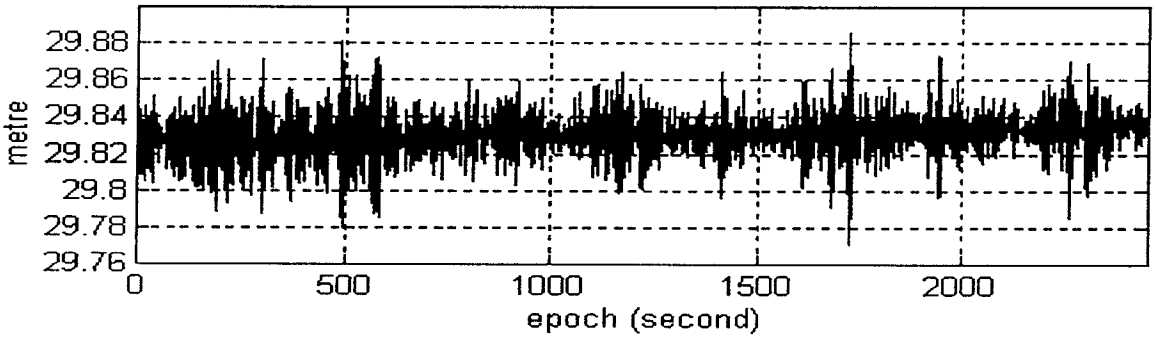

Figure 8.40. Baseline between Bow & Fun (day 28, attitude mode, ambiguity fixed).

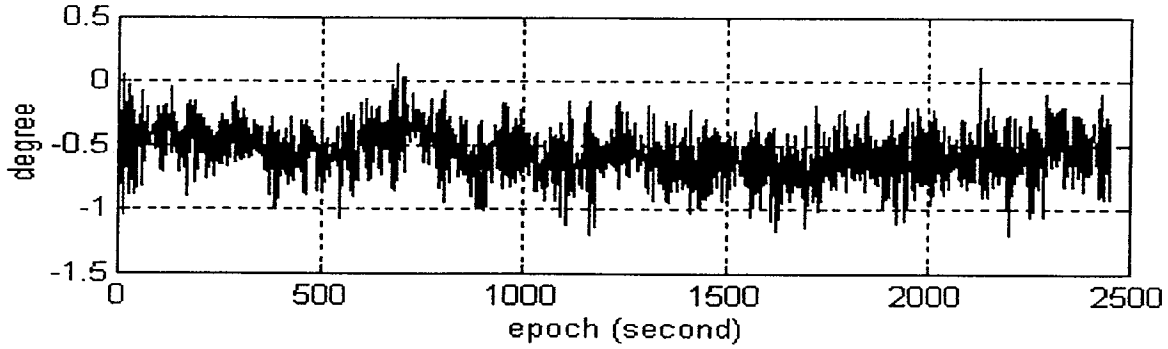

Figure 8.41. Heading difference (day 28, attitude mode, ambiguity fixed).

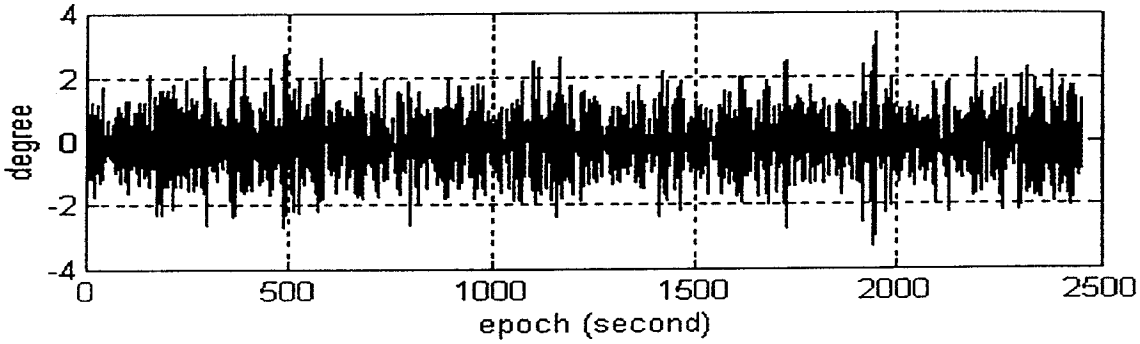

Figure 8.42. Pitch angle (day 28, attitude mode, ambiguity fixed).

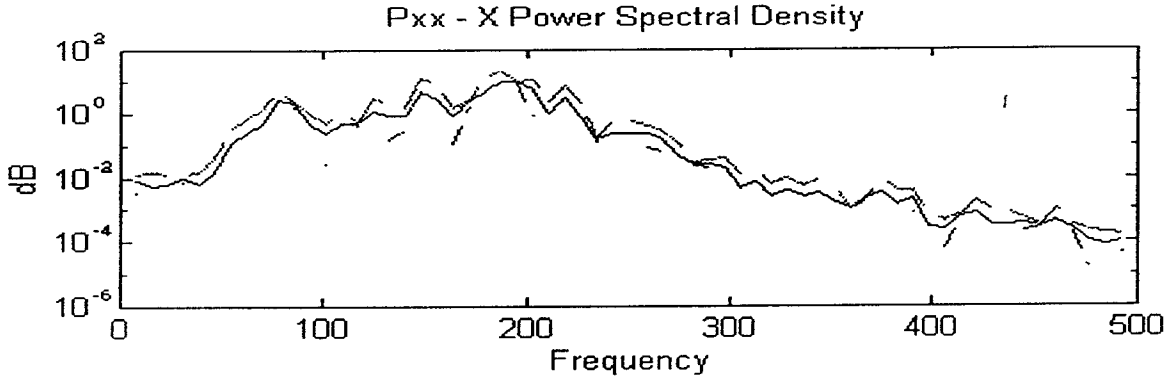

Figure 8.43. PSD of pitch (day 28, attitude mode, ambiguity fixed).

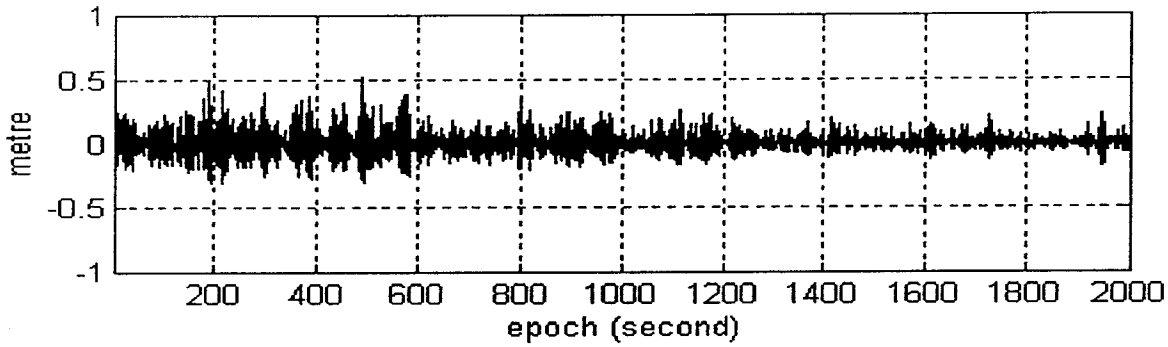

Figure 8.44. Innovation series of PRN 2-13 (day 28, attitude mode, ambiguity fixed).

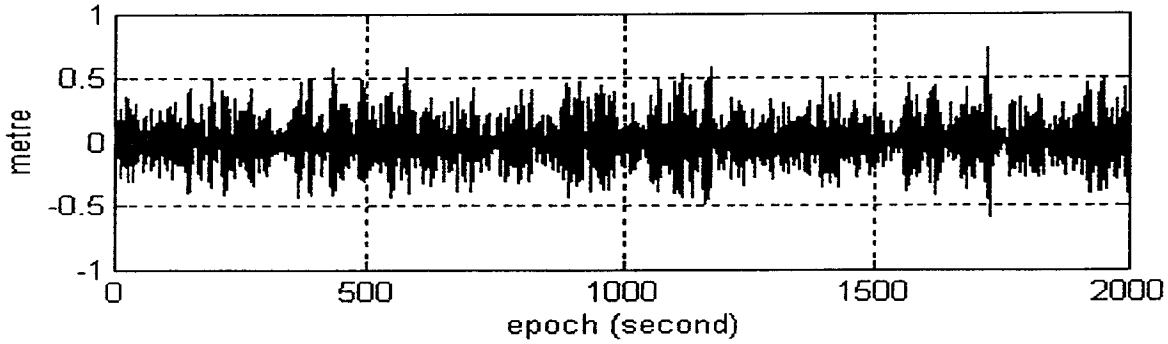

Figure 8.45. Innovation series of PRN 2-19 (day 28, attitude mode, ambiguity fixed).

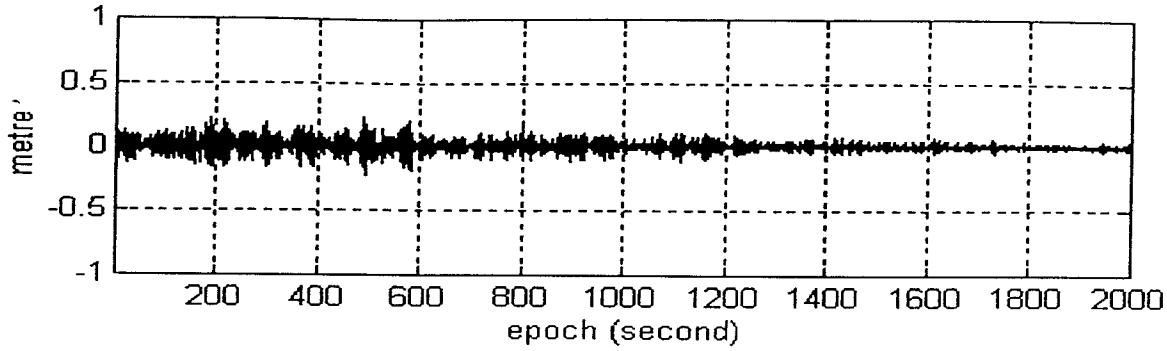

Figure 8.46. Innovation series of PRN 2-6 (day 28, attitude mode, ambiguity fixed).

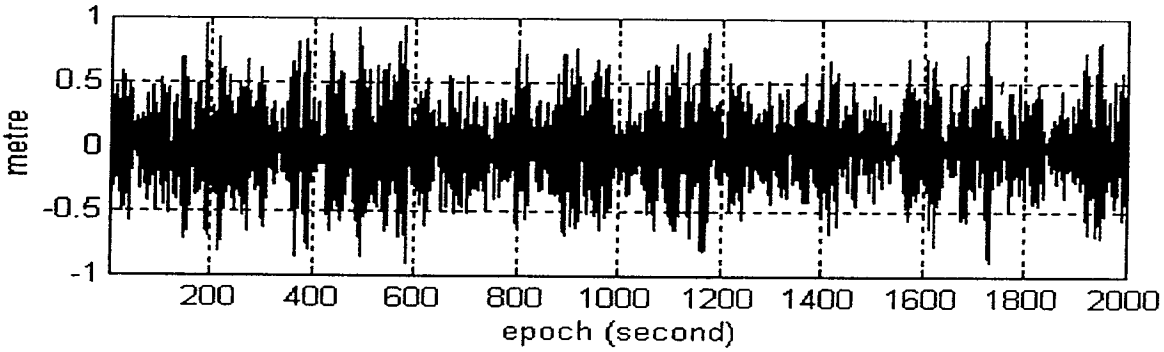

Figure 8.47. Innovation series of PRN 2-15 (day 28, attitude mode, ambiguity fixed).

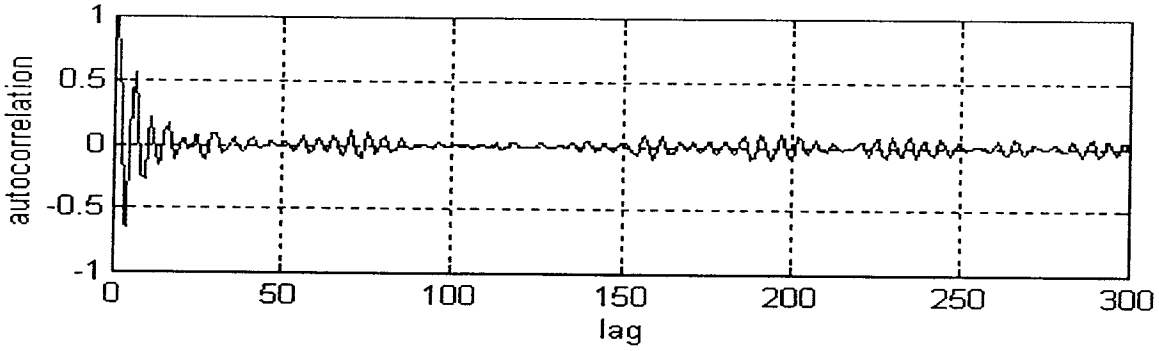

Figure 8.48. Autocorrelation of innovation series of PRN 2-13 (day 28, attitude mode).

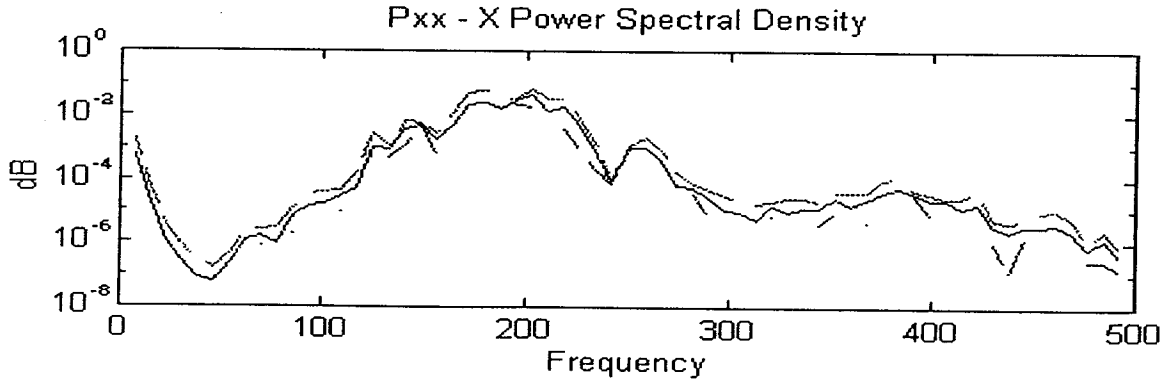

Figure 8.49. PSD of innovation series of PRN 2-13 (day 28, attitude mode).

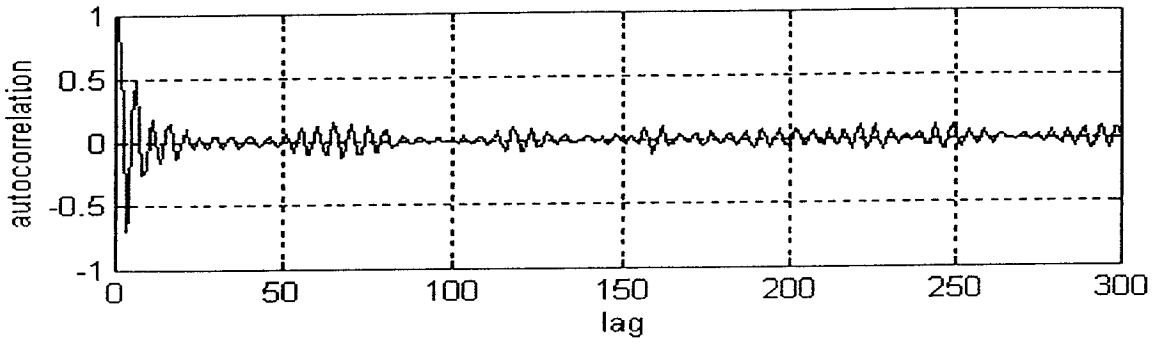

Figure 8.50. Autocorrelation of innovation series of PRN 2-19 (day 28, attitude mode).

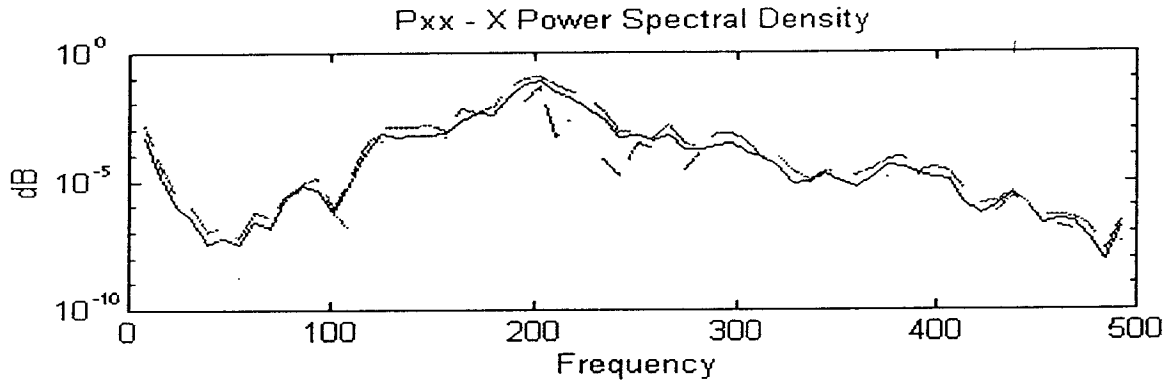

Figure 8.51. PSD of innovation series of PRN 2-19 (day 28, attitude mode).

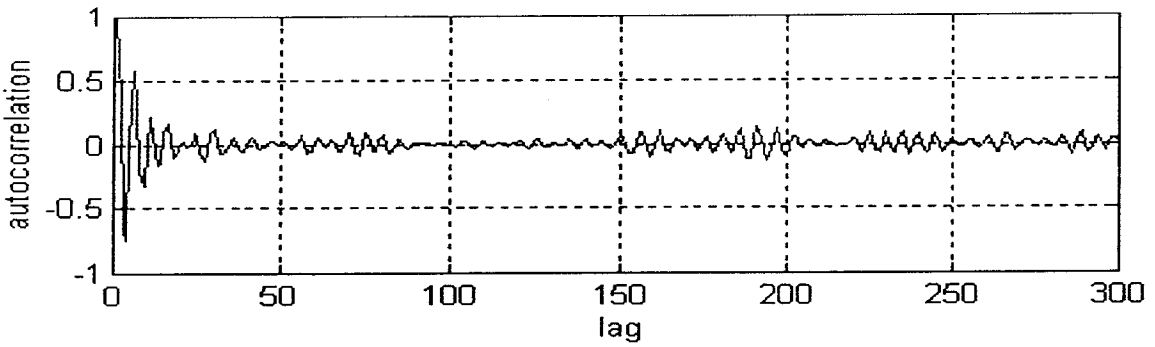

Figure 8.52. Autocorrelation of innovation series of PRN 2-6 (day 28, attitude mode).

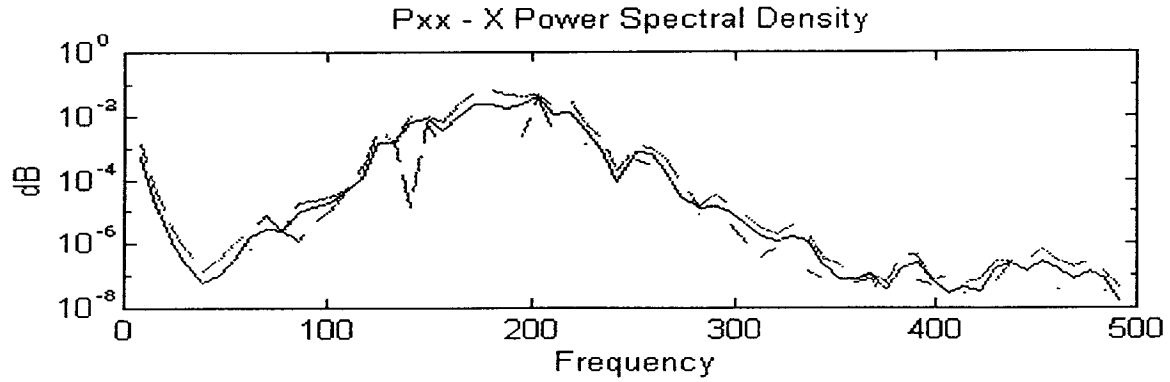

Figure 8.53. PSD of innovation series of PRN 2-6 (day 28, attitude mode).

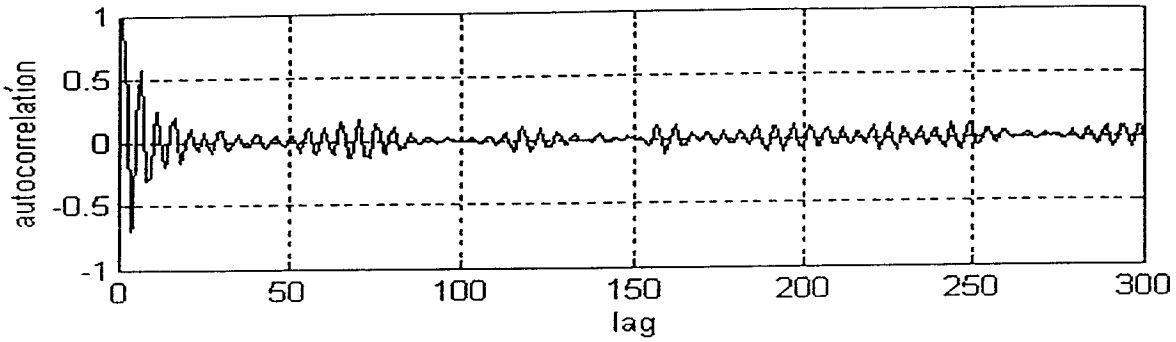

Figure 8.54. Autocorrelation of innovation series of PRN 2-15 (day 28, attitude mode).

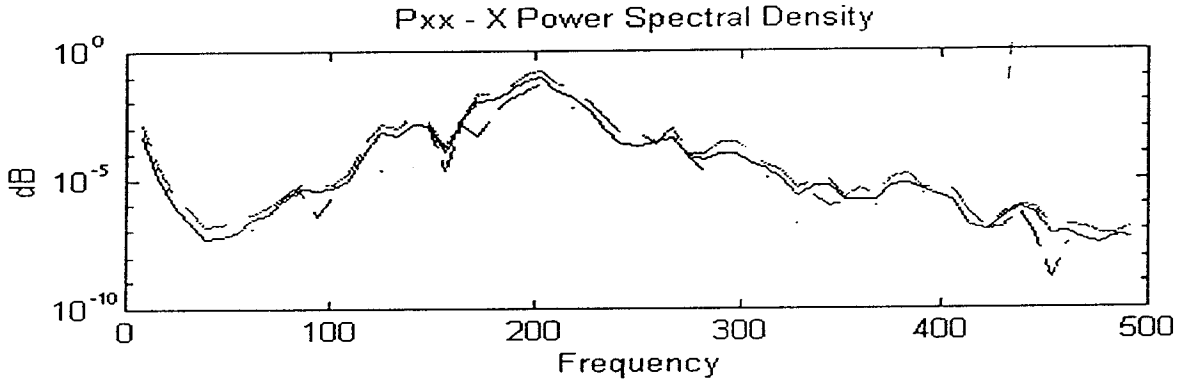

Figure 8.55. PSD of innovation series of PRN 2-15 (day 28, attitude mode).

Table 8.3. Mean values of ambiguity fixed solution (day 28).

Date Mean value	day 26	day 28
Baseline	29.8327 m	29.8295 m
Heading difference	-0.6131 deg.	-0.5664 deg.

Table 8.4. Mean values of innovation series (day 28).

PRN Antenna	2-13	2-19	2-6	2-15
Fun	0.00044 m	0.00132 m	0.00169 m	0.00045 m

8.3.3. DR mode

This mode makes use of the closed-loop DR model, introduced in section 5.2. The DR is calibrated by the C/A code and phase-rate measurements, which is similar to position-velocity calibration of an INS. The "reference station" was the Mather pillar and the "remote station" was Bow antenna. As there were no Doppler data available, the phase-rate was derived from the L1 phase measurements. The time constants of the errors of the gyrocompass, log and sea current were set to 120 minutes, 2 hours and 0.4 hours respectively. The measurement accuracies for the C/A code and phase-rate were selected as 6 metre and 1 centimetre/sec respectively. A large measurement noise was assigned to the code measurements in order to reduce their error influence, and the main contribution of the code measurements was position initialization. Because there were no information on the sea current its initial uncertainty was set to 0.5 metre/sec. 0.1 m/sec and 1 degrees were the initial uncertainties assigned to the log and gyrocompass, and small dynamic noise was put into the filter (0.2 degree, 0.001m/sec, 0.0001m/sec for gyrocompass, log and current respectively).

The results are shown in Fig.8.56 to Fig.8.83 and Tables 8.5 and 8.6. About 800 epochs were needed for the estimation to become steady, due to the requirement to separate sea current and the ship's velocity. Except for PRN 2-19, the remaining innovation series of the double-differenced C/A code measurements were nearly white with non-zero means, as shown in the autocorrelation and PSD plots, and Table 8.6. The autocorrelations of the C/A code innovation series, except of the PRN 2-19, passed the Bartlett test, but not the Portmanteau test, and the autocorrelations of small lags appear an exponential decay feature showing an AP(1) process with a positive coefficient in the C/A code measurements.The 60 second period component of the PRN 2-19 C/A code innovation series was likely cause by the SA for PRN 19, because the same phenomenon also occurred for the PRN 19 C/A code measurements of the Gas receiver (see Fig.A.7.12). The phase-rate innovation series include the ship's pitching component whose period is about 8 seconds, and also have relative large power in frequency range 0 to 0.02 π, hence there were biases in the phase-rate measurements with oscillation periods larger than 100 seconds. The biases of the double-differenced phase-rate measurements were due to the long distances between the Mather and the Bow stations.

Generally speaking, the estimated error of the gyrocompass is inversely proportional to the vessel's speed, and it can be expressed as:

$$e_G = \frac{\sigma_V}{V} = \frac{PDOP^*\sigma_D}{V} \qquad (8.1)$$

where:

- e_G gyrocompass estimate error
- σ_V velocity error
- σ_D Doppler (or phase-rate) measurement error
- V vessel's speed

For example, 0.1m/sec velocity error can causes a 0.1 degree of gyrocompass estimate error while the vessel's speed is 10 knots. The greater is the vessel's velocity, the faster is the convergence speed of the gyrocompass error estimate. In the case of day 26 and day 28 the vessel's speeds were 2.2 and 3 knots respectively, hence a long observation time was needed to obtain the steady state solutions.

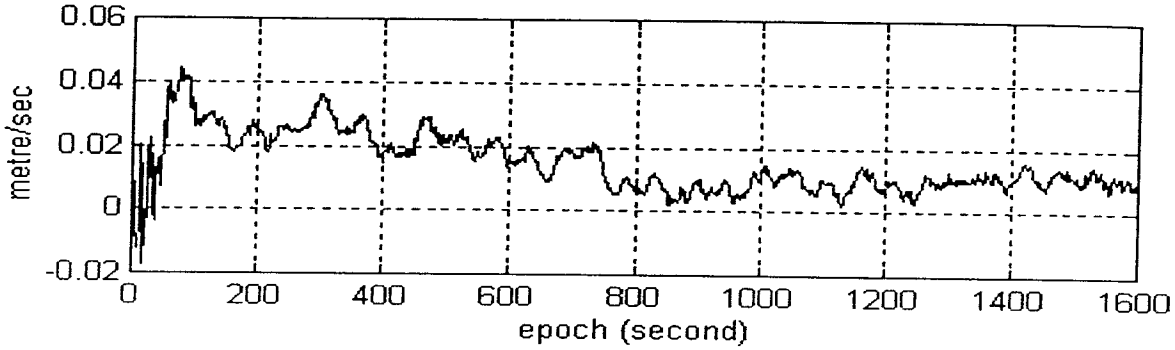

Figure 8.56. Doppler-log error (day 26, DR).

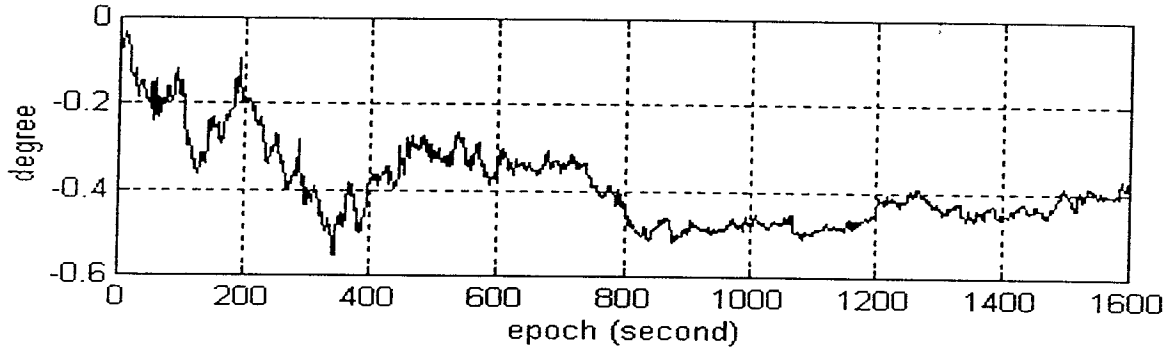

Figure 8.57. Gyrocompass error (day 26, DR)

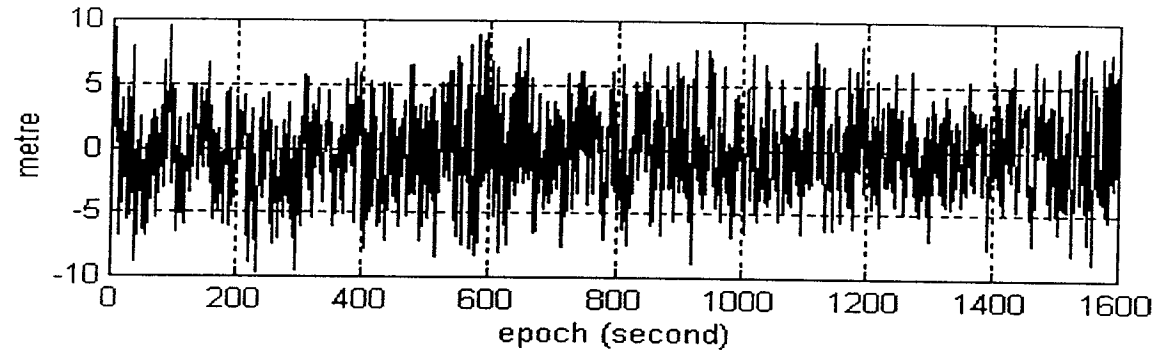

Figure 8.58 Innovation series of PRN 2-13 C/A code (day 26, DR)

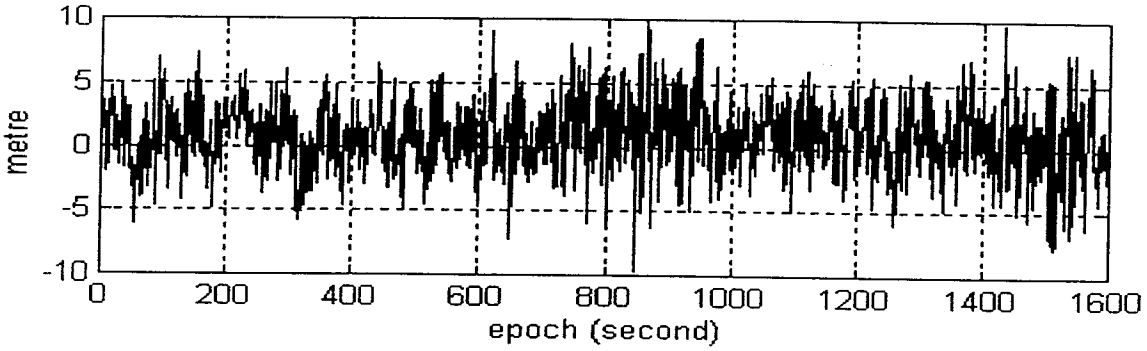

Figure 8.59. Innovation series of PRN 2-6 C/A code (day 26, DR).

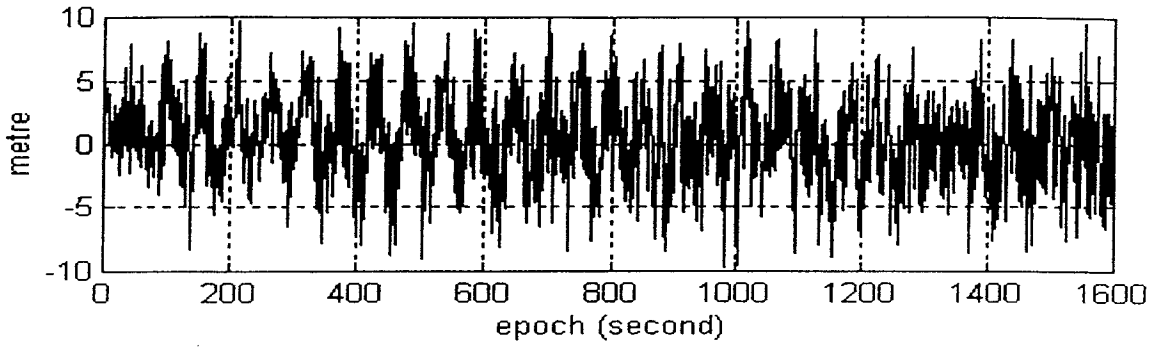

Figure 8.60. Innovation series of PRN 2-19 C/A code (day 26, DR).

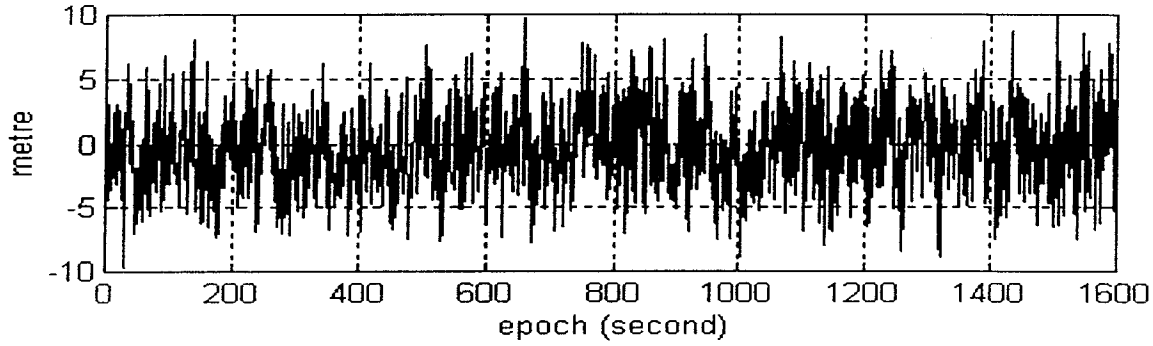

Figure 8.61. Innovation series of PRN 2-15 C/A code (day 26, DR).

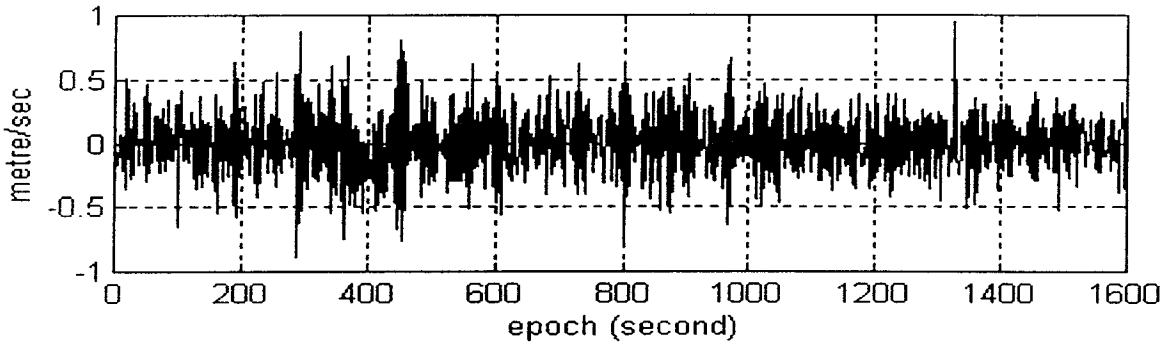

Figure 8.62. Innovation series of PRN 2-13 phase-rate (day 26, DR).

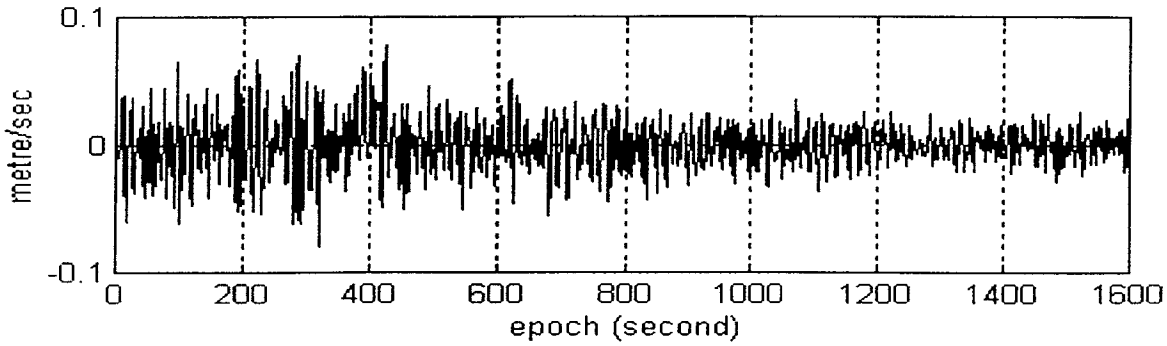

Figure 8.63. Innovation series of PRN 2-6 phase-rate (day 26, DR).

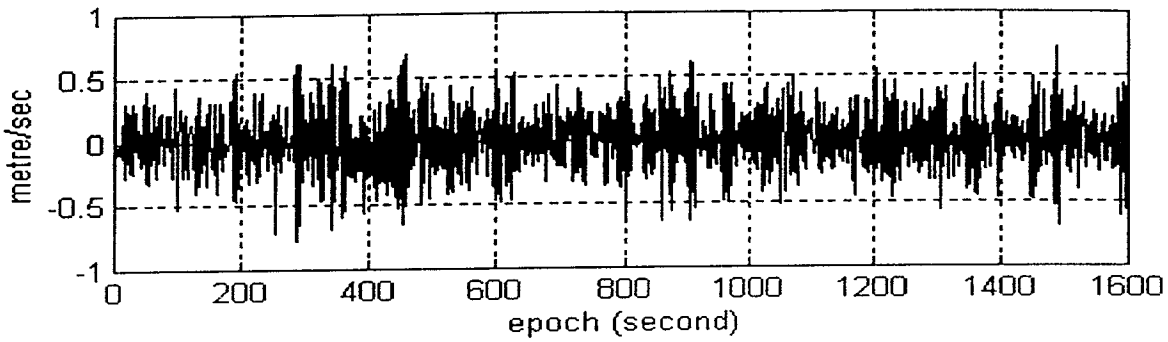

Figure 8.64. Innovation series of PRN 2-19 phase-rate (day 26, DR).

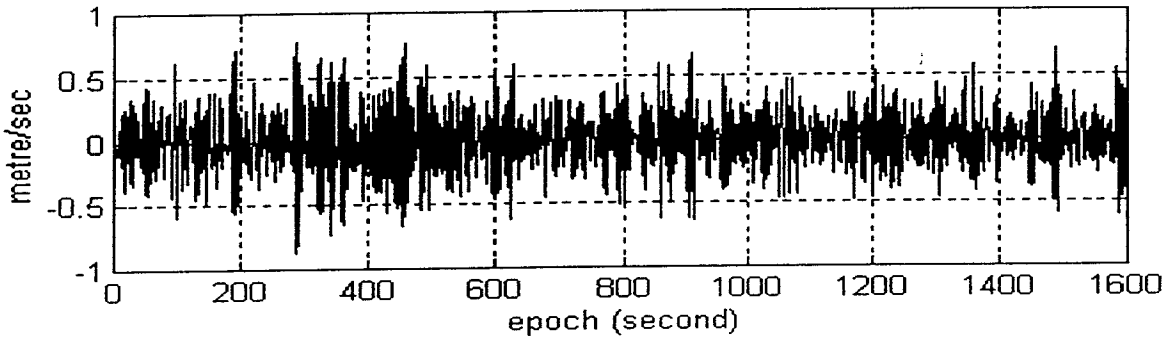

Figure 8.65. Innovation series of PRN 2-15 phase-rate (day 26, DR).

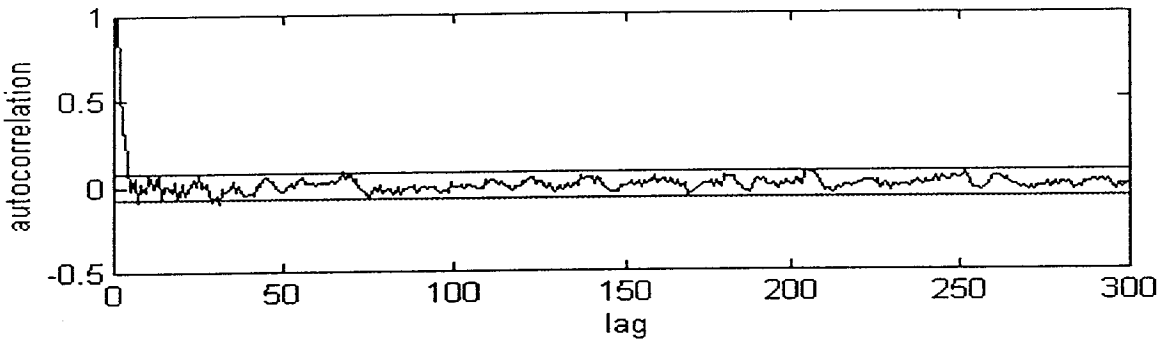

Figure 8.66. Autocorrelation of innovation series of PRN 2-13 C/A (day 26, DR).

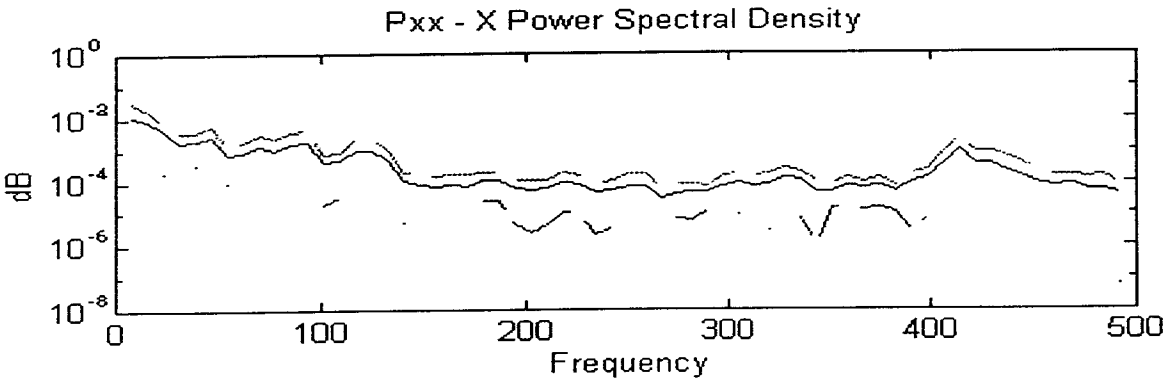

Figure 8.67. PSD of innovation series of PRN 2-13 C/A (day 26, DR).

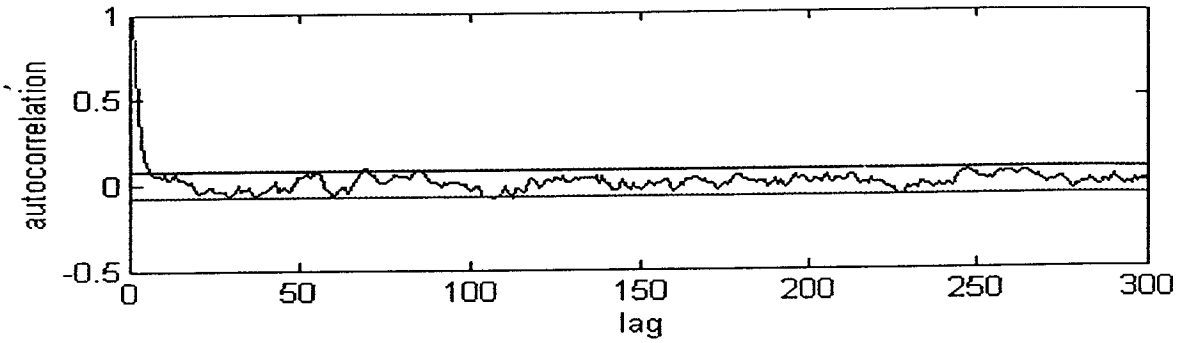

Figure 8.68. autocorrelation of innovation series of PRN 2-6 C/A (day 26, DR).

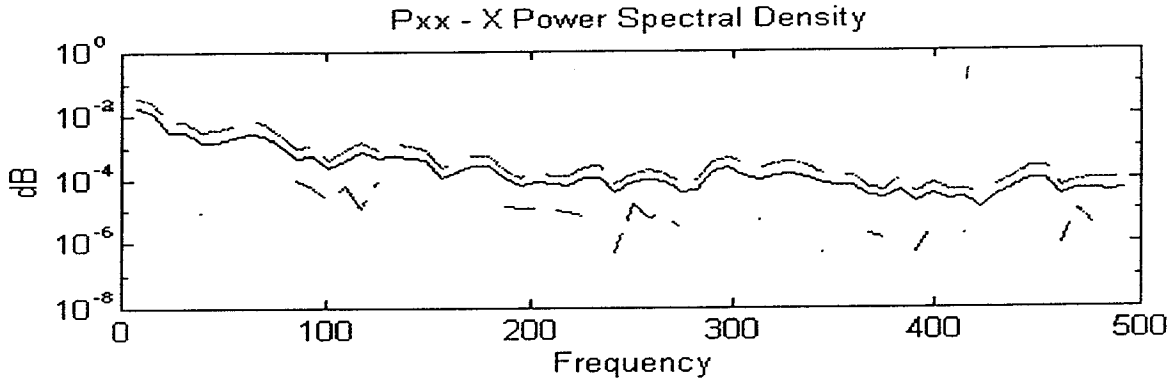

Figure 8.69. PSD of innovation series of PRN 2-6 C/A (day 26, DR).

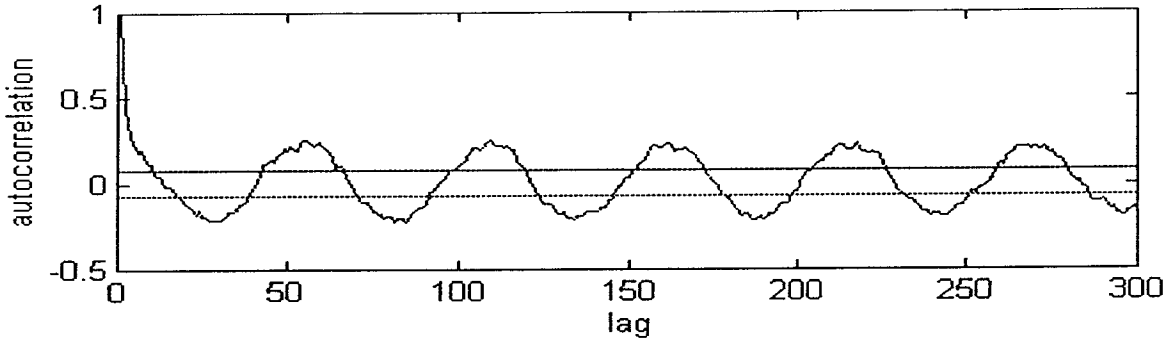

Figure 8.70. autocorrelation of innovation series of PRN 2-19 C/A (day 26, DR).

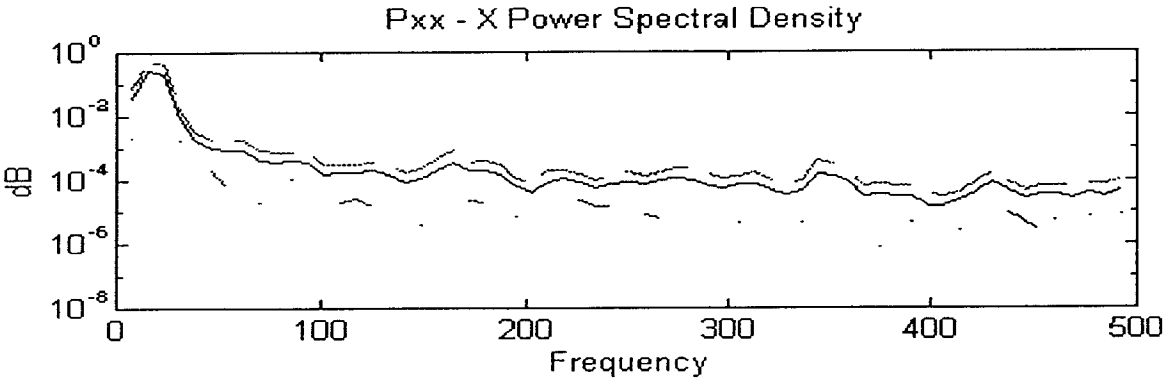

Figure 8.71. PSD of innovation series of PRN 2-19 C/A (day 26, DR).

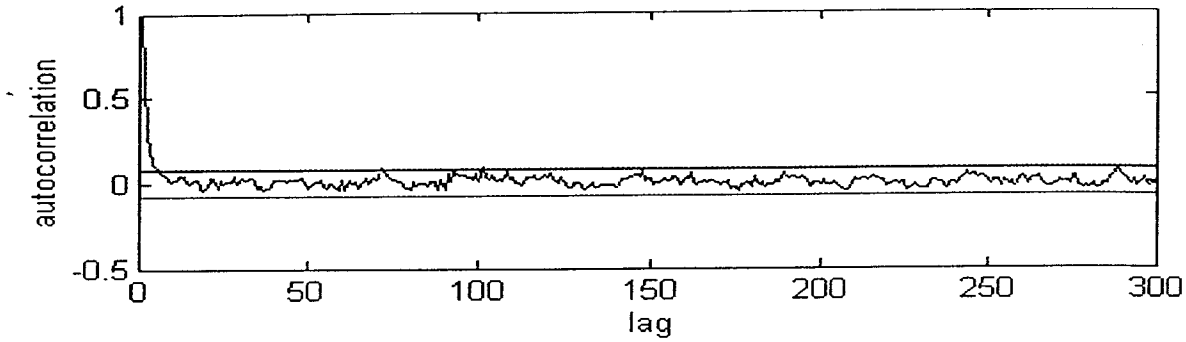

Figure 8.72. autocorrelation of innovation series of PRN 2-15 C/A (day 26, DR).

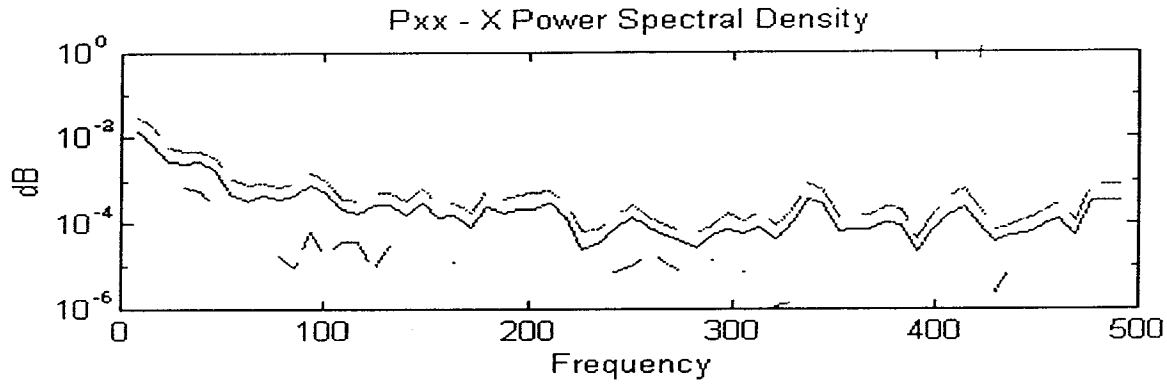

Figure 8.73. PSD of innovation series of PRN 2-15 C/A (day 26, DR).

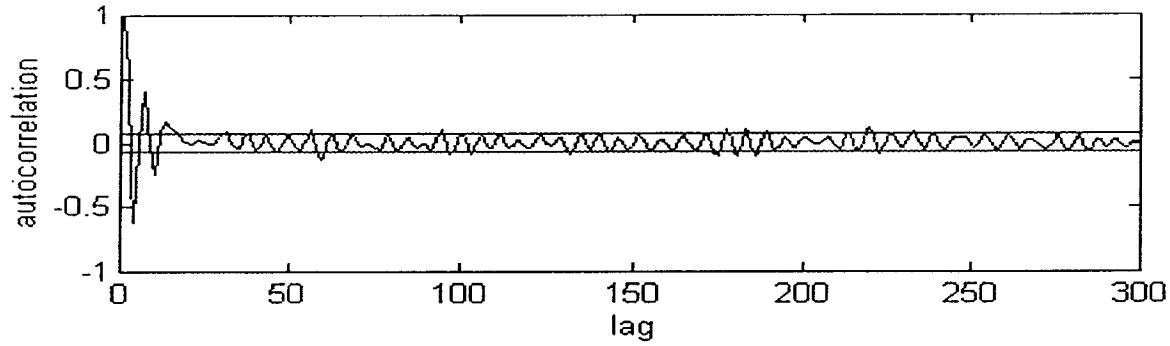

Figure 8.74. autocorrelation of innovation series of PRN 2-13 phase-rate (day 26, DR).

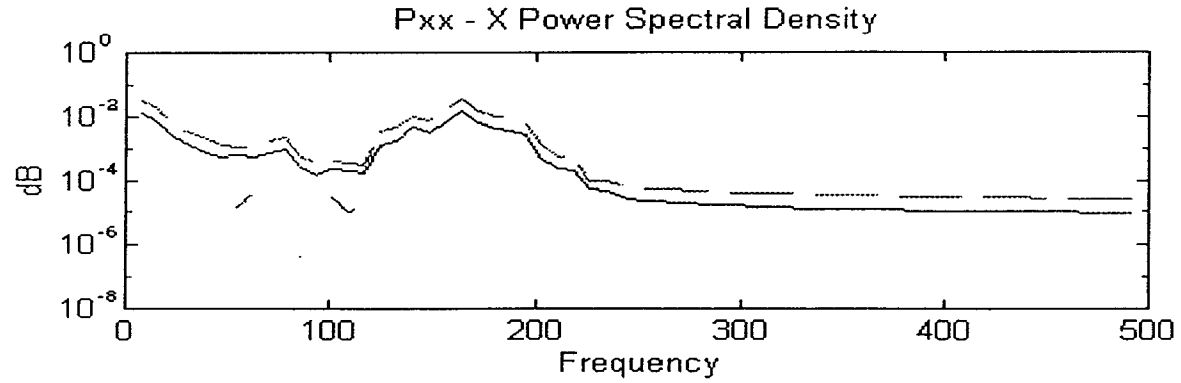

Figure 8.75. PSD of innovation series of PRN 2-13 phase-rate (day 26, DR).

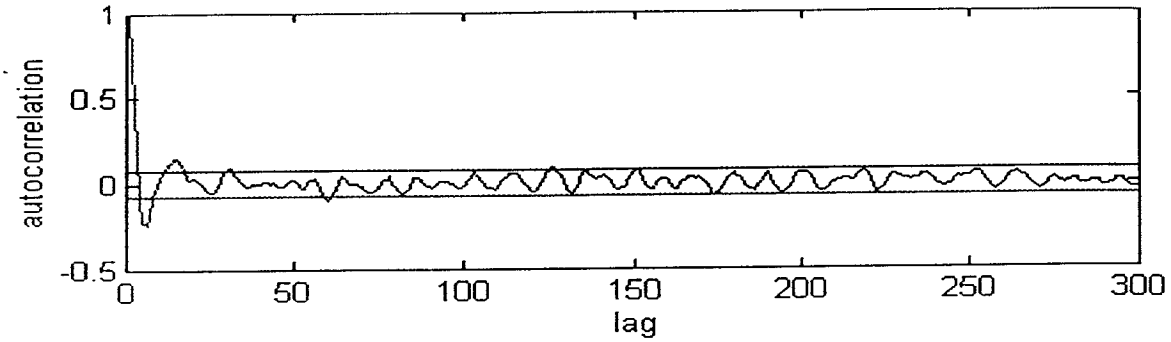

Figure 8.76. autocorrelation of innovation series of PRN 2-6 phase-rate (day 26, DR).

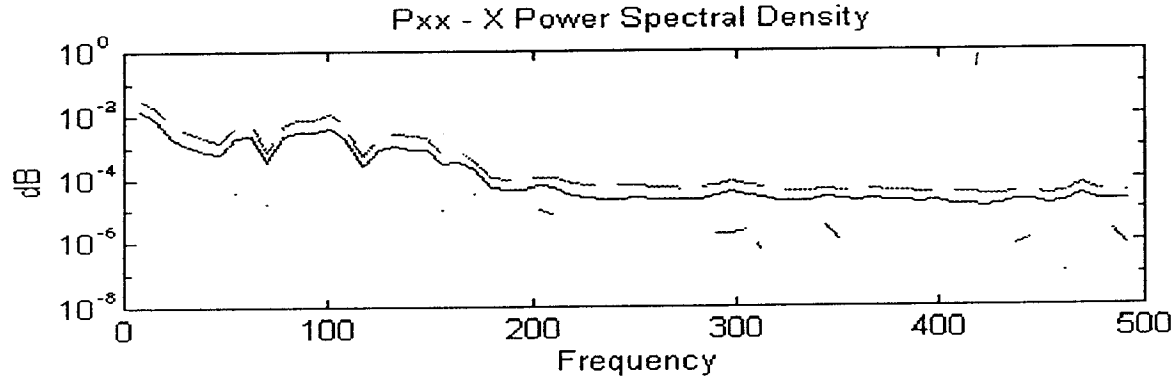

Figure 8.77. PSD of innovation series of PRN 2-6 phase-rate (day 26, DR)

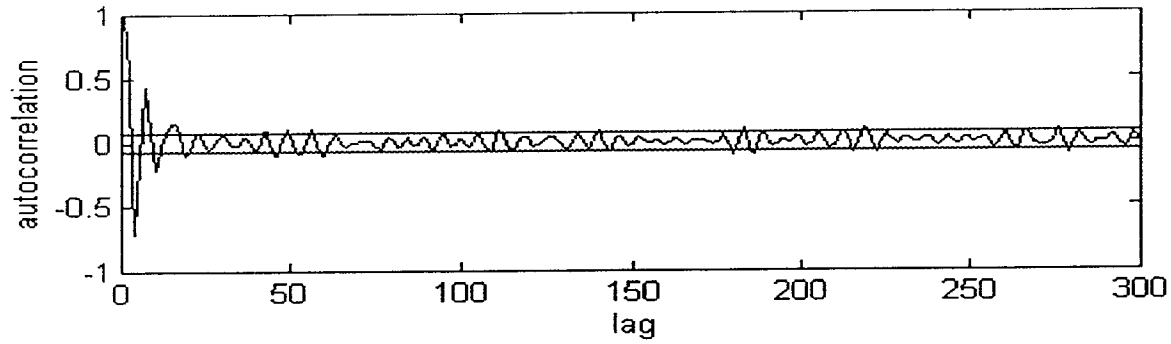

Figure 8.78. autocorrelation of innovation series of PRN 2-19 phase-rate (day 26, DR).

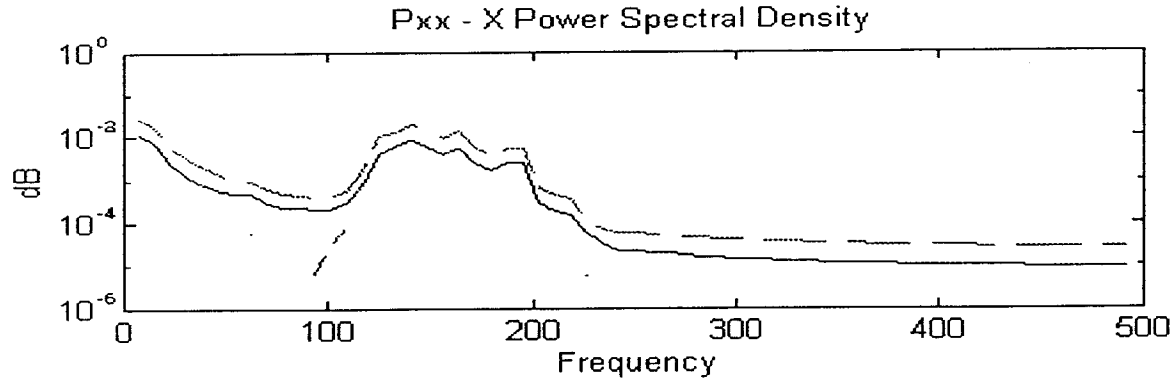

Figure 8.79. PSD of innovation series of PRN 2-19 phase-rate (day 26, DR).

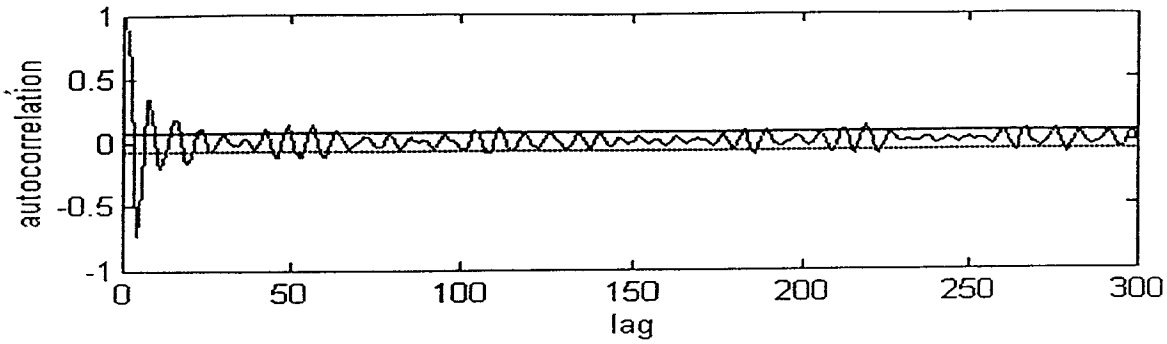

Figure 8.80. autocorrelation of innovation series of PRN 2-15 phase-rate (day 26, DR).

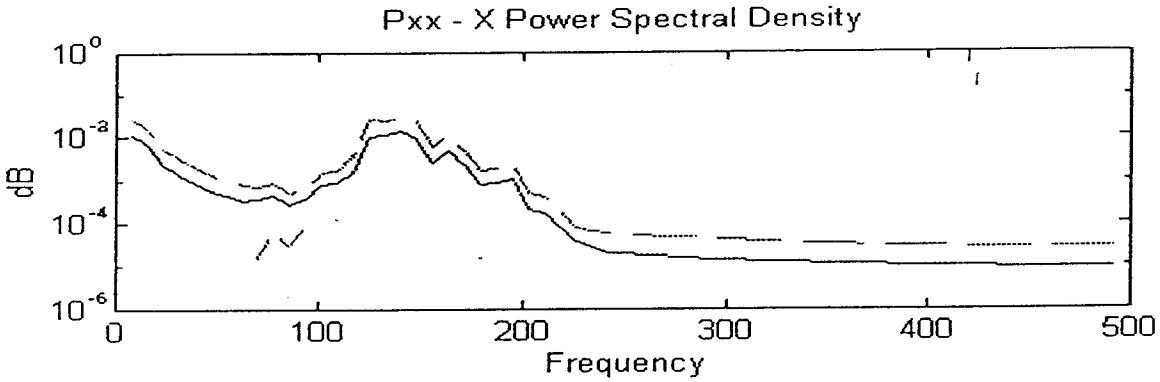

Figure 8.81. PSD of innovation series of PRN 2-15 phase-rate (day 26, DR).

Table 8.5 Mean values of steady state

Date / Type	26/05	28/05
Gyrocompass error	-0.6536 deg.	-0.5824 deg.
Log error	0.0092 m/sec	0.0253 m/sec

CHAPTER 9

CONCLUSIONS AND RECOMMENDATIONS

Extensive software development and GPS data analyses complement the significant theoretical studies undertaken and reported in this thesis. In the process of investigating GPS attitude determination several other worthwhile topics were identified and the results of these studies were incorporated into the thesis work. This thesis is a record of these investigations, and the following conclusions are drawn:

1) GPS measurement noise and biases can be depressed in the frequency domain using low-pass filters, and high-pass filters, respectively (Chapter 4, section 4.4.1.3; Chapter 7, section 7.2.1) .

2) Only constant components of the bias in time or space (zero frequency components) can be eliminated by the time-differencing or space-differencing operators. The time-differencing or space-differencing operators will only depress those components whose frequency is less than 0.25 π, while the other components will be amplified by the operators in a nearly linearly fashion (Chapter 7, section 7.2.1).

3) Dual-frequency phase smoothed code measurements have the narrowest pass-band among the phase, Doppler and Finite Impulse Response digital filter (FIR DF) smoothing processes, and its pass-band can be adjusted automatically to follow the body's dynamics (Chapter 4, section 4.4.1.2).

4) FIR DF smoothing design is dependent on the body's dynamics. A good FIR DF design and implementation will ensure the original data characteristics are not changed (the phase response of the FIR DF is linear), but introduce an output delay which is equivalent to the half-length of the DF order. A data rate which is higher than the Nyquist frequency is necessary for good DF performance. For 1 Hz code measurements, a two third noise intensity depression can easily be achieved using a 12th order FIR DF (Chapter 4, section 4.4.1.3).

5) Doppler-created phase data is an alternative application of the GPS Doppler measurements. For short baselines, centimetre accuracy is achievable in the static processing model. The additional bias introduced into the Doppler-created phase data is only receiver dependent, and for most receivers it is a constant and quite small, hence a technique has been developed for kinematic positioning, achieving cm accuracy better than that expected of a P-code solution (Chapter 4, section 4.4.2).

6) Least Squares polynomial fitting (LSPF) operates like a low-pass FIR DF. The "wiggle effect" is caused by the large sidelobe and phase distortion of the LSPF frequency response of near end point fitting. The choice of the LSPF order and fitting data point number can be easily made after studying the frequency response characteristics of both the LSPF and the data (Chapter 7, section 7.1.1).

7) The LSPF middle point fitting has the smallest sidelobe and no phase distortion. It introduces an output delay, as in the case of a FIR DF (Chapter 7, section 7.1.1).

8) A fifth order elliptic Infinite Impulse Response digital filter (IIR DF) can be used for cycle slip detection and repair of one-way GPS phase data at the 1 second data rate for low dynamic body. The cut-off frequency of the IIR is dependent on the body's dynamics (Chapter 7, section 7.1.2).

9) For all navigation models introduced here, the position variable is unstable (Chapter 6, section 6.1.1.4).

10) With the exception of the static model, all navigation models are stochastically completely controllable. This means that all of the body's state is affected by the input noise and the state can be changed by changing the input (Chapter 6, section 6.4).

11) For the navigation models introduced here, the GPS code and phase measurements are observable for all the body's states (position, velocity and acceleration), but the Doppler is only sensitive to the body's velocity and acceleration (Chapter 6, sections 6.5.1, 6.5.2, 6.5.4).

12) For the augmented measurement bias model, stationary models such as the first order Markov process are preferable from the system stability point of view. The augmented models for each bias should not have common components, otherwise the augmented models can not be separated by the filter (such as for the augmented random walk and ambiguity) (Chapter 6, sections 6.5.3, 6.5.4).

13) For the navigation models introduced here, the constant measurement bias, such as the double-differenced phase ambiguity, is observable for both the static and kinematic cases if the observation time is long enough. The observability time for the ambiguity is mainly satellite geometry dependent (Chapter 6, section 6.6.2.3).

14) The Separated-Bias Kalman Filter (SBKF) can be used for floating and fixed ambiguity estimation and for slowly changing bias estimation of GPS measurements. The filter is stable and computational efficient. For single frequency data to five observed satellite, 1500 epochs (at 1 Hz) were needed to fix the ambiguity in the kinematic case in our experiments (Chapter 7, section 7.1.4; Chapter 8, sections 8.3.1, 8.3.2).

15) The gyrocompass error estimation accuracy of the closed-loop Dead Reckoning (DR) and GPS integration implementation depends on the velocity estimation accuracy obtained from the GPS Doppler or phase-rate measurements, and is insensitive to the body's dynamics. A 0.1 degree accuracy is achievable if the velocity error is 1 cm/sec for a body of 10 knot speed (Chapter 8, section 8.3.3).

16) The same accuracy of heading is achieved using differential and attitude data processing modes, and the repeatability of the heading accuracy is better than 0.01 degree (Chapter 8, sections 8.3.1, 8.3.2).

These are several recommendations for future work, including:

1) GPS Doppler data is a very useful observable as it contains information on the GPS measurement bias-rate and the body's velocity (position change-rate) and acceleration information. Investigations should be made concerning the Doppler measurement characteristics, such as: the measurement noise and correlation, the cross-correlation with code and

phase measurements, the measurement bias model, and the effects of signal loss-of-lock on the Doppler measurement for different types of receivers.

2) A more sophisticated Doppler-created phase algorithms can be developed in order to overcome the effects of different biases and to make the Doppler-created phase behave more like "real" phase data that can then be processed using standard GPS phase reduction software.

3) Digital filters are useful tools for GPS data processing, and are especially suitable for real-time receiver applications. There are a variety of digital filters with different performance characteristics that can be used for GPS data processing. These include amplitude-limiting filters for data smoothing, notch filters for eliminating biases with periodic oscillation, etc. A further investigation of the application of digital filters to GPS data processing will therefore be rewarding.

4) Separation of the body's dynamics, measurement biases and noise can be made more effectively in the wavelet domain. The main defects of the Fourier transform, used for time-frequency domain transformation, are that the resolution for the different frequency components of the signal are the same, and there is no direct connection between the frequency components to the signal location in the time domain. The wavelet transform can overcome these problems by transforming the one-dimensional signal to a two-dimensional wavelet series in the wavelet domain (translation and scale). Hence representing the signal in both the time and frequency domains simultaneously, and the scale, or resolution, can be changed according to the signal frequency. The potential applications of the wavelet transform for GPS data processing are many, such as cycle slip detection and repair, data smoothing, ambiguity resolution, data compression and even replacing the correlator of the receiver itself because the wavelet function is itself a wide-band correlation (ambiguity) function. This is a potentially exciting area of research.

5) The ambiguity search methods (Lambda, Cholesky factorization, etc.) can fix the ambiguity to its integer value in a matter of millisecond period. The problem is that the quality, or reliability, of the fixed-ambiguity is not guaranteed. The ambiguity search methods are based on the assumption that the measurement residuals are Gaussian and white, but in reality it is rarely the case considering the residual bias effects such as multipath and

measurement correlation. The correctness of the fixed-ambiguity is difficult to verify because the statistical distribution of the ambiguity (conditional and unconditional) is difficult to establish. Therefore a long observation time (few minutes to a few tens of minutes) is still needed for real-time kinematic ambiguity resolution in order to depress the measurement noise and low frequency bias effects. As stated above, using a well-chosen mother wavelet both the low frequency bias and high frequency noise can be detected and eliminated effectively because the high frequency component of the signal can be "zoomed", and this operation can be done quite fast because the wavelet transform operates like a scaled-windowed Fourier transform and the signal is decomposed and analysed under the window bases. Hence a robust and fast ambiguity resolution can be obtained using wavelet transform technique.

6) The Separated-Bias Kalman Filter (SBKF) can be easily applied to the detection and repair of bias-jumps, such as cycle slips, and for time-varying (deterministical) bias estimation for Wide Area DGPS. A combination with traditional ambiguity search methods can reduce the ambiguity resolution time and work as a monitor of the fixed-ambiguity quality.

7) Models of the body's dynamics can be modified for non-Gaussian input noise, such as uniformly distributed noise and Possion processes which are more appropriate for low dynamics and "jinking" manoeuvres. These would need further investigation.

8) Closed-loop GPS and Dead Reckoning (DR) integration can be implemented as non-feedback federated filters. The system integrity and quality control can then be easily performed by a non-feedback federated filter implementation which separates the individual sensors and facilitates error detection and identification.

9) More and more inexpensive inertial sensors such as optic-fibre gyro and solid-state accelerometer are now available on the market. Using these sensors a cheap DR or a simple Strapdown Inertial Navigation System (SINS) can be implemented by users, and integrated with GPS. The DR and the SINS operate on a computer platform and no specific and sophisticated hardware is involved for system implementation. The integrated navigation system is assumed to be a GPS-mainly system, the DR or SINS is used to support the GPS, hence only the high frequency performance of the DR or

SINS (stability over a few seconds) is of interest. That is, only the information of the change of body's state is obtained from the inertial sensors, and this information is useful for GPS signal recovery and body's manoeuvre detection. For example, if the angle change can be measured by the inertial sensors to better than 5.5 degree during the period of GPS signal loss, there will be no necessity for ambiguity resolution for a GPS attitude determination system with 1 metre distance between the antennas. The low frequency biases, such as gyro drift and accelerometer bias, can be measured regularly by the GPS measurements and calibrated by the computer. Tests and error model developmet for the inertial sensors, in both static and dynamic bases, are necessary.

10) The GPS measurement biases are usually modelled by a deterministic function, and the bias residuals can be further modelled by time series models such as Auto-Regresive Moving-Average (ARMA) or Kalman Filter (KF), to improve the measurement precision. The ARMA and KF models are based on the analysis of the autocorrelation functions or power spectra of the measurements, and the models and the bias prediction can be updated when new measurements are available. The time series models are very useful for real-time applications, especially the KF model which can more easily deal with the non-stationary biases than the ARMA model does. For example, there are several DGPS monitor stations around the Australian coast and some ionosphere monitors stations inland. Multiple time series models of GPS ionospheric delay which are functions of time and location can be established using the measurements obtained from these stations, and used for the ionospheric delay correction for vehicles long distances away from the monitor stations.

The development of new algorithms for GPS data analysis is a never ending challenge!

References

Abidin H., 1993. **Computational and Geometrical Aspects of On-The Flying Ambiguity Resolution.** Ph.D Dissertation, Dept. of Surveying Eng., Univ of New Brunswick, Canada, 290 pp.

Adams G., Hadfield M., 1981. GEO_SPIN/IPS-2 Improvements for Precision Gravity Measurement. Proc. of 2nd International Symp. on Inertial Technology for Surveying and Geodesy, 1981, the Canadian Institude of Surveying, Banff, Canada, 245 pp.

Anderson B., Moore J., 1979. **Optimal Filtering**. Prentice Hall, New Jersey, London, 357 pp.

Bader J., 1993. Low Cost GPS/INS for UAV's. Proc. of ION GPS-93, Sixth International Technical Meeting of the Satellite Division of the Institute of Navigation, Salt Lake City, Utah, Sept. 22-24, 235-244.

Balakrishnan A., 1987. **Kalman Filtering Theory**. Optimization Software INC., New York, 252 pp.

Beggs J., 1983. **Kinematics**. Springer-Verlag, Berlin, New York, 223 pp.

Bierman G., 1973. Comments on 'Linear Filtering in the Presence of Time-Varying Bias'. IEEE Trans. Automatic Control, AC-18, No.4, 412 pp.

Bierman G., 1977. **Factorization Methods for Discrete Sequential Estimation**. Academic Press Inc, New York, London, Sydney, 241 pp.

Blewitt G., 1989. Carrier Phase Ambiguity Resolution for Global Positioning System Applied to Geodetic Baseline up to 2000 km. Journal of Geopys. Res., Vol 94, No. B6, 10187-10203.

Bosloper C., 1990. **Multipath and GPS**. Unisurv Report S-39, School of Surveying, Univ. of NSW, Australia, 206 pp.

Bowman C., Snashall G., 1987. Multiprocessor Implementations of Real-Time Multi-Sensor Integration Avionics. IEEE National Aerospace and Electronics Conference NAECON, Vol. 2, 350-358.

Britting K., 1971. **Inertial Navigation System Analysis**. Wiley-Interscience, New York, London, Sydney, 249 pp.

Brown A., Bowles W., Thorvaldsen T., 1982. Interferometric Attitude Determination Using the Global Positioning System. Draper Lab. Report P-1531, Feb.

Brown R., Evans A., 1990. GPS Pointing System Performance. Proc. of ION GPS-90, Third International Technical Meeting of the Satellite Division of the Institute of Navigation, Colorado Springs, Colorado, Sept. 19-21, 645-654.

Brown R., Ward P., 1990. A GPS Receiver with Built-in Precision Pointing Capability. IEEE PLANS, 83-93.

Brown R., 1992. Instantaneous GPS Attitude Determination. IEEE PLANS, 1992, 113-120.

Cannon M, 1987. Kinematic Positioning Using GPS Psedorange and Carrier Phase Observations. UCSE Reports No. 20019, Univ. of Calgary, Canada, 17-20.

Cannon M., 1992. Real-Time Heading Determination Using an Integrated GPS-Dead Reckoning System. Proc. of ION GPS-92, Fifth International Technical Meeting of the Satellite Division of the Institute of Navigation, Albuquerque, New Mexico, Sept. 16-18, 775-782.

Cannon M., Lachapelle G., 1992. Analysis of a High-Performance C/A-Code GPS Receiver in Kinematic Mode. **Navigation**, Vol.39, No.3, Fall, 285-300.

Cannon M., 1993. Experiences of GPS Attitude Determination within a Helicopter Pod. Proc. of ION GPS-93, Sixth International Technical Meeting of the Satellite Division of the Institute of Navigation, Salt Lake City, Utah, Sept. 22-24, 1993, 633-641.

Cannon M., Sun H., 1994. Assessment of a Non-Dedicated GPS Receiver System for Precise Airborne Attitude Determination. Proc. of ION GPS 94, 7th International Technical Meeting of the Satellite Division of the Institute of Navigation, Salt Lake City, Utah, Sept. 20-23, 645-654.

Carlson N.,1990. Federated Square Root Filter for Decentralized Parallel Processes. IEEE Trans. on Aerospace and Electronic Systems, Vol. AES-26, No. 3, 517-525.

Carlson N., Beradducci M., 1994. Federated Kalman Filter Simulation Results. **Navigation**, Journal of the Inst. of Navigation, Fall, Vol. 41, No. 3, 297-321.

Caspary W, 1987. Inertial plattformen: Messprinzip und Geodätische Nützung.Schriftenreihe Heft 22, Studiengang Vermessungswesen, Univ. Bundeswher München, 7-22.

Charles R., Amy G., 1993. Statistical testing and Analysis of Performance Factors in GPS Attitude Determining Systems (ADS). Proc. of ION GPS-93, Sixth International Technical Meeting of the Satellite Division of the Institute of Navigation, Salt Lake City, Utah, Sept. 22-24, 617-623.

Chatfield C., 1989. **The Analysis of Time Series**. Chapman and Hall, London, New York, 241 pp.

Chou H, 1990. An Anti - SA Filter for Non - differential GPS Users. Proc. of ION GPS-90, Third International Technical Meeting of The Satellite Division of the Institute of Navigation, Colorado Springs, Colorado, Sept. 19-21, 645-654.

Christou T.,1983. **Evaluation of Mathematical Models for Gyrocompass Behaviour : Error Modelling and Applications**. Department of Surveying Eng., Univ. of New Brunswick, Canada, 181 pp.

Clark D., 1968. **Plane and Geodetic Surveying**. Constable & Company Ltd., London, Vol. 2, 685 pp.

Coco D., Coker C., Dahlke S., Clynch J., 1991. Variability of GPS Satellite Differential Group Delay Biases. IEEE Trans. on Aerospace and Electronic Systems, Vol. 27, 931-938.

Cohen C., Parkinson B.,1991. Expanding the Performance Envelope of GPS Based Attitude Determination. Proc. of ION GPS-93, Fourth International Technical Meeting of the Satellite Division of the Institute of Navigation, Albuquerque, New Mexico, Sept. 11-13,1001-1011.

Cohen C., Parkinson B.,1992. Aircraft Applications of GPS-Based Attitude Determination. Proc. of ION GPS-92, Fifth International Technical Meeting of the Satellite Division of the Institute of Navigation, Albuquerque, New Mexico, Sept. 16-18, 775-782.

Cohen C., Glenn E., 1993. Space Flight Test of Attitude Determination Using GPS. Proc. of ION GPS-93, Sixth International Technical Meeting of The Satellite Division of the Institute of Navigation, Salt Lake City, Utah, Sept. 22-24, 625-632.

Colombo O., 1991. Errors in Long Distance Kinematic GPS. Proc. of ION GPS-91, Fourth International Technical Meeting of The Satellite Division of The Institute of Navigation, Albuquerque Convention Centre, Albuquerque, New Mexico, Sept. 11-13, 673-680.

Colombo O., 1992. Precise, Long-range Aircraft Positioning with GPS: the Use of Datat Compression. Proc. Sixth Inter. Geodetic Sym. on Satellite Positioning, the Ohio State Univ., Columbus, Ohio, 17 to 20 March, Vol. II, 640-649.

Cox D., 1980. Integration Of GPS With Inertial Navigation System. **Global Positioning System**. Papers published in Navigation, Vol.1,144-153.

Cross P., 1983. **Advanced Least Squares Applied to Positioning-fixing**. Working Paper No.6, Dept. of Land Surveying, North East London Polytechnic, 205 pp.

Daubechies I., 1992. **Ten Lectures on Wavelets**. Society for Industrial and Applied Mathematics, Philadephia, Penn., 357 pp.

Decker B., 1986. World Geodetic System 1984 4th International Geodetic Symposium on Satellite Positioning, 28 Apr.-2 May, 69-92.

Diefes D., Hazel G., Greenlee D., 1993. GPS Attitude Determining System for Marine Navigation. Proc. of ION GPS-93, Sixth International Technical Meeting of the Satellite Division of the Institute of Navigation, Salt Lake City, Utah, Sept. 22-24, 649-655.

Diefes D., 1994. GPS Based Attitude Determining System for Marine Navigation. IEEE PLANS, 806-812.

Eissfeller B., 1989. **Analyse einer geodätischen raumstabilisierten Inertialpalttform und Integration mit GPS**. Schriftenreihe Heft 37, Studiengang Vermessungswesen, Univ. Bundeswher München, 321 pp.

Eissfeller B., Spietz P., 1989. Basic Filter Concepts for the Integration of GPS and an Inertial Ring Laser Gyro Strapdown System. **Manuscripta Geodaetica**, Vol. 14, 166-182.

Enge P., McCullough J., 1989. Aiding GPS with Calibrated Loran-C. **Navigation**, Winter, 1988-1989, Vol. 35, No. 4, 469-482.

Fabeck W., 1980. **Kreisel - geräte**. Vogel-Verlag, Würzburg, German, 432 pp.

Farrell L., 1976. **Integrated Aircraft Navigation**. Academic Press, New York, 351 pp.

Feess W., Stephens S., 1987. Evaluation of GPS Ionospheric Time-Delay Model. IEEE Trans. on Aerospace and Electronic Systems, Vol. AES-23, No.3, May, 332-338.

Forssell B, 1991. **Radionavigation Systems**. Prentice Hall, New York, London, Sydney, 392 pp.

Friedland B., 1969. Treatment of Bias in Recursive Filtering. IEEE Trans. Automatic Control. AC-14, No.4, August, 359-367.

Friedland B., 1983. Separated-Bias Estimation and Some Applications. **Control and Dynamic System,** Vol.20, 2-45.

Frei E., 1991. **Rapid Differential Positioning with the Global Positioning System (GPS).** Geodätisch-geophysikalische Arbeiten in der Schweiz, Band 44.

Fu W., 1991. Attitude Determination at Sea Using GPS & Other Sensors. UNSW Annual Research Seminars, Sydney.

Fu W., 1992. The Application of Digital Filter to GPS Data Processing. Australian National Conf. on GPS Surveying, Sydney, 73-86.

Fu W., 1993. GPS & Doppler. UNSW Annual Research Seminars, Sydney.

Fu W., 1994. Integration of GPS & Dead Reckoning System. Conf. of International Association of Navigation, Beijing.

Fu W., 1995. Doppler-Created Phase and Baseline Computation. Satellite Navigation Technology: 1995 and Beyond, 26-28 June, Brisbane.

Gao Y., Krakiwsky E., Abousalem M., 1993. Comparison and Analysis of Cenrtalized, Decentralized, and Federated Filters. **Navigation**, Vol. 40, No. 1, Spring 1993, 69-86.

Goad C., 1990. Optimal Filtering of Pseudoranges and Phases from Single Frequency GPS Receivers. **Navigation**, Vol. 37, No. 3, Fall 1990, 249-272.

Graas F., Braasch M., 1992. GPS Interferometric Attitude and Heading Determination: Initial Flight Test Results. **Navigation**, Vol. 18, No. 4, Winter 1991-1992, 297-316.

Graupe D., 1989. **Time Series Analysis, Identification and Adaptive Filtering**. Robert E. Krieger Publishing Co., Malabar, Fl, 420 pp.

Hamming R., 1989. **Digital Filters**. Prentice Hall, Englewood Cliffs, New Jersey, 284 pp.

Hatch R., 1982. The Synergism of GPS Code and Carrier Measurements. Proc. of the Third Intl. Geod. Sym. on Satellite Doppler Positioning, Las Cruces, New Mexico, 8-12 Feb., 1213-1231 pp.

Hatch R., 1986. Dynamic Differential GPS at the Centimeter Level. The Proceedings of the Fourth International Geodetic Symposium on Satellite Positioning, 1287-1298.

Hatch R., 1989. Ambiguity Resolution in the Fast Lane. Proc. of ION GPS-89, Colorado Springs, Colorado, Sept. 27-29, 45-50.

Hatch R., 1990. Instantaneous Ambiguity Resolution. Kinematic Systems in Geodesy, Surveying, and Remote Sensing, IAG Simposium No. 107, Banff, Alberta, Canada, Sept 10-13, 299-308.

Hein G., Bauster G., Eissfeller B., Landau H., 1988. High-Precision Kinematic GPS Differential Positioning: Experiences, Results, Integration of GPS with a Ring Laser Strapdown Inertial System. Proc. of ION GPS-88, Colorado Spring, Colorado, Sept., 19-23, 129-137.

Henkel D., 1992. Developing and Expert System to Support GPS Integration. Proc. of ION GPS-92, Fifth International Technical Meeting of the Satellite Division of the Institute of Navigation, Albuquerque, New Mexico, Sept., 16-18, 257-264.

Heywood O., 1992. The U.S. Federal Radionavigation Plan. IEEE PLANS, 68-73.

Hopfield H., 1971. Tropospheric effect on Electromagnetically Measured Range: Prediction from Surface Weather Data. **Radio Science**, Vol. 6, No. 3, 357-367.

Huddle J., 1989. Advances in Strapdown Systems for geodetic Applications. **High Precision Navigation**, Springer-Verlag, Berlin, 496-530.

Ignagni M., 1981. An Alternative Derivation and Expansion of Friedland's Two-Stage Kalman Filter. IEEE Trans. Automatic Control, AC-26, No.3, 746-750.

Ishlinskii A., 1965. **Mechanics of Gyroscope Systems**. Israel Program for Scientific Translation, Jerusalem, 313 pp.

Jules G., 1991. GPS Signal Policy. Proc. of ION GPS-93, Fourth International Technical Meeting of the Satellite Division of the Institute of Navigation, Albuquerque, New Mexico, Sept. 11-13, 33-45.

Jurgens R., Rodgers C., 1991. Advances in GPS Attitude Determining Technology as Developed for the Strategic Defense Command Proceedings of ION GPS-91, Fourth International Technical Meeting of the Satellite Division of the Institute of Navigation, Albuquerque, New Mexico, Sept. 11-13, 991-999.

Jurgens R., Fan L., Diefes D., Rodgers C., 1992. Measurement of Errors in GPS Attitude Determining Systems. Proc. of ION GPS-92, Fifth International Technical Meeting of the Satellite Division of the Institute of Navigation, Albuquerque, New Mexico, Sept. 16-18, 793-799.

Karels S., Macdonald T., Ciggh M., 1994. Techniques to Achieve Ultra-Precise Attitude Determination for Large Baselines. Proc. of ION GPS- 94, 7th International Technical Meeting of the Satellite Division of the Institute of Navigation, Salt Lake City, Utah, Sept. 20-23, 667-673.

Karnick D., 1992. Low Cost Inertial Measurement Unit. IEEE PLANS, 422-425.

Kayton M., Fried R., 1969. **Avionics Navigation Systems**. John Wiley & Sons, New York, 666 pp.

Kendall M., Ord J., 1990. **Time Series**. Edward Arnold, 296 pp.

Kerr T., 1987. Decentralized Filtering and Redundancy Management for Multisensor Navigation. IEEE Trans. on Aerospace and Electronic Systems, Vol. AES-23, 83-119.

Killian K., 1994. Pointing grade Fiber Optic Gyroscope. IEEE PLANS, 168 pp.

Klein F., Sommerfeld A., 1965. **Über die Theorie des Kreisels**. Johnson Reprint Cop., New York, 966 pp.

Kleusberg A., 1993. Workshop on GPS Kinematic Positioning and Navigation, UNSW, Sydney, March 8-10.

Klobuchar J., 1987. Ionospheric Time-Delay Algorithm for Single-Frequency GPS Users. IEEE Trans. on Aerospace and Electronic Systems, Vol. AES-23, No.3, May, 321-325.

Krakiwsky E., Wells D., 1971. **Coordinate System in Geodesy**. Lecture Notes No. 16, Dept. of Surveying Eng., Univ. of New Brunswick, Canada, May, 115 pp.

Krakiwsky E., Lachapelle G., Schwarz K., 1990. **Assessment of Emerging Technologies for Future Navigation Systems in the Canadian Transportation Sector**. Dept. of Surveying Eng., Univ. of Calgary, Canada, 248 pp.

Kremer G., Kalafus R., Loomis P., Reynold J., 1989. The Effect of Selective Availability on Differential GPS Correction. Proc. of ION GPS 89, Colorado Springs, Colorado, Sept. 27-29, 307-312.

Lachapelle G., 1990. GPS observables and Error Sources for Kinematic Positioning. IAG Simposium No. 107, Banff, Alberta, Canada, Sept 10-13, 19pp.

Landau H., 1988. **Zur Nützung des Global Positioning Systems in Geodäsie und Geodynamik: Modellbildung, Software-Entwicklung und Analyse**. Uni. der Bundeswehr Munchen, 321 pp.

Last D., Searle M., Farnworth R., 1993. The North-West European Loran-C System: Coverage and Performance prediction. **Navigation**, Journal of The Institute of Navigation, Fall 1993, vol. 40, No. 3, 209-227.

Lawrence A., 1993. **Modern Inertial Technology, Navigation, Guidance, and Control.** Springer-Verlag, New York, Berlin, 268 pp.

Liang D, McMillan J., 1982. Development Analysis of a Marine Integrated Navigation System. IEEE PLANS, 233-245.

Lipp A., Gu X., 1994. Cycle-Slip Detection and Repair in Integrated Navigation Systems. IEEE PLANS, 681-688.

Liu R., Adams G., 1990. Interferometric Fiber-Optic Gyroscope: A Summary of Progress. IEEE PLANS, 31-36.

Logsdon T., 1992. **The Navstar Global Positioning System**. Van Nostrand Reinhold, New York, 256 pp.

Loomis P., Geier G., 1990. Inertially Aided Lane Recapture After GPS Carrier Lock Loss. Kinematic Systems in Geodesy, Surveying, and Remote Sensing, IAG Simposium No.107, Banff, Alberta, Canada, 309-318.

Lynn P, 1992. **Digital Signals, Processors and Noise**. MacMillan, 221 pp.

MacMillan J., 1988. MINS-B II: A Marine Integrated Navigation System. IEEE PLANS, 499-508.

Mader G., 1986. Dynamic Positioning Using GPS Carrier Phase Measurements. **Manuscripta Geodaetica**, 272-277.

Martin E., 1980. GPS User equipment Error Models. **Global Positioning System**. Papers published in Navigation, Vol. 1, 109-118.

Matchett G., 1985. Stochastic Simulation of GPS Selective Availability Errors. Technical Memorandum, TASC Contract DTRS-57-83-C-00077, June.

Mathews J, 1992. Numerical Methods for Mathematics, Science, and Engineering. Prentice-Hall International, Inc., New Jersey, London, Sydney, 646 pp.

Maybeck P., 1979. **Stochastic Models, Estimation, and Control.** Vol. 1, Academic Press, New York, London, 423 pp.

Maybeck P., 1982. **Stochastic Models, Estimation, and Control.** Vol. 2, Academic Press, New York, London, 289 pp.

Maybeck P., 1982. **Stochastic Models, Estimation, and Control.** Vol. 3, Academic Press, New York, London, 291 pp.

McMillan C., Lachapelle G., Lu G., 1994. Dynamic GPS Attitude Performance Using INS/GPS Reference. Proc. of ION GPS-94, 7th International Technical

Meeting of the Satellite Division of the Institute of Navigation, Salt Lake City, Utah, Sept. 20-23, 675-682.

McMillan C., 1994. AGPS Attitude Error Model for Kalman Filtering. IEEE PLANS, 329-336.

Meijer S., 1983. **Navigation Filter**. Delft Uni. of Technology, Dep. of Marine Technology, Section Navigation, Part 1, 112 pp.

Mendel J., 1976. Extension of Friedland's Bias Filtering Technique to a Class of Nonlinear Systems. IEEE Trans. Automatic Control, AC-21, No.2, 296-298.

Minkler G., Minkler J., 1993. **Theory and Application of Kalman Filtering**. Magellan Book Co., Palm Bay, FL, 608 pp.

Morris P., Gupta R., Wenzel C., Shirer H., 1989. Omega System Performance Assessment. **Navigation**, Journal of the Institute of Navigation, Winter, 1989-1990, Vol.36, No. 4, 345-362.

Navpapers, 1963. **Introduction to Sonar**. Navpers 10130 - A, U.S. Navy, 162 pp.

Negast W., Paschall R., 1990. Copensation of Selective Availability Using A GPS/INS Extended Kalman Filter. IEEE National Aerospace and Electronics Conference NAECON 1990, Vol. 1, 356-362.

Norling B., 1990. Accelerometers: Current and Emerging Technologies. IAG Symposium No.107, Banff, Alberta, Canada, Sept. 10-13, 70-84.

Norman S., 1992. **Control Systems Engineering**. Benjamin/Cummings Pub. Co., New York, Tokyo, Sydney, 756 pp.

O'Donnell C., 1964. **Inertial Navigation Analysis and Design**. McGraw-Hill Book Company, New York, 442 pp.

Oppenheim A., Schafer R., 1989. **Discrete-Time Signal Processing**. Prentice-Hall International, Inc, 879 pp.

Quinn P., 1993. Instantaneous GPS Attitude Determination. Proc. of ION

GPS-93, Salt Lake City, Utah, Sept. 22-24, 603-615.

Percival D., 1976. Prediction Error Analysis of Atomic Frequency Standards. Proc. of the 31th Annual Frequency Control Symposium, 319-326.

Proakis G., Manolakis G., 1992. **Digital Signal Processing**. Maxwell MacMillan International, New York, Oxford, Sydney, 969 pp.

Proakis G., Rader C., Fuyun Lin, Nikias C., 1992. **Advanced Digital Signal Processing**. Makmillan Publishing Co., New York, Oxford, Sydney, 610 pp.

Remondi B., 1992. Real-time Centimeter-accuracy GPS for Marine Applications. Proc. of U.S. Hydrographic Conference, 1992. The Hydrographic Society, Special Publication No. 28, Baltimore, MD, Feb. 25-28.

Rizos C., Grant D., 1990. Time and the Global Positioning System. Contributions to GPS Studies, UNISURV S-38, 1990, Reports in the School of Surveying, UNSW, 204 pp.

Rizos C., 1991. Principles and Practice of GPS Surveying. Lecture Notes, the School of Geomatic Eng., UNSW, Australia.

Roberts W., Cross P., 1993. The Effect of DGPS Temporal Correlation within the Kalman Filter Applied to Offshore Positioning. **The Hydrographic Journal**, No. 67, Jan., 5-11.

Rocken C., Meertens C., 1991. Monitoring Selective Availability Dither Frequency and Their Effect on GPS Data. **Bulletin Geodesique**, Vol. 65, No. 3, 162-169.

Russell S., Schaibly J., 1980. Control Segment and User Performance. **Global Positioning System**, papers published in **Navigation**, vol.1, 74-81, 1980, 74-80.

Saastamoinen J., 1973. Contribution to the Theory of Atmospheric Refraction. **Bull. Geod.**, No.107, 13-34.

Salzmann M., 1993. **Least Squares Filtering and Testing for Geodetic Navigation Applications.** Ph.D Dissertation, Netherlands Geodetic Commission, Publications of Geodesy, New series No. 37, 209 pp.

Samant V. & Sorenson H., 1974. On Reducing Computational Burden in the Kalman Filter. **Automatica**, No.10, 61-68.

Schröder D., Thong N., Wiegner S., Grafarend E., Schaffrin B., 1988. A Comparative Study of Local level and Strapdown Inertial Systems. **Manuscripta Geodaetica**, No. 13, 224-248.

Schwarz K.,1979. Grundgleichungen und Fehlermodelle für Inertiale Messsysteme. Zfv 104, 447-460.

Schwarz K.,1980. Error Propagation in Inertial Positioning. **Canadian Surveyor**, No.34, 265-276.

Schwarz K., Wei M., 1994. Aided Versus Embedded: A Comparison of Two Approaches to GPS/INS Integration. IEEE PLANS, 314-322.

Schwarz K., Zhang G., 1994. Development and Testing of a Low Cost Integrated GPS/INS. Proc. of ION GPS-94, 7th International Technical Meeting of The Satellite Division of the Institute of Navigation, Salt Lake City, Utah, Sept. 20-23, 1137-1144.

Seeber G., 1993. **Satellite Geodesy**. Walter de Gruyter, Berlin, New York, 531 pp.

Sinha P., Dedoes D., 1990. INS Alignment Using GPS Phase I I I User Equipment Computed Corrections. Proc. ION GPS, 471-481.

Smith R., Weyrauch J., 1990. Gyroscope: Current and Emerging Technologies. IAG Symposium No.107, Banff, Alberta, Canada, Sept. 10-13, 59-70.

Sonnenberg G., 1978. **Radar and Electronic Navigation**. Newnes-Butterworth, London, Boston, Sydney, 376 pp.

Spilker J., 1980. GPS Signal Structure and Performance Characteristics. **Global Positioning System**. Papers published in Navigation, Vol. 1,

29-54.

Stieler B., Winter H., 1982. Gyroscope Instruments and their Application to Flight Testing. AGARD Flight Instrumentation Series, Vol. 15, AGARDograph No.160, Neuille-sur-Seine, France, 72 pp.

Stieler B., 1982. Trägheitsnavigation. Stand der Technik und Entwicklungstendenzen. **Ortung und Navigation**, Heft 2, 262-289.

Terheyden K., Zickwolff G., 1983. **Handbuch für die Schiffsführung**. 1B, Springer-Verlag, Berlin, Heidelberg, New York, Tokyo, 269 pp.

Terheyden K., Zickwolff G., 1986. **Handbuch für die Schiffsführung**. 1C, Springer-Verlag, Berlin, Heidelberg, New York, Tokyo, 399 pp.

Teunissen P., 1990. Quality Control In Integrated Navigation System. IEEE PLANS, 158-165.

Teunissen P., 1994. A New Method for Fast Carrier Phase Ambiguity Estimation. Proc. IEEE PLANS, April 11-15, Las Vegas, 562-573.

Trimble, 1987. Final Report, GPS Heading and Attitude Determining Instrument Investigation and Prototype Development. Contract N60921-86-C-A272, Trimble Navigation Ltd., Sunnyvale, CA.

Vandaele W., 1983. **Applied Time Series & Box-Jenkins Models**. Academic Press, New York, Paris, Sydney, 417 pp.

Van Dierendonck A., Russell S., Kopitzke E., Birnbaum M., 1980. The GPS Navigation Message, **Global Positioning System**, papers published in **Navigation**, vol. 1, 55-74

Warren R., Morris P., Tench K., Gupta R., 1990. Omega Signal Coverage Prediction in the 90's. IEEE PLANS, 626-633.

Wei M., Schwarz K., 1990. Testing a Decentralized Filter for GPS/INS Integration. IEEE PLANS, 429-435.

West-Vukovich G., Zywiel J., Scherzinger B., 1988. The Honeywell/DND Helicopter Integrated Navigation System (HINS). IEEE PLANS, 416-425.

Wolfe A, Satzer J., 1982. Smoothed Track Reconstruction of Ocean-Going Vessels. IEEE PLANS, 214-220.

Wong R., Schwarz K., Cannon M., 1988. High-Accuracy Kinematic Positioning by GPS-INS. **Navigation**, Journal of the Institute of Navigation, Vol.35, No.2, Summer 1988, 275-287.

Xinhua Qin, Gourevitch S., Ferguson K., Kuhl M., Ladd J., 1992. Dynamic Short Baseline Calibration and Attitude Determination Using Ashtech 3DF System. Proc. Sixth International Geodetic Symposium on Satellite Positioning, the Ohio State Univ., Columbus, Ohio, March 17-20, 190-199.

Young L., Neilan R., Bletzacker F., 1985. GPS Satellite Multipath: an Experimental Investigation. Proc. of the First Symp. on Precise Positioning with GPS, Rockville, Maryland, April 15-19, 423-432.

APPENDIX 1 INS NAVIGATION EQUATION AND MECHANIZATION

A.1.1 Navigation Equation

The semi-analytic (platform) and analytic (strapdown) systems are based on the output of accelerometer:

$$\mathbf{a} = \frac{d\mathbf{r}^2}{d^2t} - \mathbf{G}_e \qquad \text{(A.1.1.1)}$$

where:

- $\mathbf{a}$ the output of accelerometer (specific force)
- $\mathbf{r}$ body's position vector in inertial frame
- $\mathbf{G}_e$ gravitational force of the earth.

For navigation near or on the earth's surface only the gravitational force caused by the earth needs to be considered. Hence it can assumes the non-rotating earth-centred coordinate system is an inertial frame for INS. In this earth-centred inertial system, the velocity of the body relative to inertial frame can be expressed as:

$$\frac{d\mathbf{r}}{dt} = \mathbf{V} + \Omega \times \mathbf{r} \qquad \text{(A.1.1.2)}$$

where $\mathbf{V}$ is the velocity relative to earth, Ω is the angular velocity of the earth's rotation and x denotes the vector product. The angular velocity of a body relative to the inertial frame is:

$$\rho = \Omega + \omega \qquad \text{(A.1.1.3)}$$

where ω is the angular velocity of the body relative to earth, and hence the time differentiation of eqn (A.1.1.2) relative to the inertial frame can be written as:

$$\frac{d^2\mathbf{r}}{dt^2} = \dot{\mathbf{V}} + (2\Omega + \omega) \times \mathbf{V} + \Omega \times (\Omega \times \mathbf{r}) \qquad \text{(A.1.1.4)}$$

The general INS navigation equation is obtained by combining eqn (A.1.1.1)

and eqn (A.1.1.4) as:

$$\dot{\mathbf{V}} = \mathbf{a} - (2\Omega + \omega) \times \mathbf{V} + \mathbf{g} \qquad \text{(A.1.1.5)}$$

where $\mathbf{g}$ is the acceleration due to earth gravity:

$$\mathbf{g} = \mathbf{G}_e - \Omega \times (\Omega \times \mathbf{r}) \qquad \text{(A.1.1.6)}$$

$2\Omega \times \mathbf{V}$ results from a body's motion on the rotating earth and is called the Coriolis acceleration.

A.1.2 Mechanization Equation of North-Directed System

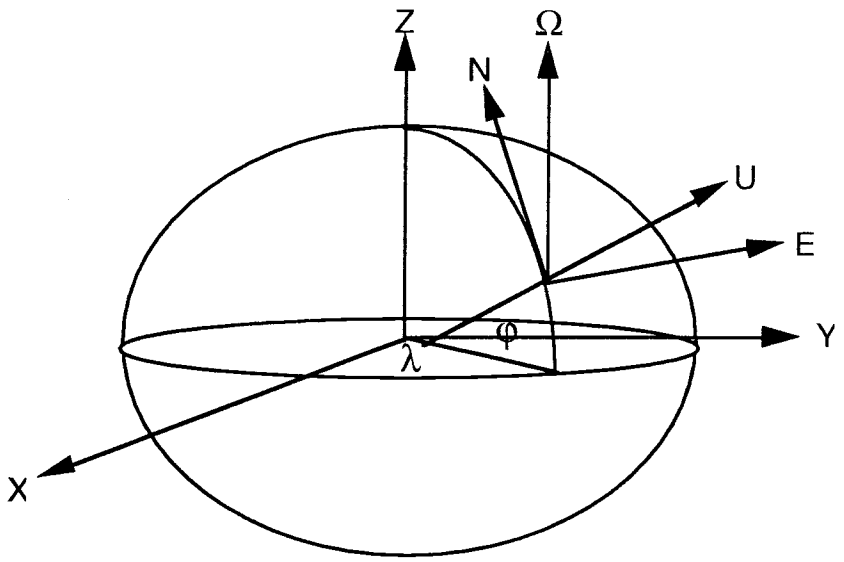

Figure A.1.1. The earth frame and the geographic frame.

In Fig. A.1.1 XYZ is the earth frame, ENU is the geographic frame and Ω is the angular velocity vector of the earth,s rotation.

The body's motion relative to the earth can be expressed as:

$$\rho = \dot{\lambda}\mathbf{i}_\Omega - \dot{\varphi}\mathbf{i}_e \qquad \text{(A.1.2.1)}$$

where $\mathbf{i}_\Omega$ and $\mathbf{i}_e$ are the unit vectors in the earth pole and east directions.

The projections of the angular velocity of the body relative to the earth in the geographic frame are:

$$\omega_e = -\dot{\varphi} = -\frac{V_n}{R_N} \qquad \text{(A.1.2.2)}$$

$$\omega_n = \dot{\lambda}\cos\varphi = \frac{V_e}{R_M} \qquad \text{(A.1.2.3)}$$

$$\omega_u = \omega_n \mathrm{tg}\varphi \qquad \text{(A.1.2.4)}$$

where ω_e, ω_n, ω_u are the eastern, northern and up components of the body's angular velocity relative to the earth.

The mechanization equation of the north-directed system can be derived by expansion of eqn (A.1.1.5):

$$\dot{V}_e = \alpha_e + (2\Omega\sin\varphi + \omega_n \mathrm{tg}\varphi)V_n - (2\Omega\cos\varphi + \omega_n)V_u \qquad \text{(A.1.2.5)}$$

$$\dot{V}_n = \alpha_n - (2\Omega\sin\varphi + \omega_n \mathrm{tg}\varphi)V_e + \omega_e V_u \qquad \text{(A.1.2.6)}$$

$$\dot{V}_u = \alpha_u - \omega_e V_n + (2\Omega\cos\varphi + \omega_n)V_e - g \qquad \text{(A.1.2.7)}$$

where:

V_n, V_e, V_u	north, east and up components of platform's velocity
α_n, α_e, α_u	outputs of accelerometers
g	acceleration due to earth gravity

Obviously the platform command which is equal to the angular velocity of the geographic frame relative to the inertial frame is:

$$\omega_{ec} = \omega_e \qquad \text{(A.1.2.8)}$$

$$\omega_{nc} = \omega_n + \Omega\cos\varphi \qquad \text{(A.1.2.9)}$$

$$\omega_{uc} = \omega_n tg\varphi + \Omega sin\varphi \qquad \text{(A.1.2.10)}$$

A.1.3 Mechanization Equation of Wander-Azimuth System

For this system ω_u of eqn (A.1.2.4) is not compensated for, and it appears as a platform azimuth wandering:

$$\dot{\alpha} = - \omega_n \, tg\varphi \qquad \text{(A.1.3.1)}$$

where α is the platform azimuth wandering angle. The platform frame xyz now rotates α around the vertical axis of the geographic frame. The angular velocity of the body's rotation relative to the earth in the platform frame has to be calculated according to the earth curvature in the wandering direction and the body's latitude:

$$\omega_x = -\left[\frac{1}{R_N} - \frac{1}{R_M}\right] V_x cos\alpha sin\alpha - \left[\frac{sin^2\alpha}{R_N} + \frac{cos^2\alpha}{R_M}\right] V_y \qquad \text{(A.1.3.2)}$$

$$\omega_y = \left[\frac{1}{R_N} - \frac{1}{R_M}\right] V_y cos\alpha sin\alpha \left[\frac{sin^2\alpha}{R_N} + \frac{cos^2\alpha}{R_M}\right] V_x \qquad \text{(A.1.3.3)}$$

$$\omega_z = 0 \qquad \text{(A.1.3.4)}$$

The projection of earth rotation to the platform frame is:

$$\Omega_x = \Omega cos\varphi cos\alpha \qquad \text{(A.1.3.5)}$$

$$\Omega_y = - \Omega cos\varphi sin\alpha \qquad \text{(A.1.3.6)}$$

$$\Omega_z = \Omega sin\varphi \qquad \text{(A.1.3.7)}$$

Using eqns (A.1.3.2)-(A.1.3.7) the mechanization equation can be derived from eqn (A.1.1.5) as:

$$\dot{V}_x = a_x - (2\Omega_y + \omega_y)V_z + 2\Omega_z V_y \qquad \text{(A.1.3.8)}$$

$$\dot{V}_y = a_y - 2\Omega_z V_x + (2\Omega_x + \omega_x)V_z \qquad \text{(A.1.3.9)}$$

$$\dot{V}_z = a_z - (2\Omega_x + \omega_x)V_y + (2\Omega_y + \omega_y)V_x - g \qquad \text{(A.1.3.10)}$$

The platform commands are:

$$\omega_{xc} = \Omega_x + \omega_x \qquad \text{(A.1.3.11)}$$

$$\omega_{yc} = \Omega_y + \omega_y \qquad \text{(A.1.3.12)}$$

$$\omega_{zc} = \Omega_z \qquad \text{(A.1.3.13)}$$

A.1.4 Mechanization Equation of Free-Azimuth System

Because the angular velocity of earth rotation is not compensated for the azimuth gyro, compared to eqn (A.1.3.1), the azimuth angle changing rate is:

$$\dot{\alpha} = -\omega_n \, tg\varphi - \Omega sin\varphi \qquad \text{(A.1.4.1)}$$

The projections of the angular velocities of the body's rotation relative to the earth and earth rotation, as well as the platform command, are in the same forms as eqns (A.1.3.2)-(A.1.3.7) and (A.1.3.11)-(A.1.3.13), except that:

$$\omega_{zc} = 0 \qquad \text{(A.1.4.2)}$$

The angular velocity of the azimuth relative to the geographic frame is:

$$\omega_z = -\Omega sin\varphi \qquad \text{(A.1.4.3)}$$

The mechanization equations are:

$$\dot{V}_x = a_x - (2\Omega_y + \omega_y)V_z - \Omega_z V_y \qquad \text{(A.1.4.4)}$$

$$\dot{V}_y = a_y + \Omega_z V_x + (2\Omega_x + \omega_x)V_z \qquad \text{(A.1.4.5)}$$

$$\dot{V}_z = a_z - (2\Omega_x + \omega_x)V_y + (2\Omega_y + \omega_y)V_x - g \qquad \text{(A.1.4.6)}$$

A.1.5 Mechanization Equation of Rotating-Azimuth System

A constant torque is applied to the azimuth gyro to make the platform rotate around the azimuth axis with an angular velocity ω_{z0}. The vertical angular velocity of the platform is now:

$$\omega_z = \omega_{z0} - \Omega\sin\varphi \qquad \text{(A.1.5.1)}$$

and the azimuth changing rate is:

$$\dot{\alpha} = \omega_{z0} - \Omega\sin\varphi - \omega_n tg\varphi \qquad \text{(A.1.5.2)}$$

Compared to the free-azimuth system, the mechanization equations can be expressed as:

$$\dot{V}_x = a_x - (2\Omega_y + \omega_y)V_z + (\omega_{z0} - \Omega_z)V_y \qquad \text{(A.1.5.3)}$$

$$\dot{V}_y = a_y + (\omega_{z0} - \Omega_z)V_x + (2\Omega_x + \omega_x)V_z \qquad \text{(A.1.5.4)}$$

$$\dot{V}_z = a_z - (2\Omega_x + \omega_x)V_y + (2\Omega_y + \omega_y)V_x - g \qquad \text{(A.1.5.5)}$$

and

$$\omega_{zc} = \omega_{z0} \qquad \text{(A.1.5.6)}$$

The other equations for angular velocity projections and platform command are the same as those of free-azimuth system.

APPENDIX 2 STRAPDOWN SYSTEM MECHANIZATION

According to eqn (A.1.5) the output of the accelerometer of a strapdown system can be expressed as:

$$\mathbf{a}_{Ib}^{b} = \dot{\mathbf{V}}_{eb}^{b} + (2\Omega_{Ib}^{b} + \omega_{eb}^{b}) \times \mathbf{V}_{eb}^{b} - \mathbf{g}_{eb}^{b} \qquad \text{(A.2.1)}$$

where:

- $\mathbf{a}_{Ib}^{b}$ output of accelerometer in the body frame
- Ω_{Ib}^{b} angular velocity of earth rotation in the body frame
- ω_{eb}^{b} angular velocity of the body relative to earth in the body frame
- $\mathbf{V}_{eb}^{b}$ velocity of the body relative to earth in the body frame
- $\mathbf{g}_{eb}^{b}$ acceleration of the earth gravity in the body frame

Assuming the direction cosine matrix from the body frame to the platform frame is $\mathbf{C}_{b}^{p}$, which functions as a mathematical platform, the output of the accelerometer can be transformed to the platform frame as:

$$\mathbf{a}_{Ib}^{p} = \mathbf{C}_{b}^{p}\, \mathbf{a}_{Ib}^{b} \qquad \text{(A.2.2)}$$

The acceleration of the body relative to the earth in the platform frame is:

$$\dot{\mathbf{V}}_{eb}^{p} = \mathbf{a}_{Ib}^{p} - (2\Omega_{Ie}^{p} + \omega_{eb}^{p}) \times \mathbf{V}_{eb}^{p} + \mathbf{g}_{eb}^{p} \qquad \text{(A.2.3)}$$

Usually the platform frame that is used is one of the local level frames and hence $\mathbf{g}_{eb}^{p}$ is the acceleration due to earth gravity.

After initial alignment, the velocity of the body can be obtained directly by integration of eqn (A.2.3). The angular velocity of the platform relative to the earth in the platform frame can be expressed as:

$$\omega_{ep}^{p} = \mathbf{C}_{v}^{\omega}\, \mathbf{V}_{eb}^{p} \qquad \text{(A.2.4)}$$

where

$$\mathbf{C}_v^{\omega} = \begin{bmatrix} -\frac{1}{\tau_a} & -\frac{1}{R_y} \\ \frac{1}{R_x} & \frac{1}{\tau_a} \end{bmatrix} \tag{A.2.5}$$

and

$$\frac{1}{R_x} = \frac{\cos^2\alpha}{R_N} + \frac{\sin^2\alpha}{R_M} \tag{A.2.6}$$

$$\frac{1}{R_y} = \frac{\sin^2\alpha}{R_N} + \frac{\cos^2\alpha}{R_M} \tag{A.2.7}$$

$$\frac{1}{\tau_\alpha} = \left[\frac{1}{R_N} - \frac{1}{R_M}\right] \cos\alpha\sin\alpha \tag{A.2.8}$$

α is the platform azimuth rotating angle.

The measurement of the gyro of a strapdown system is ω_{ib}^{b}, the angular velocity of the body relative to the inertial frame, and it can be transformed to the platform frame:

$$\omega_{ib}^{p} = \mathbf{C}_b^p \omega_{ib}^{b} \tag{A.2.9}$$

The angular velocity of the platform relative to the inertial frame is:

$$\omega_{ip}^{p} = \Omega_{ie}^{p} + \omega_{ep}^{p} \tag{A.2.10}$$

and hence the angular velocity of the body relative to the platform is:

$$\omega_{pb}^{p} = \omega_{ib}^{p} - \omega_{ip}^{p} \tag{A.2.11}$$

Finally $\mathbf{C}_b^p$ is obtained by integration of the following equation:

$$\dot{\mathbf{C}}_b^p = \omega_{pb}^{p}\, \mathbf{C}_b^p \tag{A.2.12}$$

where:

$$\mathbf{C}_b^p = \begin{bmatrix} C_{11}^\theta & C_{12}^\theta & C_{13}^\theta \\ C_{21}^\theta & C_{22}^\theta & C_{23}^\theta \\ C_{31}^\theta & C_{32}^\theta & C_{33}^\theta \end{bmatrix}$$

and

$$C_{11}^\theta = \cos\theta_z \cos\theta_p$$
$$C_{12}^\theta = \cos\theta_z \sin\theta_p \sin\theta_R$$
$$C_{12}^\theta = \cos\theta_z \sin\theta_p \sin\theta_R - \sin\theta_z \cos\theta_R$$
$$C_{13}^\theta = \cos\theta_z \sin\theta_p \cos\theta_R + \sin\theta_z \sin\theta_R$$
$$C_{21}^\theta = \sin\theta_z \cos\theta_p$$
$$C_{22}^\theta = \sin\theta_z \sin\theta_p \sin\theta_R + \cos\theta_z \cos\theta_R$$
$$C_{23}^\theta = \sin\theta_z \sin\theta_p \cos\theta_R - \cos\theta_z \sin\theta_R$$
$$C_{31}^\theta = -\sin\theta_p$$
$$C_{32}^\theta = \cos\theta_p \sin\theta_R$$
$$C_{33}^\theta = \cos\theta_p \cos\theta_R$$

The pitching, rolling and course angles θ_p, θ_R, θ_z are simply:

$$\theta_p = tg^{-1}\left[\frac{-C_{31}^\theta}{\sqrt{(C_{32}^\theta)^2 + (C_{33}^\theta)^2}}\right] \qquad \text{(A.2.13)}$$

$$\theta_R = tg^{-1}\left[\frac{C_{32}^\theta}{C_{33}^\theta}\right] \qquad \text{(A.2.14)}$$

$$\theta_z = tg^{-1}\left[\frac{C_{21}^\theta}{C_{11}^\theta}\right] \qquad \text{(A.2.15)}$$

Similarly, the transformation matrix from the platform frame to the earth frame is obtained by integration of the following equation:

$$\dot{\mathbf{C}}_p^e = \mathbf{C}_p^e \, \omega_{ep}^p \qquad \text{(A.2.16)}$$

where:

$$\mathbf{C}_p^e = \begin{bmatrix} C_{11} & C_{12} & C_{13} \\ C_{21} & C_{22} & C_{23} \\ C_{31} & C_{32} & C_{33} \end{bmatrix}$$

and

$$C_{11} = -\sin\alpha\sin\varphi\cos\lambda - \cos\alpha\sin\lambda$$
$$C_{12} = -\sin\alpha\sin\varphi\sin\lambda + \cos\alpha\cos\lambda$$
$$C_{13} = \sin\alpha\cos\varphi$$
$$C_{21} = -\cos\alpha\sin\varphi\cos\lambda + \sin\alpha\sin\lambda$$
$$C_{22} = -\cos\alpha\sin\varphi\sin\lambda - \sin\alpha\cos\lambda$$
$$C_{23} = \cos\alpha\cos\varphi$$
$$C_{31} = \cos\varphi\cos\lambda$$
$$C_{32} = \cos\varphi\sin\lambda$$
$$C_{33} = \sin\varphi$$

The platform's position and azimuth rotating angle α are:

$$\varphi = \sin^{-1}[C_{33}] \qquad \text{(A.2.17)}$$

$$\lambda = \mathrm{tg}^{-1}\left[\frac{C_{32}}{C_{31}}\right] \qquad \text{(A.2.18)}$$

$$\alpha = \mathrm{tg}^{-1}\left[\frac{C_{13}}{C_{23}}\right] \qquad \text{(A.2.19)}$$

When a body manoeuvres, its attitude matrix $\mathbf{C}_b^p$ changes rapidly. To reduce the computational burden, the direction cosine matrix can be replaced by quaternion operators (Farrell, 1976).

APPENDIX 3 PLATFORM INS ERROR ANALYSIS

A.3.1 Frames for INS

1) True frame (X_t, Y_t , Z_t):
A local level frame whose origin is at the location of the INS.

2) Platform frame (X_p, Y_p, Z_p):
The platform frame is a right-hand orthogonal triad which can be thought of as three fiducial lines physically inscribed on the platform. The origins of true frame and the platform frame are the same but the directions of their axes are different due to platform drifting.

3) Computer frame (X_c, Y_c, Z_c):
The computer frame is a local level frame which origin is at the computed location. Not only are the origins of the true frame and the computer frame different but their axis directions also.

4) Gyro frame (X_g, Y_g, Z_g):
Origin is that of the platform frame, but it is a non-orthogonal frame due to gyro assembly errors.

5) Accelerometer frame (X_a, Y_a, Z_a):
Origin is that of the platform frame, but it is a non-orthogonal frame due to accelerometer assembly errors.

6) Transformation of the frames:
The deviation angles between all frames mentioned above are small, the transformation of the frames is (see eqn (2.24)) :

$$\mathbf{C}_t^p = \begin{bmatrix} 1 & \phi_z & -\phi_y \\ -\phi_z & 1 & \phi_x \\ \phi_y & -\phi_x & 1 \end{bmatrix} \qquad \text{(A.3.1.1)}$$

$\mathbf{C}_t^p$ is the transformation matrix from the true frame to the platform frame, and the platform misalignment angles are:

$$\phi = [\phi_x \quad \phi_y \quad \phi_z]^T \tag{A.3.1.2}$$

$$\mathbf{C}_t^c = \begin{bmatrix} 1 & \theta_z & -\theta_y \\ -\theta_z & 1 & \theta_x \\ \theta_y & -\theta_x & 1 \end{bmatrix} \tag{A.3.1.3}$$

$\mathbf{C}_t^c$ is the transformation matrix from the true frame to the computer frame, and the deviation angles between the true frame and the computer frame are:

$$\theta = [\theta_x \quad \theta_y \quad \theta_z]^T \tag{A.3.1.4}$$

$$\mathbf{C}_c^p = \begin{bmatrix} 1 & \psi_z & -\psi_y \\ -\psi_z & 1 & \psi_x \\ \psi_y & -\psi_x & 1 \end{bmatrix} \tag{A.3.1.5}$$

$\mathbf{C}_c^p$ is the transformation matrix from the computer frame to the platform frame, and the platform drift angles are:

$$\psi = [\psi_x \quad \psi_y \quad \psi_z]^T \tag{A.3.1.6}$$

The relationship between the true, platform and computer frames are:

$$\phi = \psi + \theta \tag{A.3.1.7}$$

and

$$\mathbf{C}_t^p = \mathbf{C}_c^p \, \mathbf{C}_t^c \tag{A.3.1.8}$$

The transformations of the gyro and accelerometer frames are (eqn (2.26)):

$$\mathbf{C}_g^p = \begin{bmatrix} 1 & -\sigma_{xz} & \sigma_{xy} \\ \sigma_{yz} & 1 & -\sigma_{yx} \\ -\sigma_{zy} & \sigma_{zx} & 1 \end{bmatrix} \qquad \text{(A.3.1.9)}$$

$\mathbf{C}_g^p$ is the transformation matrix from the gyro frame to the platform frame, and σ_{xz}, σ_{xy}, σ_{yz}, σ_{yx}, σ_{zy}, σ_{zx} are the gyro assembly errors.

$$\mathbf{C}_p^a = \begin{bmatrix} 1 & \mu_{xz} & -\mu_{xy} \\ -\mu_{yz} & 1 & \mu_{yx} \\ \mu_{zy} & -\mu_{zx} & 1 \end{bmatrix} \qquad \text{(A.3.1.10)}$$

$\mathbf{C}_p^a$ is the transformation matrix from the accelerometer frame to the platform frame, and μ_{xz}, μ_{xy}, μ_{yz}, μ_{yx}, μ_{zy}, μ_{zx} are the accelerometer assembly errors.

A.3.2 Gyro and Accelerometer Errors

Regardless of attitude errors, the accelerometer errors can be expressed as:

$$\mathbf{a}_a = (\mathbf{I} + \mathbf{K}_a)\mathbf{C}_p^a\mathbf{a}_p + \nabla \qquad \text{(A.3.2.1)}$$

where:

- $\mathbf{a}_a$ accelerations in the accelerometer frame
- $\mathbf{a}_p$ accelerations in the platform frame
- ∇ accelerometer biases

$$\mathbf{K}_a = \begin{bmatrix} k_{ax} & 0 & 0 \\ 0 & k_{ay} & 0 \\ 0 & 0 & k_{az} \end{bmatrix} \qquad \text{(A.3.2.2)}$$

k_{ax}, k_{ay}, k_{az} are the scale factor errors of the accelerometers.

Similarly, the platform drift rate **E** can be written as:

$$\mathbf{E} = \varepsilon + \mathbf{K}_g\omega_c + \Sigma\omega_c \qquad \text{(A.3.2.3)}$$

where ε is the gyro drift-rate, consisting of two parts: a constant bias and a random error. The random error can be well modelled as a stationary random process with zero mean and a autocorrelation function $\sigma^2 e^{-\beta|\tau|}$, where σ is the standard deviation of the gyro drift-rate and β is the correlation frequency.

$$\mathbf{K}_g = \begin{bmatrix} k_{gx} & 0 & 0 \\ 0 & k_{gy} & 0 \\ 0 & 0 & k_{gz} \end{bmatrix} \qquad \text{(A.3.2.4)}$$

where k_{gx}, k_{gy}, k_{gz} are the scale factor errors of the gyros. Supposing the scale factor error of the north gyro is 0.001 and $\varphi=45^o$, it causes an equivalent platform drift-rate of about 0.01deg/h.

$$\Sigma = \mathbf{C}_g^p - \mathbf{I} \qquad \text{(A.3.2.5)}$$

$\Sigma\omega_c$ is the equivalent platform drift-rate caused by the assembly errors of the gyros. Assuming there is an assembly error of 2 arc seconds, this causes a platform drift-rate of approximately 0.0001deg/h.

According to eqn (2.34) and the definition of Ψ, the platform drift can also be written as:

$$\frac{d\psi}{dt} + \omega_c \times \psi = \mathbf{E} \qquad \text{(A.3.2.6)}$$

A.3.3 Attitude Errors

From eqns (A.3.1.6) and (A.3.2.6) the attitude error equations of the platform can be expressed as:

$$\dot{\phi} = \dot{\theta} + \psi \times \omega_c + \mathbf{E} \qquad \text{(A.3.3.1)}$$

or in component form:

$$\dot{\phi}_x = \dot{\theta}_x + \psi_y\omega_{cz} - \psi_z\omega_{cy} + E_x \qquad \text{(A.3.3.2)}$$

$$\dot{\phi}_y = \dot{\theta}_y + \psi_z\omega_{cx} - \psi_x\omega_{cz} + E_y \qquad \text{(A.3.3.3)}$$

$$\dot{\phi}_z = \dot{\theta}_z + \psi_x\omega_{cy} - \psi_y\omega_{cx} + E_z \qquad \text{(A.3.3.4)}$$

A.3.4 Velocity Errors

Considering the platform misalignments, the output of the accelerometers in the platform frame $\mathbf{a}_c$ is:

$$\mathbf{a}_c = (\mathbf{I} + \mathbf{K}_a)\mathbf{C}_p^a\,\mathbf{C}_t^p\mathbf{a} + \nabla \qquad \text{(A.3.4.1)}$$

where:

- $\mathbf{a}$ accelerations in true frame
- $\mathbf{a}_c$ accelerations input into the computer

By first order approximation, eqn (A.3.4.1) can be expanded as:

$$a_{cx} = a_x + \phi_z a_y - \phi_y a_z + n_x \qquad \text{(A.3.4.2)}$$

$$a_{cy} = a_y + \phi_x a_z - \phi_z a_x + n_y \qquad \text{(A.3.4.3)}$$

$$a_{cz} = a_z + \phi_y a_x - \phi_x a_y + n_z \qquad \text{(A.3.4.4)}$$

where:

$$n_x = k_{ax}a_x + \mu_{xz}a_y - \mu_{xy}a_z + \nabla_x \qquad \text{(A.3.4.5)}$$

$$n_y = k_{ay}a_y + \mu_{yx}a_z - \mu_{yz}a_x + \nabla_y \qquad \text{(A.3.4.6)}$$

$$n_z = k_{az}a_z + \mu_{zy}a_x - \mu_{zx}a_y + \nabla_z \qquad \text{(A.3.4.7)}$$

Defining

$$\delta\dot{V}_x = \dot{V}_{cx} - \dot{V}_x \qquad \text{(A.3.4.8)}$$

$$\delta\dot{V}_y = \dot{V}_{cy} - \dot{V}_y \qquad \text{(A.3.4.9)}$$

$$\delta\dot{V}_z = \dot{V}_{cz} - \dot{V}_z \qquad \text{(A.3.4.10)}$$

Substituting eqns (A.3.4.2) to (A.3.4.4) and (A.3.4.8) to (A.3.4.10) into eqn (A.1.1.5), and neglecting high order terms, the velocity error equations can be written as:

$$\begin{aligned}\delta\dot{V}_x = {} & \phi_z\left[\dot{V}_y + (2\Omega_z + \omega_z)V_x - (2\Omega_x + \omega_x)V_z\right] \\ & - \phi_y\left[\dot{V}_z + (2\Omega_x + \omega_x)V_y - (2\Omega_y + \omega_y)V_x + g\right] \\ & + (2\Omega_z + \omega_z)\delta V_y + (2\delta\Omega_z + \delta\omega_z)V_y \\ & - (2\Omega_y + \omega_y)\delta V_z - (2\delta\Omega_y + \delta\omega_y)V_z + n_x\end{aligned} \qquad \text{(A.3.4.11)}$$

$$\begin{aligned}\delta\dot{V}_y = {} & \phi_x\left[\dot{V}_z + (2\Omega_x + \omega_x)V_y - (2\Omega_y + \omega_y)V_x + g\right] \\ & - \phi_z\left[\dot{V}_x + (2\Omega_y + \omega_y)V_z - (2\Omega_z + \omega_z)V_y\right] \\ & + (2\Omega_x + \omega_x)\delta V_z + (2\delta\Omega_x + \delta\omega_x)V_z \\ & - (2\Omega_z + \omega_z)\delta V_x - (2\delta\Omega_z + \delta\omega_z)V_x + n_y\end{aligned} \qquad \text{(A.3.4.12)}$$

$$\begin{aligned}\delta\dot{V}_z = {} & \phi_y\left[\dot{V}_x + (2\Omega_y + \omega_y)V_z - (2\Omega_z + \omega_z)V_y\right] \\ & - \phi_x\left[\dot{V}_y + (2\Omega_z + \omega_z)V_x - (2\Omega_x + \omega_x)V_z\right] \\ & + (2\Omega_y + \omega_y)\delta V_x + (2\delta\Omega_y + \delta\omega_y)V_x \\ & - (2\Omega_x + \omega_x)\delta V_y - (2\delta\Omega_x + \delta\omega_x)V_y + \delta g + n_z\end{aligned} \qquad \text{(A.3.4.13)}$$

Generally, only a numerical solution can be obtained for eqns (A.3.4.11)-(A.3.4.13). For the stationary case, where $V_x = V_y = V_z = \dot{V}_x = \dot{V}_y = \dot{V}_z = 0$, and assuming $\delta V_z = 0$, these equations can be simplified as:

$$\delta\dot{V}_x = -\phi_y g + 2\,\Omega_z \delta V_y + \nabla_x \qquad \text{(A.3.4.14)}$$

$$\delta\dot{V}_y = \phi_x g - 2\,\Omega_z \delta V_x + \nabla_y \qquad \text{(A.3.4.15)}$$

The deviation angle rates between the true frame and the computer frame are:

$$\dot{\theta}_x = -\frac{\delta V_y}{R_x} \qquad \text{(A.3.4.16)}$$

$$\dot{\theta}_y = \frac{\delta V_x}{R_y} \qquad \text{(A.3.4.17)}$$

where R_x, R_y are the earth curvature in the x and y direction, see eqns (A.2.6) and (A.2.7). By differentiation of eqn (A.3.4.16) and (A.3.4.17) and assuming the earth is a sphere with radius R, the angular acceleration error can be written as:

$$-\ddot{\theta}_x + 2\Omega_z\dot{\theta}_y - \frac{g}{R}\theta_x = \frac{\nabla_y}{R} + \frac{g}{R}\psi_x \qquad \text{(A.3.4.18)}$$

$$\ddot{\theta}_y + 2\Omega_z\dot{\theta}_x + \frac{g}{R}\theta_y = \frac{\nabla_x}{R} - \frac{g}{R}\psi_y \qquad \text{(A.3.4.19)}$$

The azimuth errors can be obtained from eqns (A.1.2.14), (A.1.3.1), (A.1.4.1) and (A.1.5.2) for the different mechanization modes.

A.3.5. Position Errors

According to eqns (A.1.2.1) and (A.1.2.2) the latitude and longitude errors are:

$$\delta\dot{\varphi} = \frac{V_{cN} - V_N}{R} \qquad \text{(A.3.5.1)}$$

$$\delta\dot{\lambda} = \frac{V_{cE}}{R\cos(\varphi + \Delta\varphi)} - \frac{V_E}{R\cos(\varphi)} \qquad \text{(A.3.5.2)}$$

where $\Delta\varphi$ is latitude error and V_{cN}, V_{cE} are the north and east computed velocities. Supposing the true and computed azimuths are α and α_c, and θ_z is the azimuth error, then the latitude and longitude errors can be expressed as:

$$\begin{aligned}\delta\dot{\varphi} &\approx \frac{1}{R}(\delta V_x\cos\alpha - \delta V_y\sin\alpha) - \frac{1}{R}(V_x\sin\alpha + V_y\cos\alpha)\theta_z \\ &= \dot{\theta}_y\cos\alpha + \dot{\theta}_x\sin\alpha - (\omega_y\sin\alpha - \omega_x\cos\alpha)\,\theta_z\end{aligned} \qquad \text{(A.3.5.3)}$$

$$\begin{aligned}\delta\dot{\lambda} \approx & -\frac{\sec\varphi}{R}(\delta V_x\sin\alpha + \delta V_y\cos\alpha) \\ & -\frac{\sec\varphi}{R}(V_x\cos\alpha - V_y\sin\alpha)\,\theta_z \\ & -\frac{\sin\varphi\,tg\varphi}{R}(V_x\sin\alpha + V_y\cos\alpha)\,\Delta\varphi \\ = & (\dot{\theta}_x\cos\alpha - \dot{\theta}_y\sin\alpha)\sec\varphi \\ & -(\omega_y\cos\alpha + \omega_x\sin\alpha)\sec\varphi\theta_z \\ & -(\omega_y\sin\alpha - \omega_x\cos\alpha)\,tg\varphi\sec\varphi\Delta\varphi\end{aligned} \qquad \text{(A.3.5.4)}$$

For the stationary case, the latitude and longitude errors are:

$$\delta\dot{\varphi} = \dot{\theta}_y\cos\alpha + \dot{\theta}_x\sin\alpha \qquad \text{(A.3.5.5)}$$

$$\delta\dot{\lambda} = (\dot{\theta}_x\cos\alpha - \dot{\theta}_y\sin\alpha)\sec\varphi \qquad \text{(A.3.5.6)}$$

A.3.6 Error Propagation

For the stationary case, eqns (A.3.3.2) to (A.3.3.4) and (A.3.4.18) and (A.3.4.19) form a group of linear-constant coefficient differential equations, by Laplace transformation they can be written as:

$$\begin{bmatrix} S & -\Omega_z & \Omega_y & 0 & 0 \\ \Omega_z & S & -\Omega_x & 0 & 0 \\ -\Omega_y & \Omega_x & S & 0 & 0 \\ \frac{g}{R} & 0 & 0 & -2\Omega\sin\varphi S & S^2+\frac{g}{R} \\ 0 & \frac{g}{R} & 0 & S^2+\frac{g}{R} & 2\Omega\sin\varphi S \end{bmatrix} \begin{bmatrix} \psi_x(S) \\ \psi_y(S) \\ \psi_z(S) \\ \theta_x(S) \\ \theta_y(S) \end{bmatrix}$$

$$= \begin{bmatrix} \frac{E_x}{S} + \psi_x(0) \\ \frac{E_y}{S} + \psi_y(0) \\ \frac{E_z}{S} + \psi_z(0) \\ -\frac{\nabla_y}{RS} + S\,\theta_x(0) + \dot{\theta}_x(0) - 2\Omega\sin\varphi\theta_y(0) \\ \frac{\nabla_x}{RS} + S\,\theta_y(0) + \dot{\theta}_y(0) + 2\Omega\sin\varphi\theta_x(0) \end{bmatrix} \qquad \text{(A.3.6.1)}$$

where $\psi_x(0)$, $\psi_y(0)$, $\psi_z(0)$, $\theta_x(0)$, $\theta_y(0)$, $\dot{\theta}_x(0)$, $\dot{\theta}_y(0)$ are the initial values. The eigenfunction of eqn (A.3.6.1) is:

$$S(S^2 + \Omega^2)\,[(S^2 + \omega_s^2)^2 + 4S^2\Omega^2\sin^2\varphi] = 0 \qquad \text{(A.3.6.2)}$$

where the Schuler frequency is:

$$\omega_s = \sqrt{\frac{g}{R}} \qquad \text{(A.3.6.3)}$$

The roots of eqn (A.3.6.2) are:

$$S_1 = 0 \qquad \text{(A.3.6.4)}$$

$$S_{2,3} = \pm j\Omega \qquad \text{(A.3.6.5)}$$

$$S_{4,5} = \pm j(\sqrt{\omega_s^2 + \Omega^2 \sin^2\varphi} + \Omega\sin\varphi \approx \pm j(\omega_s + \Omega\sin\varphi) \quad \text{(A.3.6.6)}$$

$$S_{6,7} = \pm j(\sqrt{\omega_s^2 + \Omega^2 \sin^2\varphi} - \Omega\sin\varphi \approx \pm j(\omega_s - \Omega\sin\varphi) \quad \text{(A.3.6.7)}$$

S1 corresponds to the terms of integration which increase with time. $S_{2,3}$, $S_{4,5}$ and $S_{6,7}$ are all in the imaginary axis of the S plane and correspond to undamped oscillations. The oscillation period of $S_{2,3}$ is 24 hours, $S_{4,5}$ and $S_{6,7}$ form two beat frequencies:

$$\omega_1 = \frac{1}{2}[(\omega_s + \Omega\sin\varphi) + (\omega_s - \Omega\sin\varphi)] = \omega_s \quad \text{(A.3.6.8)}$$

$$\omega_2 = \frac{1}{2}[(\omega_s + \Omega\sin\varphi) - (\omega_s - \Omega\sin\varphi)] = \Omega\sin\varphi \quad \text{(A.3.6.9)}$$

where the period T_1 of ω_1 is nearly 84.4 minutes and is known as the Schuler period, the period T_2 of ω_2, known as the Foucault period, depends on the latitude. When $\varphi = 45^\circ$, T_2 is about 34 hours, when $\varphi = 0^\circ$ there is no Foucault oscillation, and when $\varphi = 90^\circ$, T_2 is 24 hours.

In eqn (A.3.6.1) the platform drifts and accelerometer biases are assumed to be step functions. The initial values of ψ, θ can be chosen according to a certain azimuth for different mechanization modes. The solutions of the errors corresponding to the system error sources such as platform drift, accelerometer bias and initial state are contained in Tables A.3.6.1 to A.3.6.9.

A.3.7 Random Errors of INS

Eqn (A.3.6.2) shows that each individual term of the transfer function matrix consists of a second order loop, or a cascade of second order loops. We choose one loop as an example. Assuming the bias of the east accelerometer is white noise with zero mean and its autocorrelation is $\mu\sigma^2\delta(\tau)$, μ is time factor, σ is standard deviation of the noise and $\delta(\tau)$ is the impulse function. For a second

order loop we have:

$$\delta V_x(s) = \frac{s}{s^2 + \omega_s^2} \nabla_x(s) \qquad \text{(A.3.7.1)}$$

From this equation it can be seen that the impulse response, or the weight function, of the second order loop is $\cos\omega_s$. By using the convolution theorem the variance of δV_x is given as:

$$\sigma^2_{\delta V_x} = \int_0^t \int_0^t \cos\omega_s(t-k)\cos\omega_s(t-l)\mu\sigma^2\delta(k-l)dkdl$$

$$= \mu\sigma^2\left[\frac{1}{2}t + \frac{1}{2\omega_s}\sin 2\omega_s t\right] \qquad \text{(A.3.7.2)}$$

eqn (A.3.7.2) indicates that the east velocity error caused by the random bias of the east accelerometer is divergent, and it's speed of divergence is proportional to $\sqrt{t}$. The same conclusion can be drawn for other random error source inputs.

Table A.3.6.1 Platform drifting angles due to platform drift rate

error / ψ	E_x	E_y	E_z
ψ_x	$\frac{\Omega_x^2}{\Omega^2}t+\frac{\Omega^2-\Omega_x^2}{\Omega^3}\sin\Omega t$	$\frac{\Omega_x\Omega_y}{\Omega^2}(t-\frac{\sin\Omega t}{\Omega})+\frac{\Omega_z}{\Omega^2}(1-\cos\Omega t)$	$\frac{\Omega_x\Omega_z}{\Omega^2}(t-\frac{\sin\Omega t}{\Omega})-\frac{\Omega_y}{\Omega^2}(1-\cos\Omega t)$
ψ_y	$\frac{\Omega_x\Omega_y}{\Omega^2}(t-\frac{\sin\Omega t}{\Omega})-\frac{\Omega_z}{\Omega^2}(1-\cos\Omega t)$	$\frac{\Omega_y^2}{\Omega^2}t+\frac{\Omega^2-\Omega_y^2}{\Omega^3}\sin\Omega t$	$\frac{\Omega_y\Omega_z}{\Omega^2}(t-\frac{\sin\Omega t}{\Omega})+\frac{\Omega_x}{\Omega^2}(1-\cos\Omega t)$
ψ_z	$\frac{\Omega_x\Omega_z}{\Omega^2}(t-\frac{\sin\Omega t}{\Omega})+\frac{\Omega_y}{\Omega^2}(1-\cos\Omega t)$	$\frac{\Omega_y\Omega_z}{\Omega^2}(t-\frac{\sin\Omega t}{\Omega})-\frac{\Omega_x}{\Omega^2}(1-\cos\Omega t)$	$\frac{\Omega_z^2}{\Omega^2}t+\frac{\Omega^2-\Omega_z^2}{\Omega^3}\sin\Omega t$

Table A.3.6.2 Platform drifting angle due to platform initial errors

error / ψ	ψ_{x0}	ψ_{y0}	ψ_{z0}
ψ_x	$\frac{\Omega_x^2}{\Omega^2}+(1-\frac{\Omega_x^2}{\Omega^2})\cos\Omega t$	$\frac{\Omega_x\Omega_y}{\Omega^2}(1-\cos\Omega t)+\frac{\Omega_z}{\Omega}\sin\Omega t$	$\frac{\Omega_x\Omega_z}{\Omega^2}(1-\cos\Omega t)-\frac{\Omega_y}{\Omega}\sin\Omega t$
ψ_y	$\frac{\Omega_x\Omega_y}{\Omega^2}(1-\cos\Omega t)-\frac{\Omega_z}{\Omega}\sin\Omega t$	$\frac{\Omega_y^2}{\Omega^2}+(1-\frac{\Omega_y^2}{\Omega^2})\cos\Omega t$	$\frac{\Omega_y\Omega_z}{\Omega^2}(1-\cos\Omega t)+\frac{\Omega_x}{\Omega}\sin\Omega t$
ψ_z	$\frac{\Omega_x\Omega_z}{\Omega^2}(1-\cos\Omega t)+\frac{\Omega_y}{\Omega}\sin\Omega t$	$\frac{\Omega_y\Omega_z}{\Omega^2}(1-\cos\Omega t)-\frac{\Omega_x}{\Omega}\sin\Omega t$	$\frac{\Omega_z^2}{\Omega^2}+(1-\frac{\Omega_z^2}{\Omega^2})\cos\Omega t$

Table A.3.6.3 Position error angles due to its initial errors and accelerometer biases

θ error sources	$\frac{\nabla_x}{g}$	$\frac{\nabla_y}{g}$	θ_{x0}	θ_{y0}
θ_x	$\cos\omega_s t \sin\Omega_z t$	$\cos\omega_s t \cos\Omega_z t - 1$	$\cos\omega_s t \cos\Omega_z t$	$\cos\omega_s t \sin\Omega_z t$
θ_y	$1 - \cos\omega_s t \cos\Omega_z t$	$-\cos\omega_s t \sin\Omega_z t$	$-\cos\omega_s t \sin\Omega_z t$	$\cos\omega_s t \cos\Omega_z t$

Table A.3.6.4 Position error angles due to its initial errors

θ error sources	$\dot{\theta}_{x0}$	$\dot{\theta}_{y0}$
θ_x	$\frac{1}{\omega_s}\sin\omega_s t \cos\Omega_z t$	$\frac{1}{\omega_s}\sin\omega_s t \sin\Omega_z t$
θ_y	$-\frac{1}{\omega_s}\sin\omega_s t \sin\Omega_z t$	$\frac{1}{\omega_s}\sin\omega_s t \cos\Omega_z t$

The position error angles are defined as the angles between the platform and the computed platform frames.

Table A.3.6.5 Position error angles due to platform drift rate

θ \ error sources	E_x	E_y	E_z
θ_x	$-\frac{\Omega_x^2}{\Omega^2}t-\frac{\Omega^2-\Omega_x^2}{\Omega^2}\sin\Omega_z t$ $+\frac{1}{\omega_s}\sin\omega_s\cos\Omega_z t$	$-\frac{\Omega_x\Omega_y}{\Omega^2}(t-\frac{\sin\Omega t}{\Omega})$ $-\frac{\Omega_z}{\Omega^2}(1-\cos\Omega t)$ $+\frac{1}{\omega_s}\sin\omega_s\sin\Omega_z t$	$-\frac{\Omega_x\Omega_z}{\Omega^2}(t-\frac{\sin\Omega t}{\Omega})$ $+\frac{\Omega_y}{\Omega^2}(1-\cos\Omega t)$
θ_y	$-\frac{\Omega_x\Omega_y}{\Omega^2}(t-\frac{\sin\Omega t}{\Omega})$ $+\frac{\Omega_z}{\Omega^2}(1-\cos\Omega t)$ $-\frac{1}{\omega_s}\sin\omega_s\sin\Omega_z t$	$-\frac{\Omega_y^2}{\Omega^2}t-\frac{\Omega^2-\Omega_y^2}{\Omega^2}\sin\Omega_z t$ $+\frac{1}{\omega_s}\cos\omega_s\sin\Omega_z t$	$-\frac{\Omega_y\Omega_z}{\Omega^2}(t-\frac{\sin\Omega t}{\Omega})$ $-\frac{\Omega_x}{\Omega^2}(1-\cos\Omega t)$

Table A.3.6.6 Position error angles due to platform initial errors

θ \ error sources	Ψ_{x0}	Ψ_{y0}	Ψ_{z0}
θ_x	$-\frac{\Omega_x^2}{\Omega^2}-\frac{\Omega^2-\Omega_x^2}{\Omega^2}\cos\Omega t$ $+\cos\omega_s t\cos\Omega_z t$	$-\frac{\Omega_x\Omega_y}{\Omega^2}(1-\cos\Omega t)$ $-\frac{\Omega_z}{\Omega}\sin\Omega t$ $+\cos\omega_s t\sin\Omega_z t$	$-\frac{\Omega_x\Omega_z}{\Omega^2}(1-\cos\Omega t)$ $+\frac{\Omega_y}{\Omega}\sin\Omega t$
θ_y	$-\frac{\Omega_x\Omega_y}{\Omega^2}(1-\cos\Omega t)$ $+\frac{\Omega_z}{\Omega}\sin\Omega t$ $-\cos\omega_s t\sin\Omega_z t$	$-\frac{\Omega_y^2}{\Omega^2}-\frac{\Omega^2-\Omega_y^2}{\Omega^2}\cos\Omega t$ $+\cos\omega_s t\cos\Omega_z t$	$\frac{\Omega_y\Omega_z}{\Omega^2}(1-\cos\Omega t)$ $-\frac{\Omega_x}{\Omega}\sin\Omega t$

Table A.3.6.7 Position, velocity and attitude errors due to accelerometer biases

error sources / errors	$\frac{\nabla_x}{g}$	$\frac{\nabla_y}{g}$
$\delta\varphi$	$1-\cos\omega_s t\cos\Omega_z t$	$-\cos\omega_s t\sin\Omega_z t$
$\delta\lambda$	$\sec\varphi\cos\omega_s t\sin\Omega_z t$	$\sec\varphi(\cos\omega_s t\cos\Omega_z t-1)$
$\delta\omega_x$	$\omega_s\sin\omega_s t\sin\Omega_z t$	$-\omega_s\sin\omega_s t\cos\Omega_z t$
$\delta\omega_y$	$\omega_s\sin\omega_s t\cos\Omega_z t$	$\omega_s\sin\omega_s t\sin\Omega_z t$
ϕ_x	$\cos\omega_s t\sin\Omega_z t$	$\cos\omega_s t\cos\Omega_z t-1$
ϕ_y	$1-\cos\omega_s t\cos\Omega_z t$	$-\cos\omega_s t\sin\Omega_z t$
ϕ_z	$-tg\varphi\cos\omega_s t\sin\Omega_z t$	$tg\varphi(\cos\omega_s t\cos\Omega_z t-1)$

Table A.3.6.8 Position, velocity and attitude errors due to platform drift rate

error sources / errors	E_x	E_y	E_z
$\delta\varphi$	$\frac{1}{\Omega}\sin\varphi(1-\cos\Omega t)$ $-\frac{1}{\omega_s}\sin\omega_s t\sin\Omega_z t$	$-\frac{\sin\Omega t}{\Omega}-\frac{1}{\omega_s}\sin\omega_s t\cos\Omega_z t$	$-\frac{\cos\varphi}{\Omega}(1-\cos\Omega t)$
$\delta\lambda$	$\sin\varphi tg\varphi(t-\frac{\sin\Omega t}{\Omega})$ $-\sec\varphi(t-\frac{1}{\omega_s}\sin\omega_s t\cos\Omega_z t)$	$-\frac{tg\varphi}{\Omega}(1-\cos\Omega t)$ $+\frac{1}{\omega_s\cos\varphi}\sin\omega_s t\cos\Omega_z t$	$-\sin\varphi(t-\frac{\sin\Omega t}{\Omega})$
$\delta\omega_x$	$\sin^2\varphi(1-\cos\Omega t)$ $-(1-\cos\omega_s t\cos\Omega_z t)$	$\sin\varphi\sin\Omega t$ $+\cos\omega_s t\sin\Omega_z t$	$-\cos\varphi\sin\varphi(1-\cos\Omega t)$
$\delta\omega_y$	$-\sin\varphi\sin\Omega t$ $-\cos\omega_s t\sin\Omega_z t$	$-\cos\Omega t-\cos\omega_s t\cos\Omega_z t$	$-\cos\varphi\sin\Omega t$
ϕ_x	$\frac{1}{\omega_s}\sin\omega_s t\cos\Omega_z t$	$\frac{1}{\omega_s}\sin\omega_s t\sin\Omega_z t$	negligible
ϕ_y	$-\frac{1}{\omega_s}\sin\omega_s t\sin\Omega_z t$	$\frac{1}{\omega_s}\sin\omega_s t\cos\Omega_z t$	negligible
ϕ_z	$-tg\varphi\frac{\sin\Omega t}{\Omega}$ $-\frac{1}{\omega_s}tg\varphi\sin\omega_s t\sin\Omega_z t$	$-\frac{1}{\Omega\cos\varphi}(1-\cos\Omega t)$ $-\frac{1}{\omega_s}tg\varphi\sin\omega_s t\cos\Omega_z t$	$\frac{\sin\Omega t}{\Omega}$

Table A.3.6.9 Position, velocity and attitude errors due to initial position errors

error sources / errors	$\delta\varphi_0$	$\delta\lambda_0$
$\delta\varphi$	$\cos \Omega t$	negligible
$\delta\lambda$	$\mathrm{tg}\varphi \sin \Omega t$	1
$\delta\omega_x$	negligible	$\Omega \cos\varphi \sin\varphi(\sin\varphi \sin\Omega t + \cos\omega_s t \sin\Omega_z t)$
$\delta\omega_y$	negligible	$\Omega \cos\varphi \sin\varphi(\cos\Omega t - \cos\omega_s t \cos\Omega_z t)$
ϕ_x	negligible	negligible
ϕ_y	negligible	negligible
ϕ_z	$\sec\varphi \sin\Omega t$	negligible

Table A.3.6.10 Position, velocity and attitude errors due to initial attitude errors

error sources / errors	ϕ_{x0}	ϕ_{y0}	ϕ_{z0}
$\delta\varphi$	$-\sin\varphi\sin\Omega t$ $-\cos\omega_s t\sin\Omega_z t$	$-\cos\Omega t+\cos\omega_s t\cos\Omega_z t$	$-\cos\varphi\sin\Omega t$
$\delta\lambda$	$\sin\varphi tg\varphi(1-\cos\Omega t)$ $-\sec\varphi(1-\cos\omega_s t\sin\Omega_z t)$	$-tg\varphi\sin\Omega t$ $+\sec\varphi\cos\omega_s t\sin\Omega_z t$	$-\sin\varphi(1-\cos\Omega t)$
$\delta\omega_x$	$-\omega_s\sin\omega_s t\cos\Omega_z t$	$-\omega_s\sin\omega_s t\sin\Omega_z t$	$-\Omega\cos\varphi(\sin\varphi\sin\Omega t$ $+\cos\omega_s t\sin\Omega_z t)$
$\delta\omega_y$	$\omega_s\sin\omega_s t\sin\Omega_z t$	$-\omega_s\sin\omega_s t\cos\Omega_z t$	$-\Omega\cos\varphi(\cos\Omega t$ $-\cos\omega_s t\cos\Omega_z t)$
ϕ_x	$\cos\omega_s t\cos\Omega_z t$	$\cos\omega_s t\cos\Omega_z t$	negligible
ϕ_y	$-\cos\omega_s t\sin\Omega_z t$	$\cos\omega_s t\cos\Omega_z t$	negligible
ϕ_z	$-tg\varphi(\cos\Omega t-\cos\omega_s t\cos\Omega_z t)$	$-\sec\varphi(\sin\Omega t$ $-\sin\varphi\cos\omega_s t\sin\Omega_z t)$	$\cos\Omega t$

Appendix 3.8 North-Directed INS/GPS Integration

For marine applications, the state vector of the system can be chosen as:

$$\mathbf{X} = (\delta V_x\ \delta V_y\ \delta\lambda\ \delta\varphi\ \alpha\ \beta\ \gamma\ \varepsilon_x\ \varepsilon_y\ \varepsilon_z\ a_0\ a_1)^T \qquad \text{(A.3.8.1)}$$

where a_0, a_1 are the clock bias and drift of GPS receiver.

When neglecting the assembly errors of the gyro and accelerometer the coefficient matrix **A** is obtained from Appendix 2 and 3:

$$\mathbf{A}(t) = \begin{bmatrix}
A_{11} & A_{12} & 0 & A_{14} & 0 & 0 & A_{17} & 0 & 0 & 0 & 0 & 0 \\
A_{21} & 0 & 0 & A_{24} & 0 & 0 & A_{27} & 0 & 0 & 0 & 0 & 0 \\
A_{31} & 0 & 0 & A_{34} & 0 & 0 & 0 & 0 & 0 & 0 & 0 & 0 \\
0 & A_{42} & 0 & 0 & 0 & 0 & 0 & 0 & 0 & 0 & 0 & 0 \\
0 & A_{52} & 0 & 0 & 0 & A_{56} & A_{57} & 1 & 0 & 0 & 0 & 0 \\
A_{61} & 0 & 0 & A_{64} & A_{65} & 0 & A_{67} & 0 & 1 & 0 & 0 & 0 \\
A_{71} & 0 & 0 & A_{74} & A_{75} & A_{76} & 0 & 0 & 0 & 1 & 0 & 0 \\
0 & 0 & 0 & 0 & 0 & 0 & 0 & -\tau_x & 0 & 0 & 0 & 0 \\
0 & 0 & 0 & 0 & 0 & 0 & 0 & 0 & -\tau_y & 0 & 0 & 0 \\
0 & 0 & 0 & 0 & 0 & 0 & 0 & 0 & 0 & -\tau_z & 0 & 0 \\
0 & 0 & 0 & 0 & 0 & 0 & 0 & 0 & 0 & 0 & 0 & 0 \\
0 & 0 & 0 & 0 & 0 & 0 & 0 & 0 & 0 & 0 & 0 & 1
\end{bmatrix} \qquad \text{(A.3.8.2)}$$

where:

$$A_{11} = \frac{V_y}{R} tg\varphi$$

$$A_{12} = \frac{V_x}{R} tg\varphi + 2\Omega sin\varphi$$

$$A_{14} = V_y (2\Omega cos\varphi + \frac{V_x}{R} sec^2\varphi)$$

$$A_{17} = \dot{V}_y + (2\Omega\sin\varphi + \frac{V_x}{R}\,tg\varphi)\ V_x = Y \text{ accelerometer output}$$

$$A_{21} = -2\ (\Omega\sin\varphi + \frac{V_x}{R}\,tg\varphi)$$

$$A_{24} = -V_x\ (2\Omega\cos\varphi + \frac{V_x}{R}\,\sec^2\varphi)$$

$$A_{27} = \dot{V}_x - (2\Omega\sin\varphi + \frac{V_x}{R}\,tg\varphi)\ V_y = X \text{ accelerometer output}$$

$$A_{31} = \frac{\sec\varphi}{R}$$

$$A_{34} = \frac{V_x}{R}\,\sec\varphi tg\varphi$$

$$A_{42} = -A_{52} = A_{61} = \frac{1}{R}$$

$$A_{56} = -A_{65} = \Omega\sin\varphi + \frac{V_x}{R}\,tg\varphi$$

$$A_{57} = -A_{75} = -(\Omega\cos\varphi + \frac{V_x}{R})$$

$$A_{64} = -\Omega\sin\varphi$$

$$A_{67} = -A_{76} = -\frac{V_y}{R}$$

$$A_{71} = \frac{tg\varphi}{R}$$

$$A_{74} = \Omega\cos\varphi + \frac{V_x}{R}\,\sec^2\varphi$$

The gyro drift-rates are modelled as a first order Markov process and the clock errors of GPS receiver as white noise and a random walk. The system noise is:

$$\mathbf{W}(t) = (\nabla_x \; \nabla_y \; 0 \; 0 \; 0 \; 0 \; 0 \; f_x \; f_y \; f_z \; w_{cl} \; w_{cld})^T \qquad \text{(A.3.8.3)}$$

where the accelerometer biases are considered white noise. f_x, f_y, f_z are the white noises of the east, north and azimuth gyros, w_{cl}, w_{cld} are the driving noises for the clock bias and drift.

The range and range-rate observation equations are:

$$\frac{\partial \rho}{\partial \varphi} = \frac{\partial \rho}{\partial X_r}\frac{\partial X_r}{\partial \varphi} + \frac{\partial \rho}{\partial Y_r}\frac{\partial Y_r}{\partial \varphi} + \frac{\partial \rho}{\partial Z_r}\frac{\partial Z_r}{\partial \varphi} \qquad \text{(A.3.8.4)}$$

$$\frac{\partial \rho}{\partial \lambda} = \frac{\partial \rho}{\partial X_r}\frac{\partial X_r}{\partial \lambda} + \frac{\partial \rho}{\partial Y_r}\frac{\partial Y_r}{\partial \lambda} + \frac{\partial \rho}{\partial Z_r}\frac{\partial Z_r}{\partial \lambda} \qquad \text{(A.3.8.5)}$$

$$\frac{\partial \dot{\rho}}{\partial \varphi} = \frac{\partial \dot{\rho}}{\partial X_r}\frac{\partial X_r}{\partial \varphi} + \frac{\partial \dot{\rho}}{\partial Y_r}\frac{\partial Y_r}{\partial \varphi} + \frac{\partial \dot{\rho}}{\partial Z_r}\frac{\partial Z_r}{\partial \varphi} \qquad \text{(A.3.8.6)}$$

$$\frac{\partial \dot{\rho}}{\partial \lambda} = \frac{\partial \dot{\rho}}{\partial X_r}\frac{\partial X_r}{\partial \lambda} + \frac{\partial \dot{\rho}}{\partial Y_r}\frac{\partial Y_r}{\partial \lambda} + \frac{\partial \dot{\rho}}{\partial Z_r}\frac{\partial Z_r}{\partial \lambda} \qquad \text{(A.3.8.7)}$$

$$\frac{\partial \dot{\rho}}{\partial V_x} = \frac{\partial \dot{\rho}}{\partial \dot{X}_r}\frac{\partial \dot{X}_r}{\partial V_x} + \frac{\partial \dot{\rho}}{\partial \dot{Y}_r}\frac{\partial \dot{Y}_r}{\partial V_x} + \frac{\partial \dot{\rho}}{\partial \dot{Z}_r}\frac{\partial \dot{Z}_r}{\partial V_x} \qquad \text{(A.3.8.8)}$$

$$\frac{\partial \dot{\rho}}{\partial V_y} = \frac{\partial \dot{\rho}}{\partial \dot{X}_r}\frac{\partial \dot{X}_r}{\partial V_y} + \frac{\partial \dot{\rho}}{\partial \dot{Y}_r}\frac{\partial \dot{Y}_r}{\partial V_y} + \frac{\partial \dot{\rho}}{\partial \dot{Z}_r}\frac{\partial \dot{Z}_r}{\partial V_y} \qquad \text{(A.3.8.9)}$$

where:

ρ	GPS range
X_r, Y_r, Z_r	coordinates of GPS receiver antenna

and

$$X_r = R_M \cos\varphi \cos\lambda \,, \qquad Y_r = R_M \cos\varphi \sin\lambda \,,$$

$$Z_r = R_N \sin\varphi \qquad \text{(A.3.8.10)}$$

$$\dot{X}_r = -V_x \sin\lambda - V_y \cos\lambda \sin\varphi \,, \quad \dot{Y}_r = V_x \cos\lambda - V_y \sin\lambda \sin\varphi \,,$$

$$\dot{Z}_r = V_y \cos\varphi \qquad \text{(A.3.8.11)}$$

$$\frac{\partial\rho}{\partial X_r} = \frac{\partial\dot{\rho}}{\partial\dot{X}_r} = -\left|\frac{X_s - X_r}{\rho}\right| , \quad \frac{\partial\rho}{\partial Y_r} = \frac{\partial\dot{\rho}}{\partial\dot{Y}_r} = -\left|\frac{Y_s - Y_r}{\rho}\right| ,$$

$$\frac{\partial\rho}{\partial Z_r} = \frac{\partial\dot{\rho}}{\partial\dot{Z}_r} = -\left|\frac{Z_s - Z_r}{\rho}\right| \qquad \text{(A.3.8.12)}$$

X_s, Y_s, Z_s are the coordinates of the satellite in the earth frame of the WGS 84 system.

$$\frac{\partial X_r}{\partial\varphi} = -R_M \sin\varphi\cos\lambda , \quad \frac{\partial Y_r}{\partial\varphi} = -R_M \sin\varphi\sin\lambda ,$$

$$\frac{\partial Z_r}{\partial\varphi} = -R_N \cos\varphi \qquad \text{(A.3.8.13)}$$

$$\frac{\partial X_r}{\partial\lambda} = -R_M \cos\varphi\sin\lambda , \quad \frac{\partial Y_r}{\partial\lambda} = R_M \cos\varphi\cos\lambda$$

$$\frac{\partial Z_r}{\partial\lambda} = 0 \qquad \text{(A.3.8.14)}$$

$$\frac{\partial\dot{\rho}}{\partial X_r} = \frac{\left[\dot{X}_s - \dot{X}_r\right] - \dot{\rho}\frac{\partial\rho}{\partial X_r}}{\rho} , \quad \frac{\partial\dot{\rho}}{\partial Y_r} = \frac{\left[\dot{Y}_s - \dot{Y}_r\right] - \dot{\rho}\frac{\partial\rho}{\partial Y_r}}{\rho} ,$$

$$\frac{\partial\dot{\rho}}{\partial Z_r} = \frac{\left[\dot{Z}_s - \dot{Z}_r\right] - \dot{\rho}\frac{\partial\rho}{\partial Z_r}}{\rho} \qquad \text{(A.3.8.15)}$$

$$\frac{\partial\dot{X}_r}{\partial V_x} = -\sin\lambda , \quad \frac{\partial\dot{Y}_r}{\partial V_x} = \cos\lambda , \quad \frac{\partial\dot{Z}_r}{\partial V_x} = 0 \qquad \text{(A.3.8.16)}$$

$$\frac{\partial \dot{X}_r}{\partial V_y} = -\cos\lambda\sin\varphi\ ,\ \frac{\partial \dot{Y}_r}{\partial V_y} = -\sin\lambda\sin\varphi\ ,\ \frac{\partial \dot{Z}_r}{\partial V_y} = \cos\varphi \qquad \text{(A.3.8.17)}$$

The range observation equation of GPS is:

$$Z_p = \begin{bmatrix} \frac{\partial \rho}{\partial \varphi} & \frac{\partial \rho}{\partial \lambda} & 1 \end{bmatrix} \begin{bmatrix} \Delta\varphi \\ \Delta\lambda \\ a_0 \end{bmatrix} + v_p \qquad \text{(A.3.8.18)}$$

and the range-rate observation equation is:

$$Z_d = \begin{bmatrix} \frac{\partial \dot{\rho}}{\partial V_x} & \frac{\partial \dot{\rho}}{\partial V_y} & \frac{\partial \dot{\rho}}{\partial \varphi} & \frac{\partial \dot{\rho}}{\partial \lambda} & 1 \end{bmatrix} \begin{bmatrix} \Delta V_x \\ \Delta V_y \\ \Delta\lambda \\ \Delta\varphi \\ a_1 \end{bmatrix} + v_d \qquad \text{(A.3.8.19)}$$

where v_p, v_d are zero mean white noise.

The feedback control component $\mathbf{U}(t_k)$ is obtained from the estimation of the system state $\hat{\mathbf{X}}(t_k)$ as:

$$\mathbf{U}(t_k) = -\,\mathbf{g}\,\hat{\mathbf{X}}(t_k)\ ,\quad \mathbf{g} = \begin{bmatrix} 1 & 0 & 0 & \cdots & 0 & 0 & 0 \\ 0 & 1 & 0 & \cdots & 0 & 0 & 0 \\ 0 & 0 & 1 & \cdots & 0 & 0 & 0 \\ & & & \cdots & & & \\ 0 & 0 & 0 & \cdots & 1 & 0 & 0 \\ 0 & 0 & 0 & \cdots & 0 & 0 & 0 \\ 0 & 0 & 0 & \cdots & 0 & 0 & 0 \end{bmatrix}_{(12\times12)} \qquad \text{(A.3.8.20)}$$

APPENDIX 4 BARTLETT AND PORTMANTEAU TESTS

For lags k greater than some value q beyond which the theoretical autocorrelation function may be deemed to have died out, Bartlett has shown that an approximate of the sample autocorrelation variance is given by (Vandaele, 1983):

$$Var(r_k) \approx \frac{1}{n}\left[1 + 2\sum_{i=1}^{q} r_i^2\right], \quad k > q \qquad \text{(A.4.1.1)}$$

$$r_k = \frac{c_k}{c_0}, \quad c_k = \frac{1}{n}\sum_{t}^{n-k} z_t z_{t+k} \qquad \text{(A.4.1.2)}$$

where:

n data length

z_t residual

and r_k is asympototically normally distributed a under weak condition. Its mean value is (Kendall & Steuart, 1966):

$$E(r_k) \approx -\frac{1}{n} \qquad \text{(A.4.1.3)}$$

If the residuals are white noise series, the population autocorrelation and covariance of the series should be zero for the lag k > 0. If the residual series is white, the variance of sample autocorrelation for large k can be written as:

$$Var(r_k) \approx \frac{1}{n}, \quad k > q \qquad \text{(A.4.1.4)}$$

If the value of r_k falls outside the 95% confidence limits of $-1/n \pm 2/\sqrt{n}$, which is often further approximated by $\pm 2/\sqrt{n}$, the r_k is 'significantly' different from zero at the 5% level.

The Portmanteau test is based on the Q statistic:

$$Q(k) = n(n+2) \sum_{i=1}^{k} \frac{r_i^2}{n - i} \qquad \text{(A.4.1.5)}$$

For white a noise series, the Q(k) is distributed approximately as a chi - squared distribution with k degrees of freedom. If the computed value of Q(k) is less than the table value of the chi - square statistic with k degrees of freedom, given a pre-specified significant level, the group of autocorrelations used to calculate the test can be assumed to be not 'significantly different' from zero.

APPENDIX 5 FEDERATED KALMAN FILTER

Assuming there are N local sensors or systems, the ith local system model can be expressed as:

$$\mathbf{X}_i(t_{k+1}) = \Phi_i(t_{k+1},t_k)\mathbf{X}_i(t_k) + \overline{\mathbf{G}}_i(t_k)\mathbf{w}_i(t_k) \tag{A.5.1}$$

Eqn (A.5.1) can be written as:

$$\mathbf{X}_i(t_{k+1}) = \Phi_i(t_{k+1},t_k)\mathbf{X}_i(t_k) + \mathbf{G}_i(t_k)\mathbf{w}(t_k) \tag{A.5.2}$$

$$\mathbf{Z}_i(t_k) = \mathbf{H}_i(t_k)\mathbf{X}_i(t_k) + \mathbf{v}_i(t_k) \tag{A.5.3}$$

where:

$$\mathbf{X}_i(t_k) = \begin{bmatrix} \mathbf{X}_{ic}(t_k) \\ \mathbf{X}_{iu}(t_k) \end{bmatrix} \tag{A.5.4}$$

$\mathbf{X}_{ic}$ is the common state vector, which contains the state variables common to all local systems. $\mathbf{X}_{iu}$ is the unique state vector, which contains the state variables that are unique to the ith local system. $\mathbf{v}_i$, $\mathbf{w}$ are white noise series, and $\mathbf{w}$ is the global system noise with a covariance $\mathbf{Q}$ and:

$$\mathbf{w}(t_k) = \begin{bmatrix} \mathbf{w}_1(t_k) \\ \cdots \\ \mathbf{w}_N(t_k) \end{bmatrix} \tag{A.5.5}$$

$$\mathbf{G}_i(t_k) = \overline{\mathbf{G}}_i(t_k)\left[0_{p_i \times p_1} \cdots 0_{p_i \times p_{i-1}} \; \mathbf{I}_{p_i \times p_i} \; 0_{p_i \times p_{i+1}} \cdots 0_{p_i \times p_N}\right] \tag{A.5.6}$$

where p_i is the ith local system noise dimension. Using conventional Kalman filter algorithms, a local estimate $\hat{\mathbf{X}}_i(t_k)$ and associated covariance matrix $\mathbf{P}_i(t_k)$ for each local system, based on the local system model, can be obtained. Those local estimates will be input into a global system to obtain the global estimates of the global state $\hat{\mathbf{X}}(t_k)$ and:

$$\mathbf{X}(t_k) = \begin{bmatrix} \mathbf{X}_1(t_k) \\ \cdots \\ \mathbf{X}_N(t_k) \end{bmatrix} \tag{A.5.7}$$

The global system model is:

$$\mathbf{X}(t_{k+1}) = \Phi(t_{k+1},t_k)\mathbf{X}(t_k) + \mathbf{G}(t_k)\mathbf{w}(t_k) \tag{A.5.8}$$

$$\mathbf{Z}(t_k) = \mathbf{H}(t_k)\mathbf{X}(t_k) + \mathbf{v}(t_k) \tag{A.5.9}$$

where:

$$\Phi(t_{k+1},t_k) = \begin{bmatrix} \Phi_1(t_{k+1},t_k) & \cdots & 0 \\ \vdots & \ddots & \vdots \\ 0 & \cdots & \Phi_N(t_{k+1},t_k) \end{bmatrix} \tag{A.5.10}$$

$$\mathbf{H}(t_k) = \begin{bmatrix} \mathbf{H}_1(t_k) & \cdots & 0 \\ \vdots & \ddots & \vdots \\ 0 & \cdots & \mathbf{H}_N(t_k) \end{bmatrix} \tag{A.5.11}$$

$$\mathbf{G}(t_k) = \begin{bmatrix} \mathbf{G}_1(t_k) \\ \cdots \\ \mathbf{G}_N(t_k) \end{bmatrix}, \quad \mathbf{Z}(t_k) = \begin{bmatrix} \mathbf{Z}_1(t_k) \\ \cdots \\ \mathbf{Z}_N(t_k) \end{bmatrix}, \quad \mathbf{v}(t_k) = \begin{bmatrix} \mathbf{v}_1(t_k) \\ \cdots \\ \mathbf{v}_N(t_k) \end{bmatrix} \tag{A.5.12}$$

The one-step prediction of the estimate covariance of the global system is:

$$\mathbf{P}(t_k^-) = \Phi(t_k,t_{k-1})\mathbf{P}(t_{k-1})\Phi^T(t_k,t_{k-1}) + \mathbf{G}(t_{k-1})\mathbf{Q}(t_{k-1})\mathbf{G}^T(t_{k-1}) \tag{A.5.13}$$

For simplification of the global system computation, the input of the global system is decoupled by a diagonally-blocked system noise matrix with its upper

bounds:

$$\mathbf{G}(t_k)\mathbf{Q}(t_k)\mathbf{G}^T(t_k) =$$

$$\begin{bmatrix} \mathbf{G}_1(t_k) & \cdots & 0 \\ \vdots & \ddots & \vdots \\ 0 & \cdots & \mathbf{G}_N(t_k) \end{bmatrix} \begin{bmatrix} \mathbf{Q}(t_k) & \cdots & \mathbf{Q}(t_k) \\ \vdots & \ddots & \vdots \\ \mathbf{Q}(t_k) & \cdots & \mathbf{Q}(t_k) \end{bmatrix} \begin{bmatrix} \mathbf{G}_1^T(t_k) & \cdots & 0 \\ \vdots & \ddots & \vdots \\ 0 & \cdots & \mathbf{G}_N^T(t_k) \end{bmatrix}$$

$$\leq \begin{bmatrix} \gamma_1 \mathbf{G}_1(t_k)\mathbf{Q}(t_k)\mathbf{G}_1^T(t_k) & \cdots & 0 \\ \vdots & \ddots & \vdots \\ 0 & \cdots & \gamma_N \mathbf{G}_N(t_k)\mathbf{Q}(t_k)\mathbf{G}_N^T(t_k) \end{bmatrix} = \mathbf{B}(t_k) \tag{A.5.14}$$

where:

$$\frac{1}{\gamma_1} + \cdots + \frac{1}{\gamma_N} = 1 \; ; \; \gamma_{avg} = N \; ; \; 0 \leq \frac{1}{\gamma_i} \leq 1, i = 1 \cdots N \tag{A.5.15}$$

Generally γ_i can be chosen to be equal to N. The predicted covariances can now be written as:

$$\mathbf{P}(t_k^-) = \Phi(t_k, t_{k-1})\mathbf{P}(t_{k-1})\Phi^T(t_k, t_{k-1}) + \mathbf{B}(t_{k-1}) \tag{A.5.16}$$

where $\mathbf{P}(t_k^-)$ is a block diagonal matrix with diagonal elements:

$$\mathbf{P}_i(t_k^-) = \Phi_i(t_k, t_{k-1})\mathbf{P}_i(t_{k-1})\Phi_i^T(t_k, t_{k-1}) + \gamma_i \mathbf{G}_i(t_{k-1})\mathbf{Q}(t_{k-1})\mathbf{G}_i^T(t_{k-1}) \tag{A.5.17}$$

If the covariance of the global system initial state is not diagonal, it has to be set to its upper bounds:

$$\begin{bmatrix} \mathbf{P}(t_0) & \cdots & \mathbf{P}(t_0) \\ \vdots & \ddots & \vdots \\ \mathbf{P}(t_0) & \cdots & \mathbf{P}(t_0) \end{bmatrix} \leq \begin{bmatrix} \gamma_1 \mathbf{P}(t_0) & \cdots & 0 \\ \vdots & \ddots & \vdots \\ 0 & \cdots & \gamma_N \mathbf{P}(t_0) \end{bmatrix} \tag{A.5.18}$$

where $\mathbf{P}(t_0)$ is the covariance of the initial state of the local systems.

Using eqns (A.5.16) to (A.5.18), the covariance of the global estimate $\mathbf{P}(t_k)$ is a block diagonal matrix, and the global estimate can be obtained from the Least Squares solution to minimize the performance index:

$$PI = \sum_{i=1}^{N} \left[\hat{\mathbf{X}}_i(t_k) - \hat{\mathbf{X}}_i^g(t_k)\right]^T \mathbf{P}_i^{-1}(t_k)\left[\hat{\mathbf{X}}_i(t_k) - \hat{\mathbf{X}}_i^g(t_k)\right] \tag{A.5.19}$$

where the global estimate of the ith local system state is partitioned into common and unique states:

$$\hat{\mathbf{X}}_i^g(t_k) = \begin{bmatrix} \hat{\mathbf{X}}_c^g(t_k) \\ \hat{\mathbf{X}}_{iu}^g(t_k) \end{bmatrix} \tag{A.5.18}$$

$$\mathbf{P}_i(t_k) = \begin{bmatrix} \mathbf{P}_{i,c}(t_k) & \mathbf{P}_{i,cu}(t_k) \\ \mathbf{P}_{i,uc}(t_k) & \mathbf{P}_{i,u}(t_k) \end{bmatrix} \tag{A.5.19}$$

$$\mathbf{P}_{i,c}(t_k) = E\left\{\left[\mathbf{X}_c(t_k) - \hat{\mathbf{X}}_{ic}(t_k)\right]\left[\mathbf{X}_c(t_k) - \hat{\mathbf{X}}_{ic}(t_k)\right]^T\right\} \tag{A.5.20}$$

$$\mathbf{P}_{i,cu}(t_k) = E\left\{\left[\mathbf{X}_c(t_k) - \hat{\mathbf{X}}_{ic}(t_k)\right]\left[\mathbf{X}_{iu}(t_k) - \hat{\mathbf{X}}_{iu}(t_k)\right]^T\right\} \tag{A.5.21}$$

$$\mathbf{P}_{i,uc}(t_k) = \mathbf{P}_{i,cu}^T(t_k) \tag{A.5.22}$$

$$\mathbf{P}_{i,u}(t_k) = E\left\{\left[\mathbf{X}_{iu}(t_k) - \hat{\mathbf{X}}_{iu}(t_k)\right]\left[\mathbf{X}_{iu}(t_k) - \hat{\mathbf{X}}_{iu}(t_k)\right]^T\right\} \tag{A.5.23}$$

Assuming

$$\mathbf{P}_i^{-1}(t_k) = \begin{bmatrix} \tilde{\mathbf{P}}_{i,c}(t_k) & \tilde{\mathbf{P}}_{i,cu}(t_k) \\ \tilde{\mathbf{P}}_{i,uc}(t_k) & \tilde{\mathbf{P}}_{i,u}(t_k) \end{bmatrix} \tag{A.5.24}$$

The global estimate can be expressed as:

$$\hat{\mathbf{X}}^{g}_{iu}(t_k) = \hat{\mathbf{X}}_{iu}(t_k) + \tilde{\mathbf{P}}^{-1}_{i,u}(t_k)\tilde{\mathbf{P}}_{i,uc}(t_k)\left[\hat{\mathbf{X}}_{ic}(t_k) - \hat{\mathbf{X}}^{g}_{c}(t_k)\right] \tag{A.5.25}$$

$$\hat{\mathbf{X}}^{g}_{c}(t_k) = \left\{\sum_{i=1}^{N}\left[\tilde{\mathbf{P}}_{i,c}(t_k) + \tilde{\mathbf{P}}_{i,cu}(t_k)\tilde{\mathbf{P}}^{-1}_{i,u}(t_k)\tilde{\mathbf{P}}_{i,uc}(t_k)\right]\right\}^{-1}$$

$$\times \sum_{i=1}^{N}\left[\tilde{\mathbf{P}}_{i,c}(t_k) + \tilde{\mathbf{P}}_{i,cu}(t_k)\tilde{\mathbf{P}}^{-1}_{i,u}(t_k)\tilde{\mathbf{P}}_{i,uc}(t_k)\right]\hat{\mathbf{X}}_{ic}(t_k) \tag{A.5.26}$$

The covariance of the global estimate is:

$$\mathbf{P}(t_k) = \begin{bmatrix} \mathbf{P}_{11}(t_k) & \cdots & \mathbf{P}_{1N}(t_k) \\ \vdots & \ddots & \vdots \\ \mathbf{P}_{N1}(t_k) & \cdots & \mathbf{P}_{NN}(t_k) \end{bmatrix} \tag{A.5.27}$$

where:

$$\mathbf{P}_{ij}(t_k) = \begin{bmatrix} \mathbf{P}_{c}(t_k) & \mathbf{P}^{T}_{juc}(t_k) \\ \mathbf{P}_{iuc}(t_k) & \mathbf{P}_{iju}(t_k) \end{bmatrix} \tag{A.5.28}$$

$$\mathbf{P}_{c}(t_k) \equiv E\left\{\left[\mathbf{X}_{c}(t_k) - \hat{\mathbf{X}}^{g}_{c}(t_k)\right]\left[\mathbf{X}_{c}(t_k) - \hat{\mathbf{X}}^{g}_{c}(t_k)\right]^{T}\right\} \tag{A.5.29}$$

$$\mathbf{P}_{iuc}(t_k) \equiv E\left\{\left[\mathbf{X}_{iu}(t_k) - \hat{\mathbf{X}}^{g}_{iu}(t_k)\right]\left[\mathbf{X}_{c}(t_k) - \hat{\mathbf{X}}^{g}_{c}(t_k)\right]^{T}\right\} \tag{A.5.30}$$

$$\mathbf{P}_{iju}(t_k) \equiv E\left\{\left[\mathbf{X}_{iu}(t_k) - \hat{\mathbf{X}}^{g}_{iu}(t_k)\right]\left[\mathbf{X}_{ju}(t_k) - \hat{\mathbf{X}}^{g}_{ju}(t_k)\right]^{T}\right\} \tag{A.5.31}$$

$$\mathbf{P}_c = \left\{\sum_{i=1}^{N}\left[\tilde{\mathbf{P}}_{i,c} + \tilde{\mathbf{P}}_{i,cu}\tilde{\mathbf{P}}_{i,u}^{-1}\tilde{\mathbf{P}}_{i,uc}\right]\right\}^{-1}$$

$$\sum_{i=1}^{N}\left[\tilde{\mathbf{P}}_{i,c} + \tilde{\mathbf{P}}_{i,cu}\tilde{\mathbf{P}}_{i,u}^{-1}\tilde{\mathbf{P}}_{i,uc}\right]\mathbf{P}_{i,c}\left[\tilde{\mathbf{P}}_{i,c} + \tilde{\mathbf{P}}_{i,cu}\tilde{\mathbf{P}}_{i,u}^{-1}\tilde{\mathbf{P}}_{i,uc}\right]^{T}$$

$$\left\{\sum_{i=1}^{N}\left[\tilde{\mathbf{P}}_{i,c} + \tilde{\mathbf{P}}_{i,cu}\tilde{\mathbf{P}}_{i,u}^{-1}\tilde{\mathbf{P}}_{i,uc}\right]\right\}^{-T} \qquad \text{(A.5.32)}$$

$$\mathbf{P}_{iuc} = \mathbf{P}_{i,ucM} + \tilde{\mathbf{P}}_{i,u}^{-1}\tilde{\mathbf{P}}_{i,uc}\mathbf{P}_{i,ccM} - \tilde{\mathbf{P}}_{i,u}^{-1}\tilde{\mathbf{P}}_{i,uc}\mathbf{P}_c \qquad \text{(A.5.33)}$$

$$\mathbf{P}_{i,ucM}^{T} = \left\{\sum_{j=1}^{N}\left[\tilde{\mathbf{P}}_{j,c} + \tilde{\mathbf{P}}_{j,cu}\tilde{\mathbf{P}}_{j,u}^{-1}\tilde{\mathbf{P}}_{j,uc}\right]\right\}^{-1}\left[\tilde{\mathbf{P}}_{i,c} + \tilde{\mathbf{P}}_{i,cu}\tilde{\mathbf{P}}_{i,u}^{-1}\tilde{\mathbf{P}}_{i,uc}\right]\mathbf{P}_{i,cu} \qquad \text{(A.5.34)}$$

$$\mathbf{P}_{i,ccM}^{T} = \left\{\sum_{j=1}^{N}\left[\tilde{\mathbf{P}}_{j,c} + \tilde{\mathbf{P}}_{j,cu}\tilde{\mathbf{P}}_{j,u}^{-1}\tilde{\mathbf{P}}_{j,uc}\right]\right\}^{-1}\left[\tilde{\mathbf{P}}_{i,c} + \tilde{\mathbf{P}}_{i,cu}\tilde{\mathbf{P}}_{i,u}^{-1}\tilde{\mathbf{P}}_{i,uc}\right]\mathbf{P}_{i,c} \qquad \text{(A.5.35)}$$

for i = j

$$\begin{aligned}\mathbf{P}_{iju} = \mathbf{P}_{iu} &+ \mathbf{P}_{iuc}\tilde{\mathbf{P}}_{i,cu}\tilde{\mathbf{P}}_{i,u}^{-1} + \tilde{\mathbf{P}}_{i,u}^{-1}\tilde{\mathbf{P}}_{i,uc}\mathbf{P}_{icu} - \mathbf{P}_{i,ccM}\tilde{\mathbf{P}}_{i,cu}\tilde{\mathbf{P}}_{i,u}^{-1} \\ &- \tilde{\mathbf{P}}_{i,u}^{-1}\tilde{\mathbf{P}}_{i,uc}\mathbf{P}_{i,ucM}^{T} + \tilde{\mathbf{P}}_{i,u}^{-1}\tilde{\mathbf{P}}_{i,uc}\mathbf{P}_{ic}\tilde{\mathbf{P}}_{i,cu}\tilde{\mathbf{P}}_{i,u}^{-1} \\ &- \tilde{\mathbf{P}}_{i,u}^{-1}\tilde{\mathbf{P}}_{i,uc}\mathbf{P}_{i,ucM}\tilde{\mathbf{P}}_{i,cu}\tilde{\mathbf{P}}_{i,u}^{-1} - \tilde{\mathbf{P}}_{i,u}^{-1}\tilde{\mathbf{P}}_{i,uc}\mathbf{P}_{i,ucM}^{T}\tilde{\mathbf{P}}_{i,cu}\tilde{\mathbf{P}}_{i,u}^{-1} \\ &+ \tilde{\mathbf{P}}_{i,u}^{-1}\tilde{\mathbf{P}}_{i,uc}\mathbf{P}_c\tilde{\mathbf{P}}_{i,cu}\tilde{\mathbf{P}}_{i,u}^{-1}\end{aligned} \qquad \text{(A.5.36)}$$

for $i \neq j$

$$\mathbf{P}_{iju} = - \mathbf{P}_{i,ucM}\tilde{\mathbf{P}}_{i,cu}\tilde{\mathbf{P}}_{i,u}^{-1} - \tilde{\mathbf{P}}_{i,u}^{-1}\tilde{\mathbf{P}}_{i,uc}\mathbf{P}_{i,ccM}\tilde{\mathbf{P}}_{j,cu}\tilde{\mathbf{P}}_{j,u}^{-1}$$
$$- \tilde{\mathbf{P}}_{i,u}^{-1}\tilde{\mathbf{P}}_{i,uc}\mathbf{P}_{i,ccM}^{T} - \tilde{\mathbf{P}}_{i,u}^{-1}\tilde{\mathbf{P}}_{i,uc}\mathbf{P}_{i,ccM}^{T}\tilde{\mathbf{P}}_{j,cu}\tilde{\mathbf{P}}_{j,u}^{-1}$$
$$+ \tilde{\mathbf{P}}_{i,u}^{-1}\tilde{\mathbf{P}}_{i,uc}\mathbf{P}_{c}\tilde{\mathbf{P}}_{j,cu}\tilde{\mathbf{P}}_{j,u}^{-1} \qquad \text{(A.5.37)}$$

The estimates of the local systems are reset by the estimates of the global system, and the estimate covariances of the local systems are reset by the upper bounds to make the local systems decoupled:

$$\mathbf{P}(t_k) = \begin{bmatrix} \mathbf{P}_{11}(t_k) & \cdots & \mathbf{P}_{1N}(t_k) \\ \vdots & \ddots & \vdots \\ \mathbf{P}_{N1}(t_k) & \cdots & \mathbf{P}_{NN}(t_k) \end{bmatrix}$$
$$\leq \begin{bmatrix} \gamma_1\mathbf{P}_{11}(t_k) & \cdots & 0 \\ \vdots & \ddots & \vdots \\ 0 & \cdots & \gamma_N\mathbf{P}_{NN}(t_k) \end{bmatrix} = \mathbf{P}_{UB}(t_k) \qquad \text{(A.5.38)}$$

APPENDIX 6 PHASE AND FIR SMOOTHED CODE PLOTS

A.6.1 Phase smoothed code plots of Gas station

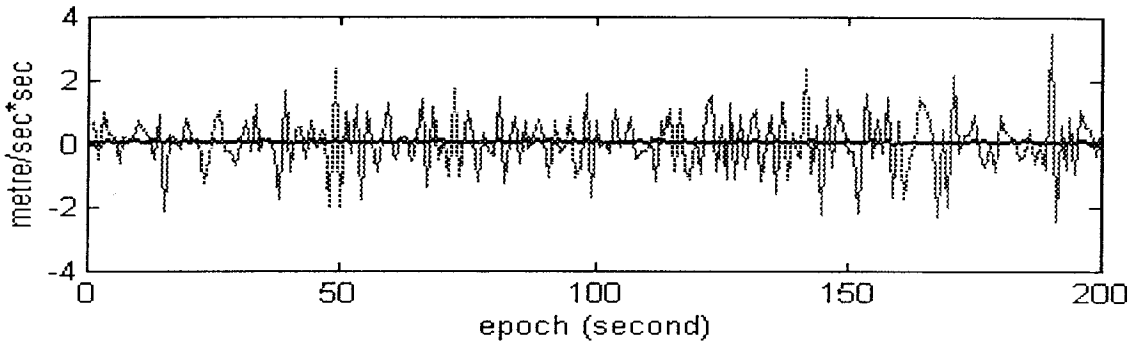

Figure A.6.1. PRN 2 accelerations of C/A and phase smoothed C/A(Gas).

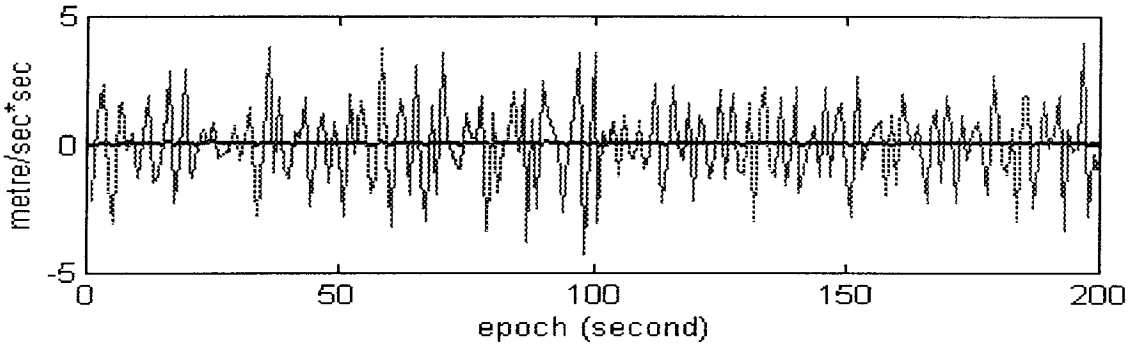

Figure A.6.2. PRN 6 accelerations of C/A and phase smoothed C/A (Gas).

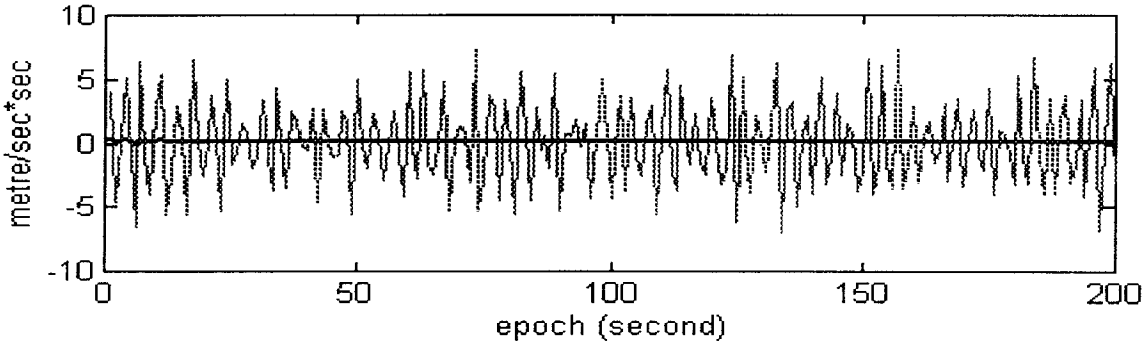

Figure A.6.3. PRN 15 accelerations of C/A and phase smoothed C/A (Gas).

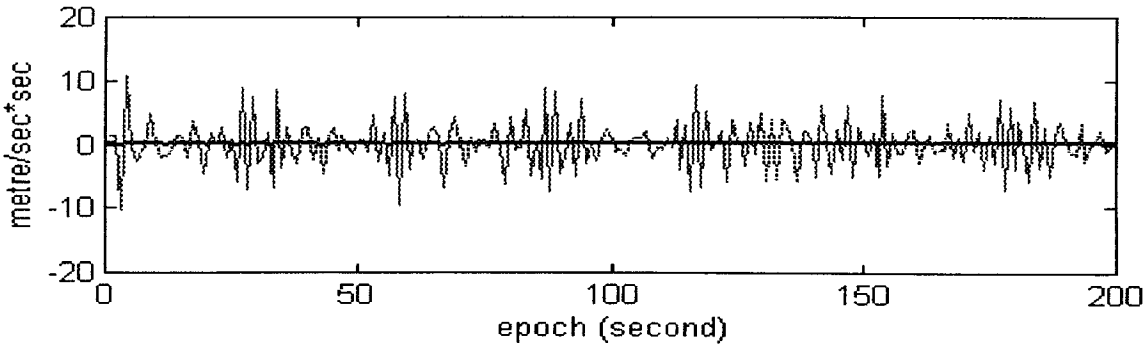

Figure A.6.4. PRN 19 accelerations of C/A and phase smoothed C/A (Gas).

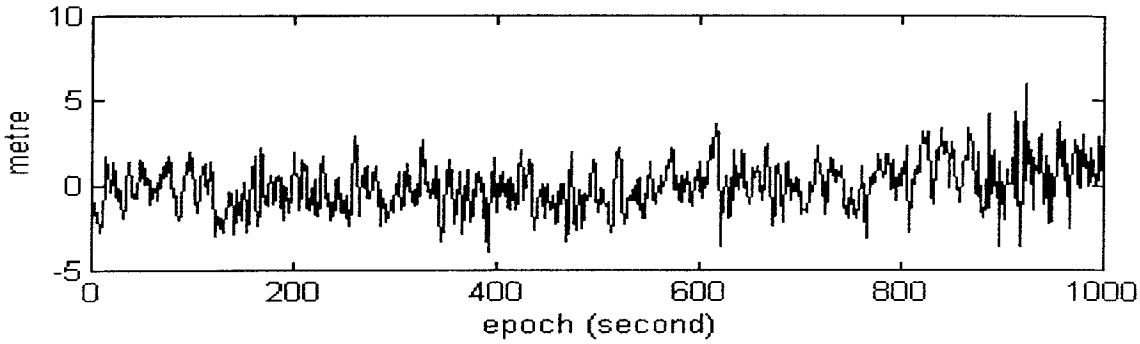

Figure A.6.5. PRN 2 phase smoothed C/A residual (Gas).

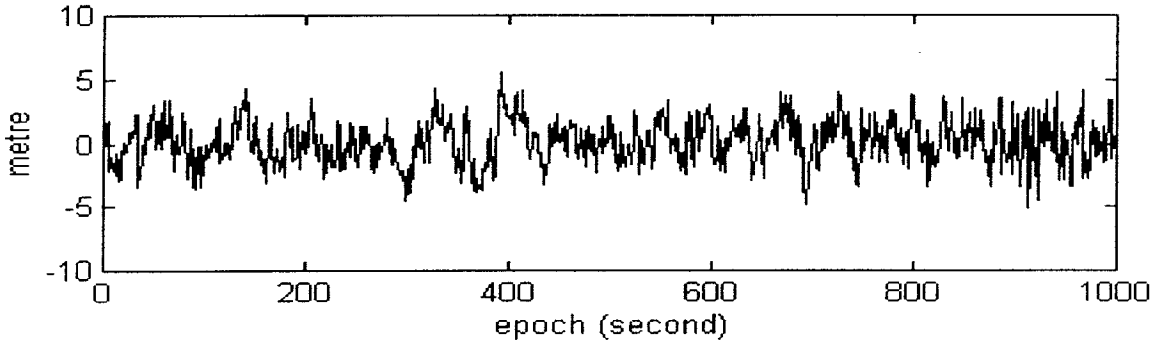

Figure A.6.6. PRN 6 phase smoothed C/A residual (Gas).

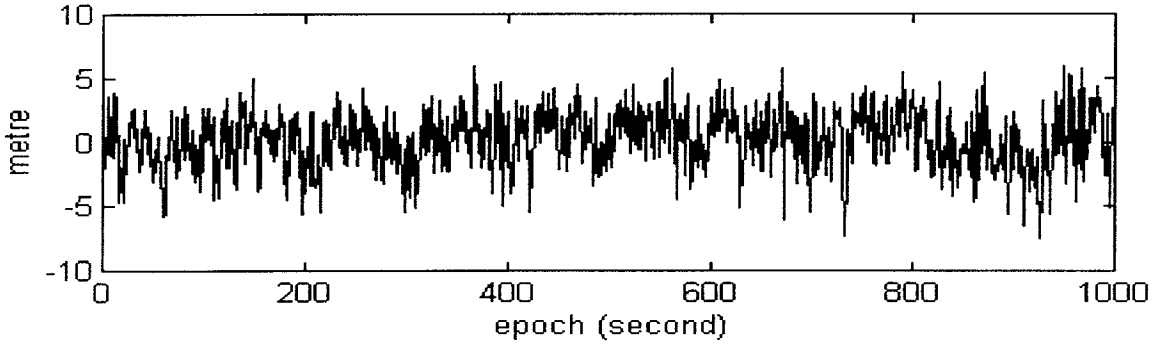

Figure A.6.7. PRN 15 phase smoothed C/A residual (Gas).

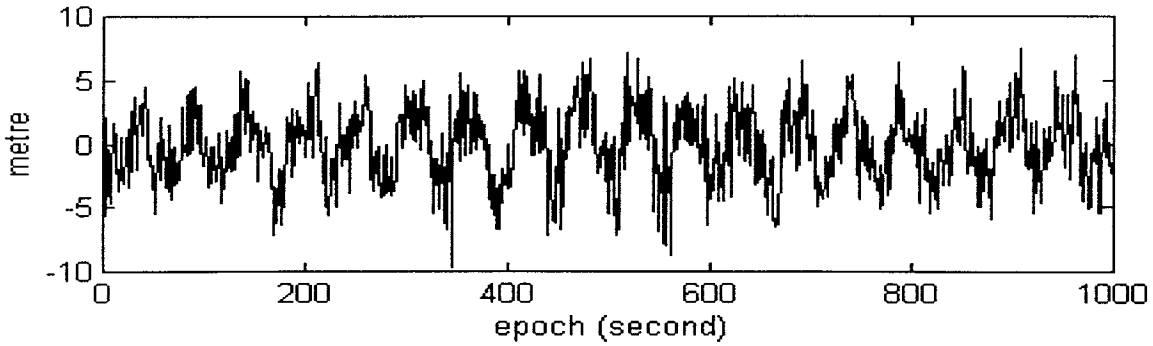

Figure A.6.8. PRN 19 phase smoothed C/A residual (Gas).

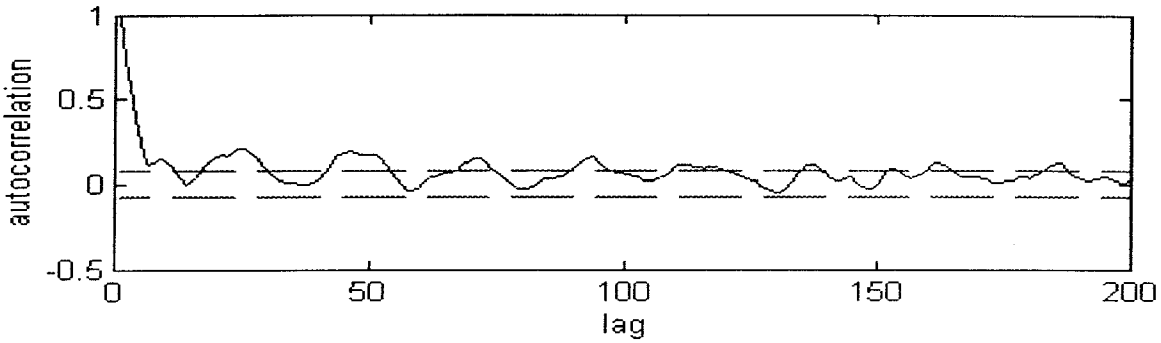

Figure A.6.9. PRN 2 phase smoothed C/A residual autocorrelation (Gas).

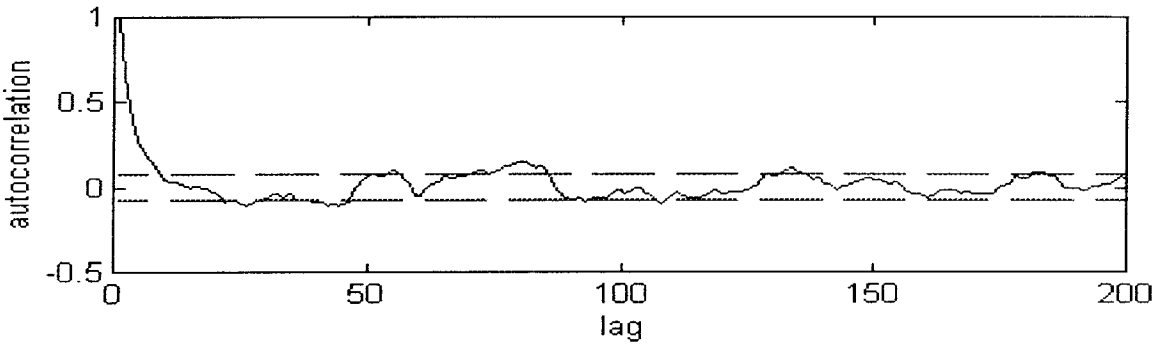

Figure A.6.10. PRN 6 phase smoothed C/A residual autocorrelation (Gas).

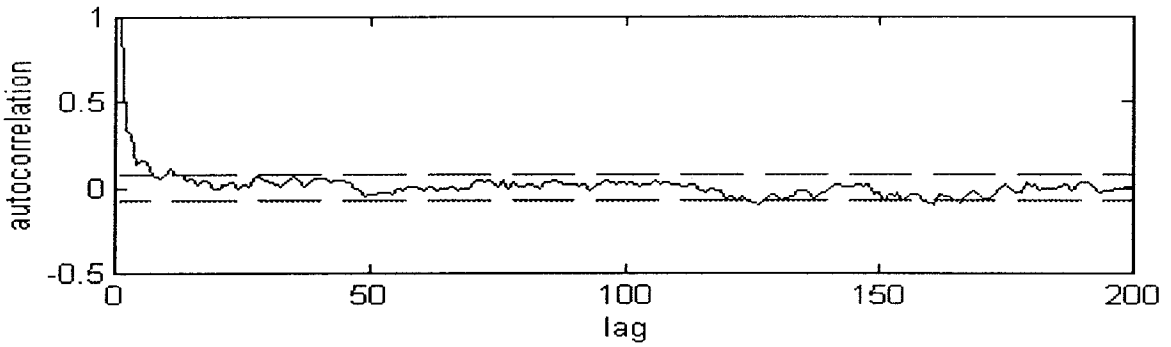

Figure A.6.11. PRN 15 phase smoothed C/A residual autocorrelation (Gas).

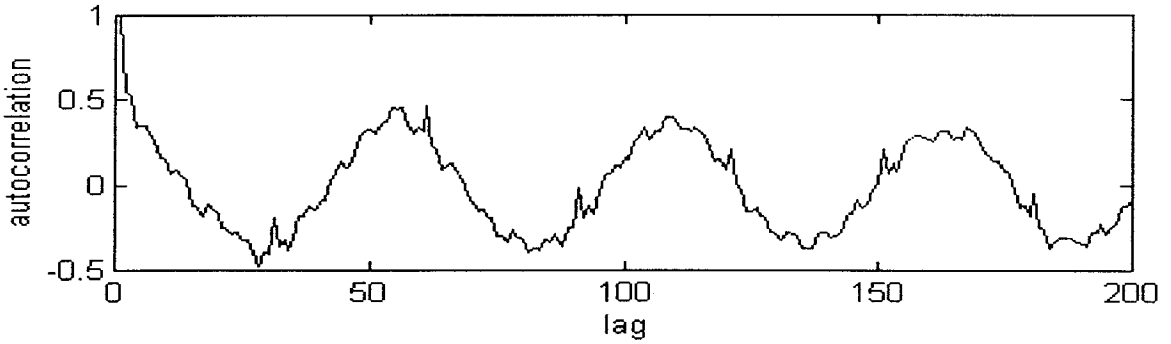

Figure A.6.12. PRN 19 phase smoothed C/A residual autocorrelation (Gas).

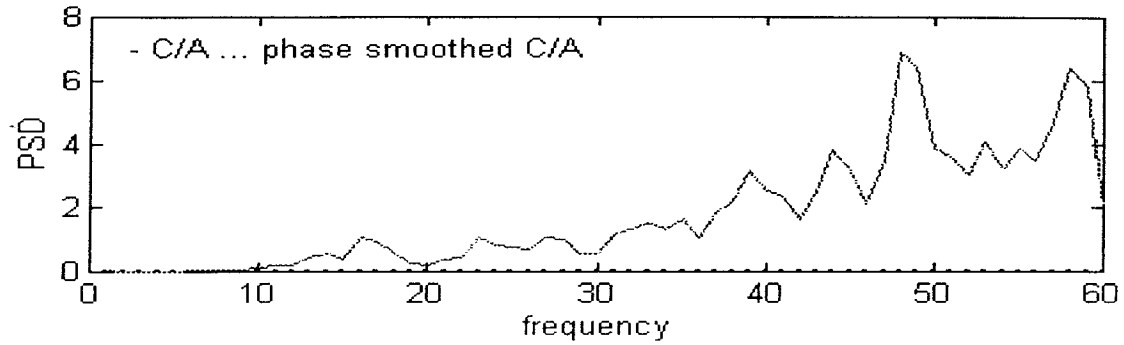

Figure A.6.13. PRN 2 PSD of C/A and phase smoothed C/A accelerations (Gas).

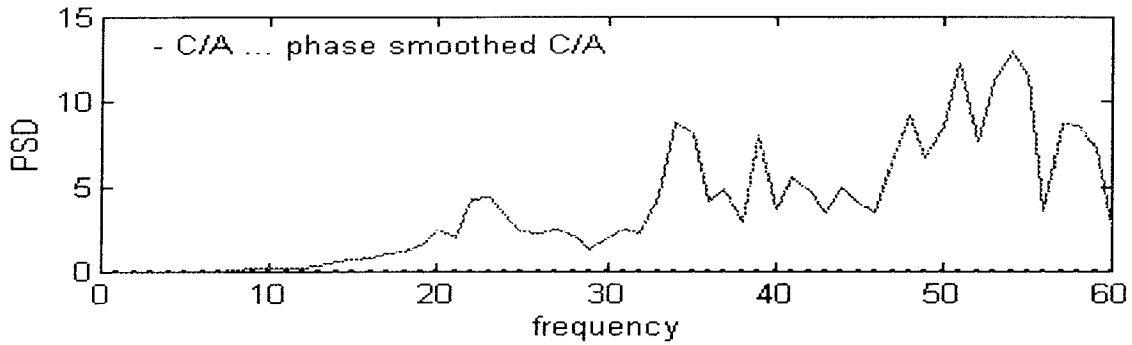

Figure A.6.14. PRN 6 PSD of C/A and phase smoothed C/A accelerations (Gas).

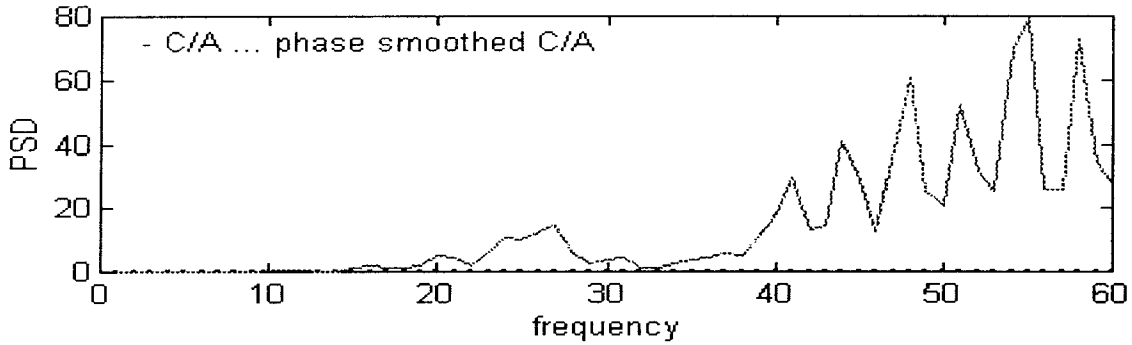

Figure A.6.15. PRN 15 PSD of C/A and phase smoothed C/A accelerations (Gas).

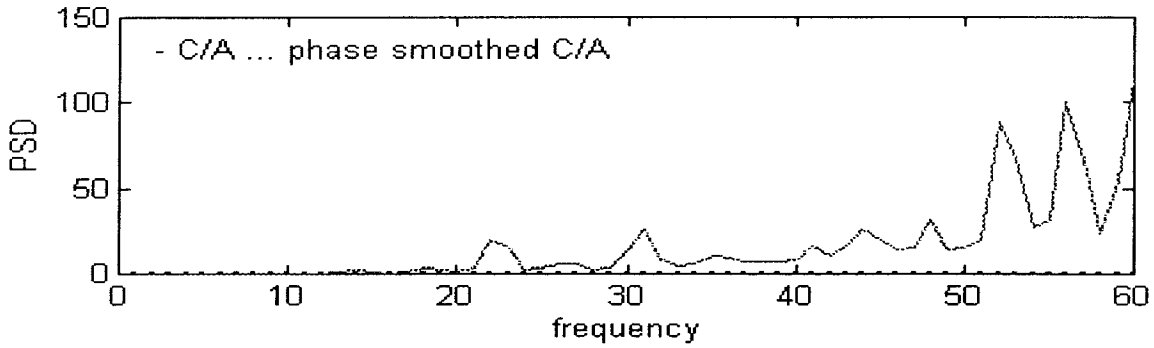

Figure A.6.16. PRN 19 PSD of C/A and phase smoothed C/A accelerations (Gas).

A.6.2 Phase smoothed code plots of Bow station

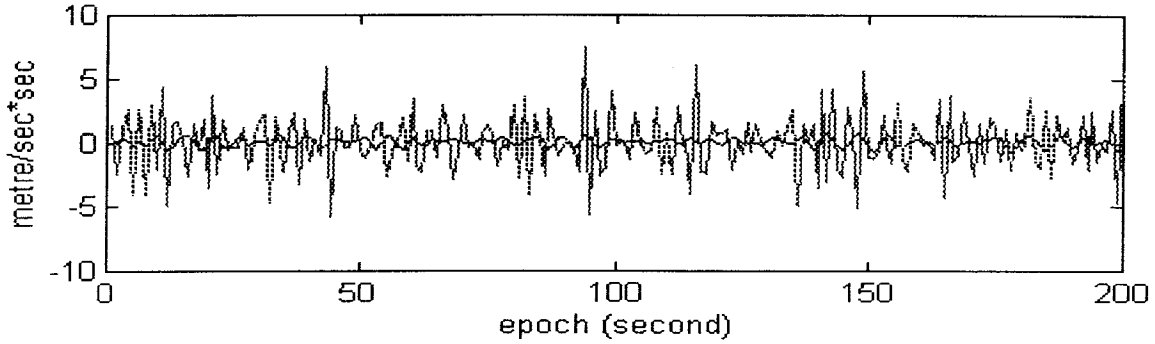

Figure A.6.17. PRN 2 accelerations of C/A and phase smoothed C/A (Bow).

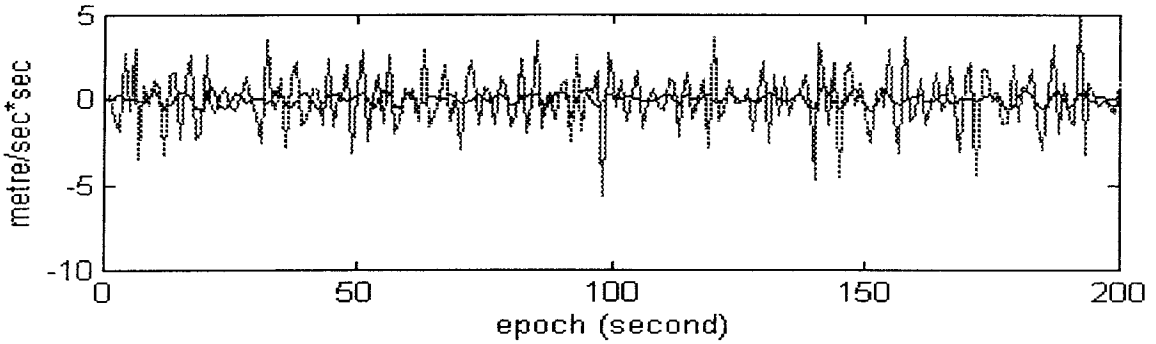

Figure A.6.18. PRN 6 accelerations of C/A and phase smoothed C/A (Bow).

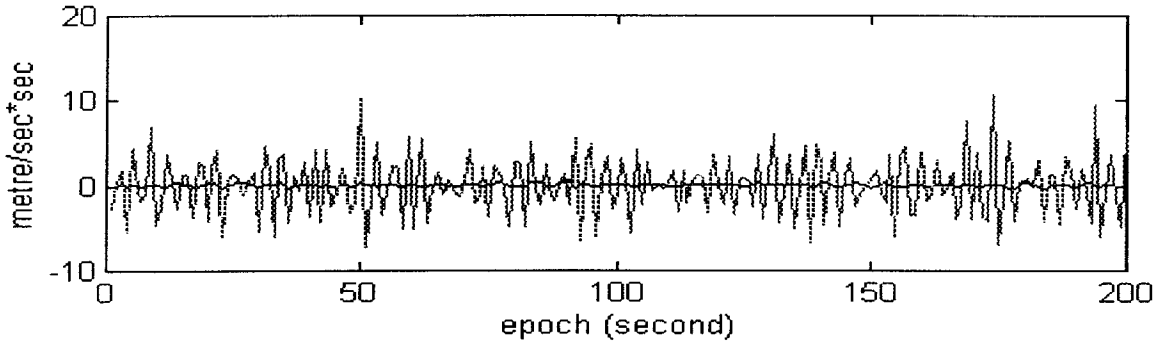

Figure A.6.19. PRN 15 accelerations of C/A and phase smoothed C/A (Bow).

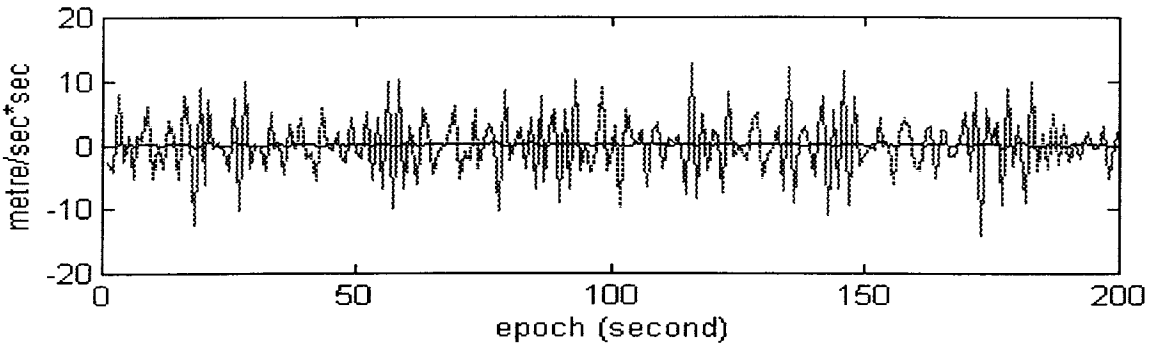

Figure A.6.20. PRN 19 accelerations of C/A and phase smoothed C/A (Bow).

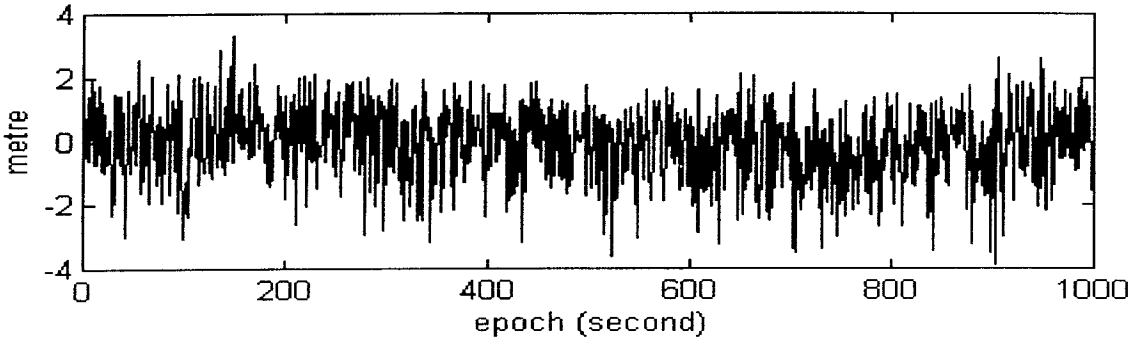

Figure A.6.21. PRN 2 phase smoothed C/A residual (Bow).

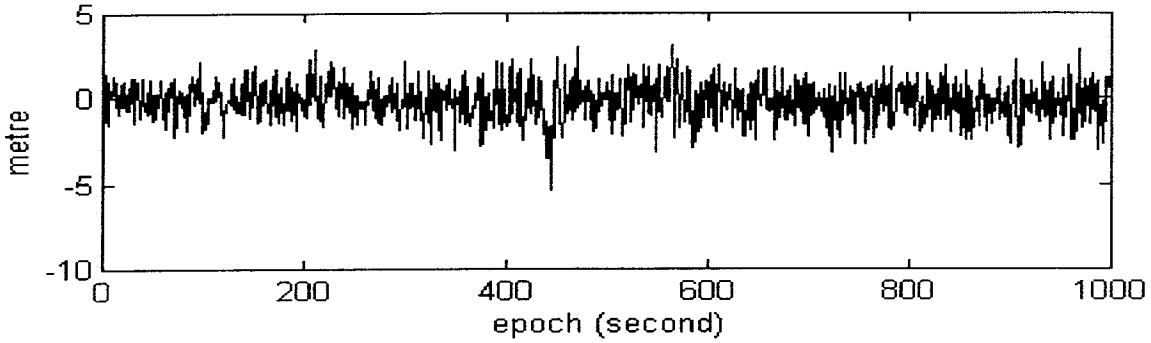

Figure A.6.22. PRN 6 phase smoothed C/A residual (Bow).

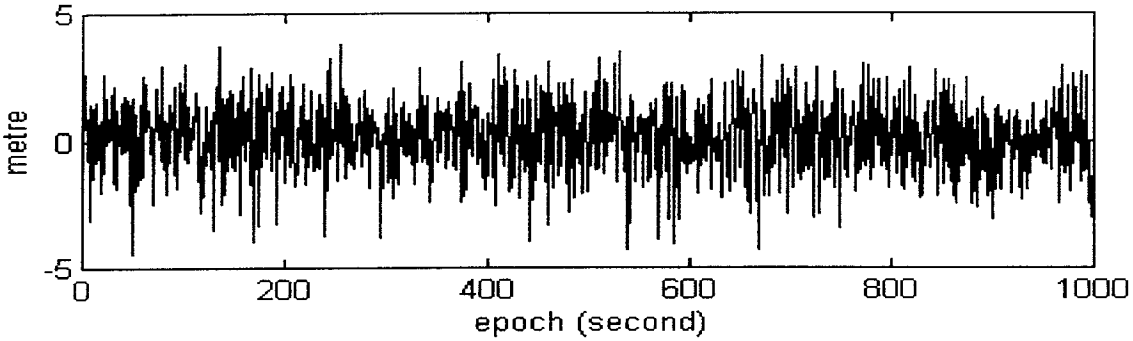

Figure A.6.23. PRN 15 phase smoothed C/A residual (Bow).

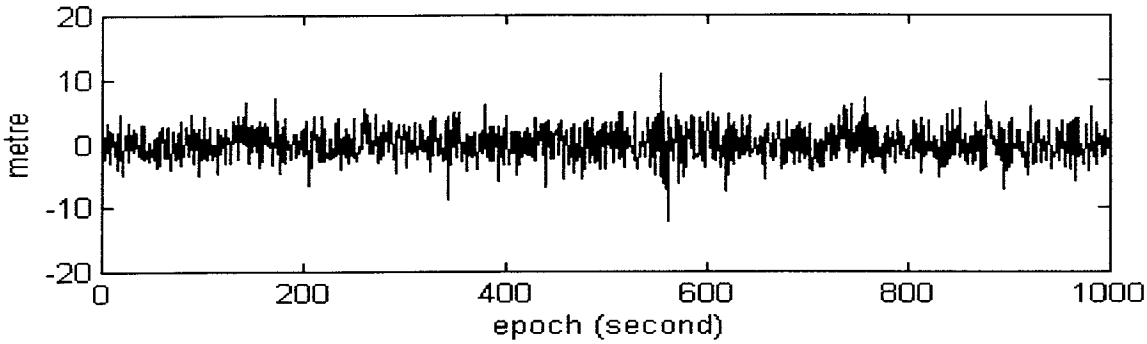

Figure A.6.24. PRN 19 phase smoothed C/A residual (Bow).

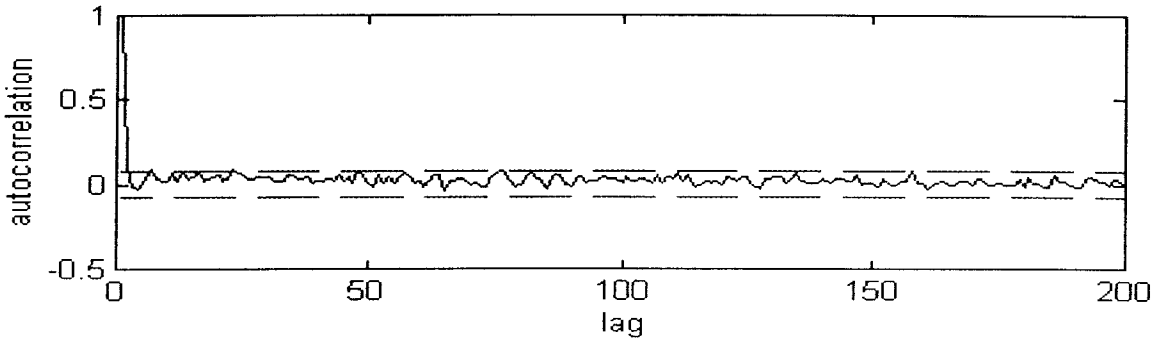

Figure A.6.25. PRN 2 phase smoothed C/A residual autocorrelation (Bow).

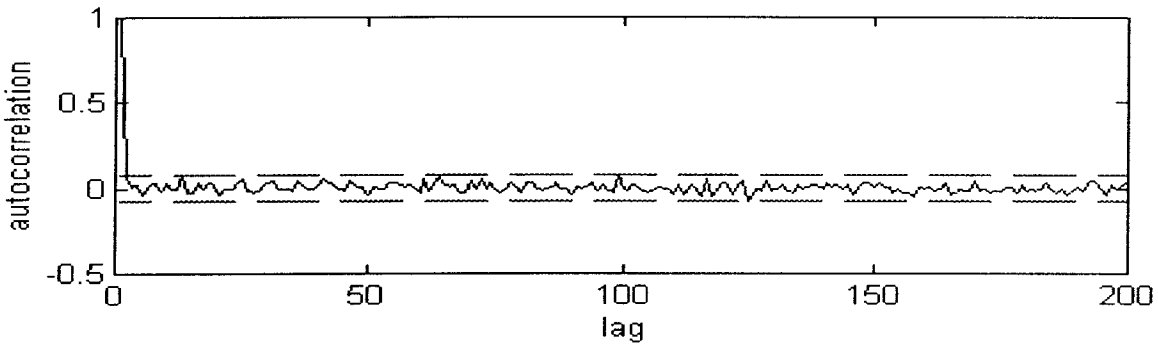

Figure A.6.26. PRN 6 phase smoothed C/A residual autocorrelation (Bow).

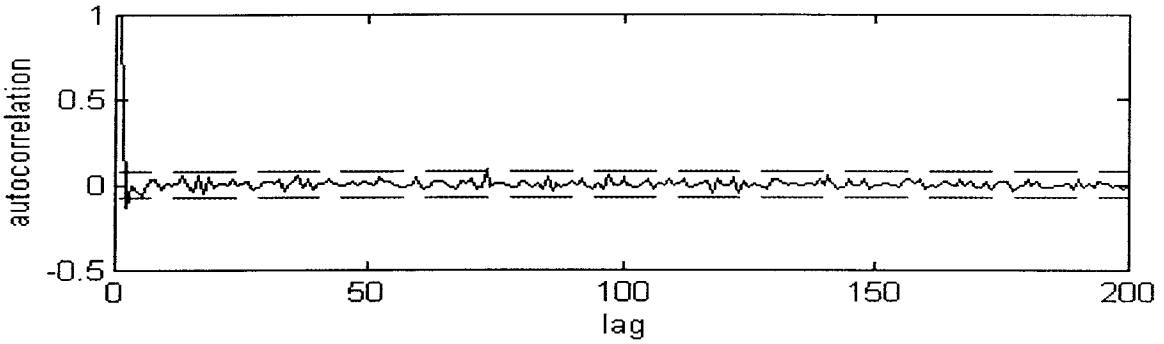

Figure A.6.27. PRN 15 phase smoothed C/A residual autocorrelation (Bow).

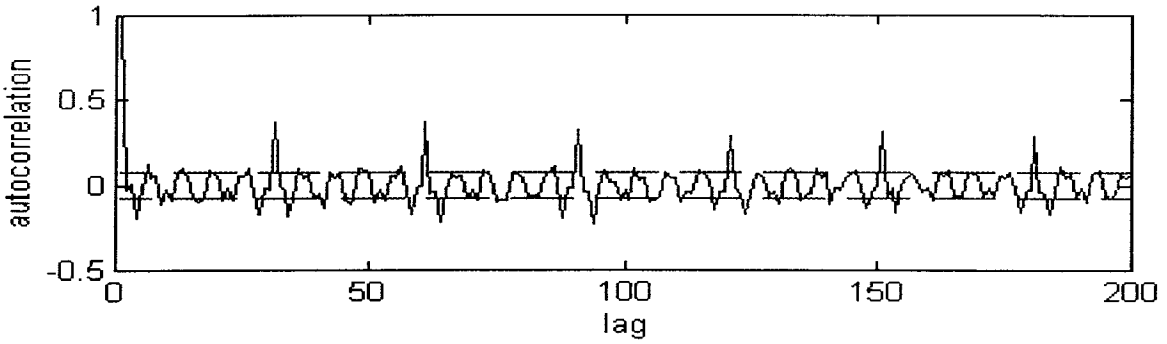

Figure A.6.28. PRN 19 phase smoothed C/A residual autocorrelation (Bow).

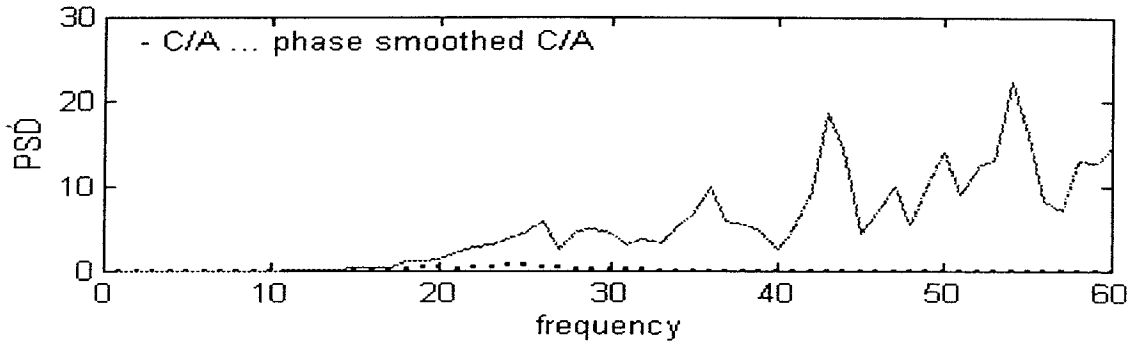

Figure A.6.29. PRN 2 PSD of C/A and phase smoothed C/A accelerations (Bow).

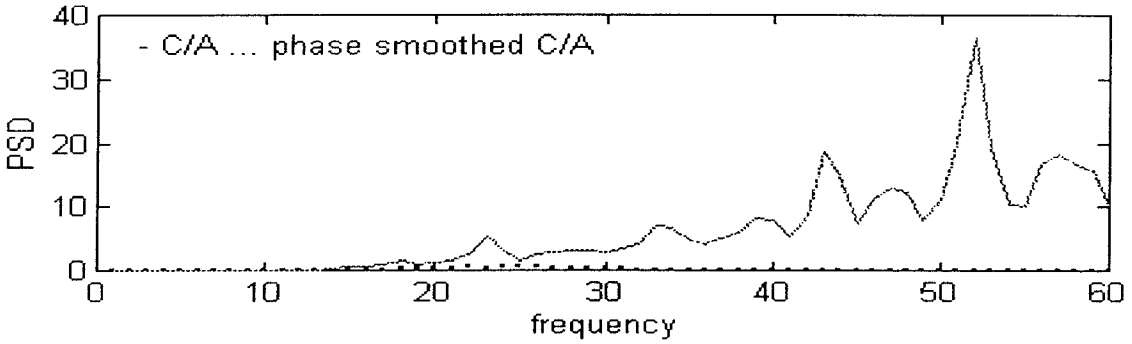

Figure A.6.30. PRN 6 PSD of C/A and phase smoothed C/A accelerations (Bow).

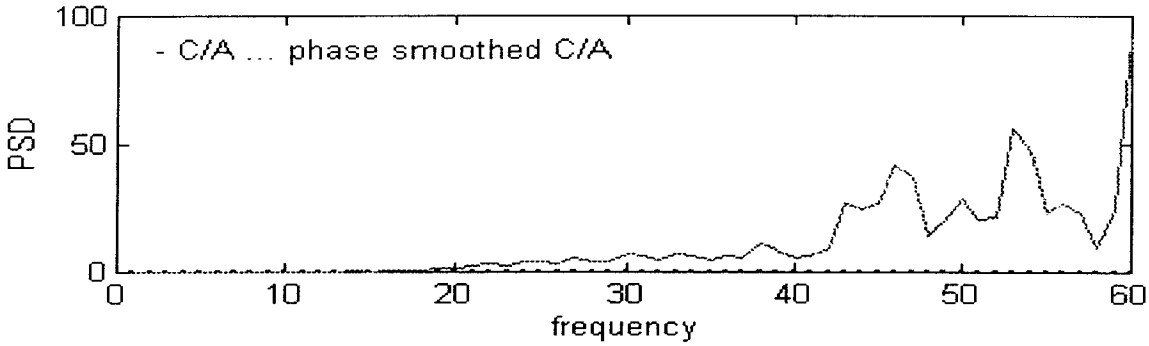

Figure A.6.31. PRN 15 PSD of C/A and phase smoothed C/A accelerations (Bow).

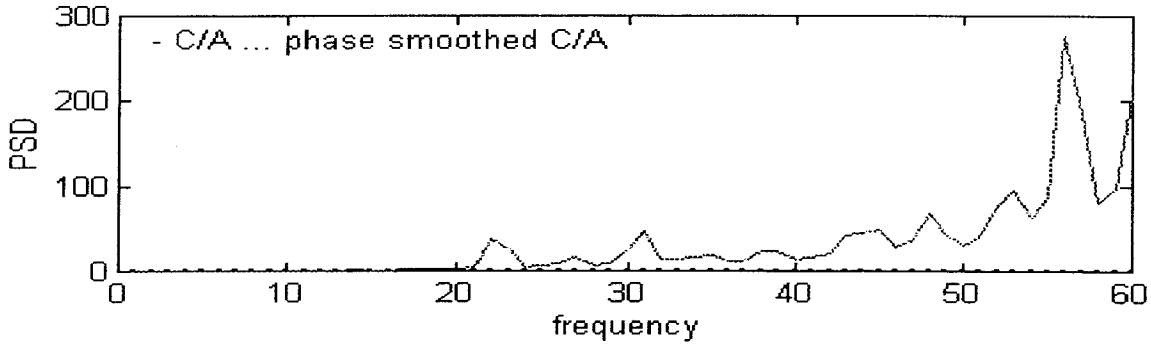

Figure A.6.32. PRN 19 PSD of C/A and phase smoothed C/A accelerations (Bow).

A.6.3 FIR smoothed code plots of Gas station

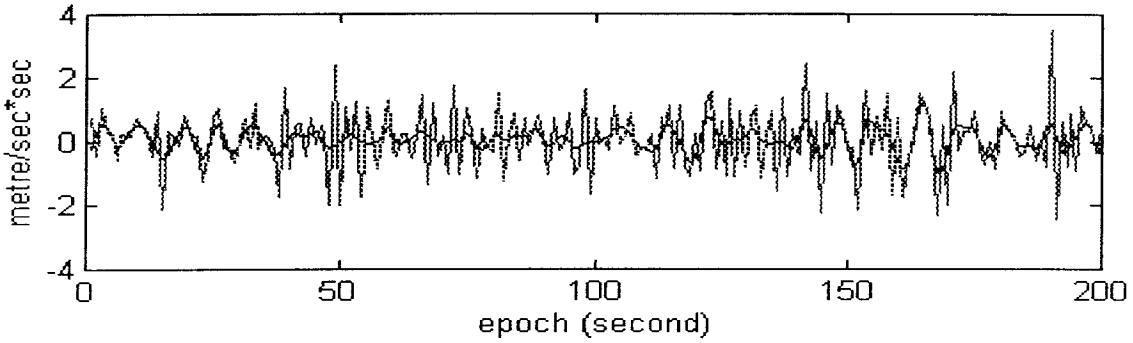

Figure A.6.33. PRN 2 accelerations of C/A and FIR smoothed C/A (Gas).

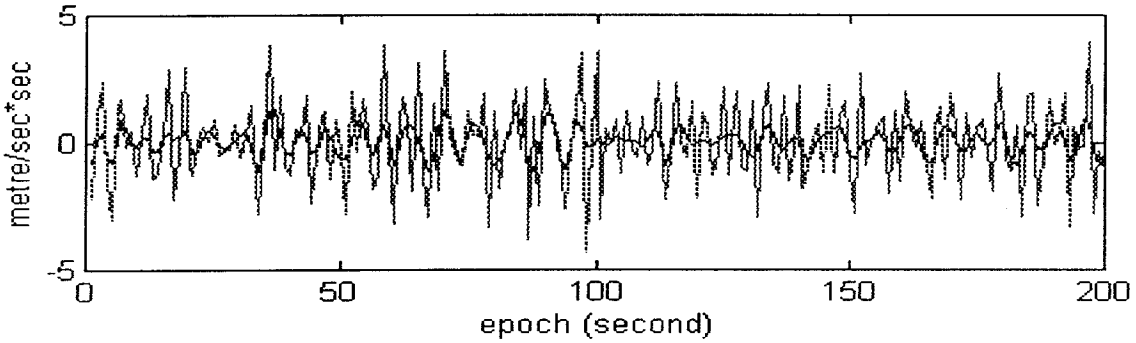

Figure A.6.34. PRN 6 accelerations of C/A and FIR smoothed C/A (Gas).

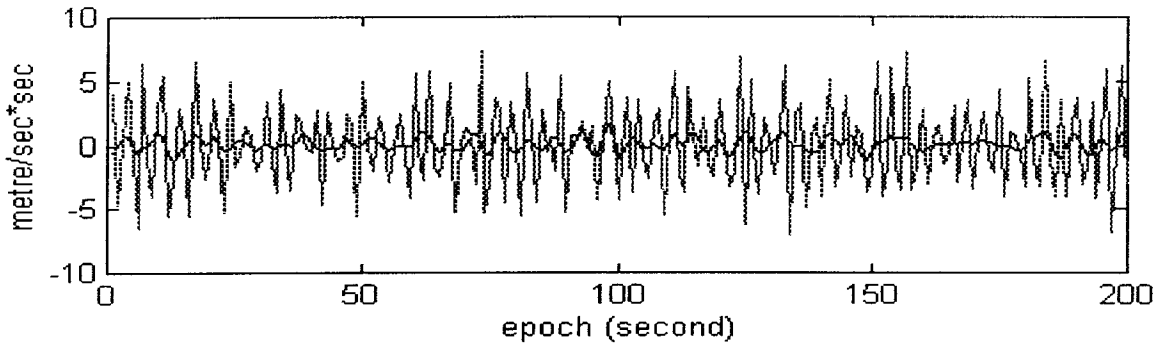

Figure A.6.35. PRN 15 accelerations of C/A and FIR smoothed C/A (Gas).

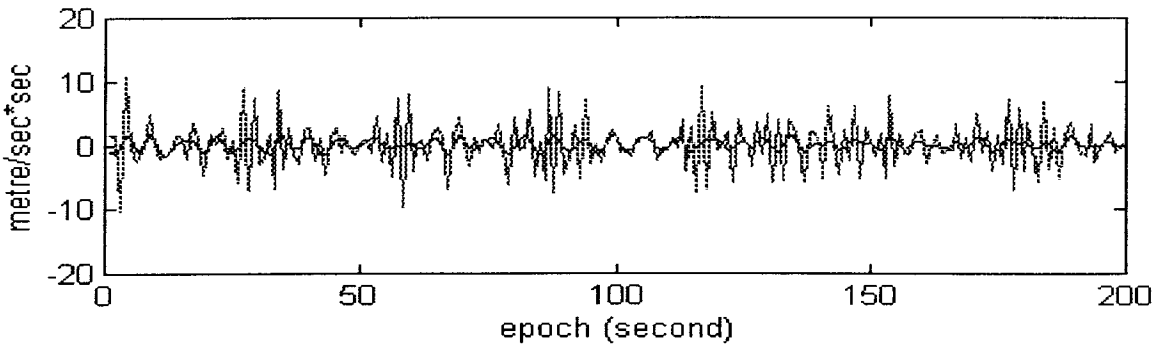

Figure A.6.36. PRN 19 accelerations of C/A and FIR smoothed C/A (Gas).

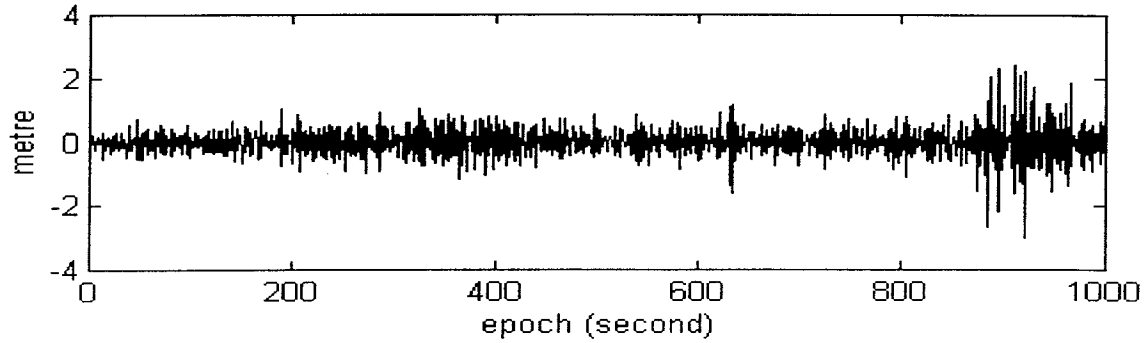

Figure A.6.37. PRN 2 FIR smoothed C/A residual (Gas).

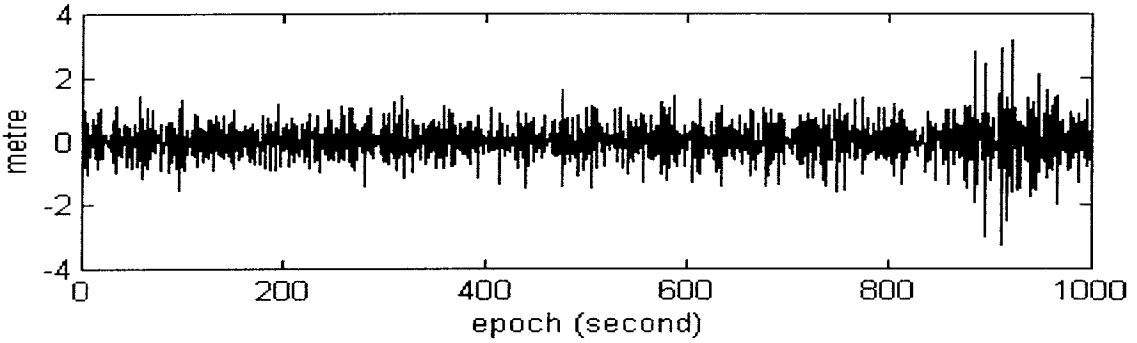

Figure A.6.38. PRN 6 FIR smoothed C/A residual (Gas).

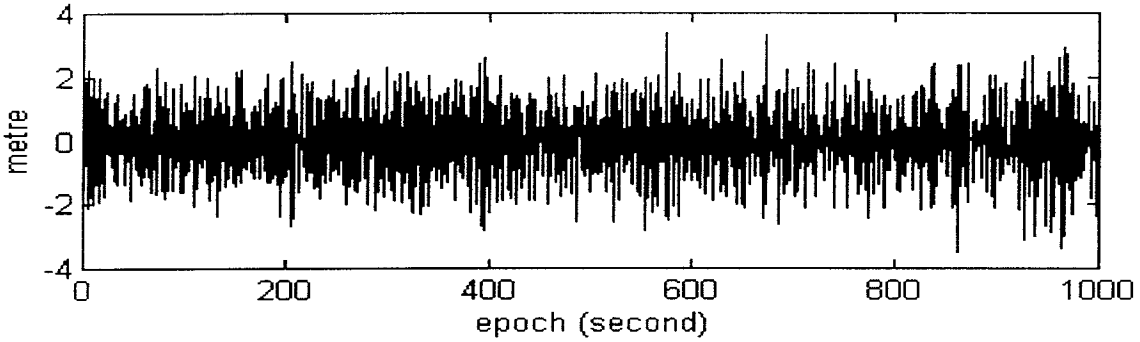

Figure A.6.39. PRN 15 FIR smoothed C/A residual (Gas).

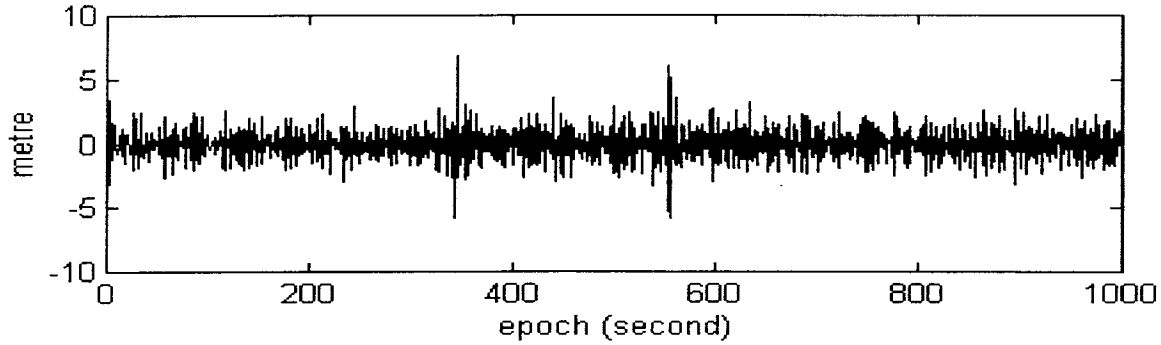

Figure A.6.40. PRN 19 FIR smoothed C/A residual (Gas).

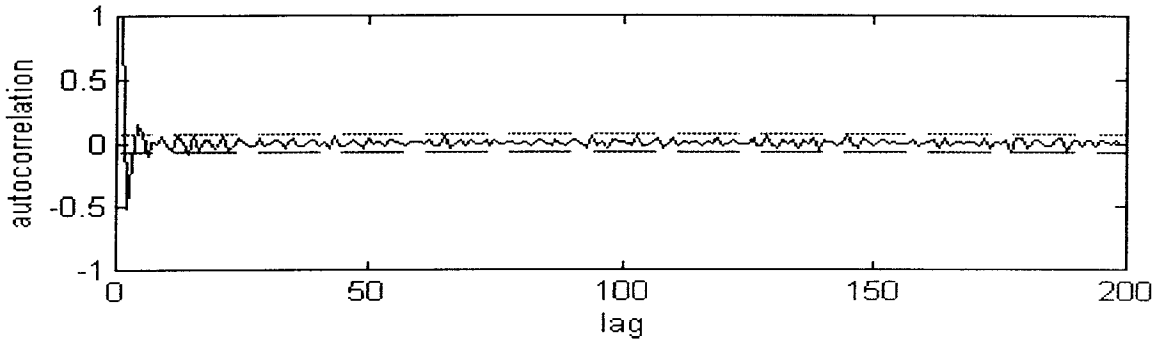

Figure A.6.41. PRN 2 FIR smoothed C/A residual autocorrelation (Gas).

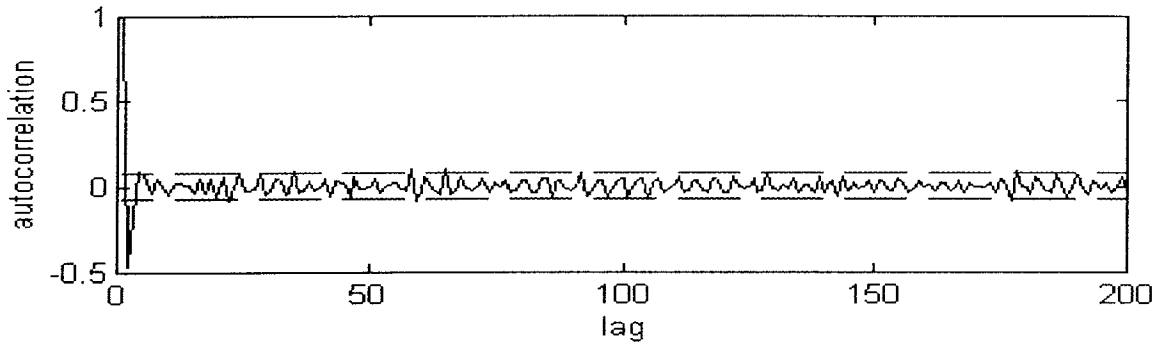

Figure A.6.42. PRN 6 FIR smoothed C/A residual autocorrelation (Gas).

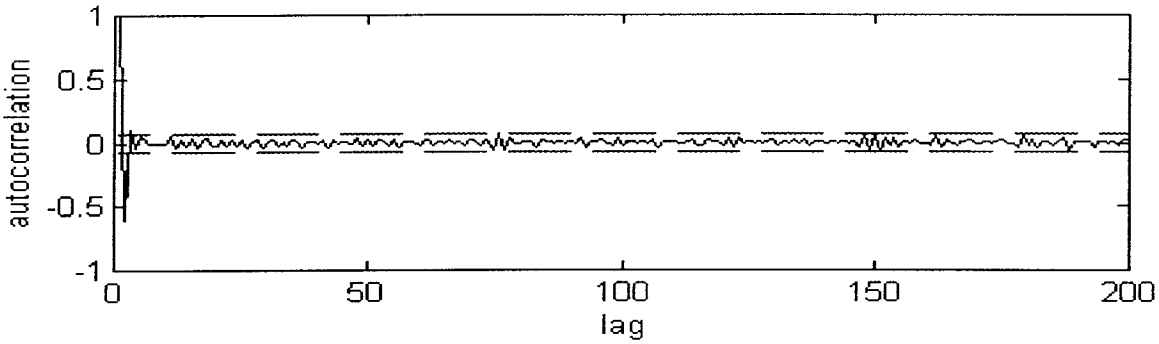

Figure A.6.43. PRN 15 FIR smoothed C/A residual autocorrelation (Gas).

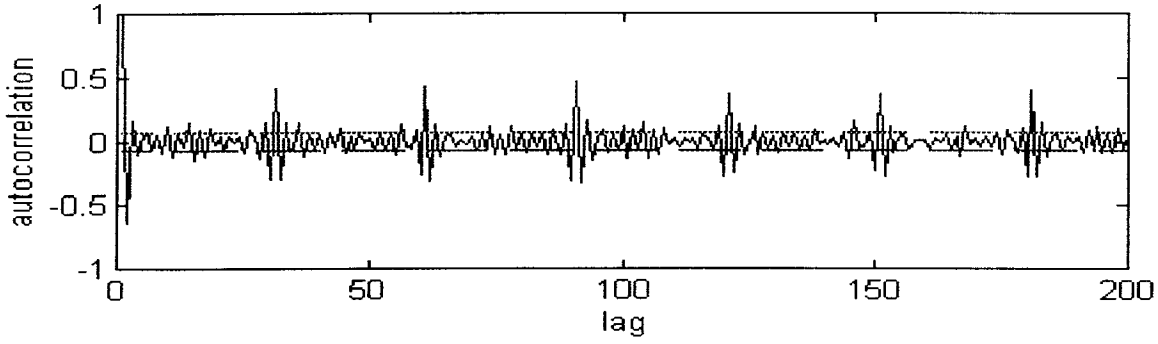

Figure A.6.44. PRN 19 FIR smoothed C/A residual autocorrelation (Gas).

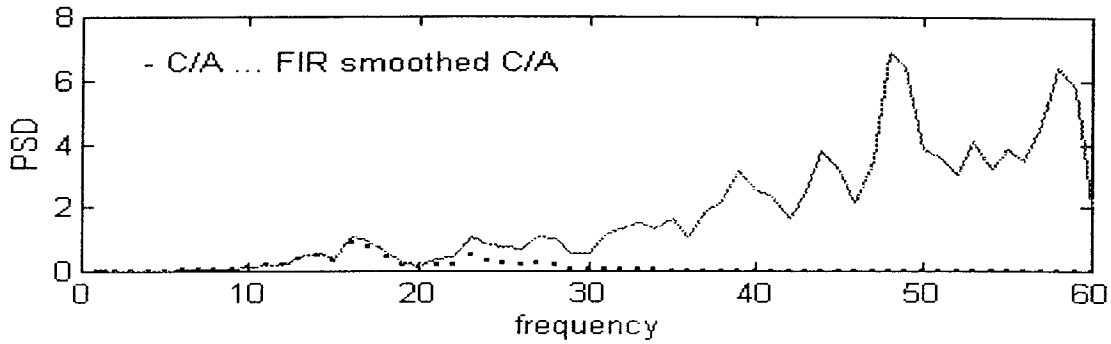

Figure A.6.45. PRN 2 PSD of C/A and FIR smoothed C/A accelerations (Gas).

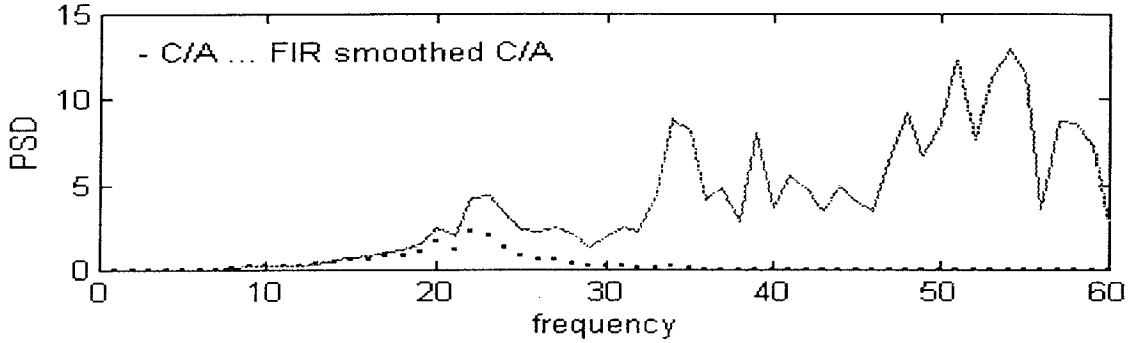

Figure A.6.46. PRN 6 PSD of C/A and FIR smoothed C/A accelerations (Gas).

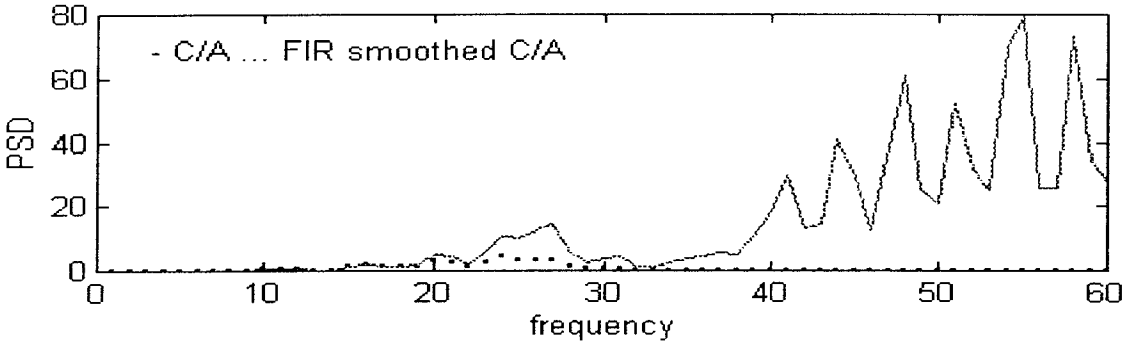

Figure A.6.47. PRN 15 PSD of C/A and FIR smoothed C/A accelerations (Gas).

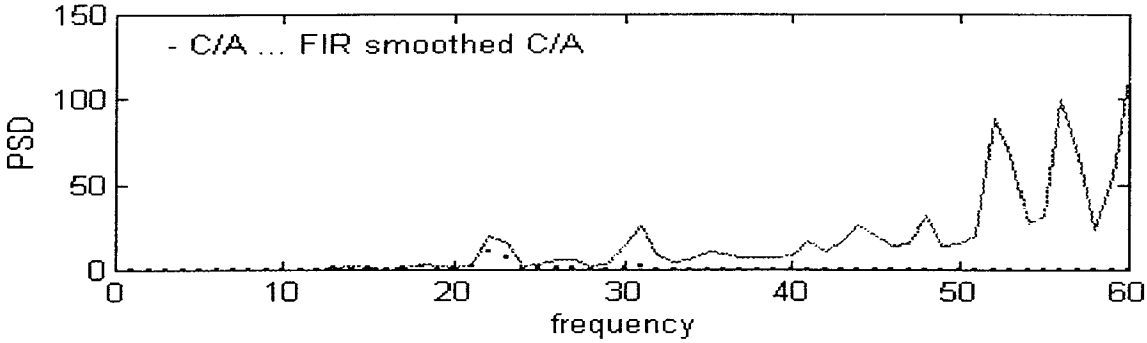

Figure A.6.48. PRN 19 PSD of C/A and FIR smoothed C/A accelerations (Gas).

A.6.4 FIR smoothed code plots of Bow station

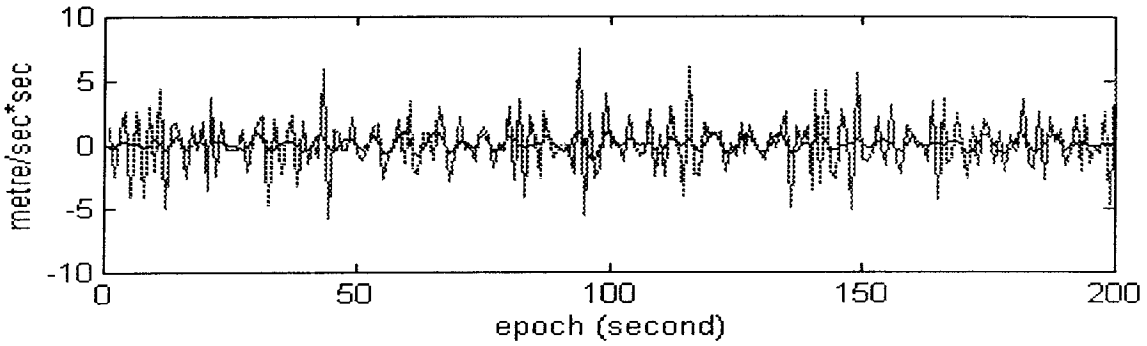

Figure A.6.49. PRN 2 accelerations of C/A and FIR smoothed C/A (Bow).

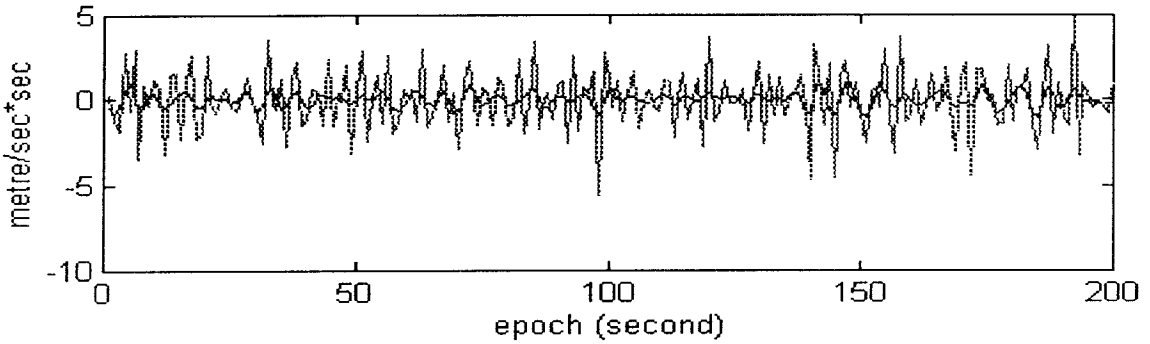

Figure A.6.50. PRN 6 accelerations of C/A and FIR smoothed C/A (Bow).

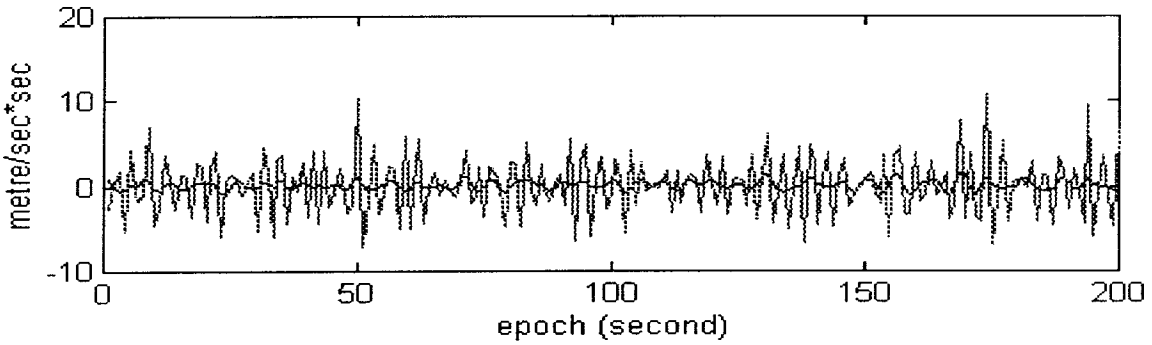

Figure A.6.51. PRN 15 accelerations of C/A and FIR smoothed C/A (Bow).

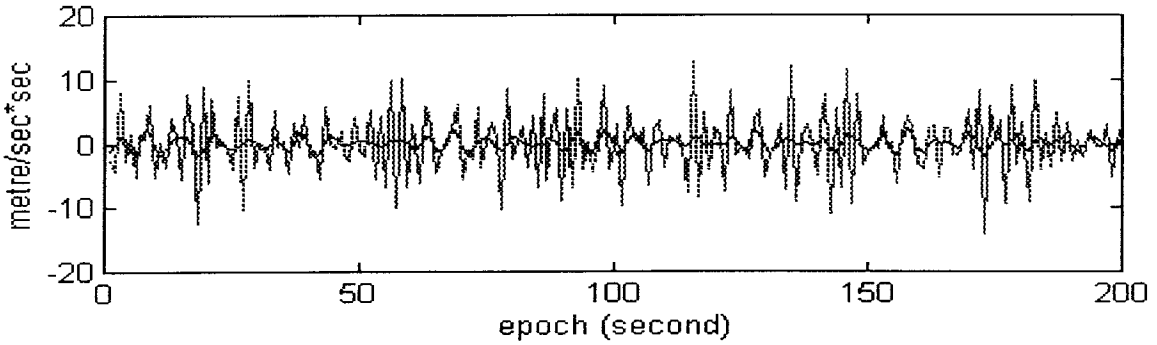

Figure A.6.52. PRN 19 accelerations of C/A and FIR smoothed C/A (Bow).

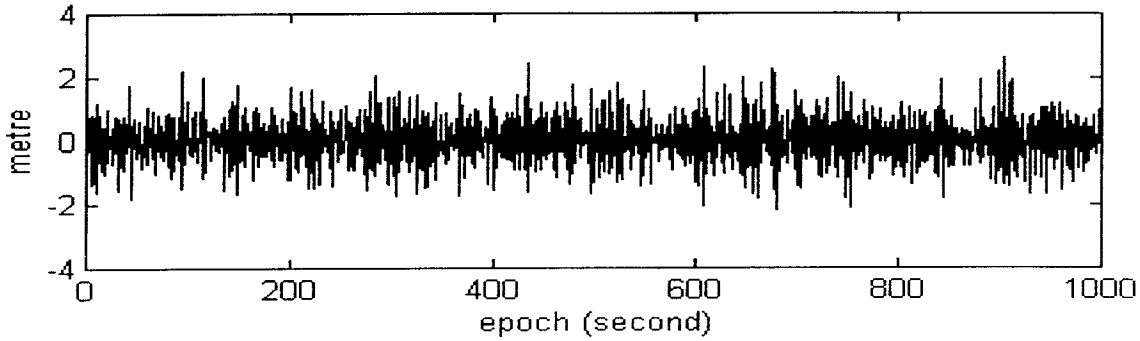

Figure A.6.53. PRN 2 FIR smoothed C/A residual (Bow).

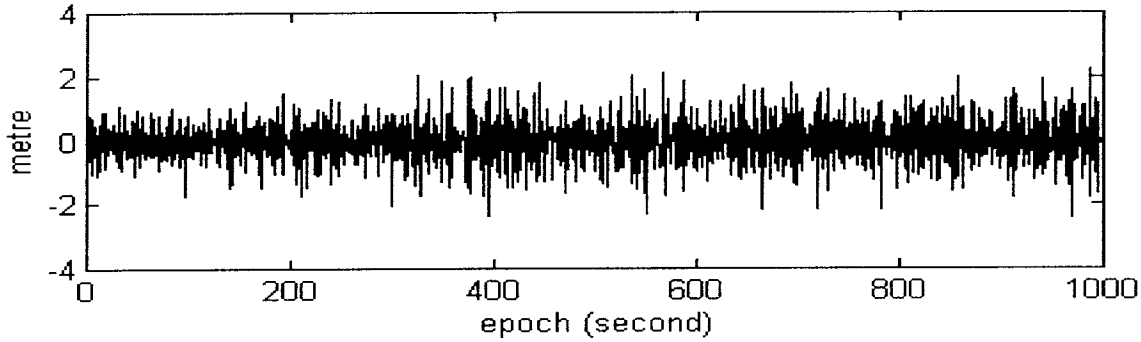

Fig.A.6.54. PRN 6 FIR smoothed C/A residual (Bow).

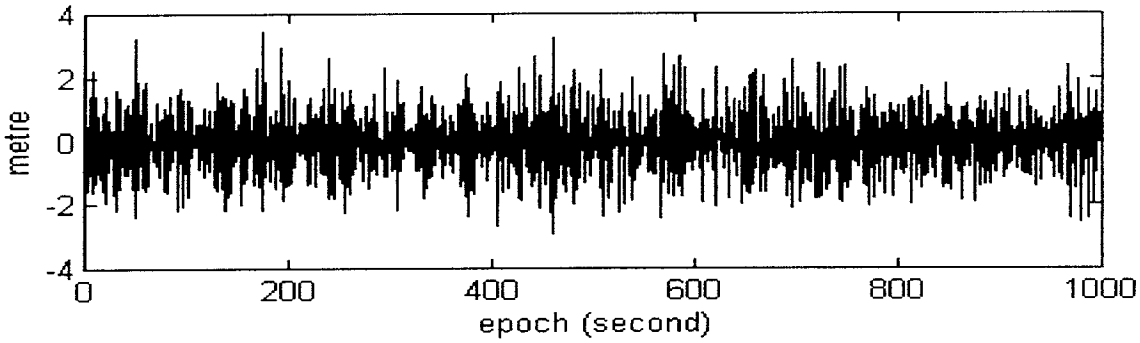

Figure A.6.55. PRN 15 FIR smoothed C/A residual (Bow).

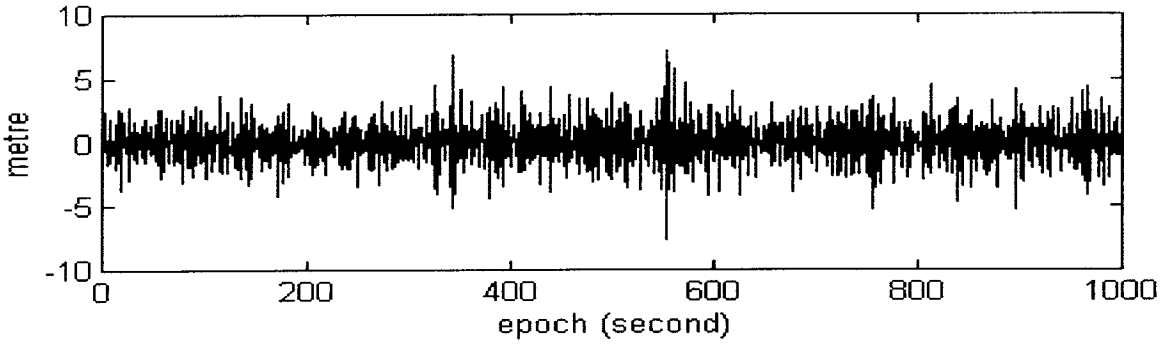

Figure A.6.56. PRN 19 FIR smoothed C/A residual (Bow).

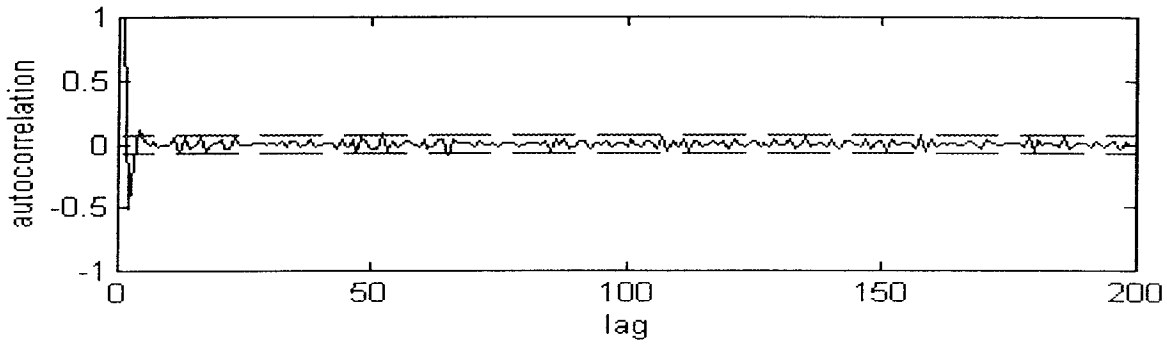

Figure A.6.57. PRN 2 FIR smoothed C/A residual autocorrelation (Bow).

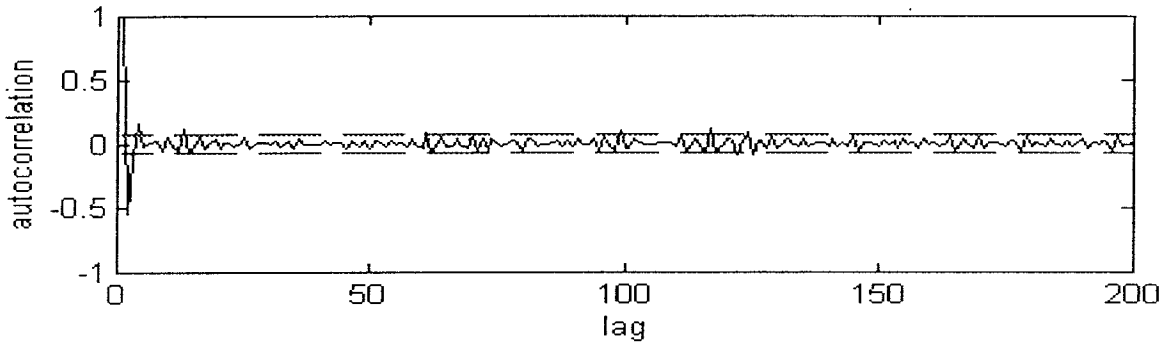

Figure A.6.58. PRN 6 FIR smoothed C/A residual autocorrelation (Bow).

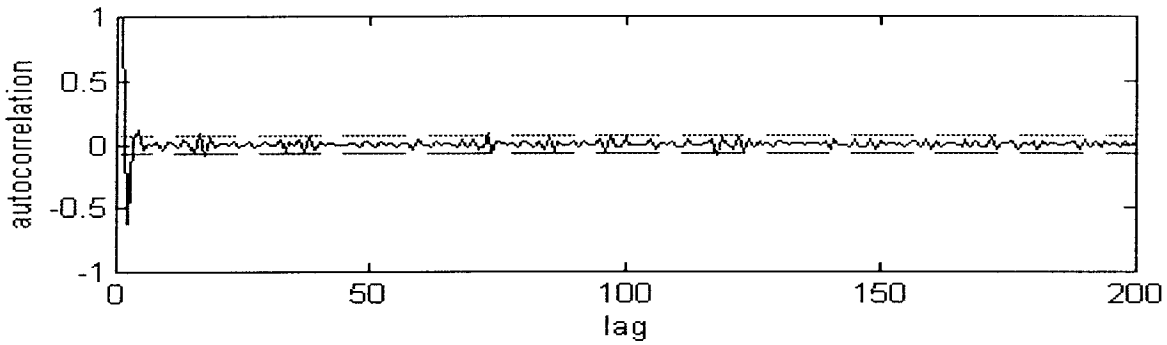

Figure A.6.59. PRN 15 FIR smoothed C/A residual autocorrelation (Bow).

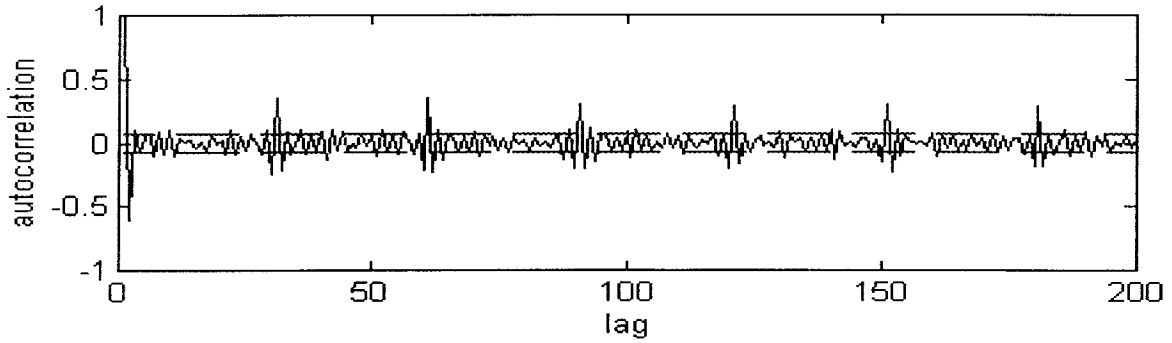

Figure A.6.60. PRN 19 FIR smoothed C/A residual autocorrelation (Bow).

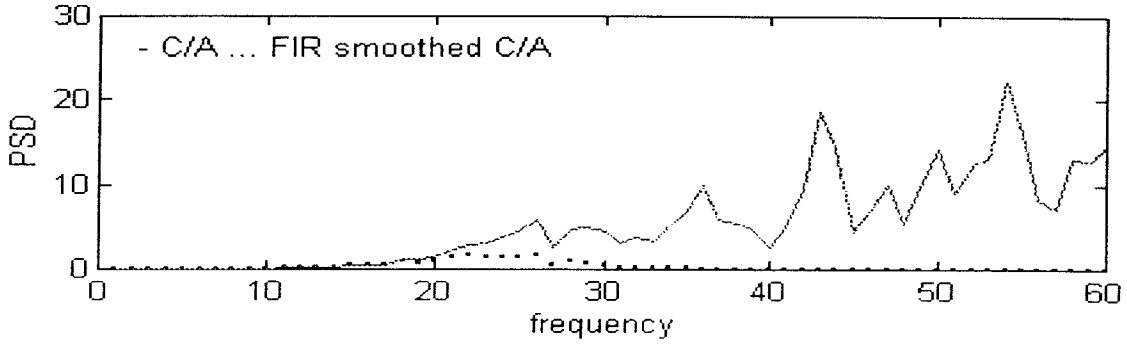

Figure A.6.61. PRN 2 PSD of C/A and FIR smoothed C/A accelerations (Bow).

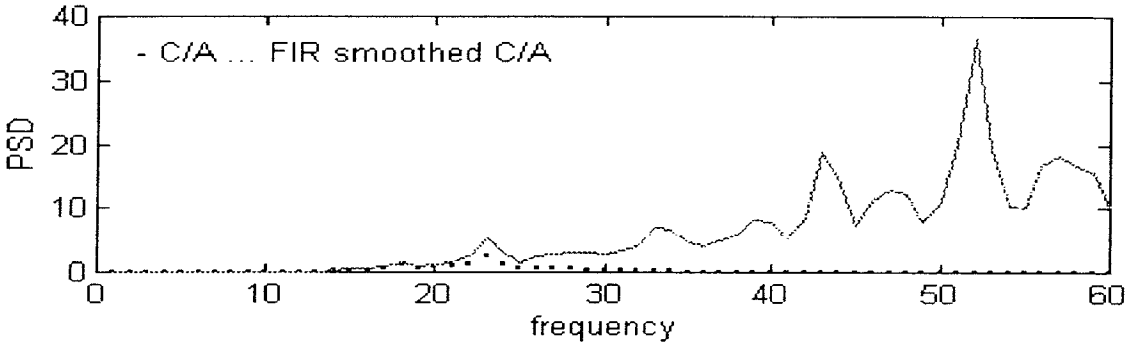

Figure A.6.62. PRN 6 PSD of C/A and FIR smoothed C/A accelerations (Bow).

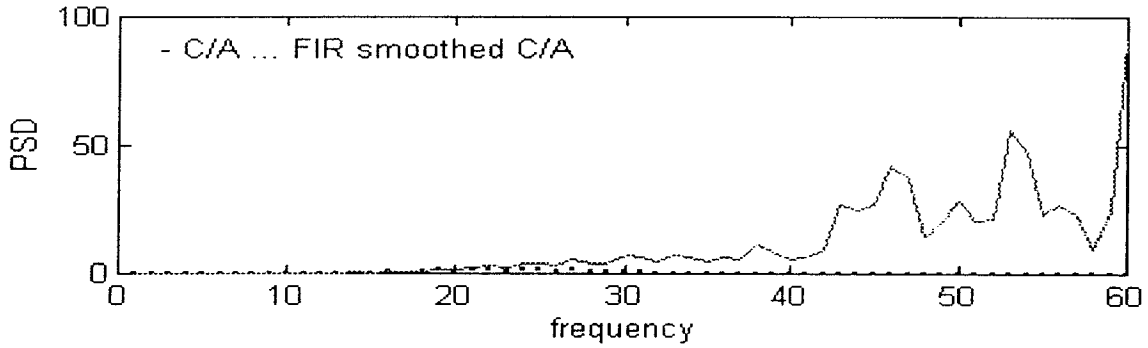

Figure A.6.63. PRN 15 PSD of C/A and FIR smoothed C/A accelerations (Bow).

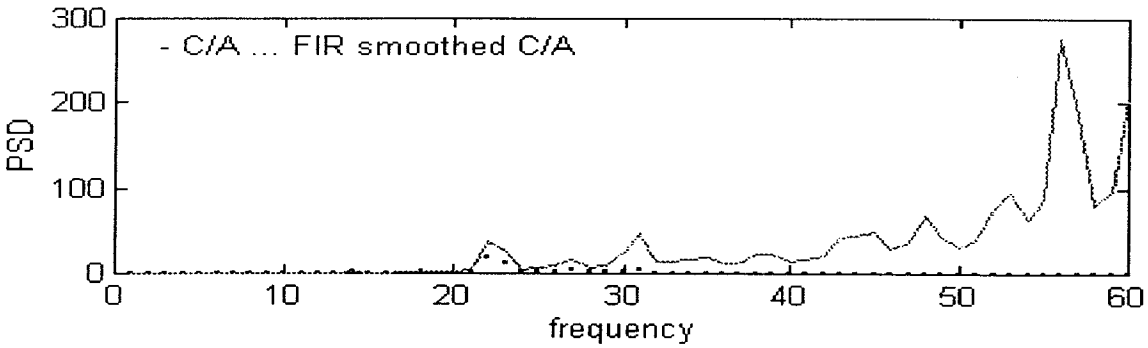

Figure A.6.64. PRN 19 PSD of C/A and FIR smoothed C/A accelerations (Bow).

Publications from

THE SCHOOL OF GEOMATIC ENGINEERING

(Formerly School of Surveying)

THE UNIVERSITY OF NEW SOUTH WALES

All prices include postage by surface mail. Air mail rates on application. (Effective September 1996)

To order, write to Publications Officer, School of Geomatic Engineering
The University of New South Wales, Sydney 2052, AUSTRALIA

NOTE: ALL ORDERS MUST BE PREPAID

UNISURV REPORTS - S SERIES

S8 - S20	Price (including postage) :		$10.00
S29 onwards	Price (including postage) :	Individuals	$25.00
		Institutions	$30.00

S8 A. Stolz, "Three-D Cartesian co-ordinates of part of the Australian geodetic network by the use of local astronomic vector systems", Unisurv Rep. S8, 182 pp, 1972.

S10 A.J. Robinson, "Study of zero error & ground swing of the model MRA101 tellurometer", Unisurv Rep. S10, 200 pp, 1973.

S12. G.J.F. Holden, "An evaluation of orthophotography in an integrated mapping system", Unisurv Rep. S12, 232 pp, 1974.

S14. Edward G. Anderson, "The Effect of Topography on Solutions of Stokes` Problem", Unisurv Rep. S14, 252 pp, 1976.

S16. K. Bretreger, "Earth Tide Effects on Geodetic Observations", Unisurv S16, 173 pp, 1978.

S17. C. Rizos, "The role of the gravity field in sea surface topography studies", Unisurv S17, 299 pp, 1980.

S18. B.C. Forster, "Some measures of urban residential quality from LANDSAT multi-spectral data", Unisurv S18, 223 pp, 1981.

S19. Richard Coleman, "A Geodetic Basis for recovering Ocean Dynamic Information from Satellite Altimetry", Unisurv S19,332 pp, 1981.

S20. Douglas R. Larden, "Monitoring the Earth's Rotation by Lunar Laser Ranging", Unisurv Report S20, 280 pp, 1982.

S29 Gary S Chisholm, "Integration of GPS into hydrographic survey operations", Unisurv S29, 190 pp, 1987.

S30. Gary Alan Jeffress, "An investigation of Doppler satellite positioning multi-station software", Unisurv S30, 118 pp, 1987.

S31. Jahja Soetandi, "A model for a cadastral land information system for Indonesia", Unisurv S31, 168 pp, 1988.

S33. R. D. Holloway, "The integration of GPS heights into the Australian Height Datum", Unisurv S33, 151 pp.,1988.

S34. Robin C. Mullin, "Data update in a Land Information Network", Unisurv S34, 168 pp. 1988.

S35. Bertrand Merminod, "The use of Kalman filters in GPS Navigation", Unisurv S35, 203 pp., 1989.

S36. Andrew R. Marshall, "Network design and optimisation in close range Photogrammetry", Unisurv S36, 249 pp., 1989.

S37. Wattana Jaroondhampinij, "A model of Computerised parcel-based Land Information System for the Department of Lands, Thailand," Unisurv S37, 281 pp., 1989.

S38. C. Rizos (Ed.), D.B. Grant, A. Stolz, B. Merminod, C.C. Mazur "Contributions to GPS Studies", Unisurv S38, 204 pp., 1990.

S39. C. Bosloper, "Multipath and GPS short periodic components of the time variation of the differential dispersive delay", Unisurv S39, 214 pp., 1990.

S40. John Michael Nolan, "Development of a Navigational System utilizing the Global Positioning System in a real time, differential mode", Unisurv S40, 163 pp., 1990.

S41. Roderick T. Macleod, "The resolution of Mean Sea Level anomalies along the NSW coastline using the Global Positioning System", 278 pp., 1990.

S42. Douglas A. Kinlyside, "Densification Surveys in New South Wales - coping with distortions", 209 pp., 1992.

S43. A. H. W. Kearsley (ed.), Z. Ahmad, B. R. Harvey and A. Kasenda, "Contributions to Geoid Evaluations and GPS Heighting", 209 pp., 1993.

S44. Paul Tregoning, "GPS Measurements in the Australian and Indonesian Regions (1989-1993)", 134 + xiii pp, 1996.

S45. Wan-Xuan Fu, "A study of GPS and other navigation systems for high precision navigation and attitude determinations", 332pp, 1996.

S46. Peter Morgan et al, "A zero order GPS network for the Australia region", 187 + xii pp, 1996.

MONOGRAPHS

Prices include postage by surface mail

M1.	R.S. Mather, "The theory and geodetic use of some common projections", (2nd edition), 125 pp., 1978.	Price	$15.00
M2.	R.S. Mather, "The analysis of the earth's gravity field", 172 pp., 1971.	Price	$8.00
M3.	G.G. Bennett, "Tables for prediction of daylight stars", 24 pp.,1974.	Price	$5.00
M4.	G.G. Bennett, J.G. Freislich & M. Maughan, "Star prediction tables for the fixing of position", 200 pp., 1974.	Price	$8.00
M8.	A.H.W. Kearsley, "Geodetic Surveying", 96 pp, (revised) 1988.	Price	$12.00
M11.	W.F. Caspary, "Concepts of Network and Deformation Analysis", 183 pp., 1988.	Price	$25.00
M12.	F.K. Brunner, "Atmospheric Effects on Geodetic Space Measurements", 110 pp., 1988.	Price	$16.00
M13.	Bruce R. Harvey, "Practical Least Squares and Statistics for Surveyors", (2nd edition), 319 pp., 1994.	Price	$30.00
M14.	Ewan G. Masters & John R. Pollard (Ed.), "Land Information Management", 269 pp., 1991. (Proceedings LIM Conference, July 1991).	Price	$20.00
M15/1	Ewan G. Masters & John R. Pollard (Ed.), "Land Information Management - Geographic Information Systems - Advance Remote Sensing Vol 1" 295 pp., 1993 (Proceedings of LIM & GIS Conference, July 1993).	Price	$30.00
M15/2	Ewan G. Masters & John R. Pollard (Ed.), "Land Information Management - Geographic Information Systems - Advance Remote Sensing Vol 2" 376 pp., 1993 (Proceedings of Advanced Remote Sensing Conference, July 1993).	Price	$30.00
M16.	A. Stolz, "An Introduction to Geodesy", 112 pp., 1994.	Price	$20.00